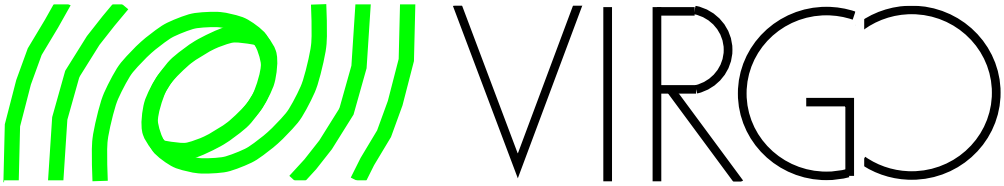

The VIRGO Physics Book, Vol. II

OPTICS and related TOPICS

The Virgo collaboration

1st release : Feb. 2001

April 21, 2006

Contents

Preface

This is one of the volumes of the Virgo Physics Book. The aim of this enterprise (VPB) is to keep track of the various theoretical or numerical studies carried out during the development of the Virgo conceipt and its realization. This is necessary for several reasons.

- The first reason is to present outside the collaboration, in a comprehensive document, the sum of the theoretical researches carried out during the R&D period (not fully over, considering future improvements), in order to show what physical effects have been studied.

- The second reason is to prevent loss of memory in the collaboration. It is convenient to be able to find in one place the state of the art in the various domains of modeling. Evolution of the technology, of the materials, etc... makes necessary to re-estimate from time to time the orders of magnitude of different sources of noise, for instance, and check wether the hierarchy is still valid. For doing this, the principles must be available.

- The third reason is to provide a reference document for the young searchers entering the collaboration allowing them to become efficiently acquainted with the principles of the experiment. In this spirit, some "frequently asked questions" are treated, even if the relation with Virgo is not direct.

The principle of the document is thus to present all theoretical contributions of the Virgo teams in a comprehensive way. This is not a compilation of Virgo notes, although obviously it contains some of them, nor a course of physics, although obviously some general principles are recalled.

It is signed by "the collaboration", because all theoretical or numerical works reported in, have been carried out on request and with the help of it as a whole.

This Volume II contains some works related to optics and other issues strongly related to optics. The principles of interferometry are recalled, then the various configurations of interferometers. The various principles of optical modeling are presented (propagation of light, simulation of cavities, of interferometers), and also the methods of analyzing mirrors. The opto-thermal problems are studied (thermal lensing, distortions), and the part of thermal noise studies related to the mirror substrates though a special volume should be dedicated to thermal noise issues. The modulation-demodulation theory is also described.

This is the present status of this document. It is clear that further contributions will be added from time to time, and this is the reason why it will not have a general paper version, but only a virtual presence on the net. Moreover, other volumes are expected,

- about General Relativity and gravitational wave theory basic background, theory of the interaction of GW with detectors...,
- about thermal noise issues,
- about seismic noise suppression and superattenuator physics
- and possibly other topics ?

and for which future contributors are known. Please report possible errors or misprints to

vinet@obs-nice.fr

N.B.:

From time to time, this document will be improved by correcting misprints and errors, or adding some new material.

Chapter 1

Theory of GW Interferometers

1.1 Shot noise limited interferometry

1.1.1 Spectral density of power equivalent to SN

Shot noise is produced by photodetectors currently used in all domains of photonics. Even with very stable lasers and cooled detectors, the photocurrent appears, at the microscopic level as a random stationnary process having a mean in agreement with a classical theory, but a variance that can be understood only by reference to quantum theory. In fact the light is produced and received as a flux of photons, and it is shown, for instance, that during a time interval Δt, the number photons that a photodiode can detect is a random variable N whose probability law is Poissonnian (a general law for all processes consisting in random arrivals). This means that the probability of detecting exactly n photons is:

$$p_n \;=\; \mathrm{e}^{-m}\,\frac{m^n}{n!}$$

where m is the only parameter of the Poisson probability distribution, and in concrete terms, represents the mean photon flux. In fact, if the mean number of photons is larger than about 50, the Poisson law is identical to a gaussian law having the same moments. It is classically shown that the expectation value of a random variable N obeying a Poisson law of parameter m is $E[N] = m$, and it variance is $V[N] = m$. On the other hand, during the time interval Δt, the energy deposited on the diode is

$$\Delta e \;=\; \eta P \Delta t \;=\; N h_P \nu$$

where P is the power of the light beam, and ν its frequency (h_P is the Planck constant). η is the *quantum efficiency* of the detector, a quantity very close to 1 in present infra-red detectors, so that we shall ignore η in all the sequel. In other words, consider P as the power actually detected. Now, it is clear that there is an equivalence between saying that N is a random variable, and saying that P is a random variable. Calling P_0 the averaged value of P, we see that

$$E[N] = \frac{P_0 \Delta t}{h_P \nu}$$

and consequently (Poisson) :

$$V[N] = \frac{P_0 \Delta t}{h_P \nu}$$

It is now possible to consider the variance of P :

$$V[P] = V[N] \frac{h_P^2 \nu^2}{\Delta t^2}$$

$$= \frac{P_0 h_P \nu}{\Delta t}$$

The quantity $1/\Delta t$ may be regarded as the ideal bandwidth of the detector, then the quantity $P_0 h\nu$ appears as a white spectral density. We shall consider in the sequel that given an incoming power P_0, the two-sided spectral density of power equivalent to shot noise is

$$S'_P(f) = P_0 h_P \nu \tag{1.1}$$

The fact that the preceding formula gives actually the two-sided SD can be shown as follows. On successive time slices of duration Δt, the detected energy (and consequently the averaged power) is a random variable of mean P_0, so that, calling x the statistical variable $P - P_0$, $x(t)$ defines a stationary centered stochastic process. We can write the function $x(t)$ as :

$$x(t) = x_k \quad \text{for} \quad k\Delta t < t < (k+1)\Delta t$$

The spectral density of any stationary centered process has the general definition :

$$S_x(\Omega) = \lim_{T \to \infty} \frac{1}{T} E \left[\left| \int_0^T \mathrm{e}^{-i\Omega t} x(t)\, dt \right|^2 \right]$$

If we choose T an integer multiple of Δt, we get easily :

$$\int_0^T \mathrm{e}^{-i\Omega t} x(t)\, dt \;=\; \sum_{k=0}^{n-1} x_k\, \mathrm{e}^{-i(k+\frac{1}{2})\Omega\Delta t}\, \Delta t\, \mathrm{sinc}(\Omega\Delta t/2)$$

so that

$$\left| \int_0^T \mathrm{e}^{-i\Omega t} x(t)\, dt \right|^2 = \sum_{k,m} x_k x_m\, \mathrm{e}^{-i(k-m)\Omega\Delta t}\, \Delta t^2\, \mathrm{sinc}(\Omega\Delta t/2)^2$$

The variables x_k are uncorrelated, so that

$$E[x_k x_m] \;=\; V[P]\, \delta_{km}$$

and

$$E\left[\left| \int_0^T \mathrm{e}^{-i\Omega t} x(t)\, dt \right|^2 \right] \;=\; \sum_k V[P] \Delta t^2\, \mathrm{sinc}(\Omega\Delta t/2)^2$$

$$=\; n\Delta t V[P] \Delta t \mathrm{sinc}(\Omega\Delta t/2)^2$$

(with the definition: $\mathrm{sinc}(x) \equiv \sin(x)/x$), and with $T = n\Delta t$, this is finally

$$S'_P(\Omega) \;=\; P_0\; h_P \nu\; \mathrm{sinc}(\Omega\Delta t/2)^2$$

One easily sees that the total variance is recovered by integrating over negative and positive frequencies (and remembering that $\int_{-\infty}^{\infty} \mathrm{sinc}(x)^2\, dx = \pi$) The single-sided spectral density is thus :

$$S_P(\Omega) \;=\; 2P_0\; h_P \nu\; \mathrm{sinc}(\Omega\Delta t/2)^2$$

The integration time Δt can be chosen very short, so that the preceding function is almost flat in the audio region, and the one sided spectral density to be used in practical problems is simply :

$$S_P(\Omega) \;=\; 2P_0\; h_P \nu$$

as for a white noise.

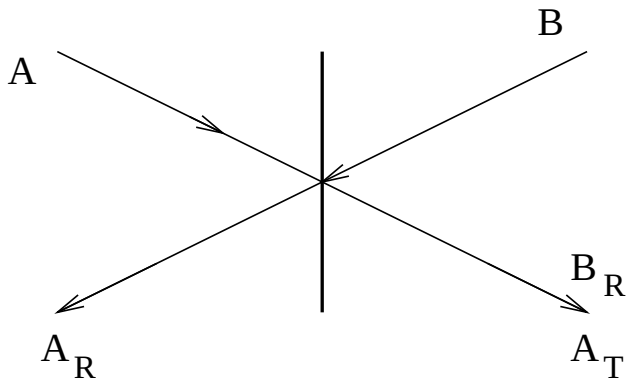

Figure 1.1: Partially reflecting mirror

1.1.2 Partially reflecting mirrors

In interferometry, a light source provides a beam that is often splitted into two or more waves propagating along different paths. It is mandatory to take into account the phase jumps caused by reflection or transmission at a mirror surface. We consider a mirror as a plane surface of vanishing thickness. There are two complex numbers z_R and z_T expressing respectively the relative reflected and transmitted waves. Namely, when a wave of complex amplitude A reaches the mirror's surface, we have (see Fig.1.1 for notation):

$$A_R \;=\; z_R A \;\;,\;\; A_T \;=\; z_T A$$

Conservation of the total power requires that

$$|z_R|^2 + |z_T|^2 \;=\; 1 - p$$

where p expresses possible absorption (dissipation) in the mirror. For our present purposes, it is mandatory to have a very small p (usually a few ppm, i.e. a few 10^{-6}). Requirements on the arguments of z_R and z_T come from the mirror viewed as a 4 ports element. If a second wave of amplitude B reaches the mirror coming from the opposite direction, the source of A being switched off, it undergoes exactly the same processes with the same coefficients (the mirror is invariant in a space reflection). When the two amplitudes are present simultaneously, we have thus:

$$A_R = z_R A + z_T B$$

$$B_R = z_T A + z_R B$$

Remark that we call A_R the sum of all waves going to the left, and B_R the sum of all waves going to the right; we could as well call B_T and A_T the same waves. If we consider the power balance, we must have

$$|A_R|^2 + |B_R|^2 = (1-p)\left(|A|^2 + |B|^2\right)$$

on the other hand, using the preceding equations, we get

$$|A_R|^2 + |B_R|^2 = \left(|z_R|^2 + |z_T|^2\right)\left(|A|^2 + |B|^2\right) + (z_R\overline{z_T} + \overline{z_R}z_T)\left(\overline{A}B + A\overline{B}\right)$$

we therefore must have

$$(z_R\overline{z_T} + \overline{z_R}z_T)\left(\overline{A}B + A\overline{B}\right) \;=\; 0$$

for any couple (A, B) of complex numbers, which clearly requires

$$z_R\overline{z_T} + \overline{z_R}z_T \;=\; 0$$

or, in terms of arguments:

$$Arg(z_R) - Arg(z_T) \;=\; (2n+1)\frac{\pi}{2} \quad (n \in \mathbf{N})$$

In order to preserve power balance at each interference occuring at the surface of a mirror, we must, in the calculation, take into account this phase jump of $\pi/2$ between the reflected and the transmitted wave. One possible choice, that will be kept throughout this document, is

$$z_R = i\,r \;,\quad z_T \;=\; t$$

where (r, t) are real numbers verifying

$$r^2 + t^2 = 1 - p$$

1.1.3 Elementary Michelson

A simple interferometer design is shown on Fig.1.2. The light coming from a laser is split into two distinct paths ended by mirrors, then reflected and recombined on the splitter where the interference occurs. We call r_s and t_s the reflection and transmission coefficients of the splitter, and k the wave

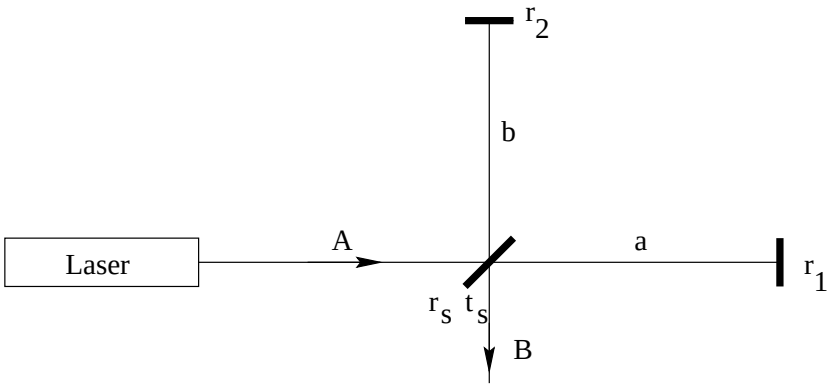

Figure 1.2: A simple Michelson experiment

number ($k \equiv 2\pi/\lambda$, λ being the wavelength. The amplitude of the laser wave is A and the outgoing is B. One has

$$B = r_s t_s \left(r_1 \mathrm{e}^{2ika} + r_2 \mathrm{e}^{2ikb} \right)$$

so that

$$B\overline{B} = r_s^2 t_s^2 A\overline{A} \left(r_1^2 + r_2^2 + 2r_1 r_2 \cos[2k(a-b)] \right)$$

Suppose now that the device aims to measure a very small variation of the length of one arm. For instance, the length of arm 1 is $a = a_0 + x(t)$, where $|x(t)| \ll \lambda$. We can consider for brevity that the splitter is well balanced and $r_s^2 = t_s^2 = 1/2$. The outgoing power is :

$$P(t) = P_{DC} + \Delta P(t)$$

with

$$P_{DC} = \frac{1}{4} P_0 \left(r_1^2 + r_2^2 + 2r_1 r_2 \cos\alpha \right)$$

where $\alpha = 2k(a_0 - b)$ is the static tuning of the interferometer. if $x(t) = 0$, we see that the outgoing power can be controlled by α. If $\alpha = 2n\pi$,

$$P_{DC,b} = \frac{(r_1 + r_2)^2}{4} P_0$$

which is almost 1 if both r_1, r_2 are reasonably near unity, we say that the interferometer is tuned at a *bright fringe*, if now $\alpha = (2n+1)\pi$,

$$P_{DC,d} = \frac{(r_1 - r_2)^2}{4} P_0$$

which can be made as small as wanted by equalizing r_1 and r_2. We say that the interferometer is tuned at a *dark fringe*. In practice, it is not so easy to make $r_1 = r_2$, and this determines the *contrast* of the inteferometer. If x is not zero, there is a time varying component

$$\Delta P(t) \;=\; r_1 r_2 P_0 k x(t) \sin\alpha$$

The question is now : What is the minimum variation x that we could detect, knowing that there is a fluctuation of the power, even in the absence of signal, due to shot noise. The answer is given by computing the signal to noise ratio ρ :

$$\rho(f) \;=\; \frac{S_{\Delta P(f)}}{S_P(f)}$$

The spectral density S_P of power equivalent to shot noise is :

$$S_P(f) \;=\; \frac{1}{2} P_0 h_P \nu \left(r_1^2 + r_2^2 + 2 r_1 r_2 \cos\alpha\right)$$

The spectral density of signal is :

$$S_{\Delta P}(f) \;=\; r_1^2 r_2^2 P_0^2 \sin^2\alpha\, k^2 S_x(f)$$

where $S_x(f)$ is the SD of x viewed as a stationnary process. We have thus

$$\rho(f) \;=\; 2 r_1^2 r_2^2 \frac{P_0}{h_P \nu} f(\alpha)\, k^2 S_x(f)$$

where

$$f(\alpha) \;=\; \frac{\sin^2\alpha}{r_1^2 + r_2^2 + 2 r_1 r_2 \cos\alpha}$$

(see Fig.1.3). It is easily seen that the optimal value α_0 is such that

$$\cos\alpha_0 = -\frac{r_<}{r_>}$$

where $r_<$ is the smallest of r_1, r_2 ,and $r_>$ the largest. One already sees that if the two coefficients are close to 1 , the tuning of the interfometer is near a dark fringe. When optimally tuned, we have

$$f(\alpha_0) \;=\; \frac{1}{r_>^2}$$

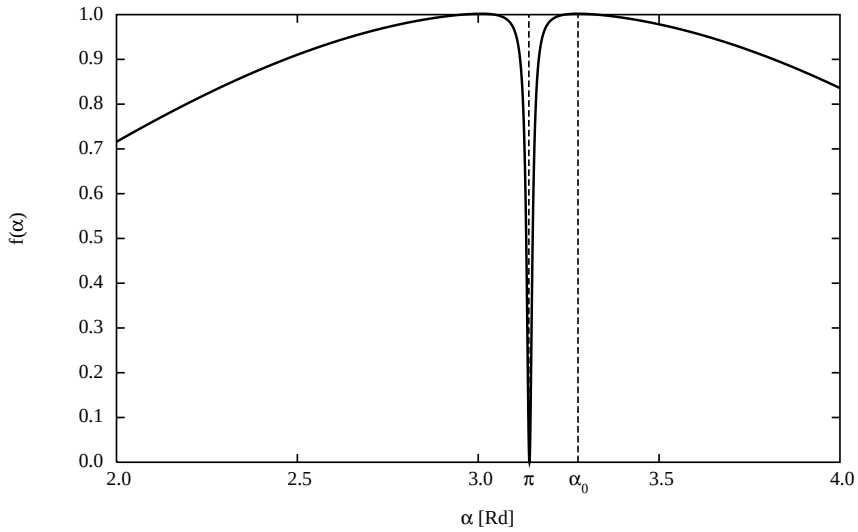

Figure 1.3: Optimization of the SNR

so that the optimal SNR is

$$\rho(f) \;=\; 2r_<^2\,\frac{P_0}{h\nu}\,k^2\,S_x(f)$$

The minimum detectable x can be evaluated by taking $\rho = 1$, and this gives

$$S_x(f)_{\rm min} \;=\; \frac{1}{2r_<^2}\frac{h_P\nu}{k^2P_0}$$

It is more physical to consider the root spectral density :

$$S_x^{1/2}(f) \;=\; \frac{\lambda}{4\pi}\sqrt{\frac{2h_P\nu}{P_0}}$$

where we have set $r_< \sim 1$. If further we assume that the small displacement $x(t)$ is caused by a gravitational wave $h(t)$, we have

$$x(t) = L\,h(t)$$

where L is the roughly equal arm lengths of the arms, and we have replaced the motion of both mirrors of $hL/2$ by a unique motion of mirror 1 by hL.

The root spectral density of h equivalent to shot noise is finally:

$$S_h^{1/2}(f) \;=\; \frac{\lambda}{4\pi L}\sqrt{\frac{2h_P\nu}{P_0}}$$

With the Virgo laser ($P_0 \sim 20$ W) and the wavelength $\lambda \sim 1.064\,\mu$m of the Nd:YAG amplifier, we get

$$S_x^{1/2}(f) \;\sim\; 1.2 \times 10^{-17}\,\mathrm{m\,Hz^{-1/2}}$$

With a 3 km arm length, this gives

$$S_h^{1/2}(f) \;\sim\; 3.8 \times 10^{-21}\,\mathrm{Hz^{-1/2}}$$

In fact, according to the theoretical litterature, this means that two orders of magnitude are missing for having some hope to detect gravitational waves. We shall see that these two orders can be gained by

- enhancing the laser power, not by upsizing the laser itself, but by creating a resonance surtension on the Michelson
- increase the arm length, not by adding kilometers of tunnels, but by creating a resonance in the 3 km arms

Creation and characterics of resonances are thus a very important item we are going to analyze and discuss in details.

1.1.4 Frequency stability requirements

The shot noise is not the only limitation to laser metrology. The laser source is not in practice a purely monochromatic source. The laser frequency is determined by the optical length of the laser cavity, which means the distance between mirrors, but also the index in the amplifier medium, and the index of the medium in between mirrors and amplifier medium. All these parameters are in general coupled to external sources of mechanical or thermal noise, so that the instantaneous frequency of the laser may be viewed as a random process. We shall represent the laser optical amplitude as:

$$A_{\mathrm{laser}} = A_0\;\mathrm{e}^{-i\omega_0 t}\,\mathrm{e}^{i\Psi(t)}$$

where $\omega_0/2\pi$ is the nominal frequency of the laser, and $\Psi(t)$ a random centered process. The power reaching the photodetector is:

$$P(t) \;=\; \frac{1}{4}\left[r_1^2 + r_2^2 + 2r_1 r_2 \cos[2k(b-a) + \Psi(t-2a/c) - \Psi(t-2b/c)]\right]$$

We have thus a spurious phase:

$$\phi(t) \;=\; \frac{1}{2}\left[\Psi(t-2a/c) - \Psi(t-2b/c)\right] \;=$$

$$\frac{1}{2}\left[\Psi(t-(a+b)/c+(b-a)/c) - \Psi(t-(a+b)/c-(b-a)/c)\right]$$

$$\simeq\; \frac{b-a}{c}\frac{\partial\Psi}{\partial t}(t-(a+b)/c)$$

assuming the difference $d \equiv b-a$ small compared to the coherence length of the laser. We have thus

$$\phi(t) \;=\; \frac{d}{c} \times 2\pi\nu(t)$$

where $\nu(t)$ is the instantaneous frequency. This implies that if we want to reduce the corresponding phase noise to a level comparable to the shot noise, which is:

$$\phi_{\rm sn} \;=\; \sqrt{\frac{2h_P\nu}{P}}$$

we must obtain a spectral density of frequency noise:

$$\delta\nu(f) < \frac{c}{2\pi d}\sqrt{\frac{2h_P\nu}{P}}$$

we see the importance of having a good symmetry (a small d) between the two arms. If we take the parameters already used above, the shot noise induced phase was about 10^{-10}Rd/Hz$^{1/2}$, if we admit a 1% relative asymmetry, this results in a requirement of

$$\delta\nu(f) < 2.10^{-4}\text{Hz/Hz}^{1/2}$$

The realistic situation is even more demanding, because firstly we want a safety margin of at least 1 order of magnitude with respect to the shot noise, secondly the shot noise will be reduced by 1 order of magnitude by recycling, and finally, the arm lengths will be seen to result from resonance effects, less easy to symmetrize than actual geometrical lengths, so that the requirement is rather in the range of 10^{-6}Hz/Hz$^{1/2}$.

1.2 The Fabry-Perot resonant cavity

1.2.1 Conventions used throughout this section

We assume a monochromatic light source, and we describe in the present section the (ideal) light beam circulating inside the interferometer as a plane wave, and moreover, we consider a given component of the electric field, so that the optical field at any place x of an optical system is of the scalar form

$$A(t,x) \;=\; A(x)\; \mathrm{e}^{-i\omega t}$$

A simple propagation step along a path of length L in a vacuum is therefore represented by a phase factor, and the relation between amplitudes will be

$$A(x+L) \;=\; \mathrm{e}^{ikL}\; A(x)$$

with $k \;=\; \omega/c \;=\; 2\pi/\lambda$, c being the velocity of light. As seen above, when a light ray encounters a mirror, it is partially reflected, transmitted and absorbed. We keep the convention explicited above: A_{in} being the incoming amplitude, A_{ref} the reflected, A_{trans} the transmitted, we have :

$$A_{ref} \;=\; ir\; A_{in} \quad , \quad A_{trans} \;=\; t\; A_{in}$$

$r,\; t$ being respectively the reflection and transmission coefficients of the mirror (real numbers).. We have the power balance :

$$r^2 + t^2 \;=\; 1 - p$$

where p is the loss coefficient, accounting for absorption in the coating or scattering into a different mode due to mirror geometrical imperfections (p can be as low as a few ppm (10^{-6}) for supermirrors as Virgo's).

A Fabry-Perot cavity is made of two parallel mirrors. When light enters the cavity through mirror 1, it is partially reflected and partially transmitted. The transmitted wave is reflected by mirror 2, then returns to mirror 1 where it is recombined with the incoming wave and partially transmitted to the exterior. On Fig.1.4, we have spatially separated the left and right propagating waves for the sake of clarity. If the phase after a round trip in the cavity allows it, the interference of the incoming wave and the returning wave is constructive and a strong intracavity wave builds up. light can be stored. We call $r_i,\; t_i \;, p_i \quad (i \;=\; 1,2)$, the parameters of the mirrors, and

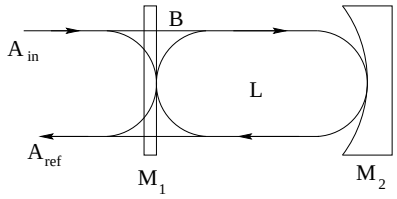

Figure 1.4: Fabry-Perot cavity

$A_{\rm in}$ the incoming wave. The length of the cavity is L. We can write the interference at M_1 for the intracavity wave as :

$$B \;=\; t_1\, A_{\rm in} \;-\; r_1 r_2\, {\rm e}^{2ikL} B$$

so that

$$B \;=\; \frac{t_1}{1 + r_1 r_2 {\rm e}^{2ikL}}\, A_{\rm in}$$

Clearly a resonance occurs when ${\rm e}^{2ikL} \;=\; -1$. We first discuss the case when the length of the cavity is fixed, and the frequency of light variable. The inverse case will be presented later. For a given L, we have a series of resonant frequencies

$$\nu_n \;=\; \left(n + \frac{1}{2}\right)\, \frac{c}{2L}$$

The spacing between two successive resonances is called *Free spectral Range* (FSR), and noted $\Delta\nu_{FSR}$.

$$\Delta\nu_{FSR} \;=\; \frac{c}{2L}$$

For a 3 kilometers cavity (as in VIRGO), the FSR is close to 50 kHz, whereas the optical frequency (at $\lambda \;=\; 1.06\,\mu$m) is about 3×10^{14} Hz, so that the integer n is close to 6×10^9. The ratio $S \;=\; B/A_{\rm in}$ is called *surtension factor* . Its maximum value is

$$S_{\rm max} \;=\; \frac{t_1}{1 - r_1 r_2}$$

Remark that if r_2 is fixed, for instance because the end mirror is assumed "Rmax", the maximum surtension is a function of r_1, which can take any value between 0 and $\sqrt{1 - p1}$. It is easily seen that the value of r_1 for which $S_{\rm max}$ is a maximum is:

$$r_{\rm opt} \;=\; (1 - p_1)\, r_2$$

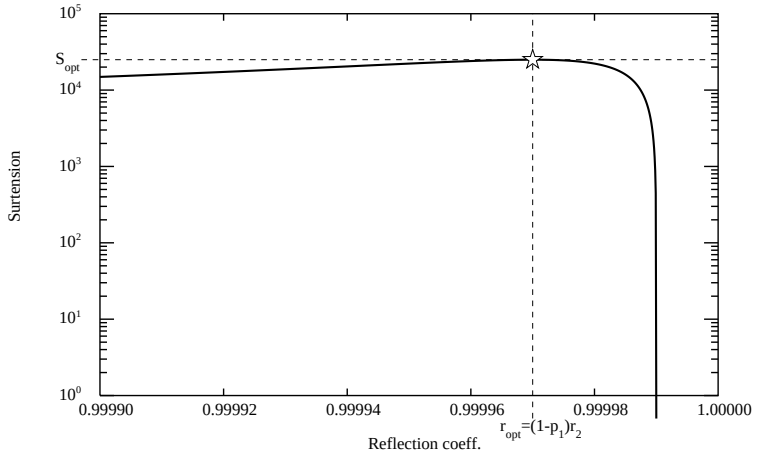

Figure 1.5: Surtension vs reflectivity of M1, assuming 20 ppm losses on each mirror, and no transmission for M2

and the corresponding value of $S_{\max}$ is

$$S_{\rm opt} \;=\; \frac{1-p_1}{1-(1-p1)(1-p2)} \;\sim\; \frac{1}{p_1+p_2}$$

(see Fig.1.5).

The width of the resonance line may be evaluated as follows. We assume that the frequency is close a resonance, so that

$$\nu \;=\; \nu_n \;+\; \delta\nu$$

with $\delta\nu \ll \Delta\nu_{FSR}$. We have

$$2kL \;=\; (2n+1)\pi \;+\; 2\pi\,\frac{\delta\nu}{\Delta\nu_{FSR}}$$

The surtension coefficient takes on the form

$$S \;=\; \frac{t_1}{1 \;-\; r_1 r_2\,\exp\left(2i\pi\frac{\delta\nu}{\Delta\nu_{FSR}}\right)}$$

Its square modulus gives the ratio between the intensities :

$$|S|^2 \;=\; \frac{t_1^2}{(1-r_1r_2)^2 \;+\; 4r_1r_2\,\sin\left(\pi\,\frac{\delta\nu}{\Delta\nu_{FSR}}\right)}$$

This is

$$|S|^2 \;=\; S^2_{\max} \times \frac{1}{1+\left[\frac{2\sqrt{r_1r_2}}{1-r_1r_2}\,\sin\left(\pi\,\frac{\delta\nu}{\Delta\nu_{FSR}}\right)\right]^2}$$

Proximity of the resonance allows to replace the sine by its argument, so that

$$|S|^2 \;=\; S^2_{\max} \times \frac{1}{1+\left[2\mathcal{F}\frac{\delta\nu}{\Delta\nu_{FSR}}\right]^2}$$

with the following definition

$$\mathcal{F} \;=\; \frac{\pi\sqrt{r_1r_2}}{1-r_1r_2} \tag{1.2}$$

for the *finesse* of the cavity. The values of $\delta\nu$ such that the surtension is half its maximum are :

$$\delta\nu \;=\; \pm\,\frac{\Delta\nu_{FSR}}{2\mathcal{F}}$$

and the *Full Width at Half Maximum* (FWHM) of the resonance is finally :

$$\delta\nu_{FWHM} \;=\; \frac{\Delta\nu_{FSR}}{\mathcal{F}}$$

One can note that we have described the cavity by an extra set of parameters $\mathcal{F}$ and $\Delta\nu_{FSR}$ equivalent to r_1r_2 and L. $\mathcal{F}$ contains only a photometric information about mirrors, whereas $\Delta\nu_{FSR}$ contains a geometrical information about the cavity. The exact expression for the resonance can be written under the form

$$|S|^2/S^2_{\max} \;=\; \frac{1}{1+\left[\frac{2\mathcal{F}}{\pi}\,\sin\left(\pi\,\frac{\delta\nu}{\Delta\nu_{FSR}}\right)\right]^2}$$

see Fig.1.6. The wave reflected off the cavity can be computed by

$$A_{\rm ref} \;=\; ir_1A_{\rm in} \;+\; ir_2t_1{\rm e}^{2ikL}B$$

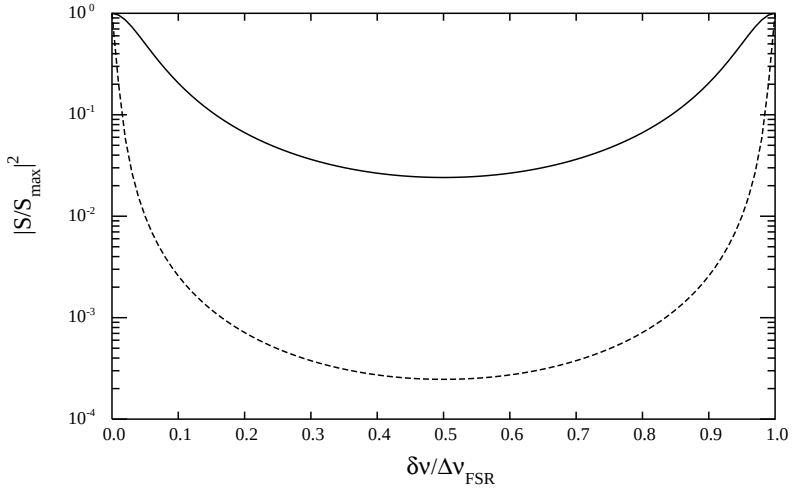

Figure 1.6: Resonance line shape for a finesse of $\mathcal{F} = 10$ (solid line), and $\mathcal{F} = 100$ (dotted line). Frequency unit is $\Delta\nu_{FSR}$

by substituting the value of B, we get

$$A_{\rm ref} \;=\; i\,\mathcal{R}\,A_{\rm in}$$

Where $\mathcal{R}$ is the reflectance of the cavity, defined as

$$\mathcal{R} \;=\; \frac{r_1 \;+\; (1-p_1)r_2\,{\rm e}^{2ikL}}{1 \;+\; r_1 r_2\,{\rm e}^{2ikL}} \tag{1.3}$$

For a cavity operated in the reflection mode, having a finite reflectivity of the input mirror (M_1), a high reflectivity end mirror (M_2) and reasonable losses (p_1, p_2), it can be seen that the global reflectance is about unity, with a small peak of absorption at resonance. The phase of the reflected wave undergoes a rapid transition of 2π when crossing the resonance (see Fig.1.7 and Fig.1.8). This is classical in all oscillators, and can be better understood in a simplified model. Note that $\delta\nu = \pm\,0.5 \times \delta\nu_{FWHM}$ correspond to half the maximum absorption and to a dephasing of $\pm\pi/2$ with respect to resonance. If now, the frequency of the light source is fixed and the length of the cavity variable, which is ideally the case in a GW interferometer, instead of resonant frequencies, we have resonant lengths given by

$$L_n \;=\; \left(n + \frac{1}{2}\right)\;\frac{\lambda}{2}$$

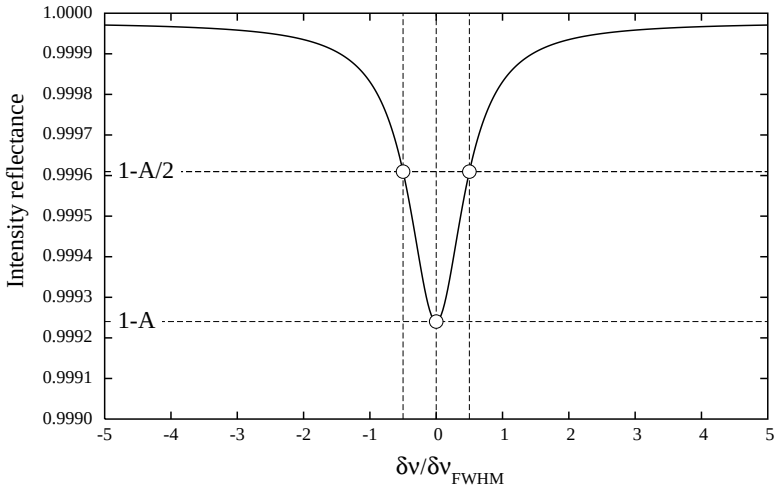

Figure 1.7: Absorption line of a cavity for r_1=0.85 and r_2=0.99998.(Finesse $\mathcal{F} \simeq 19.3$). A is the maximum of absorption.

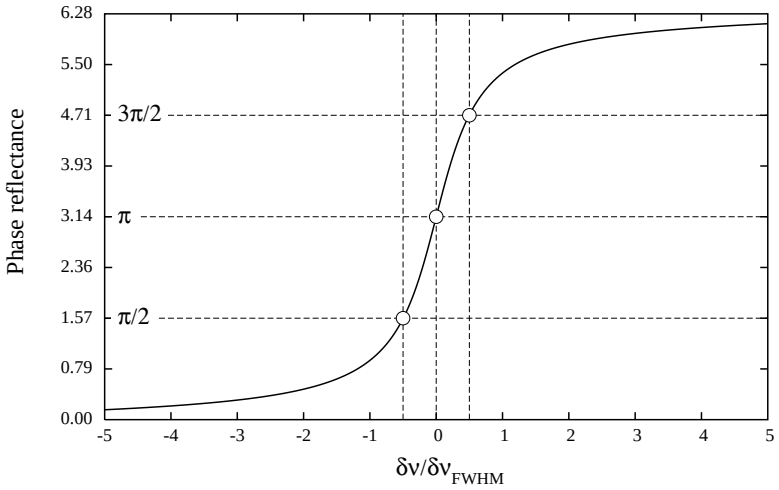

Figure 1.8: Phase reflectance of a cavity for r_1=0.85 and r_2=0.99998

showing that the displacement separating two successive resonances is :

$$\Delta L_{FSR} \;=\; \frac{\lambda}{2}$$

It is easy to show that the width of the resonance, in terms of displacement, is

$$\delta L_{FWHM} \;=\; \frac{\lambda}{2\mathcal{F}}$$

We develop now an approximate model of a cavity relying on the fact that the finesse is large compared to unity. It will prove useful for our further discussions of more complex systems involving cavities. A key parameter is indeed the finesse, defined by eq.(1.2) and depending only on the parameter $r_1 r_2$. Conversely, it is possible to compute $r_1 r_2$ from $\mathcal{F}$:

$$r_1 r_2 \;=\; 1 - \frac{\pi}{\mathcal{F}}\sqrt{1+\frac{\pi^2}{4\mathcal{F}^2}} - \frac{\pi^2}{2\mathcal{F}^2}$$

If $\mathcal{F}$ is much larger than 1, we can limit the expression at the first order in $1/\mathcal{F}$, and take

$$r_1 r_2 \;=\; 1 - \frac{\pi}{\mathcal{F}}$$

Consider now the reflectance of the cavity Eq.(1.3), and the phase factor $2kL$. We assume a frequency ν that is slightly detuned with respect ot resonance by an amount $\delta\nu$ so that :

$$2kL \;=\; 2k_0 L + 2\pi\frac{\delta\nu}{\Delta\nu_{FSR}} \;=\; \pi + \;2\pi\,\frac{1}{\mathcal{F}}\,f$$

where the *reduced frequency* f is the ratio of the offset to linewidth :

$$f \equiv \frac{\delta\nu}{\delta\nu_{FWHM}}$$

with $2k_0 L \equiv \pi \bmod[2\pi]$, we have :

$$r_2\mathcal{R} = \frac{r_1 r_2 - (1-p_1) r_2^2\, \mathrm{e}^{2i\pi f/\mathcal{F}}}{1 - r_1 r_2\, \mathrm{e}^{2i\pi f/\mathcal{F}}} \tag{1.4}$$

We set $(1-p_1)r_2^2 = (1-p)$, where p accounts for all losses in the cavity. By expanding $r_2\mathcal{R}$ at first order in $1/\mathcal{F}$ we get :

$$r_2\mathcal{R} \;=\; -\;\frac{1 - p\mathcal{F}/\pi + 2if}{1-2if}$$

The quantity $\sigma = p\mathcal{F}/\pi$ is called *coupling rate* and it is easily seen that $0 < \sigma < 2$. We have indeed obviously

$$0 < r_1^2 < 1 - p_1$$

$$\rightarrow 0 < r_1^2 r_2^2 < (1 - p_1) r_2^2 = 1 - p$$

then, assuming p very small,

$$\rightarrow 0 < r_1 r_2 < \sqrt{1 - p} = 1 - p/2$$

whence

$$0 < 1 - \frac{\pi}{\mathcal{F}} < 1 - p/2$$

$$\rightarrow 0 < \frac{p\mathcal{F}}{\pi} < 2$$

Most of the properties of the FP cavity can be known by only knowing its coupling rate. The reflectance of the cavity can thus be written (by putting $r_2 \simeq 1$ at this point) :

$$\mathcal{R} \;=\; -\frac{1 - \sigma + 2if}{1 - 2if}$$

We see that the reflectance at resonance is

$$\mathcal{R}(0) \;=\; -(1 - \sigma)$$

so that $\sigma = 1$ corresponds to total absorption of light, or *optimal coupling.* For σ running from 0 to 1 the cavity is overcoupled, this means that, at resonance, the incoming field is increasingly absorbed by the cavity until total absorption. then past 1, the field is decreasingly absorbed until total reflection. The intensity reflection coefficient is :

$$|\mathcal{R}|^2 \;=\; 1 - \frac{\sigma(2 - \sigma)}{1 + 4f^2}$$

The reflected phase is :

$$\mathrm{Arg}\,[\mathcal{R}] = \pi + \tan^{-1}\left(\frac{2f}{1 - \sigma}\right) + \tan^{-1}(2f) \tag{1.5}$$

Increasing values of σ progressively decouples the cavity from the incoming field, the reflectivity becomes near unity (because the input mirror becomes

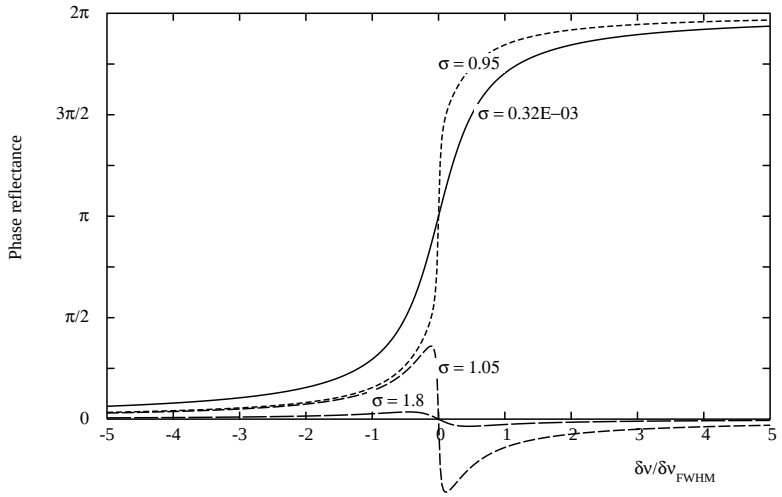

Figure 1.9: Transition from over to undercoupling. (NB : For σ=1, there is no reflected wave)

the only part of the FP visible from the exterior) , and the reflected phase becomes more and more unsensitive to frequency detuning (see Fig.1.9). Note that the coupling is strong when the coupling constant is weak, and vice-versa. We should better therefore, call σ the *undercoupling constant*, but we keep the present definition for the sake of brevity. The surtension coefficient is defined by

$$\mathcal{S} \;=\; \frac{t_1^2}{|1 + r_1 r_2 \mathrm{e}^{2ikL}|^2}$$

In the coupling rate notations, it becomes

$$\mathcal{S} \;=\; \frac{\sigma(2-\sigma)}{p\,(1+4f^2)}$$

showing that the maximum of intracavity power is reached at optimal coupling ($\sigma = 1$). In general, at resonance we have therefore

$$\mathcal{S}_0 \;=\; \frac{2\mathcal{F}}{\pi}\left(1 - \frac{\sigma}{2}\right)$$

and simply

$$\mathcal{S}_0 \;=\; \frac{2\mathcal{F}}{\pi}$$

in the strong overcoupling regime ($\sigma \ll 1$). The phase reflectance (see eq.1.5) is

$$\Phi(f) \;=\; \pi + \tan^{-1}\left(\frac{2f}{1-\sigma}\right) + \tan^{-1}(2f)$$

For f very small, this is at first order :

$$\Phi(f) \;=\; \frac{2(2-\sigma)}{1-\sigma}\, f \;=\; \frac{2(2-\sigma)}{1-\sigma}\, \mathcal{F}\, \frac{\delta\nu}{\Delta\nu_{FSR}}$$

In terms of the coupling rate, and absolute frequency detuning, the slope of $\Phi(\delta\nu)$ is

$$\frac{d\Phi}{d\delta\nu} \;=\; \frac{2\sigma(2-\sigma)}{1-\sigma}\, \frac{\pi}{p\,\Delta\nu_{FSR}}$$

In terms of the coupling rate and absolute displacement of the mirrors, we have the slope

$$\frac{d\Phi}{d\delta L} \;=\; \frac{2\sigma(2-\sigma)}{1-\sigma}\, \frac{2\pi}{p\,\lambda}$$

It could seem that the optimum detectivity is near the optimal coupling, where the slope is a maximum. The infinite slope at optimal coupling is very appealing, but unfortunately corresponds to total absorption, so that there is no reflected wave... This will be discussed later, in the Michelson interferometer section, when we shall study the conversion of a phase change into an amplitude change, detectable by a diode. If the coupling rate is small (i.e. the losses small and the finesse moderate), which is the current case in GW interferometers, the slope is simply :

$$\frac{d\Phi}{d\delta L} \;=\; \frac{8\mathcal{F}}{\lambda}$$

This allows to find a relation with an equivalent number n of non interfering round trips in a multipass cell of same length : in such a situation, the slope would be:

$$\frac{d\Phi}{d\delta L} \;=\; \frac{4\pi n}{\lambda}$$

so that

$$n \;\sim\; 2\mathcal{F}/\pi$$

note that this is exactly the surtension at resonance :

$$n \;=\; \mathcal{S}_0$$

In the undercoupling regime ($1 < \sigma < 2$), the phase reflectance has two extrema, for

$$f = \pm\frac{1}{2}\sqrt{\sigma - 1}$$

these two extrema being

$$\Phi = \pm \tan^{-1}\left(\frac{2-\sigma}{\sigma\sqrt{\sigma-1}}\right)$$

showing that the phase reflectance becomes flat as $\sigma \to 2$.

1.2.2 The Pound-Drever scheme

As a first example of application of this simple model of a reflection operated cavity, we consider the so-called Pound-Drever servo scheme, in which the goal is to keep a given light source in resonance with a reference cavity. In order to act for correction upon the frequency of the source, an error signal is needed. It is obtained by a modulation technique : the light source is phase modulated at frequency ν_{mod}, which means that after passing the modulator crystal, the amplitude entering the cavity is of the form :

$$A(t) = A_0 \exp\left[i\epsilon\cos(2\pi\nu_{mod}t)\right] \times \exp[-2i\pi\nu_L t]$$

where ν_L is the frequency of the source, i.e. the variable to be servoed. ϵ is the modulation depth, and if it is small, we can expand at first order the preceding expression, yielding

$$A(t) = A_0\,\mathrm{e}^{-2i\pi\nu_L t} + i\,\frac{\epsilon}{2}A_0\,\mathrm{e}^{-2i\pi(\nu_L+\nu_{mod})t} + i\,\frac{\epsilon}{2}A_0\,\mathrm{e}^{-2i\pi(\nu_L-\nu_{mod})t}$$

We can recognize in this sum, the carrier and two sidebands added by the modulator. Each of these three waves is differently reflected by the cavity. If we call $B(t)$ the reflected amplitude, we have :

$$B(t) = A_0\left[R\,\mathrm{e}^{-2i\pi\nu_L t} + i\,\frac{\epsilon}{2}\,R_+\,\mathrm{e}^{-2i\pi(\nu_L+\nu_{mod})t} + i\,\frac{\epsilon}{2}\,R_-\,\mathrm{e}^{-2i\pi(\nu_L-\nu_{mod})t}\right]$$

where R represents the reflectance of the cavity for the carrier, and $R_\pm$ the reflectance for the two sidebands. This amplitude is partially directed to a photodiode delivering thus a current proportional to

$$B(t)\overline{B(t)} = A_0\overline{A_0}\left[R\overline{R} - i\,\frac{\epsilon}{2}\,(R\overline{R_-} - \overline{R}R_+)\mathrm{e}^{-2i\pi\nu_{mod}t} - i\,\frac{\epsilon}{2}\,(R\overline{R_+} - \overline{R}R_-)\mathrm{e}^{2i\pi\nu_{mod}t}\right]$$

The demodulation consists in mixing the latter current with the modulation current with a variable dephasing Φ. The demodulation current is :

$$D(t) = \mathrm{e}^{i\Phi}\mathrm{e}^{2i\pi\nu_{mod}t} \; + \; \mathrm{e}^{-i\Phi}\mathrm{e}^{-2i\pi\nu_{mod}t}$$

For Φ=0, the demodulation is said *in phase*, and *in quadrature* for $\Phi = \pi/2$. The demodulated signal is the product $B\overline{B} \times D$, and considering that a low pass filter retains only the DC terms in the result, we get for the demodulated filtered current (DFC) :

$$\mathrm{DFC} \;=\; i\,\frac{\epsilon}{2}A_0\overline{A_0}\left[\mathrm{e}^{i\Phi}(\overline{R}R_+ - R\overline{R_-}) \;+\; \mathrm{e}^{-i\Phi}(\overline{R}R_- - R\overline{R_+})\right]$$

The approximate model presented above allows to compute this expression. We have, denoting by f the offset of the source frequency with respect to resonance in linewidth units :

$$R \;=\; -\,\frac{1-\sigma+2if}{1-2if}$$

It is assumed that f does not exceed 1. Now for the sidebands, we assume the modulation frequency antiresonant, i.e. such that it is shifted by half a FSR from resonance. At antiresonance, the reflectance of the cavity, and consequently $R_\pm$, is practically 1, so that the DFC becomes explicitly :

$$\mathrm{DFC} \;=\; i\,\frac{\epsilon}{2}A_0\overline{A_0}\left[X\,\mathrm{e}^{i\Phi} + \overline{X}\,\mathrm{e}^{-i\Phi}\right]$$

with

$$X \;=\; \overline{R} \;-\; R$$

or finally

$$X = \frac{4i(2-\sigma)\,f}{1+4f^2}$$

This shows that the demodulation must be in quadrature. The error curve has the following appearance (see Fig.1.10). Note that the frequency interval between the two extrema is nothing but the FWHM of the resonance. We see that there exists a range of frequency on which the error signal is practically proportional to the frequency excursion, and this is the starting point of the Pound-Drever-Hall technique for servoing cavities on laser light or conversely.

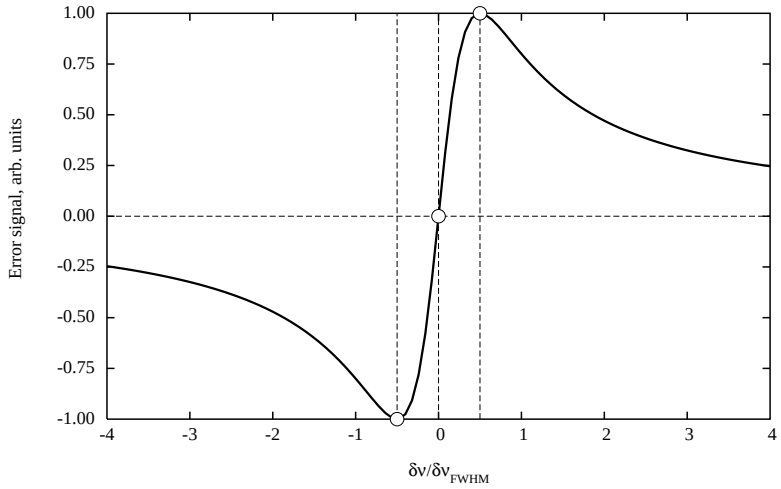

Figure 1.10: Pound-Drever error signal for laser stabilization on a reference cavity

1.2.3 The double Fabry-Perot cavity

It is interesting to investigate what happens when we install a Fabry-Perot cavity inside a Fabry-Perot cavity, because it is the basis of the so-called "power recycling" setup, used in GW interferometers for enhancing the laser power, that we shall discuss in details in a foregoing section. The system we are considering is described on Fig.1.11: it consists of three mirrors, M_1, M_2, M_3, spaced by distances l and L. We assume $L \gg l$. This offers us the opportunity to calculate the transmittance of a Fabry-Perot cavity having mirrors M_1, M_2. Call r_1, r_2, t_1, t_2 the corresponding parameters, and for the sake of simplicity, let us neglect the losses, and in the same spirit, take $r_3 = 1$. We can write the stored amplitude when M_3 is removed:

$$B \;=\; A\,\frac{t_1}{1 + r_1 r_2\,\mathrm{e}^{2ikl}}$$

as already seen. Now the amplitude tranmitted through mirror M_2 in absence of mirror M_3 defines the transmittance:

$$\mathcal{T} \;=\; \frac{t_1 t_2 \mathrm{e}^{ikl}}{1 + r_1 r_2\,\mathrm{e}^{2ikl}}$$

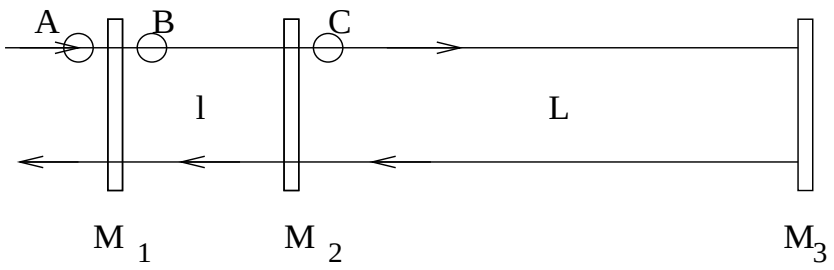

Figure 1.11: Double Fabry-Perot

whereas the reflectance for a wave coming from the right is, according to a preceding study:

$$\mathcal{R} \;=\; \frac{r_2 + r_1 \mathrm{e}^{2ikl}}{1 + r_1 r_2 \, \mathrm{e}^{2ikl}}$$

For the compound cavity, we can evaluate the amplitude C just as we would do for a cavity having a virtual mirror of parameters $\mathcal{R}$, $\mathcal{T}$, and an end mirror M_3:

$$C \;=\; \frac{\mathcal{T}}{1 + \mathcal{R} \, \mathrm{e}^{2ikL}} \, A$$

Now the question is: How to choose the phases $2kl$ and $2kL$ in order to maximize the intracavity power $|C|^2$? It is worth to compute explicitly the result:

$$C \;=\; \frac{t_1 t_2 \, \mathrm{e}^{ikl}}{1 + r_1 r_2 \, \mathrm{e}^{2ikl} + \mathrm{e}^{2ikL} \, (r_2 + r_1 \, \mathrm{e}^{2ikl})} \, A$$

we see that for $2kl \equiv 0 \ [\mathrm{mod}\ 2\pi]$, and $2kL \equiv \pi \ [\mathrm{mod}\ 2\pi]$, we get

$$|C|^2 \;=\; \frac{t_1^2 t_2^2}{(1 - r_1)^2 (1 - r_2)^2} \, |A|^2$$

which is clearly the maximum value. It means that the short cavity must be *antiresonant*, and the long one resonant. We can write the result as a global surtension:

$$S_0 \;=\; \left[\frac{|C|^2}{|A|^2} \right]_{\mathrm{reso}} \;=\; \frac{(1 + r_1)(1 + r_2)}{(1 - r_1)(1 - r_2)}$$

We know that a cavity at antiresonance is far more reflective than any of its two simple mirrors: if we assume $r_1 = 1 - \varepsilon_1$ and $r_2 = 1 - \varepsilon_2$, with $\varepsilon_1, \varepsilon_2 \ll 1$,

we have

$$\mathcal{R}_{\text{antireso}} \;=\; \mathcal{R}_0 \;=\; \frac{r_1+r_2}{1+r_1r_2} \;\sim 1-\frac{\varepsilon_1\varepsilon_2}{2}$$

which shows that the global transmittance is second order with respect to the individual transmittances. Moreover, we know that both the transmittance and the reflectance of an antiresonant cavity are almost independent on the frequency over a large interval in between two successive resonances. If we assume $L \gg l$, the free spectral range Δ_L of the long cavity is much shorter than that Δ_l of the short cavity. If we therefore take a frequency excursion $\delta\nu$ small compared to Δ_L, it will be a fortiori small compared to Δ_L, and owing to the preceding remark, we can consider $\mathcal{T}$ and $\mathcal{R}$ as constants. Its is easy to check that the phase of $\mathcal{R}$ changes by a negligible amount. We have:

$$2kl \;=\; 2\pi\frac{\delta\nu}{\Delta_l}$$

so that

$$\begin{aligned}\mathcal{R} \;&=\; \frac{r_2+r_1+2i\pi r_1\delta\nu/\Delta_l}{1+r_1r_2+2i\pi r_1r_2\delta\nu/\Delta_l}\\ &=\; \mathcal{R}_0\,\frac{1+2i\pi\frac{r_1}{r1+r_2}\frac{\delta\nu}{\Delta_l}}{1+2i\pi\frac{r_1r_2}{1+r_1r_2}\frac{\delta\nu}{\Delta_l}}\\ &=\; \mathcal{R}_0\,\left\{1+2i\pi\frac{\delta\nu}{\Delta_l}\left[\frac{r_1(1-r_2^2)}{(r_1+r_2)(1+r_1r_2)}\right]\right\}\end{aligned}$$

thus, not only $\delta\nu/\Delta_l$ is much smaller than $\delta\nu/\Delta_L$, but it is multiplied by $(1-r_2)$. We can consequently definitely neglect the phase change in $\mathcal{R}$. We have

$$2kL \;\equiv\; \pi + 2\pi\frac{\delta\nu}{\Delta_L}$$

and the surtension is

$$S \;=\; \frac{|C|^2}{|A|^2} \;=\frac{|\mathcal{T}|^2}{\left|1-\mathcal{R}\mathrm{e}^{2i\pi\delta\nu/\Delta_L}\right|^2}$$

where $\mathcal{R}$, $\mathcal{T}$ have their antiresonant values. This is:

$$S \;=\; \frac{\mathcal{T}^2}{1+\mathcal{R}^2-2\mathcal{R}\cos\left(2\pi\frac{\delta\nu}{\Delta_L}\right)}$$

$$= S_0 \frac{1}{1 + \frac{4\mathcal{R}\sin^2(\pi\delta\nu/\Delta_L)}{(1-\mathcal{R})^2}}$$

If we replace the sine by its argument, this gives:

$$S = S_0 \frac{1}{1 + \left(2\mathcal{F}_{\rm super}\frac{\delta\nu}{\Delta_L}\right)^2}$$

where $\mathcal{F}_{\rm super}$ is the *superfinesse*, defined by

$$\mathcal{F}_{\rm super} \equiv \frac{\pi\sqrt{\mathcal{R}}}{1-\mathcal{R}}$$

The linewidth is accordingly:

$$\delta_L = \frac{\Delta_L}{\mathcal{F}_{\rm super}}$$

For instance, assume the length of the long cavity to be $L = 3$ km. The free spectral range is thus $\Delta_L \sim 50$ kHz. If we put a simple input mirror with reflectivity $r_2^2 = 0.882$, the finesse is near 50, so that the linewidth of the cavity is near 1 kHz. Now if we add a second mirror, of same reflectivity $r_1^2 = 0.882$ and if we tune the short cavity at antiresonance, we get a reflectance of 0.998 for the short cavity, giving a superfinesse of 1595, and a linewidth of ~ 31 Hz.

1.3 Optics in a wave Space-Time

1.3.1 Retarded time in a GW - Simplified picture

When studying gravitational waves (GW), some arbitrary in the choice of the coordinates allows simplifications by partially removing this arbitrariness. In the so-called TT-gauge, the Space-Time metrics is of the form

$$g_{\mu\nu} = \eta_{\mu\nu} + h_{\mu\nu}$$

where $\eta_{\mu\nu} = \mathrm{diag}(1,-1,-1,-1)$ is the Minkowski tensor of Special Relativity, and $h_{\mu\nu} \ll 1$ the gravitational perturbation propagating as a wave. This

tensor reduces to two independent components, called h_+ and $h_\times$. Assume that the GW is propagating along the z direction, then we have :

$$h_{\mu\nu} = \begin{pmatrix} 0 & 0 & 0 & 0 \\ 0 & h_+ & h_\times & 0 \\ 0 & h_\times & -h_+ & 0 \\ 0 & 0 & 0 & 0 \end{pmatrix}$$

We shall assume in what follows that the z direction is orthogonal to the plane of the optics laboratory (or of the antenna), and consider the propagation of a light ray along the x, y directions. We know that in a vacuum, light follows a null geodesic, i.e. if dx^μ represents the space-time elementary vector separating two events encountered by the light ray, we can write :

$$g_{\mu\nu}\ dx^\mu dx^\nu = 0$$

or in detail, taking $dx^\mu = (c\,dt,\ dx,\ dy,\ dz)$,

$$0 = c^2dt^2 - dx^2 - dy^2 - dz^2 + 2h_\times dx\,dy\ + h_+\left(dx^2 - dy^2\right)$$

where $h_{+,\times}$ are functions of t, z only. It can be shown that there is no change of direction of the light ray during its interaction with the GW as long as the GW frequency is negligible compared to the EM frequency, which is safely verified for known GW sources. In this case, the only effect is a phase change during propagation. Let us see this in detail : For a path lying along the x direction we have simply :

$$0 = c^2dt^2 - dx^2 + h_+dx^2$$

or as well, h_+ being so small,

$$dx = \pm cdt\left[1 + \frac{1}{2}h_+(t)\right] \tag{1.6}$$

where the sign depends obviously on the propagation direction. Now, consider the round trip experiment, in which a light ray is firstly emitted from abscissa 0 at time t_0, then received at abscissa $L > 0$ at time t_1 : we have using (1.6) with the + sign :

$$L = c(t_1 - t_0) + \frac{1}{2}\,c\int_{t_0}^{t_1} h_+(u)\,du$$

then the light ray is reflected back and returns to the origin at time t_2, we have then, using again (1.6) but with the - sign :

$$-L \;=\; c(-t_2+t_1) - \frac{1}{2}\,c\,\int_{t_1}^{t_2} h_+(u)\,du$$

by subtracting the last equation to the preceding, we get

$$2L \;=\; t_2 - t_0 + \frac{1}{2}\,c\,\int_{t_0}^{t_2} h_+(u)\,du$$

In the sequel we shall omit the index + in the GW amplitude and write simply $h(t)$ instead of $h_+(t)$. Assume now that $t_2 \;=\; t$ is the detection time, and $t_0 \;=\; t_r$ the unknown time at which the light ray was emitted (retarded time). We have the relation :

$$t_r \;=\; t \;-\; \frac{2L}{c} + \frac{1}{2}\int_{t_r}^{t} h(u)\,du$$

This is an implicit equation in t_r but very easy to solve at first order in h :

$$t_r \;=\; t \;-\; \frac{2L}{c} + \frac{1}{2}\int_{t-2L/c}^{t} h(u)\,du$$

If we consider a monochromatic wave of frequency $\nu_g \;=\; \Omega/2\pi$, such that $h(t) \;=\; h\cos(\Omega t)$, the result is

$$t_r \;=\; t \;-\; \frac{2L}{c} + h\frac{L}{c}\mathrm{sinc}(\Omega L/c)\cos\left(\Omega(t-L/c)\right)$$

Clearly the result is identical for a round trip along the y axis, except that the first order term must be changed of sign. We have generally :

$$t_r \;=\; t \;-\; \frac{2L}{c} + \;\epsilon h\frac{L}{c}\mathrm{sinc}(\Omega L/c)\cos\left(\Omega(t-L/c)\right)$$

where $\epsilon \;=\; 1$ along the x axis and $\epsilon \;=\; -1$ along the y axis. One way of detecting gravitational waves could be to measure the excess time delay between emission and back detection of light. Some experiments have been proposed using this principle, for instance by analyzing solar system radar ranging data (in the microwave domain, but the principle is the same).

1.3.2 Retarded time in a GW - General picture

The preceding analysis assumed a normally incident gravitational wave, having an optimal polarization state. The results found are useful in order to determine signal-to-noise ratios, as will be done later. A quite different purpose is to analyze the angular response of an antenna. We shall therefore assume now a gravitational signal propagating along a direction $(\theta,\, \phi)$. We know that there exist a coordinate system defined by the basis $(\vec{w},\ \vec{a},\ \vec{b})$ (we assume the basis orthonormal), in which the perturbation to the metric tensor is

$$h_{\mu\nu} \;=\; \begin{pmatrix} 0 & 0 & 0 & 0 \\ 0 & h_+(t) & h_\times(t) & 0 \\ 0 & h_\times(t) & -h_+(t) & 0 \\ 0 & 0 & 0 & 0 \end{pmatrix}$$

we use the vector $\vec{w}$ used above, and vectors $\vec{\theta}$, $\vec{\phi}$, defined as

$$\vec{w} \;=\; \begin{pmatrix} \sin\theta\cos\phi \\ \sin\theta\sin\phi \\ \cos\theta \end{pmatrix} \quad , \quad \vec{\theta} \;=\; \begin{pmatrix} \cos\theta\cos\phi \\ \cos\theta\sin\phi \\ -\sin\theta \end{pmatrix} \quad , \quad \vec{\phi} \;=\; \begin{pmatrix} -\sin\phi \\ \cos\phi \\ 0 \end{pmatrix}$$

these unit vectors build an orthonormal frame. The transverse vectors $(\vec{a},\ \vec{b})$ are related to $(\vec{\theta},\ \vec{\phi})$ by some rotation of angle ψ :

$$\begin{cases} \vec{a} \;=\; \cos\psi\,\vec{\theta} - \sin\psi\,\vec{\phi} \\ \vec{b} \;=\; \sin\psi\,\vec{\theta} + \cos\psi\,\vec{\phi} \end{cases}$$

In terms of the basis vectors $(\vec{w},\ \vec{a},\ \vec{b})$, the spatial part of $h_{\mu\nu}$ can be expressed as

$$h_{ij} \;=\; h_+(a_ia_j - b_ib_j) + h_\times(a_ib_j + a_jb_i)$$

In terms of vectors $(\vec{\theta},\ \vec{\phi})$, we get :

$$h_{ij} \;=\; (h_+\cos 2\psi + h_\times \sin 2\psi)(\theta_i\theta_j - \phi_i\phi_j) + (-h_+\sin 2\psi + h_\times\cos 2\psi)(\theta_i\phi_j + \theta_j\phi_i)$$

which shows that up to a rotation, we can express the wave amplitude (with new $h_{+,\times}$) as

$$h_{ij} \;=\; h_+(\theta_i\theta_j - \phi_i\phi_j) + h_\times(\theta_i\phi_j + \theta_j\phi_i)$$

This being said, consider now a light ray starting from point A (of coordinates $\vec{r}_A$), going to point B (of coordinates $\vec{r}_B$) and returning to A. We denote by

L the ordinary (i.e. in the unperturbed space) distance from A to B. The general expression of the space-time element is

$$ds^2 \;=\; c^2dt^2 - d\vec{r}^2 - h_{ij}dx^i dx^j$$

for a trip from A to B

$$\vec{r} = \vec{r}_A + \lambda\vec{n}$$

where $0 \leq \lambda \leq L$ and $\vec{n}$ is the unit vector directed along AB. Along the path of a photon from A to B, we have thus :

$$0 \;=\; c^2dt^2 - d\lambda^2 - h_{ij}n^i n^j d\lambda^2$$

from what we obtain

$$d\lambda \;=\; \pm c\,dt\,\left[1 + \frac{1}{2}\,H(t - \vec{w}.\vec{r}/c)\right]$$

where $H \equiv h_{ij}n^i n^j$. If the trip begins at time t_r, the position $\vec{r}$ of the photon can be parametrized by

$$\vec{r}(t) \;=\; \vec{r}_A + c(t - t_r)\,\vec{n}$$

so that

$$d\lambda \;=\; \pm c\,dt\,\left\{1 + \frac{1}{2}\,H\left[t - \vec{w}.\left(\vec{r}_A + c(t - t_r)\,\vec{n}\right)\right]\right\}$$

If we denote by t_m the time of arrival at B, we get, after integration :

$$L \;=\; c(t_m - t_r) \;-\; \frac{c}{2}\int_{t_r}^{t_m} H\left[(1 - \vec{w}.\vec{n})t' - \vec{w}.\vec{r}_A/c + \vec{w}.\vec{n}\,t_r\right]\,dt' \qquad (1.7)$$

during the return trip from B to A, the position of the photon is now parametrized by

$$\vec{r}(t) \;=\; \vec{r}_A - c(t - t_m)\,\vec{n}$$

and after a similar calculation, we get

$$-L \;=\; -c(t - t_m) \;+\; \frac{c}{2}\int_{t_m}^{t} H\left[(1 + \vec{w}.\vec{n})t' - \vec{w}.\vec{r}_B/c - \vec{w}.\vec{n}\,t_m\right]\,dt' \qquad (1.8)$$

By subtracting (1.8) from (1.7), we get :

$$2L \;=\; c(t - t_r) \;-\; \frac{c}{2}\int_{t_r}^{t_m} H\left[(1 - \vec{w}.\vec{n})t' - \vec{w}.\vec{r}_A/c + \vec{w}.\vec{n}\,t_r\right]\,dt' \;-$$

$$- \frac{c}{2}\int_{t_m}^{t} H\left[(1+\vec{w}.\vec{n})t' - \vec{w}.\vec{r}_B/c - \vec{w}.\vec{n}\, t_m\right] dt'$$

At zeroth order in h, we have

$$t_m \;=\; t - L/c \;,\quad t_r \;=\; t - 2L/c$$

So that the expression of the retarded time is :

$$t_r \;=\; t - \frac{2L}{c} \;-\; \frac{1}{2}\int_{t-2L/c}^{t-L/c} H\left[(1-\vec{w}.\vec{n})t' - \vec{w}.\vec{r}_A/c + \vec{w}.\vec{n}\,(t-2L/c)\right] dt' -$$

$$- \frac{1}{2}\int_{t-L/c}^{t} H\left[(1+\vec{w}.\vec{n})t' - \vec{w}.\vec{r}_B/c - \vec{w}.\vec{n}\,(t-L/c)\right] dt' \qquad (1.9)$$

Consider now a particular gravitational frequency $f_g = \Omega/2\pi$, we have

$$H(t) \;=\; \frac{1}{2}\left[H\,\mathrm{e}^{-i\Omega t} + \overline{H}\,\mathrm{e}^{i\Omega t}\right]$$

We can write eq.1.9 under the form

$$t_t \;=\; t - \frac{2L}{c} \;-\; \frac{1}{4}\left(H\,\Delta t_r + \overline{H}\,\overline{\Delta t_r}\right)$$

where

$$\Delta t_r \;=\; \int_{t-2L/c}^{t-L/c} \exp\left\{-i\omega\;\left[(1-\vec{w}.\vec{n})t' - \vec{w}.\vec{r}_A/c + \vec{w}.\vec{n}\,(t-2L/c)\right]\right\} dt' +$$

$$+\int_{t-2L/c}^{t} \exp\left\{-i\omega\;\left[(1+\vec{w}.\vec{n})t' - \vec{w}.\vec{r}_B/c - \vec{w}.\vec{n}\,(t-L/c)\right]\right\}$$

after some straightforward algebra, we find

$$\Delta t_r \;=\; \frac{L}{c}\mathrm{e}^{-i\Omega(t-L/c)}\mathrm{e}^{i\Omega\vec{w}.\vec{r}_M/c}\left\{\mathrm{e}^{i\Omega L/2c}\mathrm{sinc}\left[(1-\vec{w}.\vec{n})\Omega L/2c\right] +\right.$$

$$\left.+\mathrm{e}^{-i\Omega L/2c}\mathrm{sinc}\left[(1+\vec{w}.\vec{n})\Omega L/2c\right]\right\}$$

where $\vec{r}_M = (\vec{r}_A + \vec{r}_B)/2$ epresents the coordinates of the middle of the segment AB. Note that in the case where $\vec{w}$ is orthogonal to the plane containing the optical path, and assuming this plane to contain the origin of the coordinates, we have $\vec{w}.\vec{n} = \vec{w}.\vec{r}_M = 0$, so that

$$\Delta_r^{\perp} \;=\; \frac{2L}{c}\,\mathrm{e}^{-i\Omega(t-L/c)}\,\mathrm{sinc}(\Omega L/c)$$

exactly as in the preceding subsection. Now, returning to eq.1.9, we can write it under the compact form

$$t_r \;=\; t - \frac{2L}{c} - \frac{1}{2}\,H\,\frac{L}{c}\xi(\vec{r}_M,\theta,\phi)\mathrm{e}^{-i\Omega(t-L/c)} - \frac{1}{2}\,\overline{H}\,\frac{L}{c}\overline{\xi}(\vec{r}_M,\theta,\phi)\,\mathrm{e}^{-i\Omega(t-L/c)}$$

where the function ξ is defined, for the sake of brevity by

$$\xi(\vec{r}_M,\theta,\phi) \;=\; \frac{1}{2}\,\mathrm{e}^{i\Omega\vec{w}.\vec{r}_M/c}\left[\mathrm{e}^{i\Omega L/2c}\mathrm{sinc}\left[(1-\vec{w}.\vec{n})\Omega L/2c\right] \;+\right.$$

$$\left.+\mathrm{e}^{-i\Omega L/2c}\mathrm{sinc}\left[(1+\vec{w}.\vec{n})\Omega L/2c\right]\right]$$

Now, if we assume

$$h_{+,\times}(t) = \frac{1}{2}\left(h_{+,\times}\mathrm{e}^{-i\Omega t} + \overline{h}_{+,\times}\mathrm{e}^{i\Omega t}\right)$$

we can write

$$H \;=\; h_+\left[(\vec{\theta}.\vec{n})^2 - (\vec{\phi}.\vec{n})^2\right] + 2\,h_\times\,(\vec{\theta}.\vec{n})(\vec{\phi}.\vec{n})$$

Let us now consider a whole interferometer, having arms directed along the x and y directions respectively. Along the north arm (x), for instance, we have a unit vector $\vec{n}_1$, and along the west arm (y), a unit vector $\vec{n}_2$. If we note $\vec{r}_0$ the coordinates of the splitter, we have for the middles of the north and west arms respectively :

$$\vec{r}_{M,1} \;=\; \vec{r}_0 + \vec{n}_1 L/2\;,\quad \vec{r}_{M,2} \;=\; \vec{r}_0 + \vec{n}_2 L/2$$

so that apart from a common phase factor we can drop out by changing the origin of the time, we have the north and west functions :

$$\xi_{1,2} \;=\; \frac{1}{2}\,\mathrm{e}^{i\Omega\vec{w}.\vec{n}_{1,2}L/2c}\left[\mathrm{e}^{i\Omega L/2c}\mathrm{sinc}\left[(1-\vec{w}.\vec{n}_{1,2})\Omega L/2c\right] \;+\right.$$

$$\left.+\mathrm{e}^{-i\Omega L/2c}\mathrm{sinc}\left[(1+\vec{w}.\vec{n}_{1,2})\Omega L/2c\right]\right]$$

The same way, we have the north and west gravitational amplitudes

$$H_{1,2} \;=\; h_+\left[(\vec{\theta}.\vec{n}_{1,2})^2 - (\vec{\phi}.\vec{n}_{1,2})^2\right] + 2\,h_\times\,(\vec{\theta}.\vec{n}_{1,2})(\vec{\phi}.\vec{n}_{1,2})$$

And the north and west excesses in round trip dephasing for an optical wave of circular frequency ω is : can be written as :

$$\Delta\Phi_{1,2} \;=\; \frac{\omega L}{2c}\,H_1\,\xi_1\mathrm{e}^{-i\Omega t}\mathrm{e}^{i\Omega L/c} + \mathrm{c.c.}$$

The Michelson topology is essentially designed for monitoring $\Delta\Phi_1 - \Delta\Phi_2$, and consequently, if we are interested in the directivity pattern of a Michelson, whatever the various enhancements will be, the antenna pattern will be given by

$$\Xi(\theta,\phi) \;=\; |H_1\xi_1 - H_2\xi_2|$$

we have explicitly

$$H_1 \;=\; h_+(\cos^2\theta\cos^2\phi - \sin^2\phi) - h_\times\cos\theta\sin 2\phi$$

$$H_2 \;=\; h_+(\cos^2\theta\sin^2\phi - \cos^2\phi) + h_\times\cos\theta\sin 2\phi$$

and also ($\alpha \equiv \Omega L/2c$) :

$$\xi_1 \;=\; \frac{1}{2}\mathrm{e}^{i\alpha\sin\theta\cos\phi}\left\{\mathrm{e}^{i\alpha}\mathrm{sinc}\left[(1-\sin\theta\cos\phi)\alpha\right] + \mathrm{e}^{-i\alpha}\mathrm{sinc}\left[(1+\sin\theta\cos\phi)\alpha\right]\right\}$$

$$\xi_2 \;=\; \frac{1}{2}\mathrm{e}^{i\alpha\sin\theta\sin\phi}\left\{\mathrm{e}^{i\alpha}\mathrm{sinc}\left[(1-\sin\theta\sin\phi)\alpha\right] + \mathrm{e}^{-i\alpha}\mathrm{sinc}\left[(1+\sin\theta\sin\phi)\alpha\right]\right\}$$

At high frequencies, when $\alpha = \Omega L/2c$ is not negligible, we have a frequency dependent antenna pattern. For arms as long as 3 km, we have at 1 kHz, $\alpha = \pi/100$, so that the dependence of the ξ's in frequency can be neglected, and we can take simply $\xi_1 = \xi_2 = 1$, so that

$$\Xi(\theta,\phi) \;\simeq\; |H_1 - H_2|$$

or,

$$\Xi(\theta,\phi) \;=\; |\; h_+(1+\cos^2\theta)\,\cos 2\phi - 2h_\times\cos\theta\,\sin 2\phi\;|$$

In the case of purely h_+ sources (binaries in a plane perpendicular to the line of sight), we have the following pattern (see fig.1.12).

1.3.3 The A133 Algebra

Let us now turn to wave optics. Our light ray is in fact a monochromatic plane wave of frequency $\nu = \omega/2\pi$. Call $B(t)$ the (complex) amplitude at the end of the round trip, and $A(t)$ its value at the beginning. We have

$$B(t) \;=\; A(t_r)$$

If we note

$$A(t) \;=\; A\mathrm{e}^{-i\omega t}$$

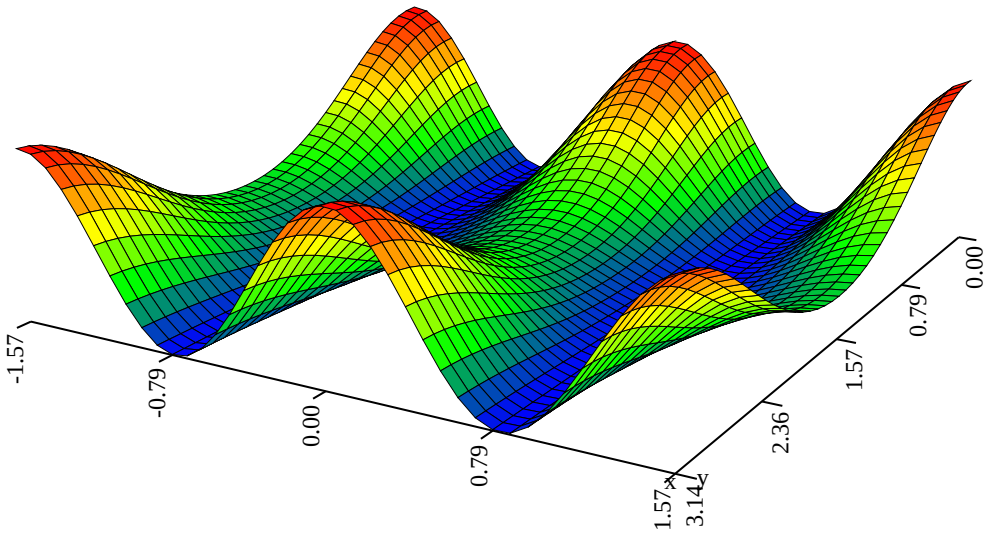

Figure 1.12: Directivity pattern for h_+ sources. Angle θ runs from 0 to π, angle ϕ from $-\pi/2$ to $\pi/2$.

we get

$$B(t) \;=\; A\mathrm{e}^{-i\omega t_r} \;=\; A\mathrm{e}^{-i\omega(t-2L/c)}\;\exp\left[ih\frac{\omega L}{c}\mathrm{sinc}(\Omega L/c)\cos\left(\Omega(t-L/c)\right)\right]$$

Since we are always at first order in h, we write

$$\begin{aligned} B(t) \;&=\; A\mathrm{e}^{-i\omega t}\mathrm{e}^{2i\omega L/c} \;+ \\ &\tfrac{i}{2}hA\;\tfrac{\omega L}{c}\mathrm{sinc}(\Omega L/c)\;\mathrm{e}^{2i\omega L/c}\mathrm{e}^{i\Omega L/c}\mathrm{e}^{-i(\omega+\Omega)t} \;+ \\ &\tfrac{i}{2}hA\;\tfrac{\omega L}{c}\mathrm{sinc}(\Omega L/c)\;\mathrm{e}^{2i\omega L/c}\mathrm{e}^{-i\Omega L/c}\mathrm{e}^{-i(\omega-\Omega)t} \end{aligned}$$

It clearly appears that the action of the GW was to create two sidebands of very low amplitude, of frequencies $\nu \pm \nu_g$ from one single frequency ν. Now let us see what happens if the incoming optical wave is already modulated and exhibits two sidebands. This is necessary because in interferometers, light undergoes several times the action of the GW in order to enhance the signal production. Let the incoming amplitude be of the form

$$A(t) \;=\; \left(A_0 \;+\; \frac{1}{2}\,h\,A_1\mathrm{e}^{-i\Omega t} \;+\; \frac{1}{2}\,h\,A_2\mathrm{e}^{i\Omega t}\right)\mathrm{e}^{-i\omega t}$$

The scaling factor is h because we assume the GW to be the only cause of generation of sidebands in the whole (unknown) optical system. We have then

$$\begin{aligned} B(t) \;=\; A(t_r) \;&=\left[A_0+\frac{1}{2}hA_1\mathrm{e}^{-i\Omega t}\mathrm{e}^{2i\eta}+\frac{1}{2}hA_2\mathrm{e}^{i\Omega t}\mathrm{e}^{-2i\eta}\right]\;\times \\ &\times\;\mathrm{e}^{-i\omega t}\mathrm{e}^{2i\xi}\mathrm{e}^{-i\epsilon h\xi\mathrm{sinc}(\eta)\cos(\Omega t-\eta)} \end{aligned}$$

For shortening the formula, we have used the abbreviations: $\xi \equiv \omega L/c$ and $\eta \equiv \Omega L/c$. After a 1st order expansion of the exponential, we get

$$B(t) \;=\; \left(B_0 \;+\; \frac{1}{2}\,h\,B_1\mathrm{e}^{-i\Omega t} \;+\; \frac{1}{2}\,h\,B_2\mathrm{e}^{i\Omega t}\right)\mathrm{e}^{-i\omega t}$$

with the following notation :

$$\begin{aligned} B_0 \;&=\; \mathrm{e}^{2i\xi}A_0 \\ B_1 \;&=\; \mathrm{e}^{2i(\xi+\eta)}A_1 - i\epsilon\xi\mathrm{sinc}(\eta)\mathrm{e}^{i(2\xi+\eta)}A_0 \end{aligned}$$

$$B_2 \;=\; \mathrm{e}^{2i(\xi-\eta)}A_2 - i\epsilon\xi\mathrm{sinc}(\eta)\mathrm{e}^{i(2\xi-\eta)}A_0$$

We see that if we define "generalized amplitudes" as rank 3 vectors having the carrier amplitude, the upper sideband and the lower sideband respectively as coordinates, by setting

$$\mathcal{A} \;=\; (A_0,\; A_1,\; A_2)$$

and

$$\mathcal{B} \;=\; (B_0,\; B_1,\; B_2)$$

the amplitude after a round trip that we have precedently computed may be written in the form :

$$\mathcal{B} \;=\; \mathbf{X}\mathcal{A}$$

where $\mathbf{X}$ is the linear round trip operator defined as

$$\mathbf{X} \;=\; \begin{pmatrix} \mathrm{e}^{2i\xi} & 0 & 0 \\ -i\epsilon\xi\mathrm{sinc}(\eta)\mathrm{e}^{i(2\xi+\eta)} & \mathrm{e}^{2i(\xi+\eta)} & 0 \\ -i\epsilon\xi\mathrm{sinc}(\eta)\mathrm{e}^{i(2\xi-\eta)} & 0 & \mathrm{e}^{2i(\xi-\eta)} \end{pmatrix} \tag{1.10}$$

It is easy to check that the set of all operators having the form

$$\mathbf{O} \;=\; \begin{pmatrix} O_{00} & 0 & 0 \\ O_{10} & O_{11} & 0 \\ O_{20} & 0 & O_{22} \end{pmatrix}$$

is stable for any algebraic operation, and even may be given a structure of non-commutative algebra isomorphous to the algebra of first order expansions. We call it "A133" for brevity. The basic algebraic operations are defined by

- The sum :

$$(\mathbf{A}+\mathbf{B})_{ij} \;=\; \mathbf{A}_{ij} \;+\; \mathbf{B}_{ij}$$

- The product :

$$(\mathbf{A}\;\mathbf{B})_{ii} \;=\; \mathbf{A}_{ii}\mathbf{B}_{ii}$$
$$(\mathbf{A}\;\mathbf{B})_{i0} \;=\; \mathbf{A}_{i0}\mathbf{B}_{00} \;+\; \mathbf{A}_{ii}\mathbf{B}_{i0}$$

- The inverse :

$$(\mathbf{A}^{-1})_{ii} \;=\; \frac{1}{\mathbf{A}_{ii}}$$
$$(\mathbf{A}^{-1})_{i0} \;=\; -\,\frac{\mathbf{A}_{i0}}{\mathbf{A}_{00}\;\mathbf{A}_{ii}}$$

An A133 operator may be associated to any optical element of a complex optical system. The diagonal elements $\mathbf{O}_{ii}$ represent action of that element on the carrier and the sidebands. Often (mirrors, lenses) there is no frequency dependence because the gravitational perturbation causes a negligible frequency shift, well inside the tolerances of the mirror coatings, and in this case, the corresponding operator is simply scalar. In fact the only non-diagonal operators are those corresponding to propagation of light in a vacuum over long distances. The result is that, after some (A133) algebra, the whole optical system has an associated A133 operator describing its behaviour.

1.4 Signal to Noise Ratio

We can start with a pure monochromatic wave

$$\mathcal{A}_{\text{in}} \;=\; (A,\ 0\ ,0)$$

S being the A133 system operator, we know that the output wave is given by :

$$\mathbf{A}_{\text{out}} \;=\; A\left[S_{00} + \frac{h}{2}S_{10}\,\mathrm{e}^{-i\Omega t} + \frac{h}{2}S_{20}\,\mathrm{e}^{i\Omega t}\right]\mathrm{e}^{-i\omega t}$$

The corresponding detectable power is, up to a normalization factor, and calling P_{in} the incoming power :

$$P(t) \;=\; \mathbf{A}_{\text{out}}\,\overline{\mathbf{A}_{\text{out}}} \;=$$

$$=\; P_{\text{in}}\left[|S_{00}|^2 + \frac{h}{2}\left(S_{10}\overline{S_{00}} + \overline{S_{20}}S_{00}\right)\mathrm{e}^{-i\Omega t} + \frac{h}{2}\left(S_{20}\overline{S_{00}} + \overline{S_{10}}S_{00}\right)\mathrm{e}^{i\Omega t}\right]$$

The signal amplitude at frequency ν_g is thus

$$S(\nu_g) \;=\; |S_{10}\overline{S_{00}} + \overline{S_{20}}S_{00}|$$

The DC component of the output is proportional to $|S_{00}|^2$, so that our main concern, the SNR is proportional to :

$$\mathrm{SNR}(\nu_g) \;\propto\; |S_{10}\,\mathrm{e}^{-i\varphi_{00}} + \overline{S_{20}}\,\mathrm{e}^{i\varphi_{00}}|$$

where φ_{ij} is the argument of S_{ij}. We have as well, with the correct normalisation :

$$\mathrm{SNR}(\nu_g) \;=\; \sqrt{\frac{P_{\mathrm{in}}}{2h_P\nu}}\,\left|\,|S_{10}| + |\overline{S_{20}}|\,\mathrm{e}^{i(\varphi_{10}+\varphi_{20}-2\varphi_{00})}\right|\,h(\nu_g) \tag{1.11}$$

Inversely, the spectral density $h_{\mathrm{SN}}(\nu_g)$ equivalent to the quantum noise is obtained by taking a unitary SNR :

$$h_{\mathrm{SN}}(\nu_g) \;=\; \sqrt{\frac{2h_P\nu}{P_{\mathrm{in}}}}\,\frac{|S_{00}|}{|S_{10}\overline{S_{00}} + \overline{S_{20}}S_{00}|}$$

We see that evaluation of the SNR of any optical GW detector eventually reduces to calculation of the S_{i0} of the whole system.

1.5 Resonant cavities in a GW

The first element we need, before addressing more complex structures, is the A133 operator associated to a Fabry-Perot cavity. We take the same notations as in Fig.1.6. The intracavity (vector) amplitude $\mathcal{B}$ obeys:

$$\mathcal{B} \;=\; t_1\mathcal{A}_{\mathrm{in}} - r_1r_2\mathbf{X}\,\mathcal{B}$$

where $\mathbf{X}$ is the round trip operator just defined above (Eq.1.10). We have thus

$$\mathcal{B} \;=\; [1 + r_1r_2\mathbf{X}]^{-1}\; t_1\,\mathcal{A}_{\mathrm{in}}$$

The reflected amplitude is :

$$\mathcal{A}_{\mathrm{ref}} \;=\; i\,r_1\,\mathcal{A}_{\mathrm{in}} + i\,t_1r_2\,\mathbf{X}\,\mathcal{B}$$

$$=\; i\,[r_1 + (1-p_1)r_2\,\mathbf{X}]\,[1 + r_1r_2\mathbf{X}]^{-1}\;\mathcal{A}_{\mathrm{in}}$$

so that the reflectance of the cavity is the operator

$$\mathbf{F} \;=\; [r_1 + (1-p_1)r_2\,\mathbf{X}]\,[1 + r_1r_2\mathbf{X}]^{-1} \tag{1.12}$$

It is possible to compute the components of $\mathbf{F}$:

$$\mathbf{F} \;=\; \begin{pmatrix} F & 0 & 0 \\ G_+ & F_+ & 0 \\ G_- & 0 & F_- \end{pmatrix}$$

F is the ordinary reflectance of the FP for the carrier, $F_\pm$ the ordinary reflectance of the FP for the upper and lower sidebands respectively. For the sake of simplicity, we use again the notation :

$$\begin{aligned} \xi &= kL \\ \eta &= \Omega L/c \end{aligned}$$

(recall that $\Omega/2\pi$ is the GW frequency). We have then, after direct evaluation of $\mathbf{F}$ according to Eq.1.12 :

$$F = \frac{r_1 + (1-p_1) r_2 \mathrm{e}^{2i\xi}}{1 + r_1 r_2 \mathrm{e}^{2i\xi}}$$

$$F_\pm = \frac{r_1 + (1-p_1) r_2 \mathrm{e}^{2i(\xi\pm\eta)}}{1 + r_1 r_2 \mathrm{e}^{2i(\xi\pm\eta)}} \tag{1.13}$$

$$G_\pm = -i\epsilon \frac{t_1^2 r_2 \xi \mathrm{sinc}(\eta) \mathrm{e}^{i(2\xi\pm\eta)}}{(1 + r_1 r_2 \mathrm{e}^{2i\xi})\,(1 + r_1 r_2 \mathrm{e}^{2i(\xi\pm\eta)})} \tag{1.14}$$

In the coupling rate (σ) formalism, this can be approximated by

$$F = -\frac{1 - \sigma + 2i\Delta f}{1 - 2i\Delta f} \tag{1.15}$$

$$F_\pm = -\frac{1 - \sigma + 2i(\Delta f \pm f_g)}{1 - 2i(\Delta f \pm f_g)} \tag{1.16}$$

$$G_\pm = i\epsilon \frac{2\mathcal{F}L}{\lambda} \frac{2 - \sigma}{(1 - 2i\Delta f)\,[1 - 2i(\Delta f \pm f_g)]} \tag{1.17}$$

where $\Delta f = \delta\nu/\delta\nu_{\mathrm{FWHM}}$ is the reduced detuning of the light source from resonance, and $f_g = \nu_g/\delta\nu_{\mathrm{FWHM}}$ the reduced gravitational frequency. When we vary the detuning, we see that the modulus of G_+ has a resonance for $\Delta f = 0$ (resonance of the carrier) and a second resonance when $\Delta f = -f_g$, the upper sideband becoming resonant. The modulus of G_- has also a resonance for $\Delta f = 0$ and for $\Delta f = f_g$, the lower sideband becoming resonant (see Fig.1.13). A symmetrical figure can be obtained with $|G_+|$.

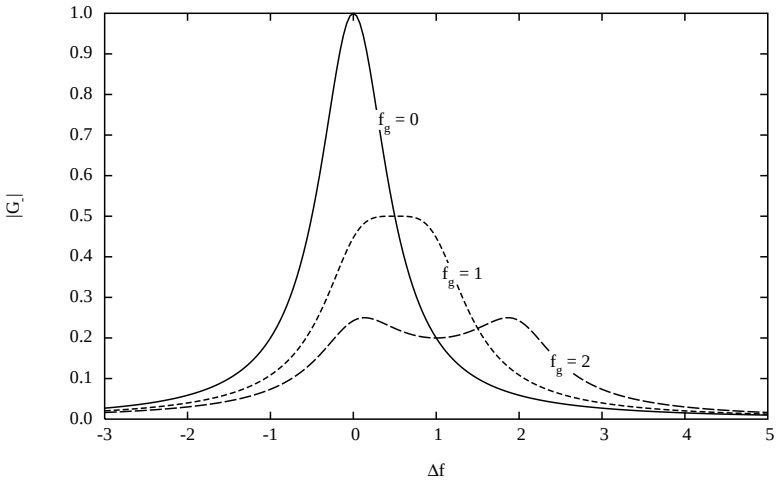

Figure 1.13: Efficiency of lower sideband generation vs detuning of the source for three reduced GW frequencies. Solid line :$f_g = 0$, short dashed line : $f_g = 1$, long dashed line : $f_g = 2$

1.6 Michelson Interferometer involving FP cavities

We take the classical Michelson geometry, but replace the end mirrors by two identical Fabry-Perot cavities, F_1 and F_2. Note that even when optically identical, the effect of a GW on them will be different, and consequently we must denote the corresponding operators by different notations (see Fig.1.14). We neglect in this first aapproach, small phases of order $2\pi\nu_g a/c$. The transmitted amplitude is

$$\mathcal{A}_{\rm trans} \;=\; -r_s t_s \left(\mathrm{e}^{2ika}\mathbf{F}_1 + \mathrm{e}^{2ikb}\mathbf{F}_2\right) \mathcal{A}_{\rm in}$$

whereas the reflected amplitude is

$$\mathcal{A}_{\rm ref} \;=\; i\left(t_s^2\mathrm{e}^{2ika}\mathbf{F}_1 - r_s^2\mathrm{e}^{2ikb}\mathbf{F}_2\right) \mathcal{A}_{\rm in}$$

Note that we neglect phases of the order of $2\pi\nu_g a/c$. The expressions of $\mathbf{F_1}$ and $\mathbf{F_2}$ for perfectly identical but orthogonal cavities lying respectively along

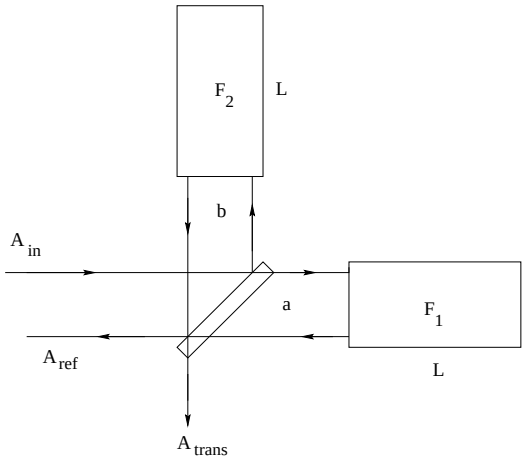

Figure 1.14: Geometry of a Michelson with FP cavities

the x and y directions, are :

$$\mathbf{F}_1 = \begin{pmatrix} F & 0 & 0 \\ G_+ & F_+ & 0 \\ G_- & 0 & F_- \end{pmatrix} \quad , \quad \mathbf{F}_2 = \begin{pmatrix} F & 0 & 0 \\ -G_+ & F_+ & 0 \\ -G_- & 0 & F_- \end{pmatrix}$$

The opposite signs of the off-diagonal elements reflect the signature of a + polarized gravitational wave having the x, y axes as polarization directions. We can define a transmittance and a reflectance A133 operator an obvious way, by

$$\begin{aligned} \mathcal{A}_{\rm trans} &= \mathbf{T}_{\rm Mic}\, \mathcal{A}_{\rm in} \\ \mathcal{A}_{\rm ref} &= i\, \mathbf{R}_{\rm Mic}\, \mathcal{A}_{\rm in} \end{aligned}$$

The elements of these operators are as follows, assuming a perfectly symmetrical splitter ($r_s = t_s = \sqrt{1-p_s}/2$), for the transmittance:

$$\begin{aligned} T_{\rm Mic,00} &= -(1-p_s)\mathrm{e}^{ik(a+b)} \cos[k(a-b)]\, F \\ T_{\rm Mic,11} &= -(1-p_s)\mathrm{e}^{ik(a+b)} \cos[k(a-b)]\, F_+ \\ T_{\rm Mic,22} &= -(1-p_s)\mathrm{e}^{ik(a+b)} \cos[k(a-b)]\, F_- \\ T_{\rm Mic10} &= -i(1-p_s)\mathrm{e}^{ik(a+b)} \sin[k(a-b)]\, G_+ \\ T_{\rm Mic20} &= -i(1-p_s)\mathrm{e}^{ik(a+b)} \sin[k(a-b)]\, G_- \end{aligned}$$

and for the reflectance :

$$\begin{aligned} R_{\mathrm{Mic},00} &= i(1-p_s)\mathrm{e}^{ik(a+b)}\sin[k(a-b)]\,F \\ R_{\mathrm{Mic},11} &= i(1-p_s)\mathrm{e}^{ik(a+b)}\sin[k(a-b)]\,F_+ \\ R_{\mathrm{Mic},22} &= i(1-p_s)\mathrm{e}^{ik(a+b)}\sin[k(a-b)]\,F_- \\ R_{\mathrm{Mic},10} &= (1-p_s)\mathrm{e}^{ik(a+b)}\cos[k(a-b)]\,G_+ \\ R_{\mathrm{Mic},20} &= (1-p_s)\mathrm{e}^{ik(a+b)}\cos[k(a-b)]\,G_- \end{aligned}$$

It is evident that when the interferometer is tuned at a dark fringe for the carrier, the sidebands are transmitted, and conversely. The SNR takes the form :

$$\mathrm{SNR}(\nu_g) \;\propto\; (1-p_s)\sin[k(a-b)]\left|G_+\frac{\overline{F}}{|F|}-\overline{G_-}\frac{F}{|F|}\right| \qquad (1.18)$$

If we assume the carrier at a dark fringe, we get

$$\mathbf{T}_{\mathrm{Mic}} = (1-p_s)\mathrm{e}^{ik(a+b)}\begin{pmatrix} 0 & 0\,0 \\ -iG_+ & 0\,0 \\ -iG_- & 0\,0 \end{pmatrix} \;,\; \mathbf{R}_{\mathrm{Mic}} = (1-p_s)\mathrm{e}^{ik(a+b)}\begin{pmatrix} iF & 0 & 0 \\ 0 & iF_+ & 0 \\ 0 & 0 & iF_- \end{pmatrix}$$

This allows to study the SNR of a simple Michelson having FP cavities as arms. We have in the coupling rate formalism, neglecting p_s at this level :

$$\mathrm{SNR}(f_g) \;\propto\; \frac{4\mathcal{F}L}{\lambda}\frac{2-\sigma}{\sqrt{1+4\Delta f^2}}\frac{1}{2}\left|\frac{\mathrm{e}^{i\Psi_+}}{\sqrt{1+4(\Delta f+f_g)^2}}+\frac{\mathrm{e}^{-i\Psi_-}}{\sqrt{1+4(\Delta f-f_g)^2}}\right|$$

where

$$\begin{aligned} \Psi_+ &= \tan^{-1}\left(2(\Delta f+f_g)\right)-\tan^{-1}\left(\frac{2\Delta f}{1-\sigma}\right) \\ \Psi_- &= \tan^{-1}\left(2(\Delta f-f_g)\right)-\tan^{-1}\left(\frac{2\Delta f}{1-\sigma}\right) \end{aligned}$$

After some algebra, we find the following result :

$$\mathrm{SNR}(f_g) \;\propto\; \frac{8(1-\sigma/2)\mathcal{F}L}{\lambda}\times$$

$$\left[\frac{(1-\sigma+4\Delta f)^2+4(1-\sigma)^2f_g^2}{(1+4\Delta f)^2\left((1-\sigma)^2+4\Delta f)^2\right)\left(1+8(\Delta f^2+f_g^2)+16(\Delta f^2-f_g^2)^2\right)}\right]^{1/2} \qquad (1.19)$$

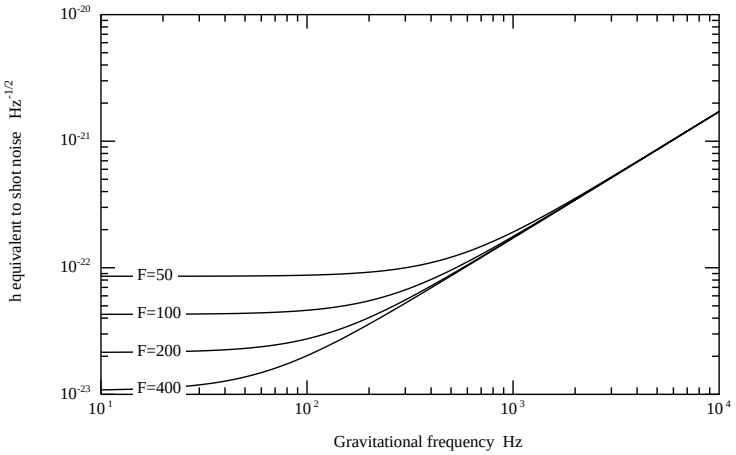

Figure 1.15: Simple Michelson with FP cavities : Spectral density of h equivalent to shot noise

if the cavities are at resonance ($\Delta f = 0$), we have simply

$$\mathrm{SNR}(f_g) \;=\; \frac{8\mathcal{F}L}{\lambda}\,\frac{1-\sigma/2}{\sqrt{1+4f_g^2}}\,\sqrt{\frac{P_L}{2h_P\nu}}\,h(f_g)$$

q we plot hereafter the spectral density of equivalent h for various values of $\mathcal{F}$ for a 20W light source at $\lambda = 1.064\,\mu$m. (see Fig.1.15). The sensitivity at low frequency is a function of $\mathcal{F}$. The optimum value of $\mathcal{F}$ occurs theoretically for $\sigma = 1$, i.e. for the optimal coupling of the cavities. This corresponds to $\mathcal{F} = \pi/p$. For $p = 3\,10^{-5}$, this corresponds to a finesse of 10^5. On the other hand, when $\sigma = 1$, the surtension coefficient is $\mathcal{S} = 1/p$, and this means here a surtension of $\simeq 3\,10^4$. For a 10 W laser source, this is is 0.3 MW stored light power. Let us keep however in mind that the improvement due to increasing the finesse occurs only at low frequency. But at low frequency, the limitation of the sensitivity is due to thermal noise, and it is worthless to try higher finesses as long as a means of reducing thermal noise has'nt been found . Better idea is to increase the laser power, because the whole curve is then globally lowered. But 20W (as assumed in Fig.1.15) is the maximum presently reasonable for a CW monomode, stabilized laser. For

gaining 1 order of magnitude, we would have to lock in phase an array of 3 such lasers. This is quite feasible, but the result can be achieved with a much more elegant and convenient solution, as explained hereafter. Let us remark that for given ν_g, the SNR is of the form

$$SNR \;=\; \frac{8\pi L}{\lambda}\,\frac{1}{p}\,\frac{\sigma(1-\sigma/2)}{\sqrt{1+q^2\sigma^2}}\,\sqrt{\frac{P_L}{2h_P\nu}}\,h(\nu_g)$$

with $q \equiv 2\pi\nu_g/p\Delta\nu_{\rm FSR}$ and consequently is a maximum for a finite value of σ. The parameter q is very high even for $\nu_g = 10\,$Hz, and a good approximation of the optimal coupling rate is :

$$\sigma_{opt} \;=\; \left(\frac{2}{q^2}\right)^{1/3} \;=\; \left(\frac{p\Delta\nu_{\rm FSR}}{\sqrt{2}\,\pi\nu_g}\right)^{2/3}$$

The optimal finesse is therefore :

$$\mathcal{F}_{opt}(\nu_g) \;=\; \left(\frac{\pi}{p}\right)^{1/3}\left(\frac{\Delta\nu_{\rm FSR}}{\nu_g}\right)^{2/3}$$

For instance, with $p = 3\,10^{-5}$, $\Delta\nu_{\rm FSR} = 50\,$kHz, this gives

$$\mathcal{F}_{opt}(\nu_g) \;=\; 13782 \times \left(\frac{10{\rm Hz}}{\nu_g}\right)^{2/3}$$

But the maximum is very flat, and it is not necessary to require the true optimum. A value of σ such that $q\sigma = 2$ is quite sufficient, the SNR differing from its true optimum by only 10%. this corresponds to

$$\mathcal{F}_{opt}(\nu_g) \;=\; \frac{\Delta\nu_{\rm FSR}}{\nu_g}$$

The pseudo-optimal finesse for $\nu_g = 1$ kHz is for instance $\mathcal{F} = 50$. The pseudo-optimal finesse depends of a reference frequency $\nu_g^{(0)}$ which is an equivalent parameter, the length of the cavities being fixed. In terms of this reference frequency, we have :

$$\mathrm{SNR}(\nu_g) \;=\; \frac{4\,\frac{\nu_{\rm opt}}{\nu_g^{(0)}}}{\sqrt{1+\left(2\,\frac{\nu_g}{\nu_g^{(0)}}\right)^2}}\sqrt{\frac{P_L}{2h_P\nu}}h(\nu_g)$$

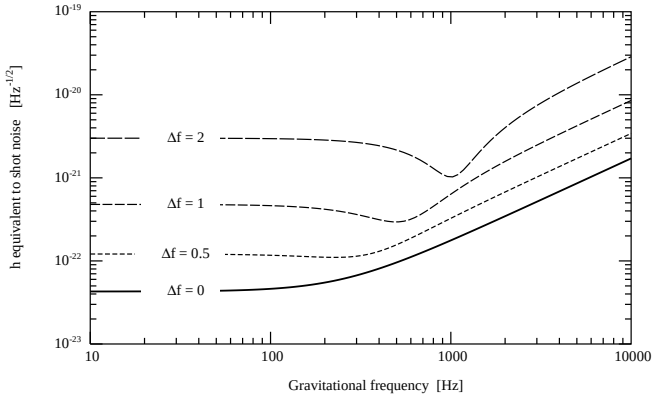

Figure 1.16: Michelson with detuned cavities (F=100)

where $\nu_{\rm opt}$ is the optical frequency. This formula is valid except for too small values of $\nu_g^{(0)}$. For the interval [10 Hz, 10kHz], it is valid. We see the huge scale factor provided by the cavities. When the two cavities have a common detuning, the SNR is reduced, as can be red directy on Eq.(1.19). But a resonance occurs when the upper sideband created by the GW becomes resonant (for $f_g = \Delta f$). At this frequency, the loss due to the frequency offset of the carrier is somewhat compensated by the resonance (see Fig1.6) One important point is that, working out of resonance, the reflectances of the cavities are much higher than in the tuned case. This regime of operation, of no benefit in the simple Michelson configuration, becomes interesting when recycling is applied, as will be shown later.

1.7 Recycling

1.7.1 standard power recycling

It is clear from conservation laws in general, and namely from the previous section that when tuned at a dark fringe, the transmittance of the Michelson being a minimum, its reflectance is a maximum. It has been proposed a long time ago by R. Drever to build a cavity with one extra mirror (the recycling mirror) and the Michelson as a second mirror (see Fig.1.17 for notation).

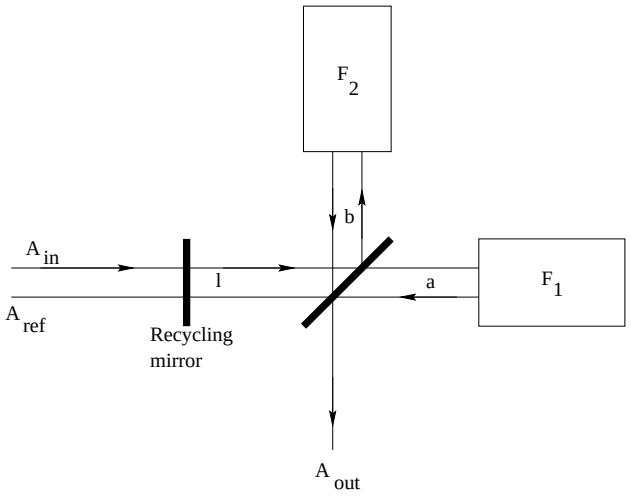

Figure 1.17: Recycled Michelson with FP cavities

By controlling the resonance of this *recycling cavity* , the surtension coefficient enhances the power reaching the splitter, and the SNR is increased. The A133 operator corresponding to this configuration is easily obtained by copying the simple Fabry-Perot operators. The Michelson operators for reflection and transmission being respectively $\mathbf{R}_{\rm Mic}$ and $\mathbf{T}_{\rm Mic}$, and l the length of the recycling cavity, we have for the reflectance and transmittance of the complete interferometer :

$$\mathbf{R}_{\rm Itf} \;=\; \left[r_r + (1-p_r)\mathrm{e}^{2ikl}\mathbf{R}_{\rm Mic}\right]\,\left[1+\mathrm{e}^{2ikl}r_r\mathbf{R}_{\rm Mic}\right]^{-1} \tag{1.20}$$

$$\mathbf{T}_{\rm Itf} \;=\; \mathrm{e}^{ikl}t_r\mathbf{T}_{\rm Mic}\left[1+\mathrm{e}^{2ikl}r_r\mathbf{R}_{\rm Mic}\right]^{-1} \tag{1.21}$$

We are especially interested in the $T_{\rm Itf\ 10,20}$ components, giving the SNR. Using the preceding results about the Michelson operators, after some algebra, we obtain ($\delta \equiv k(a-b)$) :

$$T_{\rm Itf\ 10,20} \;=\; -i\,\frac{t_r(1-p_s)\mathrm{e}^{ik(l+a+b)}\,G_{\pm}\left[\sin\delta + i\,r_r(1-p_s)\mathrm{e}^{ik(2l+a+b)}\,F_{\pm}\right]}{D\,D_{\pm}}$$

$$T_{\rm Itf\ 00} \;=\; -\,\frac{t_r(1-p_s)\mathrm{e}^{ik(l+a+b)}\,\cos\delta\,F}{D}$$

with the following definition ($a = -1, 0, 1$) :

$$D_a \;=\; 1 + i\, r_r(1-p_s)\mathrm{e}^{ik(2l+a+b)} \sin\delta\, F_a$$

It is always possible to tune the path difference between the two arms at a dark fringe ($\delta \equiv \pi/2[\mathrm{mod}2\pi]$), and the length l of the recycling cavity in order to obtain resonance, i.e. :

$$D \;=\; 1 - r_r(1-p_s)\,|F|$$

where F refers to the (assumed common) reflectance of the cavities. At this point, the SNR is simply the SNR of a Michelson, multiplied by the surtension factor :

$$\mathrm{SNR}(f_g) \;=\; \mathrm{SNR}_{\mathrm{Mic}}(f_g) \times \frac{t_r}{1 - r_r(1-p_s)\,|F|} \tag{1.22}$$

In the so called *standard recycling* sheme, we assume the FP cavities at resonance ($\Delta f = 0$). The SNR takes on the simple form

$$\mathrm{SNR} \;=\; \frac{4\frac{\mathcal{F}L}{\lambda}(2-\sigma)}{\sqrt{1+4f_g^2}}\; \frac{t_r(1-p_s)}{1 - r_r(1-p_s)|1-\sigma|}\; \sqrt{\frac{P_L}{2h_P\nu}}\; h(\nu_g)$$

Where we see directly how increasing the coupling factor increases the Michelson SNR, but decreases the recycling factor. Anyway, we are free to choose the best recycling reflectance r_r, i.e. that maximizing the recycling surtension factor. This happens when

$$r_{r\ opt} \;=\; (1-p_r)(1-p_s)|1-\sigma|$$

giving

$$S_{r\ opt} \;=\; (1-p_s)\sqrt{\frac{1-p_r}{1-(1-p_r)(1-p_s)^2(1-\sigma)^2}}\; \frac{4\frac{\mathcal{F}L}{\lambda}(2-\sigma)}{\sqrt{1+4f_g^2}}\; \sqrt{\frac{P_L}{2h_P\nu}}\; h(\nu_g)$$

The mirror losses will be taken very small (of the order of 10 ppm), and we have seen that the coupling rate in a simple Michelson must be relatively small. It will be even smaller here, because the recycling factor would be

destroyed by a large cavity absorption. It is therefore not unrealistic to consider that the total losses are dominated by the cavity resonant absorption, and however, small ($p_r + 2p_s \ll 2\sigma \ll 1$). The optimal SNR is then

$$\mathrm{SNR}(\nu_g) \;=\; \frac{4\pi L}{\sqrt{2}\lambda}\,\frac{1}{p}\;\frac{\sigma^{1/2}(2-\sigma)}{\sqrt{1+\left(2\pi\frac{\nu_g}{p\Delta\nu_{\mathrm{FSR}}}\,\sigma\right)^2}}\,\sqrt{\frac{P_L}{2h_P\nu}}\,h(\nu_g)$$

When searching for the optimal value of σ, we get the following equation, with $q = 2\pi\nu_g/p\Delta\nu_{\mathrm{FSR}}$:

$$\frac{1}{2}q^2\sigma^3 + q^2\sigma^2 + \frac{3}{2}\sigma^2 - 1 \;=\; 0$$

for avoiding an exact but useless and cumbersome resolution of this equation, we rather solve it in q:

$$q^2 \;=\; \frac{1-3\sigma^2/2}{\sigma^2(1+\sigma/2)}$$

Now we remark that, even for low GW frequencies (10 Hz), q^2 is very large: Consequently, σ must be very small, and we can take the approximation

$$\sigma_{opt} \;=\; \frac{1}{q}$$

or, in terms of finesse,

$$\mathcal{F}_{opt} \;=\; \frac{\Delta\nu_{\mathrm{FSR}}}{2\nu_g^{(0)}}$$

Where $\nu_g^{(0)}$ is the GW frequency for which the SNR is optimized. But here, the maximum is sharp (see Fig.1.18). Remark that this value is half the pseudo-optimum for the simple Michelson. This sharp maximum makes the SNR very sensitive to the GW frequency at which the SNR is optimized. With physically significant parameters (frequencies in the detection range [10 Hz,10 kHz], and small losses), the SNR can be approximated by a simple formula. Call p_{ITF} the losses encountered in the recycling mirror and the splitter, i.e. the losses external to FP's : we have

$$1 - p_{\mathrm{ITF}} \;=\; (1-p_r)(1-p_s)^2 \;\Rightarrow p_{\mathrm{ITF}} \;\simeq\; p_r + 2p_s$$

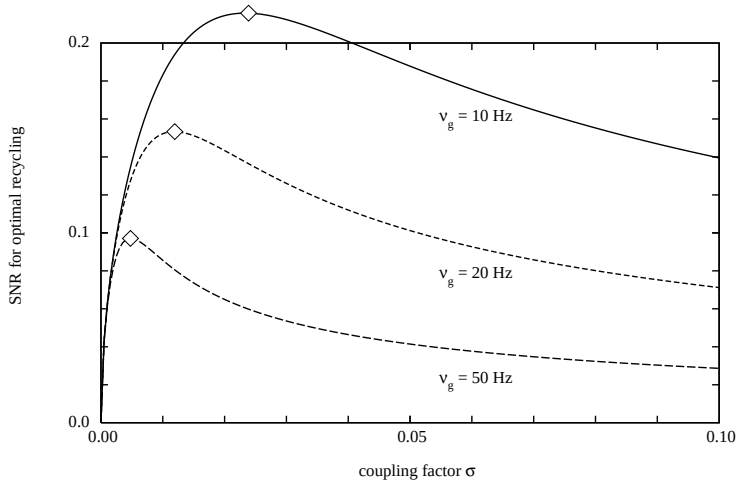

Figure 1.18: SNR vs σ for three GW frequencies. The small diamonds show the approximate optima theoretically derived

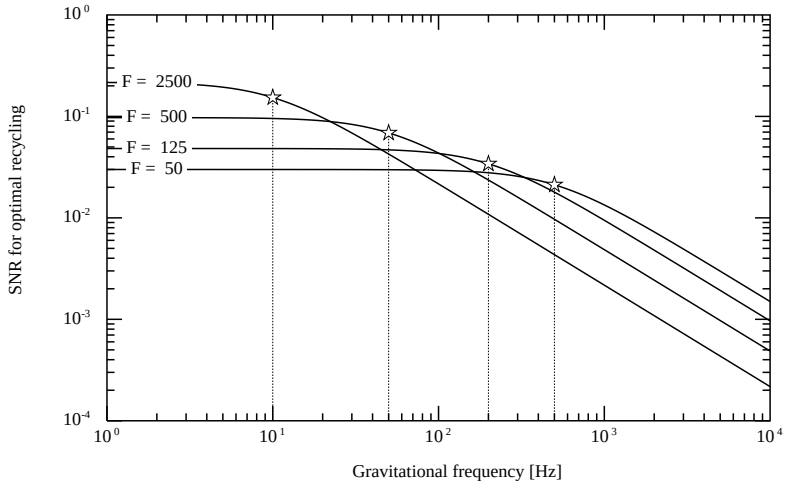

Figure 1.19: SNR vs frequency for four finesses. The small stars point the GW frequency at which the SNR was optimized.

The losses internal to FP's are still $p = 1-(1-p_1)r_2^2$. Neglecting non essential small terms leads to :

$$\mathrm{SNR}(\nu_g) \;=\; \frac{1}{\sqrt{p_{\mathrm{ITF}} + \frac{p\Delta\nu_{\mathrm{FSR}}}{\pi\nu_g^{(0)}}}} \; \frac{2\frac{\nu_{\mathrm{opt}}}{\nu_g^{(0)}}}{\sqrt{1+\left(\frac{\nu_g}{\nu_g^{(0)}}\right)^2}} \sqrt{\frac{P_L}{2h_P\nu}}\, h(\nu_g) \qquad (1.23)$$

the parameter $p\Delta\nu_{\mathrm{FSR}}/2\pi$ has the dimension of a frequency, and is of order 1 Hz. The first term represents the gain due to optimal recycling, the second is the SNR of a simple Michelson. We can conclude that a power recycled Michelson, having an optimal recycling rate, and an optimal finesse for a given GW frequency is not significantly better that a simple Michelson when that frequency is very low. In this subsection and in the next one, we see how the reflectivity of the Fabry-Perot cavities play a central role. The efficiency of recycling crucially depends on the quality of the reflectivity. This is the reason why at low frequency, a high finesse being needed, the coupling rate increases, the reflectivity decreases, and the effect of recycling becomes negligible. This strong requirement of very reflecting cavities was the cause of a number of numerical optics studies that in turn, motivated section 3.

The amplitude in the recycling cavity has a peak at the recycling resonance. It is interesting to evaluate the width of the resonance line when the frequency of the source varies. The surtension factor reads :

$$S_r \;=\; \left|\frac{t_r}{1+ir_r(1-p_s)\,\mathrm{e}^{ik(2l+a+b)}\sin\delta F}\right|^2$$

in this expression, the dominating phase is obviously given by the reflectance F. Since the phase reflected by cavities has already a sharp slope, we can expect this slope to be reinforced by the recycling finesse. We can take for the modulus of the reflectance its value $|F| = 1-\sigma$ at resonance, assume $\delta = \pi/2$ and $\pi/2 + k(2l+a+b) \equiv \pi$. The only frequency dependent quantity (in this approximation) is the phase Φ of the reflectance, given by

$$\Phi \;\sim\; 2\tan^{-1}(2\Delta f)$$

where we have assumed a small σ. If the frequency excursion is small compared to the cavity linewidth, then Δf is small, so that we can write :

$$S_r \;=\; S_r^{(0)} \left|\frac{1}{1+(4\mathcal{F}_R\Delta f/\pi)^2}\right|^2$$

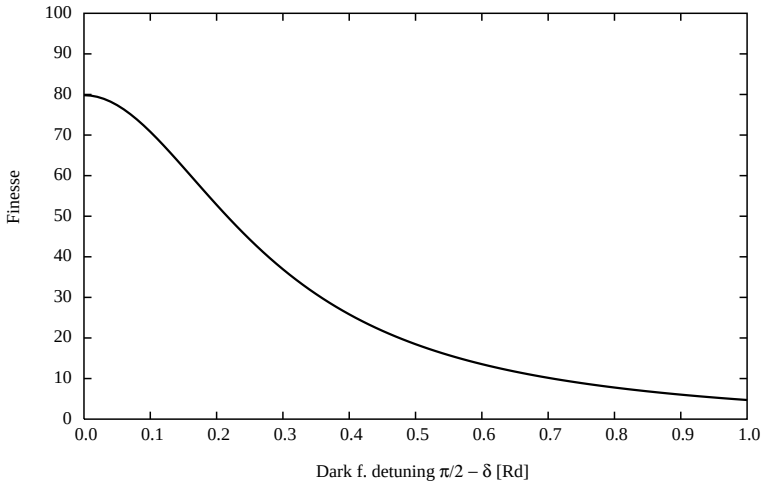

Figure 1.20: Variable finesse by detuning the dark fringe

where $S_r^{(0)}$ is the peak height for a given detuning of the dark fringe δ, Δf the reduced frequency excursion, and

$$\mathcal{F}_R \;=\; \frac{\pi\sqrt{r_r(1-p_s)(1-\sigma)\sin\delta}}{1-r_r(1-p_s)(1-\sigma)\sin\delta}$$

the recycling finesse. This finesse depends obviously of the tuning of the Michelson. Detuning reduces the reflectance of the Michelson, as can be seen on Fig.1.20.

The full width at half maximum of the surtension peak can be therefore estimated by

$$\delta\nu_{\rm rec} \;=\; \frac{\pi}{2\mathcal{F}_R}\,\delta\nu_{\rm FWHM}$$

(recall that $\delta\nu_{\rm FWHM}$ i the linewidth of the cavity). For standard values, say $p_s = 2\ 10^{-5}$, $S_r^{(0)} = 50$, (hence $r_r = 0.962$, $\sigma = 6.366\ 10^{-4}$, (corresponding to a cavity finesse of 50), we find $\mathcal{F}_R \sim 78$. For a 3 km long, 50 finesse cavity, the linewidth is 1 kHz, so that

$$\delta\nu_{\rm rec} \;\sim\; 20{\rm Hz}$$

very near the exact value, numerically obtained, of 19.64 Hz (on Fig. 1.21, we show the exact line shape for such parameters). It is also clear that

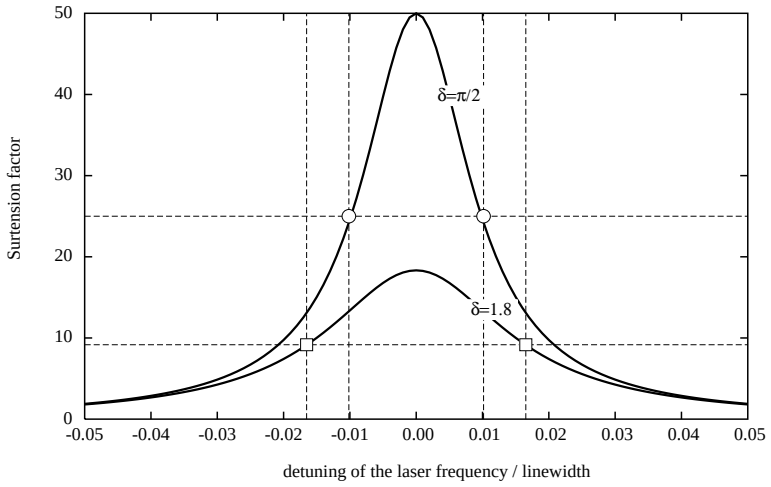

Figure 1.21: Linewidth of the recycling cavity / linewidth of the long cavities. A detuning wrt darkfringe increases the recycling width

a detuning with respect to the dark fringe ($\delta \neq \pi/2$) not only decreases the maximum recycling gain, but also increases the recycling linewidth. On Fig.1.22 the full width at half maximum of the recycling width is plotted. This helps tuning the interferometer.

1.7.2 detuned power recycling

We consider the case of a power recycled Michelson with detuned cavities. The basic idea is to exploit at the same time the resonance (frequency ν_0) of a cavity for one sideband (such that $\nu_L \pm \nu_g = \nu_0$) and the fact that the carrier being out of resonance, the reflectivity of the cavities is enhanced, and consequently the recycling efficiency also. We restrict our attention to two special cases giving the same result for the SNR : The *symmetrical* detuning, in which the two cavities have the same detuning Δf, and the *antisymmetrical* detuning, in which one cavity is detuned by Δf, and the other one by $-\Delta f$. In the first case, the upper sideband is resonant in the two arms, and never the lower sideband, in the second case, the upper sideband is resonant in the first arm, and the lower sideband in the second arm, so that finally, the effect is identical. We develop the symmetrical case. Owing

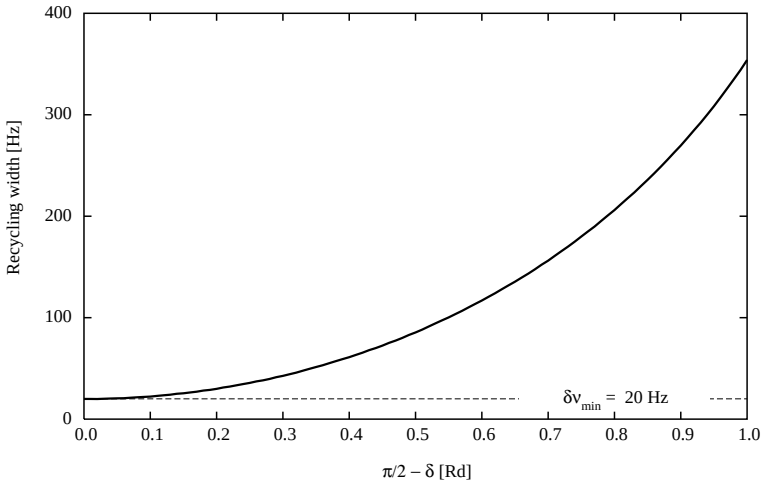

Figure 1.22: Linewidth of the recycling cavity vs dark fringe detuning $\delta \equiv 2\pi(a-b)/\lambda$

to the general Eq.1.19, the SNR for a detuned, power recycled Michelson is :

$$\mathrm{SNR}(f_g) \;=\; \frac{8\mathcal{F}L(1-\sigma/2)}{\lambda}\,\frac{t_r}{1-r_r(1-p_s)\rho}\,\sqrt{S}\,\sqrt{\frac{P_L}{2h_P\nu}}\,h(\nu_g)$$

where $\rho(\Delta f)$ is the FP's modulus reflectance, and

$$S \;=\; \frac{(1-\sigma+4\Delta f^2)^2+4(1-\sigma)^2 f_g^2}{(1+4\Delta f^2)((1-\sigma)^2+4\Delta f^2)(1+8(\Delta f^2+f_g^2)+16(\Delta f^2+f_g^2)^2)}$$

recall that

$$\rho(\Delta f) \;=\; \sqrt{1-\frac{\sigma(2-\sigma)}{1+4\Delta f^2}}$$

The optimal recycling is obtained when

$$r_r \;=\; (1-p_r)(1-p_s)^2\rho^2$$

The efficiency of recycling essentially depends on the reflectivity of the cavities. When the detuning is not zero, it simultaneously happens, for $f_g = \Delta f$ that one of the sidebands is resonant, and the reflectivity of the cavities,

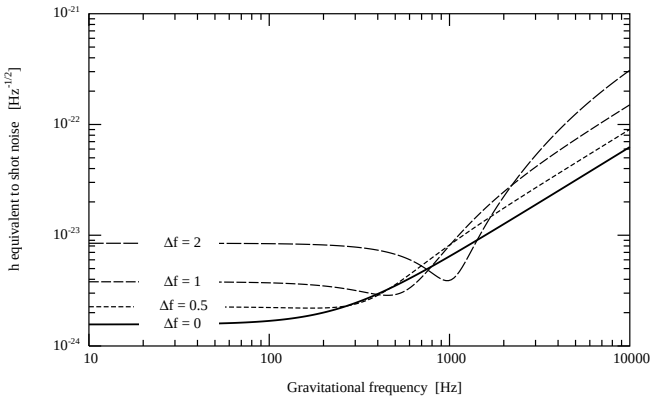

Figure 1.23: Detuned recycled Michelson (F=100)

higher than when the carrier is resonant. This is the reason why it is possible to have a better SNR for f_g in the neighborhood of Δf. (see Fig.1.23).

The maximum SNR is

$$\mathrm{SNR_{max}} = \frac{8\mathcal{F}L(1-\sigma/2)}{\lambda}\frac{1}{\sqrt{1-(1-p_r)(1-p_s)\rho^2}}\times$$

$$\times\sqrt{\frac{(1-\sigma)^2+4(1-\sigma)(3-\sigma)\Delta f^2+16\Delta f^4}{(1+4\Delta f^2)((1-\sigma)^2+4\Delta f^2)(1+16\Delta f^2)}}\sqrt{\frac{P_L}{2h_P\nu}}\,h(\nu_g)$$

1.7.3 Synchronous Recycling

The title of the present section could have been "how to make a narrow band optical detector by 6 orders of magnitude better than bar detectors". The basic idea of synchronous recycling is to have two identical cavities, and a coupling. In such a system a system of *supermodes* exists, corresponding to combinations of the individual eigenmodes of one cavity. For instance, to a given $\mathrm{TEM_{00}}$ mode of frequency ν_0, corresponds two supermodes, a symmetrical (S) and an antisymmetrical (A). The eigenfrequencies ν_S, ν_A differ from ν_0 by an amount depending of the coupling. When the coupling tends to zero, the frequencies ν_S, ν_A tend to the same limit ν_0, and to degeneracy. If the coupling is very weak, the difference $\nu_S - \nu_A$ may fall in

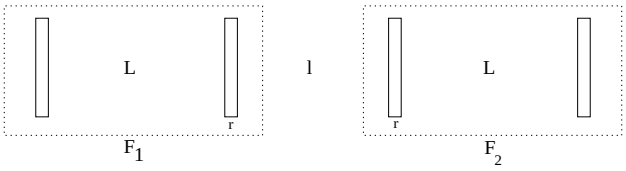

Figure 1.24: System of coupled cavities

the audio range, and a gravitational perturbation is able to pump energy from one mode in the other. The principle of operation is thus to tune the coupling at a minimum, the light source on the A mode, and waiting the signal on the S frequency (or vice-versa). Another way of understanding what happens in coupled cavities is to consider the beat note between these A and S modes. The result is that the stored energy is periodically exchanged between the two cavities, at a frequency which is the gap $\nu_S - \nu_A$ (Think to coupled pendulums). We feel that if the GW frequency is exactly this beat note, the light will accumulate positive phase shifts during the first half GW period, then will be transferred to the second cavity at the moment when the phase becomes negative in the first, and positive in the second, so that, roughly speaking, it sees always a long arm, (or a short one) and we can expect the phase modulation to increase indefinitely. It has been first proposed by Ph. Bernard and E. Picasso [4] to use this effect in high Q superconducting microwave cavities.

It is worth studying the effect on a simplified model involving only two coupled optical cavities (see Fig.1.24). The two cavities (of length L) are facing each other. The light can be transmitted through the central region of length l. In fact, this region is itself a cavity and we call it the central cavity. Without changing the two FP's, it is possible to tune the central cavity by changing the distance l. When the central cavity is at resonance, its tranmittance is a maximum, and the coupling is strong. When the central cavity is at antiresonance, its transmittance is a minimum, and the coupling is weak. We assume in the following simple model no losses, a reflectivity of 1 for the two end mirrors, and of r for the two inner mirrors. Let us consider the resonance condition for a wave to remain stored in the system. If we call F the reflectances of the (identical) cavities, we have for a round trip in the central cavity :

$$(iF\,\mathrm{e}^{ikl})^2 = 1$$

Two series of solutions can be obtained by taking

$$iF\,\mathrm{e}^{ikl} = 1 \quad \text{symmetrical mode}$$

$$iF\,\mathrm{e}^{ikl} = -1 \quad \text{antisymmetrical mode}$$

in case of zero losses, the reflectance of one cavity is of modulus 1 :

$$F \;=\; \frac{r+\mathrm{e}^{2ikL}}{1+r\,\mathrm{e}^{2ikL}} \;=\; \mathrm{e}^{2ikL}\,\frac{1+r\,\mathrm{e}^{-2ikL}}{1+r\,\mathrm{e}^{2ikL}}$$

If we take the resonance as a reference frequency, we can write

$$2kL \;=\; \frac{4\pi\nu_0 L}{c} + \frac{4\pi L\delta\nu}{c}$$

where ν_0 is the resonance frequency of the (isolated) cavity, and $\delta\nu$ the unknown detuning giving a resonance in the coupled system. We have thus $4\pi\nu_0/\lambda \equiv \pi\,[\mathrm{mod}2\pi]$, and we can work with the reduced detuning already used above, $\Delta f = \delta\nu/\delta\nu_{\mathrm{FWHM}}$ which is simply the ratio of the detuning to the linewidth of the cavity. The round trip phase becomes simply

$$2kL = \pi + \frac{2\pi}{\mathcal{F}}\,\Delta f$$

so that the reflectance reduces to the pure phase factor

$$\mathrm{Arg}(F) = \pi + \frac{2\pi}{\mathcal{F}}\,\Delta f + 2\,\tan^{-1}\left[\frac{r\,\cos(2\pi\Delta f/\mathcal{F})}{1-r\,\sin(2\pi\Delta f/\mathcal{F})}\right]$$

For the phase factor corresponding to the central cavity, we have

$$kl = \frac{2\pi\nu_0 l}{c} + \frac{\pi l}{\mathcal{F}\,L}\,\Delta f$$

The constant phase $\varphi = 2\pi\nu_0 l/c$ can be considered as the tuning of the central cavity. The resonance conditions become

$$2\,\tan^{-1}\left[\frac{r\,\cos(2\pi\Delta f/\mathcal{F})}{1-r\,\sin(2\pi\Delta f/\mathcal{F})}\right] \;=\; (2n+1)\pi - \frac{\pi}{2} - \varphi - \frac{2\pi}{\mathcal{F}}\Delta f - \frac{\pi l}{\mathcal{F}\,L}\,\Delta f$$

leading to the S-modes equation :

$$\frac{r\,\cos(2\pi\Delta f/\mathcal{F})}{1-r\,\sin(2\pi\Delta f/\mathcal{F})} \;=\; \tan\left[\frac{\varphi}{2} + \frac{\pi}{4} + \left(1+\frac{l}{2L}\right)\Delta f\right]^{-1} \qquad (1.24)$$

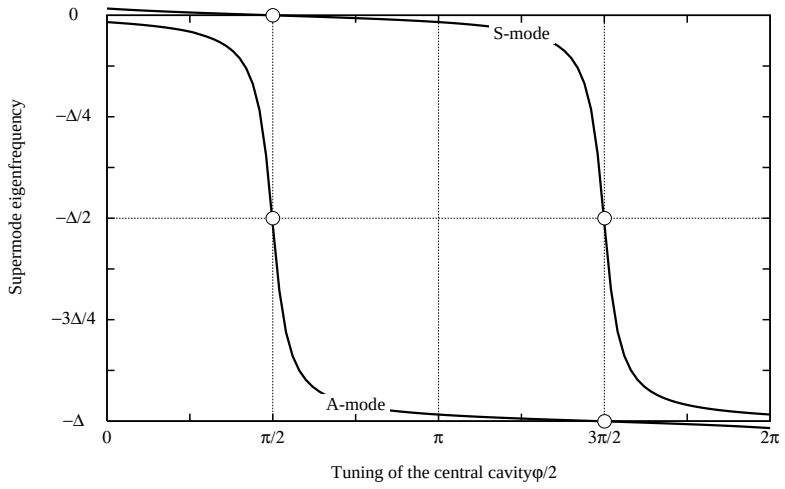

Figure 1.25: Relative detuning of the A and S supermodes vs tuning of the central cavity

The A-modes equation can be obtained a similar way :

$$\frac{r\,\cos(2\pi\Delta f/\mathcal{F})}{1-r\,\sin(2\pi\Delta f/\mathcal{F})} \;=\; -\tan\left[\frac{\varphi}{2}+\frac{\pi}{4}+\left(1+\frac{l}{2L}\right)\Delta f\right] \qquad (1.25)$$

These are implicit equations in the unknown detuning Δf. The numerical solutions are plotted on Fig.1.25. The round trip phase in the central cavity is equal to 2φ. The value $\varphi = 0$ corresponds thus to *antiresonance*, then to a minimum of coupling, and a weak splitting of the resonance lines. The tuning has period π, so that we retrieve a similar situation at $\varphi = \pi$ where the S-frequency is near the preceding A-frequency. The value $\varphi = \pi/2$ corresponds to *resonance* of the central cavity, thus to a maximum of coupling, and a maximum of line splitting This maximum is half the FSR (the interval between the two white spots on the figure). In order to study the minimum of coupling, and the frequency gap between the A and S modes at this tuning, we turn to our simplified model, which will be of some use anyway in the sequel. For zero losses, the parameter σ is zero, and we have for the phases :

$$\frac{\pi}{2}+2\,\tan^{-1}(2\Delta f)+\frac{2\pi l}{c}\,(\nu_0+\delta\nu) \;\equiv\; 0 \quad (\mathrm{S}-\mathrm{modes})$$

$$\frac{\pi}{2} + 2\,\tan^{-1}(2\Delta f) + \frac{2\pi l}{c}\,(\nu_0 + \delta\nu) \;\equiv\; \pi \quad (\mathrm{A-modes})$$

We can write as well

$$\Delta f_S \;=\; \frac{1}{2}\tan\left[\frac{\varphi}{2} + \frac{\pi}{4} + \frac{\pi l}{2\mathcal{F}L}\Delta f_S\right]^{-1}$$

The term $\pi l/2\mathcal{F}L$ is very small for kilometric cavities of finesse $\simeq 100$ and a metric central cavity. If we neglect it, we have the very simple results :

$$\Delta f_S \;=\; \frac{1}{2}\tan\left[\frac{\varphi}{2} + \frac{\pi}{4}\right]^{-1}$$

$$\Delta f_A \;=\; -\frac{1}{2}\tan\left[\frac{\varphi}{2} + \frac{\pi}{4}\right]$$

The following plot (Fig.1.26) is to be compared with the preceding. The approximation used is valid only for detunings much smaller than the FSR. For $\varphi = \pi/2$, we have seen that the detuning of the A-mode is half the FSR, the model consequently fails, this is the reason of the divergence of the A-mode at this point. The same reason causes the divergence of the S-mode at $-\pi/2$. If we restrict our attention to the neighbourhood of $\varphi = 0$, i.e. the validity range of the present model, we can see a good agreement with the exact calculation. It is in particular easy to compute the minimum line splitting :

$$[\Delta f_S - \Delta f_A]_{\min} \;=\; \frac{1}{2}\left[\frac{1}{\tan(\pi/4)} + \tan(\pi/4)\right] \;=\; 1$$

corresponding, in terms of frequency, to

$$[\delta\nu_S - \delta\nu_A]_{\min} \;=\; \delta\nu_{\mathrm{FWHM}} \;=\; \frac{c}{2\mathcal{F}L}$$

In other words, the minimum splitting is nothing but the linewidth of the cavity. If we intend to use this device to detect GW by coupling the A and S modes with the gravitational perturbation, we see that we have to use high finesse and long cavities. For the current situation (L=3 km and $\mathcal{F}$=100), the frequency gap is ν_g=500 Hz. Higher values can be obtained by a different tuning of the central cavity : The general result is

$$\nu_g \;=\; \delta\nu_S - \delta\nu_A \;=\; \frac{1}{\cos\varphi}\,\frac{c}{2\mathcal{F}L}$$

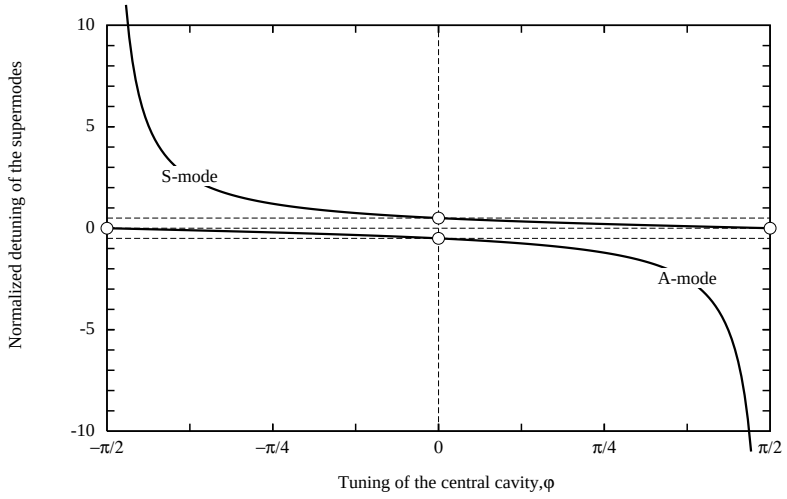

Figure 1.26: Approximate model of degeneracy removing by coupling

We have now to study the response of a real system involving a light source and a detector. The scheme of Fig.1.27 was suggested years ago by R. Drever [3] after a very different approach than Ph. Bernard & E. Picasso. The coupled cavities are in what we call *ring cavity* on the figure. The optical path has been split for clarity, and it could seem strange to separate between the incident and the reflected wave off a cavity. It is however possible by using polarization rotators and polarization sensitive reflectors, so that the situation is almost that of the figure. If (as likely) these switching elements induce losses, these losses can be localized in the mirror r_t. The splitter and the square path allow to launch two rotating waves in the ring cavity, one clockwise and one counterclockwise, these waves are recombined on the splitter. We first consider the counterclockwise wave (see Fig.1.28) and evaluate the A133 reflection operator. We have firstly for the intracavity wave :

$$B \;=\; t_r A_{in} + r_r r_t \mathrm{e}^{2ikl} \mathbf{F_2 F_1}\, B$$

or :

$$B \;=\; t_r \left[1 - r_r r_t \mathrm{e}^{2ikl} \mathbf{F_2 F_1}\right]^{-1}$$

then

$$A_{out} = i\, r_r\, A_{in} - i\, t_r r_t \mathrm{e}^{2ikl} \mathbf{F_2 F_1}\, B$$

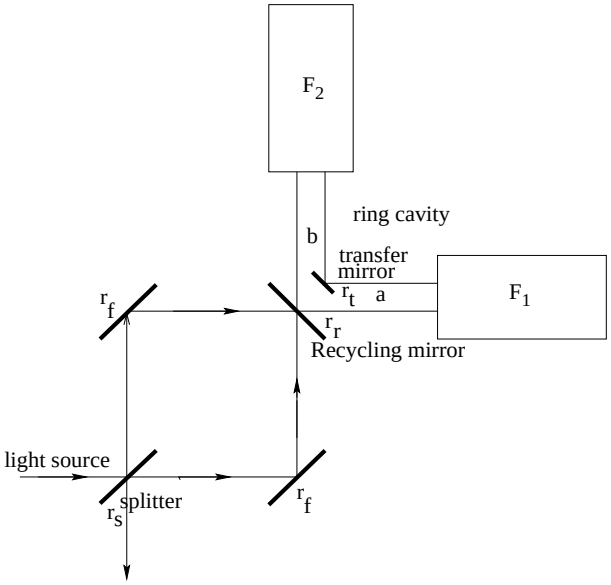

Figure 1.27: Sketch of the synchronous recycling configuration

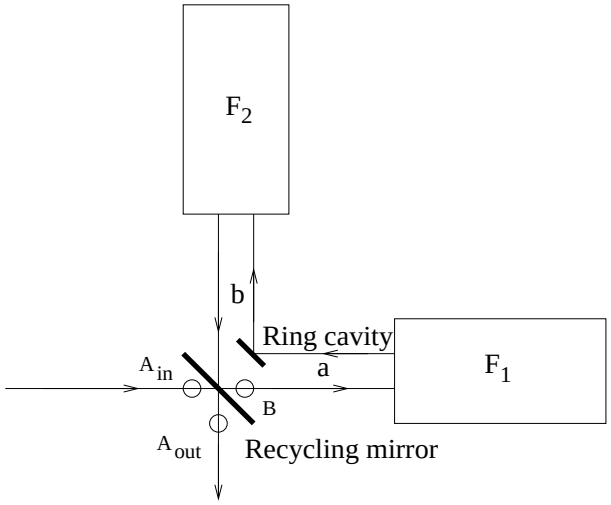

Figure 1.28: Ring cavity and counterclockwise optical path

so that the reflectance is :

$$\mathbf{R}_+ = r_r - t_r^2 r_t \mathrm{e}^{2ikl}\mathbf{F_2F_1}\left[1 - r_r r_t \mathrm{e}^{2ikl}\mathbf{F_2F_1}\right]^{-1}$$

$$= \left[r_r - (1-p_r) r_t \mathrm{e}^{2ikl}\mathbf{F_2F_1}\right]\left[1 - r_r r_t \mathrm{e}^{2ikl}\mathbf{F_2F_1}\right]^{-1}$$

Obviously, for the clockwise optical path, we have the reflectance :

$$\mathbf{R}_- = \left[r_r - (1-p_r) r_t \mathrm{e}^{2ikl}\mathbf{F_1F_2}\right]\left[1 - r_r r_t \mathrm{e}^{2ikl}\mathbf{F_1F_2}\right]^{-1}$$

Now, if we return to the splitter, we can compute the transmittance of the whole system :

$$\mathbf{T} = -i\, t_s^2 r_f^2\, \mathrm{e}^{i\phi}\mathbf{R}_- + i r_s^2 r_f^2\, \mathrm{e}^{i\phi}\mathbf{R}_+$$

Where the two transfer mirrors of the square cavity have been assumed identical. ϕ is the optical path inside the square cavity. If further we assume a perfectly symmetrical splitter, we can write

$$\mathbf{T} = -i\,\frac{1}{2}(1-p_s) r_f^2 \mathrm{e}^{i\phi}\,(\mathbf{R}_- - \mathbf{R}_+)$$

A direct calculation gives

$$[R_- - R_+]_{10} = -t_r^2 r_t\, \mathrm{e}^{2ikl}\,\frac{2G_+(F_-F_+)}{DD_+}$$

Where the definitions of $G_\pm$, $F_\pm$ are the same as in section 7 , and

$$D_a = 1 - r_r r_t\, \mathrm{e}^{2ikl} F_a^2 \quad (a = -1, 0, 1)$$

The [10] component of $\mathbf{T}$ is thus :

$$T_{10} = \frac{\mathcal{F}L}{\lambda}\,\frac{4i(2-\sigma)^2(1-p_s) r_f^2 r_t \mathrm{e}^{i\phi} t_r^2 f_g}{(1-2i\Delta f)^2[1-2i(\Delta f + f_g)]^2\,[1 - r_r r_t \mathrm{e}^{2ikl}F^2]\,[1 - r_r r_t \mathrm{e}^{2ikl}F_+^2]}$$

One would obtain a similar expression for T_{20} by changing the sign of f_g. The preceding expression exhibits a sharp resonance peak when the resonance condition

$$2kl + 2\mathrm{Arg}(F) \equiv 0 \quad [\mathrm{mod} 2\pi]$$

is met. The difference of π with respect to the preceding subsection (two isolated cavities) is due to the fact that we have now two extra mirrors, for

recycling (M_r) and transfer (M_t) each adding a phase of $\pi/2$. This should be kept in mind in any comparison. In particular, the resonance condition for the central cavity is now $2kl \equiv 0$, and the antiresonance is $2kl \equiv \pi$. We assume the laser frequency given, so that kl is a constant, representing the tuning of the central cavity. The long cavities are detuned by a microscopic change in length making their new resonance shifted by an amount Δf. For Δf corresponding to a resonance of the ring cavity, we have thus to solve

$$\tan^{-1}\left(\frac{2\Delta f}{1-\sigma}\right) + \tan^{-1}(2\Delta f) \;=\; -kl$$

or,

$$\frac{2(2-\sigma)\Delta f}{1-\sigma-4\Delta f^2} = -\tan(kl)$$

this gives two solutions :

$$\Delta f_S \;=\; \frac{1}{2}\left[\frac{1-\sigma/2}{\tan(kl)} + \sqrt{\left(\frac{1-\sigma/2}{\tan(kl)}\right)^2 + 1 - \sigma}\right]$$

and

$$\Delta f_A \;=\; \frac{1}{2}\left[\frac{1-\sigma/2}{\tan(kl)} - \sqrt{\left(\frac{1-\sigma/2}{\tan(kl)}\right)^2 + 1 - \sigma}\right]$$

Note that

$$\Delta f_A \times \Delta f_S \;=\; -\frac{1-\sigma}{4} \tag{1.26}$$

and

$$\Delta f_S - \Delta f_A \;=\; \sqrt{\left(\frac{1-\sigma/2}{\tan(kl)}\right)^2 + 1 - \sigma} \tag{1.27}$$

We remark that the minimum frequency gap, is

$$[\Delta f_S - \Delta f_A]_{\min} = \sqrt{1-\sigma}$$

For having a large SNR at the normalized GW frequency $f_g^{(0)} \;>\; \sqrt{1-\sigma}$, we follow the following scheme :

- Tune the central cavity in such a way that $\Delta f_S - \Delta f_A = f_g^{(0)}$, which happens for

$$kl = \tan^{-1}\left[\frac{1-\sigma/2}{\sqrt{f_g^{(0)2} - (1-\sigma)}}\right]$$

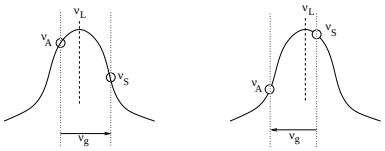

Figure 1.29: Gravito-optical pumping

- Δf_A and Δf_S are now determined. Tune the cavities in such a way that $\Delta f = \Delta f_A$.

Obviously, a similar process can be carried out starting from the upper frequency Δf_S and going to the lower level Δf_A : this is described by the T_{20} component of the A133 transmittance (see Fig.1.29). Unfortunately, only one of the two components T_{10} and T_{20} can be made resonant. If we work on T_{10}, we can therefore neglect T_{20}, and vice-versa. At the end of this process, we see that the resonance condition is met simultaneously, for

$$1 - r_r r_t \mathrm{e}^{2ikl} F^2 = 1 - r_r r_t \rho_A^2$$

because the tuning satisfies the modes A equation, and for

$$1 - r_r r_t \mathrm{e}^{2ikl} F_+^2 = 1 - r_r r_t \rho_S^2$$

because the tuning satisfies the modes S equation when $f_g = f_g^{(0)}$. ρ_A and ρ_S are the modulus reflectances :

$$\rho_{A,S}^2 = 1 - \frac{\sigma(2-\sigma)}{1 + 4\Delta f_{A,S}^2}$$

We have then, at resonance, when $f_g = f_g^{(0)}$,

$$|T_{10}| = \frac{\mathcal{F}L}{\lambda} \frac{16(1-\sigma/2)^2 t_r^2 f_g^{(0)}}{(1+4\Delta f_A^2)(1+4\Delta f_S^2)(1-r_r r_t \rho_A^2)(1-r_r r_t \rho_S^2)}$$

We can still fix the recycling rate by opimizing T_{10} with respect to r_r. In the general case, when the gravitational frequency is larger than the minimum gap, it is cumbersome to derive the optimal r_r. We have :

$$[r_r]_{\mathrm{opt}} = \frac{1 + (1-p_r) r_t^2 \rho_A^2 \rho_S^2}{r_t(\rho_A^2 + \rho_S^2)} - \sqrt{\left(\frac{1 + (1-p_r) r_t^2 \rho_A^2 \rho_S^2}{r_t(\rho_A^2 + \rho_S^2)} \right)^2 - (1-p_r)}$$

If we use the definitions of ρ_A and ρ_S, it is possible to show that

$$\rho_A \times \rho_S = 1 - \sigma$$

which is particularly remarkable, being independent on the tuning of the cental cavity. After that, the sum $\rho_A^2 + \rho_S^2$ will obviously depend on the tuning :

$$\rho_A^2 + \rho_S^2 = 1 + (1-\sigma)^2 - \frac{\sigma^2(2-\sigma)^2}{\sigma^2 + 4f_g^{(0)2}}$$

It is however reasonable to optimize the SNR for the lowest possible GW frequency, i.e when $f_g^{(0)} = f_m = \sqrt{1-\sigma}$, situation in which we have $\rho_A = \rho_S = \sqrt{1-\sigma}$. The optimum value of the recycling mirror reflection coefficient is simply

$$[r_r]_{\rm opt} = (1-p_r) r_t (1-\sigma)$$

And the optimal peak value of $|T_{10}|$ is

$$|T_{10}|_{\rm peak} = \frac{2\pi L}{\lambda p} K(\sigma)$$

with the form factor

$$K(\sigma) = \frac{2\sigma\sqrt{1-\sigma}}{1-(1-p_{RC})(1-\sigma)^2}$$

and $1 - p_{RC} = (1-p_r) r_t^2$. The form factor K has the maximum value 1, obtained for the approximate value $\sigma = (2p_{RC})^{1/3}$. But the shape of the curve is so flat, that this value is misleading, a value of K very close to 1 is obtained already for the pseudo- optinum $\sigma \simeq 20 p_{sr}$ (see fig.1.30). The peak SNR at resonance is therefore

$$\mathrm{SNR}_{\rm peak,Max} = \frac{2\pi L}{\lambda p} \sqrt{\frac{P_L}{2h_P\nu}}\, h(\nu_g)$$

for a wide range of reference GW frequencies. For $f^{(0)}$ too small, however, the SNR falls to zero. Remark that this peak value scales as $1/p$, whereas the zero frequency limit of the (wideband) power recycling scales as $1/\sqrt{p}$. The spectral density of h equivalent to shot noise is :

$$h(f_0) = \sqrt{\frac{2h_P\nu}{P_L}} \frac{1}{\mathrm{SNR}_{\rm peak,Max}}$$

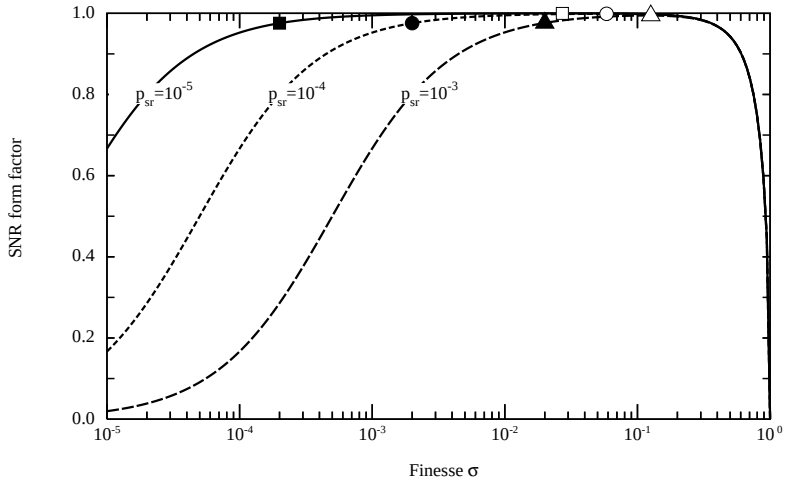

Figure 1.30: Form factor K for the SNR vs finesse $\sigma = p\mathcal{F}/\pi$. The white dots are the strict optima, the black dots mark the pseudo-optima

For cavity losses $p = 3\,10^{-5}$, l=3 km, $\lambda = 1.064\,10^{-6}$ m, P_L=20W, we have

$$h(f_0) \;\simeq\; 2.3\;10^{-25}\mathrm{Hz}^{-1/2}$$

It is now necessary to study the width of the resonance. For this purpose, we assume the laser being locked on the antisymmetric resonance, and the gravitational frequency in the neighbourhood of the gap $f_g^{(0)}$, i.e. $f_g = f_g^{(0)} + \delta f$, so that $\Delta f_A + f_g \;=\; \Delta f_S + \delta f$. Consider the SNR :

$$\mathrm{SNR}(\delta f) \propto \frac{16\mathcal{F}L}{\lambda}\,\frac{(1-\sigma/2)^2 t_r^2 f_g}{(1+4\Delta f_A^2)(1+4(\Delta f_A+f_g)^2)(1-r_r r_t \rho_A^2)\,(1-r_r r_t \rho_+^2 \mathrm{e}^{2i\Phi})}$$

In this expression, the varying terms are :

- The fast varying phase

  $$\Phi \;=\; \tan^{-1}\left[\frac{2(\Delta f_S+\delta f)}{1-\sigma}\right] + \tan^{-1}\left[2(\Delta f_S+\delta f)\right] - \tan^{-1}\left[\frac{2\Delta f_S}{1-\sigma}\right] - \tan^{-1}\left[2\Delta f_S\right]$$

  expanded at first order in δf this gives

  $$\Phi \;=\; A\delta f \quad \text{with} \quad A \;=\; \frac{4(2-\sigma)(1-\sigma+4\Delta f_S^2)}{[(1-\sigma)^2+4\Delta f_S^2]\,[1+4\Delta f_S^2]}$$

- The reflectivity of the cavities for the upper sideband :

$$\rho_+^2 \;=\; 1 - \frac{\sigma(2-\sigma)}{1+4(\Delta f_S + \delta f)^2}$$

This differs from unity by a small amount, whose variation is like second order. More specifically, the second order expansion gives

$$\rho_+^2 \;=\; \rho_S^2 + \frac{8\sigma(2-\sigma)\Delta f_S}{(1+4\Delta f_S^2)}\,\delta f + \frac{4\sigma(2-\sigma)(1-12\Delta f_S^2)}{(1+4\Delta f_S^2)^3}$$

We have already seen that the best value of σ is very small, in order to have a good reflectivity of the cavities. It can be thus understood, and numerically checked that the variations of ρ_+^2 around the S resonance can be neglected.

- The term,

$$\frac{f_g^{(0)} + \delta f}{1+4(\Delta f_S + \delta f)^2}$$

which varies very little.

The study of the shape of the resonance line can thus be carried out on the only term :

$$|1 - r_r r_t \rho_+^2 \mathrm{e}^{2i\Phi}| \;\simeq\; \left[(1 - r_r r_t \rho_S^2)^2 + 4 r_r r_t \sin^2(A\delta f)\right]^{1/2}$$

$$= \;(1 - r_r r_t \rho_S^2)\left[1 + \left(\frac{2\sqrt{r_r r_t \rho_S^2}\,\sin(A\delta f)}{1 - r_r r_t \rho_S^2}\right)^2\right]^{1/2}$$

expression very similar to a cavity resonance, with the *superfinesse*

$$\mathcal{SF} \;=\; \frac{\pi\sqrt{r_r r_t \rho_S^2}}{1 - r_r r_t \rho_S^2}$$

The linewidth (FWHM) od the SNR is thus :

$$\Delta f_g = \frac{\sqrt{3}(1 - r_r r_t \rho_s^2)}{A\sqrt{r_r r_t \rho_S^2}}$$

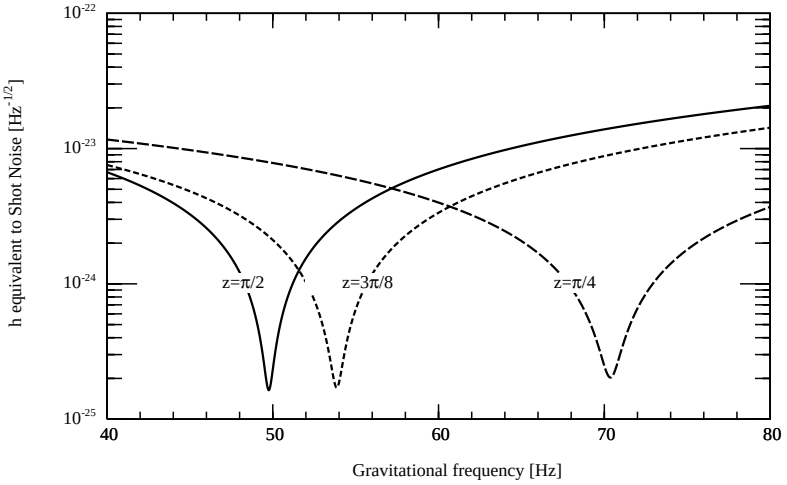

Figure 1.31: Effect of the detuning of the central cavity on the response of synchronous recycling interferometer

A simplified model will help to get simple estimates of the peak value and the linewidth of the SNR. We have seen that small values of σ are pseudo-optimal. We can then try a first order approximation in σ and a fortiori in the various losses. The SNR (with optimized recycling rate) becomes :

$$\mathrm{SNR}(f_g) \;=\; \frac{16\mathcal{F}L}{\lambda}$$

$$\frac{(1-\sigma)f_g(p_{RC}+2\sigma)}{(1+4\Delta f_A^2)(1+4\Delta f_S^2)(1-(1-p_{RC})(1-\sigma)\rho_A^2)|1-(1-p_{RC})(1-\sigma)\rho_S^2\,\mathrm{e}^{2i\Phi}|}\;\times$$

$$\times\;\sqrt{\frac{P_L}{2h_P\nu}}\,h(\nu_g)$$

It is easy to see that the 1st order expressions for the S and A detunings are respectively :

$$\Delta f_S \;=\; \frac{1-\sigma/2}{2\tan(z/4)}$$

$$\Delta f_A \;=\; -\frac{(1-\sigma/2)\tan(z/4)}{2}$$

where $z = 2kl$ is the tuning of the central cavity. we find then

$$1 + 4\Delta f_S^2 = \frac{1 - \sigma\cos^2(z/4)}{\sin^2(z/4)}$$

$$1 + 4\Delta f_A^2 = \frac{1 - \sigma\sin^2(z/4)}{\cos^2(z/4)}$$

whence

$$(1 + 4\Delta f_S^2)(1 + 4\Delta f_A^2) = \frac{4(1-\sigma)}{\sin^2(z/2)}$$

and also

$$\rho_S^2 = 1 - 2\sigma\sin^2(z/4)$$
$$\rho_A^2 = 1 - 2\sigma\cos^2(z/4)$$

The gravitational resonance frequency is

$$f_g^{(0)} = \Delta f_S - \Delta f_A = \frac{1 - \sigma/2}{\sin(z/2)}$$

If we can neglect the ring cavity losses p_{RC} (a few 10^{-5}) with respect to σ (up to 1%), we have simply

$$1 - (1 - p_{RC})(1 - \sigma)\rho_S^2 \simeq \sigma[1 + 2\sin^2(z/4)]$$

$$1 - (1 - p_{RC})(1 - \sigma)\rho_A^2 \simeq \sigma[1 + 2\cos^2(z/4)]$$

For the varying phase factor, we have

$$\Phi = 4(1 - \sigma/2)\sin^2(z/4)\,\delta f$$

The SNR is :

$$\mathrm{SNR} = \frac{8\pi L}{\lambda p}\,\frac{(1-\sigma/2) f_g^{(0)}\sin(z/2)}{(1-\sigma)[1+2\cos^2(z/4)][1+2\sin^2(z/4)]}$$
$$\times \left[1 + \left(\frac{8\sin^2(z/4)}{\sigma[1+2\sin^2(z/4)]}\,\delta f\right)^2\right]^{-1/2} \sqrt{\frac{P_L}{2h_P\nu}}\; h(\nu_g)$$

and finally :

$$\mathrm{SNR} = \frac{2\pi L}{\lambda}\,\frac{1}{p}\,(1-\sigma/2)\,\frac{4\sin(z/2)}{3+\sin^2(z/2)}$$

$$\times \left[1+\left(\frac{8\sin^2(z/4)}{\sigma[1+2\sin^2(z/4)]}\,\delta f\right)^2\right]^{-1/2} \sqrt{\frac{P_L}{2h_P\nu}}\; h(\nu_g)$$

from where we conclude that the overall peak value, corresponding to $z=\pi/2$ is

$$\mathrm{SNR}_{peak,max} \;=\; \frac{2\pi L}{\lambda}\frac{1}{p} \tag{1.28}$$

This peak corresponds to the resonance frequency

$$f_g^{(0)} \;=\; 1-\sigma/2$$

in other words, the minimum resonance frequency is given by the linewidth of the cavity, and the minimum gravitational linewidth (FWHM) :

$$\delta f_{FWHM,min} \;=\; \sigma\sqrt{3}$$

In terms of gravitational frequencies, we find the relation with the cavity linewidth :

$$\Delta\nu_{g,FWHM,min} \;=\; \sqrt{3}\;\times\;\delta\nu_{FWHM}$$

Let us summarize the results for small σ and z not far $\pi/2$:

- By varying the tuning of the central cavity, it is possible to adjust the resonance for a GW frequency equal to or larger than the linewidth of the cavities. The general formula is :

$$\nu_g^{(0)} \;=\; \frac{1-\sigma/2}{\sin(z/2)}\;\times\;\delta\nu_{FWHM} \tag{1.29}$$

- The best response of the interferometer is obtained for the lowest GW frequency, when the central cavity is exactly antiresonant ($z=\pi/2$), the value of the SNR resonance peak is:

$$\mathrm{SNR}_{peak} = \mathrm{SNR}_{peak,max}\times P(z) \tag{1.30}$$

where the maximum peak value has been expressed above (Eq. 1.28), and $P(z)$ is a form factor, taking the value 1 for $z=\pi/2$:

$$P(z) \;=\; \frac{4\sin(z/2)}{3+\sin^2(z/2)} \tag{1.31}$$

- When the central cavity is progressively detuned from antiresonance, the GW resonance frequency increases, the sensitivity decreases, and the GW linewidth increases. The general formula for the GW linewidth is :

$$\delta\nu_{g,FWHM} \;=\; \sigma\sqrt{3} \;\times\; \frac{1+2\sin^2(z/4)}{4\sin^2(z/4)} \;\times\; \delta\nu_{FWHM} \qquad (1.32)$$

These approximations remain true as long as σ does'nt exceed a few %. For very low gravitational frequencies, the linewidth has to be very thin, and the finesse very high, σ cannot more be kept small and the approximation fails. In fact we already know from the preceding study that the SNR tends to zero when the resonance peak tends to zero. The ratio $\nu_g/\delta\nu_{g,FWHM}$ gives an idea of the equivalent Q of the resonator. For the optimal operation point ($z = \pi/2$), we have

$$Q \;\simeq\; \frac{1}{\sigma\sqrt{3}} \;=\; \frac{\pi}{\sqrt{3}p\mathcal{F}}$$

1.7.4 Signal recycling

Signal recycling was proposed some years ago by B. Meers [2]. The idea is to add one more mirror after the output port of the interferometer in order to store the sidebands generated by the GW. The dark fringe port plus the signal recycling mirror form a resonant cavity whose reflectivity can be tuned. The gravitational frequencies creating a sideband for which the signal cavity is *antiresonant* are enhanced. This allows to modify the sensitivity curve and have a gain factor at a given frequency range of special interest. We have seen other methods giving a comparable result. Here, one more benefit is to enhance the constrast of the interferometer by the spatial filtering effect of the extra Fabry-Perot installed at the output (But this is out of the scope of the present chapter). The sketch of the setup and the notation are shown on Fig.1.32. The lengths of the short arms are a and b, the length of the power recycling cavity is l, and the length of the dual recycling cavity is z. The parameters of the mirrors are labeled by r,s,d. The A133 operator corresponding to the whole setup may be constructed by successive shells. We first consider the Michelson (mic) as a black box having two inputs, West (as in the preceding sections) and South (because the dual recycling reinjects from the South). It has therefore an A133 reflectance R^W_{mic} and a transmittance $T^W_m ic$ (see Fig.1.33). It has also a reflectance R^S_{mic} and a

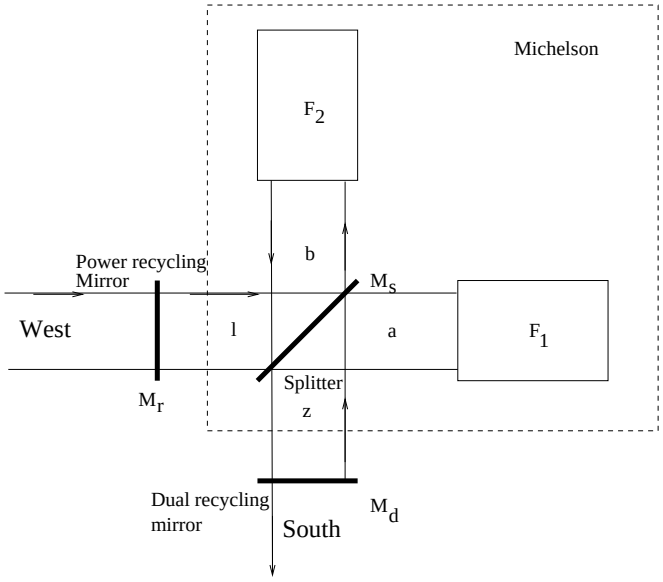

Figure 1.32: sketch of the Dual recycling configuration

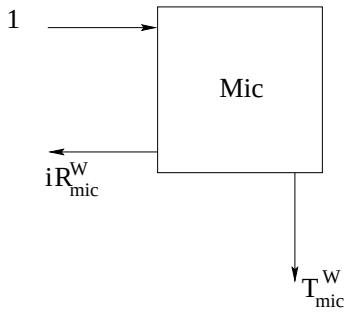

Figure 1.33: West input

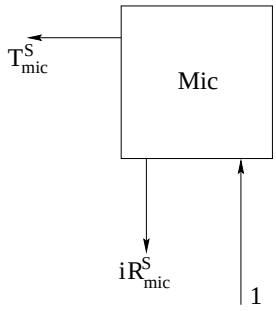

Figure 1.34: South input

transmittance T^S_{mic} for the South input port : The corresponding operators are easy to compute :

$$\begin{aligned} R^W_{mic} &= t_s^2 \mathrm{e}^{2ika} F_1 - r_s^2 \mathrm{e}^{2ikb} F_2 \\ T^W_{mic} &= -r_s t_s \left(\mathrm{e}^{2ika} F_1 + \mathrm{e}^{2ikb} F_2 \right) \\ R^S_{mic} &= -r_s^2 \mathrm{e}^{2ika} F_1 + t_s^2 \mathrm{e}^{2ikb} F_2 \\ T^S_{mic} &= -r_s t_s \left(\mathrm{e}^{2ika} F_1 + \mathrm{e}^{2ikb} F_2 \right) \end{aligned}$$

If we assume the splitter to be strictly symmetrical, and the Michelson tuned at a black fringe, we have simply, after setting $m = (a+b)/2$,

$$R^W_{mic} = -R^S_{mic} = \frac{i}{2}(1-p_s)\mathrm{e}^{2ikm}(F_1+F_2) = R_{mic}$$

$$T^W_{mic} = T^S_{mic} = -\frac{i}{2}(1-p_s)\mathrm{e}^{2ikm}(F_1-F_2) = T_{mic}$$

with

$$F_1 = \begin{pmatrix} F & 0 & 0 \\ G_+ & F_+ & 0 \\ G_- & 0 & F_- \end{pmatrix} \quad , \quad F_2 = \begin{pmatrix} F & 0 & 0 \\ -G_+ & F_+ & 0 \\ -G_- & 0 & F_- \end{pmatrix}$$

F, $F_\pm$ and $G_\pm$ having the definitions set in section 8. Now the power recycled interferometer (pritf) (see Fig.1.35 and Fig.1.36) has a transmittance T_{pritf} for a west input, and a reflectance R_{pritf} for a south input. The corresponding operators are :

$$T_{pritf} = t_r \mathrm{e}^{ikl} T_{mic} \left[1 + r_r \mathrm{e}^{2ikl} R_{mic} \right]^{-1}$$

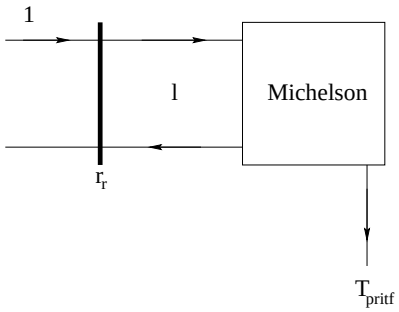

Figure 1.35: West input on a power recycled Michelson

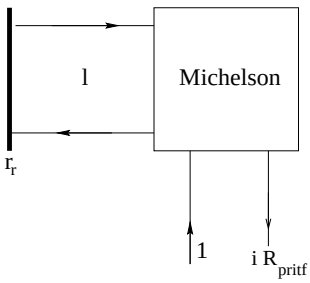

Figure 1.36: South input on a power recycled Michelson

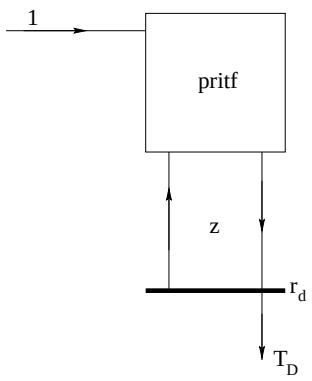

Figure 1.37: West input on a power and dual recycled Michelson

$$R_{pritf} = -R_{mic} + r_r e^{2ikl} T_{mic} \left[1 + r_r e^{2ikl} R_{mic}\right]^{-1} T_{mic}$$

Finally, the dual recycling setup (see Fig.1.37) has a transmittance for a west input T_D.

$$T_D = t_d e^{ikz} \left[1 + r_d e^{2ikz} R_{pritf}\right]^{-1} T_{pritf}$$

After some elementary algebra, we find :

$$T_{D,10} = -i \frac{t_r t_d (1-p_s) e^{ik(l+2m+z)} G_+}{[1 - i(1-p_s) r_d e^{2ik(m+z)} F_+]\,[1 + i(1-p_s) r_r e^{2ik(l+m)} F]} \quad (1.33)$$

$$T_{D,20} = -i \frac{t_r t_d (1-p_s) e^{ik(l+2m+z)} G_-}{[1 - i(1-p_s) r_d e^{2ik(m+z)} F_-]\,[1 + i(1-p_s) r_r e^{2ik(l+m)} F]} \quad (1.34)$$

It is easy ro recognize in these formulas the SNR for a power recycled Michelson, as already derived in a previous section, multiplied by an extra surtension factor :

$$S_D = \frac{t_d}{1 - i(1-p_s) r_d e^{2ik(m+z)} F_+}$$

Remark the opposite signs in the two factors of the denominators : The best efficiency is obtained for resonance in the recycling cavity, and antiresonance in the signal cavity. Obviously, the two sidebands cannot be both antiresonant (except at zero gravitational frequency). if we choose for instance, to make the (10)-component resonant. It is possible

- to tune the long Fabry-Perot's at resonance, so that $Arg(F) = \pi$,

- to tune the power recycling cavity so as to obtain resonance, by taking

$$2k(l+m)+\frac{\pi}{2} \equiv \pi$$

the signal surtension factor may be written as

$$S_D = \frac{t_d}{1-r_d(1-p_s)\,\rho_+\,\mathrm{e}^{i[\pi/2+2k(m+z)+Arg(F_+)]}}$$

where, f being the gravitational reduced frequency,

$$\rho_+ = 1-\frac{\sigma(2-\sigma)}{1+4f^2}$$

$$Arg(F_+) = \pi + \tan^{-1}\left[\frac{2f}{1-\sigma}\right]+\tan^{-1}[2f]$$

clearly, it is always possible to tune the dual recycling cavity to meet resonance, with the condition :

$$2k(m+z)+\tan^{-1}\left[\frac{2f}{1-\sigma}\right]+\tan^{-1}[2f] \equiv \frac{\pi}{2}$$

The sharpness of the dual resonance is a function of r_d (see Fig.1.38) If σ is small, we conclude that the detuning giving the sensitivity peak at given f_0 is

$$\delta \sim \frac{\pi}{2}-2\tan^{-1}(2f_0)$$

where we have set $\delta \equiv 4\pi(m+z)/\lambda$. (see Fig.1.39)

1.7.5 The signal extraction regime

We remark that for $\delta=-\pi/2$, which corresponds to $f_0=\infty$, the sensitivity is almost flat (there is a knee at a higher frequency). This regime, exhibiting a broadband response (broader than the standard recycling, and thus losing in maximum sensitivity, for the same finesse) was called 'Signal extraction' by J. Mizuno [5], [6]. The explanation is that the flat curve is the result of a conflict between the low-pass response of the Michelson $(1/(1+4f^2)$ and the signal-recycling gain factor which starting from a low value at $f=0$ (the SNR is out of resonance though the FP's are resonant), increases sharply to a high and

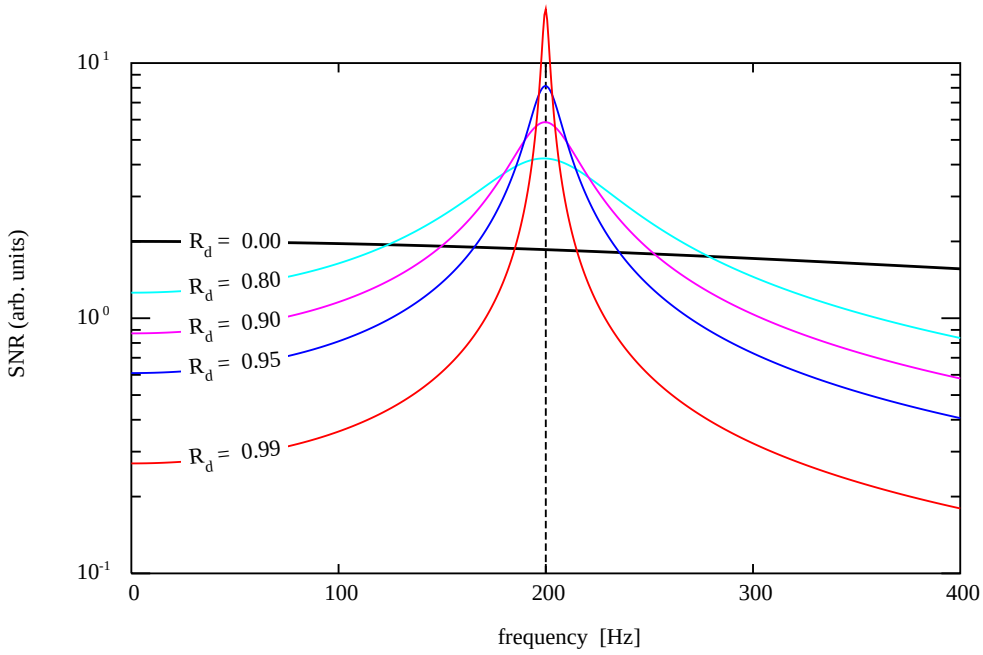

Figure 1.38: SNR of dual recycling configuration for various recycling rates (values of r_d)

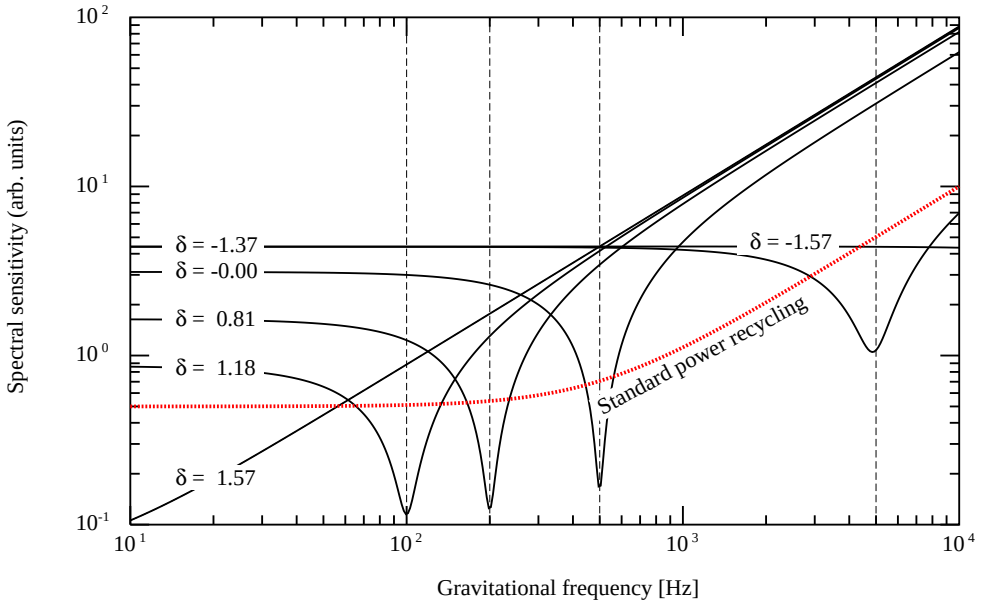

Figure 1.39: Spectral sensitivity of dual recycling configuration for various detunings of the signal recycling cavity $\delta \equiv 4\pi(m+z)/\lambda \pmod{2\pi}$

constant value when the FP's arrive to anti-resonance. (recall that there is a phase flip when a FP transits from resonance to anti, that the antiresonance frequency range is much larger than the resonance, especially at high finesses, and that the reflectance modulus is much higher at antiresonance than at resonance). This result can be understood by looking at the expression of the SNR (1.33). Recall that, when the cavities are at resonance, the upper sideband generated by the GW in one cavity is

$$G_+ \;=\; i\frac{2\mathcal{F}L(2-\sigma)}{\lambda}\;\frac{1}{1-2if_g}$$

and the reflectance of the cavity for that upper sideband is

$$\rho_+ \;=\; -\;\frac{1-\sigma+2if_g}{1-2if_g}$$

where f_g is the normalized gravitational frequency, i.e. the ratio of the gravitational frequency to the linewidth of the cavity ($f_g = \nu_g/\delta\nu$), and σ the coupling coefficient. The SNR takes thus the form (up to a phase factor and neglecting the length of the SR cavity), when power recycling is resonant and signal recycling antiresonant :

$$T_{D,10} \;=\; \frac{2\mathcal{F}L(2-\sigma)}{\lambda}\;\frac{1}{1-2if_g}\;G_r\;\frac{t_d}{1+(1-p_s)r_d\,\frac{1-\sigma+2if_g}{1-2if_g}}$$

where G_r is the resonant power recycling gain (unsensitive to GW frequency) :

$$G_r \;=\; \frac{t_r}{1-(1-p_s)r_r(1-\sigma)}$$

This yields

$$|T_{D,10}| \;=\; \frac{2\mathcal{F}L(2-\sigma)}{\lambda}\;G_r\left|\frac{t_d}{1-2if_g+(1-p_s)r_d\,[1-\sigma+2if_g]}\right| \;=$$

$$\frac{2\mathcal{F}L(2-\sigma)}{\lambda}\;G_r\left|\frac{t_d}{1+(1-p_s)(1-\sigma)r_d\;-2if_g\,[1-(1-p_s)r_d]}\right|$$

Which makes clear that the bandwidth is now

$$\delta\nu_g \;=\; \frac{\delta\nu}{1-(1-p_s)r_d}$$

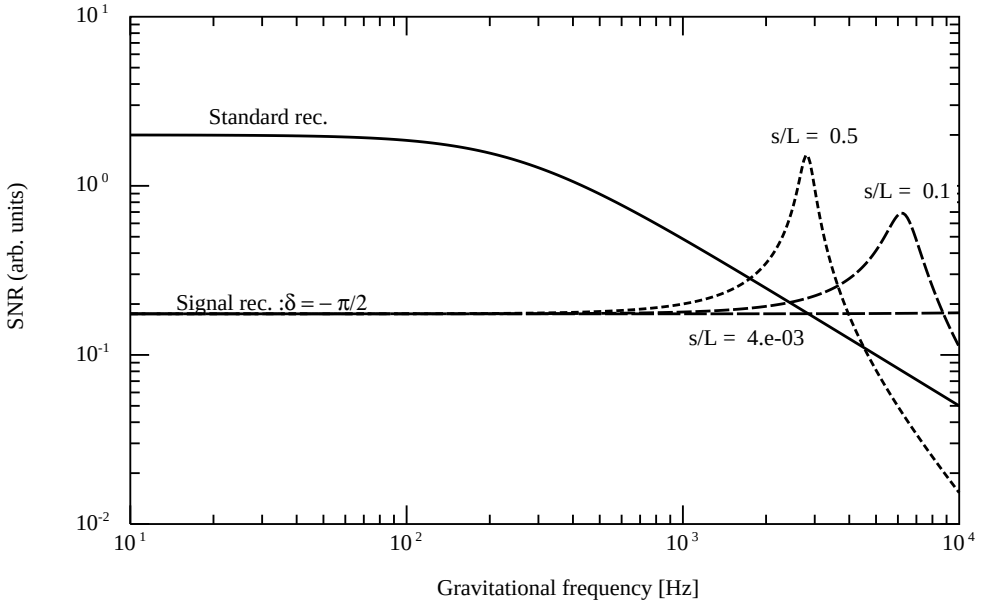

Figure 1.40: SNR in the regime of "signal extraction", i.e. $\delta \equiv -\pi/2 \pmod{2\pi}$, for several ratios s/L of the signal cavity. L is the length of the arms

so that, even if the finesse is very high, by increasing the recycling rate r_d, it is possible to keep constant the product $\mathcal{F}[1-(1-p_s)r_d]$ and thus the bandwidth of the detector.

It is even possible to play with the length of the signal cavity, assuming lengths much longer than the recycling cavity (see Fig.1.40). This creates local resonance effects.

It is interesting to note that it is possible, due to the effect mentionned above, to have almost exactly the same SNR spectral profile with standard power recycling, and with power recycling + signal extraction. The following extreme example will help to understand it.

- Assume a power recycling interferometer having finesse 100 long FP cavities. The optimum power recycling rate corresponds to a surtension ~ 800. Starting from a 20 W laser, this gives ~ 18 kW on the splitter, and finally about 500 kW in the FP cavities.

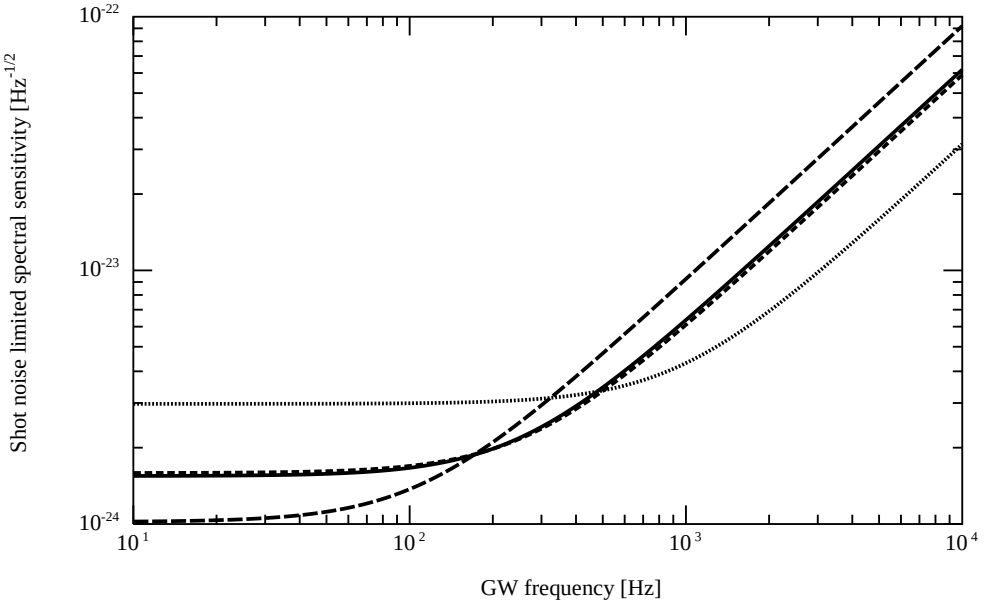

Figure 1.41: Solid curve : Standard power recyling, with $\mathcal{F} = 100$ and optimal recycling. Short dashed curve : Dual recycling-Signal extraction, $\mathcal{F} = 1000$, optimal recycling, $r_d^2 = 0.69$. Long dashed curve : $r_d^2 = 0.4$. Dotted line : $r_d^2 = 0.9$.

- Assume now a dual recycling interferometer in the signal extraction regime. The finesses of the long FP cavities are 1000, and under optimal power recycling, the power surtension is only ~ 80, which is ~ 1.6 kW on the splitter. The reflection coefficient of the signal recycling mirror is $r_d^2 = 0.69$. The power stored in the FP's is still about 500 kW.

- we can compare the SNR in the two situations (see Fig.1.41).

- the coincidence is caused by the particular choice of r_d. A smaller value would give a standard power recyling type response peaked at $f = 0$, a higher value would give a flat response but with a loss of sensitivity.

We see that the drawbacks caused by high powers (thermal lensing, thermal distortions, radiation pressure, ...) are identical in the FP cavities in both

cases, but very different in the power recycling cavity. This is of some importance when power dissipation is taken into account (see further chapters). The ultimate logics of the signal extraction regime is reached when the cavities are optimally coupled (all the light power is absorbed in the FP's), the power recycling rate being zero, and nevertheless, the bandwidth large.

Chapter 2

Beam optics and Interferometers

2.1 introduction

In interferometric GW detectors, we need to store light in long cavities in which light propagates back and forth. We have seen that a good reflectivity of these cavities is a key condition for efficiency in recycling. This reflectivity, combined with the ability to achieve a dark fringe have been an actual worry at the beginning of interferometer projects, and have triggered a lot of optical simulations of FP cavities and interferometers. It was essential to have theoretical models for light propagation. The theory used up to now for this purpose is the Scalar Diffraction Theory (SDT) (this seemed sufficient, owing to the very weak departure of the optical elements from an ideal shape). The basis of the SDT is the Kirchhoff equation, it seemed therefore useful to recall it and its derivation, in order to see clearly what means the paraxial approximation which is in fact more widely used.

2.2 A short theory of diffraction

2.2.1 The Helmholtz equation

A component of the the real Electric field, say $\mathcal{E}(x, y, z)$ in a homogeneous dielectric medium of refractive index n, obeys the wave equation ($c = 2.997925 \times$

10^8km.s^{-1} being the speed of light in a vacuum)

$$\left[\Delta - \frac{n^2}{c^2}\,\frac{\partial^2}{\partial t^2}\right]\,\mathcal{E}(t,x,y,z) \;=\; 0 \tag{2.1}$$

The light coming from a laser can be viewed, in a naive representation as a pure monochromatic wave. In fact, real lasers have a finite linewidth, and a finite coherence range. So far as the dimensions of an optical system are small compared to the coherence range, the monochromatic approximation remains valid. The lasers used in gravitational wave interferometers are highly stabilised in frequency and have huge coherence ranges. Even kilometric optical systems may be treated assuming purely monochromatic waves. For a monochromatic wave of frequency $\nu \;=\; \omega/2\pi$, we can set

$$\mathcal{E}(x,y,z) \;=\; \frac{1}{2}\left(E(x,y,z)\;\mathrm{e}^{-i\omega t} + \overline{E}(x,y,z)\;\mathrm{e}^{i\omega t}\right) \tag{2.2}$$

and for the amplitude E of the electric field, we obtain the Helmholtz equation

$$\left[\Delta \;+\; k^2\right] E(x,y,z) \;=\; 0 \tag{2.3}$$

where $k \;\equiv\; n\omega/c$.

2.2.2 The Kirchhoff integral

This is usually the most delicate part in optics books, and often skipped by stressed readers. The role and the status of the Kirchhoff theory is therefore seldom known: Is it "exact" or "approximate", then with respect to what ? We try to address these issues and give answers at the end of the present section. Recall that for two arbitrary fields A and B, we have a relation between a volume integral and an integral on the surface bounding the same volume, known as Green's theorem:

$$\int_{\mathcal{V}} (A\Delta B - B\Delta A)\,d\vec{r} \;=\; -\oint_{\mathcal{S}}\left[A\,\frac{\partial B}{\partial n} - B\,\frac{\partial A}{\partial n}\right] ds \tag{2.4}$$

$\vec{n}$ represents the inward normal to the surface $\mathcal{S}$ surrounding the volume $\mathcal{V}$ (see Fig.2.1). The following notation has been used:

$$\frac{\partial}{\partial n} \;\equiv\; \vec{n}\cdot\vec{\nabla}$$

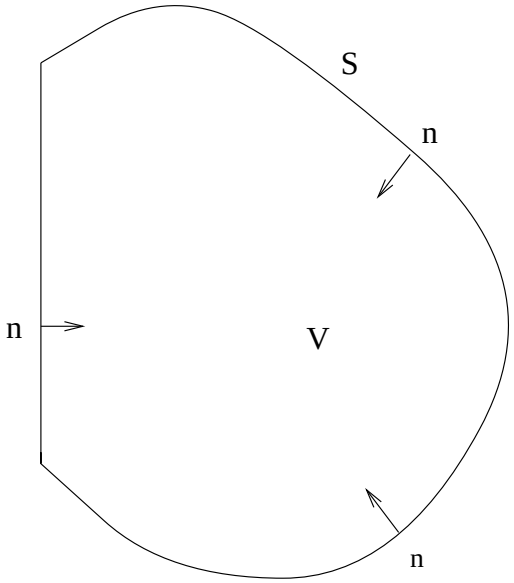

Figure 2.1:

Consider now a solution $E(x,y,z) = E(\vec{r})$ of the Helmholtz equation (2.3), and $G(\vec{r})$ a Green function, i.e. satisfying

$$\left[\Delta + k^2\right] G(\vec{r}) = -\delta(\vec{r}) \tag{2.5}$$

We have as well, Δ' involving 2d order derivatives with respect to the primed coordinates,

$$\left[\Delta' + k^2\right] G(\vec{r} - \vec{r'}) = -\delta(\vec{r} - \vec{r'}) \tag{2.6}$$

by multiplying both sides by $E(\vec{r'})$, we can write

$$E(\vec{r'}) \left[\Delta' + k^2\right] G(\vec{r} - \vec{r'}) = -\delta(\vec{r} - \vec{r'})\, E(\vec{r'})$$

and obviously, with (2.3):

$$G(\vec{r} - \vec{r'}) \left[\Delta' + k^2\right] E(\vec{r'}) = 0$$

by subtracting these two equations, we get:

$$E(\vec{r'})\, \Delta'\, G(\vec{r} - \vec{r'}) - G(\vec{r} - \vec{r'})\, \Delta'\, E(\vec{r'}) = -\delta(\vec{r} - \vec{r'})\, E(\vec{r'})$$

Consider now a volume $\mathcal{V}$ in which Eq.(2.3) holds, bounded by a closed surface $\mathcal{S}$. By integrating the preceding equation over the volume, we get:

$$E(\vec{r}) \;=\; -\int_{\mathcal{V}} \left[E(\vec{r'})\;\Delta'\;G(\vec{r}\;-\vec{r'})\;-\;G(\vec{r}\;-\vec{r'})\;\Delta'\;E(\vec{r'})\right] d\vec{r'}$$

by using Green's theorem, this becomes:

$$E(\vec{r}) \;=\; \oint_{\mathcal{S}} \left[E(\vec{r'})\;\vec{n'}\cdot\vec{\nabla}'G(\vec{r}\;-\;\vec{r'}) - G(\vec{r}\;-\;\vec{r'})\vec{n'}\cdot\vec{\nabla}'E(\vec{r'})\right] ds'$$

provided the point $\vec{r}$ is inside the closed surface $\mathcal{S}$. If the point is outside, the integral vanishes, and this property will be exploited below. Assume now that the surface $\mathcal{S}$ extends to infinity. There are thus two half spaces that we refer to as the left half space, and the right half space respectively. On the surface at infinity, it can be shown that the surface integral vanishes, due to the radiation condition on the field (outgoing waves, no source at infinity). The result is that at any point $\vec{r}$ in the right half space we have:

$$E(\vec{r}) \;=\; \oint_{\mathcal{S}} \left[E(\vec{r'})\;\vec{n'}\cdot\vec{\nabla}'G(\vec{r}\;-\;\vec{r'}) - G(\vec{r}\;-\;\vec{r'})\vec{n'}\cdot\vec{\nabla}'E(\vec{r'})\right] ds' \qquad (2.7)$$

whereas for $\vec{r}$ in the left half space, we have:

$$\oint_{\mathcal{S}} \left[E(\vec{r'})\;\vec{n'}\cdot\vec{\nabla}'G(\vec{r}\;-\;\vec{r'}) - G(\vec{r}\;-\;\vec{r'})\vec{n'}\cdot\vec{\nabla}'E(\vec{r'})\right] ds' \;=\; 0 \qquad (2.8)$$

Now it is well known that a solution of Eq.(2.5) is the simple spherical wave:

$$G(\vec{r}) \;=\; \frac{\mathrm{e}^{ikr}}{4\pi r} \qquad (2.9)$$

so that by taking

$$G_1(\vec{r}\;-\;\vec{r'}) \;=\; \frac{\mathrm{e}^{ik\rho'}}{4\pi\rho'}$$

with $\rho' \;=\; |\vec{r}\;-\;\vec{r'}|$, we have a Green function. Let us define $\vec{r'} \;=\; [x', y', z']$. Now, if we consider

$$G_2(\vec{r} - \vec{r''}) = \frac{e^{ik\rho''}}{4\pi\rho''} \tag{2.10}$$

with $\rho'' = |\vec{r} - \vec{r''}|$ and $\vec{r''} = [x', y', -z']$, we note that it is the symmetrical of the preceding with respect to the plane $z = 0$. If the surface $\mathcal{S}$ is this plane, any point in the right half space, will give a non-zero contribution by the G_1 integral, and a zero contribution by the G_2 integral, the equations (2.7,2.8) being exchanged. We may thus add any multiple of G_2 to G_1 without changing the result:

$$E(\vec{r}) = \iint_{z=0} \left[E(\vec{r'})\ \vec{n'} \cdot \vec{\nabla}' G(\vec{r}, \vec{r'}) - G(\vec{r}, \vec{r'}) \vec{n'} \cdot \vec{\nabla}' E(\vec{r'}) \right]\ dx'\ dy' \tag{2.11}$$

where $G = G_1 + \beta\, G_2$ with β arbitrary. The special choice

$$G(\vec{r}, \vec{r'}) = G_1(\vec{r} - \vec{r'}) - G_2(\vec{r} - \vec{r''}) \tag{2.12}$$

is especially interesting, because it gives a Green function that is zero on the surface $z = 0$, which greatly simplifies the equation. We obtain simply

$$E(\vec{r}) = \iint_{z=0} E(\vec{r'})\ \vec{n'} \cdot \vec{\nabla} G(\vec{r}, \vec{r'})\ dx'\ dy' \tag{2.13}$$

this is the Kirchhoff equation

2.2.3 Application of the Kirchhoff equation

The preceding equation, establishing a relation between the field inside a volume and the field at the boundary is exact, but taken in the strict sense, of almost no practical interest: It could seem that in order to compute E, we first need to know E, because the correct way to impose boundary values is out of this theory. It can however be widely exploited, by slightly changing its meaning, in the following situation. Assume that the surface $z = 0$ contains a hole, and that a primary electromagnetic wave is coming from the left (see Fig.2.2). We can assume that at the immediate right of the surface $z = 0$, the field is simply the field at the left, transmitted through the hole. This means that on the right side of the plane, the field is zero outside the hole, and identical to the field coming from the left, within the hole. We can change the sense of the Kirchhoff equation (2.13) by introducing two fields, one is the coming one $E_1(\vec{r})$, which is assumed to be given throughout the aperture

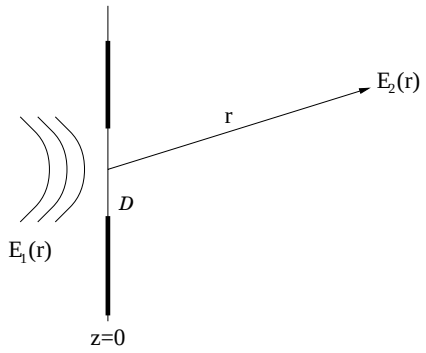

Figure 2.2:

D, and the second one $E_2(\vec{r})$, which is to be computed from the preceding one by using a Kirchhoff-like formula:

$$E_2(\vec{r}) \;=\; \iint_D E_1(\vec{r'})\; \vec{n'} \cdot \vec{\nabla} G(\vec{r}, \vec{r'})\; dx'\; dy' \tag{2.14}$$

The function $K(\vec{r}, \vec{r'}) \;\equiv\; \vec{n'} \cdot \vec{\nabla} G(\vec{r}, \vec{r'})$ is called the Diffraction Kernel. It can be explicitly computed:

$$K(\vec{r}, \vec{r'}) \;=\; -\,\frac{i}{\lambda}\,\frac{\mathrm{e}^{ik\rho}}{\rho}\,\left(1 \;+\; \frac{i}{k\rho}\right)\,\frac{z}{\rho}$$

where $\rho \equiv \sqrt{(x-x')^2 + (y-y')^2 + z^2}$.
With this explicit formula, we obtain:

$$E_2(\vec{r}) \;=\; -\,\frac{i}{\lambda}\,\iint_D E_1(\vec{r'})\,\frac{\mathrm{e}^{ik\rho}}{\rho}\,\left(1 \;+\; \frac{i}{k\rho}\right)\,\frac{z}{\rho}\;\; dx'\; dy' \tag{2.15}$$

For a numerical implementation of Eq.(2.15), it is necessary to extract the rapidly oscillating term in $\exp(ik\rho)$ by writing, with $\mu^2 \;\equiv\; (x-x')^2 + (y-y')^2$,

$$\rho \;=\; z \;+\; \sqrt{\mu^2 + z^2} \;-\; z \;= z \;+\; \frac{\mu^2}{\sqrt{z^2+\mu^2} \;+\; z}$$

so that

$$\mathrm{e}^{ik\rho} \;=\; \mathrm{e}^{ikz} \;\times\; \exp\left[\frac{ik\mu^2}{z + \sqrt{z^2+\mu^2}}\right] \tag{2.16}$$

The first exponential, rapidly oscillating represents pure propagation, and goes out of the integral, whereas the second exponential is slowly oscillating, which is much more convenient, numerically. As a first example, we compute the diffraction pattern of a rectangular aperture illuminated by a constant amplitude. The aperture has its length [-b=-1cm,b=1cm] directed along y, and its width [-a=-0.5cm,a=0.5cm] along x. The distance of the observation plane is z=1 km, the wavelength is $\lambda = 1$ μm. The computational window containing the source was [-1 cm, 1 cm] $\times$ [-1 cm, 1 cm],and the discretization grid was 200 $\times$ 200 points. The well known far field theory [7] gives a central spot of rectangular shape, with its longer dimension along x, and its shorter along y. The dark lines correspond to solutions of

$$\sin\left[\frac{kax}{z}\right] = 0$$

i.e.

$$x_n = \frac{n\lambda z}{2a} = n \times 10.6 \text{ cm}$$

and

$$\sin\left[\frac{kby}{z}\right] = 0$$

i.e

$$y_m = \frac{m\lambda z}{2b} = m \times 5.3 \text{ cm}$$

The plot is logarithmic with respect of the light intensity (Fig.2.3)

As a second example we compute using Eq.(2.15) the diffraction pattern of a circular aperture illuminated by a constant amplitude. The radius of the aperture is $a = 1$ cm, the distance of the observator is $z = 1$ km, the wavelength is $\lambda = 1$ μm. The window containing the source was [-1 cm, 1 cm] $\times$ [-1 cm, 1 cm], and the discretization grid used for numerical integration was 200 $\times$ 200 points. The far field theory foresees a central spot surrounded by rings, the dark rings correspond to solutions r_{dark} of

$$J_1\left(\frac{2\pi a}{\lambda z}\, r\right) = 0$$

the first zeros of the Bessel functions J_1 are

$$\zeta_1 = 3.83171 \quad \Rightarrow \quad r_{\text{dark},1} \approx 6.5 \text{ cm}$$

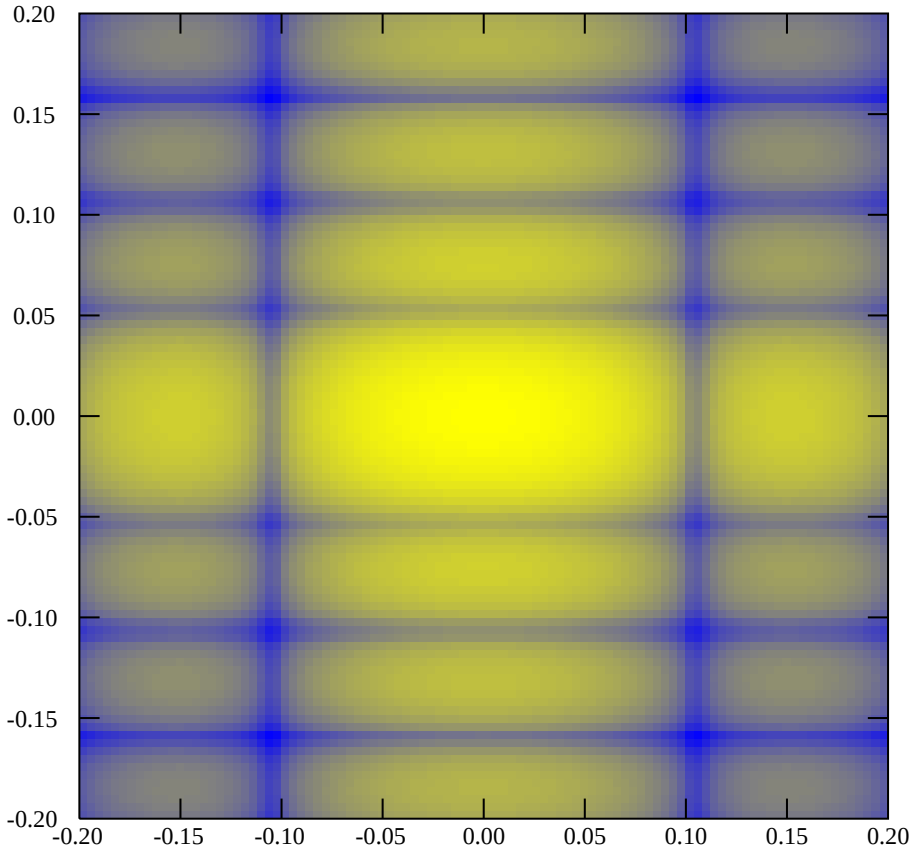

Figure 2.3: Diffraction pattern of a uniform rectangular aperture a =1 cm, b=0.5cm, at z=1 km for the Nd:YAG wavelength: Distribution of log(I)

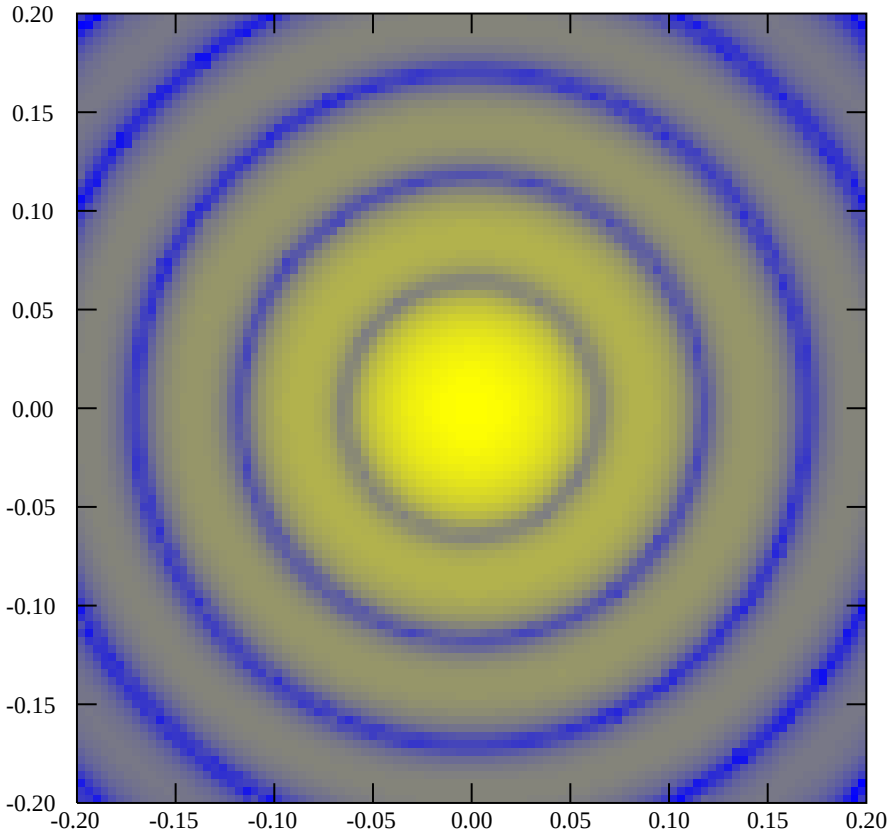

Figure 2.4: Diffraction pattern of a uniform circular aperture a =1 cm at z=1 km for the Nd:YAG wavelength: Distribution of log(I), longitudinal cut

$$\zeta_2 = 7.01559 \Rightarrow r_{\text{dark},2} \approx 11.9 \text{ cm}$$
$$\zeta_3 = 10.17347 \Rightarrow r_{\text{dark},3} \approx 17.2 \text{ cm}$$

The plot (Fig.2.4) is logarithmic with respect to the light intensity. it can be seen that the dark rings coming out of the numerical calculation are in agreement with the far field theory. The near field theory of this case is analytically difficult. Numerical exploitation of the Kirchhoff formula, give access to the near field. See for instance a longitudinal (i.e. along the propagation direction z) cut of the intensity distribution (Fig.2.5). In this case, the circular aperture had 0.1mm radius. The transmitted field is computed starting from z = 0.01 mm. The two precedent diffraction

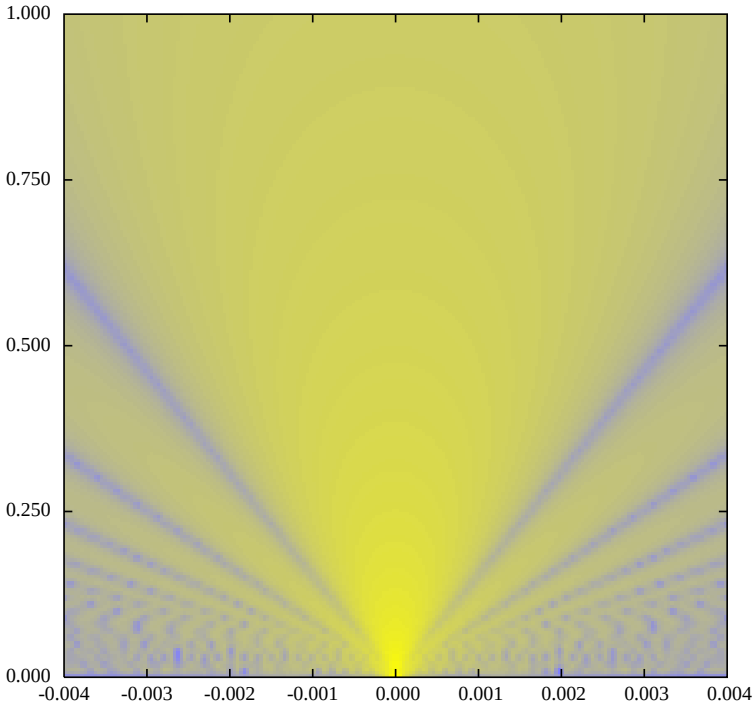

Figure 2.5: Diffraction pattern of a uniform circular aperture $a = 0.1$ mm for the Nd:YAG wavelength: Distribution of log(I)

patterns are roughly known after their far-field approximation (see below). But let us consider a rather exotic window shape, as for instance a regular 5 folded star (seee. fig.2.6). Even the far field is rather intricate to estimate. Use of the Kirchhoff integral gives however the result at any distance: (see Fig.2.7). We give this example, because it cannot be treated analytically due to the complexity of the aperture, nor even by the numerical (to be presented farther) Fourier transforms methods because of its sharp edges, this is a case where use of the Kirchhoff formula is necessary. Finally let we consider the gaussian beam (this will be studied later in detail), of amplitude

$$E(x,y,0) \;\propto\; \exp\left[-\frac{x^2+y^2}{w_0^2}\right]$$

in the plane $z = 0$. For w_0=2 cm, this is the amplitude of the light taken at the input mirrors of the Virgo cavities. It seems to diffract without any lobe, as can be seen on Fig.2.8. In fact, the amplitude extends to infinity, even if it becomes negligible for radial distances larger than w_0, whereas the computing window is finite. It is necessary to take a window much larger than the gaussian radius of the beam. Too narrow windows are understood like a diaphragm, and spurious rings are generated. In the preceding case, even with a computing window as wide as 30 cm, faint lobes can be observed on a logarithmic plot (see Fig.2.9).

2.2.4 Consistency of the Kirchhoff equation

It is not obvious by only looking at the Kirchhoff formula (2.15), that the secondary field E_2 will reduce to the input field E_1 when $z \;\rightarrow\; 0$, i.e. that the diffraction kernel tends to a delta function for $z \;\rightarrow\; 0$. Because we have changed the meaning of the surface integral, the question of the agreement of the approximation done in the preceding subsection with reality could be raisen: Let us try to discuss this issue. The Kirchhoff equation can be written under the form:

$$E_2(x,y,z) \;=\; \int_{-\infty}^{\infty} dx' \int_{-\infty}^{\infty} dy' \left[\partial_{z'}\left(\frac{\mathrm{e}^{ik\rho'}}{4\pi\rho'} \;-\; \frac{\mathrm{e}^{ik\rho''}}{4\pi\rho''}\right)\right]_{z'=0} E_1(x',y',0) \tag{2.17}$$

with

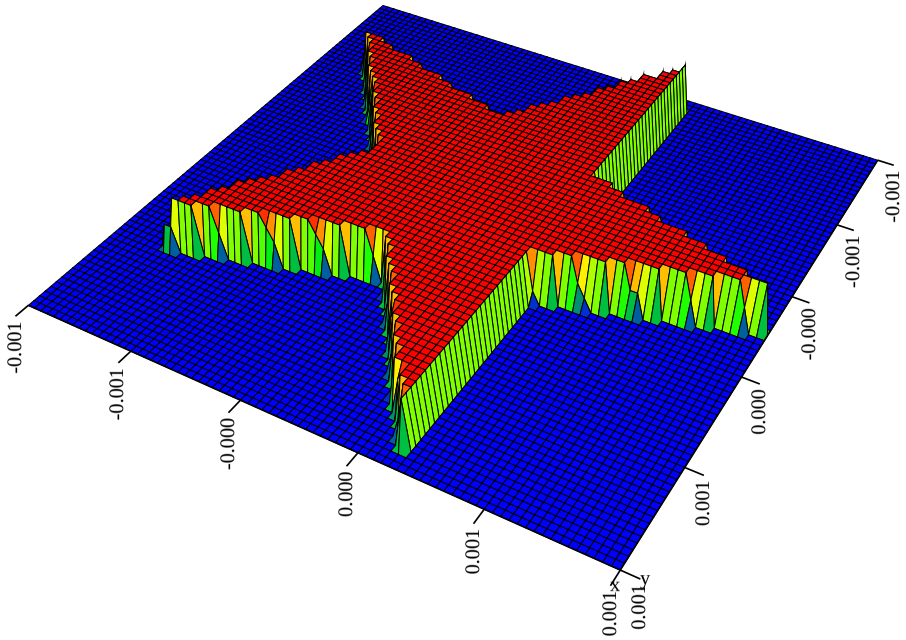

Figure 2.6: A starred pupil: a regular polygon in a circle of radius 1 mm

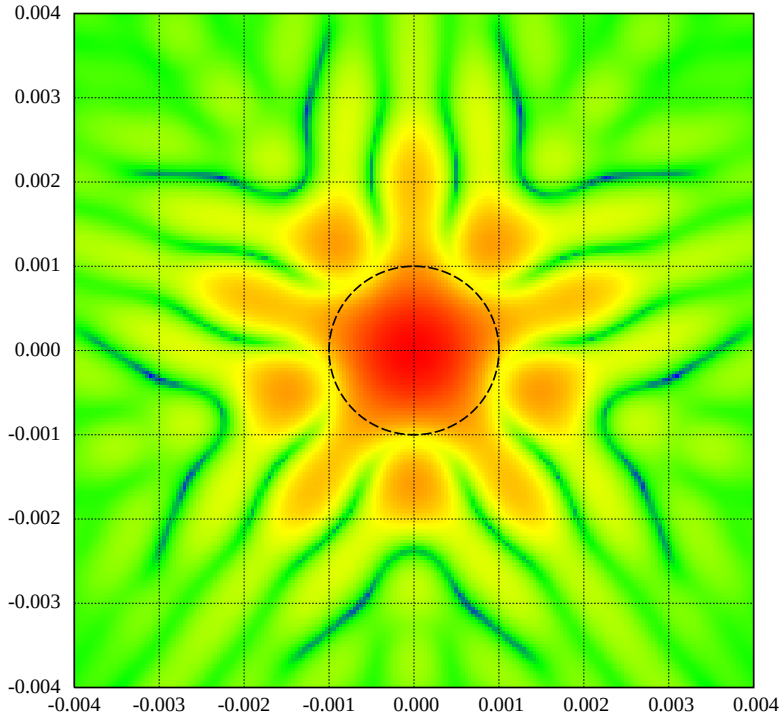

Figure 2.7: diffraction pattern at 1 m from the starred source. The thin circle indicates the size of the initial starred window.

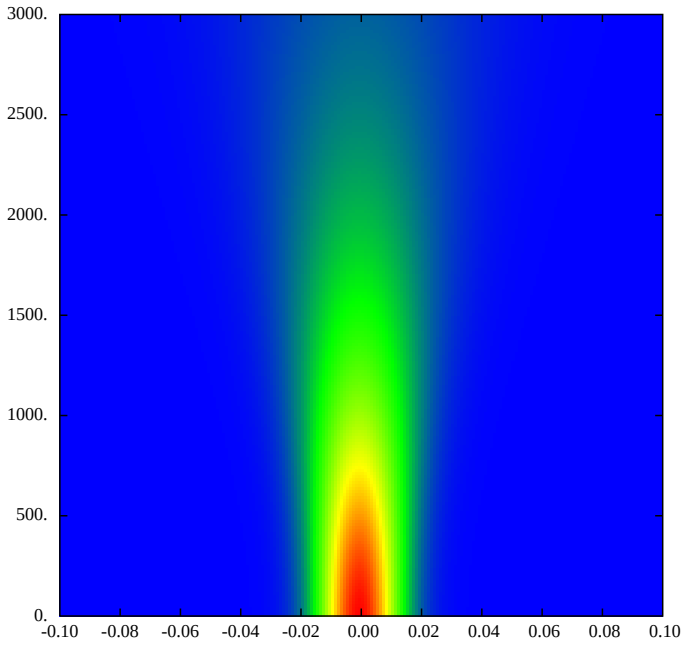

Figure 2.8: Diffraction of a gaussian wave from 100 m to 3 km

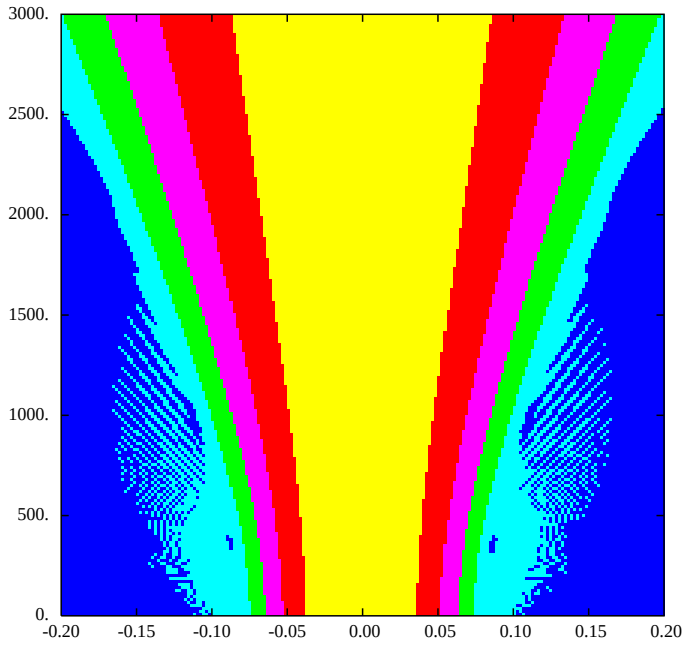

Figure 2.9: Diffraction of a gaussian wave from 100 m to 3 km,logarithmic plot

$$\begin{aligned}\rho' &= \sqrt{(x-x')^2+(y-y')^2+(z-z')^2} \\ \rho'' &= \sqrt{(x-x')^2+(y-y')^2+(z+z')^2}\end{aligned}$$

It is clear that the integral may be viewed as a 2D convolution product, and therefore may be transformed into a simple algebraic product by a 2D Fourier tranform in the variables (x', y'). Recall that the 2D Fourier Transform of any function $f(x, y)$ of integrable square modulus is defined by:

$$\tilde{f}(p,q) = \int_{\mathbf{R}} dx \int_{\mathbf{R}} dy \; \mathrm{e}^{ipx}\mathrm{e}^{iqy} \; f(x,y) \tag{2.18}$$

and the reciprocal transform by

$$f(x,y) = \frac{1}{4\pi^2} \int_{\mathbf{R}} dp \int_{\mathbf{R}} dq \; \mathrm{e}^{-ipx}\mathrm{e}^{-iqy} \; \tilde{f}(p,q) \tag{2.19}$$

A useful result can be found in [9]. The function

$$g(x,y,z) = \frac{\mathrm{e}^{ik\sqrt{x^2+y^2+z^2}}}{2\pi\sqrt{x^2+y^2+z^2}}$$

has the following FT:

$$\tilde{g}(p,q,z) = i \, \frac{\mathrm{e}^{iz\sqrt{k^2-p^2-q^2}}}{\sqrt{k^2-p^2-q^2}}$$

After a Fourier transform, the Kirchhoff equation becomes, using this result:

$$\widetilde{E_2}(p,q,z) = \left[\partial_{z'}\left(i \, \frac{\mathrm{e}^{i(z-z')\sqrt{k^2-p^2-q^2}}}{2\sqrt{k^2-p^2-q^2}} - i \, \frac{\mathrm{e}^{i(z+z')\sqrt{k^2-p^2-q^2}}}{2\sqrt{k^2-p^2-q^2}}\right)\right]_{z'=0} \times$$

$$\times \; \widetilde{E_1}(p,q,0)$$

and eventually reduces to

$$\widetilde{E_2}(p,q,z) = \mathrm{e}^{iz\sqrt{k^2-p^2-q^2}} \times \widetilde{E_1}(p,q,0) \tag{2.20}$$

which shows that the **propagator**, defined as the Fourier Transform of the diffraction kernel has the very simple form

$$\tilde{G}(p,q,z) \;=\; \mathrm{e}^{iz\sqrt{k^2-p^2-q^2}} \tag{2.21}$$

We see that this is perfectly consistent with the Helmholtz equation, which becomes, after a FT:

$$\left(\partial_z^2 \;+\; k^2 - \;p^2 \;-q^2\;\right)\;\tilde{E}(p,q,z) \;=\; 0$$

Anyway, for $z \to 0$, the propagator reduces to 1, showing that the diffraction kernel reduces to $\delta(\vec{r} \;-\; \vec{r'})$, and the diffraction to

$$\widetilde{E_2}(p,q,0) \;=\; \widetilde{E_1}(p,q,0) \;\Rightarrow E_2(x,y,0) \;=\; E_1(x,y,0)$$

as could be expected. We can conclude that, despite a serious change of meaning with respect to the Green theorem, the Kirchhoff formula is strictly equivalent to the wave equation, at least in the case where initial data are given on a plane screen. It follows that if convenient, it is possible to split space into successive slices along the propagation direction, the final data of slice #n being the initial data for slice #(n+1), provided that reflections at each cut do not exist or are ignored. This scheme can be used in compound systems with interfaces, and as will be seen later on, in resonant cavities. We can add the following remark: If we interpret the 2D Fourier transform in the transverse plane as a continuous expansion on plane waves of various directions, by identifying

$$p \;=\; k\sin\theta\,\cos\phi \quad , \quad q \;=\; k\sin\theta\,\sin\phi$$

where (θ,ϕ) denote that direction, we see that the propagator is nothing but the phase change along the z axis of this special plane wave:

$$\tilde{G}(p,q,z) \;=\; \tilde{G}(\theta,\phi,z) \;=\; \mathrm{e}^{ikz\,\cos\theta}$$

2.2.5 The Fresnel approximation and the paraxial diffraction equation (PDE)

The Fresnel approximation

As soon as the distance z separating the input aperture from the observation plane is much larger than the wavelength, the $1/k\rho$ term in Eq.(2.15) becomes negligible, and we can write:

$$E_2(\vec{r}) \;=\; -\,\frac{i}{\lambda}\;\oint_D E_1(\vec{r'})\;\frac{\mathrm{e}^{ik\rho}}{\rho}\;\cos(\theta)\;ds' \qquad (2.22)$$

where θ is the angle under which the element of aperture centered at (x', y') is seen from the observation point (x, y). Eq.2.22 is often referred to as the "Huyghens-Fresnel" equation. It can be (and was) derived heuristically by considering all points of the aperture as elementary sources of spherical waves: At any point of the right hand side half space, the amplitude is the sum of all these wavelets, and we can for instance say that the elementary amplitude created at $\vec{r}$ by the small elementary source

$$ds(x', y') \;=\; E_1(x', y')dx'\,dy'$$

is:

$$dE_2(x, y) \;=\; \kappa\;\iint_D \frac{\mathrm{e}^{ik\rho}}{\rho} E_1(x', y')\,dx'\,dy'$$

where κ is some coefficient to be determined. For this purpose, we can require that the propagation of an indefinite plane wave is the same plane wave, up to a phase factor. This means that

$$\mathrm{e}^{ikz} \;=\; \kappa\;\iint_{\mathrm{R}^2} \frac{\mathrm{e}^{ik\rho}}{\rho}\,dx'\,dy'$$

The integral is easy to compute, being the value at $p = q = 0$ of the Fourier transform of $\mathrm{e}^{ik\rho}/\rho$ that is known, as said above, we have thus

$$\mathrm{e}^{ikz} \;=\; \kappa\;\left[2i\pi\,\frac{\mathrm{e}^{iz\sqrt{k^2-p^2-q^2}}}{\sqrt{k^2-p^2-q^2}}\right]_{p=q=0} \;=\; \frac{2i\pi\mathrm{e}^{ikz}}{k}\;\kappa$$

It is therefore necessary that $\kappa \;=\; -i/\lambda$. This was known long before Kirchhoff's theory, which is the mathematical justification to the Huyghens principle and to the Fresnel formula. If θ in Eq.2.22 is small, we are in the paraxial regime. If the observation point is near the optical axis, and the distance Z long enough, we can neglect the quantity

$$\sqrt{(x-x')^2+(y-y')^2}$$

with respect to z, except in the phase factor. This leads to the paraxial diffraction integral:

$$E_2(x,y,z) \;=\; -\,\frac{i}{\lambda z}\;\exp(ikz)\;\times \tag{2.23}$$

$$\times \iint_D E_1(x',y',0)\;\exp\left[ik\frac{(x-x')^2+(y-y')^2}{2z}\right]\;dx'\;dy'$$

All consequences of this formula are said having been obtained within the Fresnel approximation. Remark that this equation is the convolution product of the field $E(z=0)$ with the simplified (paraxial) diffraction kernel

$$K_{\rm P}(x,y,z) \;=\; -\,\frac{i}{\lambda z}\;\exp\left[ik\frac{x^2+y^2}{2z}\right]$$

Use of the Fourier transform is especially convenient here, because the Fourier transform of $K_{\rm P}$ is easy to compute. For a function of the form

$$G(x,y) \;=\; \mathrm{e}^{-Z(x^2+y^2)}$$

where Z is any complex number of positive real part, it can be shown that

$$\tilde{G}(p,q) \;=\; \frac{\pi}{Z}\;\mathrm{e}^{-\frac{p^2+q^2}{4Z}} \tag{2.24}$$

in particular the propagator is

$$\widetilde{K_{\rm P}}(p,q,z) \;=\; \exp\left[-i\frac{z(p^2+q^2)}{2k}\right] \tag{2.25}$$

Obviously, we could have deduced it from the "exact" propagator

$$\tilde{G}_{\rm exact}(p,q,z) \;=\; \mathrm{e}^{iz\sqrt{k^2-p^2-q^2}}$$

by assuming that the values of p,q are restricted to small values due to the behavior of the function to be propagated ("small" means $p,q \;\ll\; k$). This is one more version of the paraxial approximation, the diffraction is "adiabatic" along z (if z is regarded as an evolution parameter), so that the angles of the rays with respect to the axis are small. $p,q,\sqrt{k^2-p^2-q^2}$ may be thought of as the coordinates of the wave vector of an elementary plane wave. Then , θ being the direction of that elementary wave, we have $\theta \simeq \sin\theta \;=\; \sqrt{p^2+q^2}/\sqrt{k^2-p^2-q^2}$. If θ is small, we can thus write:

$$\tilde{G}(p,q,z) \;=\; \mathrm{e}^{ikz} \;\times\; \mathrm{e}^{-i\frac{z(p^2+q^2)}{2k}}$$

An alternative way of computing E_2 is therefore:

$$E_2(x,y,z) \;=\; \widetilde{K_{\mathrm{P}}}(p,q,z) \;\widetilde{\times}\; \widetilde{E_1}(p,q,0) \tag{2.26}$$

This is a very convenient way, as will be shown later.

The Paraxial Diffraction Equation

One can derive from the Helmholtz equation an approximate equation called **The paraxial diffraction equation** (PDE) which is equivalent to the paraxial diffraction integral. Consider the Helmholtz equation:

$$\left[\Delta + k^2\right] \mathcal{E} \;=\; 0 \tag{2.27}$$

If the field is expected to propagate mainly in the z direction, with a slow expansion in the transverse plane, we can use the slowly varying envelope approximation scheme, i.e.

$$\mathcal{E}(x,y,z) \;=\; \mathrm{e}^{ikz} \times\; E(x,y,z)$$

in which the envelope $E(x,y,z)$ is assumed to depend slowly on z, the rapidly oscillating factor having been extracted. More specifically, we intend to use the approximation

$$\frac{\partial E}{\partial z} \;\ll\; k\; E$$

for neglecting second order derivatives of E, so that the Helmholtz equation becomes:

$$\left[2ik\;\partial_z \;+\; \Delta_{\mathrm{T}}\right]\; E \;=\; 0 \tag{2.28}$$

where

$$\Delta_{\mathrm{T}} \;\equiv\; \partial_x^2 + \partial_y^2$$

is the transverse Laplace operator.This is the PDE. It is clearly equivalent to the Fresnel integral, for by taking the Fourier transform of Eq.(2.28) with respect to x, y, we obtain:

$$\left[2ik\ \partial_z\ -\ (p^2+q^2)\right]\tilde{E}(p,q,z)\ =\ 0$$

the solution of which is of the form

$$\tilde{E}(p,q,z+\Delta z)\ =\ \tilde{E}(p,q,z)\times\exp\left[-\ i\frac{(p^2+q^2)\Delta z}{2k}\right]$$

in which we recover the propagator (2.25).

2.2.6 The Fraunhofer approximation

The ultimate approximation for a diffracted wave holds when the very far field is considered. The Fresnel-Huyghens integral can be written as:

$$E(x,y,z)\ =\ -\ \frac{i}{\lambda z}\ \exp\left[i\pi\frac{x^2+y^2}{\lambda z}\right]\ \times$$

$$\int_{\mathbf{R}^2}\ \exp\left[i\pi\frac{x'^2+y'^2}{\lambda z}\right]\exp\left[-2i\pi\frac{xx'}{\lambda z}\right]\exp\left[-2i\pi\frac{yy'}{\lambda z}\right]\ E(x',y',0)\ dx'\,dy'$$

If we assume the transverse extension of the initial amplitude bounded by a radius a, the order of magnitude of the argument of the quadratic term in the complex exponential is

$$\delta\ <\ \pi\frac{a^2}{\lambda z}\ =\ \pi\times\ N_F$$

N_F is called *Fresnel number*. If the observation distance is so large that N_F may be neglected, we can write simply

$$E(x,y,z)\ =\ -\ \frac{i}{\lambda z}\ \exp\left[i\pi\frac{x^2+y^2}{\lambda z}\right]\ \times$$

$$\int_{\mathbf{R}^2}\ \exp\left[-2i\pi\frac{xx'}{\lambda z}\right]\exp\left[-2i\pi\frac{yy'}{\lambda z}\right]\ E(x',y',0)\ dx'\,dy'$$

which is nothing but the Fourier transform of the incoming amplitude:

$$E(x,y,z)\ =\ -\ \frac{i}{\lambda z}\ \exp\left[i\pi\frac{x^2+y^2}{\lambda z}\right]\ \tilde{E}\left(\frac{2\pi x}{\lambda z}\ ,\ \frac{2\pi y}{\lambda z}\ ,\ 0\right)$$

This is the Fraunhoffer approximation, and allows to compute quickly the properties of the diffracted field for z very large. For instance, for a rectangular and uniform aperture $[-a,a]\times[-b,b]$, one finds immediately

$$|E(x,y,z)|^2 \;=\; \frac{16a^2b^2}{\lambda^2z^2}\;\left[\mathrm{sinc}\left(\frac{2\pi x}{\lambda z}\right)\mathrm{sinc}\left(\frac{2\pi y}{\lambda z}\right)\right]^2$$

explaining the pattern of Fig.2.3. For a uniform circular aperture, $r<a$, we find

$$|E(r,z)|^2 \;=\; \left[\frac{a}{r}\,J_1\left(\frac{2\pi ar}{\lambda z}\right)\right]^2$$

explaining the pattern of Fig.2.4. Anyway, in the very far field, when r/z is sufficiently small, we have

$$I(0) \;\sim\; I_0\times\left(\frac{S}{\lambda z}\right)^2$$

S being the area enclosed within the aperture, I(0) the intensity on axis in the far field, and I_0 the initial intensity. If we consider the total power P_0 passing through the aperture , we get

$$I(0) \;\sim\; \left(\frac{S}{\lambda^2z^2}\right)\,P_0$$

The total power received by an equal area in the far field is $P_1 = S\,I(0)$, so that we have the ratio

$$\frac{P_1}{P_0} \;=\; \left(\frac{S}{\lambda z}\right)^2$$

2.2.7 Representation of optical elements

The action of thin optical elements, like thin lenses or nearly flat mirrors on the optical amplitudes can be modelled without using a diffraction integral. Consider for instance the reflection off a curved mirror of curvature radius R_c and diameter D. Assume the mirror to close the aperture in the plane $z=0$ (see Fig.2.10). Strictly speaking, the field arriving on the mirror's surface should be computed fromn the field in the plane by Kirchhoff's equation. It is more convenient to discuss in the Fourier space. Calling $E_1(x,y,0)$ the field in the plane $z=0$, and $E_2(x,y,z)$ the field on the mirror's surface, we have as seen in (2.20):

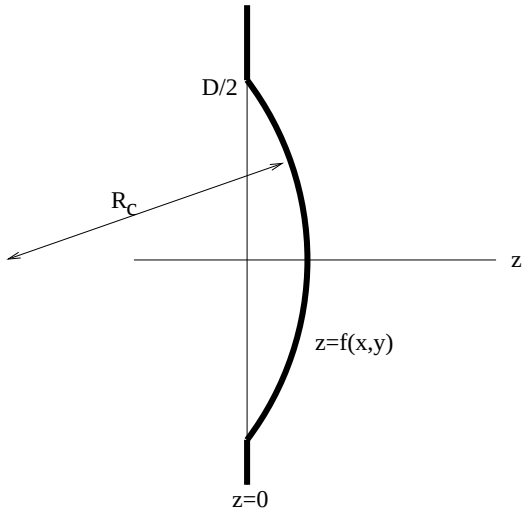

Figure 2.10: reflection off a curved mirror

$$\widetilde{E_2}(p,q,z) \;=\; \mathrm{e}^{iz\sqrt{k^2-p^2-q^2}} \;\times\; \widetilde{E_1}(p,q,0)$$

The argument of the imaginary exponential can be written as:

$$z\sqrt{k^2-p^2-q^2} \;=\; kz \;+\; z\left(\sqrt{k^2-p^2-q^2}-k\right)$$

or

$$z\sqrt{k^2-p^2-q^2} \;=\; kz \;-\; \frac{z(p^2+q^2)}{2k}\,\frac{2}{1+\sqrt{1-\frac{p^2+q^2}{k^2}}}$$

It is necessary to estimate the different orders of magnitude of these terms.

- The quantity p^2+q^2 is determined by the spatial behavior of the input wave. If the spatial frequencies are of the order of magnitude of w_0, for instance for a TEM mode of Fourier transform

$$\tilde{\phi}(p,q) \;=\; \exp\left(-\frac{w_0^2(p^2+q^2)}{4}\right)$$

we have

$$\frac{p^2+q^2}{k^2} \;\sim\; \frac{4}{k^2w_0^2} \;\sim\; \left(\frac{\lambda}{\pi w_0}\right)^2 \;\sim\; \theta_g^2$$

θ_g being nothing but the divergence angle of the beam. For long baseline interferometers, this aperture is of the order of tens of microradians, for Virgo, $\theta_g = 1.7 \times 10^{-5}$Rd. It is clear that we can neglect this term.

- The argument of the imaginary exponential therefore reduces to

$$z\sqrt{k^2 - p^2 - q^2} = kz - \frac{z(p^2+q^2)}{2k}$$

but

$$\frac{z(p^2+q^2)}{2k} \sim \frac{z\lambda}{\pi w_0^2} \sim \frac{z}{z_R}$$

where z_R is the Rayleigh parameter of the beam (see below), about 1km for GW interferometers, whereas z is of the order of tens of micrometers. More precisely, we have for a parabolic mirror $z_{\max} = D^2/8R_c$, on the other hand, the Rayleigh parameter is related to the curvature radius (in a flat/parabolic cavity of length L) by

$$z_R = \sqrt{L(R_c - L)} = \frac{1}{\alpha} \times R_c$$

where

$$\alpha = \frac{R/L}{\sqrt{R/L - 1}}$$

the factor α is of the order of the unity (For Virgo, $\alpha \simeq 2.97$). We have thus:

$$\frac{z(p^2+q^2)}{2k} \sim \frac{\alpha}{8}\left(\frac{D}{R_c}\right)^2$$

Taking again Virgo figures (D=35 cm, R_c=3.45 km) this is:

$$\frac{z(p^2+q^2)}{2k} \sim 3.8 \times 10^{-9}$$

The conclusion is that we can write with a good accuracy

$$\widetilde{E_2}(p,q,z) \;=\; \mathrm{e}^{ikz} \;\times\; \widetilde{E_1}(p,q,0)$$

which by inverse Fourier transform gives simply

$$E_2(x,y,z) \;=\; \mathrm{e}^{ikz} \;\times\; E_1(x,y,0)$$

In other words, in the Fresnel equation

$$E_2(x,y,z) \;=\; \mathrm{e}^{ikz} \int K_p(x-x',y-y',z)\, E_1(x',y',0)\, dx'\, dy'$$

we have shown that the kernel K_p is a 2-D delta function for small z, so that if we consider the amplitude on a surface of equation $z = f(x,y)$, we can write simply

$$E_2(x,y) \;=\; \mathrm{e}^{ikf(x,y)} \;\times\; E_1(x,y)$$

For the reflected wave $E_3(x,y,z)$, we reverse the point of view. If we would compute E_2 knowing E_3 we would find (the propagation direction being reverse)

$$E_2(x,y) \;=\; \mathrm{e}^{-ikf(x,y)} \;\times\; E_3(x,y)$$

Therefore

$$E_3(x,y) \;=\; \mathrm{e}^{2ikf(x,y)} \;\times\; E_1(x,y)$$

and the reflection operator is simply the phase factor ;

$$R \;=\; \mathrm{e}^{2ikf(x,y)} \tag{2.29}$$

Let us recall that this only holds for "thin" optical elements, in the above discussed sense. In particular, for a parabolic mirror, well adapted to gaussian beams in the paraxial approximation, we have

$$R \;=\; \exp\left[i\, \frac{2\pi(x^2+y^2)}{\lambda R_c} \right] \tag{2.30}$$

2.3 Fundamental TEM mode

It is possible to find a special solution of 2.28 under the axially symmetrical form depending on two unknown functions of z:

$$\Psi(r,z) \;=\; \mathrm{e}^{\mathrm{A(z)}}\,\mathrm{e}^{ikr^2/2q(z)}$$

substituting this expression in 2.28 provides two coupled differential equations:

$$\frac{dq}{dz} \;=\; 1 \quad \text{and} \quad \frac{dA}{dz} \;=\; -\,\frac{1}{q}$$

from where we get firstly

$$q(z) \;=\; q_0 + z$$

It is convenient to choose the constant q_0 in such a way that at $z = 0$, the wave is a real gaussian function of parameter w_0. (i.e. of the form $\exp(-r^2/w_0^2)$). This clearly happens if

$$q_0 \;=\; -i\frac{kw_0^2}{2} \;=\; -i\,b$$

The parameter $b = kw_0^2/2$ is called **Rayleigh range**. We have then $q(z) = z - i\,b$, so that

$$A(z) \;=\; \ln\left[\frac{1}{z - i\,b}\right] + C$$

The arbitrary integration constant C may be chosen in order to have $A(0) = 0$, i.e. $C = -\ln(-1/ib)$, and then

$$A(z) \;=\; \ln\left[\frac{1}{1 + iz/b}\right]$$

or as well

$$A(z) \;=\; \ln\left[\frac{1}{\sqrt{1 + z^2/b^2}}\right] \;-\; i\,\arctan(z/b)$$

on the other hand we have, separating the real from the imaginary part of $1/q$:

$$\frac{ik}{2q(z)} \;=\; \frac{1}{z + b^2/z} + \frac{i}{b + z^2/b}$$

defining two new real functions , $w(z)$ and $R(z)$:

$$\frac{ik}{2q(z)} = -\frac{1}{w^2(z)} + \frac{ik}{2R(z)}$$

The definitions of $w(z)$ and $R(z)$ are consequently:

$$w(z) = w_0\sqrt{1+z^2/b^2}$$

$$R(z) = z(1+b^2/z^2)$$

$w(z)$ is the beam half-width at abscissa z, and $R(z)$ is the curvature radius at the same point. These two real functions have concrete optical meanings, but contain the same information as the complex function $q(z)$ often called **complex curvature radius** We have finally the complete solution for the envelope:

$$\Psi(r,z) = \frac{1}{\sqrt{1+z^2/b^2}}\, \mathrm{e}^{-r^2/w(z)^2}\, \mathrm{e}^{ikr^2/2R(z)}\, \mathrm{e}^{-i\arctan(z/b)}$$

The factor $\exp(ikz)$ may be added for representing the rapidly varying part. The extra phase $\arctan(z/b)$ appearing during propagation with respect to a plane wave is called **Gouy phase**. The solution $\Psi(r,z)$ is a very special one. One can find other solutions by considering the product of $\Psi(r,z)$ by polynomials in the variables $(x/w\ , y/w)$. The solution $\Psi(r,z)$ is called $\mathrm{TEM}_{(0,0)}$ propagation mode. It is the fundamental mode of two families of modes discussed below.

2.4 Discrete bases for free space propagation

The set $\mathcal{L}^2$ of all complex functions $f(x,y)$ of integrable square modulus may be given the structure of a Hilbert vector space, by introducing the scalar product:

$$\langle\ f\ ,\ g\ \rangle = \int_{\mathbf{R}^2} dx\ dy\ \overline{f(x,y)}g(x,y) \tag{2.31}$$

If we think to these functions in terms of optical amplitudes at a given point of the path of a light beam having the preferred propagation direction z, we see that

$$\|f\|^2 = \langle\ f\ ,\ f\ \rangle = \int_{\mathbf{R}^2} dx\ dy\ |f(x,y)|^2 \tag{2.32}$$

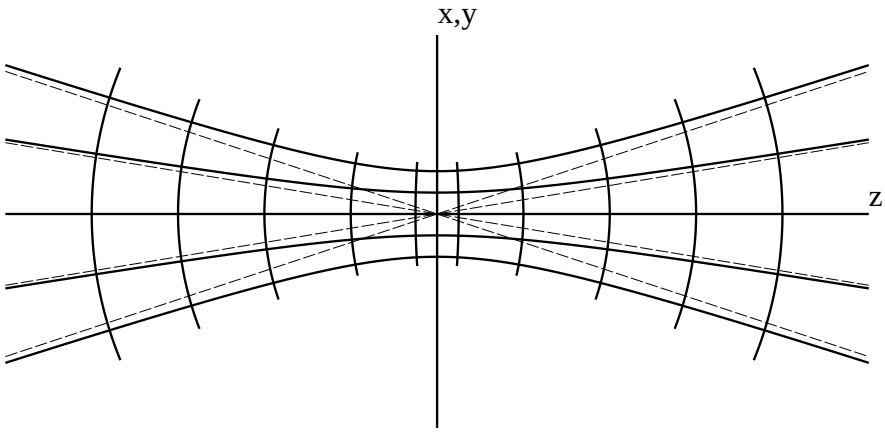

Figure 2.11: Diffraction of a gaussian wave: equal intensity and equal phase surfaces

is nothing but the light power of the beam crossing the transverse plane at z: restriction to $\mathcal{L}^2$ is therefore not too demanding. Obviously, a number of bases can be constructed for this Hilbert space. It is possible to find discrete bases, whose corresponding vectors are called Transverse Electromagnetic Modes, and are labelled by two indices: $\mathrm{TEM}_{(\mathrm{m,n})}$. The more often employed bases for studying cavities and laser beams, are the Hermite-Gauss modes $\mathrm{HG}_{(\mathrm{m,n})}$ when rectangular coordinates are convenient, and the Laguerre-Gauss modes $\mathrm{LG}_{(\mathrm{m,n})}$ when polar coordinates are convenient. The fundamental mode has been defined above as: $\mathrm{TEM}_{(0,0)}(x,y;z) = \mathrm{HG}_{(0,0)}(x,y;z) = \mathrm{LG}_{(0,0)}(x,y;z)$ is, with $r^2 \equiv x^2+y^2$,

$$\mathrm{TEM}_{(0,0)}(x,y;z) = \sqrt{\frac{2}{\pi\, w(z)^2}}\ \mathrm{e}^{ikz}\ \ \mathrm{e}^{-i\arctan(z/b)}\mathrm{e}^{-r^2/w(z)^2}\ \mathrm{e}^{ikr^2/2R(z)} \quad (2.33)$$

where $w(z)$ gives the radius of the beam, $R(z)$ the curvature radius of the phase surface, b the Rayleigh range. The form of $w(z)$ suggests a widening of the beam (see Fig.2.11) during propagation, an angle aperture can be evaluated by

$$\lim_{z\to\infty}\ \frac{w(z)}{z}$$

This gives the gaussian aperture angle

$$\theta_g \;=\; \frac{\lambda}{\pi w_0}$$

2.4.1 Hermite-Gauss modes

Extended solution

The fundamental solution found above can be extended in the following scheme. Let us look for solutions of the form:

$$\Psi(x,y,z) \;=\; \mathrm{e}^{A(z)}\mathrm{e}^{ikr^2/2q(z)}P[u(z)x]\,Q[u(z)y]$$

where A and q are complex functions of z alone, whereas u is a real function of z, and P, Q real functions. The reason for these choices are firstly a separation of the variables x and y, and secondly the clear necessity to include a variable scaling factor in the transverse plane accounting for the extension of the wavefront, as seen in the fundamental mode. In this spirit, we expect the unknown function $u(z)$ to be inversely proportional to $w(z)$. After straightforward calculations, the paraxial diffraction equation becomes:

$$\begin{aligned} 2ik\left(\frac{\partial A}{\partial z}+\frac{1}{q}\right)\,P(X)\,Q(Y) + \frac{k^2r^2}{q^2}\left(\frac{\partial q}{\partial z}-1\right)\,P(X)\,Q(Y) + \\ +\,2ik\left(\frac{\partial u}{\partial z}+\frac{u}{q}\right)\left(x\frac{\partial P}{\partial X}Q(Y)+y\frac{\partial Q}{\partial Y}P(X)\right) \\ +u^2\left(\frac{\partial^2 P}{\partial X^2}Q(Y)+\frac{\partial^2 Q}{\partial Y^2}P(X)\right) \;=\; 0 \end{aligned} \tag{2.34}$$

where we used the notations $X \equiv u(z)x$ and $Y \equiv u(z)y$. Now we require the function $q(z)$ to be the same as in the fundamental solution, i.e.

$$\frac{\partial q}{\partial z}-1 \;=\; 0$$

in order to keep the same dependence for the width of the beam, and for the curvature radius of the wavefront. Now we furthermore require that separately:

$$u^2\,\frac{\partial^2 P}{\partial X^2}+2ikx\left(\frac{\partial u}{\partial z}+\frac{u}{q}\right)\frac{\partial P}{\partial X}+\Lambda' P \;=\; 0 \tag{2.35}$$

and

$$u^2 \frac{\partial^2 Q}{\partial Y^2} + 2iky \left(\frac{\partial u}{\partial z} + \frac{u}{q} \right) \frac{\partial Q}{\partial Y} + \Lambda'' Q \;=\; 0 \tag{2.36}$$

where Λ', Λ'' are real arbitrary constants. Owing to the fact that u must be real, as also P and Q, it is necessary that

$$\frac{\partial u}{\partial z} + \frac{u}{q}$$

be purely imaginary. This is

$$\Re \left\{ \frac{\partial u}{\partial z} + \frac{u}{z - ib} \right\} \;=\; 0$$

or

$$\frac{1}{u} \frac{\partial u}{\partial z} \;=\; - \frac{z}{z^2 + b^2}$$

which gives the obvious solution

$$u(z) \;=\; \frac{\mu}{\sqrt{b^2 + z^2}}$$

where μ, an arbitrary constant, may be chosen in such a way that $u(0) = \sqrt{2}/w_0$. This is finally

$$u(z) \;=\; \frac{\sqrt{2}}{w(z)}$$

$w(z)$ being the function defined above in the fundamental solution. But now, we have:

$$\frac{\partial u}{\partial z} + \frac{u}{q} \;=\; \frac{ibu}{z^2 + b^2}$$

$$=\; i \frac{2\sqrt{2}}{kw^3}$$

so that eq.2.35 becomes:

$$\frac{2}{w^2} \frac{\partial^2 P}{\partial X^2} - \frac{4}{w^2} X \frac{\partial P}{\partial X} + \Lambda' P \;=\; 0$$

or

$$\frac{\partial^2 P}{\partial X^2} - 2X \frac{\partial P}{\partial X} + \frac{\Lambda' w^2}{2} P \;=\; 0 \tag{2.37}$$

We know that polynomial solutions of eq.2.37 exist, if

$$\frac{\Lambda' w^2}{2} \;=\; 2n$$

where n is any integer; in this case, eq.2.37 defines the Hermite polynomial of order n.

$$P(X) \;\equiv\; H_n(X)$$

Obviously, the same discussion holds for eq.2.36, and with

$$\frac{\Lambda'' w^2}{2} \;=\; 2m$$

we find

$$Q(Y) \;\equiv\; H_m(Y)$$

Now, eq.2.34 reduces to:

$$2ik\left(\frac{\partial A}{\partial z} + \frac{1}{q}\right) - (m+n)\frac{4}{w^2} \;=\; 0$$

or

$$\frac{\partial A}{\partial z} + \frac{1}{z - ib} + \frac{i(m+n)}{b(1 + z^2/b^2)} \;=\; 0$$

so that:

$$A(z) \;=\; \ln\left(\frac{1}{z - ib}\right) - i(m+n)\arctan\left(\frac{z}{b}\right)$$

and

$$\mathrm{e}^{A(z)} \;=\; (1 + z^2/b^2)^{-1/2}\,\mathrm{e}^{-i(m+n+1)\arctan(z/b)}$$

The HG basis

It has been shown that the PDE has Hermite-Gauss solutions of the form

$$\mathrm{HG}_{(m,n)}(x,y;z) \;=\; c_{m,n}\;\mathrm{e}^{ikz}\;H_m\left(\sqrt{2}\frac{x}{w(z)}\right)\;H_n\left(\sqrt{2}\frac{y}{w(z)}\right)\;\times$$

$$\mathrm{e}^{-i(m+n+1)\arctan(z/b)}\;\mathrm{e}^{-r^2/w(z)^2}\;\mathrm{e}^{ikr^2/2R(z)} \qquad (2.38)$$

where the functions $H_n(X)$ are the Hermite polynomials and $c_{m,n}$ a normalization constant to be defined later.

Several properties of these functions are very convenient, and we recall them herafter without any proof.

- The Hermite polynomials are defined by:

$$H_n(x) \;=\; \mathrm{e}^{x^2}\left(-\frac{d}{dx}\right)^n \mathrm{e}^{-x^2} \tag{2.39}$$

- The explicit expression is:

$$H_n(x) \;=\; \sum_{s=0}^{[n/2]} (-1)^s \;\frac{n!}{(n-2s)!s!}\;(2x)^{n-2s} \tag{2.40}$$

(the bracket means the integer part)

- They obey the following differential equation:

$$H_n''(x) - 2xH'n(x) + 2nH_n(x) \;=\; 0$$

- Their derivatives are given by:

$$H_n'(x) \;=\; 2n\; H_{n-1}(x)$$

- They obey a recurrence relation:

$$H_{n+1}(x) \;=\; 2x\; H_n(x) \;-\; 2n\; H_{n-1}(x) \tag{2.41}$$

- They obey an orthogonality relation

$$\int_{-\infty}^{\infty} H_m(x)\, H_n(x)\; \mathrm{e}^{-x^2} dx \;=\; \sqrt{\pi}\; 2^m m!\, \delta_{mn} \tag{2.42}$$

The normalization constants for the HG modes are therefore:

$$c_{m,n} \;=\; \left[\frac{2}{\pi w^2}\;\;\frac{1}{2^{m+n} m!\; n!}\right]^{1/2} \tag{2.43}$$

- They obey as well a closure relation:

$$\frac{1}{\sqrt{\pi}} \sum_p \frac{1}{2^p p!}\; H_p(x) H_p(x')\; \mathrm{e}^{-(x^2+x'^2)/2} \;=\; \delta(x-x') \tag{2.44}$$

- There is a translation formula:

$$H_n(x+\Delta/2) \;=\; \sum_{k=0}^{n} C_n^k \; H_{n-k}(x)\; \Delta^k \tag{2.45}$$

(it can be shown using the recursion formula)

- There is a scaling formula:

$$H_n(\beta x) \;=\; \sum_{k=0}^{[n/2]} \frac{n!}{k!(n-2k)!}\, \beta^{n-2k}\, \left(\beta^2-1\right)^k \; H_{n-2k}(x) \tag{2.46}$$

- There is a reduction formula:

$$H_m(x)\, H_n(x) \;=\; \sum_{s=0}^{\min(m,n)} \frac{m!\, n!\, 2^s}{(m-s)!(n-s)!s!}\; H_{m+n-2s}(x) \tag{2.47}$$

- It is possible to give the general expression of the Fourier Transform of any mode ; We even give a more general formula under the following form. Let

$$\Psi_{(m,n)}(Z,x,y) \;=\; H_m\left(\sqrt{2}\frac{x}{w}\right)\; H_n\left(\sqrt{2}\frac{y}{w}\right)\; \exp\left(-Z\;\frac{x^2+y^2}{w^2}\right)$$

where Z is any complex number of positive real part. The Hermite-Gauss functions correspond to $Z=1$. The Fourier Transform is:

$$\widetilde{\Psi}_{(m,n)}(Z,p,q) \;=\; \frac{\pi w^2}{Z}\;\left(\frac{i}{Z}\right)^{m+n}\left(2Z-Z^2\right)^{(m+n)/2}\;\times$$

$$H_m\left(\frac{pw}{\sqrt{2}\sqrt{2Z-Z^2}}\right)\; H_n\left(\frac{qw}{\sqrt{2}\sqrt{2Z-Z^2}}\right)\; \exp\left[-\frac{w^2(p^2+q^2)}{4Z}\right] \tag{2.48}$$

For $Z=1$ (HG functions) this is simply:

$$\widetilde{\Psi}_{(m,n)}(1,p,q) \;=\; \pi w^2\, i^{m+n}\, H_m\left(\frac{pw}{\sqrt{2}}\right)\; H_n\left(\frac{qw}{\sqrt{2}}\right)\; \exp\left[-\frac{w^2(p^2+q^2)}{4}\right]$$

In a certain sense, we see that the HG modes are eigenvectors of the Fourier transform. The special case $Z=2$ gives

$$\widetilde{\Psi}_{(m,n)}(2,p,q) \;=\; \frac{\pi w^2}{2}\;\left(\frac{ipw}{2\sqrt{2}}\right)^m\;\left(\frac{iqw}{2\sqrt{2}}\right)^n\; \exp\left[-\frac{w^2(p^2+q^2)}{8}\right]$$

- There is a useful Fourier transform:

$$\frac{1}{\sqrt{\pi}} \int \mathrm{e}^{-x^2} H_n(x)\, \mathrm{e}^{ipx}\, dx \;=\; (ip)^n \mathrm{e}^{-p^2/4} \tag{2.49}$$

  note that this formula has nothing to do with the Fourier transform of a TEM mode, rather with the FT of the product of two modes.

- A consequence of the preceding integral (or an application of the generating function as well) is the expansion of a plane wave in terms of Hermite polynomials:

$$\mathrm{e}^{ipx} \;=\; \mathrm{e}^{-p^2/4} \sum_{n\geq 0} \frac{(ip)^n}{2^n n!} H_n(x)$$

- The first Hermite polynomials are explicitly:

$$H_0(x) \;=\; 1$$

$$H_1(x) \;=\; 2x$$

$$H_2(x) \;=\; 4x^2 - 2$$

$$H_3(x) \;=\; 8x^3 - 12x$$

$$H_4(x) \;=\; 16x^4 - 48x^2 + 12$$

$$H_5(x) \;=\; 32x^5 - 160x^3 + 120x$$

$$H_6(x) \;=\; 64x^6 - 480x^4 + 720x^2 - 120$$

  etc...

The intensity pattern of some HG functions is shown on the figures 2.12, 2.13, 2.14.

2.4.2 The Laguerre-Gauss modes

Using polar coordinates (r, ϕ) instead of (x, y) in the transverse plane, a new class of solutions to the PDE can be found, of the form

$$\mathrm{LG_{m,n}}(r, \phi; z) \;=\; c_{m,n}\, \mathrm{e}^{ikz} \left(\sqrt{2}\frac{r}{w(z)}\right)^n \; L_m^{(n)}(2r^2/w(z)^2)\times$$

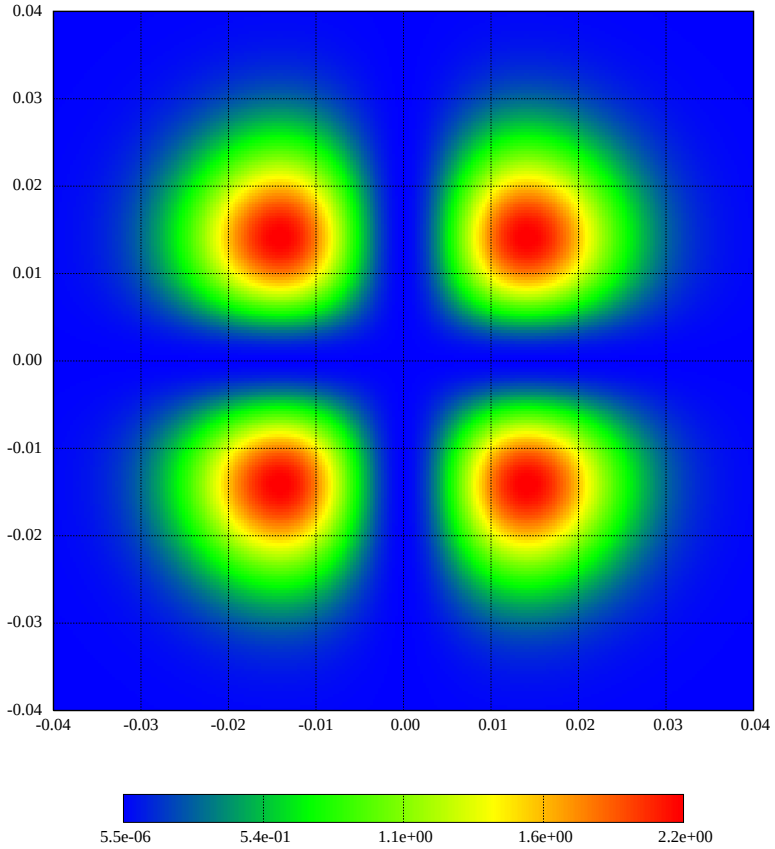

Figure 2.12: Intensity pattern of a HG_{11} mode for $w_0 = 0.02$ m

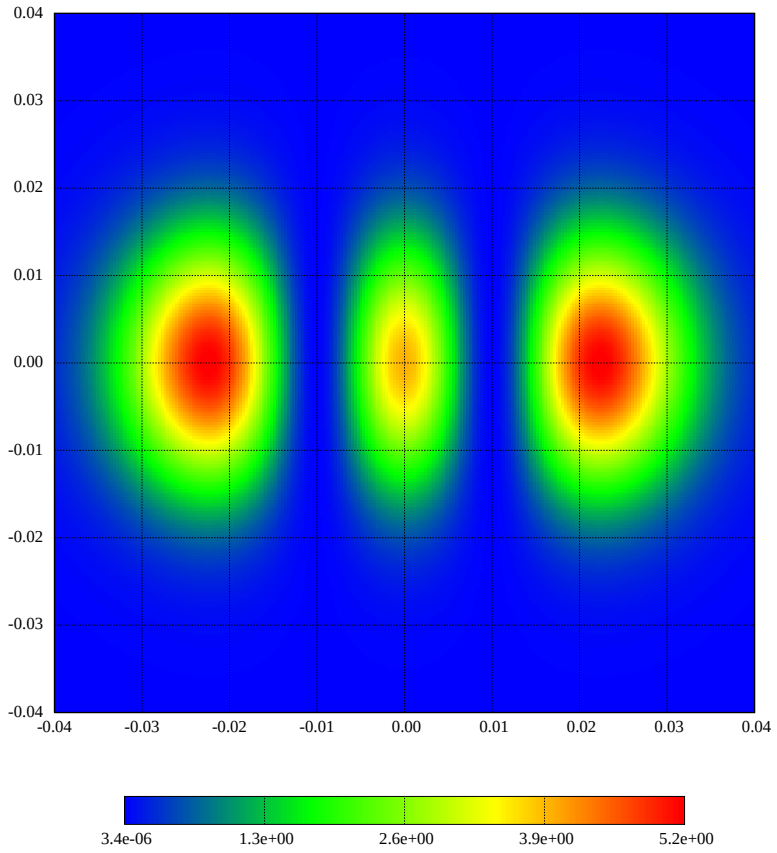

Figure 2.13: Intensity pattern of a HG_{20} mode for $w_0 = 0.02$ m

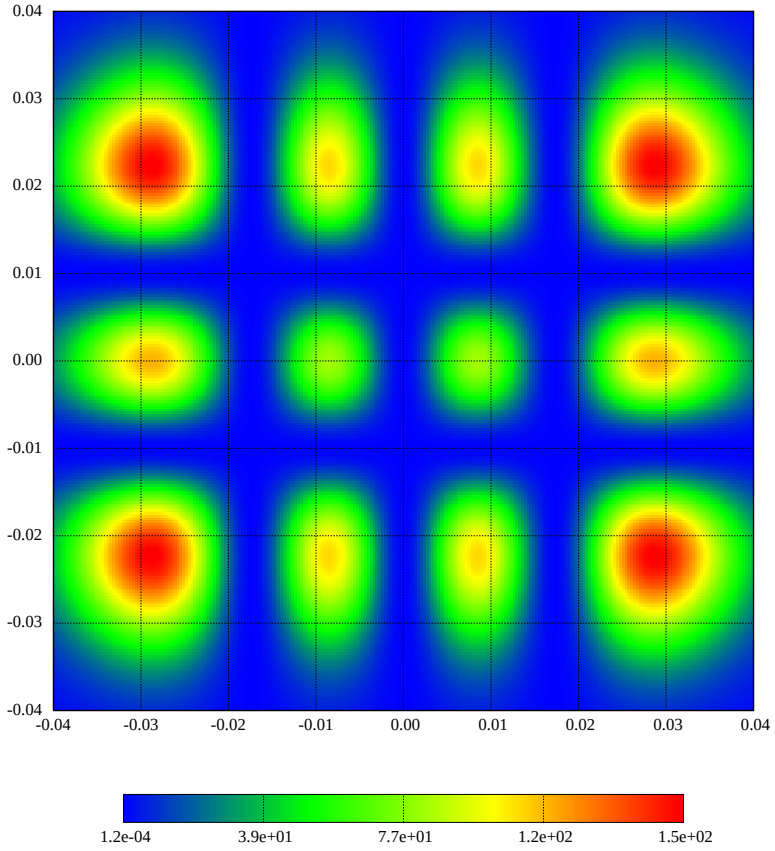

Figure 2.14: Intensity pattern of a HG_{32} mode for $w_0 = 0.02$ m

$$\mathrm{e}^{-i(2m+n+1)\arctan(z/b)}\ \mathrm{e}^{-r^2/w(z)^2}\ \mathrm{e}^{ikr^2/2R(z)}\ \cos(n\phi) \tag{2.50}$$

The functions $L_m^{(n)}(X)$ are the generalized Laguerre polynomials. They are defined by

$$L_m^{(n)}(x) \ = \ \frac{\mathrm{e}^x}{m!\ x^n}\ \left(\frac{d}{dx}\right)^m \left(x^{n+m}\mathrm{e}^{-x}\right)$$

They obey the recursion relation:

$$(m+1)L_{m+1}^{(n)}(x) \ = \ (2m+n+1-x)L_m^{(n)}(x) \ - \ (m+n)L_{m-1}^{(n)}(x)$$

The first ones are as follows:

$$L_0^{(n)}(x) \ = \ 1$$

$$L_1^{(n)}(x) \ = \ n+1-x$$

$$L_2^{(n)}(x) \ = \ \frac{(n+1)(n+2)}{2} - (n+2)\,x + \frac{x^2}{2}$$

$$L_3^{(n)}(x) \ = \ \frac{(n+1)(n+2)(n+3)}{6} \ - \frac{(n+2)(n+3)}{2}\,x \ + \ \frac{n+3}{2}\,x^2 \ - \ \frac{x^3}{6}$$

$$L_4^{(n)}(x) \ = \ \frac{(n+1)(n+2)(n+3)(n+4)}{24} \ - \frac{(n+2)(n+3)(n+4)}{6}\,x \ + \\ + \ \frac{(n+3)(n+4)}{4}\,x^2 \ - \ \frac{n+4}{6}\,x^4 \ + \ \frac{x^4}{24}$$

The normalization relation for the Laguerre polynomials comes from [11]:

$$\int_0^\infty L_m^{(n)}(x)^2\,x^n\,\mathrm{e}^{-x}\,dx \ = \ \frac{(m+n)!}{m!}$$

so that the normalization constants c_{mn} are:

$$c_{mn} \ = \ \frac{2}{w}\sqrt{\frac{m!}{\pi\,(1+\delta_{n0})\,(m+n)!}}$$

As a special case, we see that the $\mathrm{LG}_{m,0}$ modes have all the same normalization:

$$c_{m,0} \ = \ \sqrt{\frac{2}{\pi\,w^2}}$$

The intensity pattern of some LG modes is given in the maps 2.15,2.16,2.17,.

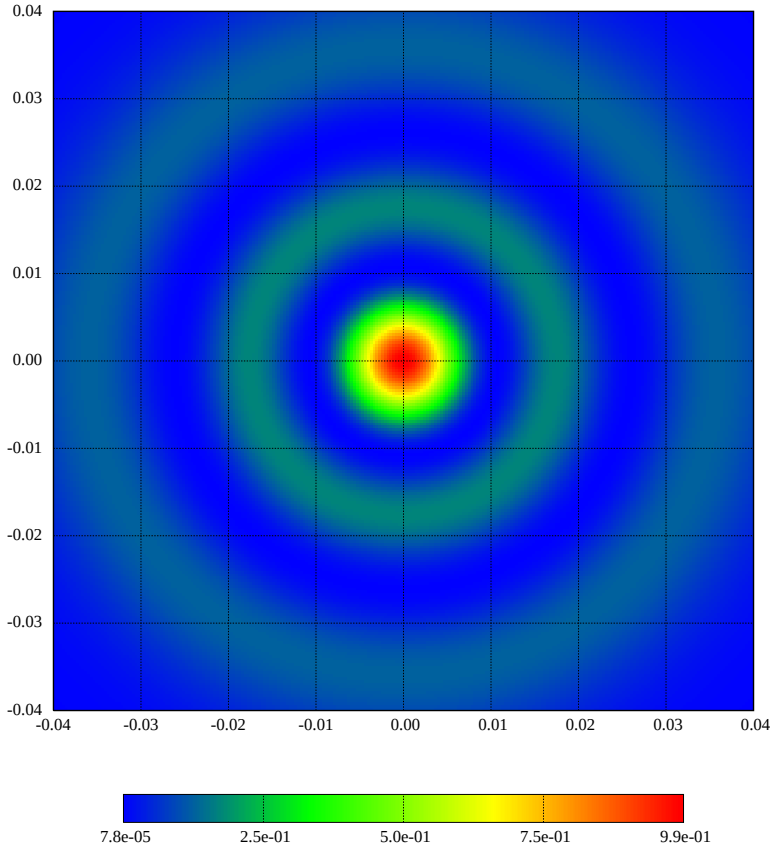

Figure 2.15: Intensity pattern of a LG_{20} mode for $w_0 = 0.02$ m

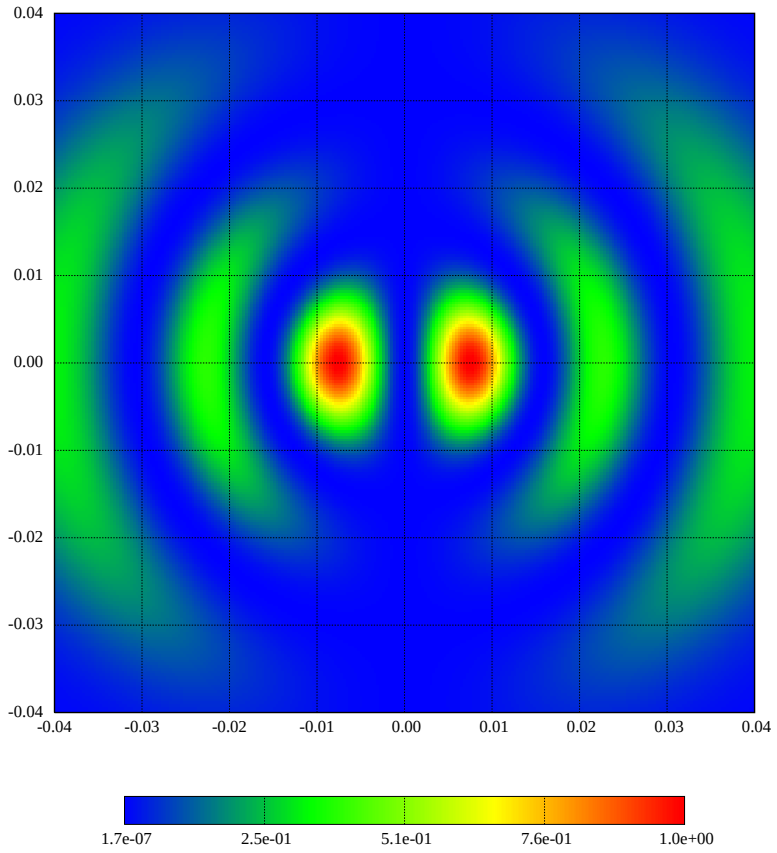

Figure 2.16: Intensity pattern of a LG_{21} mode for $w_0 = 0.02$ m

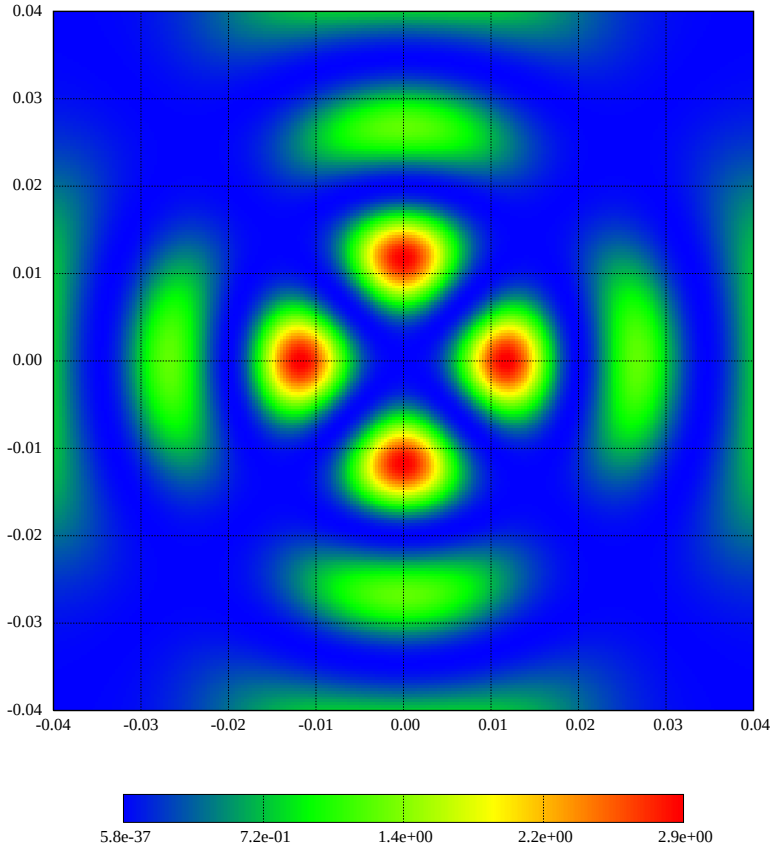

Figure 2.17: Intensity pattern of a LG_{22} mode for $w_0 = 0.02$ m

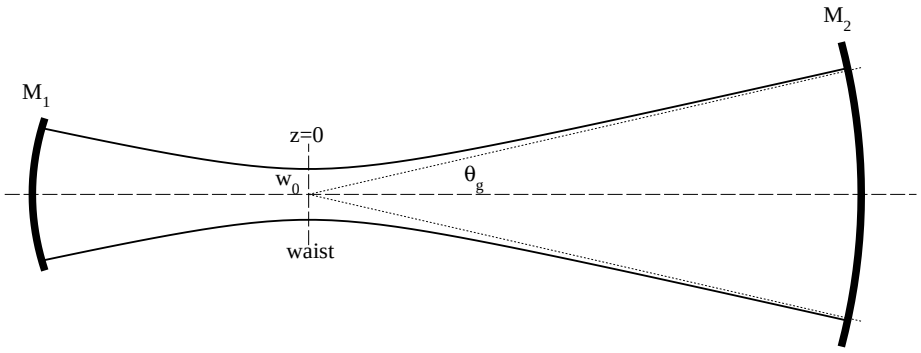

Figure 2.18: Any Fabry-Perot cavity with curved mirrors

2.5 Fabry-Perot: paraxial approximation

It has been seen that the free space propagation operator has, in a certain sense eigenmodes called $\mathrm{TEM_{m,n}}$ modes. They have the significant two following properties:

- They are of finite transverse extension, there is already a storage in the transverse plane
- They have a parabolic equiphase surface

The second property allows to make "matched" mirrors, of shape adapted to the equiphase surface, reflecting the mode on itself (see Fig.2.18) A mode matching two parabolic mirrors not always exists, depending on the curvature radii of the mirrors and on the cavity length. Consider for instance a plane-spherical cavity with a plane input mirror M_1, and a spherical mirror M_2 of curvature radius R_c, at a distance L. in order to be matched to M_1, the stored wave must be at its waist at $z = 0$ on the input plane. Then, the

stored wave must have a phase curvature radius of R_c at $z = L$, so that we can write

$$R_c \;=\; L\left(1 \;+\; \frac{b^2}{L^2}\right)$$

b (Rayleigh parameter) having the definition previously encountered. This gives

$$b \;=\; \sqrt{L(R_c - L)}$$

Clearly, this is possible only if $R_c > L$. This is a stability condition for that type of cavity. If this condition is fulfilled, the cavity is able to store any $\mathrm{TEM_{m,n}}$ mode, provided it is near resonance. The size of the waist is

$$w_0 \;=\; \sqrt{\lambda b/\pi}$$

The resonance condition, assuming a $\pi/2$ dephasing at each reflection, is :

$$\pi \;-\; 2(m+n+1)\tan^{-1}\left(\frac{L}{b}\right) \;\equiv\; 2p\pi$$

the eigenmodes of the cavity are thus labeled by 3 integers, exactly as the modes of a closed box. The frequency spacing between modes is a very important feature in a cavity. If two modes have by chance close eigenfrequencies, a class of perturbations of the mirrors having the right symmetry will pump power from one mode to the other due to the finite linewidths (see below). In particular, if the cavity is operated on its fundamental mode, it is better to choose the geometrical parameters in such a way that the nearest transverse modes $(m,n) \neq (0,0)$ are well separated from the reference mode. The $\mathrm{TEM_{0,1}}$ and $\mathrm{TEM_{1,0}}$ modes are especially well coupled with the $\mathrm{TEM_{0,0}}$ in case of misalignment of mirrors. Let us discuss this issue now. We call $\Phi_{m,n,p}$ the total dephasing of the m,n,p mode over a round trip in the cavity. We have:

$$\Phi_{m,n,p} \;=\; \frac{4\pi\nu_{m,n,p}L}{c} \;-\; 2(m+n+1)\tan^{-1}\left(\frac{L}{b}\right) \;+\; \pi \;=\; 2p\pi$$

We see that the frequency gap between two successive longitudinal resonances, or Free Spectral Range (FSR), $(\Delta p = \pm 1)$, is $\Delta\nu_{FSR} \;=\; c/2L$. we see that the frequencies of the modes are given by

$$\nu_{m,n,p} \;=\; \Delta\nu_{FSR}\left(p - \frac{1}{2} + (m+n+1)\alpha\right)$$

with $\alpha = \tan^{-1}(L/b)/\pi$. Assume the operation mode has frequency $\nu_{0,0,p_0}$, the distances of the other modes are:

$$\delta\nu_{m,n,p} = \nu_{m,n,p} - \nu_{0,0,p_0} = (p - p_0 + (m+n)\alpha)\ \Delta\nu_{FSR} \qquad (2.51)$$

The distribution of resonances being periodic, it is sufficient to study it over a FSR. Given the length L of the cavity, the curvature radius R_c can be chosen under the following constraints:

- it must be larger than L
- it must not cause a too large magnification factor between the input mirror and the end mirror
- it must give a value of α such that equation 2.51 has no zero solutions for (m, n) small.

In the case of Virgo, the length of the arms is $L = 3$km and the curvature radius of the end mirror $R_c = 3.45$ km, so that $\alpha \simeq 0.38238$. The frequency offsets of the 15 nearest tranverse modes are given in the following table.

Mode order (m+n)	*Frequency offset* (Hz)
8	2950.62
3	7352.16
11	10302.78
6	14704.32
14	17654.94
1	19105.86
9	22056.48
4	26458.02
12	29408.64
7	33810.18
15	36760.79
2	38211.72
10	41162.34
5	45563.88
13	48514.49

Remark that the (0,1) and (1,0) modes are well separated from the (0,0), and that there is no coincidence for orders lower than 15. The nearest are the family (m+n=8) which are not easy to couple to (0,0) by a simple perturbation.

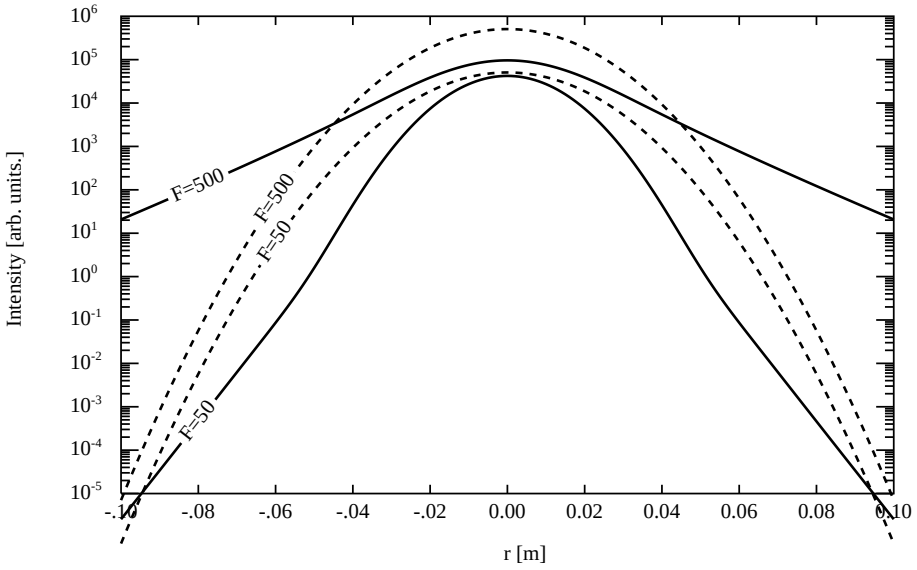

Figure 2.19: Intracavity mode intensity (solid lines) in a 12 m long flat/flat cavity for gaussian input wave w_0=2 cm for two finesses. Dashed lines : gaussian input wave times the surtension

2.6 flat cavities

It is intersting to check what happens when a gaussian mode is launched in a cavity involving flat mirrors. This would happen in the Virgo central zone, in the absence of cavity end mirrors. This is also what happens to the sidebands when antiresonant. Assume the input wave at its waist, of half width w_0. The reflection on flat and perfect mirrors does not affect the diffraction of the beam, so that the mode inside the cavity, of amplitude $E(r)$ can be expressed as the sum of gaussian waves with increasing width, curvature radius and Gouy phase. Let L be the length of the cavity and $b \equiv \pi w_0^2/\lambda$ the Rayleigh parameter of the beam. We have:

$$E(r) \;=\; t \sum_{n=0}^{\infty} R^n \, \mathrm{e}^{2inkL} \frac{w_0}{w_n} \exp\left[-\frac{r^2}{w_n^2} + i\,\frac{kr^2}{2R_n} - i \arctan 2inL/b \right]$$

where $R \equiv r_1\, r_2$ (the product of the reflectivities of the mirrors, t the transmission of the input mirror, and:

$$w_n = \sqrt{1 + \left(\frac{2nL}{b}\right)^2}$$

$$R_n = 2nL + \frac{b^2}{2nL}$$

It is easy to check that this is as well:

$$E(r) = t \sum_{n=0}^{\infty} R^n \, \mathrm{e}^{2inkL} \frac{1}{Z_n} \exp\left[-\frac{r^2}{w_0^2 Z_n}\right]$$

A numerical investigation shows that the maximum surtension is obtained for $2kL \equiv \pi$, and confirms the intuitive idea that the intracavity mode is close to the incoming one multiplied by the surtension of the cavity (see Fig.2.19), for a moderate finesse, and is widely spread for a high finesse. The reflected wave may have a distorted wavefront for high cavity finesses (see Fig.2.20).

2.7 Hypergaussian modes

2.7.1 construction

It will be shown in a foregoing section that the thermal noise (random motion of the mirror's surface) depends on the area of the light spot on the mirror. Large spots are better than sharp. With this respect, it appears than gaussian modes are not the best choice. The idea of constructing more homogeneous modes has been proposed long time ago by laser scientists in order to better exploit amplifier media: such modes are called hypergaussian. A way of constructing almost flat modes has been explored by D'Ambrosio ([16]). In this work, D'A. was dealing with a symmetrical cavity. In the case of plane-spherical cavities, we try a similar method. On the assumed flat input mirror, we consider the field as a superposition of gaussian modes according to :

$$\Psi(x, y, 0) = \frac{1}{\pi b^2} \int_{\Delta} dx_0\, dy_0\; \phi(x - x_0, y - y_0)$$

where Δ is the disk of radius b, centered at $(x = 0, y = 0)$, and where

$$\phi(x, y) = \sqrt{\frac{2}{\pi w_0^2}} \exp\left[-\frac{x^2 + y^2}{w_0^2}\right]$$

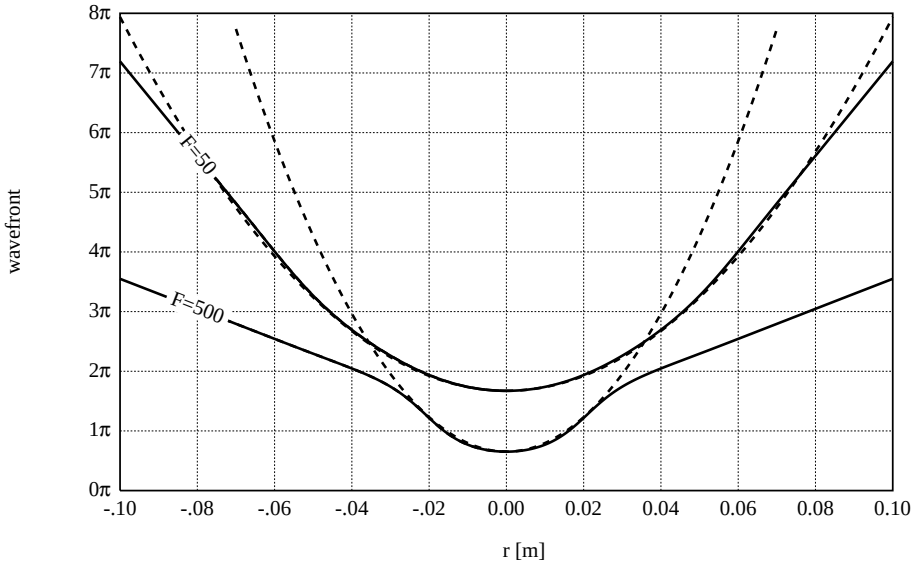

Figure 2.20: Wavefront of reflected wave (solid lines) in a 12 m long flat/flat cavity for gaussian input wave w_0=2 cm for two finesses. Dashed lines : fit of spherical wavefronts: R=3000 m for F=50, R=1300 m for F=500

is a classical TEM_{00} mode. In other words, Ψ is the superposition of such modes with various offsets, uniformly distributed on the disk of radius b. Remark (though it is fairly clear) that $\Psi(x,y,z)$ is actually a solution of the paraxial diffraction equation, for it is a linear combination of solutions. It is straightforward to express the field propagated at a distance z, propagation of each elementary gaussian mode being known:

$$\Psi(x,y,z) \;=\; 2\sqrt{\frac{2}{\pi w^2}}\,\frac{w^2}{b^2}\;\psi_{00}(r,z)\mathrm{e}^{-iArctan(z/z_R)} \qquad (r \;\equiv\; \sqrt{x^2+y^2})$$

with

$$\psi_{00}(r,z) \;\equiv\; \int_0^{b/w} \mathrm{e}^{-Z(r/w-u)^2}\;\mathrm{e}^{-2Zru/w}\;I_0(2Zru/w)\;u\,du$$

where $Z \equiv 1 - iz/z_R$ ($z_R \equiv \pi w_0^2/\lambda$ being the Rayleigh parameter), and where $I_0(z)$ denotes the 1st kind modified Bessel function. w is the beam width at the distance z, i.e.

$$w = w_0\sqrt{1+z^2/z_R^2}$$

Following E.d'A, we have taken the following values (L being the length of the cavity):

$$w_0 \;=\; \sqrt{\frac{\lambda L}{\pi}} \;\simeq\; 3.2\ \mathrm{cm}$$

$$b \;=\; 4w_0 \;\simeq\; 12.8\ \mathrm{cm}$$

The integral $\psi_{00}(r,z)$ can be evaluated numerically by a simple Simpson numerical integration technique, the function $\exp(-z)I_0(z)$ having a quite simple behavior. The initial intensity profile is as shown on Fig.2.21 The intensity profile after 3 km propagation is plotted on Fig.2.22. The wavefront is shown on Fig.2.23

2.7.2 Angular aperture and Fourier transform

It is remarkable that the mode is practically unchanged along the propagation. The difficult point is to make a mirror having the profile shown on Fig.2.23. The aperture angle of the beam is obviously much smaller than the gaussian's. On the flat mirror, The beam may be viewed as the convolution product of a gaussian of waist w_0 with a uniform distribution on the disk $r < b$. The Fourier transform of the beam amplitude is therefore the simple

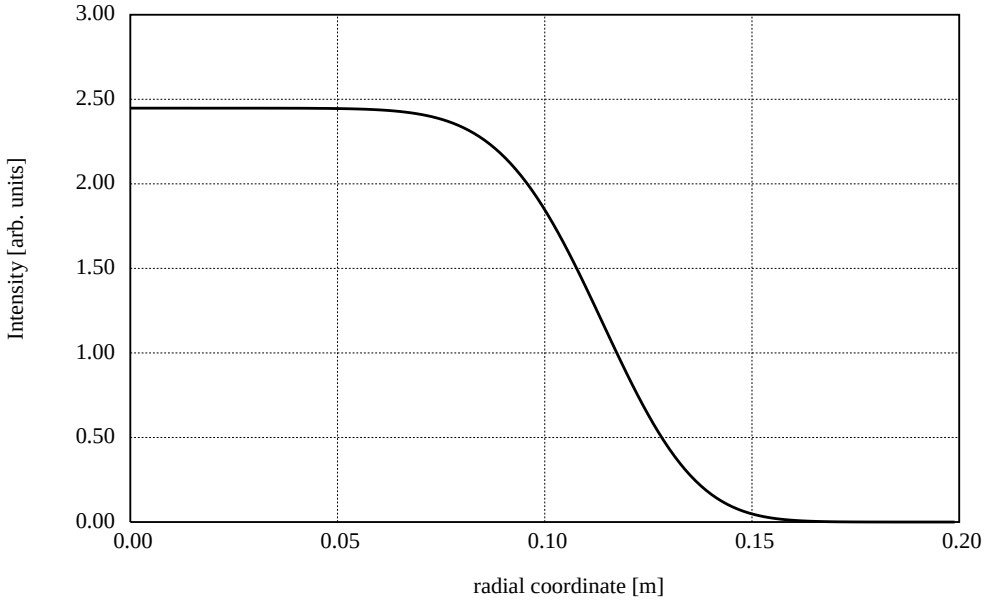

Figure 2.21: Intensity profile on the flat input mirror

product of the Fourier transform of the elementary gaussian beam with that of the disk. A detailed calculation gives thus,

$$\tilde{\Psi}(p,q,0) \;=\; 2\sqrt{2\pi w_0^2}\,\exp\left(-w_0^2\rho^2/4\right)\;\frac{J_1(\rho b)}{\rho b}$$

where $\rho^2 \equiv p^2+q^2$. By identifying $\rho = k\,\theta$, we get

$$|\tilde{\Psi}(p,q,0)|^2 \;=\propto\; \exp\left(-2\theta^2/\theta_g^2\right)\;\left[\frac{2J_1(\theta/\theta_b)}{\theta/\theta_b}\right]^2$$

where $\theta_g = \lambda/\pi w_0$ is the gaussian aperture angle, and $\theta_b = \lambda/2\pi b$ is the Bessel aperture angle. For $w_0 = 2$ cm and $b = 10$ cm, θ_b happens to be 10 times smaller than θ_g, and the aperture angle is practically determined by θ_b (see Fig. 2.24). This is consistent with the fact that the width of the beam is practically constant along the diffraction length.

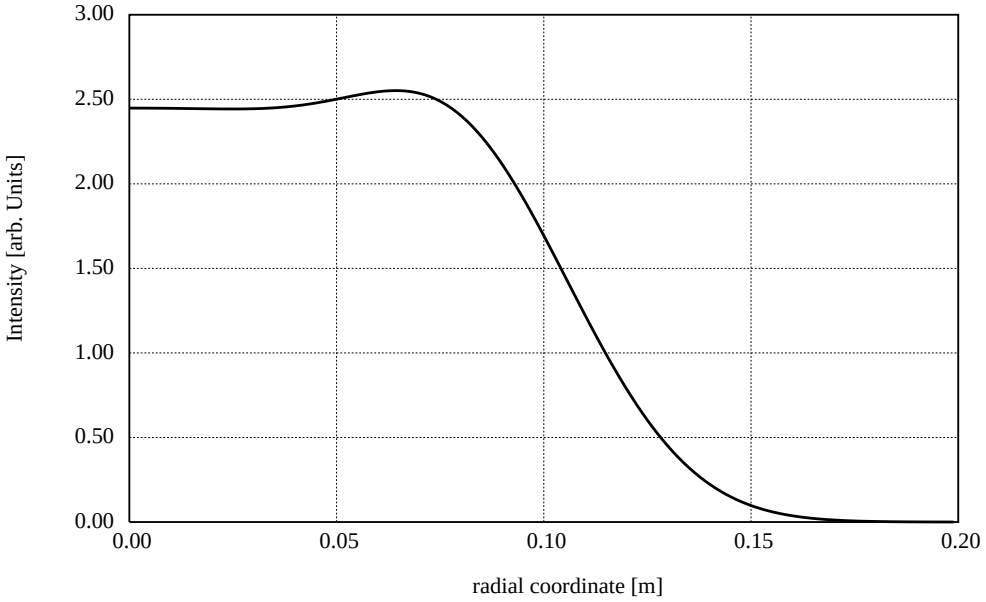

Figure 2.22: Intensity profile at 3 km

2.7.3 Normalization

It is difficult to compute directly the power carried by such a mode by simply integrating the intensity in the plane (x, y). Instead, we do it in the Fourier space. Owing to the Parseval-Plancherel theorem, we can write for the norm P:

$$P \;=\; \int |\Psi(x,y)|^2\, dx\, dy \;=\; \frac{1}{4\pi^2} \int |\tilde{\Psi}(p,q,0)|^2\, dp\, dq \tag{2.52}$$

so that, using a precedent result:

$$P \;=\; 2\,\frac{w_0^2}{b^2} \;\times\; 2 \int_0^\infty \exp(-w_0^2 x^2/2b^2)\, \frac{J_1(x)^2}{x}\, dx \tag{2.53}$$

The integral can be carried out, yielding:

$$P(w_0, b) \;=\; 2\,\frac{w_0^2}{b^2}\, F_{00} \tag{2.54}$$

with

$$F_{00} \;\equiv\; 1 \;-\; \exp(-b^2/w_0^2)\, \Big[I_0(b^2/w_0^2) + I_1(b^2/w_0^2) \Big]$$

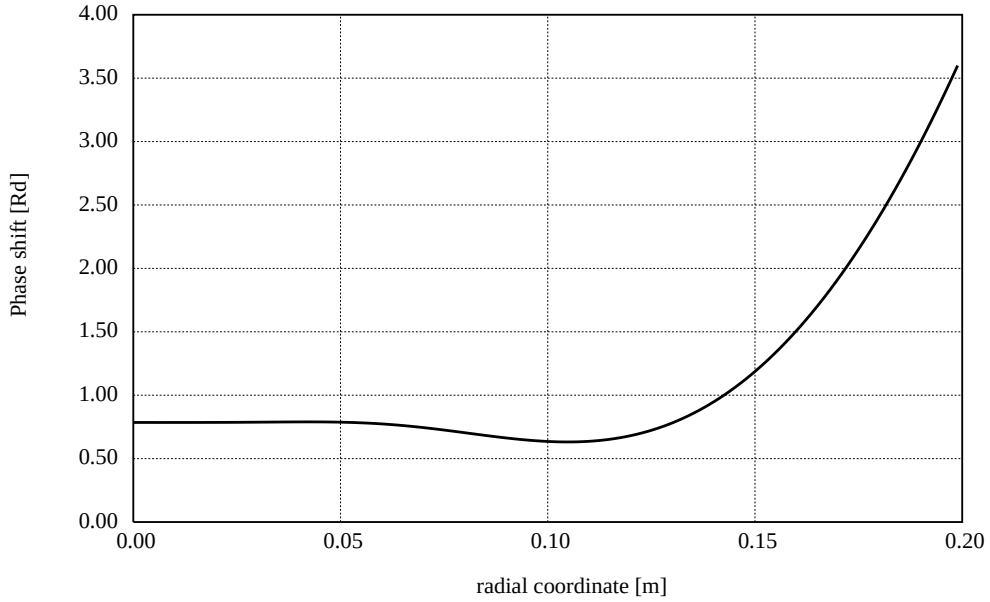

Figure 2.23: Wavefront at 3 km

where $I_0(z)$ and $I_1(z)$ are the modified Bessel functions of the 1st kind. When w_0 is small, so that b/w_0 is large, using the asymptotic values of the Bessel functions we get:

$$F_{00} \equiv 1 - \frac{2w_0}{\sqrt{\pi}b}\left[1 - \frac{w_0^2}{8b^2} - \frac{3w_0^4}{128b^4} - \frac{45w_0^6}{3072b^6} - ...\right] \tag{2.55}$$

The normalized flat mode at its waist is:

$$\Psi(x,y,0) = \frac{1}{\pi\, b\, w_0\, \sqrt{2F_{00}}} \int_\Delta dx_0\, dy_0\ \phi(x-x_0, y-y_0) \tag{2.56}$$

and finally, at any distance z:

$$\Psi(x,y,z) = \mathrm{e}^{-i\arctan(z/z_R)} \times$$
$$\times \frac{2w}{w_0 b\sqrt{\pi\, F_{00}}} \int_0^{b/w} \exp\left[-Z(r/w-\rho)^2\right] \exp(-2Zr\rho/w)\, I_0(2Zr\rho/w)\, \rho\, d\rho \tag{2.57}$$

with the same notation as above:

$$Z \equiv 1 - iz/z_R,\ z_R \equiv \pi w_0^2/\lambda, \quad w \equiv w_0\sqrt{Z.\overline{Z}}$$

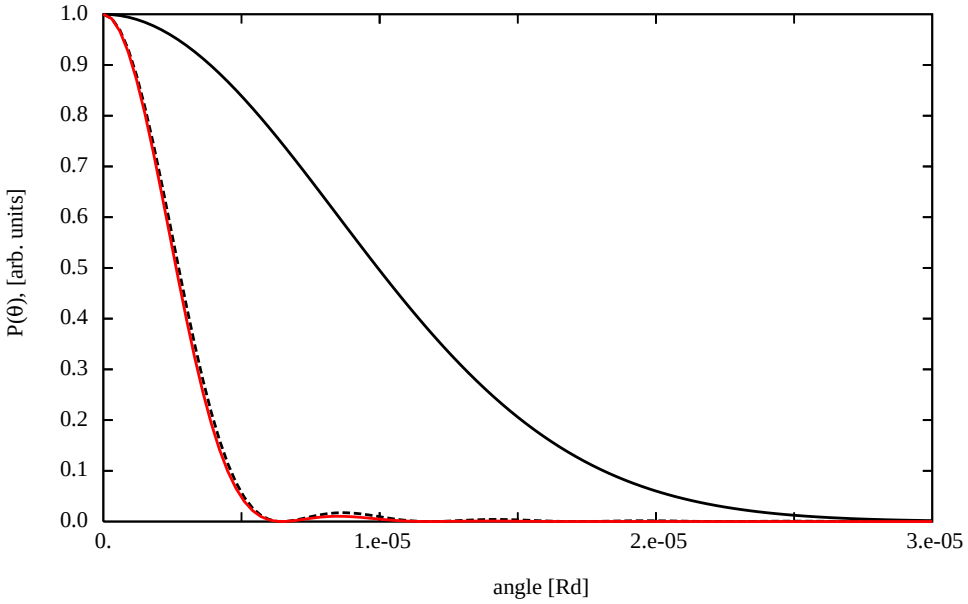

Figure 2.24: Angular distribution of the flat beam. Solid line: gaussian distribution, dashed line: circular aperture. Red dashed line: resulting angular distribution

2.7.4 Coupling with gaussian beams

It is of some importance to know the coupling rate of such flat beams with ordinary gaussian modes. We can for this compute the scalar product of the flat mode $\Psi(x,y)$ with for instance the fundamental gaussian mode of waist w : $\phi_{00}(x,y)$, at their common waist:

$$\Gamma_{00} \equiv \langle \Psi, \phi_{00} \rangle = \sqrt{\frac{2}{\pi w^2}} \sqrt{\frac{2}{\pi w_0^2}} \frac{1}{\pi b^2} \int_\Delta dx_0\, dy_0 \int_{\mathrm{R}^2} dx\, dy$$
$$\exp\left[-\frac{x^2+y^2}{w^2}\right] \exp\left[-\frac{(x-x_0)^2+(y-y_0)^2}{w_0^2}\right] \tag{2.58}$$

after some elementary algebra, we find:

$$\Gamma_{00} = \frac{2w_0 w}{b^2} \left\{ 1 - \exp\left[-\frac{b^2}{w_0^2+w^2}\right] \right\} \tag{2.59}$$

The power directly coupled from a gaussian beam into a flat beam (i.e. Γ_{00}^2) is thus extremely weak. We give on Fig.2.25 a plot of this power transfer versus the waist of the incoming gaussian beam, showing that only a few percent of the power can be this way injected in a flat beam. The coupling becomes worse and worse as the parameter b increases, and as the parameter w_0 decreases (the most the flat beam is interesting for thermal noise, the worst is its direct coupling to a gaussian beam). It is thus necessary to devise other ways of coupling power into flat-beam cavities.

2.7.5 Diffraction losses of flat beams

Flat beams have been seen to have a wide extension on the mirrors (this is exactly the reason why they have been designed). It may be useful to have an idea of the diffraction losses for such modes. How the clipping of the beam by a finite mirror reduces the reflected power. The following figure (2.26) shows the decrease of diffraction losses for two cases :b = 10 cm, 12 cm and w_0 = 3.2 cm. We see that for Virgo-like mirrors (a = 17.5 cm), the diffraction losses are negligible.

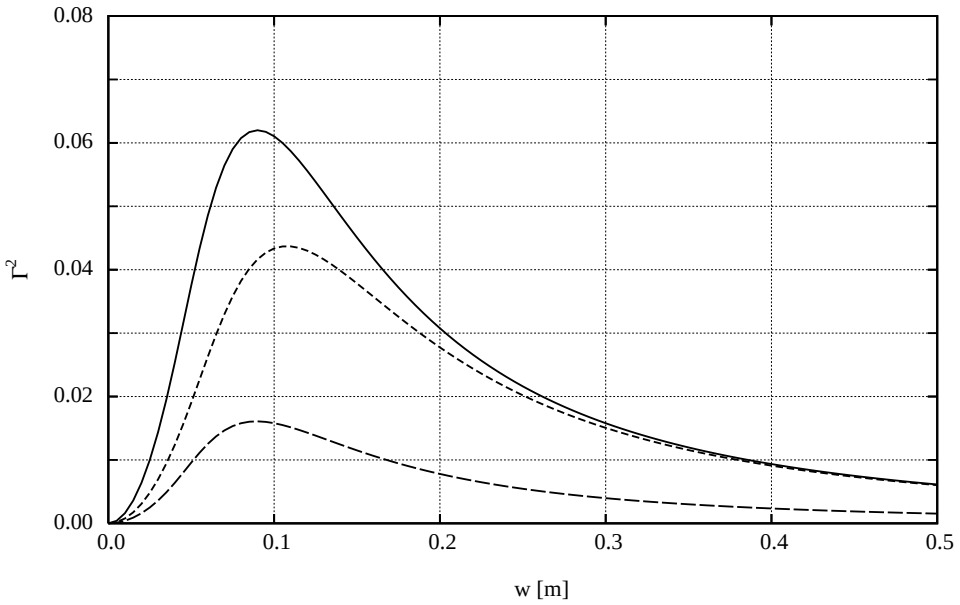

Figure 2.25: Coupling rate of a gaussian beam of waist w into a flat mode of parameters w_0, b. Solid line: $b = 10$ cm, $w_0 = 2$ cm. Short dashed line : $b = 12$ cm,$w_0 = 2$ cm. Long dashed line : $b = 10$ cm, $w_0 = 1$ cm.

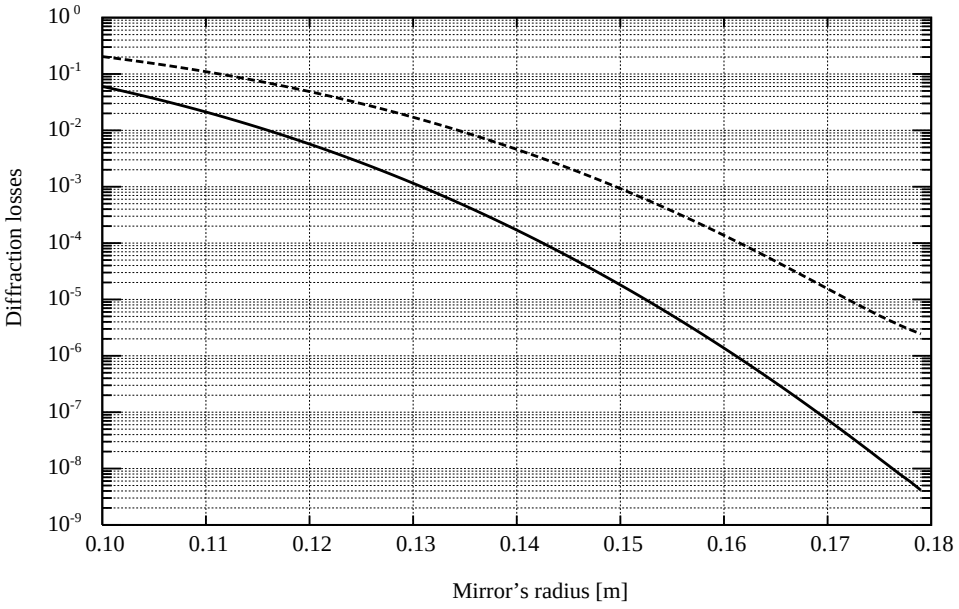

Figure 2.26: Diffraction losses of a flat beam of parameters $b = 10$ cm (solid line), $b = 12$ cm (dashed line) and $w_0 = 3.2$ cm

Chapter 3

Numerical methods

An optical instrument is generally composed of optical elements like lenses, mirrors, and of space between them. For studying any property of the instrument, we have to represent the action of each of these elements on a light beam. Everyone understands that space produces a diffraction of the beam, thin lenses or almost flat mirrors pure refraction or reflection, and thick lenses both. There are a lot of ways of representing numerically a light beam, for, instance:

- by sampling its complex amplitude on a rectangular grid in the x, y plane
- by mapping it on a polar mesh in the (r, θ) plane
- by expanding it on a discrete basis of modes

to each of these decisions correspond a special way of computing the field diffracted at a distance z. The method to choose depends obviously of the type of effects we want to analyze. In the case of axial symmetry, the polar representation will be convenient. In case of very small misalignments of mirrors in a resonant cavity, the modal expansion will do the job. Anyway, each of the corresponding algorithm belong to the class of "spectral methods" expanding the optical amplitudes on a basis of simple functions for which the diffraction/refraction problem is already solved. These simple functions will be

- plane waves in the case of Fourier (or Hankel) transform based methods
- $\mathrm{TEM_{m,n}}$ modes (HG or LG) in the modal methods

3.1 Numerical propagation using Fourier transforms

3.1.1 On the discrete Fourier transform

When the complex amplitude is sampled on a rectangular grid with equally spaced sampling points, it is possible to use a discrete 2D Fourier Transform to propagate the field. The Discrete Fourier Transform (DFT) comes from the crude approach of the numerical Fourier Transform of any function $\Phi(t)$ which is zero outside the interval [0,T]. The Fourier Transform then reduces to:

$$\tilde{\Phi}(f) \;=\; \int_0^T \mathrm{e}^{2i\pi ft}\;\Phi(t)\;dt$$

For a numerical integration, we can cut the interval in N slices of width $\Delta t \;=\; T/n$, and write approximately:

$$\tilde{\Phi}(f) \;=\; \frac{T}{N}\sum_{j=0}^{N-1}\mathrm{e}^{2i\pi fjT/N}\Phi(jT/N)$$

Now it is possible to sample the function in the frequency domain too. The smallest frequency interval we can consider is obviously $\Delta f \;=\; 1/T$, because the longest time interval on which the function Φ can be studied is T. The sampling will thus be:

$$f_m \;=\; m\times\frac{1}{T}$$

and the samples of the Fourier Transform are:

$$\widetilde{\Phi}_m \;\equiv\; \tilde{\Phi}(m/T) \;=\; \frac{1}{N}\sum_{j=0}^{N-1}\mathrm{e}^{2i\pi mj/N}\Phi_j \qquad (3.1)$$

with the notation $\Phi_j \;=\; \Phi(jT/N)$. Eq.(3.1) expresses the DFT.
If we consider the vector $\widetilde{\Phi}_m$, several remarks arise

- It is easily seen that

  $$\widetilde{\Phi}_{m+N} \;=\; \widetilde{\Phi}_m$$

  showing that the DFT has period N with respect to m, it is therefore sufficient to compute $\{\widetilde{\Phi}_m \;;\; m=0,\ldots,N-1\}$.

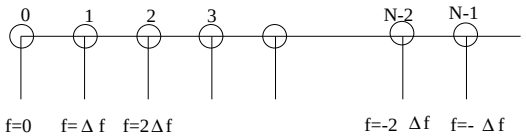

Figure 3.1: Assign frequencies to the DFT samples

- Clearly $m = 0$ corresponds to the mean of the function $\Phi(t)$, and thus to the value at $f = 0$ of its Fourier transform. Now, it is easily seen that

$$\widetilde{\Phi}_{N-m} \;=\; \widetilde{\Phi}_{-m}$$

  and as a result, the second half of the vector $\{\widetilde{\Phi}_m\}$ contains the negative frequencies (see Fig.(3.1))

- The maximum frequency is thus

$$f_{\max} \;=\; \left[\frac{N}{2}\right]\frac{1}{T}$$

- Consider a Fourier transform followed by the reciprocal:

$$\widetilde{\Phi}_m \;=\; \frac{1}{N}\sum_{j=0}^{N-1} \mathrm{e}^{2i\pi mj/N}\Phi_j$$

  (as already seen, the time element is T/N, and the frequency element is $1/T$, so that the time $\times$ frequency element is $1/N$) then

$$\widetilde{\widetilde{\Phi}}_n \;=\; \frac{1}{N}\sum_{m=0}^{N-1}\sum_{j=0}^{N-1} \mathrm{e}^{2i\pi m(j-n)/N}\Phi_j$$

  but $-N+1 \;\leq\; j-n \;\leq\; N-1$, so that

$$\sum_{m=0}^{N-1} \mathrm{e}^{2i\pi m(j-n)/N} \;=\; \frac{\mathrm{e}^{2i\pi(j-n)}-1}{\mathrm{e}^{2i\pi(j-n)/N}-1} \;=\; \begin{cases} 0 \text{ if } j \neq n \\ N \text{ if } j = n \end{cases}$$

  and consequently,

$$\tilde{\tilde{\Phi}}_n \;=\; \Phi_n \tag{3.2}$$

which shows that the "approximate" of the inverse FT is the exact inverse of the "approximate" FT. Practically, when implementing any DFT algorithm, this is the first property to check.

- Let us denote here by

$$\widetilde{\Phi_{N,m}}$$

the N-points DFT of Φ. Assume that $N = 2N'$ even, and $m = 2m'$ too. We can write

$$\widetilde{\Phi_{N,m}} \;=\; \frac{T}{N}\sum_{j=0}^{N-1} \mathrm{e}^{2i\pi mj/N}\Phi_j \;=\; \frac{T}{2N'}\sum_{j=0}^{2N'-1} \mathrm{e}^{2i\pi m'j/N'}\Phi_j$$

By splitting the sum into two segments we get

$$\widetilde{\Phi_{N,m}} \;=\; \frac{1}{2}\frac{T}{N'}\sum_{j=0}^{N'-1} \mathrm{e}^{2i\pi m'j/N'}\Phi_j \;+\; \frac{1}{2}\frac{T}{N'}\sum_{j=N'}^{2N'-1} \mathrm{e}^{2i\pi m'j/N'}\Phi_j$$

and by renaming $j = j' + N'$ in the second sum,

$$\widetilde{\Phi_{N,m}} \;=\; \frac{1}{2}\frac{T}{N'}\sum_{j=0}^{N'-1} \mathrm{e}^{2i\pi m'j/N'}\Phi_j \;+\; \frac{1}{2}\frac{T}{N'}\sum_{j'=0}^{N'-1} \mathrm{e}^{2i\pi m'j'/N'}\Phi_{j'+m}$$

if we note $\Phi^{(1)}$ and $\Phi^{(2)}$ the two halves (of lengths $N' = N/2$) of the input vector Φ (of length N), we have the following property

$$\widetilde{\Phi_{2N',2m'}} \;=\; \frac{1}{2}\left(\widetilde{\Phi^{(1)}_{N',m'}} + \widetilde{\Phi^{(2)}_{N',m'}}\right) \tag{3.3}$$

In the case where $m = 2m' + 1$ is odd, we have:

$$\widetilde{\Phi_{N,m}} \;=\; \frac{1}{2}\frac{T}{N'}\sum_{j=0}^{N'-1} \mathrm{e}^{2i\pi m'j/N'}\mathrm{e}^{i\pi j/N'}\Phi_j \;-\; \frac{1}{2}\sum_{j'=0}^{N'-1} \mathrm{e}^{2i\pi m'j'/N'}\mathrm{e}^{i\pi j/N'}\Phi_{j'+m}$$

If we introduce the new function $\Psi_j \equiv e^{2i\pi j/N} \times \Phi_j$, we see that the preceding equation reads:

$$\widetilde{\Phi_{2N',2m'}} = \frac{1}{2}\left(\widetilde{\Psi^{(1)}_{N',m'}} + \widetilde{\Psi^{(2)}_{N',m'}}\right) \tag{3.4}$$

and the conclusion is that the N-ranks Discrete Fourier Transform essentially reduces to two $N/2$-rank partial transformations of the two halves of the input vector. This is the fundamental remark that led to FFT algorithms. FFT routines allow to compute rank N DFT's with $N\mathrm{Log}_2 N$ algorithms instead of N^2. The result is a tremendous increase of the computational speed of Fresnel diffraction (FFT) compared to the general Kirchhoff integral. The gain is for a 2 dimensional FT:

$$\left[\frac{N}{\mathrm{Log}_2 N}\right]^2$$

for $N = 128$ this is a gain larger than 300 ! But this is at the price of a restriction of the validity of the method (very small diffraction angles).

It must be clear that the result of a DFT is not a sampling of the result of the continuous transformation. The finite step integration which was at the starting point of the algorithm can only converge towards the true FT as N increases. The linear algebra involving vectors of size N and rank N DFT's is perfectly closed due to eq.(3.2), but it represents a world different from reality. We give for instance the result of a basic experiment. We consider the function

$$F(t) = \exp\left(-\frac{t^2}{2\tau^2}\right)$$

in our experiment, we take the time constant τ=1s. Its Fourier transform is:

$$\tilde{F}(f) = \sqrt{2\pi}\,\tau \exp\left(-\frac{1}{2}(2\pi f\tau)^2\right)$$

and we compare a N-sample of the continous FT of F to the DFT of a N-sample of F (see table (3.1.1)). The interval over which the function is sampled is called window. The size of the window must be chosen such that the function takes vanishing values near the ends of the window. Moreover, there is an optimal density of samples, which implies that when the size of the sample is changed, the size of the window giving the optimal agreement changes too.

Sample size	*Optimal window*	*rms error*
16	10s	$6.9\ 10^{-7}$
32	14s	$1.8\ 10^{-12}$
64	17s	$7.2\ 10^{-17}$

In this case, it can be seen that increasing the size of the sample is useless, since at N=64, the ultimate precision of the computer is reached.

We have seen that the DFT has the dichotomic property, reducing in principle a N-DFT to two $N/2$-DFT's. The basic of the FFT is to recursively compute any N-DFT from a series of initial 2-DFT's. In this elementary scheme (due to J. Cooley and J. Tukey [10]), N has obviously to be an integer power of 2. Moreover, it is clear that the number of recursions is $\log_2(N)$, so that the number of operations, grows as $N \times \log_2(N)$, which is a tremendous improvement with respect to the naive DFT scheme. For instance, in a 2D Fourier Transform, if a 1024×1024 2D sample is needed, FFT provides a factor of roughly 10^4 gain in CPU time. All other properties are exactly those described for the DFT.

The Fourier Transform of the paraxial diffraction kernel

$$K(x,y,\Delta z) \;=\; -\,\frac{i}{\lambda\Delta z}\;\exp\left(-i\frac{k(x^2+y^2)}{2\Delta z}\right)$$

is:

$$\widetilde{K}(p,q,\Delta z) \;=\exp\left(-i\frac{\Delta z(p^2+q^2)}{2k}\right)$$

Now, if we intend to use a DFT for computing the diffraction integral according to the scheme

$$E_2(x,y,z+\Delta z) \;=\; \widetilde{K_{\rm P}}(p,q,\Delta z)\;\widetilde{\times}\;\;\widetilde{E_1}(p,q,z) \tag{3.5}$$

we need the discretization of $\widetilde{K}(p,q,\Delta z)$ with respect to p,q. We remember that the frequency increment in the DFT is $\delta f \;=\; 1/T$ where T is the time window. In terms of spatial circular frequencies, the increment will be $\delta p \;= 2\pi/F_x$, where F_x is the x side of the 2D spatial window. We have also $\delta q \;= 2\pi/F_y$. The discretization is therefore of the form:

$$\widetilde{K}(m,n,\Delta z) \;=\; \exp\left[-\;i\;\pi\lambda\Delta z\left(\frac{m^2}{F_x^2}\;+\frac{n^2}{F_y^2}\right)\right]$$

If we remember that the DFT has a specific way of sorting the frequencies, we could think that we have to correctly arrange the FFT of the input field, before multiplying by $\tilde{K}$. Clearly, it is more efficient not to correct the FFT's, but rather write the propagator according to the same convention. For a square computation window of size `window` the FORTRAN sequence calculating $\widetilde{K}(i,j,z)$, could be:

```
mil=n/2+1
do i=1,n
   if (i.le.mil) then
      ind1=i-1
   else
      ind1=i-1-n
   endif
   do j=1,n
      if (j.le.mil) then
         ind2=j-1
      else
         ind2=j-1-n
      endif
      square=ind1**2+ind2**2
      phase=-pi*lambda*z*square/window**2
      ktilde(i,j)=cmplx(cos(phase),sin(phase))
   enddo
enddo
```

3.1.2 FFT-based propagation algorithms

A step Δz of propagation will be carried out following the scheme showed on Fig.3.2, and propagation steps can be linked into series corresponding to the various interfaces of an optical system. The optical amplitudes are sampled on a rectangular grid (it is not necessary to use a square grid. If we have spatially squeezed beams, one direction can be larger and more sampled than the other). Call `a(i,j)` the complex array (of size $n \times n$) representing the amplitude at $z = 0$. The propagation step is for instance

```
c-------------------------------------------------------------
c     the subroutine named cfft2d(m,n,ar,iflag) represents any
```

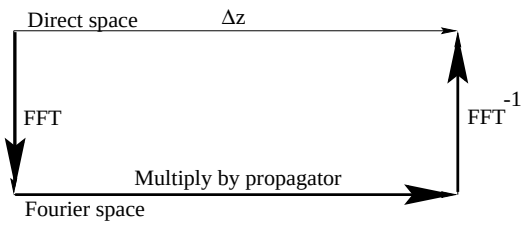

Figure 3.2: propagation step

```
c     procedure carrying out the 2D-FT of a complex array
c
c     m,n : size of the array to be transformed
c     ar : the array to be transformed, and on return, the
c          transformed array
c     iflag = 1 : direct transform
c     iflag = -1: inverse transform
c-------------------------------------------------------------
      call cfft2d(n,n,a,1)
      do i=1,n
        do j=1,n
           a(i,j)=a(i,j)*ktilde(i,j)
        enddo
      enddo
      call cfft2d(n,n,a,-1)
c-------------------------------------------------------------
```

after what `a(i,j)` represents the propagated amplitude. Mirrors are sampled on the same grid, and represented by complex arrays:

```
c-------------------------------------------------------------
      subroutine defmirr(n,window,reflect,radius,curvature,mir)
c
c     returns an array of samples of the phase equivalent
c     of the mirror for given parameters
c
c       n         : rank of the arrays
c       window    : computation window
c       reflect   : photometric amplitude reflectivity
```

```
c       radius    : radius (half size) of the mirror
c       curvature : inverse of curvature radius
c       mir       : returned array representing the mirror
c
      implicit none
c
      integer n,i,j
      real*8 reflect,radius,curvature,pi,x,y,rp2
      real*8 window,lambda,dx,phase
      complex*16 ci,mir(n,n)
c
      data pi/3.141592653589793d0/
      data ci/(0.d0,1.d0)/
      data lambda/1.064d-6/
c
      dx=window/n
      do i=1,n
         x=(i-1)*dx-window/2
         do j=1,n
            y=(j-1)*dx-window/2
            rp2=x*x+y*y
            if (rp2.gt.radius*radius) then
               mir(i,j)=0
            else
               phase=2*pi*rp2*curvature/lambda
               mir(i,j)=ci*reflect*dcmplx(dcos(phase),-dsin(phase))
            endif
         enddo
      enddo
      return
      end
```

A reflection will then be carried out by a simple term to term product of the amplitude by the mirror :

```
      do i=1,n
         do j=1,n
            aref(i,j)=ain(i,j)*mir(i,j)
         enddo
```

```
enddo
```

The main example we shall study is the case of a Fabry-Perot cavity. In fact, round trips in the cavity will be implicitly replaced by a direct propagation through a series of thin lenses. It is remarkable that propagation looks just like a lens (see below) in the Fourier space, so that diffraction and refraction processes are exchanged by the FT. As an example we can make the following numerical experiment. Start from the TEM_{00} amplitude at its waist (this situation exists at the corner mirrors of the Virgo cavities, with $w_0 \simeq 2$ cm, then propagate over the distance L =3 km, first by using the analytical formula giving the continuous paraxial result, second by using one step of the FFT scheme, with a sampling of n×n over a grid of size s. Then make numerically the two wave interfere. For measuring the distance between two complex amplitude arrays, we use the Hilbert Space metrics:

$$d(e_1, e_2) \;=\; \left[\frac{s}{n}\sum_{i,j=0}^{n-1} |e_{2,ij} \;-\; e_{1,ij}|^2\right]^{1/2}$$

which maybe interpreted as the square root of the total power in the interference of the two waves. The following table gives an idea of the convergence of the discrete world towards continuous.

Sample size	*Optimal window*	*rms error*
32	34 cm	$4.9\ 10^{-5}$
64	49 cm	$1.6\ 10^{-8}$
128	70 cm	$4.9\ 10^{-15}$
256	81 cm	$8.3\ 10^{-15}$

Now, we can also propagate a TEM_{00} wave having such a waist ($w_0 \sim 2$ cm) that the curvature radius of its wavefront matches a 3.45 km curvature radius mirror. In the paraxial theory, starting from the waist (plane wave), the reflected wave exactly coincide, after the return trip, with the original. We can carry out this experiment by numerical propagation, and compare the image after the round trip with the original. The result depends of the size of the window, and on the sampling rate. We see on (Fig.3.3) these dependences. The difference between the theoretical propagated mode and the numerically propagated one can be visualized as an interference (see Fig.3.4). The shown intensity distribution represents the computational noise, and the cross pattern reflects the square grid used for the discrete sampling in the window.

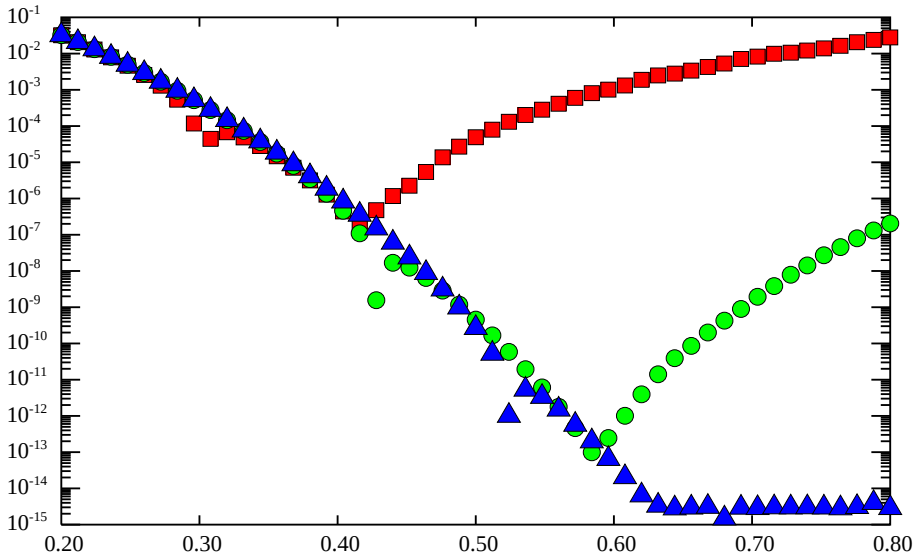

Figure 3.3: Round trip error vs window size (m). n=50 (squares) n=100 (circles), n=150 (triangles)

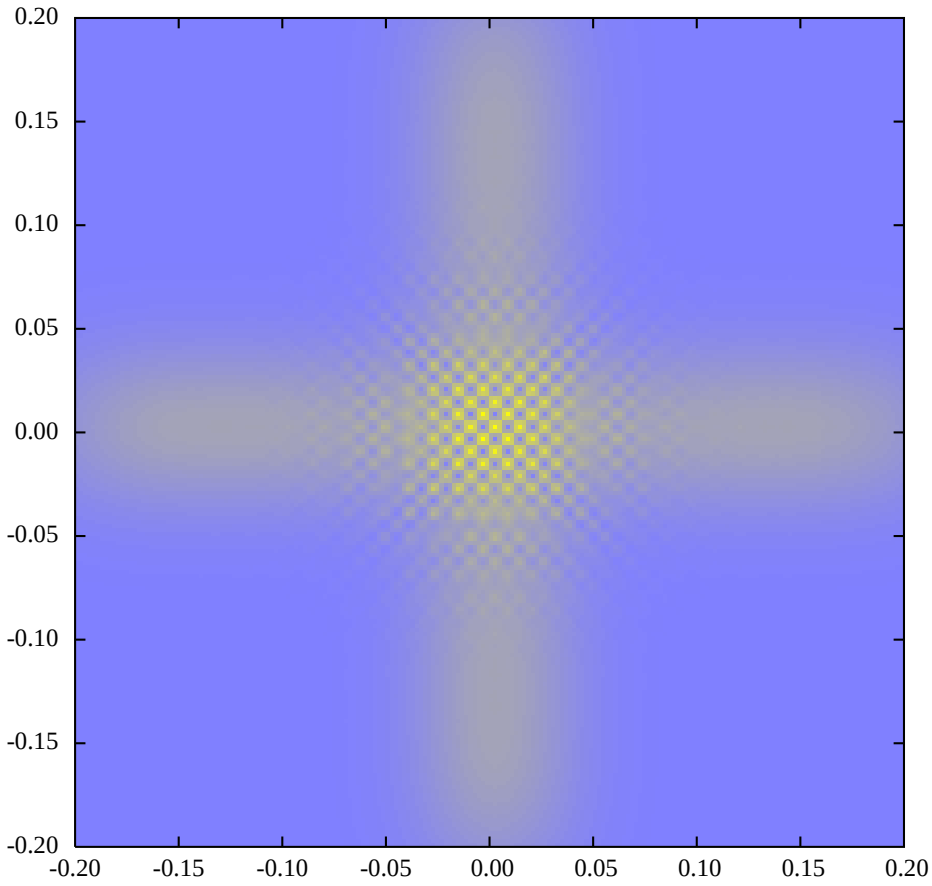

Figure 3.4: Interference fringe between exact and numerically propagated TEM_{00}

3.1.3 Finding the field reflected off a resonant cavity

Assume an amplitude $E_{in}(x,y)$ is entering a Fabry-Perot cavity. The intracavity field $B(x,y)$ obeys the following equation:

$$B \;=\; t_1\; E_{in} \;-\; r_1 r_2\; M_1 \times P_L \times M_2 \times P_L\; B \tag{3.6}$$

(see Fig.1.6 for notation). $M_{1,2}$ are the reflection operators on the two mirrors respectively, for instance given by (2.30). Mathematically, this is an implicit linear equation, and it could be in principle solved by matrix inversion. But for a n×n sampling grid, the linear operator P_L is a $n^2 \times n^2$ rank operator, which, for large n would lead to invert huge matrices. It is therefore much more convenient if possible, to solve eq.(3.6) by successive iterations, provided some inital guess of the intracavity field. For instance, if we study small geometrical defects of the mirrors surfaces, the initial guess could be the ideal TEM_{00} mode $\Phi_{00}(x,y)$, with the correct surtension coefficient:

$$B_{guess}(x,y) \;=< E_{in}, \Phi_{00} > \;\frac{t_1}{1 \;-\; r_1 r_2}\; \Phi_{00}(x,y)$$

But other choices are possible. The speed of the convergence to the solution depends on the finesse of the cavity. Once the intracavity field $B(x,y)$ is found, the reflected amplitude is obtained by

$$E_{out} \;=\; M_1^* E_{in} + P_L \times M_2 \times P_L B$$

. It is possible to bring into evidence the various eignemodes of a parabolic Fabry-perot cavity. In the following numerical experiment we try to scan the different resonances of a VIRGO type cavity by adding a varying phase $\Phi \in [0, 2\pi]$ to the propagator, in order to simulate the fine tuning of the cavity. The inital tuning is assumed to correspond to a TEM_{00}. If the input field is a pure TEM_{00}, we see only the resonances of the fundamental (Fig3.5), other modes being orthogonal to the input field are never excited. In order to excite higher order modes, we have to take an input field not strictly orthogonal to the TEM_{00}. For instance, adding terms in $x,\; y^2\;, x^3,\; \ldots$ to the phase of the input wave allows resonances of $\mathrm{TEM}_{\mathrm{mn}}$ up to $m+n=4$, as can be seen on fig.3.6. A more accurate study shows that the resonances are slightly different from their theoretical values. This is a consequence of the discretization of the field, of the mirrors, of the propagator. The discrete world has different rules. By increasing the order of the calculation (the

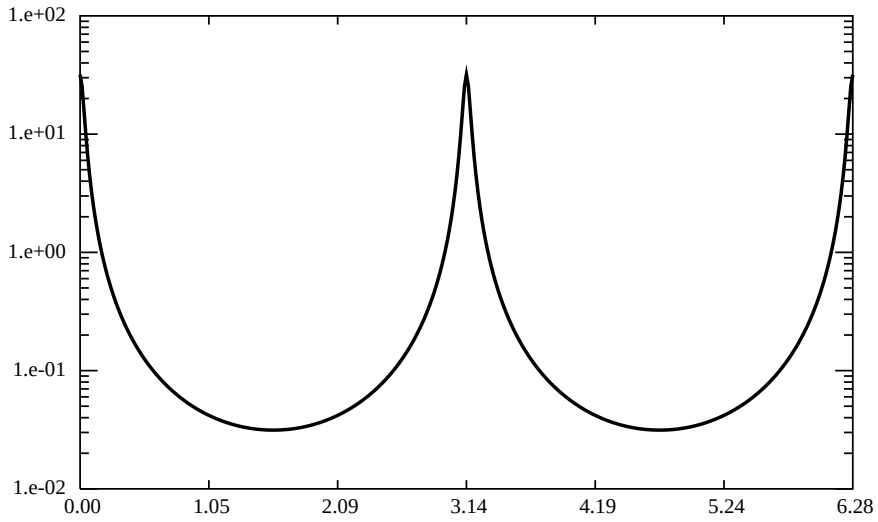

Figure 3.5: Fabry-Perot cavity : resonances of the fundamental mode

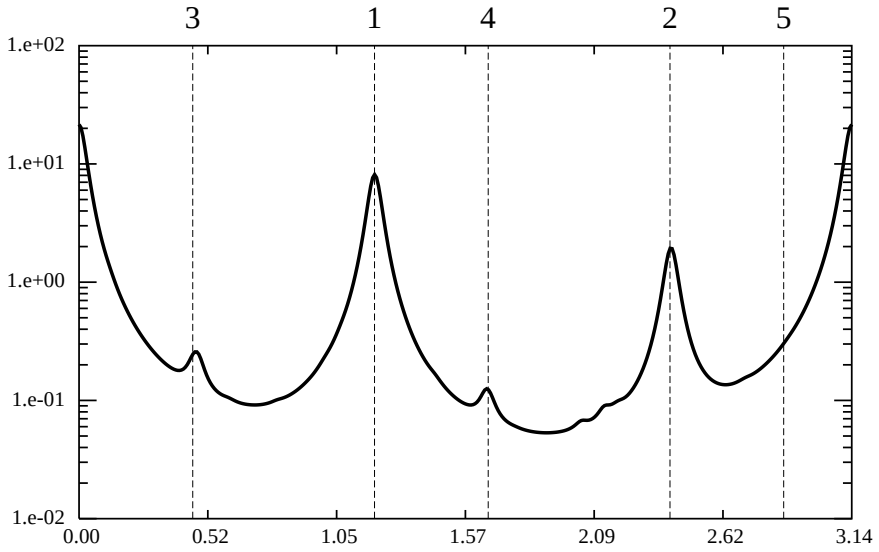

Figure 3.6: Fabry-Perot cavity : excitation of the $TEM_{m,n}$ modes. Dashed lines correspond to the first theoretical resonances, and are labeled by $m+n$.

preceding was carried out on a 64×64 grid), this small discrepancy vanishes. In order to drive the cavity exactly at resonance, it is necessary to achieve a fine tuning of the propagator. The brute force method would consist in computing the power in the intracavity field for various values of the varying phase precedingly introduced, and search for the maximum, but this would result in a very time costly code. It is better to use the following scheme. Let us denote by $\mathcal{C}$ the cavity operator:

$$\mathcal{C} \;=\; M_1 \;\times\; P_L \;\times\; M_2 \;\times\; P_L$$

and ϕ an arbitrary phase representing the fine tuning of the cavity. The intracavity field B obeys the implicit equation

$$B \;=\; t_1\, A \;+\; \mathrm{e}^{i\phi}\mathcal{C}\; B \tag{3.7}$$

where A is the input field. If the input field is the fundamental mode TEM_{00} with an amplitude a, and if for the sake of simplicity we note $\{\psi_p \;;\; p = 1, 2, \ldots, \infty\}$ (with a unique index) the basis of TEM modes, we can write:

$$B \;=\; b_0\psi_0 \;+\; \sum_{p>0} b_p\psi_p$$

For a small perturbation, the coefficients $\{b_p \;;\; p > 0\}$ are first order quantities. By taking the scalar product of eq.3.7 with the fundamental, we get

$$b_0 \;=\; t_1 a \;+\; \mathrm{e}^{i\phi}\left[b_0 < \psi_0 \;,\; \mathcal{C}\;\psi_0 > \;+\; \sum_{p>0} b_p < \psi_0 \;,\; \mathcal{C}\;\psi_p >\right]$$

At the lower order we get

$$b_0 \;=\; \frac{t_1\; a}{1 \;-\; \mathrm{e}^{i\phi} < \psi_0 \;,\; \mathcal{C}\;\psi_0 >}$$

making clear that the value of ϕ which corresponds to resonance is

$$\phi \;=\; -\mathrm{Arg}\,[< \psi_0 \;,\; \mathcal{C}\;\psi_0 >]$$

The one way propagator must therefore be corrected by the phase factor

$$\mathrm{e}^{i\phi/2}$$

The phase discrepancy ϕ of discrete vs continuous eigenmodes of the cavity is given in the following table.

Sample size	*Optimal window*	*phase corr.*
32	34 cm	-7.4 10^{-8} Rd
64	49 cm	-4.5 10^{-15} Rd
128	70 cm	-6.1 10^{-16} Rd

3.1.4 The Michelson Interferometer

It is easy to model a Michelson interferometer having two cavities as arms, for instance is order to study the field reflected off a cavity having imperfect mirrors, we take a perfect reference cavity and recombine the two reflected fields. Denoting by E_1 , E_2 the amplitides reflected by the two cavities, the total output field is

$$E_{\rm tot} \;=\; E_1 \;+\; {\rm e}^{i\phi}\; E_2$$

where ϕ represents the differential optical path between the two arms. It is necessary to adjust this phase to obtain the darkest field. In the ideal case, the phase is π and the resulting field is zero. In the general case, let

$$< E_1 \;, E_2 > = \;\; |E_1|.|E_2|\; {\rm e}^{i\alpha}$$

it is easy to obtain the following equation for the power ;

$$P_{\rm tot} \;=\; \left(\sqrt{P_1} - \sqrt{P_2}\right)^2 \;+\; 4\sqrt{P_1\;P_2}\sin^2[(\phi\;-\alpha)/2]$$

so that it is clear that we must take $\phi \;=\; \alpha$, i.e.

$${\rm e}^{i\phi} \;=\; \frac{< E_1 \;, E_2 >}{|E_1|.|E_2|}$$

As an example, we consider a Michelson having the same parameters as Virgo, and in which one spherical mirror has a wrong curvature radius (1% error): After computation, we read that the relative power on the dark fringe is $1.6\,10^{-3}$, the intensity field having the structure shown on Fig.3.7. The interference between the two slightly differently curved wavefronts gives a series of rings of which one is visible in the non zero zone of the globally gaussian intensity. Another example corresponds to a misalignment of a mirror. For instance a corner mirror of one cavity has a pointing error of 10^{-8} Rd. The relative power on the dark fringe is 4.810^{-8}. The structure of the fringe (see Fig.3.8) is analogous to the intensity pattern of a $\rm TEM_{01}$ mode.

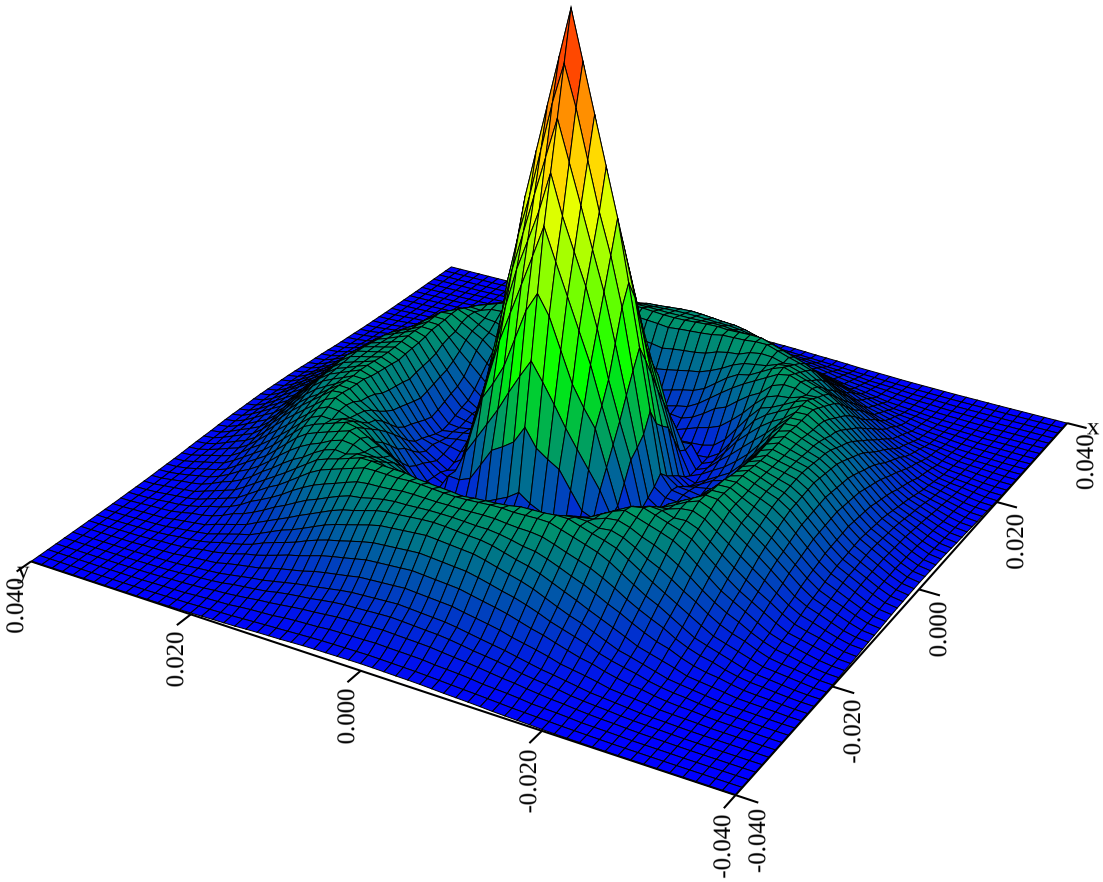

Figure 3.7: Michelson interferometer: Dark fringe pattern for 1% curvature radius error on a far mirror

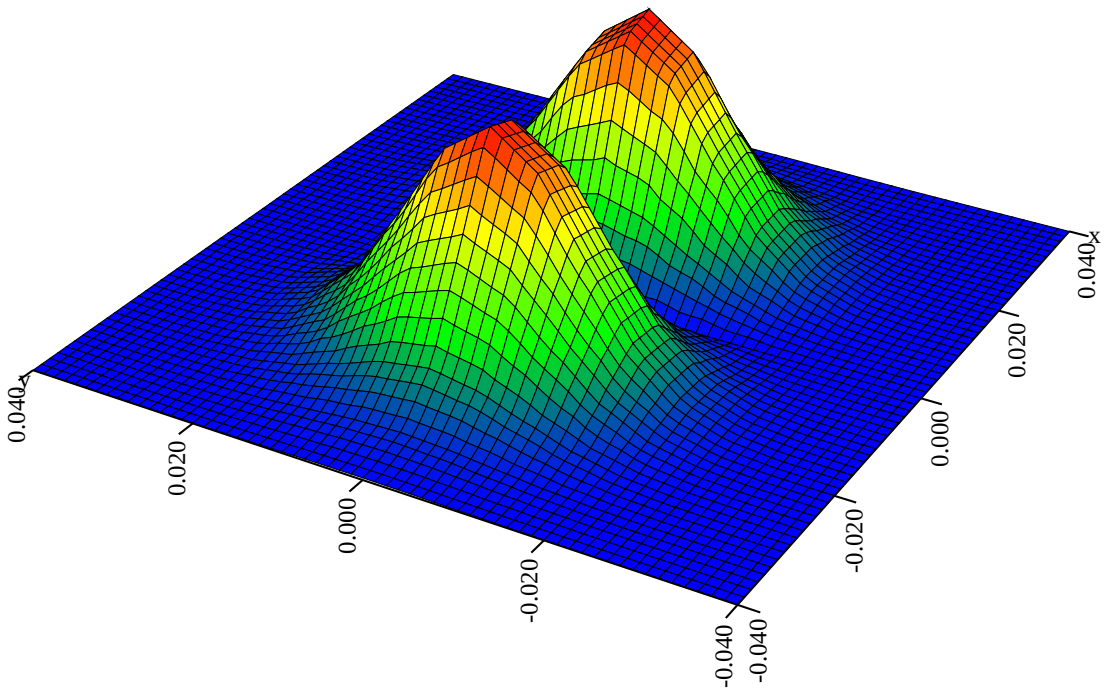

Figure 3.8: Michelson interferometer: Dark fringe pattern for 10^{-8} Rd pointing error on a corner mirror

3.1.5 The power-recycled Michelson interferometer

It is possible to model a power recycled interferometer by an external loop, starting on an estimate of the recycled field E then involving two subloops for describing the two FP cavities. A such code would be however very time consuming without necessity. It is much more convenient to use one loop. We begin by a first estimate of the recycled field E and of the two intracavity fields F_1 and F_2 (see Fig.3.9 for notation) We denote by R_i, T_i respectively the operators associated to the reflection and the transmission of mirror M_i. The 6 mirrors involved are: the recycling mirror $M_{\rm R}$, the corner mirror M_{11} and the far mirror M_{12} of the North cavity, and the corresponding M_{21}, M_{22} for the West cavity. The splitter is M_S. We start from three estimates (E, F_1, F_2) of the internal fields corresponding to the easily computed ideal situation (perfect mirrors), then new estimates can be computed according to the following scheme:

$$E^{\rm new} = T_R A + R_R \left[\mathcal{P}_1 R_{11} \mathcal{P}_1 + \mathcal{P}_2 R_{21} \mathcal{P}_2\right] E^{\rm old} + R_R \mathcal{P}_1 T_{11} \mathcal{C}_1 F_1^{\rm old} + R_R \mathcal{P}_2 T_{21} \mathcal{C}_2 F_2^{\rm old}$$

$$F_1^{\rm new} = T_{11} \mathcal{P}_1 E^{\rm old} + R_{11} \mathcal{C}_1 F_1^{\rm old}$$

$$F_2^{\rm new} = T_{21} \mathcal{P}_2 E^{\rm old} + R_{21} \mathcal{C}_2 F_2^{\rm old}$$

where $\mathcal{C}_i$ denotes a round trip in cavity #i (*i.e.* propagation/reflection/propagation), $\mathcal{P}_1$ a propagation along the North short arm through the splitter, and $\mathcal{P}_2$ a propagation from South to West by reflection on the splitter. Then the process is iterated until the hilbertian distance between two successive estimates is small enough. At the end, the field in the dark fringe is B given by

$$B = \left[R_S \mathcal{P'}_1 R_{11} \mathcal{P}_1 + T_S \mathcal{P'}_2 R_{21} \mathcal{P}_2\right] E + R_S \mathcal{P'}_1 T_{11} \mathcal{C}_1 F_1 + T_S \mathcal{P'}_2 T_{21} \mathcal{C}_2 F_2$$

For instance, we have taken the maps of two recently produced end mirrors (C01077 and C02017 respectively), and used the preceding algorithm for checking the best mutual attitude of both when installed in a power-recycled interferometer. The two mirrors are not perfectly identical, as well for the curvature radius than for the roughness pattern. The following table summarizes the main parameters:

Mirror #	Curv. Rad.	Matched Waist	RMS roughness
C01077	3584 m	2.12 cm	2.8 nm
C02017	3624 m	2.15 cm	3.6 nm

The roughness maps are shown on Fig.3.10 and Fig.3.11 respectively

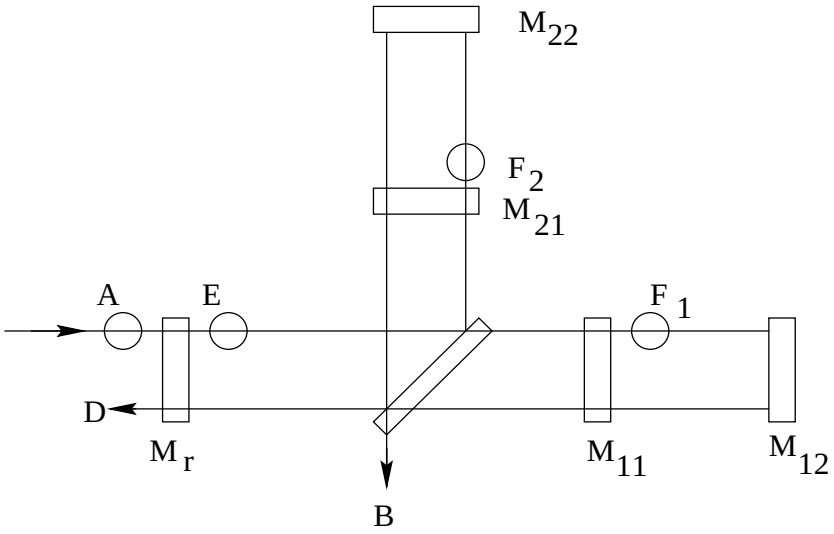

Figure 3.9: Sketch of a power recycled Michelson

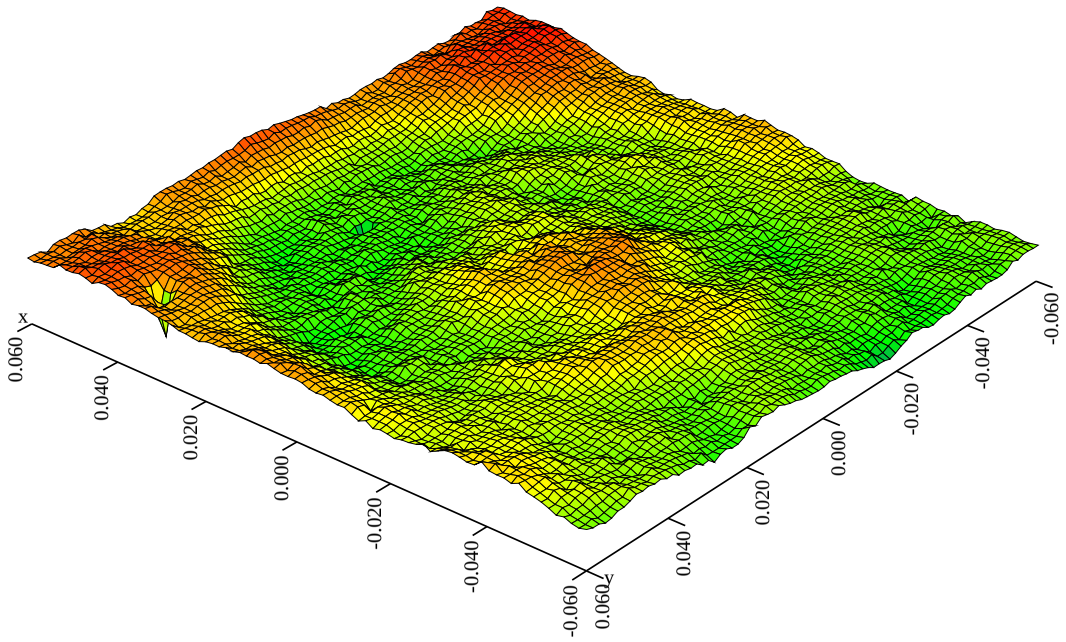

Figure 3.10: Roughness in the axial zone of C01077

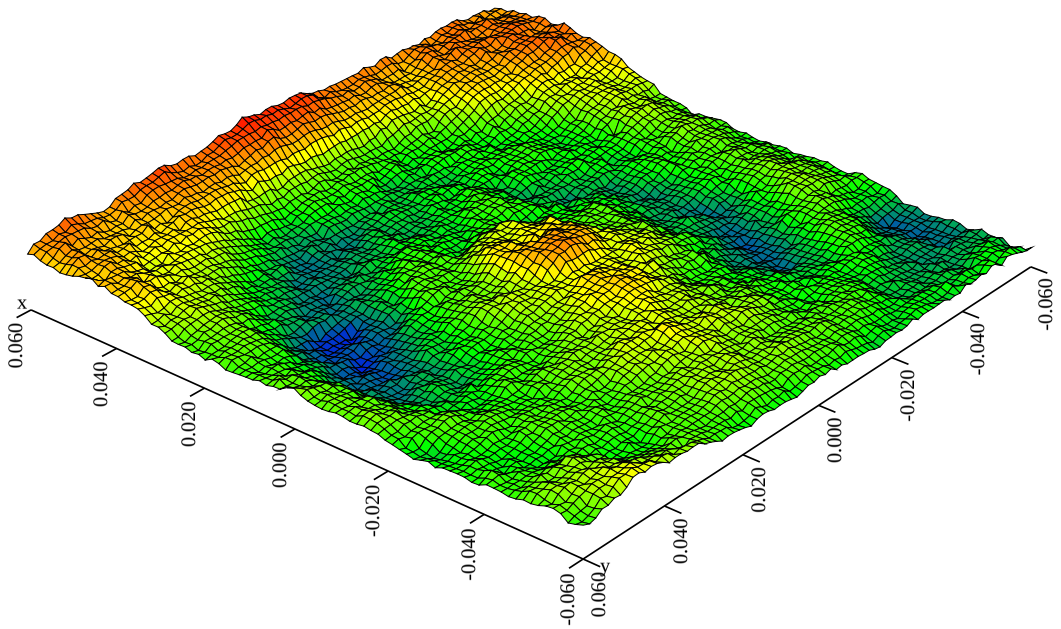

Figure 3.11: Roughness in the axial zone of C02017

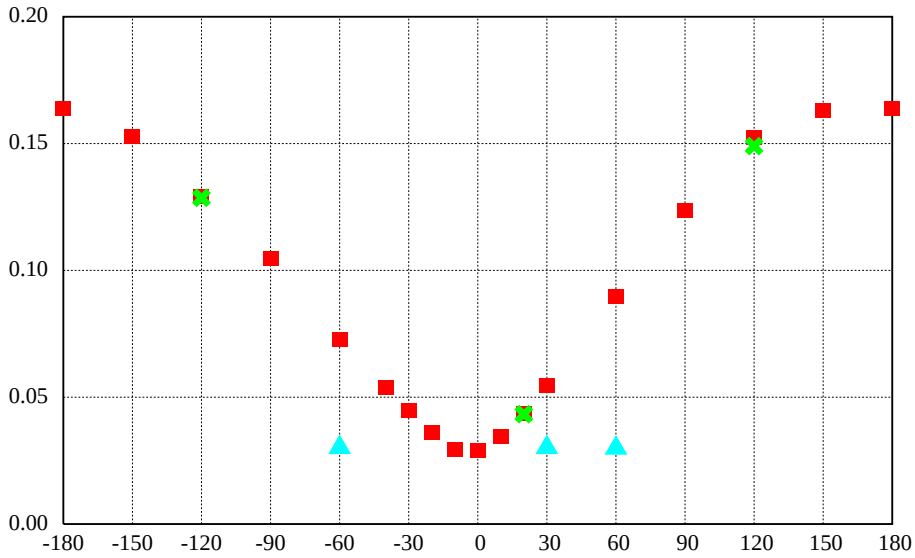

Figure 3.12: Power on dark fringe for various mutual angles (see text for comments)

It is instructive to run the code with different mutual angles. The two surface maps may be rotated in the (x, y) plane by angles θ_1 and θ_2 respectively, and the dark fringe computed as above. The results are summarized in the following plot (Fig.3.12): The various types of dots correspond to consistence tests. The red squares are obtained by setting the rotation angle of map #1 to zero and varying the roation angle of map #2. The green crosses are obtained by the inverse calculation: map #1 is left unchanged, and map #2 rotated by opposite angles. Cyan triangles are obtained by rotating the two mirrors by indentical angles. The fact that the values found for the same angular difference but different offsets are only almost equal is due to the necessary interpolation that causes some fluctuations of the mirrors surfaces. A merit figure proportional to the SNR can be evaluated according to the formula

$$M = \sqrt{\frac{P_{\rm ic1}\, P_{\rm ic2}}{P_{\rm rec}}}$$

where $P_{\rm ic1}$ (resp. $P_{\rm ic2}$) is the power in cavity #1 (resp. # 2), and $P_{\rm rec}$ the power in the recycling cavity. It is known (Chapter I) that the signal to noise ratio of a recycled Michelson with FP cavities is

- proportional to the finesse of the two cavities. The finesse of a cavity can be estimated by
$$\mathcal{F} \;=\; \frac{\pi}{2}\,\frac{P_{\rm ic}}{P_{\rm in}}$$
where $P_{\rm in}$ is the incoming power. We have here $P_{\rm in} \sim P_{\rm rec}/2$, so that, for our two cavities:
$$\mathcal{F}_{1,2} \;=\; \pi\,\frac{P_{\rm ic1,2}}{P_{\rm rec}}$$
The two cavities having in general different finesses, we take the geometric average, so that:
$$\mathcal{F} \;=\; \pi\,\sqrt{\frac{P_{\rm ic1}\,P_{\rm ic2}}{P_{\rm rec}^2}}$$
- also proportional to the square root of the power stored in the recycling cavity,

This explains the structure of the merit factor. Its optimum value corresponds to a recycling surtension of 50 and cavity finesses of 50. For 1 W laser power, this is $P_{\rm rec} = 50$ W, so that the power entering the cavities is $P_{\rm in} = 25$ W, and the intracavity power $P_{ic} = 25{\rm W} \times 2 \times 50/\pi = 795.8$ W. The maximum merit factor is therefore

$$M_{\rm max} = 795.8/\sqrt{50} = 112.54\,{\rm W}^{1/2}$$

The quantity plotted on Fig.3.13 (red squares) is $M/M_{\rm max} \equiv {\rm SNR}/{\rm SNR}_{\rm max}$

Because the mirrors have not exactly the same curvature radii, the question of the mode to be injected in the interferometer could be raised. It seems reasonable to choose a waist such that the curvature radius of the wavefront matches the averaged curvature radius of the two mirrors, i.e. 3604 m. In Fig.3.14 we have varied the input waist and computed the corresponding merit factor. In Fig.3.14,

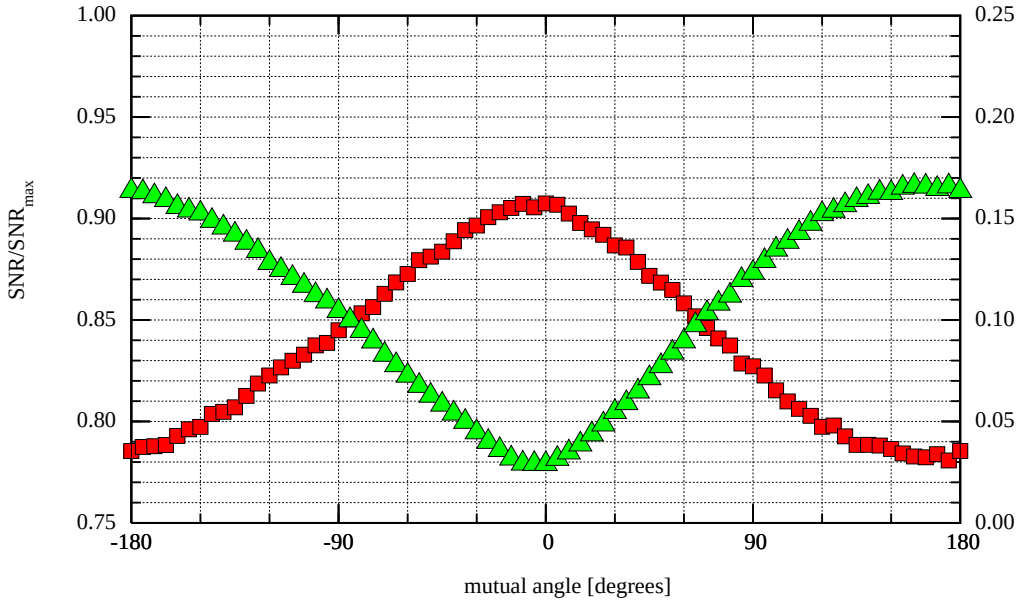

Figure 3.13: SNR vs mutual angle of end mirrors (red squares), relative power on the dark fringe (green triangles)

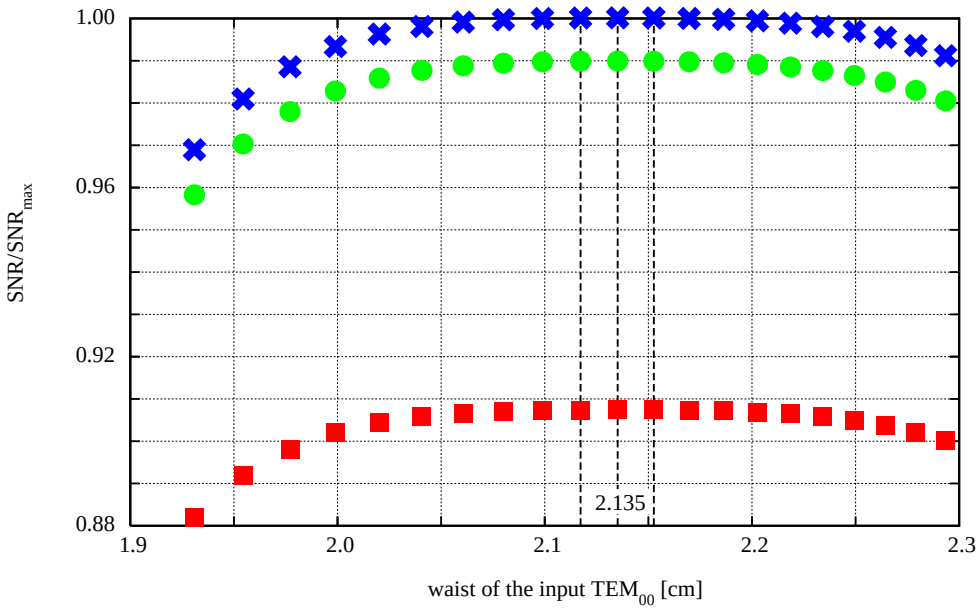

Figure 3.14: SNR vs waist of input mode

the red sqares correspond to the actual SMA mirrors in the nominal reciprocal attitude (marks up). The green disks correspond to the same situation (different curvature radii) but with zero residual roughness. The blue crosses correspond to two identical mirrors without roughness, of same curvature radius 3604 m. In all cases, mirrors have a finite size (35 cm diameter). The computation grid was a 1m side square, giving 256×256 samples. The three dotted vertical lines correspond to values of w_0 such that the wavefront has respectively 3854m, 3604m, 3624m curvature radius. Finally, in the best situation, the dark fringe has the following pattern (see Fig.3.15):

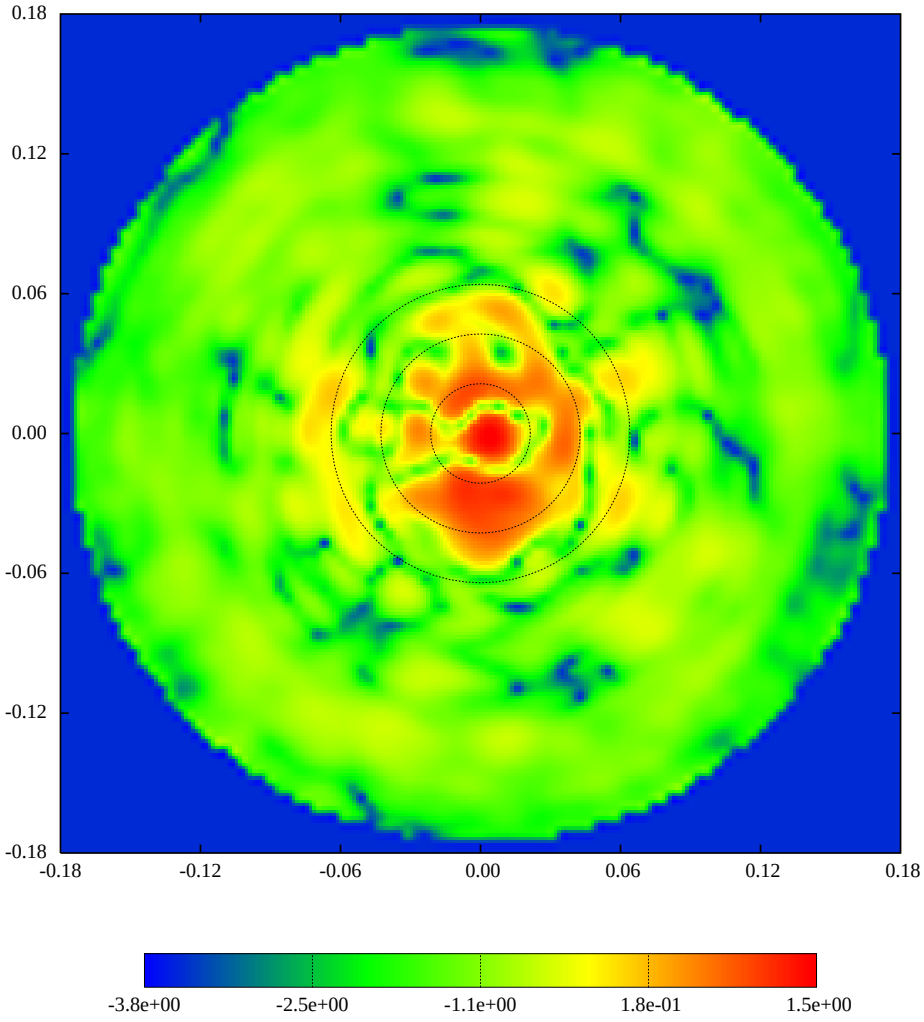

Figure 3.15: darkest fringe: intensity pattern (logarithmic plot)

The three black circles have diameters respectively $w_0 = 2.135$ cm, $2w_0$ and $3w_0$, where w_0 is the waist (gaussian radius of the spot on the mirror).

3.1.6 On the intrinsic limitation to basic DFT-based algorithms

When chosing the spatial window and the rank of the transform, special care must be taken of the angular limitation induced by the finite sampling of optical amplitudes. We know that the maximum spatial frequency, for the rank N and the window F is

$$p_{\max} = \frac{N\pi}{F}$$

This is a limitation on the structure of the admissible optical amplitudes: if their variations are of scale shorter than $\Lambda_{\min} \equiv 2\pi/p_{\max} = 2F/N$, corresponding to the Shannon frequency, aliasing will follow, and the algorithm fails. The Fourier variable p being interpreted as a transverse component of an oblique wave vector, we can set $p_{\max} \equiv k\theta_{\max}$ where θ represents the propagation direction with respect to the main optical axis. We can thus write:

$$\theta_{\max} = \frac{N\lambda}{2F} = \frac{\lambda}{2D}$$

D being the size of the sampling interval. This means that larger divergences are forbidden. For a gaussian beam of amplitude

$$f(r) = \exp\left[-r^2/w_0^2\right]$$

having a Fourier transform given by

$$\tilde{f}(\rho) = \frac{\pi}{w_0}\exp\left[-\rho^2 w_0^2/4\right]$$

with $\rho^2 = p^2 + q^2$, by substituting $\rho = k\theta$, we get

$$\tilde{f}(\theta) = \frac{\pi}{w_0}\exp\left[-\theta^2 / \theta_g^2\right]$$

where $\theta_g \equiv \lambda/\pi w_0$ is the gaussian divergence angle of the beam. The spectrum becomes negligible for $\theta_0 = \sigma \times \theta_g$ where σ of the order of 3 or 4. Owing to the condition $\theta_0 < \theta_{\max}$, we get the condition

$$D < \frac{\pi w_0}{2\sigma}$$

On the other hand, the window must be significantly larger than w_0, say $F > \sigma\ w_0$, so that we get the new limitation

$$D\ >\ \frac{\sigma w_0}{N}$$

The compatibility of these two conditions requires that

$$N\ >\ \frac{2\sigma^2}{\pi}$$

which is easily met. However, we would have serious troubles if after diffraction, the intensity distribution were out of, or larger than the computation window.

3.1.7 Propagation with magnification

If a beam is foreseen as very divergent, it may be difficult to choose a window and a sampling rate adapted to the situation. For intance assume we want to propagate a TEM_{00} mode of waist $w_0\ = 5$ mm, over a distance of $L =$ 3 km (the wavelength is about 1 μm). The beam width after diffraction on the distance L is $w_1\ \sim 203$ mm. If we decide to take a common square computation window at both ends of the path, we see that is must be much larger than w_1, say $F \sim 10 \times\ w_1\ \sim 2$m. This implies that the maximum spatial frequency is

$$p_{\max} = \frac{2\pi}{F} \times \frac{N}{2}$$

where N is the sampling rate. Now, the Fourier transform of the input beam is

$$\tilde{\phi}(p,q) = \sqrt{2\pi w_0^2}\exp\left[-(p^2+q^2)w_0^2/4\right]$$

so that the maximum frequency can be estimated at about

$$p_{\max} = 5/w_0\ =\ 10^3\ \mathrm{m}^{-1}$$

by comparing with th epreceding expression of $p_{\max}$, we get

$$N \sim 640$$

which is very demanding in terms of memory and cpu time. Moreover, in the initial window, the wavefront is certainly undersampled, and the preceding

rough estimation based on a pure TEM is still optimistic for a distorted wavefront. It is therefore sometimes mandatory to use a modified paraxial algorithm based on a function and coordinates transform. Let us return to the paraxial diffraction equation:

$$(2ik\partial_z + \Delta_T)\,\Psi \;=\; 0$$

where $\Psi(x,y,z)$ is the unknown wave function, and $\Delta_T \;\equiv\; \partial_x^2 + \partial_y^2$. After an idea proposed by Sziklas and Siegman ([13]), consider a new wave function $F(x,y,z)$ defined by

$$\Psi(x,y,z) \;=\; \frac{1}{z}\;\exp\left[ikr^2/2z\right]\;\;F(x,y,z)$$

F obeys the following partial differential equation:

$$\left[2ik\partial_z + \Delta_T + \frac{2ik}{z}\,(x\partial_x + y\partial_y)\right]\;\;F \;=\; 0$$

If now we introduce the new coordinates:

$$x' = \frac{\alpha x}{z} \tag{3.8}$$

$$y' = \frac{\alpha y}{z} \tag{3.9}$$

$$z' = \alpha^2\left[\frac{1}{z_0} - \frac{1}{z}\right] \tag{3.10}$$

where α and z_0 are arbitrary constants, it is easily seen that the diffraction equation becomes

$$(2ik\partial_{z'} + \Delta'_T)\;\;F \;=\; 0$$

in other words, the paraxial diffraction equation is invariant under the combined transformation of function and coordinates. We can exploit this fact, in the case of strong focusing or defocusing to remove the convergent or divergent part of the field. Consider a freely diffracting wave which has a beam width w_0 at $z = 0$, and a beam width w_1 at $z = L$ (see Fig.3.16), we may choose the constants α and z_0 in such a way that the change of coordinates follows the transverse extension of the field, namely take $\alpha = z_0$ and

$$\frac{z_0 + L}{z_0} \;=\; \frac{w_1}{w_0}$$

this determines z_0:

$$z_0 \;=\; \frac{L}{w_1/w_0 - 1}$$

the new coordinates are now

$$x' = \frac{z_0}{z}\, x \tag{3.11}$$

$$y' = \frac{z_0}{z}\, y \tag{3.12}$$

$$z' = z_0 - \frac{z_0^2}{z} \tag{3.13}$$

so that the initial plane is located at $z = z_0$ where

$$z_0' = 0, \quad x_0' = x, \quad y_0' = y$$

and the final plane at $z = z_0 + L$, where

$$z_1' = \frac{w_0}{w_1}\, L, \quad x_1' = \frac{w_0}{w_1}\, x, \quad x_1' = \frac{w_0}{w_1}\, y$$

Consequently, the coordinate change is smooth on the initial plane; in other words, the initial data may be given in the initial coordinates. The procedure for numerical propagation is therefore the following:

- The initial wave function $\Psi_0(x, y, z)$ is given, and the propagation step L is fixed.
- On computes the magnification factor w_1/w_0 for the propagation step (this can be estimated by analogy with a gaussian beam).
- One changes of wave function by the formula

  $$F_0 \;=\; \exp\left[-ikr^2/2z_0\right]\; \Psi_0$$

  where $z_0 \equiv L/(w_1/w_0 - 1)$.
- one chooses the window appropriate for F_0, and propagates the field using the propagator

  $$P_L \;=\; \exp\left[-i\,\frac{(p^2+q^2)\Delta z'}{2k}\right]$$

  where $\Delta z' \equiv w_0 L/w_1$.

- get the propagated wavefunction $F_1(x', y')$, and return to the true wave function by

$$\Psi_1(x', y') = \frac{z_0}{z_0 + L} \exp\left[ikr^2/2(z_0 + L)\right] = \frac{w_0}{w_1} \exp\left[ik\frac{r'^2(z_0 + L)}{2z_0^2}\right] F_1(x', y')$$

  be aware that the transverse coordinates are now rescaled according to the magnification factor.

It may be very instructive to examine step by step what happens to a pure TEM_{00} (an analytic calculation is possible) when treated this way. The initial wave function is:

$$\Psi_0(x, y) = \mathrm{e}^{-r^2/w_0^2}$$

z_0 being computed, we obtained the corrected wave function

$$F_0(x, y) = \mathrm{e}^{-r^2/w_0^2}\, \mathrm{e}^{-ikr^2/2z_0} = \exp\left[-\frac{r^2}{w_0^2}\left(1 + i\,\frac{b}{z_0}\right)\right]$$

where $b \equiv \pi w_0^2/\lambda$. The Fourier transform is:

$$\widetilde{F_0}(p, q) = \frac{\lambda b}{1 + ib/z_0} \exp\left[-\frac{w_0^2(p^2 + q^2)}{4(1 + ib/z_0)}\right]$$

we obtain the propagated wave in the Fourier space by

$$\widetilde{F_1} = P(\Delta z') \times \widetilde{F_0}$$

where $(\Delta z' \equiv Lz_0/(z_0 + L))$:

$$P(\Delta z') = \exp\left[-\,i\,\frac{w_0^2(p^2 + q^2)\Delta z'}{4b}\right]$$

we find, after a reciprocal Fourier transform:

$$F_1(x', y') = \frac{1}{1 + i\Delta z'(1 + ib/z_0)/b} \exp\left[-\,\frac{r'2}{w_0^2}\,\frac{b(1 + ib/z_0)}{b + i\Delta z'(1 + ib/z_0)}\right]$$

the propagated function is thus

$$\Psi_1(x', y') = \frac{z_0}{z_0 + L}\,\frac{1}{1 + i\Delta z'(1 + ib/z_0)/b} \times$$

$$\times \ \exp\left\{ -\ \frac{r'2}{w_0^2}\left[\frac{b(1+ib/z_0)}{b+i\Delta z'(1+ib/z_0)} - i\frac{b(z_0+L)}{z_0^2}\right]\right\}$$

or as well

$$\Psi_1(x',y') \ = \ \frac{1}{1+iL/b}\ \exp\left[-\ \frac{r'2}{w_0^2}\ w_1^2 w_0^2\ \frac{1}{1+iL/b}\right]$$

$$= \ \frac{w_0}{w_1}\ \exp\left[-i\ \mathrm{atan}(L/b) - \frac{r^2}{w_1^2}\ + ik\,\frac{r^2}{2R}\right]$$

with $R \equiv L(1+b^2/L^2)$, which is the classical result (see a preceding section) of gaussian optics. It is thus checked that the preceding method gives the same result as the direct calculation giving directly Ψ_1 from Ψ_0. This result is not very interesting by itself, but the detailed calculation allows to understand how the new algorithm maps a diverging beam onto a collimated one. Let us examine the nature of the corrected waves F_0 and F_1 used as intermediary data. We have firstly

$$\Psi_0 = \mathrm{e}^{-r^2/w_0^2}$$

we know from the theory of gaussian beams that

$$w_1 \ = \ w_0\sqrt{1+L^2/b^2} \ = \ w_0\sqrt{1+\zeta^2}$$

($\zeta \equiv L/b$); consequently,

$$z_0 = L/(\sqrt{1+\zeta^2}-1)$$

the corrected function is then:

$$F_0 \ = \ \exp\left\{-\ \frac{r^2}{w_0^2}\ \left[1+i\,\frac{\sqrt{1+\zeta^2}-1}{\zeta}\right]\right\}$$

the propagator may be written as:

$$P(p,q) \ = \ \exp\left[-\ i\ \frac{w_0^2(p^2+q^2)}{4}\ \frac{\zeta}{\sqrt{1+\zeta^2}}\right]$$

by taking the Fourier transform of F_0, multiplying by P and applying a reciprocal Fourier transform, gives the propagated corrected wave function as:

$$F_1(x',y') \ = \ \exp\left\{-\ \frac{r'^2}{w_0^2}\ \left[1-i\,\frac{\sqrt{1+\zeta^2}-1}{\zeta}\right]\right\}$$

where we see that the new wave has the same width w_0 and an opposite radius of curvature. The initial wave has been transformed into a collimated wave propagating without magnification between z_0 and $z_0 + L$. The diverging behavior of the wave is recovered through the homothetic transformation of coordinates at the end.

3.1.8 Off-axis propagation

When the incidence angle is not zero, the Fourier transform of the incoming amplitude may exceed the limits of the Fourier window, although the behavior of the field is quite reasonable. It is possible to suppress this effect simply by translating the Fourier transform. Assume the incidence angles are (θ, ϕ) and set $p_0 \equiv k\theta\cos\phi, \quad q_0 \equiv k\theta\sin\phi$. If the incoming amplitude is denoted by $\Psi_1(x, y)$, it is likely that its Fourier trnasform is peaked at (p_0, q_0) and possibly out of the Fourier window. Let us define a *corrected* field by

$$F_1(x, y) \;=\; \Psi_1(x, y) \;\times\; \mathrm{e}^{-ip_0 x}\,\mathrm{e}^{-iq_0 y}$$

the desired effect follows immediately:

$$\tilde{F}_1(p, q) \;=\; \tilde{\Psi}_1(p - p_0, q - q_0)$$

showing that the FT has been translated in the Fourier plane to reach a central position. Now, we can propagate the corrected field over a distance L. If the propagated field is Ψ_2 and the corrected propagated field F_2, we can write:

$$\tilde{F}_2(p, q) \;=\; \exp\left[ikL - i\frac{L}{2k}(p^2 + q^2)\right]\;\tilde{\Psi}_1(p - p_0, q - q_0)$$

and by taking the reciprocal transform:

$$F_2(x, y) \;=\; \mathrm{e}^{ikL}\;\frac{1}{4\pi^2}\;\int dp\,dq\,\mathrm{e}^{-iL(p^2+q^2)/2k}\;\tilde{\Psi}_1(p - p_0, q - q_0)$$

$$=\; \mathrm{e}^{ikL}\mathrm{e}^{-ip_0 x - iq_0 y}\frac{1}{4\pi^2}\;\int dp\,dq\,\mathrm{e}^{-iL[(p+p_0)^2+(q+q_0)^2]/2k}\;\tilde{\Psi}_1(p, q)$$

$$=\; \exp\left[ikL\left(1 - \frac{p_0^2 + q_0^2}{2k^2}\right)\right]\;\mathrm{e}^{-ip_0 x - iq_0 y}\;\mathrm{e}^{-ikL}\Psi_2(x + Lp_0/k, y + Lq_0/k)$$

the factor of $\exp(-ikL)$ comes from the fact that our definition of Ψ_2 (the propagated field) implicitly includes a pure propagation phase of $\exp(ikL)$. by returning to the incidence angles, we get

$$F_2(x,y) \;=\; \mathrm{e}^{ikL(1-\theta^2/2)}\,\mathrm{e}^{-ikx\theta\cos\phi}\,\mathrm{e}^{-iky\theta\sin\phi}\;\left[\mathrm{e}^{-ikL}\times\Psi_2(x+\theta L\cos\phi, y+\theta L\sin\phi)\right]$$

where we have put into evidence the following facts:

- the propagated wave function has been translated, so that the field is expressed in the new cordinates

  $$x' = x+\theta L\cos\phi, \quad y' = y+\theta L\sin\phi$$

  so as to follow the angular direction of the beam, and keep the amplitude map at the center of the window,

- the angular direction of the beam is preserved

- the pure propagation phase is

  $$kL(1-\theta^2/2) \quad \text{instead of} \quad kL$$

  this accounts for the removed obliquity that introduces a factor of $\cos\theta$ which can be easily corrected if necessary.

The situation is summarized on Fig.3.17

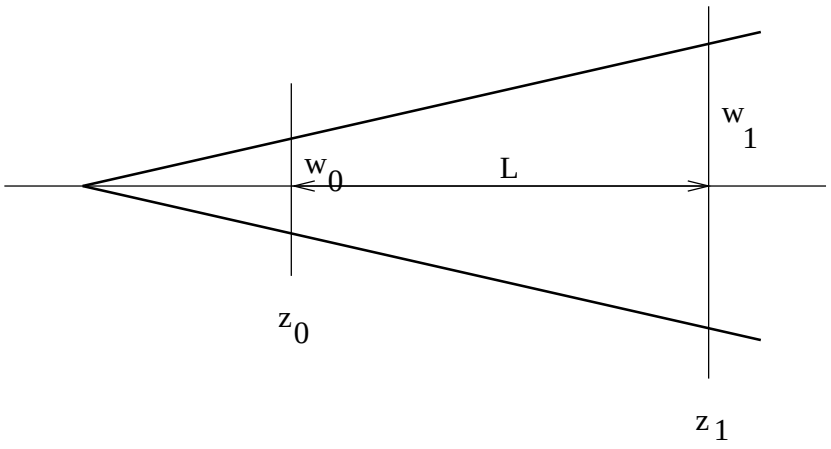

Figure 3.16: Beam divergence

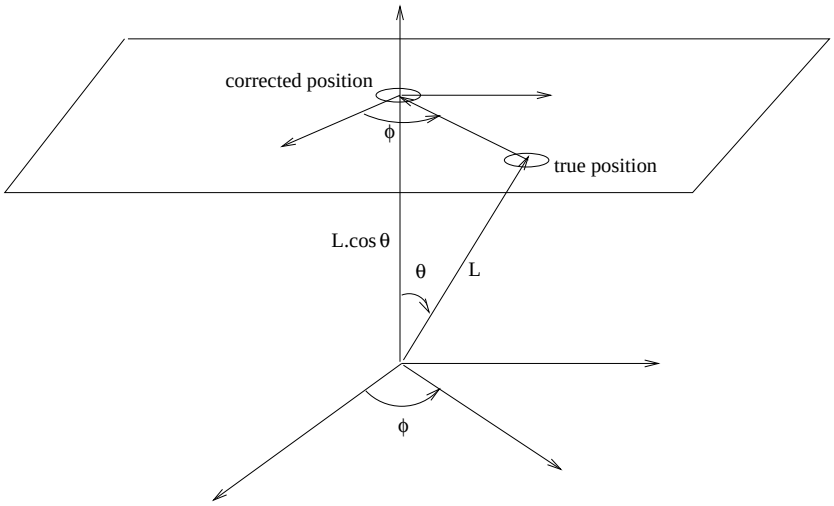

Figure 3.17: Corrected off-axis propagation

3.2 Hankel transform methods

The preceding numerical methods were designed to study situations having no symmetry. In certain cases, we may assume the optical elements and the optical field itself having the axial symmetry. This happens namely in the case of thermally induced distortions caused by the beam. We can neglect the beam's imperfections, and assume a pure TEM_{00} mode as the source of heat, owing to what, almost all distortions will keep axial symmetry. In such cases, we can take benefit of the symmetry and reduce the computational demands by specifying explicitly the symmetry in the calculations. In the case of the Fourier transform approach, this results in the Hankel transform.

3.2.1 Theory

The 2D Fourier Transform of a function $f(x, y)$ is

$$\tilde{f}(p, q) \;=\; \int_{\mathbf{R}} \mathrm{e}^{ipx}\mathrm{e}^{iqy} f(x, y)\, dx\, dy$$

In order to have polar coordinates both in the direct and in the Fourier space, we define (r, ϕ) and (ρ, ψ) by:

$$\begin{aligned} x &= r\cos\phi, \;\; y \;=\; r\sin\phi \\ p &= \rho\cos\psi, \;\; q \;=\; \rho\sin\psi \end{aligned}$$

the transform is now:

$$\tilde{f}(\rho, \psi) \;=\; \int_0^{2\pi} d\phi \int_0^{\infty} r\; dr\; \mathrm{e}^{i\rho r\cos(\phi-\psi)}\; f(r, \phi)$$

If the initial function f is axially symmetrical, i.e. independent of ϕ, then its transform $\tilde{f}$ is also axially symmetrical in the Fourier space, the ϕ integration can be carried out, and we obtain:

$$\tilde{f}(\rho) \;=\; 2\pi \int_0^{\infty} J_0(\rho r)\; f(r)\; r\; dr$$

Integrals of this type, involving a Bessel function, are called Hankel transforms. The inverse Fourier transform reads

$$\tilde{f}(r) \;=\; \frac{1}{2\pi} \int_0^{\infty} J_0(\rho r)\; \tilde{f}(\rho)\; \rho\; d\rho$$

It is cumbersome to keep these factors of 2π throughout all foregoing calculations. It is much more convenient to use here a different convention in the definition of the Fourier Transform:

$$\tilde{f}(p) \;=\; \frac{1}{\sqrt{2\pi}} \int_{-\infty}^{\infty} \mathrm{e}^{ipx} f(x)\; dx \tag{3.14}$$

In this case, the 2D Fourier transform of $f(r)$ is simply the Hankel transform:

$$\tilde{f}(\rho) \;=\; \int_0^{\infty} J_0(\rho r)\; f(r)\; r\; dr \tag{3.15}$$

and its inverse is

$$f(r) \;=\; \int_0^{\infty} J_0(\rho r)\; \tilde{f}(\rho)\; \rho\; d\rho \tag{3.16}$$

We are dealing with special physical solutions of the wave equation, i.e. amplitudes of finite spatial extension (or almost), such as gaussian waves, which are practically zero for $x^2 + y^2 > 10w_0^2$, and of finite extension in the Fourier space (again gaussian waves). There exists a circle of radius a outside of which the amplitude is negligible, and there exists a circle of radius b in the Fourier plane outside of which the Fourier transform of the amplitudes is negligible. It is well known that there exists a family of orthogonal functions on the disk $\mathcal{D}_a \;\equiv\; \{r < a\}$, i.e. the functions

$$\varphi_\beta(r) \;=\; J_0(\zeta_\beta r/a), \quad \beta = 1, 2, \ldots, \infty$$

where the $\zeta_\beta, \quad \beta = 1, 2, \cdots, \infty$ are the zeros of $J_1(z)$. The orthogonality relation is:

$$\int_0^a \varphi_\beta(r)\; \varphi_\alpha(r)\; r\; dr \;=\; \frac{a^2}{2} J_0^2(\zeta_\alpha)\; \delta_{\alpha\beta} \tag{3.17}$$

Let us note

$$p_\alpha \;=\; \frac{a^2}{2} J_0^2(\zeta_\alpha)$$

Obviously, if $\mathcal{D}_b \;\equiv\; \{\rho < b\}$ is the disk in the Fourier space, it admits a corresponding family of functions:

$$\psi_\beta(\rho) \;=\; J_0(\zeta_\beta \rho/b), \quad \beta = 0, 1, \ldots, \infty$$

with the notation

$$q_\alpha \;=\; \frac{b^2}{2} J_0^2(\zeta_\alpha)$$

we have the orthogonality relation:

$$\int_0^b \psi_\beta(\rho)\ \psi_\alpha(\rho)\ \rho\ d\rho \;=\; q_\alpha\ \delta_{\alpha\beta} \tag{3.18}$$

We call B_a the set of all functions of r negligible outside $\mathcal{D}_a$, and B_b the set of functions of ρ negligible outside $\mathcal{D}_b$. We can assume in the formulas of the Hankel Transform (3.15,3.16), that $\tilde{f} \;\in\; B_b$, and expand it on the basis. Such an expansion is called Dini expansion:

$$\tilde{f}(\rho) \;=\; \sum_{\beta=0}^{\infty} f'_\beta \psi_\beta(\rho) \;=\; \sum_{\beta=0}^{\infty} f'_\beta\ J_0(\zeta_\beta \rho/b)$$

by substituting in (3.16) we get:

$$f(r) \;=\; \sum_{\beta=0}^{\infty} f'_\beta\ \int_0^{\infty} J_0(\rho r)\ J_0(\zeta_\beta \rho/b)\ \rho\ d\rho$$

We can sample the values of $f(r)$ by choosing an elementary distance in the plane. It is convenient to take $\delta r \;=\; 1/b$ as the distance element and sample the radii according to

$$r_\alpha \;=\; \zeta_\alpha / b$$

so that there is a strong link between the coefficients f'_β introduced in the Dini expansion of $\tilde{f}$ and the samples $f(r_\alpha)$:

$$f_\alpha \;\equiv\; f(r_\alpha) \;=\; \sum_{\beta=0}^{\infty} f'_\beta\ \int_0^b J_0(\rho\zeta_\alpha/b)\ J_0(\zeta_\beta\rho/b)\ \rho\ d\rho$$

Remark that the transform integral stops to b instead of ∞ because we know that the function $\tilde{f}(\rho)$ is zero outside $\mathcal{D}_b$. Owing to the orthogonality relation gives:

$$f'_\alpha \;=\; \frac{f_\alpha}{q_\alpha}$$

by substituting in the expansion of $\tilde{f}$ we get:

$$\tilde{f}(\rho) \;=\; \sum_{\beta=0}^{\infty} \frac{f_\beta \; J_0(\zeta_\beta \rho/b)}{q_\beta}$$

We can now also sample the values of $\tilde{f}(\rho)$ by chosing the elementary frequency as $\delta\rho \;=\; 1/a$, and the spectrum samples will be evaluated at $\rho_\alpha \;=\; \zeta_\alpha/a$. The preceding expression, after sampling becomes:

$$\tilde{f}_\alpha \;\equiv\; \tilde{f}(\rho_\alpha) \;=\; \sum_{\beta=0}^{\infty} \frac{1}{q_\alpha} \; f_\alpha \; J_0(\zeta_\beta \zeta_\alpha/ab)$$

This is the discrete expression of the Hankel Transform, a linear relation between the vector $\tilde{f}_\alpha$ and the vector f_α:

$$\tilde{f}_\alpha \;=\; \sum_{\beta=0}^{\infty} H^{(+)}_{\alpha\beta} \; f_\beta$$

The direct transform is thus represented by the matrix

$$H^{(+)}_{\alpha\beta} \;=\; \frac{2J_0(\zeta_\alpha \zeta_\beta/ab)}{b^2 J_0^2(\zeta_\beta)} \tag{3.19}$$

Obviously, a similar treatment can be carried out for the inverse transform. The previously introduced function $f \;\in\; \mathcal{D}_a$ admits a Dini expansion of the form

$$f(r) \;=\; \sum_{\beta=0}^{\infty} \tilde{f}'_\beta \; J_0(\zeta_\beta \; r/a)$$

so that the expression (3.15) of the continuous direct Hankel Transform becomes:

$$\tilde{f}(\rho) \;=\; \sum_{\beta=0}^{\infty} \tilde{f}'_\beta \; \int_0^a J_0(\rho r) \; J_0(\zeta_\beta \; r/a) \; r \; dr$$

Now, in the Fourier plane, we can sample the conjugated variable ρ according to $\rho_\alpha = \zeta_\alpha/a$, so that we have the discrete version:

$$\tilde{f}_\alpha \;\equiv\; \tilde{f}(\rho_\alpha) \;=\; \sum_{\beta=0}^{\infty} \tilde{f}'_\beta \; \int_0^a J_0(\zeta_\alpha \; r/a) J_0(\zeta_\beta \; r/a) \; r \; dr$$

from the orthogonality relation we obtain:

$$\tilde{f}'_\alpha \;=\; \frac{\tilde{f}_\alpha}{p_\alpha}$$

the Dini expansion of $f(r)$ is now determined, and we have:

$$f(r) \;=\; \sum_{\beta=0}^{\infty} \frac{1}{p_\beta} \tilde{f}_\beta \; J_0(\zeta_\beta \; r/a)$$

Sampling of the values of f according to $r_\alpha \;=\; \zeta_\alpha / b$ leads to the inverse Hankel Transform:

$$f_\alpha \;=\; \sum_{\beta=0}^{\infty} H^{(-)}_{\alpha\beta} \; \tilde{f}_\beta$$

with

$$H^{(-)}_{\alpha\beta} \;=\; \frac{2 J_0(\zeta_\alpha \zeta_\beta / ab)}{a^2 J_0^2(\zeta_\beta)} \tag{3.20}$$

The fact that the studied function f is in the set B_a implies that it takes negligible values for $r > a$. The sampling r_α can therefore stop at $r = a$, and we have:

$$\zeta_\alpha \; / b \;\leq\; a \;\Rightarrow\; \zeta_\alpha \;<\; ab$$

The same result is obviously obtained by considering the Fourier space. If the transformed function $\tilde{f}$ takes negligible values for $\rho > b$, then the sampling of ρ must stop at b:

$$\zeta_\alpha \; / a \;\leq\; b \;\Rightarrow\; \zeta_\alpha \;<\; ab$$

We can freely decide the size of the computation window a. Then we can still freely decide the maximum number N of zeros we shall take into account in the infinite sums encountered in the expressions of the Discrete Hankel Transformn (DHT). This being done, we have

$$\alpha \;=\; 0, 1, 2, \ldots, N$$

$$ab \;=\; \zeta_N \;\Rightarrow\; b \;=\; \zeta_N / a$$

The radial sampling is thus:

$$r_\alpha \;=\; a\,\zeta_\alpha/\zeta_N$$

and the spatial frequency sampling:

$$\rho_\alpha \;=\; \zeta_\alpha/a$$

The expressions for the Transforms (FDHT) are finite rank matrix algebra:

$$\tilde{f}_\alpha \;=\; \sum_{\beta=0}^{N} H^{(+)}_{\alpha\beta}\; f_\beta \quad , \quad \alpha \;=\; 0,1,2,\ldots,N$$

with $H^{(\pm)}_{\alpha\beta}$ having the following definitions:

$$H^{(+)}_{\alpha\beta} \;=\; \frac{2a^2 J_0(\zeta_\alpha\zeta_\beta/\zeta_{\rm N})}{\zeta^2_{\rm N} J^2_0(\zeta_\beta)} \tag{3.21}$$

$$H^{(-)}_{\alpha\beta} \;=\; \frac{2J_0(\zeta_\alpha\zeta_\beta/\zeta_{\rm N})}{a^2 J^2_0(\zeta_\beta)} \tag{3.22}$$

The Hermitian scalar product of two functions $f(r)\ ,\ g(r)$ is defined in the direct Hilbert space by

$$< f\ ,\ g > = \int_0^\infty f(r)^*\; g(r)\; r\; dr$$

if moreover, $f, g \;\in\; \mathcal{D}_a$, then the integral can be stopped at $r \;=\; a$ and $f\ ,\ g$ may be replaced by their Dini expansions on the φ_α, so that, using the orthogonality,

$$< f\ ,\ g > = \sum_\alpha \tilde{f'}^*_\alpha\; \tilde{g'}_\alpha\; p_\alpha$$

or,

$$< f\ ,\ g > = \sum_\alpha \tilde{f}^*_\alpha\; \tilde{g}_\alpha\; /p_\alpha$$

The Hermitian scalar product is invariant by a Fourier Transform, so that we have as well:

$$< f\ ,\ g > = < \tilde{f}\ ,\ \tilde{g} >$$

it is easily seen that

$$< \tilde{f}\ ,\ \tilde{g} > = \sum_\alpha {f^*}_\alpha g_\alpha/q_\alpha$$

these formula provide the way of computing the scalar product either in the spatial or in the frequency space. The power carried by a given amplitude f is now

$$P(f) \ = < f \ , \ f >$$

and we have a distance in the Hilbert space, defined for two functions f, g by

$$\mathrm{d}(f,g) \ = \ \sqrt{P(f-g)}$$

3.2.2 Numerical implementation

If efficient FFT routines are available in all mathematical computer libraries, this is not the same for DHT, this is the reason why we give here the basic ideas for building specific libraries. All preceding formulas deal with the two numerical tables of the zeros of J_1 (including 0), ζ_α and $J_0(\zeta_\alpha)$. It is easy to obtain the table ζ_α by the following scheme. An initial guess of ζ being given, a better estimate is found by the Newton formula:

$$\zeta_{new} \ = \ \zeta_{old} \ - \frac{J_1(\zeta_{old})}{J_1'(\zeta_{old})}$$

which can be iterated until a given accuracy is met. Now, using the well known relation

$$J_1'(z) \ = \ J_0(z) \ - \ \frac{1}{z} \ J_1(z)$$

this is

$$\zeta_{new} \ = \ \zeta_{old} \ \left[1 \ - \ \frac{J_1(\zeta_{old})/J_0(\zeta_{old})}{\zeta_{old} \ - \ J_1(\zeta_{old})/J_0(\zeta_{old})} \right]$$

The problem reduces to the calculation of $J_1(z)/J_0(z)$. This can be done using a well known algorithm based on the recursion formula for Bessel functions, namely

$$J_n(z) \ = \ \frac{2(n+1)}{z} \ J_{n+1} \ - \ J_{n+2}$$

The recursion begins by taking arbitrarily $J_M = 0$ and $J_{M-1} = 1$, and then descending to J_1 and finally J_0 by the preceding formula. M must be chosen sufficiently large depending on the argument. If during the recursion the J_n's become to large, leading to a possible overflow, all the terms of the recursion can be divided by a common arbitrary renormalization constant. Finally, the ratio of the two last terms gives the value of $J_1(z)/J_0(z)$. The calculation

of $J_0(z)$ is identical, except that the last term of the recursion gives $J_0(z)$ only after normalization. This normalization is done using the well known relation

$$1 \;=\; J_0(z) \;+\; 2\sum_{n=1}^{\infty} J_{2n}(z)$$

Finally, the determination of all $\{\zeta_\alpha \;;\; \alpha \;=\; 0, 1, \ldots, N\}$ is done by taking the first ones from any mathematical handbook:

$$\zeta_0 \;=\; 0 \;,\; \zeta_1 \;=\; 3.83 \;,\; \zeta_2 \;=\; 7.02$$

(values already encountered in the diffraction problem for a uniform circular aperture) as initial guesses for initializing the Newton refinement process. Then for all higher indices, the initial guess for ζ_α is $\zeta_{\alpha-1} + \pi$. One can easily imagine routines providing at the same time the two families ζ_α and $J_0(\zeta_\alpha)$.

The question "is the inverse HT actually the algebraic inverse of the direct HT ?" must be considered, because it is not manifest that

$$\sum_{\sigma=0}^{N} H^{(\pm)}_{\alpha\sigma} H^{(\mp)}_{\sigma\beta} \;=\; \delta_{\alpha\beta} \;(?)$$

In fact this is not true. What is true is that the linear operator $H^{(-)}\, H^{(+)}$ is a projector on B_a , and $H^{(+)}\, H^{(-)}$ a projector on B_b, for N infinite. Practically, this means that for a given function f negligible outside $\mathcal{D}_a$, and for N large enough, we have

$$f_\alpha \;\simeq\; \sum_{\beta=0}^{N} \sum_{\sigma=0}^{N} H^{(-)}_{\alpha\sigma} H^{(+)}_{\sigma\beta}\; f_\beta$$

and the corresponding formula in the Fourier space, with an accuracy depending on the window size a and the rank N. To be more specific, it is possible to reach the limit accuracy of the computer ($\simeq 10^{-15}$) in `double` , or `REAL*8` , by suitably chosing the window a. We conclude that the situation is theoretically different from the 2D DFT, in which the product $\mathrm{DFT}^{-1} \times \mathrm{DFT}$ is exactly the unity operator, regardless of the rank of the transform or the window size, but practically, the window being correctly chosen, the numerical accuracy is the same. If we consider a gaussian wave at its waist ($w_0 = 2$ cm) and compare it with its double DHT, we obtain the following results:

Sample size	*Optimal window*	*rms error*
10	8 cm	$5.2\ 10^{-7}$
20	11 cm	$1.8\ 10^{-13}$
50	17 cm	$1.0\ 10^{-15}$

Thus, with N about 50 , there is no significant numerical discrepancy between the DFT and the DHT

The correspondance between an initial field distribution $e_0(r)$ and the field $e_z(r)$ diffracted at a distance z is represented by a matrix that can be computed explicitly. The paraxial propagator, as seen previously, is expressed in the Fourier variables p , q, by

$$\widetilde{G}(p,q,z) \;=\; \exp\left[-\,i\,\frac{z}{2k}\left(p^2\;+\;q^2\right)\right]$$

with $\rho^2 \;=\; p^2 \;+\; q^2$, and using the sampling $\rho_\alpha \;=\; \zeta_\alpha/a$, we have

$$\widetilde{G}_\alpha \;=\; \exp\left[-\,i\,\frac{\lambda z}{4\pi a^2}\,\zeta_\alpha^2\right]$$

The Fourier tranform of the initial field is:

$$\tilde{e}_{1,\alpha} \;=\; \sum_{\beta=0}^{N} H_{\alpha\beta}^{(+)}\;e_{1,\beta}$$

The Fourier Transform of the final field is

$$\tilde{e}_{2,\alpha} \;=\; \widetilde{G}_\alpha \;\times\; \tilde{e}_{1,\alpha}$$

And the final field itself is

$$e_{2,\alpha} \;=\; \sum_{\beta=0}^{N} H_{\alpha\beta}^{(-)}\;\tilde{e}_{2,\beta}$$

All this can be summarized by the simple linear operation

$$e_{2,\alpha} \;=\; \sum_{\beta=0}^{N} P_{\alpha\beta}\;e_{1,\alpha} \tag{3.23}$$

Where the matrix P is:

$$P_{\alpha\beta} = \sum_{\sigma=0}^{N} H^{(-)}_{\alpha\sigma} \, \widetilde{G}_{\sigma} \, H^{(+)}_{\sigma\beta} \tag{3.24}$$

In order to compare with the 2D DFT, we do the same numerical experiment, and we propagate a normalised TEM_{00} from its waist ($w_0 = 2\mathrm{cm}$) over a distance $z = 3\mathrm{km}$. We compare in the following table the numerically propagated wave with the theoretical.

Sample size	*Optimal window*	*rms error*
10	13 cm	$6.3\ 10^{-3}$
20	18 cm	$3.1\ 10^{-5}$
50	29 cm	$9.5\ 10^{-13}$
100	40 cm	$1.8\ 10^{-15}$

The intensity of the field can be represented on a radial plot (see Fig.3.18). The sampling has been represented by small spots. The red profile corresponds to the initial gaussian wave, the blue to the diffracted one.

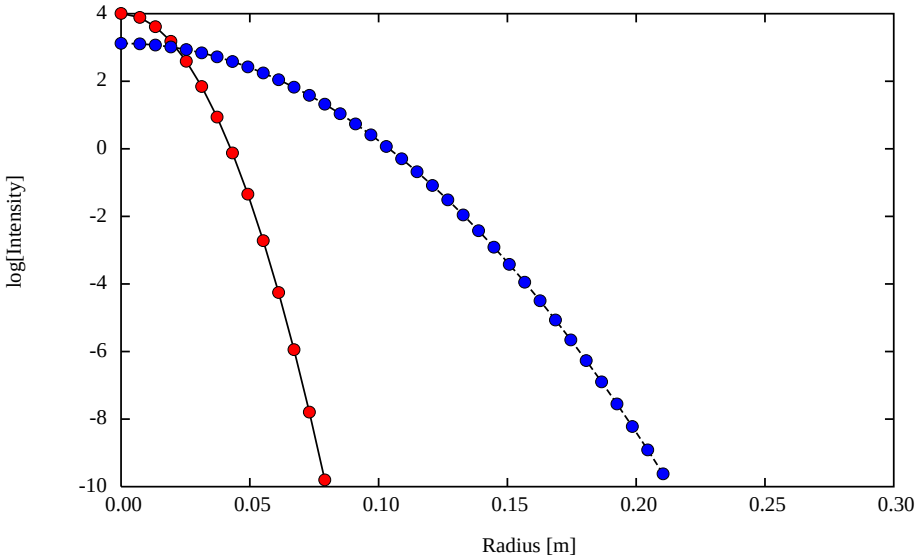

Figure 3.18: Diffraction of a gaussian wave, N=50 samples, window = 30 cm. dots: HT samples, solid line: diffraction theory

The difference between a numerically propagated mode and its exact value is represented on Fig.3.19, the same experiment as reported on the previous Fig.3.4:

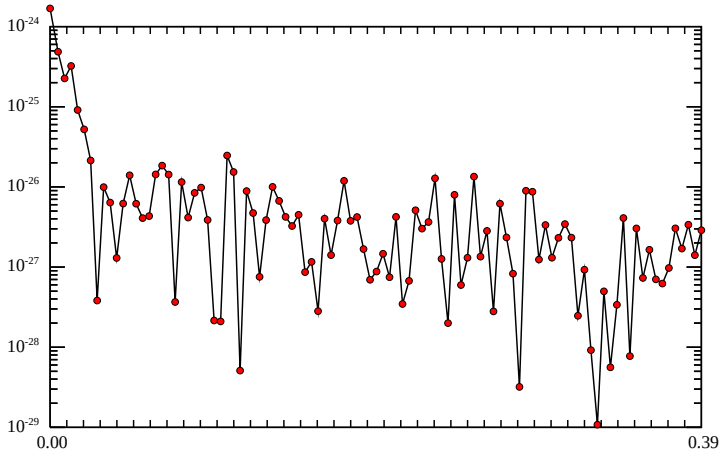

Figure 3.19: Interference fringe between a numerically propagated TEM_{00} and its exact value

The optical system being assumed axially symmetrical, the mirror surfaces are sampled along a radius. A mirror will be defined by the diagonal operator

$$M_\alpha \;=\; i\; r_P \;\exp\left[i\; k\; \frac{a\zeta_\alpha^2}{2R_c\;\zeta_N^2} \;+\; i\; k\; f(a\zeta_\alpha/\zeta_N)\right]$$

where r_P is the photometric reflection coefficient, and R_c the curvature radius. The function $f(r)$ represents possible geometrical defects of the mirror. Action on an optical amplitude, giving $A_{\rm ref}$ from $A_{\rm in}$ is:

$$A_{{\rm ref},\alpha} \;=\; M_\alpha A_{{\rm in},\alpha}$$

It follows that to any optical system involving distances and mirrors (or thin lenses) can be associated a single matrix which represents explicitly the optical transfer function. An example is treated below.

Finding the field stored in a resonant cavity is especially convenient in the DHT scheme because it can be done by one matrix inversion. Recall that if the input amplitude is A, the intracavity field B obeys the implicit equation

$$B \;=\; t_1\; A \;+\; r_1 r_2\; {\rm e}^{i\phi}\,[\; M_1\; P\; M_2\; P\;]\,B$$

where the phase ϕ determines the tuning of the cavity, and P is the diffraction operator described above. Calling $\mathcal{C} \;=\; M_1\; P\; M_2\; P$ the cavity operator, representing the effect of a round trip, we see from the preceding subsection that $\mathcal{C}$ is an explicitly known matrix. The solution of the preceding equation can therefore be found as

$$B \;=\; \left[\mathcal{I} \;-\; r_1 r_2 {\rm e}^{i\phi}\mathcal{C}\right]^{-1}\; t_1 A$$

where $\mathcal{I}$ is the identity matrix. Instead of a series of iterations, as in the DFT scheme, we may now solve the problem by a single $N \times N$ matrix inversion. In case of moderate finesse ($r_1 r_2$ not too close to 1), this is a huge benefit. If the finesse is high, the iteration scheme in the FFT method converges very slowly, but the matrix inversion may become problematic too, due to the very small diagonal elements. An idea of the accuracy of the algorithm can be drawn from the following experiment: We consider a resonant cavity of finesse 50, tuned on the fundamental mode, and we check the relative accuracy on the solution of the implicit cavity equation, i.e:

$$\epsilon \;=\; \|\; B - t_1 A + r_1 r_2 {\rm e}^{i\phi}\mathcal{C}\;\|$$

Sample size	*Optimal window*	*rms error*
20	17 cm	$4.8\ 10^{-5}$
50	29 cm	$1.7\ 10^{-12}$
100	39 cm	$3.0\ 10^{-15}$

For the reflected field, we have

$$A_{\rm ref} \;=\; M_1^\dagger\ A \;+\; t_1\ B$$

so that the reflection off the cavity reduces to a matrix product:

$$A_{\rm ref} \;=\; \Big[M_1^\dagger \;+\; t_1\left(\mathcal{I} \;-\; r_1 r_2 {\rm e}^{i\phi}\mathcal{C}\right)\ t_1\Big]^{-1}\ A$$

3.3 Modal expansion

The principle of a modal expansion is to expand the optical amplitudes on a discrete basis of functions having a known behavior in diffracting. Examples of such functions have been already presented as the Hermite-Gauss (HG) functions and the Laguerre-Gauss (LG) functions respectively. A perfect beam in a perfect cavity would be precisely a HG_{00} or a LG_{00} as well. This suggests that in case of very small perturbations of the system, the actual amplitudes could be described with a small number of HG or LG functions, saving much computational power. A general numerical approach of small perturbations must involve small displacements, including rotations, of the mirrors. In this case, the HG functions are highly recommended, as will be seen, and consequently, will be kept for other perturbations having the axial symmetry, even if this increases the complexity. The ideal field of application of modal expansion is the simulation of the small motions of mirrors in any degree of freedom.

3.3.1 Return to the HG family of modes

The set of Hermite-Gauss functions $\{HG_{mn}(x,y), \quad m,n = 0,1,\ldots,\infty\}$ is a complete set. Thus any optical amplitude admits a unique expansion of the type

$$E(x,y) \;=\; \sum_{m,n} E_{mn}\; HG_{z;m,n}(x,y)$$

This kind of representation has the key advantage that, dealing with its eigenfunctions, the propagation operator has a diagonal matrix representation. In fact, in a perfect system where all mirrors are matched, the propagation problem completely decouples in independent scalar equations, one for each mode. linear coupling of these modes are caused by perturbations of the optical elements. In all what follows, we take the normalized $HG_{m,n}$ functions as the basis. This means that at all optical element, there is a basis of functions

$$\phi_{z;m,n}(x,y) \;=\; c_{mn}\, H_m\left(\sqrt{2}x/w(z)\right) H_n\left(\sqrt{2}y/w(z)\right) \;\times$$

$$\times\; \exp\left[-\frac{x^2+y^2}{w(z)^2}\right] \exp\left[i\,\frac{\pi\,(x^2+y^2)}{\lambda R(z)}\right]$$

having a $w(z)$ parameter equal to what diffraction imposes. The normalisation constant is:

$$c_{mn} \;=\; \sqrt{\frac{2}{\pi w(z)^2}\,\frac{1}{2^{m+n}\,m!\,n!}}$$

In other words, we have one Hilbert space per element, and all these Hilbert spaces are connected by the coordinate z. For instance, at the waist, we have the basis $\phi_{w_0;m,n}(x,y)$, and at the end mirror, at a distance $z=L$, the basis $\phi_{w_1;m,n}(x,y)$, where $w_1 \;=\; w_0\sqrt{1+L^2/b^2}$

The optical elements we shall consider as examples are weak curvature matched mirrors having defects or wrong location. In general, the effect of such a mirror on an incoming wave $E_{mn,\ in}$ will be represented by a matrix operation

$$E_{mn,\mathrm{out}} \;=\; ir\sum_{k,l} R_{mn,kl}\,E_{kl,\mathrm{in}}$$

where r is the photometric coefficient, and where the coefficients $R_{mn,kl}$ are given by

$$R_{mn,kl} \;=\; c_{mn}c_{kl}\int_{\mathbf{R^2}} H_m\left(\sqrt{2}\frac{x}{w}\right)H_n\left(\sqrt{2}\frac{y}{w}\right)\;\times$$

$$H_k\left(\sqrt{2}\frac{x}{w}\right)H_l\left(\sqrt{2}\frac{y}{w}\right)\exp\left(-2\frac{x^2+y^2}{w^2}\right)\exp\left(2ikf(x,y)\right)\,dx\,dy$$

The total curvature phase factor vanishes, because if we represent the incoming wave's by $e^{i\phi}$, the matched mirror is $e^{-2i\phi}$, and the reflected wave $e^{-i\phi}$. Then we take the scalar product of this wave with the inversely directed wave which contains $e^{-i\phi}$, and eventually, ϕ disappears. The function $f(x,y)$ represents consequently only the departure of the surface with respect to the ideal paraboloid. We take the opportunity to remark that in kilometric FP cavities, curved mirrors can be considered as well as spherical or parabolic. The apex equation of a sphere of radius R_c osculating the plane $z=0$ is:

$$z = R_c \;-\; \sqrt{R_c^2-x^2-y^2}$$

The expansion for large R_c gives

$$z \;=\; \frac{x^2+y^2}{2R_c^2} \;-\; \frac{\left(x^2+y^2\right)^2}{8R_c^3} \;+\mathcal{O}(a^6/R_c^5)$$

(a being the radius of the mirror). The first term is the parabolic approximation, and the second is bounded by

$$\delta z_{\max} \;=\; \frac{a^4}{8R_c^3}$$

For typical values, $a = 17.5$ cm, and $R_c = 3.45$ km, we have $\delta z_{\max} \simeq 3. \times 10^{-15}$ m, so that there is no significant difference between the paraboloid and the sphere. The scalar product can be written

$$R_{mn,kl} \;=\; \frac{w^2}{2}\, c_{mn} c_{kl} \int_{\mathbf{R^2}} H_m(X)\, H_n(Y)\, H_k(X)\, H_l(Y) \;\times \qquad (3.25)$$

$$\exp(-X^2)\, \exp(-Y^2) \exp\left(2ikf(wX/\sqrt{2}, wY/\sqrt{2})\right)\, dx\, dy$$

3.3.2 Tilted mirrors

The first case we shall examine is the rotation of a mirror. Obviously we consider small rotation angles. The general apex equation of a parabolic mirror, as already said, is, in the X, Y, Z coordinates

$$Z \;=\; \frac{X^2 + Y^2}{2R_c}$$

Suppose that the X, Y, Z frame is rotated by an azimutal angle ϕ and a colatitude angle θ from the reference frame x, y, z. We need the apex equation in that reference frame. We have

$$\begin{aligned} X &= x\, \cos\theta\, \cos\phi \;+\; y\, \cos\theta\, \sin\phi \;-\; z\, \sin\theta \\ Y &= -\, x\, \sin\phi \;+\; y\, \cos\phi \\ Z &= x\, \sin\theta\, \cos\phi \;+\; y\, \sin\theta\, \sin\phi \;+\; z\, \cos\theta \end{aligned}$$

By substituting in the apex equation, we get a second order equation in z, whose solution is

$$z \;=\; \frac{x^2 + y^2}{2R_c\, \cos\theta} \;-\; u\, \tan\theta \;+\; \frac{u^2 \sin^2\theta}{2R_c \cos\theta} \;+\; \mathcal{O}(1/R_c^2)$$

where we have set

$$u \;=\; x\, \cos\phi + y\, \sin\phi$$

Consider now orders of magnitude. A sophisticated numerical model is useful if the mirrors are aligned enough to allow some interference in the system. If not, geometrical optics models are quite sufficient to describe what happens to the light. If the waves interfere, it means that the rotation angles allow some light off a mirror to reach the opposite one. In other words, the colatitude angle θ is less than $\theta_{\max} = a/L$ where a is the radius of the mirror. This is less than 10^{-4} Rd. With 3.45 km curvature we see that the neglected terms were less than 10^{-21} m. Now, x and y being at most of order w, the third kept term is less than 10^{-14} m. It is therefore possible to take, with a very good accuracy, neglecting lengths of order $w^2\theta^2/R_c$:

$$z = \frac{x^2+y^2}{2R_c} - \tan\theta\,(x\,\cos\phi + y\,\sin\phi)$$

as the rotated-mirror apex equation. It means that the function $f(x,y)$ introduced above is simply

$$f(x,y) = - \tan\theta\,(x\,\cos\phi + y\,\sin\phi)$$

In order to compute the rotation matrix, we have to calculate integrals of the form

$$I_{mk}(p) = \int_{-\infty}^{\infty} H_m(X)\,H_k(X)\,\mathrm{e}^{-X^2}\,\mathrm{e}^{ipX}\,dx \tag{3.26}$$

with either $p = -\sqrt{2}kw\tan\theta\cos\phi$ or $p = -\sqrt{2}kw\tan\theta\sin\phi$. It is easy to compute the integral 3.26 by using the translation formula 2.45. We can write indeed:

$$I_{mk}(p) = \mathrm{e}^{-p^2/4}\int_{-\infty}^{\infty}\mathrm{e}^{-(X-ip/2)^2}H_m(X)\,H_k(X)\,dX$$

By considering a closed loop in the complex plane and using the Cauchy theorem, it can be immediately seen that

$$I_{mk}(p) = \mathrm{e}^{-p^2/4}\int_{-\infty}^{\infty}\mathrm{e}^{-X^2}H_m(X+ip/2)\,H_k(X+ip/2)\,dX$$

now, with the translation formula this is

$$I_{mk}(p) = \mathrm{e}^{-p^2/4}\sum_{s=0}^{m}\sum_{t=0}^{k}C_m^s\,C_k^t\,(ip)^{m-s+k-t}\int_{-\infty}^{\infty}\mathrm{e}^{-X^2}H_s(X)\,H_t(X)\,dX$$

and with the orthogonality relation of the Hermite polynomials, this gives

$$I_{mk}(p) \;=\; \mathrm{e}^{-p^2/4} \sum_{s=0}^{m} \sum_{t=0}^{k} C_m^s \, C_k^t \, (ip)^{m-s+k-t} \, \sqrt{\pi} 2^s s! \delta_{st}$$

or, finally

$$I_{mk}(p) \;=\; \sqrt{\pi}\, i^{m+k}\, \mathrm{e}^{-p^2/4} \sum_{s=0}^{\min(m,k)} (-2)^s \, \frac{m!\, k!}{s!\,(m-s)!\,(k-s)!} \, p^{m+n-2k}$$

the same result can be found by using formula 2.47 and 2.49. It is thus natural to introduce the *displacement polynomials*

$$Q_{mk}(x) \;=\; \sum_{s=0}^{\min(m,k)} (-2)^s \, \frac{m!\, k!}{s!\,(m-s)!\,(k-s)!} \, x^{m+k-2s} \tag{3.27}$$

so that our result can be expressed as:

$$I_{mk}(p) \;=\; \sqrt{\pi}\, i^{m+k}\, \mathrm{e}^{-p^2/4}\, Q_{mk}(p) \tag{3.28}$$

The rotation matrix takes on the form

$$R_{mn,kl}(\theta,\phi) \;=\; \frac{i^{m+n+k+l}}{\sqrt{2^{m+n+k+l} m!n!k!l!}} \;\times \tag{3.29}$$

$$Q_{mk}\left(-\sqrt{2}kw \tan\theta \cos\phi\right) Q_{nl}\left(-\sqrt{2}kw \tan\theta \sin\phi\right) \mathrm{e}^{-k^2w^2 \tan\theta^2/2}$$

Some more details on displacement polynomials will be discussed in a following section. Remark that

$$\frac{k\theta w}{2} \;=\; \frac{\theta}{\theta_g} \frac{w}{w_0}$$

where $\theta_g \;=\; \lambda/\pi w_0$ is the divergence of the gaussian beam.

3.3.3 Parallel translations of the beam

Consider now a parallel displacement of the beam in a region of null curvature. The incoming beam was

$$E_{\text{in}} \;=\; \sum_{mn} E_{mn} \phi_{mn}(x,y)$$

and the translation operator T acts as

$$T.E_{\text{in}} \;=\; E_{\text{in}}(x+\Delta x, y+\Delta y)$$

The matrix elements of the operator are:

$$T_{mn,kl} \;=\; \frac{w^2}{2}\, c_{mn} c_{kl} \;\times$$

$$\times \int_{-\infty}^{\infty} dX \int_{\infty}^{\infty} dY \;\exp\left[-\frac{(X+\Delta X)^2+(Y+\Delta Y)^2}{2}\right] \exp\left[-\frac{X^2+Y^2}{2}\right] \;\times$$

$$H_m(X)\, H_n(Y)\, H_k(X+\Delta X) H_l(Y+\Delta Y)$$

with $\Delta X \;\equiv\; \sqrt{2}\Delta x/w$. A change of variables leads to

$$T_{mn,kl} \;=\; \frac{w^2}{2}\, c_{mn} c_{kl} \int_{-\infty}^{\infty} dX \int_{-\infty}^{\infty} dY \;\exp\left[-\frac{(X+\Delta X/2)^2+(Y+\Delta Y/2)^2}{2}\right] \;\times$$

$$\exp\left[-\frac{(X-\Delta X/2)^2+(Y-\Delta Y/2)^2}{2}\right] \;\times$$

$$H_m(X-\Delta X/2)\, H_n(Y-\Delta Y/2)\, H_k(X+\Delta X/2) H_l(Y+\Delta Y/2)$$

By using again the translation formula, we get successively

$$T_{mn,kl} \;=\; \frac{w^2}{2}\, c_{mn} c_{kl}\, (-1)^{k+l}\, \pi\, Q_{mk}(\Delta X)\, Q_{nl}(\Delta Y) \;\exp\left[-\frac{\Delta X^2+\Delta Y^2}{4}\right]$$

then

$$T_{mn,kl} \;=\; \frac{(-1)^{k+l}}{\sqrt{2^{m+n+k+l}\, m!n!k!l!}}\, Q_{mk}(\sqrt{2}\Delta x/w)\, Q_{nl}(\sqrt{2}\Delta y/w) \times \qquad (3.30)$$

$$\exp\left[-\frac{\Delta x^2+\Delta y^2}{2w^2}\right]$$

3.3.4 Mismatching

When the wavefront incoming on a mirror of curvature radius R_c has curvature radius R, if $R \neq R_c$ there is mismatching. This may happen for instance if the mirror has been displaced along the optical axis. Assume for instance the reference beam is a TEM_{mn} HG-mode:

$$\varphi_{mn}(x,y) = c_{mn} \mathrm{e}^{ikr^2/2R}\ \mathrm{e}^{-r^2/w^2}\ H_m(\sqrt{2}x/w)\, H_n(\sqrt{2}y/w)$$

where the c_{mn} are the normalization constants. The mirror operator is:

$$M(x,y) = \mathrm{e}^{-ikr^2/R_c}$$

so that the mirror's matrix elements being defined as

$$M_{mnkl} \ = \ \langle \varphi^*_{kl}, M\varphi_{mn} \rangle$$

where φ^*_{kl} is the phase-conjugate of φ_{kl}, we get

$$M_{mnkl} \ = \ c_{mn}c_{kl} \int_{-\infty}^{\infty} \mathrm{e}^{-2r^2/w^2} \mathrm{e}^{ikr^2/R} \mathrm{e}^{-ikr^2/R_c} \times$$

$$\times\ H_m(\sqrt{2}x/w)\, H_n(\sqrt{2}y/w)\ H_k(\sqrt{2}x/w)\, H_l(\sqrt{2}y/w)\ dx\, dy$$

or

$$M_{mnkl} \ = \ \frac{\pi w^2}{2}\ c_{mn}c_{kl}\ I_{m,k}(\alpha)\ I_{n,l}(\alpha)$$

where we have set

$$\alpha \equiv \frac{\pi w^2}{\lambda}\ \left[\frac{1}{R'} - \frac{1}{R}\right]$$

and introduced the following integrals:

$$I_{m,k}(\alpha) \ = \ \frac{1}{\sqrt{\pi}} \int_{-\infty}^{\infty} \mathrm{e}^{-(1+i\alpha)x^2} H_m(x)\ H_k(x)\ dx$$

First of all, it is clear that the $I_{m,k}$ are non zero only if m and k have the same parity. By using the reduction formula (2.47), we get for instance

$$H_{2m}(x)H_{2k}(x) \ = \ \sum_{s=0}^{\min[2m,2k]} \frac{2m!2k!2^s}{(2m-s)!(2k-s)!s!}\ H_{2m+2k-2s}(x)$$

moreover, one can show from the scaling formula (2.46) and the Cauchy theorem on a trivial path in the complex plane that, for any complex number Z of positive real part:

$$\int_{\mathrm{R}} \mathrm{e}^{-Zx^2} H_{2n}(x)\,dx \;=\; \frac{2n!}{n!} Z^{-1/2}(1/Z-1)^n$$

we have thus the following result:

$$I_{2m,2k} \;=\; Z^{-1/2}\mu_{mk}(1/Z-1)$$

where $Z \equiv 1+i\alpha$, and $\mu_{mk}(x)$ is a even-matching polynomial defined as:

$$\mu_{mk}(x) \;=\; \sum_{s=0}^{\min[2m,2k]} \frac{2m!2k!2^s(2m+2k-2s)!}{(2m-s)!(2k-s)!(m+k-s)!s!} x^{m+k-s}$$

The same calculation can be done for the odd-odd integral:

$$I_{2m-1,2k-1} \;=\; Z^{-3/2}\nu_{mk}(1/Z-1)$$

which defines the odd-matching polynomial

$$\nu_{mk}(x) \;=\; \frac{1}{1+x} \sum_{s=0}^{\min[2m-1,2k-1]} \frac{(2m-1)!(2k-1)!2^s(2m+2k-2s-2)!}{(2m-1-s)!(2k-1-s)!(m+k-s-1)!s!} x^{m+k-s-1}$$

the factor $1/(1+x)$ comes from the fact that the preceding sum happens to be divisible by $1+x$. These two explicit formulas allow in principle to compute any matrix element, but are not optimal for an efficient numerical computation. It is better to know the first orders and find higher orders by recurrence. The well-known recurrence formula for Hermite polynomials induces the following recurrence scheme:

$$\mu_{m,k}(x) \;=\; 2(2m-1)x\mu_{m-1,k}(x) + 4k(x+1)^2\nu_{m,k}(x)$$

$$\nu_{m,k}(x) \;=\; 4(m-1)x\nu_{m-1,k}(x) + 2(2k-1)\mu_{m-1,k-1}$$

This crossed recurrence scheme can be initiated for instance from the following explicitly known matching polynomials, for $n \geq 0$:

$$\mu_{0,n}(x) \;=\; \frac{2n!}{n!} x^n$$

$$\mu_{1,n}(x) = 2x^{n-1}\frac{2n!}{n!}\Big[(2n+1)x^2+4nx+2n\Big]$$

$$\mu_{2,n}(x) = 4x^{n-2}\frac{2n!}{n!}\Big[(2n+3)(2n+1)x^4+8n(2n+1)x^3+12n(2n-1)x^2+$$
$$+16n(n-1)x+4n(n-1)\Big]$$

and for $n \geq 1$:

$$\nu_{1,n}(x) = \frac{2n!}{n!}x^{n-1}$$

$$\nu_{2,n}(x) = 2x^{n-2}\frac{2n!}{n!}\Big[(2n+1)x^2+4(n-1)x+2(n-1)\Big]$$

$$\nu_{3,n} = 4x^{n-3}\frac{2n!}{n!}\Big[(2n+3)(2n+1)x^4+8(n-1)(2n+1)x^3+4(n-1)(6n-7)x^2+$$
$$+16(n-1)(n-2)x+4(n-1)(n-2)\Big]$$

the symmetry breaking between the two indices is only apparent. The matrix elements have the following expressions:

$$M_{2m,2n,2k,2l}(\alpha) = \frac{1}{1+i\alpha}\frac{\mu_{mk}(z)\mu_{nl}(z)}{\sqrt{2^{2m+2n+2k+2l}2m!2n!2k!2l!}}$$

where $z \equiv -i\alpha/(1+i\alpha)$, and

$$M_{2m-1,2n,2k-1,2l}(\alpha) = \frac{1}{(1+i\alpha)^2}\frac{\nu_{mk}(z)\mu_{nl}(z)}{\sqrt{2^{2m+2n+2k+2l-2}(2m-1)!2n!(2k-1)!2l!}}$$

$$M_{2m,2n-1,2k,2l-1}(\alpha) = \frac{1}{(1+i\alpha)^2}\frac{\mu_{mk}(z)\nu_{nl}(z)}{\sqrt{2^{2m+2n+2k+2l-2}2m!(2n-1)!2k!(2l-1)!}}$$

$$M_{2m-1,2n-1,2k-1,2l-1}(\alpha) = \frac{1}{(1+i\alpha)^3}\frac{\nu_{mk}(z)\nu_{nl}(z)}{\sqrt{2^{2m+2n+2k+2l-4}(2m-1)!(2n-1)!(2k-1)!(2l-1)!}}$$

Some examples for the first orders of self-coupling:

$$M_{00,00}(\alpha) = \frac{1}{1+i\alpha}$$

$$M_{01,01}(\alpha) = \frac{1}{(1+i\alpha)^2}$$

$$M_{02,02}(\alpha) = \frac{1}{1+i\alpha}(1+2z+3z^2/2)$$

$$M_{11,11}(\alpha) \;=\; \frac{1}{(1+i\alpha)^3}$$

for coupling of 00 to higher orders:

$$M_{00,2m,2n}(\alpha) \;=\; \frac{1}{1+i\alpha}\,\frac{\sqrt{2m!2n!}}{2^{m+n}m!n!}\,z^{m+n}$$

for coupling of 01 to higher orders ($n \geq 1$):

$$M_{01,2m,2n-1}(\alpha) \;=\; \frac{1}{(1+i\alpha)^2}\,\frac{\sqrt{2m!2n!}}{2^{m+n}m!n!}\,\sqrt{2n}\,z^{m+n-1}$$

3.3.5 Clipped mirrors

Real mirrors are of finite size. The ideal TEM_{00} beam is, strictly speaking, of indefinite transversal extension, but it is so sharply peaked that, in practice, mirrors having radii about 2.5 times the half-width of the beam can be considered almost indefinite, which exactly means that "one can neglect the diffraction losses". It is interesting to quantify these losses in terms of power coupled in higher order modes. The finite sizing of an otherwise perfectly matched mirror can be considered as a perturbation, and we address the question of computing the matrix elements of that perturbation in the Hermite-Gauss basis. If we denote by $\phi_{m,n}(x,y)$ the elements of the basis, the matrix elements have the form

$$\Gamma_{m,n,k,l} \;=\; \langle \phi_{m,n}, M\phi_{k,l}\rangle$$

M being the mirror operator. Due to the perfect matching of the mirror curvature radius, this scalar product reduces to

$$\Gamma_{m,n,k,l} \;=\; c_{mn}c_{kl}\int_0^{2\pi} d\phi \int_0^a r\,dr\,\mathrm{e}^{-2r^2/w^2} H_m(\sqrt{2}r\cos\phi/w)\,H_n(\sqrt{2}r\sin\phi/w)\times$$

$$\times\; H_k(\sqrt{2}r\cos\phi/w)\,H_l(\sqrt{2}r\sin\phi/w)$$

where a is the finite radius of the mirror. When $a \to \infty$, we expect the bracket to vanish unless $m=k,\ n=l$, due to the orthogonality of the basis. After a change of variables, the integral becomes

$$\Gamma_{m,n,k,l} \;=\; c'_{mn}c'_{kl}\,2\int_0^{\rho} \mathrm{e}^{-R^2}\,R\,dR$$

$$\times \frac{1}{2\pi}\int_0^{2\pi} d\phi\, H_m(R\cos\phi)\, H_n(R\sin\phi)\, H_k(R\cos\phi)\, H_l(R\sin\phi)$$

where $\rho \equiv \sqrt{2}a/w$. The new normalization constants are

$$c'_{mn} \;=\; \frac{1}{\sqrt{2^{m+n}m!\,n!}}$$

It is convenient to take a shorthand notation

$$[m,n,k,l](\phi) \;=\; 2\int_0^{\rho} \mathrm{e}^{-R^2} R\,dR\, H_m(R\cos\phi)\, H_n(R\sin\phi)\, H_k(R\cos\phi)\, H_l(R\sin\phi)$$

for the radial integral. For the angular average, we take the abbreviation

$$(f) \;\equiv\; \frac{1}{2\pi}\int_0^{2\pi} d\phi\, f(\phi)$$

so that the matrix element is

$$\Gamma_{m,n,k,l} \;=\; \langle mn|M|kl\rangle \;=\; c'_{mn}c'_{kl}\,([m,n,k,l])$$

From the definition of the Hermite polynomials we get immediately:

$$H_m(R\cos\phi) \;=\; \sum_{s=0}^{[m/2]} (-1)^s \frac{m!}{s!\,(m-2s)!}\,(2R)^{m-2s}\,(\cos\phi)^{m-2s} \tag{3.31}$$

and obviously:

$$H_m(R\sin\phi) \;=\; \sum_{s=0}^{[m/2]} (-1)^s \frac{m!}{s!\,(m-2s)!}\,(2R)^{m-2s}\,(\sin\phi)^{m-2s} \tag{3.32}$$

It is however clear that averaging over angles will eliminate a number of terms, we have in particular:

$$(\cos^{2n+1}\phi) = (\sin^{2n+1}\phi) = 0$$

moreover,

$$(\cos^{2n}\phi\;\sin^{2m}\phi) \;=\; \frac{2m!\,2n!}{2^{2m+2n}m!\,n!\,(m+n)!} \tag{3.33}$$

so that we see immediately that the only nonzero elements are:

$$\Gamma_{2m,2n,2k,2l},\;\Gamma_{2m,2n+1,2k,2l+1},\;\Gamma_{2m+1,2n,2k+1,2l},\;\Gamma_{2m+1,2n+1,2k+1,2l+1}$$

It is straightforward to derive from the recurrence relation obeyed by the Hermite polynomials, the following:

$$[m,n,k,l] \;=\; [m,n-1,k,l+1]+2l\,[m,n-1,k,l-1]-2(n-1)\,[m,n-2,k,l] \tag{3.34}$$

$$[m,n,k,l] \;=\; [m-1,n,k+1,l]+2k\,[m-1,n,k-1,l]-2(m-1)\,[m-2,n,k,l] \tag{3.35}$$

allowing to compute any matrix element, once some initial elements are known. The point is that a whole family of elements can be computed explicitly in terms of the incomplete Gamma function. We firstly have:

$$2\int_0^\rho \mathrm{e}^{-R^2} R^{2n+1}\,dR \;=\; n!\left[1-\mathrm{e}^{-\rho^2}\sum_{s=0}^{n}\frac{\rho^{2s}}{s!}\right]$$

so that in particular, we have simply:

$$([0,0,0,0]) \;=\; 1-\mathrm{e}^{-\rho^2} \tag{3.36}$$

then, by using the definitions (3.31,3.32), formula (3.33) and some algebra, it is possible to show that, for $k+l\neq 0$ (the special case $k+l=0$ is known):

$$([0,0,2k,2l]) \;=\; (-1)^{k+l}\frac{2k!\,2l!}{k!\,l!\,(k+l)!}\,\rho^2\mathrm{e}^{-\rho^2}C_{k+l-1}(\rho^2) \tag{3.37}$$

where the $C_m(x)$ are the *clipping polynomials* defined by

$$C_m(x) \;=\; \sum_{s=0}^{m}(-1)^s\,C_m^s\,\frac{(m+1)!}{(s+1)!}\,x^s \tag{3.38}$$

The first clipping polynomials are as follows:

$$C_0(x) \;=\; 1$$

$$C_1(x) \;=\; 2-x$$

$$C_2(x) \;=\; 6-6x+x^2$$

$$C_3(x) \;=\; 24-36x+12x^2-x^3$$

$$C_4(x) \;=\; 120-240x+120x^2-20x^3+x^4$$

They obey the following recurrence relation ($n>0$):

$$C_n(x) \;=\; -(x-2n)\,C_{n-1}(x) \;-\; n(n-1)\,C_{n-2}(x)$$

Moreover, with (3.34):

$$([0,1,2k,2l-1]) \;=\; (-1)^{k+l}\frac{2k!\,2l!}{k!\,l!\,(k+l)!}\,\rho^2\mathrm{e}^{-\rho^2}\left[C_{k+l-1}(\rho^2)-(k+l)\,C_{k+l-2}(\rho^2)\right] \tag{3.39}$$

One can introduce the family $C_m^{(1)}(x) \;\equiv\; C_m(x)-(m+1)C_{m-1}(x)$, (for $m>0$) and show that

$$C_m^{(1)}(x) \;=\; \frac{x}{m}\,\frac{d}{dx}C_m(x) \quad (m>0)$$

or

$$C_m^{(1)}(x) \;=\; -x\sum_{s=0}^{m-1}(-1)^s C_{m-1}^s\;\frac{(m+1)!}{(s+2)!}x^s$$

so that

$$([0,1,2k,2l-1]) \;=\; (-1)^{k+l}\frac{2k!\,2l!}{k!\,l!\,(k+l)!}\;\rho^2\mathrm{e}^{-\rho^2}C_{k+l-1}^{(1)}(\rho^2)$$

The first $C^{(1)}$ plynomials are:

$$C_1^{(1)}(x) \;=\; -x$$

$$C_2^{(1)}(x) \;=\; -3x+x^2$$

$$C_3^{(1)}(x) \;=\; -12x+8x^2-x^3$$

$$C_4^{(1)}(x) \;=\; -60x+60x^2-15x^3+x^4$$

The $C^{(1)}$ polynomials obey the following recurrence relation ($n>1$):

$$C_n^{(1)}(x) \;=\; -(x-2n+1)\,C_{n-1}^{(1)}(x)-n(n-2)\;C_{n-2}^{(1)}(x)$$

These two results, added to the recurrence relations and to the symmetry in the pairs (m,k) and (n,l), allow to recursively compute any matrix element. We have namely ($n>0$):

$$\Gamma_{m,n,k,l} \;=\; \sqrt{\frac{l+1}{n}}\,\Gamma_{m,n-1,k,l+1} \;+\; \sqrt{\frac{l}{n}}\,\Gamma_{m,n-1,k,l-1} \;-\; \sqrt{\frac{n-1}{n}}\,\Gamma_{m,n-2,k,l}$$

and ($m>0$):

$$\Gamma_{m,n,k,l} \;=\; \sqrt{\frac{k+1}{m}}\,\Gamma_{m-1,n,k+1,l} \;+\; \sqrt{\frac{k}{m}}\,\Gamma_{m-1,n,k-1,l} \;-\; \sqrt{\frac{m-1}{m}}\,\Gamma_{m-2,n,k,l}$$

The clipping polynomials are orthogonal in the following sense:

$$\int_0^\infty \mathrm{e}^{-x} C_m(x)\, C_n(x)\; x\, dx \;=\; \delta_{mn} n!\,(n+1)!$$

Result (3.37) allows already to study the coupling of the TEM_{00} with higher order modes. The complete expression of the coupling coefficient is ($c'_{00} = 1$):

$$\Gamma_{0,0,0,0} \;=\; 1 - \mathrm{e}^{-\rho^2}$$

$$\Gamma_{0,0,2k,2l} \;=\; c'_{2k,2l}\,([0,0,2k,2l]) \quad (k+l \neq 0)$$

or

$$\Gamma_{0,0,2k,2l} \;=\; \frac{(-1)^{k+l}\sqrt{2k!\,2l!}}{2^{k+l} k!\, l!(k+l)!}\, \rho^2\, \mathrm{e}^{-\rho^2}\, C_{k+l-1}(\rho^2) \quad (k+l \neq 0)$$

(recall that $\rho^2 \equiv 2a^2/w^2$). In Fig.3.20, one can see the dependence on a of the coupling factor (power). We see that for small values of a, there is a huge loss of power, and thus the coupling is weak, then it increases and finally returns to zero when a is large, due to orthogonality of the modes. The explicit values for the first matrix elements expressing the coupling of the TEM_{00} are:

$$\Gamma_{0,0,0,2} \;=\; -\frac{\sqrt{2}}{2}\, \rho^2\, \mathrm{e}^{-\rho^2}$$

$$\Gamma_{0,0,0,4} \;=\; \frac{\sqrt{3}}{2\sqrt{2}}\, \rho^2\, \mathrm{e}^{-\rho^2}(1 - \rho^2/2)$$

$$\Gamma_{0,0,0,6} \;=\; -\,\frac{\sqrt{5}}{4}\, \rho^2\, \mathrm{e}^{-\rho^2}(1 - \rho^2 + \rho^4/6)$$

$$\Gamma_{0,0,0,8} \;=\; \frac{\sqrt{35}}{8\sqrt{2}}\, \rho^2\, \mathrm{e}^{-\rho^2}(1 - 3\rho^2/2 + \rho^4/2 - \rho^6/24)$$

$$\Gamma_{0,0,2,2} \;=\; \frac{1}{2}\, \rho^2\, \mathrm{e}^{-\rho^2}(1 - \rho^2/2)$$

$$\Gamma_{0,0,2,4} \;=\; -\frac{\sqrt{3}}{4}\, \rho^2\, \mathrm{e}^{-\rho^2}(1 - \rho^2 + \rho^4/6)$$

$$\Gamma_{0,0,2,6} \;=\; \frac{\sqrt{5}}{4\sqrt{2}}\, \rho^2\, \mathrm{e}^{-\rho^2}(1 - 3\rho^2/2 + \rho^4/2 - \rho^6/24)$$

$$\Gamma_{0,0,4,4} \;=\; \frac{3}{8}\, \rho^2\, \mathrm{e}^{-\rho^2}(1 - 3\rho^2/2 + \rho^4/2 - \rho^6/24)$$

$$\Gamma_{0,0,4,6} = -\frac{\sqrt{30}}{16}\,\rho^2\,\mathrm{e}^{-\rho^2}(1-2\rho^2+\rho^4-\rho^6/6+\rho^8/120)$$

$$\Gamma_{0,1,0,3} = -\frac{\sqrt{6}}{4}\,\rho^4\,\mathrm{e}^{-\rho^2}$$

$$\Gamma_{0,1,0,5} = \frac{\sqrt{30}}{8}\,\rho^4\,\mathrm{e}^{-\rho^2}(1-\rho^2/3)$$

$$\Gamma_{0,1,2,1} = -\frac{1}{2\sqrt{2}}\,\rho^4\,\mathrm{e}^{-\rho^2}$$

$$\Gamma_{0,1,2,3} = \frac{\sqrt{3}}{4}\,\rho^4\,\mathrm{e}^{-\rho^2}(1-\rho^2/3)$$

$$\Gamma_{0,2,0,4} = -\frac{\sqrt{3}}{4}\,\rho^2\,\mathrm{e}^{-\rho^2}(1-\rho^2+5\rho^4/6)$$

In order to initiate any recursive scheme, we need the coupling factors for the TEM_{01} mode ($k>0, l>1$):

$$\Gamma_{0,1,2k,2l-1} = \frac{(-1)^{k+l}\sqrt{2k!\,(2l-1)!}}{2^{k+l-1}k!\,(l-1)!(k+l)!}\,\rho^2\,\mathrm{e}^{-\rho^2}\,\left[C_{k+l-1}(\rho^2)-(k+l)C_{k+l-2}(\rho^2)\right]$$

And for autocoupling of higher order modes, we get for instance:

$$\Gamma_{0,1,0,1} = 1-\mathrm{e}^{-\rho^2}(1+\rho^2)$$

$$\Gamma_{0,2,0,2} = 1-\mathrm{e}^{-\rho^2}(1+\rho^2/2+3\rho^4/4)$$

$$\Gamma_{1,1,1,1} = 1-\mathrm{e}^{-\rho^2}(1+\rho^2+\rho^4/2)$$

$$\Gamma_{0,3,0,3} = 1-\mathrm{e}^{-\rho^2}(1+\rho^2-\rho^4/4+5\rho^6/12)$$

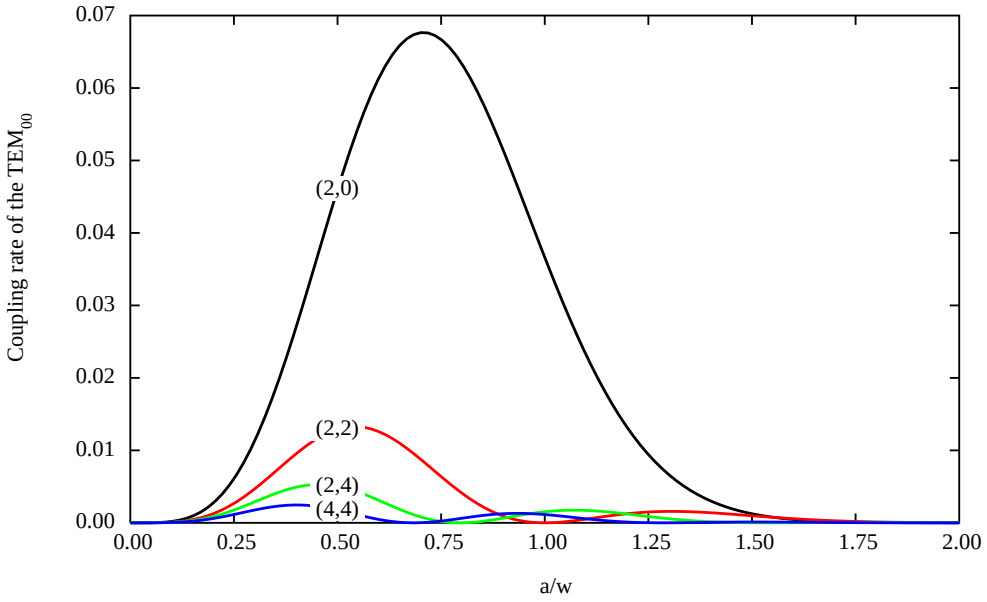

Figure 3.20: Relative power coupled from the TEM_{00} into the first higher order modes vs. radius of the diaphragm

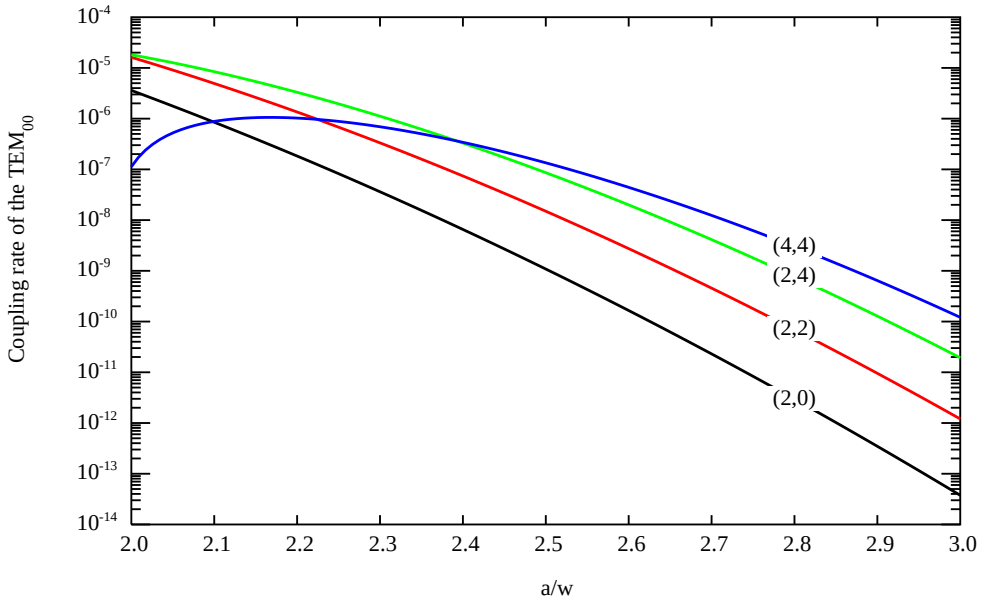

Figure 3.21: Relative power coupled from the TEM_{00} into the first higher order modes vs. radius of the diaphragm

For realistic values of a/w, a logarithmic scale is preferrable (Fig.3.21):

It may be also interesting to see how the incident power is ditributed in the coupled modes by seeing the cumulated coupling coefficients.

$$P(n) \;=\; \sum_{s=0}^{n}\sum_{k=0}^{s} \Gamma^2_{0,0,2s-2k,2k}$$

In (Fig.3.22), we show the case of a small diaphragm aperture: the convergence is very slow, because the intense perturbation spread the incident power among almost more all the modes. In Fig.3.3.5, we have the cases of realistic values of w/a, and we have plotted $1 - P(n)$.

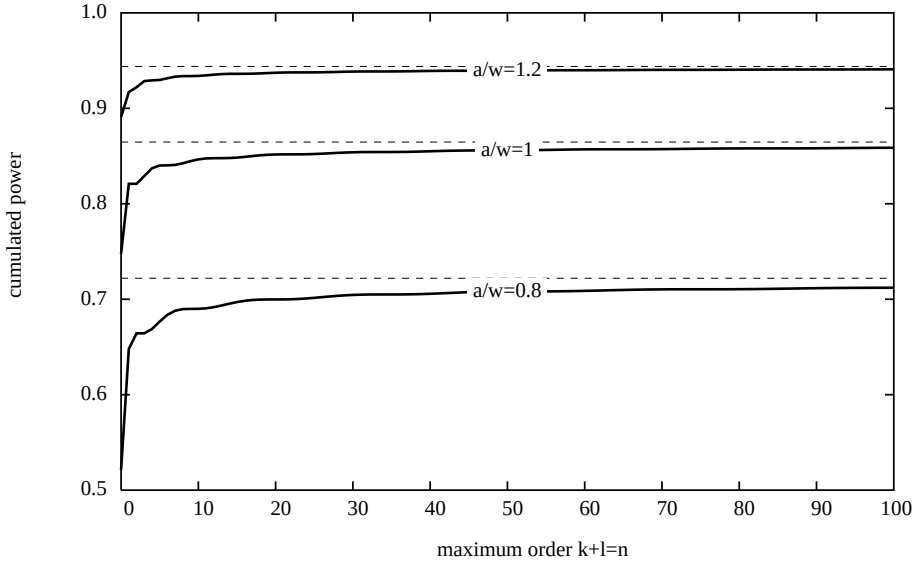

Figure 3.22: Cumulated relative power coupled from the TEM_{00} into the first modes vs. maximum order. The dashed lines indicate the total power i.e. $1 - \exp(-2a^2/w^2)$

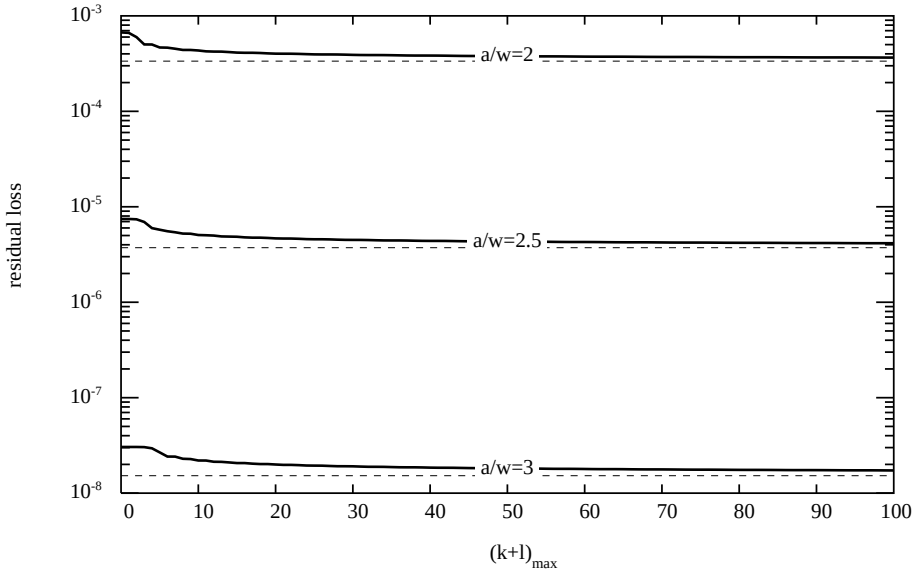

Figure 3.23: Residual relative power coupled from the TEM_{00} into the higher order modes vs. maximum order. The dashed lines indicate the total losses, i.e. $\exp(-2a^2/w^2)$.

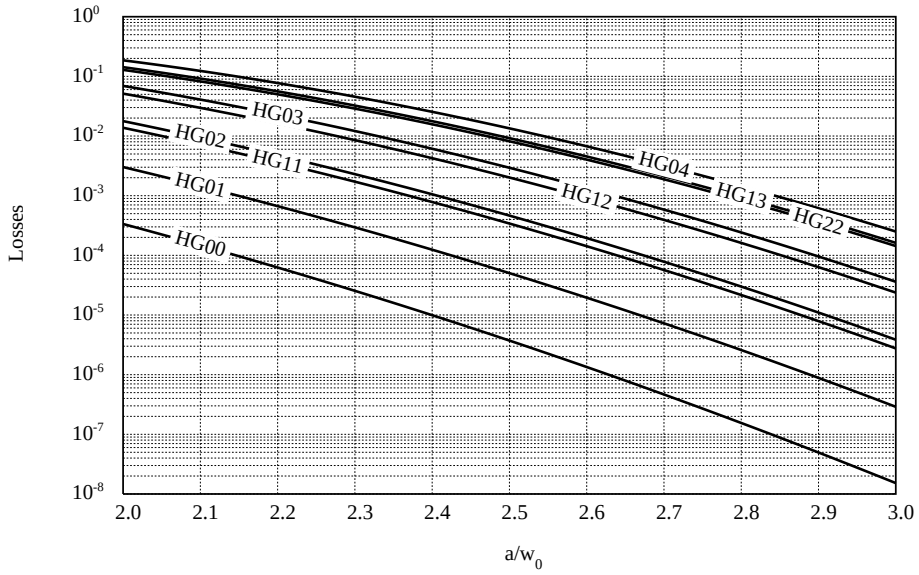

Figure 3.24: Losses caused by a finite circular aperture in $\mathrm{TEM}_{m,n}$ modes (clipping losses)

Passing a $\mathrm{TEM}_{m,n}$ mode through a circular aperture of radius r, or reflection on a mirror of radius a, causes losses by cutting the tail of the gaussian profile of the mode. These losses can be evaluated by computing the $\Gamma_{m,n,m,n}$ coefficients, expressing the power coupled from the mode into itself, after the aperture. The preceding plot (Fig.3.24) shows these losses vs radius of the aperture for the first modes.

It is interesting to see how the found modal expansion allows to compute the field propagated at a given distance. The coefficients $\Gamma_{0,0,2m,2n}$ are assumed calcultated for a given gaussian beam of waist w_0 and a circular aperture of radius a. We assume the incoming field at its waist on the aperture. The parameters for the experiment are : $w_0 = 2$ cm and $a = 1$ cm. The reconstruction formula for the field at any distance z from the aperture is:

$$A(x,y,z) \;=\; \sum_{m=0}^{\infty}\sum_{n=0}^{\infty} \Gamma_{0,0,2m,2n}(a/w_0)\,\Psi_{2m,2n}(x,y,z)$$

where the $\Psi_{2m,2n}(x,y,z)$ are the normalized Hermite-Gauss modes. it is intersting to check that we recover the incoming field at $z = 0$. The field, though gaussian does not vary significantly in the (narrow) aperture, so that we expect the clipped amplitude to be nearly constant throughout a disk of radius a. On Fig.3.25, one sees the reconstructed field with modes up to order 100.

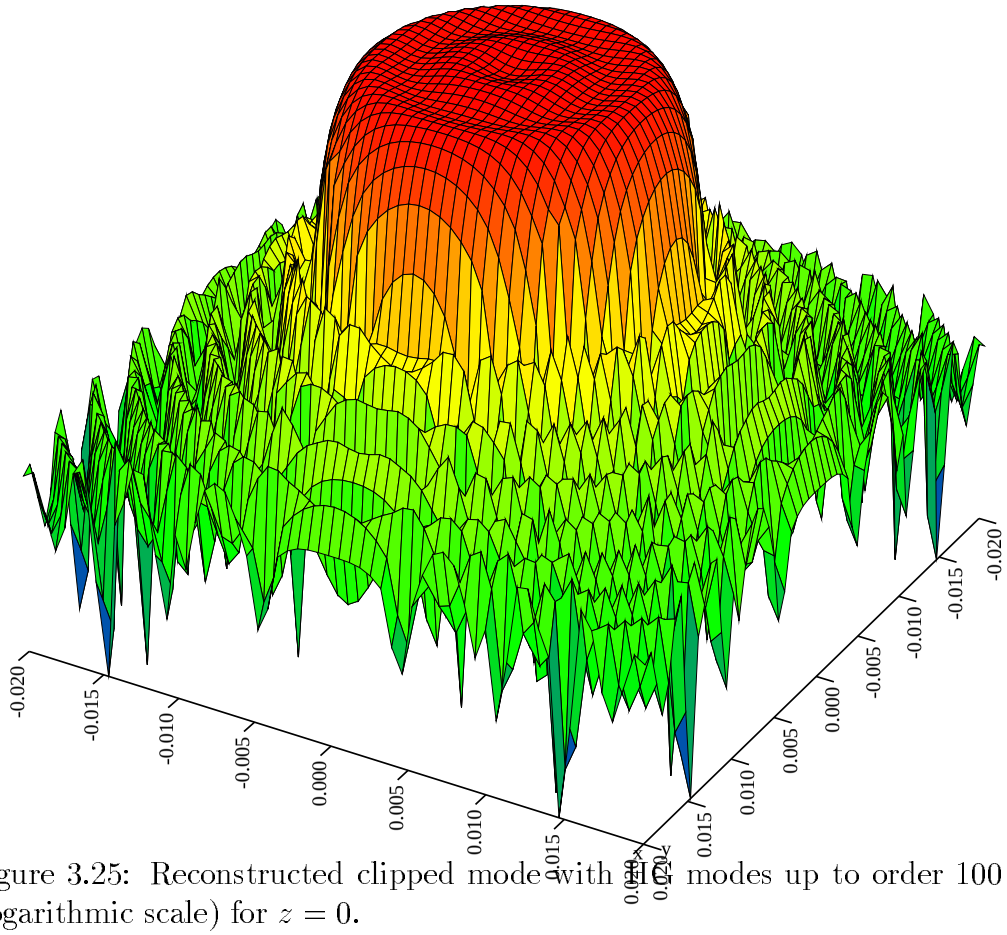

Figure 3.25: Reconstructed clipped mode with FLT modes up to order 100 (logarithmic scale) for $z = 0$.

In this case of a narrow aperture compared to the gaussian waist, we are not far from the case of a circular aperture uniformly illuminated. In the far field, we retrieve a field intensity very close to the well-known annular pattern. Fig.3.26 shows this pattern at distance of $z = 1000$ m.

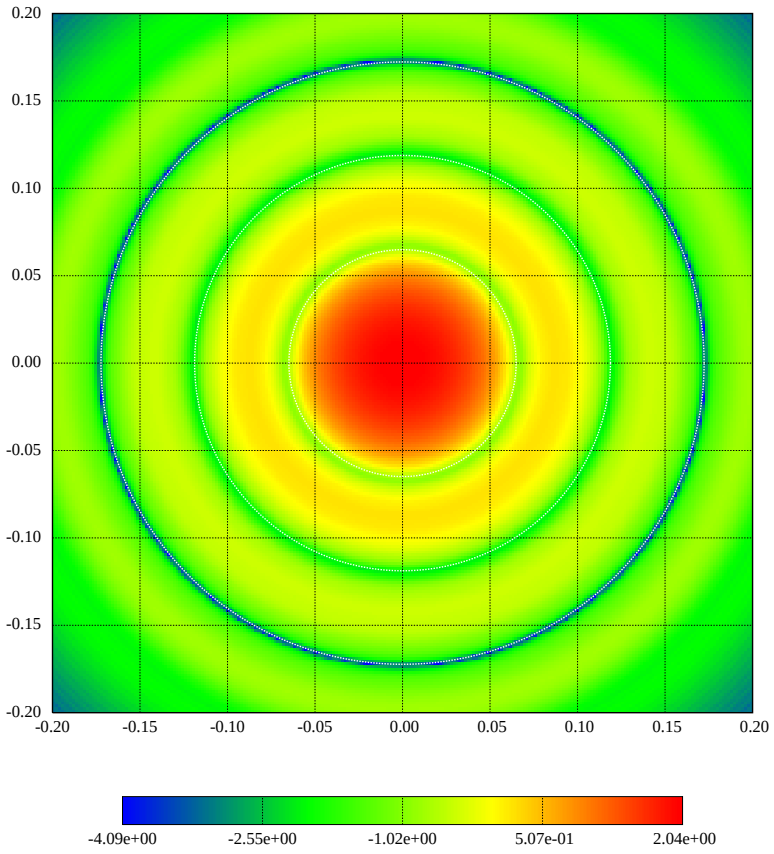

Figure 3.26: Reconstructed clipped mode with HG modes up to order 100 (logarithmic scale) for $z = 1000$ m. The white circles mark the zeroes $r_{1,2,3}$ of $J_1(2\pi ar/\lambda z)$

3.3.6 Offset and clipping

We consider the case where the beam being translated by δ from the optical axis, it is then clipped by a mirror. For instance, the recycling mirror having a radius of order 5 cm, one may worry about a possible angular displacement of the beam making it interacting with the edges. We assume without loss of generality a displacement along the x direction. The power transmission factor is:

$$\Gamma \;=\; \frac{2}{\pi w^2}\int_{C(a)} \exp\left[-2\,\frac{(x-\delta)^2+y^2}{w^2}\right] dx\,dy$$

where $C(a)$ is the area delimited by the circle of radius a representing the mirror's edge. This is

$$\Gamma \;=\; \frac{1}{\pi}\,\mathrm{e}^{-2\delta^2/w^2}\int_0^{2\pi} d\phi \int_0^{\sqrt{2}a/w} \rho\,d\rho\,\mathrm{e}^{-\rho^2+2\rho\delta\cos\phi}$$

or

$$\Gamma \;=\; 2\mathrm{e}^{-2\delta^2/w^2}\int_0^{\sqrt{2}a/w} \rho\,d\rho\,\mathrm{e}^{-\rho^2} I_0(2\sqrt{2}\rho\delta/w)$$

where I_0 is the modified Bessel function of the 1st kind. The preceding integral can be numerically computed for arbitrary δ, but if we assume a displacement small compared to w we can replace I_0 by its Taylor expansion up to 2d order:

$$I_0(z) \;\sim\; 1+z^2/4$$

so that

$$\begin{aligned}\Gamma \;&=\; 2\mathrm{e}^{-2\delta^2/w^2}\left[\int_0^{\sqrt{2}a/w}\rho\,d\rho\,\mathrm{e}^{-\rho^2} \;+\; \frac{2\delta^2}{w^2}\int_0^{\sqrt{2}a/w}\rho^3\,d\rho\,\mathrm{e}^{-\rho^2}\right]\\
&=\; \mathrm{e}^{-2\delta^2/w^2}\left[1-\mathrm{e}^{-2a^2/w^2}+\frac{2\delta^2}{w^2}\left(1-(1+2a^2/w^2),\mathrm{e}^{-2a^2/w^2}\right)\right]\\
&=\; 1-\mathrm{e}^{-2a^2/w^2} \;-\; \frac{2a^2}{w^2}\,\frac{2\delta^2}{w^2}\,\mathrm{e}^{-2a^2/w^2} \;+\; \mathcal{O}(\delta^4/w^4)\end{aligned}$$

If the offset δ is a random process $\delta(t)$, we see that it induces a power noise:

$$\frac{\Delta P(t)}{P_0} \;=\; \gamma\,\frac{2\delta(t)^2}{w^2}$$

with the scaling factor

$$\gamma \;=\; \frac{2a^2}{w^2}\,\mathrm{e}^{-2a^2/w^2}$$

For a recycling mirror of radius 5 cm, we have $a/w \sim 2.5$, so that $\gamma \sim 5\times 10^{-5}$

3.3.7 Mismatched beams

The first case of mismatching occurs when for instance a beam ψ of the TEM_{00} type of waist w_1 enters a cavity having a system of eigenmodes of waist w_2. We assume the waist precisely on the input flat mirror. We have thus to expand the incoming beam on the basis of the HG functions of parameter w_2. This is done by computing the matrix elements:

$$\Gamma_{m,n} \;=\; \langle \psi, \phi_{m,n} \rangle$$

where the $\phi_{m,n}$ are the eigen HG functions:

$$\phi_{m,n}(x,y) \;=\; \sqrt{\frac{2}{\pi w_2^2}} \sqrt{\frac{1}{2^{m+n}\, m!\, n!}} \exp\left[-\frac{x^2+y^2}{w_2^2}\right] H_m(\sqrt{2}\, x/w_2)\, H_n(\sqrt{2}\, y/w_2)$$

The scalar product is thus reducible to

$$\Gamma_{m,n} \;=\; \sqrt{\frac{2}{\pi w_1^2}} \sqrt{\frac{2}{\pi w_2^2}} \sqrt{\frac{1}{2^{m+n}\, m!\, n!}} \;\times$$

$$\times \int \exp\left[-\frac{r^2}{w_2^2}\left(1+\frac{w_2^2}{w_1^2}\right)\right] \; H_m(\sqrt{2}\, x/w_2)\, H_n(\sqrt{2}\, y/w_2)\, dx\, dy$$

we are in the case of formula 2.48 giving a Fourier transform, in the special case $p = q = 0$, which yields a non zero result only for even orders both in m and in n. For even orders, we get

$$\Gamma_{2m,2n} \;=\; \sqrt{\frac{2}{\pi w_1^2}} \sqrt{\frac{2}{\pi w_2^2}} \sqrt{\frac{1}{2^{m+n}\, m!\, n!}} \;\times$$

$$\times \frac{\pi w_2^2}{1+w_2^2/w_1^2} \; \left[\frac{-1}{(1+w_2^2/w_1^2)^2}\right]^{m+n} (1-w_2^4/w_1^4)^{m+n} \; (-1)^m \frac{2m!}{m!} \; (-1)^n \frac{2n!}{n!}$$

so that, at the end,

$$\Gamma_{2m,2n} \;=\; \frac{\sqrt{2m!\, 2n!}}{2^m 2^n m! n!} \; \frac{2 w_1 w_2}{w_1^2+w_2^2} \; \left[\frac{w_1^2-w_2^2}{w_1^2+w_2^2}\right]^{m+n}$$

The arithmetic factor (under the square root) has a very low decreasing rate, as m, n grow, so that if w_1 and w_2 are very different, the coupling coefficients are very small and very slowly decreasing with the order (as could

be foreseen). Note that $w_1 = w_2$ yields $\Gamma_{2m,2n} = 0$ for $m, n \neq 0$, and $\Gamma_{0,0} = 1$. It is easy to check that the total power is conserved, for the arithmetic factors can be recognized as those in the Taylor expansion of $(1-x^2)^{-1/2}$. In fact:

$$(1-x^2)^{-1/2} \;=\; \sum_k \frac{2k!}{2^{2k}k!^2}x^{2k} \quad (|x|<1)$$

so that,

$$\sum_{m,n} \frac{2m!\,2n!}{2^{2m+2n}m!^2\,n!^2}\left[\frac{w_1^2-w_2^2}{w_1^2+w_2^2}\right]^{2m+2n} = \left[\sum_m \frac{2m!}{2^{2m}m!^2}\left[\frac{w_1^2-w_2^2}{w_1^2+w_2^2}\right]^{2m}\right]^2 = \frac{(w_1^2+w_2^2)^2}{4w_1^2w_2^2}$$

and thus

$$\sum_{m,n} |\Gamma_{2m,2n}|^2 \;=\; 1$$

Now, if the input amplitude and the TEM_{mn} basis are not taken at the waist, the formula for coupling the TEM_{00} mode of parameters $(w_1,\ R_1)$ with the TEM_{mn} mode of parameters $(w_2,\ R_2)$ is simply:

$$\Gamma_{2m,2n} \;=\; \frac{\sqrt{2m!\,2n!}}{2^m 2^n m!n!}\,\frac{2w_1w_2}{w_1^2+w_2^2-i\frac{k}{2}w_1^2w_2^2(1/R_1-1/R_2)}$$

$$\times\;\left[\frac{w_1^2-w_2^2+i\frac{k}{2}w_1^2w_2^2(1/R_1-1/R_2)}{w_1^2+w_2^2-i\frac{k}{2}w_1^2w_2^2(1/R_1-1/R_2)}\right]^{m+n}$$

(with $k \;\equiv\; 2\pi/\lambda$).

3.3.8 Coupling of astigmatic beams

Consider an astigmatic normalized optical amplitude of the following type:

$$A(x,y) = \sqrt{\frac{2}{\pi w_1 w_2}}\;\exp\left[-\frac{x^2}{w_1^2}-\frac{y^2}{w_2^2}\right]$$

The wavefront is assumed flat at $z=0$. After diffraction over a distance L, the amplitude becomes, up to uniform phases (propagation+Gouy):

$$B(x,y) = \sqrt{\frac{2}{\pi W_1 W_2}}\;\exp\left[-\frac{x^2}{W_1^2}-\frac{y^2}{W_2^2}\right]\;\exp\left[-i\frac{\pi}{\lambda R_1}x^2 - i\frac{\pi}{\lambda R_2}y^2\right]$$

where $W_1,\ W_2$ on one hand, et $R_1,\ R_2$ on the other, are derived from $w_1,\ w_2$ and from the distance L through the ordinary gaussian formulas:

$$W_1 = w_1\sqrt{1+\frac{L^2}{b_1^2}}$$

$$W_2 = w_2\sqrt{1+\frac{L^2}{b_2^2}}$$

$$R_1 = L\left[1+\frac{b_1^2}{L^2}\right]$$

$$R_2 = L\left[1+\frac{b_2^2}{L^2}\right]$$

$b_1,\ b_2$ are the two Rayleigh parameters corresponding to the two astigmatism directions:

$$b_1 \equiv \pi w_1^2/\lambda, \quad b_2 \equiv \pi w_2^2/\lambda$$

Suppose now a TEM_{00} mode:

$$\phi(x,y) = \sqrt{\frac{2}{\pi w_0^2}}\ \exp\left[-\frac{x^2+y^2}{w_0^2}\right]$$

Let us compute the scalar product

$$\Gamma = \langle \phi, B \rangle$$

The result is:

$$|\Gamma|^2 = \frac{4w_0^2 W_1 W_2}{\sqrt{(w_0^2+W_1^2)^2+\frac{b^2W_1^4}{R_1^2}}\sqrt{(w_0^2+W_2^2)^2+\frac{b^2W_2^4}{R_2^2}}}$$

where $b \equiv \pi w_0^2/\lambda$ is the usual Rayleigh parameter for the TEM_{00} mode. This expresses the rate of incoming power one can couple in a perfect TEM_{00} mode when the incoming amplitude is astigmatic in such a way that the intensity has two different widths along x and y, and the wavefront two different curvatures along x and y.

3.3.9 Properties of the Displacement polynomials

The $\{Q_{mn}\}$ polynomials have useful properties, that we summarize below without proof. All can be obtained after some elementary algebra, using the recurrence relations of the Hermite polynomials.

- Definition:

$$Q_{mn}(x) \;=\; \sum_{k=0}^{\min(m,n)} \frac{(-2)^k\; m!n!}{k!\,(m-k)!\,(n-k)!}\; x^{m+n-2k} \tag{3.40}$$

  making clear the symmetry with respect to m and n.

- Value at $x = 0$:

$$Q_{mn}(0) \;=\; 0 \quad (m \neq n) \tag{3.41}$$

$$Q_{mm}(0) \;=\; (-2)^m\, m! \tag{3.42}$$

- Recurrence relation:

$$Q_{m+1,n}(x) \;=\; x\, Q_{mn}(x) - 2n\, Q_{m,n-1}(x) \tag{3.43}$$

  or as well

$$Q_{m,n+1}(x) \;=\; x\, Q_{mn}(x) - 2m\, Q_{m-1,n}(x) \tag{3.44}$$

- Orthogonality:

$$\sum_{k\geq 0} \frac{1}{2^k k!}\; Q_{mk}(x)\; Q_{kn}(x) \;=\; 2^m m!\; \mathrm{e}^{x^2/2}\; \delta_{mn} \tag{3.45}$$

- Addition law:

$$\sum_{k\geq 0} \frac{(-1)^k}{2^k k!}\; Q_{mk}(x)\; Q_{kn}(y) \;=\; \mathrm{e}^{-xy/2}\; Q_{mn}(x+y) \tag{3.46}$$

- Derivative:

$$\frac{dQ_{mn}(x)}{dx} \;=\; mQ_{m-1,n}(x) + nQ_{m,n-1}(x) \tag{3.47}$$

- Some of the first polynomials:

	0	1	2	3
0	1	x	x^2	x^3
1	x	x^2-2	x^3-4x	x^4-6x^2
2	x^2	x^3-4x	x^4-8x^2+8	x^5-12x^3+24x
3	x^3	x^4-6x^2	x^5-12x^3+24x	$x^6-18x^4+72x^2-48$
4	x^4	x^5-8x^3	$x^6-16x^4+48x^2$	$x^7-24x^5+144x^3-192x$
5	x^5	x^6-10x^4	$x^7-20x^5+80x^3$	$x^8-30x^6+240x^4-480x^2$

The first lines are simple:

$$Q_{0n}(x) = x^n \tag{3.48}$$

$$Q_{1n}(x) = x^{n+1} - 2n\,x^{n-1} \tag{3.49}$$

$$Q_{2n}(x) = x^{n+2} - 4n\,x^n + 4n(n-1)\,x^{n-2} \tag{3.50}$$

$$Q_{3n}(x) = x^{n+3} - 6n\,x^{n+1} + 12n(n-1)\,x^{n-1} - 8n(n-1)(n-2)\,x^{n-3} \tag{3.51}$$

- Miscellaneous:

$$\sum_{n\geq 0} \frac{Q_{mn}(x)}{n!} = (x-2)^m\ \mathrm{e}^x$$

3.3.10 Structural properties of Displacement matrices

Practical use of the displacement operators raises several questions.

Energy conservation The energy coming under the form of a given mode (m,n) is in general spread over all others after any non perfect optical element. We have seen that rotations and translations can be represented by operators of the form

$$U_{mn,kl}(p,q) = \left(\frac{1}{\sqrt{2}}\right)^{m+n+k+l} \frac{u^{m+n+k+l}}{\sqrt{m!n!k!l!}}\, Q_{mk}(p)\ Q_{nl}(q)\ \mathrm{e}^{-(p^2+q^2)/4}$$

where u is a unitary complex number, and (p,q) a couple of parameters representing the two degrees of freedom of the displacement. Conservation of the energy brought by any (m,n) mode requires the following relation:

$$1 = \sum_{k,l} |U_{mn,kl}(p,q)|^2$$

This leads to compute $|Q_{mk}|^2$. We do it for definiteness in the case of rotations, but the method is quite general. We first take the formula 3.28 defining the Q polynomials, this yields

$$Q_{mk}(p) \;=\; (-i)^{m+k}\;\frac{1}{\sqrt{\pi}}\;\mathrm{e}^{p^2/4}\;I_{mk}(p)$$

then the formula 3.26 giving the definition of the I_{mk} integrals:

$$I_{mk}(p) \;=\; \int_{\mathbf{R}} dx\;\mathrm{e}^{-x^2}\mathrm{e}^{ipx}\;H_m(x)H_k(x)$$

So that

$$|Q_{mk}(p)|^2 \;=\; \frac{1}{\pi}\,\mathrm{e}^{p^2/2}\int_{\mathbf{R^2}} dx\,dx'\,\mathrm{e}^{-(x^2+x'2)}\,\mathrm{e}^{ip(x-x')}\;H_m(x)\,H_m(x')\,H_k(x)\,H_k(x')$$

We have consequently

$$\sum_k \frac{1}{2^k k!}|Q_{mk}(p)|^2 \;=\; \frac{1}{\pi}\,\mathrm{e}^{p^2/2}\times$$

$$\times\int_{\mathbf{R^2}} dx\,dx'\,\mathrm{e}^{-(x^2+x'2)}\;\mathrm{e}^{ip(x-x')}\;H_m(x)\,H_m(x')\;\sum_k\frac{1}{2^k k!}H_k(x)\,H_k(x')$$

Due to the closure relation 2.44, we have

$$\sum_k \frac{1}{2^k k!}H_k(x)\,H_k(x') \;=\; \sqrt{\pi}\mathrm{e}^{(x^2+x'2)/2}\delta(x-x')$$

from what we get

$$\sum_k \frac{1}{2^k k!}|Q_{mk}(p)|^2 \;=\; \frac{1}{\sqrt{\pi}}\;\mathrm{e}^{p^2/2}\int_{\mathbf{R}} dx\,\mathrm{e}^{-x^2}\,H_m(x)^2$$

and due to the normalization relation 2.43, we find

$$\sum_k \frac{1}{2^k k!}|Q_{mk}(p)|^2 \;=\; 2^m m!\;\mathrm{e}^{p^2/2} \tag{3.52}$$

(This is an indirect proof of eq.3.45 for $m = n$). Now, if we return to the energy balance, we have

$$\sum_{k,l}|U_{mn,kl}(p,q)|^2 \;=\; \frac{1}{2^{m+n}m!\,n!}\,\mathrm{e}^{-(p^2+q^2)/2}\;\left[\sum_k\frac{1}{2^k k!}|Q_{mk}(p)|^2\right]\left[\sum_l\frac{1}{2^l l!}|Q_{nl}(q)|^2\right] \;=\; 1$$

owing to eq. 3.52.

Transitivity Given any two displacements of parameters (p_1, q_1) and (p_2, q_2) respectively, the result of the sequence is a displacement of parameters $(p_1 + p_2, q_1 + q_2)$.

$$\sum_{kl \geq 0} D_{mn,kl}(p_1, q_1)\ D_{kl,st}(p_2, q_2) \ = \ D_{mn,st}(p_1 + p_2, q_1 + q_2)$$

This is a direct consequence of the addition law 3.46.

Inversion Given any displacement of parameters (p, q), represented by matrix $D_{mn,kl}(p, q)$, the inverse displacement $(-p, -q)$ is represented by $D_{mn,kl}(-p, -q)$, and we have

$$\sum_{kl \geq 0} D_{mn,kl}(p, q)\ D_{kl,st}(-p, -q) \ = \ \delta_{ms}\, \delta_{lt}$$

This was *a priori* expected, but it is instructive to see that it is one more consequence of the addition law 3.46. It also can be deduced from transitivity, for

$$D_{mn,kl}(0, 0) \ = \ \delta_{mk}\, \delta_{nl}$$

3.3.11 Magnitude of displacement matrix elements

Consider for instance the rotation matrix:

$$R_{mnkl}(\theta, \phi) \ = \ R'_{mk}(\theta, \phi)\, R'_{nl}(\theta, \phi)$$

We can set as previously

$$p \equiv \sqrt{2}\, \frac{2\pi}{\lambda}\, w\, \theta \cos(\phi) \quad , \quad q \equiv \sqrt{2}\, \frac{2\pi}{\lambda}\, w\, \theta \sin(\phi)$$

so that, setting

$$R'_{mk}(x) \ \equiv \ \frac{i^{m+k}}{\sqrt{2^{m+k} m! k!}}\, Q_{mk}(x)\, \mathrm{e}^{-x^2/4}$$

we have

$$R_{mnkl}(\theta, \phi) \ = \ R'_{mk}(p) \times R'_{nl}(q)$$

It is interesting to check the numerical values of these matrix coefficients. For instance, we can study the coupling of the TEM_{00} mode with higher order ones (see Fig.3.27). we see that the coupling efficiency is very small

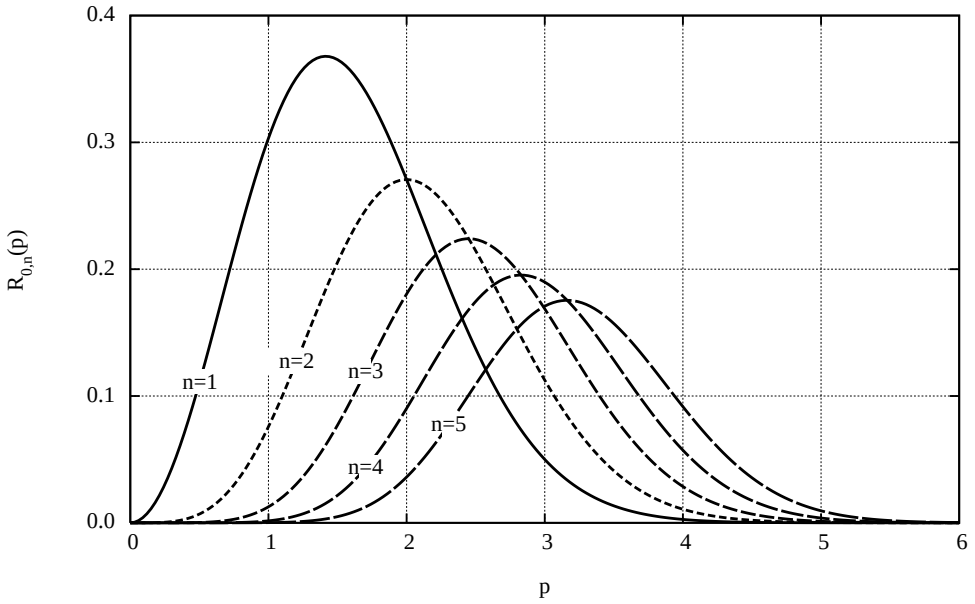

Figure 3.27: Power coupled from the TEM_{00} mode into higher order modes (TEM_{0n}) through rotation of a mirror

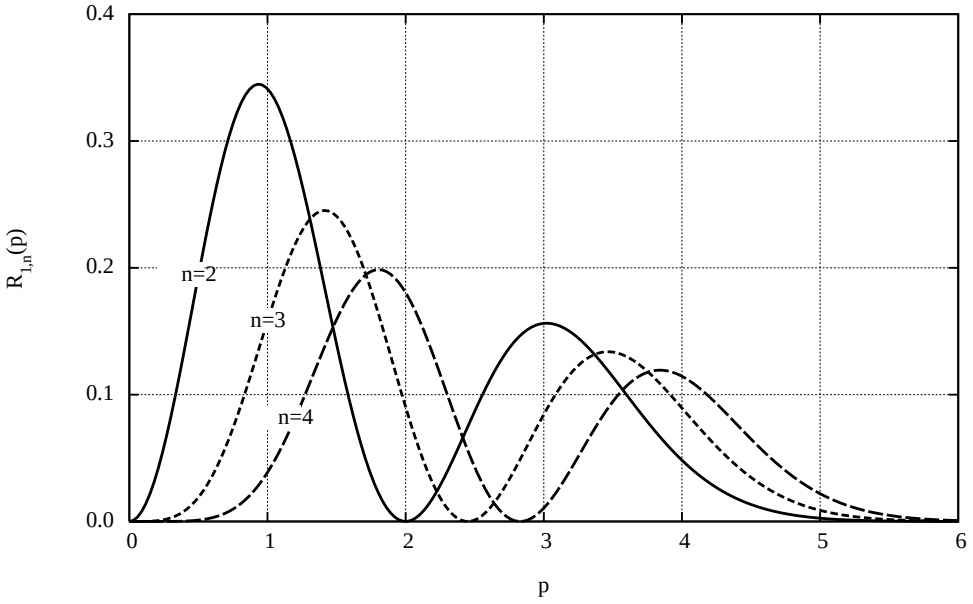

Figure 3.28: Power coupled from the TEM_{10} mode into higher order modes (TEM_{1n}) through rotation of a mirror

for orders larger than 2 and values of p smaller than 1. If we assume (Virgo parameters) a waist of 2 cm on the cavity input mirror, a curvature radius of 3.45 km of the far mirror, the width on that far mirror is about 5.5 cm, and the correspondance between p and the rotation angle θ is:

$$\theta \;=\; p \;\times\; 2.18\,10^{-6}\ \mathrm{Rd}$$

so that $p = 1$ corresponds to about 13% of the gaussian aperture $\theta_g = \lambda/\pi w_0$. The gaussian aperture corresponds to $p \sim 7.8$. In this angular region, it makes sense to assume a very weak rate of modes having orders larger that 2. It is also interesting to see how the TEM_{10} and TEM_{20} modes, for instance, couple to higher orders (see Figs.3.28 and 3.29): This shows that a light initially (00) is weakly directly coupled into the (20) mode, as well as indirectly through (10). This makes consistent an approximate model (see next subsection) involving only first orders modes, when θ is small. Finally,

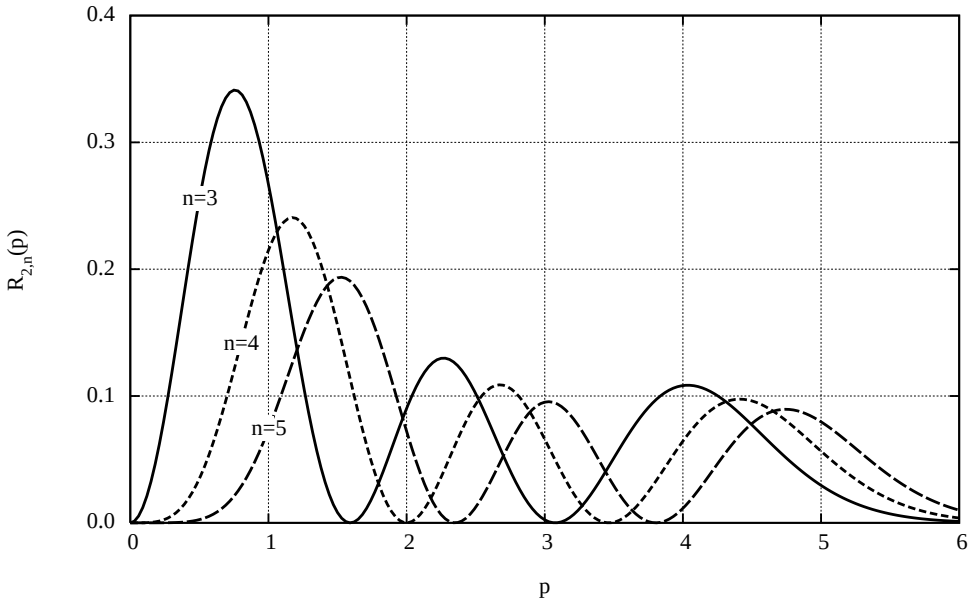

Figure 3.29: Power coupled from the TEM_{20} mode into higher order modes through rotation of a mirror

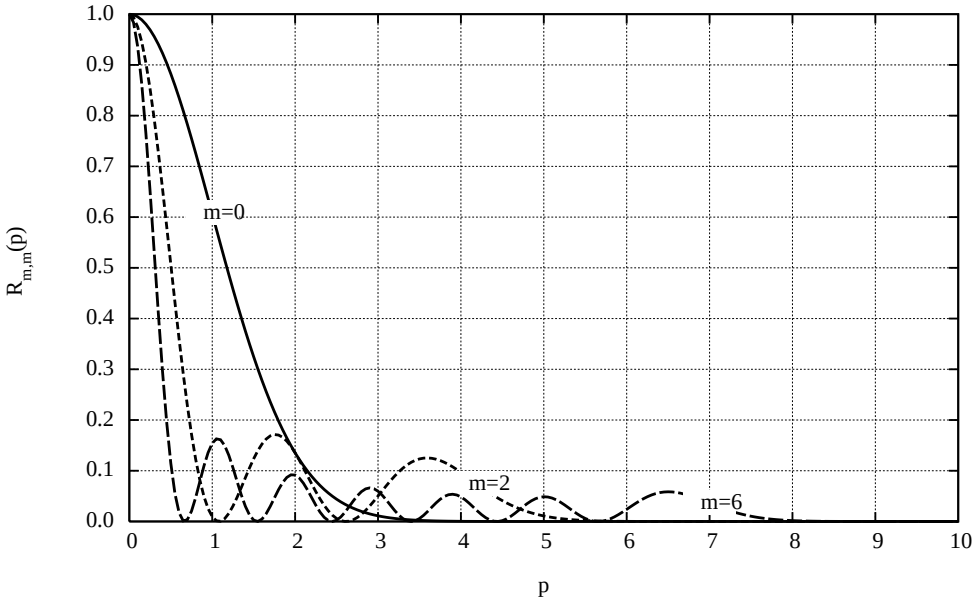

Figure 3.30: Power coupled from the $\mathrm{TEM_{mm}}$ mode into itself

we show how the first orders are coupled into themselves (see Fig.3.30): The complete map of the rotation matrix squared modulus in the (p, q) plane has the following pattern (the example of $R_{0055}(p, q)$ is shown on Fig.3.31). The four maxima correspond to the maxima already shown on Fig.3.27.

3.3.12 Numerical results

We check here the results we can obtain from a modal expansion limited to orders up to 2. This means that we restrict the expansion to the 6 modes (00), (10), (01), (20), (11),and (02). Namely, we consider a flat/spherical cavity where the spherical mirror is rotated by an angle θ, and we study firstly the displacement of the intracavity mode. We classically expect a transversal displacement of $\Delta x = R_c \times \theta$: see Fig.3.33. When the misalignment angle θ increases, the stored poser decreases: see Fig.3.34. We can also study the field reflected by the cavity. Fig.3.35 shows the evolution of the

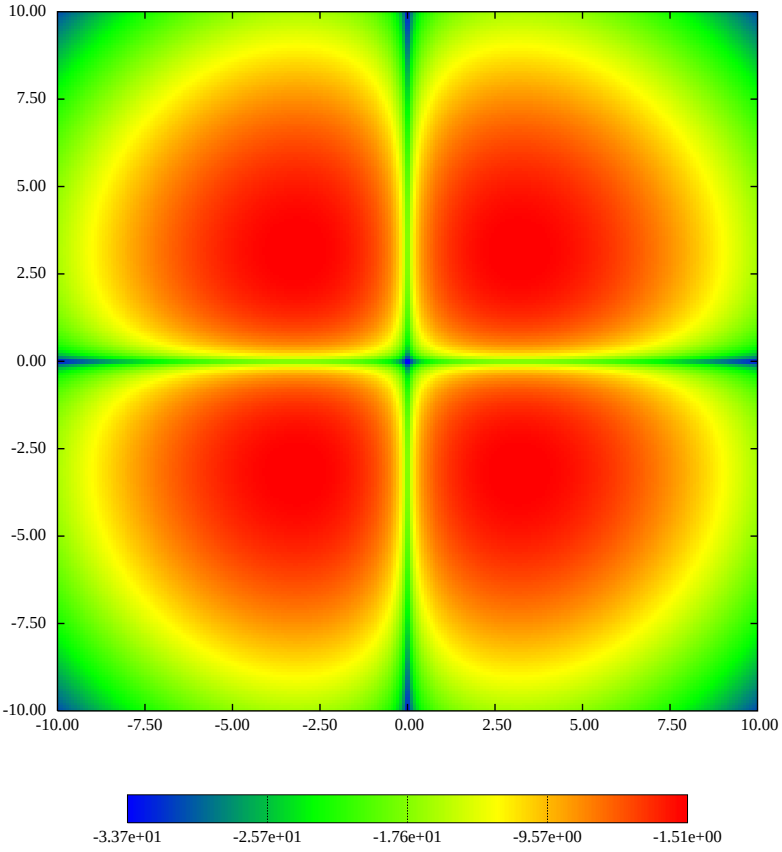

Figure 3.31: Power coupled from the TEM_{00} mode into TEM_{55} after a rotation, ((p, q) plane, logarithmic scale)

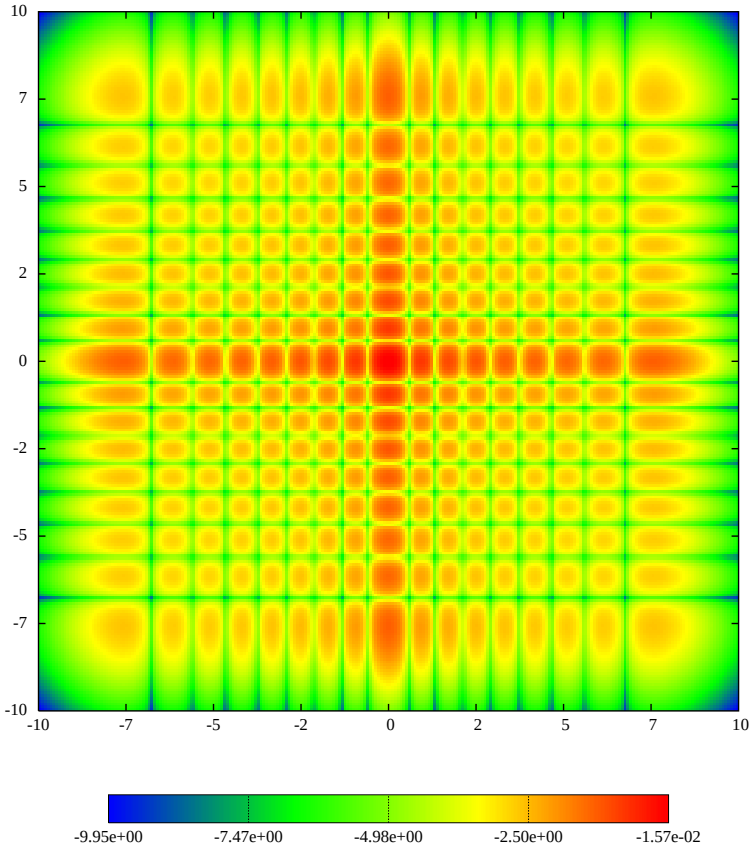

Figure 3.32: Power coupled from the TEM_{88} mode into itself ((p, q) plane, logarithmic scale)

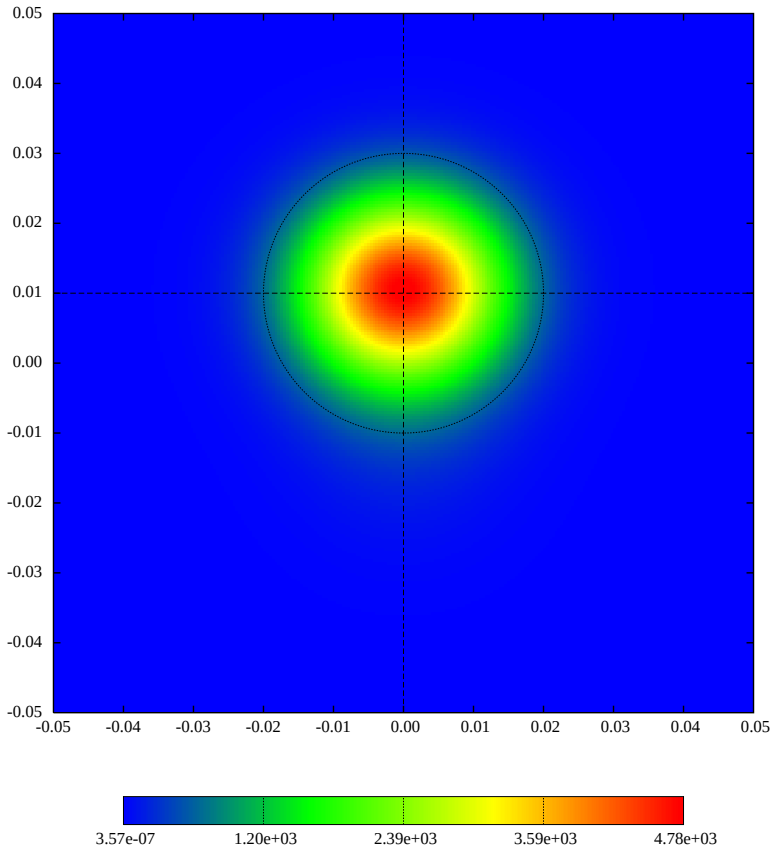

Figure 3.33: Map of the intracavity mode for $\theta = 2.9$ μRd misaligment of the far miror (A rather extreme case). The circle shows the theoretical location of the mode.

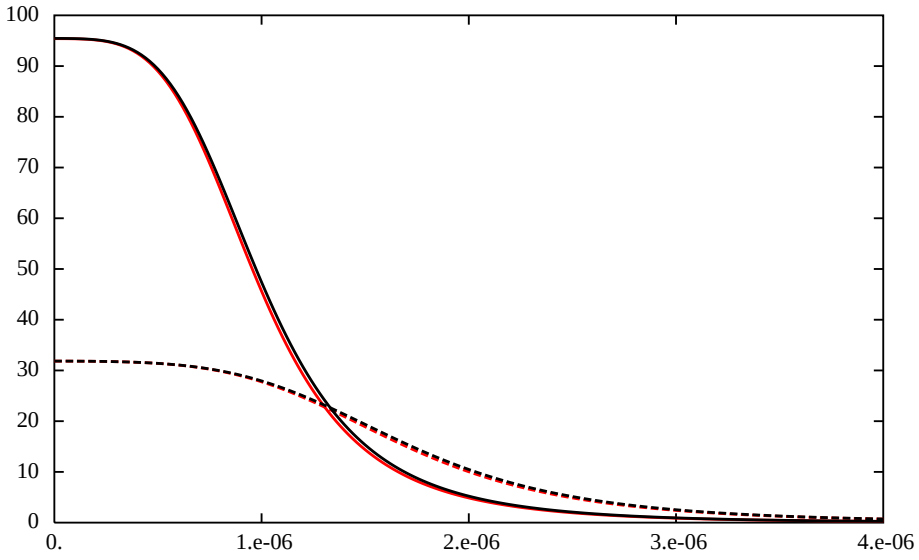

Figure 3.34: Intracavity power vs misalignment of the far mirror. Finesse=150 (solid line), Finesse=50 (dashed line). The red curves are obtained from a full FFT simulation over 512×512 samples

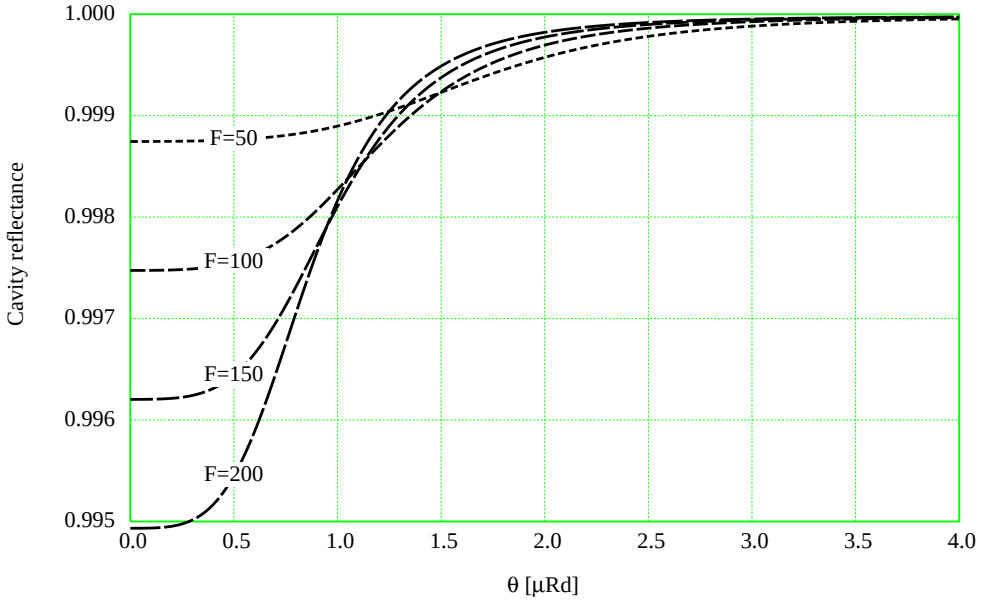

Figure 3.35: Power reflectance of a cavity for increasing tilt angle and for several finesses

reflected amplitude from a cavity having a tilted far mirror. We see that tilting the mirror has a negligible effect for small angles, and for larger values is equivalent to a detuning, so that the reflectance increases. It is worth to emphasize that this is not due to the longitudinal displacement of the mirror, which has been corrected as if a servo loop were present. The rotation angle being θ, the apex equation of the mirror (of curvature radius R_c) is:

$$z = \frac{x^2+y^2}{2R_c} + \theta x \;=\; \frac{(x+\theta R_c)^2+y^2}{2R_c} + \frac{1}{2}\theta^2 R_c$$

a corrective phase of

$$\delta\Phi \;=\; -\pi R_c \theta^2/\lambda$$

is therefore introduced in the propagator. For higher tilt angles, the reflectance of the cavity progressively reaches a constant value which is nothing but the bare reflectance of the input mirror: the far mirror can not more

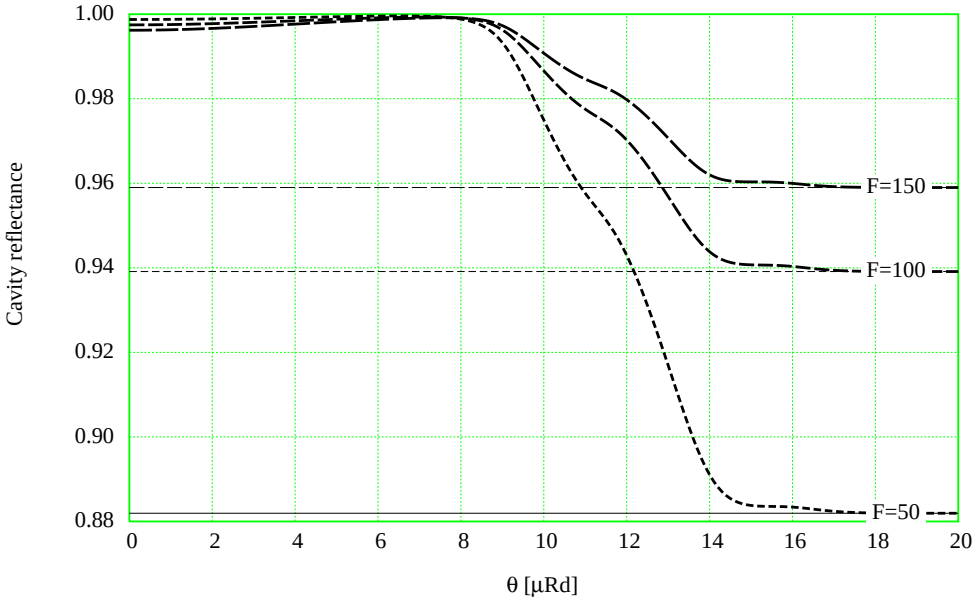

Figure 3.36: Power reflectance of a cavity for increasing tilt angle and for several finesses. The horizontal lines represent the power reflectance of the input mirror corresponding to the different finesses

produce interferences in the cavity. This happens when the tilt angle reaches values comparable with the beam aperture: see Fig.3.36. Remark that if the tilt angle is equal to the beam gaussian aperture, the transverse displacement of the intracavity beam is:

$$\Delta x \;=\; \theta_g R_c \;=\; \frac{\lambda}{\pi w_0} R_c$$

so that

$$\Delta x / w_0 \;=\; R_c / b$$

where b is the Rayleigh parameter. For the Virgo parameters, this is $\Delta x / w_0 \sim 3$, so that the input beam is mostly out the intracavity beam. Even if the input field is a pure TEM_{00}, a small misaligment introduces a second resonance

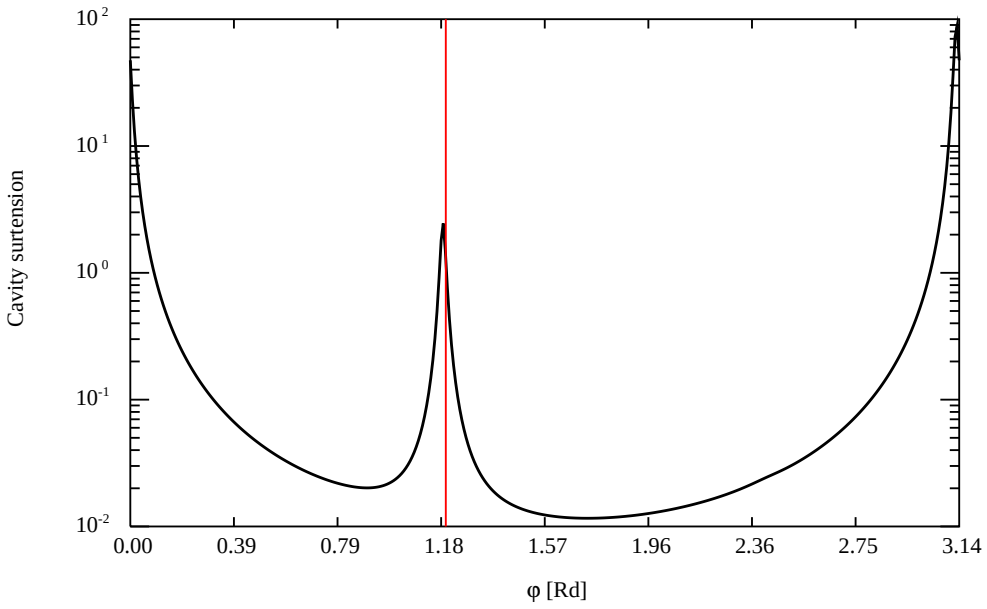

Figure 3.37: Resonances of a Fabry Perot cavity with a small misalignment. The red line is the theoretical position of the TEM_{10} mode

at the frequency (or cavity length corresponding to higher order modes, especially the TEM_{10} or the TEM_{01} depending on the direction of the tilt. On Fig.3.37, we have scanned the free spectral range and compared the numerical peak with the theoretical position of the (10) resonance. Finally, it is possible to build a Michelson having a reference arm (ideal cavity) and a second arm having a tilted far mirror. The dark finge pattern exhibits a characteristic TEM_{10} signature. (Fig.3.38).

3.3.13 Modal expansion of flat modes

The interest of flat modes already presented int the Beam Optics chapter, will be developped in a foregoing chapter devoted to thermal noise. It is however the right place to study the modal expansion of such modes. We recall that flat modes can be viewed as a superposition of elementary gaussian modes of

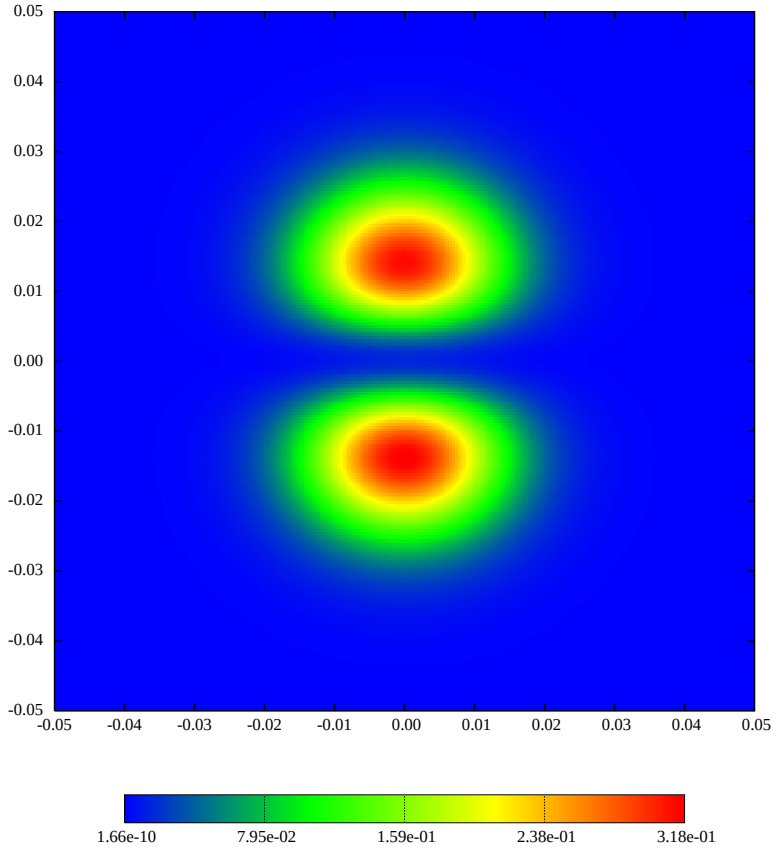

Figure 3.38: Dark fringe on the output port of a Michelson for .1 μRd tilted far mirror on one arm

waists w_0 uniformly distributed on a disk of radius b in the plane transverse to propagation direction. Namely, at the abscissa $z = 0$ where the wavefront is flat, we have for the fundamental flat mode:

$$\Psi_{00}(x, y, 0) \;=\; \frac{1}{\pi b^2} \int_\Delta \phi_{00}(x - x_0, y - y_0, 0) dx_0\, dy_0 \tag{3.53}$$

where $\phi_{00}(x, y, z)$ is a TEM_{00} mode of waist w_0. Owing to the modal properties of gaussian beams precedingly presented, we have

$$\phi_{00}(x - x_0, y - y_0, 0) \;=\; \sum_{m,n} T_{00mn}(x_0, y_0)\, \phi_{mn}(x, y, 0)$$

where T_{klmn} is the displacement matrix defined above. This provides a mean to expand flat modes on the HG basis of the elementary gaussian modes of parameter w_0. We have in particular:

$$T_{00mn}(x_0, y_0) \;=\; \frac{(-)^{m+n}}{\sqrt{2^{m+n} m!\, n!}}\, Q_{0m}(\sqrt{2} x_0/w_0)\, Q_{0n}(\sqrt{2} y_0/w_0)\, \exp\left(-\frac{x_0^2 + y_0^2}{2w_0^2}\right)$$

where the Q_{km} functions are the displacement polynomials. In this special case, we have seen that:

$$Q_{0m}(x) \;=\; x^n$$

so that the integral 3.53 becomes:

$$\Psi_{00}(x, y, 0) \;=\; \sum_{m,n} \Gamma_{00mn} \phi_{mn}(x, y)$$

with

$$\Gamma_{00mn} \;=\; \frac{1}{\pi b^2} \frac{(-)^{m+n}}{\sqrt{2^{m+n} m!\, n!}} \times$$

$$\times \int_0^{2\pi} d\phi \int_0^b \left(\frac{x_0\sqrt{2}}{w_0}\right)^m \left(\frac{y_0\sqrt{2}}{w_0}\right)^n \exp\left(-\frac{r_0^2}{2w_0^2}\right) r_0\, dr_0$$

where (r_0, ϕ) are the polar coordinates equivalent to (x_0, y_0). It is easily seen that the coefficients Γ_{mn} having at least one index odd are zero, moreover, we have:

$$\frac{1}{2\pi} \int_0^{2\pi} \cos^{2m}\phi\, \sin^{2n}\phi\; d\phi \;=\; \frac{2m!\, 2n!}{2^{2m+2n}\, m!\, n!\, (m+n)!}$$

on the other hand, we know that:

$$\int_0^R \rho^{2k+1} \mathrm{e}^{-\rho^2}\, d\rho \;=\; \frac{k!}{2}\left[1 - \mathrm{e}^{-R^2} \sum_{s=0}^{k} \frac{R^{2s}}{s!}\right]$$

Putting these together, we find that the non zero coefficients are:

$$\Gamma_{0,0,2m,2n} \;=\; \frac{\sqrt{2m!\,2n!}}{2^{m+n}\, m!\, n!}\, \gamma_{m+n}(b^2/2w_0^2)$$

where the functions $\gamma_k(x)$ (closely related to the incomplete Gamma function) are defined by:

$$\gamma_k(x) \;\equiv\; \frac{1}{x}\left[1 - \mathrm{e}^{-x} \sum_{s=0}^{k} \frac{x^s}{s!}\right]$$

an equivalent form, useful for small arguments, is:

$$\gamma_k(x) \;=\; \frac{x^k}{(k+1)!} \sum_{s=0}^{\infty} \frac{(-x)^s}{s!}\, \frac{k+1}{k+1+s}$$

The dependence of the Γ_{mn} on the indices is shown on Fig.3.39 in the special case $b = 10$ cm and $w_0 = 2$ cm: The same treatment can be applied to the (1,0) mode. We have, for the non zero coefficients:

$$\Gamma_{1,0,2m+1,2n} \;=\; -\frac{w_0^2}{2}\, \frac{1}{\sqrt{2^{2m+2n+2}(2m+1)!2n!}} \int_0^{2\pi} d\Phi \;\times$$

$$\times \int_0^{\sqrt{2}b/w_0} Q_{2m+1,1}(R\cos\Phi)\, Q_{2n,0}(R\sin\Phi)\, \mathrm{e}^{-R^2/4}\, R\, dR$$

and the result is:

$$\Gamma_{1,0,2m+1,2n} \;=\; \frac{\sqrt{(2m+1)!\,2n!}}{2^{m+n} m!\, n!}\, \left[\gamma_{m+n}(b^2/2w_0^2) - \gamma_{m+n+1}(b^2/2w_0^2)\right] \qquad (3.54)$$

or, as well

$$\Gamma_{1,0,2m+1,2n} \;=\; \frac{\sqrt{(2m+1)!\,2n!}}{2^{m+n} m!\, n!(m+n+1)!} \mathrm{e}^{-b^2/2w_0^2} \left(\frac{b^2}{2w_0^2}\right)^{m+n}$$

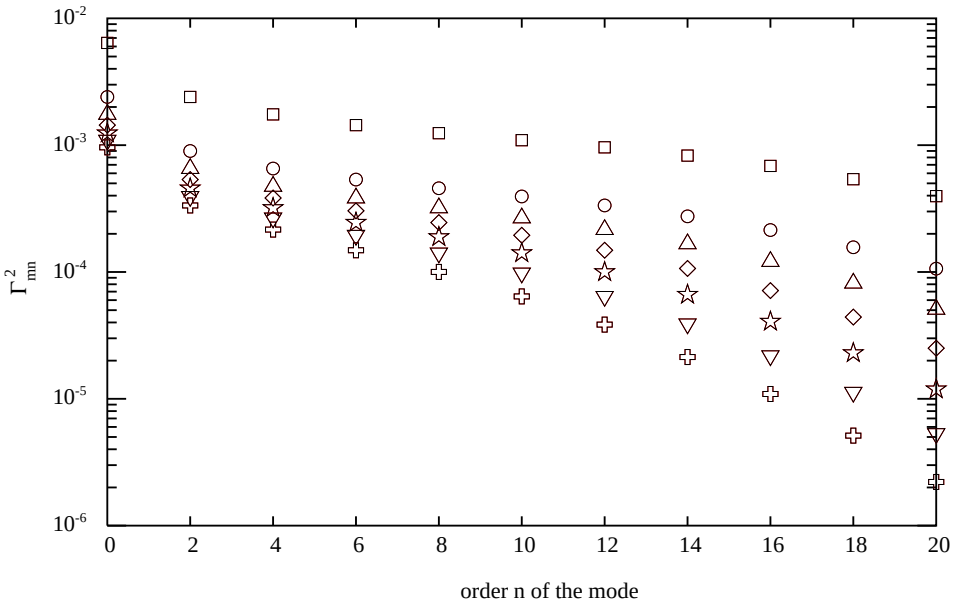

Figure 3.39: Power coupling coefficients Γ^2_{mn} for various orders.Squares : m=0, Circles: m=2, Up triangles: m=4, Diamonds: m=6, Stars: m=8, Down triangles: m=10, Crosses: m=12

3.3.14 The A266 Algebra

We often need a fast simulation code for a dynamical model of misaligned and detuned interferometer, in order for instance to study the global control of the system. If the angles are small compared to the divergence of the beam, it is possible to limit at 2d order the modal expansion for each mirror. Moreover, we see fom the preceding table that the modes of order m, n are coupled to the TEM_{00} at the $m+n$ order. A consistent 2d order expansion will thus involve the only first 6 modes, and we shall see that it is possible to carry out all calculations using a 2d order, rank 6×6 matrix algebra that we call A266. If we limit the expansion to the second order, the expression of the mirror operator, using the notation

$$p \;=\; \sqrt{2}kw\theta\cos\phi, \quad q \;=\; \sqrt{2}kw\theta\sin\phi$$

has the expression

$$R_{mnkl}(p,q) \;=\; \mathrm{e}^{-(p^2+q^2)/4}\;\mathcal{R}_{mnkl}(p,q)$$

where $\mathcal{R}_{mnkl}(p,q)$ is the following table:

	00	10	01	20	11	02
00	1	$i\frac{p}{\sqrt{2}}$	$i\frac{q}{\sqrt{2}}$	$-\frac{p^2}{2\sqrt{2}}$	$-\frac{pq}{2}$	$-\frac{q^2}{2\sqrt{2}}$
10	$i\frac{p}{\sqrt{2}}$	$1-\frac{p^2}{2}$	$-\frac{pq}{2}$	ip	$i\frac{q}{\sqrt{2}}$	0
01	$i\frac{q}{\sqrt{2}}$	$-\frac{pq}{2}$	$1-\frac{q^2}{2}$	0	$i\frac{p}{\sqrt{2}}$	iq
20	$-\frac{p^2}{2\sqrt{2}}$	ip	0	$1-p^2$	$-\frac{pq}{\sqrt{2}}$	0
11	$-\frac{pq}{2}$	$i\frac{q}{\sqrt{2}}$	$i\frac{p}{\sqrt{2}}$	$-\frac{pq}{\sqrt{2}}$	$1-p^2-q^2$	$-\frac{pq}{\sqrt{2}}$
02	$-\frac{q^2}{2\sqrt{2}}$	0	iq	0	$-\frac{pq}{\sqrt{2}}$	$1-q^2$

There is an apparent inconsistency in keeping the exponential not expanded, but this is not necessary for numerical computations, and gives much better accuracy when the expansion parameter (for instance θ/θ_g is not infinitesimal. The free propagation along the optical axis is represented by the diagonal operator

$$P_{mn,pq} \;=\; \exp\left[-i(m+n)\arctan\left(\frac{L}{b}\right)\right]\delta_{mp}\delta_{nq}$$

where L is the propagation distance and b the Rayleigh Range. It is therefore clear that all operators involved in A266 are of the form

$$M \;=\; M_0 + M_1 \;+\; M_2$$

where the partial operators M_i $(i = 1, 2, 3)$ contain respectively the zeroth order in the perturbation strength (θ/θ_g or $\Delta x/w$), the first order and the second. Moreover, each partial operator has a special structure. We note $\mathcal{O}_3$, $\mathcal{O}_{12}$ and $\mathcal{O}_{18}$ the sets of operators having these structures. Namely, $\mathcal{O}_3$ is the set of 6×6 operators of the form

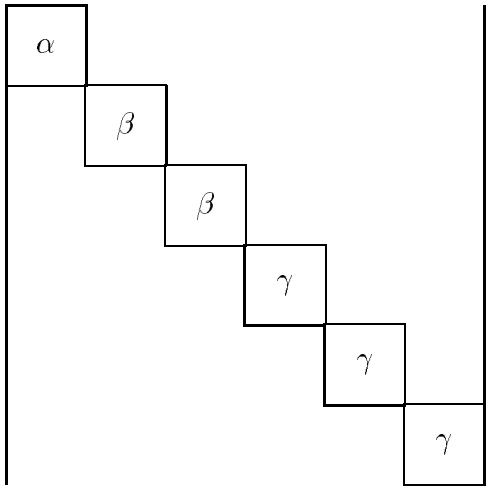

to which obviously belongs the propagation operator, and the zeroth order of any operator, $\mathcal{O}_{12}$ is the set of 6×6 operators of the form

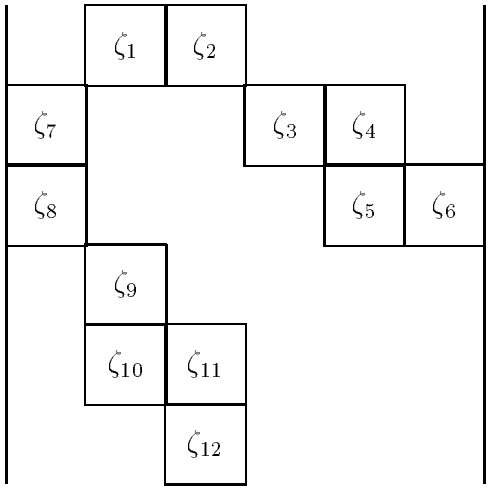

to which belongs the first order part of the operators. $\mathcal{O}_{18}$ is the set of 6×6 operators of the form

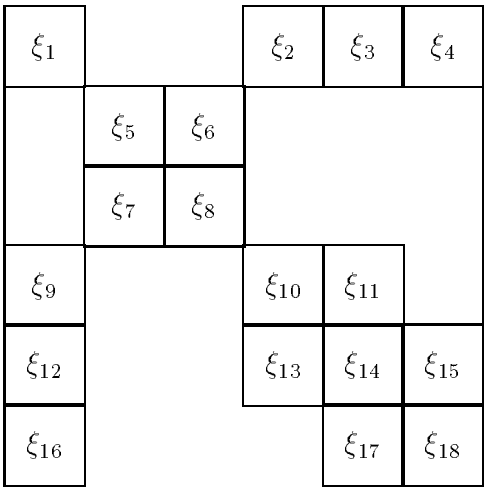

to which belongs the second order part of the operators. This kind of storage requires $3 + 12 + 18 = 33$ places instead of 36 in the general case: There is no waste of memory. The global structure is stable by the elementary algebraic operations. More specifically, it is obvious that if $A, B \in \mathcal{O}_3$, then $AB \in \mathcal{O}_3$. if $A \in \mathcal{O}_3$ and $B \in \mathcal{O}_{12}$ resp $\mathcal{O}_{18}$ then $AB \in \mathcal{O}_{12}$ resp $\mathcal{O}_{18}$. What is more remarkable is the following property which is the basis of A266: if $A, B \in \mathcal{O}_{12}$ then $AB \in \mathcal{O}_{18}$. The separation in three partial operators is therefore stable, and any algebraic operation reduces to trivial sums and products. We give below the most necessary.

- The sum of two operators is trivially defined by

  $$(A + B)_0 = A_0 + B_0, \quad (A + B)_1 = A_1 + B_1, \quad (A + B)_2 = A_2 + B_2$$

- The product of two operators is defined by

  $$(AB)_0 = A_0B_0, \quad (AB)_1 = A_0B_1 + A_1B_0 \quad (AB)_2 = A_0B_2 + A_1B_1 + A_2B_0$$

  note that the structure allows algorithms faster than the standard matrix product.

- The inverse of an operator is defined recursively by

  $$(A^{-1})_0 = A_0^{-1}$$

  which is a trivial operation, A_0 being diagonal, then

  $$(A^{-1})_1 = -(A^{-1})_0 A_1 (A^{-1})_0$$

$$(A^{-1})_2 \;=\; -(A^{-1})_0 \left[A_1 (A^{-1})_1 + A_2 (A^{-1})_0\right]$$

Remark that there is no need for a matrix inversion algorithm: In fact this is the main reason for the efficiency of A266.

- The square root X of an operator A is defined recursively by the following scheme:

$$X_0 \;=\; \sqrt{A_0}$$

which is a trivial operation, A_0 being diagonal, then

$$X_{1,ij} \;=\; \frac{A_{1,ij}}{X_{0,ii} + X_{0,jj}}$$

$$X_{2,ij} \;=\; \frac{A_{2,ij} - (X_1^2)_{ij}}{X_{0,ii} + X_{0,jj}}$$

3.4 Monte-Carlo methods

If the system in which light propagates has a complex geometry, and if the information carried by the phase is not essential, it is possible to represent light by particles following straight trajectories between reflections or diffusion processes. This is approximately the Newton theory of light. We call "photons" these particles for brevity, though the quantum nature of light is completely ignored in this approach. By launching randomly a large number of such photons, statistics can tell us where the light goes and how we can forbid certain areas to it (e.g. stray light studies). What is interesting is that the diffraction phenomena can be represented up to a certain extent by this particle description, leading to realistic models of light propagation.

3.4.1 Spatial spectra, plane waves and photons

We consider on an initial plane, a given complex amplitude of light $A(x, y)$. We can interpret the normalized square modulus of the amplitude as a probability density for a photon to be launched:

$$\frac{dP'}{ds}(x, y) \;=\; |A(x, y)|^2$$

This doesn't tell us the direction of the photon. We know that the angular information on the angles can be extracted from the Fourier transform of

the amplitude. The 2D Fourier transform of the amplitude is nothing but an expansion in terms of plane waves having for transverse components of $\vec{k}$, the conjugated variables (p, q). If we consider the square modulus of the latter, we have, due to the Parseval-Plancherel theorem:

$$\int_{\mathbf{R}^2} dp\, dq\, |\tilde{A}(p,q)|^2 \;=\; 4\pi^2$$

On the other hand, by using the substitution

$$p \;=\; k\sin\theta\cos\phi \quad , \quad q \;=\; k\sin\theta\sin\phi$$

we obtain

$$\int_{\mathbf{R}^2} dp\, dq\, |\tilde{A}(p,q)|^2 \;=\; k^2 \int_0^{2\pi} d\phi \int_0^{\pi} d\theta\, |\tilde{A}(\theta,\phi)|^2$$

and consequently:

$$\frac{1}{\lambda^2} \int_0^{2\pi} d\phi \int_0^{\pi} d\theta\, |\tilde{A}(\theta,\phi)|^2 \;=\; 1$$

which shows that we can obtain a probability density for the angular distribution by taking

$$\frac{dP''}{d\Omega}(\theta,\phi) \;=\; \frac{1}{\lambda^2}\, |\tilde{A}(\theta,\phi)|^2$$

Propagation of the light described by the complex amplitude $A(x, y)$ will thus be described by the two densities of probabilities: The departure point of a photon will obey the statistics corresponding to dP'/ds, and its direction, the statistics defined by $dP''/d\Omega$.

3.4.2 Propagation

After having chosen the departure point (x, y) and the direction of the photon (θ, ϕ), its trajectory is defined, and it is possible to compute the point (X, Y) at which it hits the plane $z = d$ (see Fig.3.40). It is even possible to compute the probability density dP'/dS of the arrival point. The conditional probability for a photon starting from (x, y) at $z = 0$ to hit the small target of area $dXdY$, is

$$\frac{dP'}{dS}(X,Y,x,y)dXdY \;=\; \frac{dP''}{d\Omega}(\theta,\phi)d\Omega$$

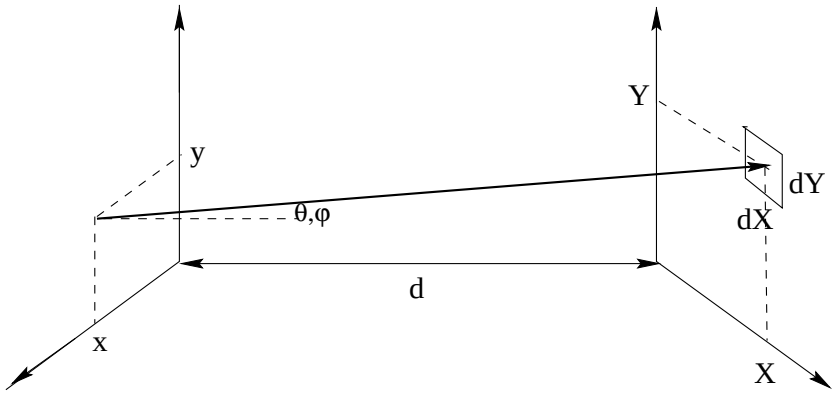

Figure 3.40: propagation from plane to plane

where $d\Omega = dXdY/\rho^2$ is the elementary solid angle corresponding to the target seen from the initial point, $\rho(x, y, X, Y)$ being defined by

$$\rho(x, y, X, Y) = \sqrt{(x - X)^2 + (y - Y)^2 + d^2}$$

For the full density, we get thus:

$$\frac{dP'}{dS}(X, Y) =$$

$$\int_{\mathbf{R}^2} dx\, dy\, \frac{1}{\rho^2(x, y, X, Y)}\, \frac{dP''}{d\Omega}(\theta(x, y, X, Y), \phi(x, y, X, Y))\, \frac{dP'}{ds}(x, y)$$

This is the integral expressing the transfer of the probability density from $z = 0$ to $z = d$. If we adopt the paraxial approximation, we can replace ρ by d, and θ by $\sqrt{(x - X)^2 + (y - Y)^2}/d$, so that:

$$\frac{dP'}{dS}(X, Y) =$$

$$\frac{1}{d} \int_{\mathbf{R}^2} dx\, dy\, \frac{dP''}{d\Omega} \left(\sqrt{(x - X)^2 + (y - Y)^2}/d, \phi(x, y, X, Y) \right)\, \frac{dP'}{ds}(x, y)$$

We can show on a very simple example how it works. Take a TEM_{00} normalized mode defined by the amplitude:

$$A(x, y) = \sqrt{\frac{2}{\pi w^2}} \exp\left(- \frac{x^2 + y^2}{w^2} \right)$$

The Fourier transform is:

$$\tilde{A}(p,q) \;=\; \sqrt{2\pi w^2}\,\exp\left(-\,\frac{w^2(p^2+q^2)}{4}\right)$$

We have thus:

$$\frac{dP'}{ds}(x,y) \;=\; \frac{2}{\pi w^2}\,\exp\left(-\,\frac{2(x^2+y^2)}{w^2}\right) \tag{3.55}$$

and

$$\frac{dP''}{d\Omega}(\theta,\phi) \;=\; \frac{2\pi w^2}{\lambda^2}\,\exp\left(-\,\frac{k^2w^2\theta^2}{2}\right) \tag{3.56}$$

And the transfer equation is:

$$\frac{dP'}{d\Omega}(X,Y) \;=$$

$$\frac{4}{\lambda^2 d^2}\int_{\mathbf{R}^2} dx\,dy\,\exp\left(-\,\frac{2(x^2+y^2)}{w^2}\right)\exp\left(-2\,\frac{\pi^2w^2[(x-X)^2+(y-Y)^2]}{\lambda^2d^2}\right)$$

This can be calculated either directly or by Fourier transform (being a convolution product) and the result is

$$\frac{dP'}{dS}(X,Y) \;=\; \frac{2}{\pi w'^2}\,\exp\left(-2\,\frac{X^2+Y^2}{w'^2}\right)$$

with

$$w' \;=\; w\sqrt{1+\left(\frac{\pi w^2}{\lambda d}\right)^2}$$

exactly as in paraxial wave optics. See Fig.3.41 for an example based on the Virgo parameters: The initial waist is w_0 =2 cm, the photons are assumed emitted at a point given by the 2D gaussian random variable (x,y) at $z=0$, of parameter w_0, the joint probability density being given by (3.55), then the direction of flight is given by a new 2D gaussian random variable (ξ,η) of parameter $\theta_g = \lambda/\pi w_0$, the joint probability density being given by (3.56). and the hit point at $z=d$ is calculated as

$$X = x + d\,\xi \quad , \quad Y = y + d\,\eta$$

We see the agreement between the wave optics theory (lines) and the Monte-Carlo result (histograms)

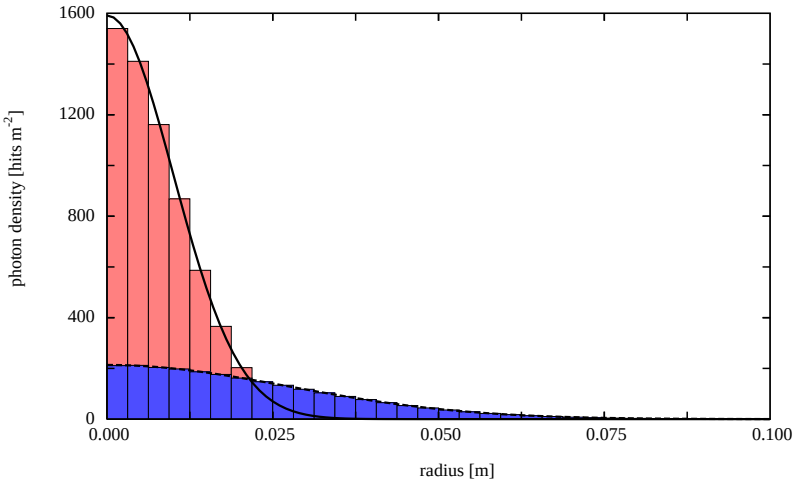

Figure 3.41: Diffraction spot at 3 km of a 2 cm waist initial TEM mode. Histogram: Monte-Carlo simulation. Solid curve: Diffraction theory

3.4.3 Diffraction patterns

It is not always possible to know the Fourier transform of the incoming amplitude. This is generally possible at the initial plane, where a clean source is assumed installed, but after propagation in a complex system, photons randomly emitted propagating as in a billiard, and reaching a given plane, do not allow to reconstruct the complex amplitude necessary to determine $dP''/d\Omega$. A very interesting procedure has been proposed in [19]. As they pass near the edge of any aperture, the photons are scattered at random angles, the standard deviation being inversely proportional to the distance at the edge. The heuristic argument is borrowed from quantum mechanics: a particle being at the distance Δx of the edge of a screen may be seen as having its location determined with accuracy Δx. Consequently, the accuracy on its momentum is $\Delta p_x = h/4\pi\Delta x$ (h is Planck's constant). Now, the momentum of a photon is known to be $p = hk/2\pi$, The relation $\Delta p_x/p = \tan\theta^*$ allows then to compute the standard deviation θ^* corresponding to the uncertainty Δp_x:

$$\theta^* = \arctan\left(\frac{\lambda}{4\pi\Delta x}\right)$$

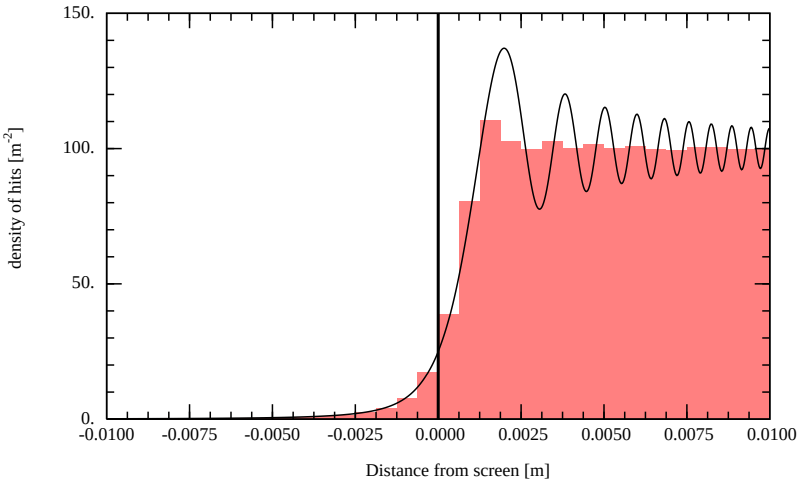

Figure 3.42: Diffraction by a half-plane. The screen is at $d = 5$m, the wavelength is $\lambda = 1.06\,\mu$m. Number of photons launched: 10^6. Histogram: Monte-Carlo simulation. Solid curve: Diffraction theory

We can test the procedure on the well-known problem of diffraction by a half plane. We assume a wide and uniform light beam centered at $x = y = 0$ falling on a blade masking half of the plane ($x < 0$). If we consider a white screen at $z = d$ behind, the intensity of the light on it is given [7] by

$$I(x) = I_0 \times \frac{1}{2}\left[\left(\frac{1}{2} + C\left(\sqrt{\frac{2}{\lambda d}}x\right)\right)^2 + \left(\frac{1}{2} + S\left(\sqrt{\frac{2}{\lambda d}}x\right)\right)^2\right] \qquad (3.57)$$

Where $C(x)$ and $S(x)$ are the Fresnel functions (see[20]). We assume a uniform random law for launching photons at x off the interval $[-x_M, x_M]$, then, x being randomly chosen, if $x < 0$ the process stops and a new photon is launched. if $x > 0$, its direction θ is drawn as a random deviate knowing its standard deviation θ^* (a gaussian deviate works). The hit point on a screen at distance d is $X = x + \theta d$. The statistics is reported on Fig.3.42 (histogram), the line represents the wave optics theory with $I_0 = 1/2x_M$ (Eq.3.57). Remark the excellent agreement in the shadow region, and the averaged behavior in the fringes region, due to the loss of information about the phase.

Chapter 4

Real mirrors

In this section, we present a more concrete representation of mirrors generally involved in laser optical systems. The fact that the light source has a very narrow linewidth around the nominal wavelength allows using mirrors having a selective reflectance at the same wavelength. This is fortunate, because all wavelengths mirrors, like metallic layers, have irreducible losses due to finite conductivity (using superconducting metallic mirrors is still a dream, or more exactly a nightmare, in realistic interferometers). This selective reflectance can be achieved by superposing thin dielectric material layers as a coating on a transparent block of dielectric material (substrate). The global quality of such a mirror results from the quality of the substrate, and from the quality of the coating.

4.1 Multilayer coatings

It is well known that light arriving at an interface separating two dielectric media of different refraction indices gives rise to both a reflected and an transmitted wave. A slice of dielectric material surrounded by other dielectric materials with different indices may thus be expected to behave like a Fabry-Perot cavity. By adjusting the round-trip phase inside, it is possible to enhance the reflectance of the slice. Superposing more and more alternatively high and low index layers produces a cascade of Fabry-Perot's, and the global reflectivity increases towards unity.

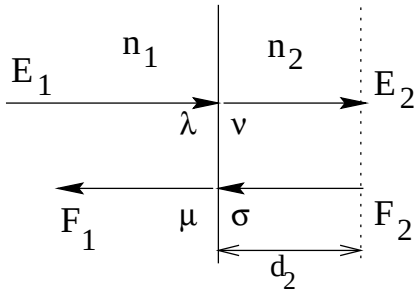

Figure 4.1: waves at a plane boundary

4.1.1 Dioptric matrix

We naively represent light in a dielectric medium of index n as a pair of monochromatic plane waves, propagating along the z direction, one electric $\mathcal{E}$, one magnetic $\mathcal{H}$, of the form

$$\mathcal{E}(t,x,y,z) \;=\; \begin{pmatrix} \mathrm{e}^{-i\omega t}\,\mathrm{e}^{inkz} \\ 0 \\ 0 \end{pmatrix}$$

$$\mathcal{H}(t,x,y,z) \;=\; \begin{pmatrix} 0 \\ n\,\frac{k}{|k|}\,\mathrm{e}^{-i\omega t}\,\mathrm{e}^{inkz} \\ 0 \end{pmatrix}$$

where $|k| \equiv \omega/c$. According to the sign of k, the wave is left or right propagating. Once given $\mathcal{E}$, the Maxwell equations impose the form of $\mathcal{H}$. Recall that the Maxwell equations also impose the continuity of the tangential components of both $\mathcal{E}$ and $\mathcal{H}$ at a boundary separating two dielectric media. Consider namely a plane $z = 0$, separating a medium of index n_1 (the left half-space) and a medium of index n_2 (the right half-space) (see Fig.4.1), where a right-propagating wave E, and a left-propagating wave F are crossing each other. The electric and magnetic fields are (we forget the $\mathrm{e}^{-i\omega t}$ time dependence) :

$$\mathbf{E}(z) \;=\; \begin{pmatrix} \lambda \mathrm{e}^{in_1 kz} \;+\; \mu \mathrm{e}^{-in_1 kz} \\ 0 \\ 0 \end{pmatrix}$$

$$\mathbf{H}(z) \;=\; \begin{pmatrix} 0 \\ \lambda\, n_1 \mathrm{e}^{in_1 kz} \;-\; \mu\, n_1 \mathrm{e}^{-in_1 kz} \\ 0 \end{pmatrix}$$

in the left half-space, and

$$\mathbf{E}(z) \;=\; \begin{pmatrix} \nu \mathrm{e}^{in_2 kz} \;+\; \sigma \mathrm{e}^{-in_2 kz} \\ 0 \\ 0 \end{pmatrix}$$

$$\mathbf{H}(z) \;=\; \begin{pmatrix} 0 \\ \nu\, n_2 \mathrm{e}^{in_1 kz} \;-\; \sigma\, n_2 \mathrm{e}^{-in_1 kz} \\ 0 \end{pmatrix}$$

for the right half-space. λ, μ, ν, σ are constant amplitudes. λ and σ are given and we want to determine ν and μ. Continuity of $\mathrm{E_x}$ and $\mathrm{H_y}$ brings the two equations :

$$\begin{cases} \lambda + \mu \;=\; \nu + \sigma \\ n_1(\lambda - \mu) \;= n_2(\,\nu - \sigma) \end{cases}$$

from where we get

$$\nu \;=\; \frac{n_2 - n_1}{n_2 + n_1}\,\sigma \;+\; \frac{2n_1}{n_2 + n_1}\,\lambda$$

$$\mu \;=\; \frac{2n_2}{n_2 + n_1}\,\sigma \;+\; \frac{n_1 - n_2}{n_1 + n_2}\,\lambda$$

This allows a convenient quadrupole representation of the interface. Given the incoming fields, namely E_1 from the left and F_2 from the right, we find the outgoing E_2 to the right and F_1 to the left, assuming that the fields are expressed, in the medium 2 at a distance d_2 from the interface (d_2 will represent the layer thickness), with $\varphi_2 \equiv kn_2 d_2$, we get under the matrix form :

$$\begin{pmatrix} E_2 \\ F_1 \end{pmatrix} \;=\; \begin{pmatrix} t_{12}\; r_{22} \\ r_{11}\; t_{21} \end{pmatrix} \begin{pmatrix} E_1 \\ F_2 \end{pmatrix} \tag{4.1}$$

We call Q_{12} the matrix operator. Owing to the preceding calculation, we have

$$Q_{12} \;=\; \begin{pmatrix} t_{12} = \frac{2n_1}{n_2+n_1}\,\mathrm{e}^{i\varphi_2} & r_{22} = \frac{n_2-n_1}{n_2+n_1}\,\mathrm{e}^{2i\varphi_2} \\ t_{21} = \frac{2n_2}{n_2+n_1}\,\mathrm{e}^{i\varphi_2} & r_{11} = \frac{n_1-n_2}{n_2+n_1} \end{pmatrix}$$

Obviously, the relevant coefficients (Q_{21}) to apply when the two media are exchanged are easily deduced from the preceding by simply exchanging the

subscripts 1 and 2. We thus have the two quadrupole operators respectively attached to a low index and a high index layer, assuming $n_2 > n_1$:

$$q_{\text{high}} = \begin{pmatrix} \frac{2n_1}{n_2+n_1}\, e^{i\varphi_2} & \frac{n_2-n_1}{n_2+n_1}\, e^{2i\varphi_2} \\ \frac{n_1-n_2}{n_2+n_1} & \frac{2n_2}{n_2+n_1}\, e^{i\varphi_2} \end{pmatrix} \tag{4.2}$$

$$q_{\text{low}} = \begin{pmatrix} \frac{2n_2}{n_2+n_1}\, e^{i\varphi_1} & \frac{n_1-n_2}{n_2+n_1}\, e^{2i\varphi_1} \\ \frac{n_2-n_1}{n_2+n_1} & \frac{2n_1}{n_2+n_1}\, e^{i\varphi_2} \end{pmatrix} \tag{4.3}$$

4.1.2 Models of stacks

The stack of N layers taken as a whole, has also a quadrupole operator Q_{stack}. It can be obtained from q_{low} and q_{high}. But the composition law of Q-like operators is more complicated than ordinary linear algebra. Assume for instance that the operator Q associated to a stack of $n-1$ layers is of the form

$$Q = \begin{pmatrix} T & P \\ R & \Theta \end{pmatrix}$$

and we want to add one more layer at the right, either low or high index. Let q be the layer operator :

$$q = \begin{pmatrix} t & \rho \\ r & \theta \end{pmatrix}$$

Introducing intermediate fields, we can write

$$\begin{pmatrix} E_2 \\ F_1 \end{pmatrix} = Q \begin{pmatrix} E_1 \\ F_2 \end{pmatrix}$$

for the uncomplete stack, and

$$\begin{pmatrix} E_3 \\ F_2 \end{pmatrix} = q \begin{pmatrix} E_2 \\ F_3 \end{pmatrix}$$

for the extra layer. By solving the system with respect to (E_1, F_3), we get

$$\begin{pmatrix} E_3 \\ F_1 \end{pmatrix} = Q \otimes q \begin{pmatrix} E_1 \\ F_3 \end{pmatrix}$$

where the operator $Q \otimes q$ is given by

$$Q \otimes q \;=\; \begin{pmatrix} \frac{tT}{1-Pr} & \frac{\rho+P(t\theta-r\rho)}{1-Pr} \\ \frac{R+r(T\Theta-RP}{1-Pr} & \frac{\theta\Theta}{1-Pr} \end{pmatrix} \tag{4.4}$$

This is the Q-product of two operators. It is now easy to construct the operator corresponding to a given stack, when for instance the first layer is low index : assume Q_0 is the operator corresponding to this layer of low index with vacuum in the left half-space (Q_0 is a special case of q_{low} with n_2 replaced by 1). Then the complete stack operator is obtained as

$$Q_n \;=\; (((Q_0 \otimes q_{\text{high}}) \otimes q_{\text{low}}) \otimes q_{\text{high}}) \otimes q_{\text{low}} \cdots$$

The tuning of the elementary Fabry-Perot's is determined by the thickness of the deposit. The best reflectivity is obtained with $\varphi_2 = \varphi_1 = \pi/2$ (quarter wave) and $\varphi_0 = \pi$ for the initial layer.

4.1.3 Numerical codes

An explicit analytical calculation is obviously untractable and even useless when n is larger than 2 or 3, but the algorithm is very well adapted to numerical methods. The following plot 4.2 shows the reflectance of a 30 layers stack : the indices were $n_1 = 1.4783$ and $n_2 = 2.10225$. The reflectivity for the nominal wavelength would be $1 - 4 \times 10^{-9}$. We see that the reflectivity remains high even for up to 20% variation of the wavelength.

4.2 Surface maps

In order to test mirrors before and after coating, measurements of the surface height are performed by interferometric means. The result is a 2D data set $\{z_{ij}\}$, containing samples measured a the nodes $\{x_{ij}, y_{ij}\}$ of a grid. This is for instance the result of a measurement of a 7 cm diameter mirror (see Fig.4.3) : one easily sees a tilt of the mirror axis.

4.2.1 Collimation and flattening

In general the method of measurement introduces a wedge, i.e. a non zero angle between the symmetry axis of the surface and the optical axis. It is

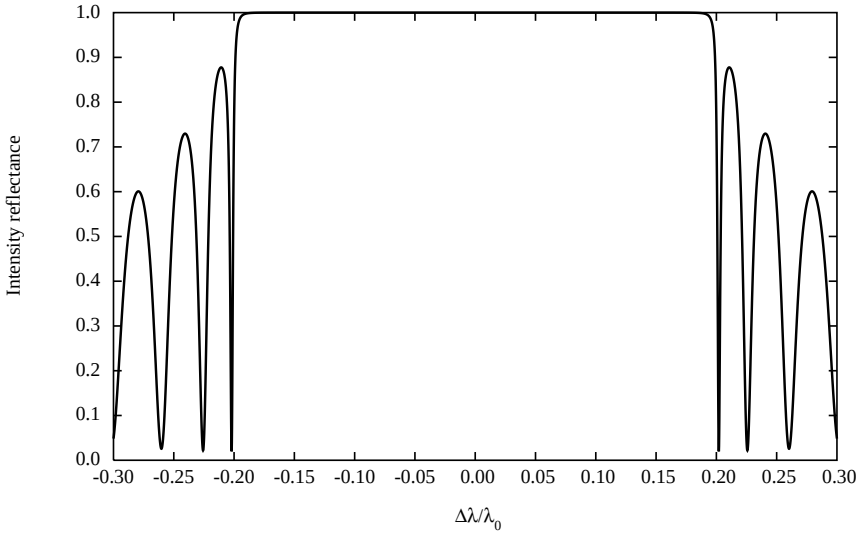

Figure 4.2: Variations of reflectance vs wavelength

thus necessary to re-orient the surface. We can define the surface axis by the normal to the mean plane. The mean plane is defined by the linear equation

$$z \;=\; a\,x \;+\; b\,y \;+c$$

where $(a,\ b,\ c)$ are parameters to be defined by a leat-square criterion, giving the normal equations

$$\begin{cases} a \;<x^2> \;+\; b \;<xy> \;+\, c \;<x> \;=\; <xz> \\ a \;<xy> \;+\; b \;<y^2> \;+\, c \;<y> \;=\; <yz> \\ \qquad a \;<x> \;+\; b \;<y> \;+\, c \;=\; <z> \end{cases} \tag{4.5}$$

where the average symbol $< \ldots >$ has the following definition for any quantity X defined on the grid :

$$<X> \;=\; \frac{\sum_{ij} w_{ij} X_{ij}}{\sum_{ij} w_{ij}} \tag{4.6}$$

The w_{ij} are weights, chosen according to the parameter w of the beam :

$$w_{ij} \;=\; \exp\left(-2(x_{ij}^2 + y_{ij}^2)/w^2\right)$$

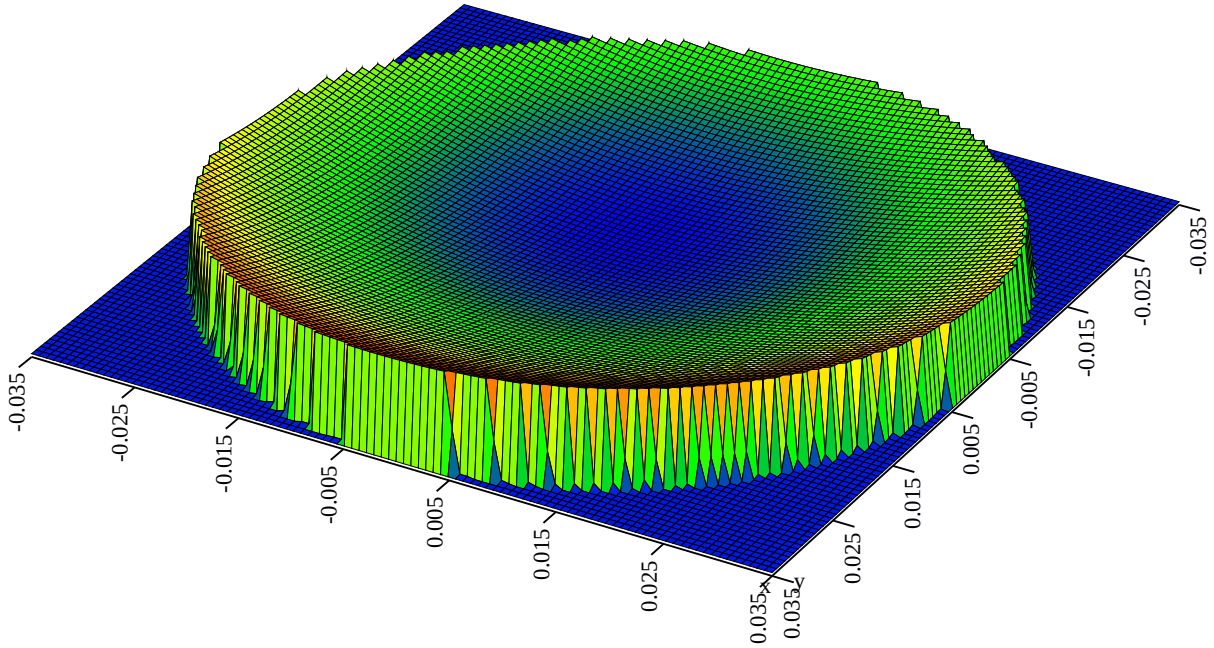

Figure 4.3: Susbstrate of mirror : surface as measured

The solution is

$$a = \frac{V(y)Cov(x,z) - Cov(x,y)\,Cov(y,z)}{V(x)V(y) - Cov(x,y)^2}$$

$$b = \frac{V(x)Cov(y,z) - Cov(x,y)\,Cov(x,z)}{V(x)V(y) - Cov(x,y)^2}$$

$$c = < z > -a < x > -b < y >$$

where the variances-covariances have the usual definition

$V(x) =< x^2 > - < x >^2$, $V(y) =< y^2 > - < y >^2$, $Cov(x,y) =< xy > - < x >< y >$

The collimation is obtained by the correction

$$z_{ij} \to z_{ij} - a\,x_{ij} - b\,y_{ij} - c$$

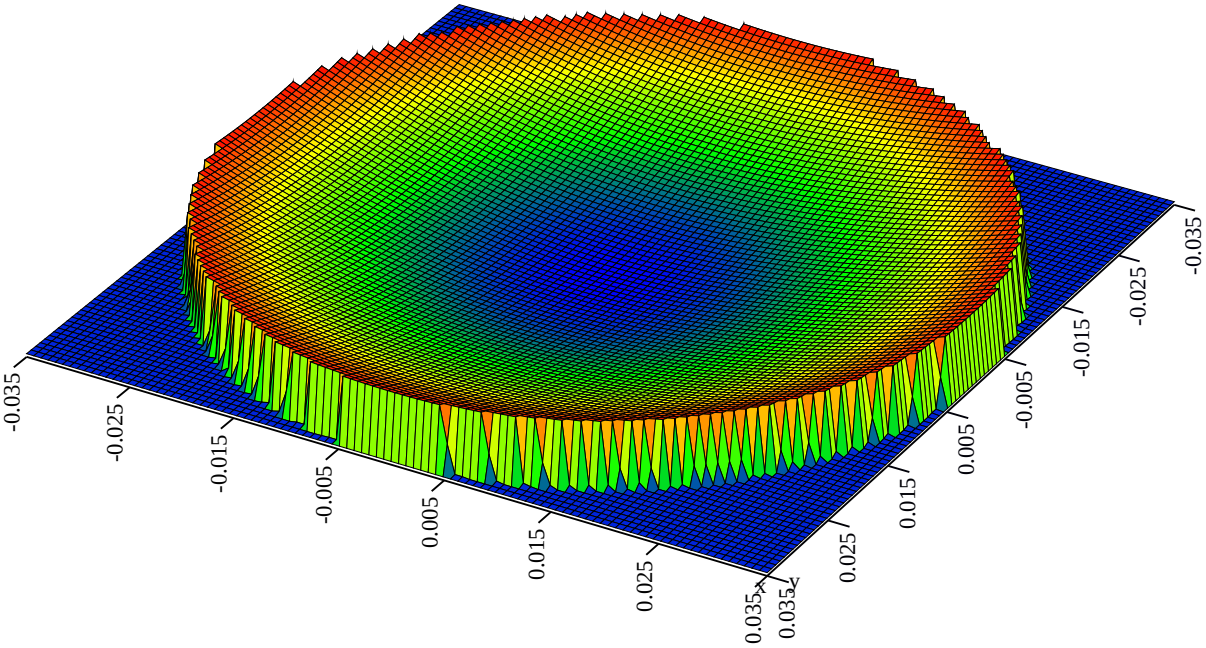

Figure 4.4: Collimated surface

one sees the same mirror map after collimation (see Fig.4.4). The next step is to extract the curvature radius of the surface. This can be done by fitting a model of the type

$$z = m\, r^2 \; + \; p \quad (r^2 \equiv x^2 + y^2)$$

The normal equations are satisfied by

$$m \;\; = \;\; \frac{< r^2 z > - < r^2 >< z >}{< r^4 > - < r^2 >^2}$$

$$p = < z > - m < r^2 >$$

c is related to the curvature radius R_c of the mirror by $R_c \;\; = \;\; 1/2m$ The determination of the curvature was done by a procedure in which the width w of the light beam is known. But if the mirror is involved in a cavity, this

width is precisely determined by the curvature, and it seems that it becomes an implicit problem. As customary, it can be solved by iterations : one begins with an initial guess of the curvature (it is not likely that we have no idea a priori of the curvature), then we compute the corresponding w, which allows a better estimate of the curvature, and so on. In fact, a reasonable initial guess gives a good corrected value within one cycle only.

4.2.2 Weighted RMS roughness

Once found the coefficients (m, p), one can make the correction

$$z_{ij} \rightarrow z_{ij} - m\, r_{ij}^2 - p$$

This is the flattening operation. The result of the curvature correction is the residual departure of the mirror from the nearest paraboloid (see Fig.4.5). The statistics

$$\sigma \;=\; \sqrt{< z^2 > - < z >^2}$$

with the already precised meaning of $< \ldots >$, and applied to the collimated and flattened surface, gives information on the roughness, we call it the weighted RMS roughness. It is the relevant parameter for scattering losses estimation (see below).

4.2.3 2D interpolation techniques

The mirror map has its own sampling grid, and the numerical propagation program has also its (different) own. It is therefore in general necessary to convert a map from an initial grid to another. This is done by interpolation. Interpolation in 1D data series is straightforward, but in a 2D data array, it is more difficult, this is a reason for giving here the basic ideas. The problem reduces eventually to find an estimation of a function $f(x, y)$, knowing its values on a grid $\{x_i,\ y_j\}$. We assume, for the sake of simplicity that the sampling grid is equally spaced, i.e.

$$x_{i+1} - x_i = \Delta x$$

$$y_{j+1} - y_j = \Delta y$$

so that knowing x and y determines easily the cell $(i, j) - (i+1, j+1)$ where the estimation point falls. The only point is thus to estimate $f(x, y)$ knowing

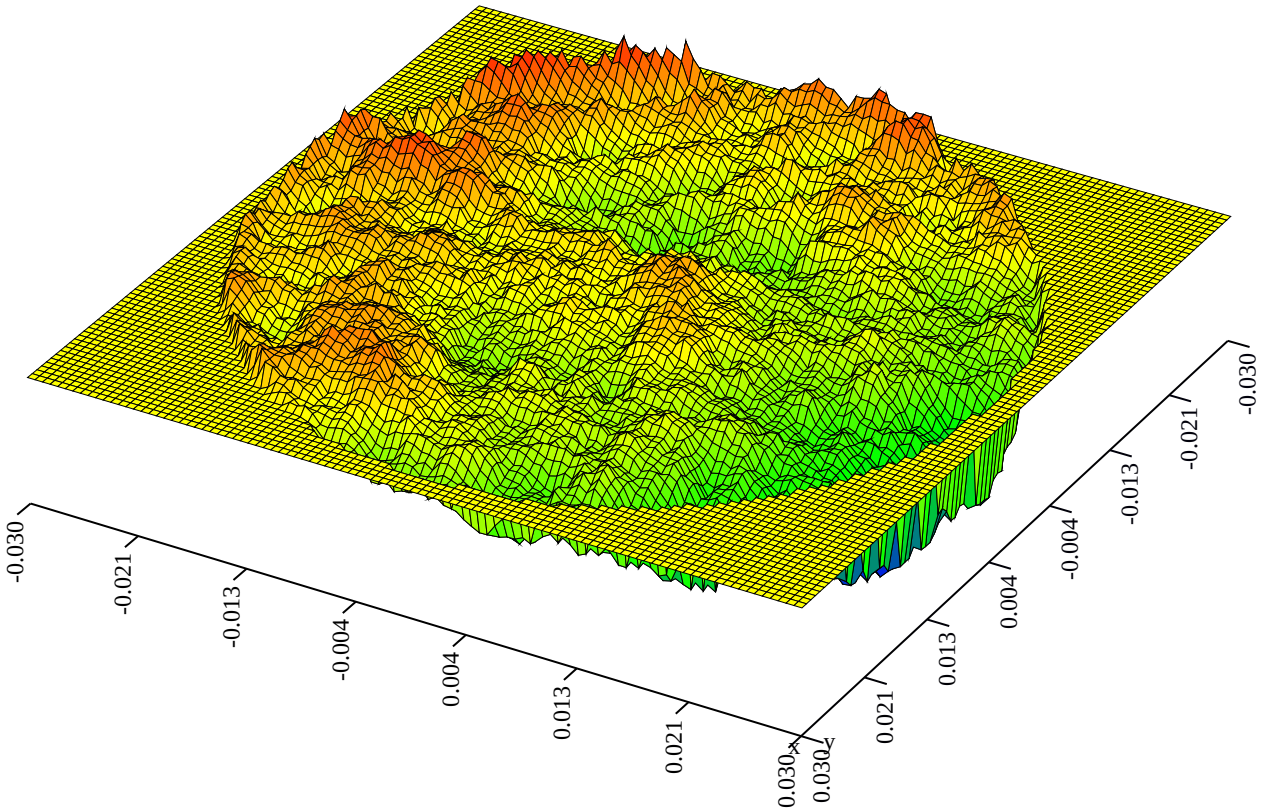

Figure 4.5: Oriented and flattened surface : An example of a residual roughness

the surrounding data : f_{ij}, $f_{i+1\,j}$, $f_{i\,j+1}$, $f_{i+1\,j+1}$, Δx, Δy. where we have set $f_{ij} \equiv f(x_i, y_j)$.

A linear interpolation formula is of the type

$$z = a\,\xi + b\,\eta + c$$

where $\xi \equiv (x - x_i)/\Delta x$ and $\eta \equiv (y - y_j)/\Delta y$. it depends on three parameters, and three data are necessary to determine them. We have the choice between two solutions (see Fig.4.6), the point $M(x, y)$ may be viewed, for instance, as either in the ABC or in the BCD triangle. These two triangles determine two different planes, and consequently two estimations of $f(\xi, \eta)$. We could

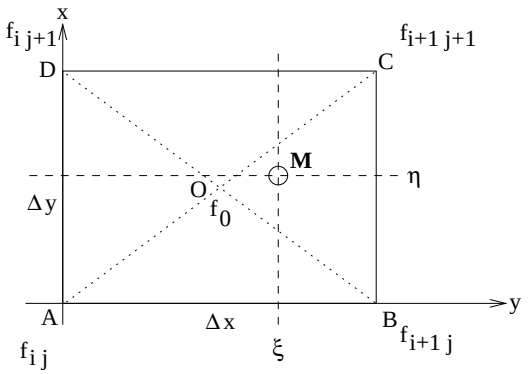

Figure 4.6: 2D interpolation problem

take the average of them. In fact this is equivalent to the following procedure : call O the center of the rectangular cell. Assign to O the estimate f_0 taken as the average of the surrounding values, i.e. $f_0 = (f_{ij} + f_{i+1\,j} + f_{i\,j+1} + f_{i+1\,j+1})/4$. We have now four triangles (AOB, BOC, COD, DOA) with known node values. It is easy to see to which of them M belongs, and use the corresponding plane to estimate f_M. For instance in the case of Fig.4.6, we would have

$$f(\xi,\eta) = \frac{f_{i+1\,j+1} + f_{i+1\,j} - f_{i\,j+1} - f_{ij}}{2}\ \xi$$

$$+\ (f_{i+1\,j+1} - f_{i+1\,j})\ \eta\ +\ \frac{f_{i+1\,j} + f_{i\,j+1} - f_{i+1\,j+1} + f_{ij}}{2}$$

and obviously different formulas, depending on the relevant triangle.

A quadratic interpolation is of the form

$$z = a\ + b\,\xi + c\,\eta + d\,\xi\eta$$

and the four coefficients are completely determined by the four corners of the cell ; the result is

$$f(\xi,\eta) = f_{ij} + (f_{i+1\,j} - f_{ij})\,\xi\ \ + (f_{i\,j+1} - f_{ij})\,\eta +$$

$$+\ (f_{i+1\,j+1} + f_{ij} - f_{i+1\,j} - f_{i\,j+1})\,\xi\eta$$

The two methods give the exact values on the nodes, and reduce to ordinary (1D) linear interpolation on the edges. The quadratic interpolation introduces a curvature of the interpolating surface that may give spurious effects.

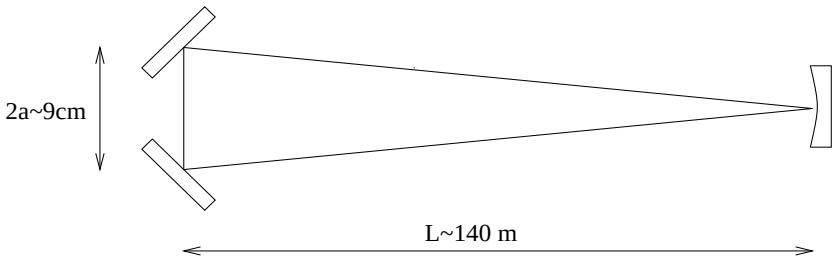

Figure 4.7: sketch of the modecleaner

Higher order polynomials can even allow to have continuous derivatives at the edges, smoothing the surface.

4.2.4 Backcoupling due to roughness

An example of direct application of the preceding methods has been found in the issue caused by the so-called mode-cleaner installed on the beam, just before entering the interferometer. The mode-cleaner consists in a three-mirrors ring cavity having the shape of a long equilateral triangle having thus a very sharp angle. The length of the basis is approximately 9 cm, whereas the length of one of the long sides is about 140 m. The two mirrors forming the basis (see Fig.4.7 are flat and nearly othogonal, and the far mirror is spherical with a curvature radius about 180 m. The reason for such a ring cavity is to avoid spurious reflection of the laser beam off the input mirror. Only one propagation direction is in principle allowed in the ring, say clockwise. But the incidence angle on the curved mirror is so sharp (about $3\ 10^{-4}$ Rd) that a fraction of the light scattered by the surface may be sent in the counterclockwise mode, resulting in interferences on the photodiode used to lock the system, and eventually causing instabilities. We can study and evaluate the effect on the roughness map of the spherical mirror as follows. The coordinates are such that the z axis is the spherical mirror axis. the x, y axes are orthogonal and within the plane tangent to the mirror. We denote by $\varphi_0(x, y)$ an incoming gaussian beam, matched to the mirror, and incident with angles (θ, ϕ). We have

$$\varphi_0(x,y) = \sqrt{\frac{2}{\pi w^2}}\ \exp\left[-(x^2+y^2)/w^2\right] \exp\left[-ik(x^2+y^2)/2R\right]\ \times$$

$$\times\ \exp\left[-ik\theta(x\cos\phi + y\sin\phi)\right]$$

The mirror operator is

$$M(x,y) = \exp\left[2ikf(x,y)\right]$$

where $f(x,y)$ refers to the wavefront map of the mirror, including the mean paraboloid plus the residual roughness. The reflected beam is thus

$$\varphi_R(x,y) = M(x,y) \times \varphi_0(x,y)$$

The counter propagating beam $\varphi_c$is the phase conjugate of φ_0 :

$$\varphi_c = \overline{\varphi_0}$$

the coupling coefficient $\Gamma(\theta,\phi)$ between the reflected and the counterpropagating beams is given by the hermitian scalar product:

$$\Gamma(\theta,\phi) = \langle \varphi_c, \varphi_R \rangle$$

or, in detail :

$$\Gamma(\theta,\phi) = \int_{\mathbf{R^2}} I(x,y) \exp\left[2ik\left(f(x,y) - \frac{x^2+y^2}{2R}\right)\right] \exp\left[-2ik\theta(x\cos\phi + y\sin\phi)\right]\, dx\, dy$$

where $I(x,y)$ is the normalized intensity distribution in the beam. Note that the function $\delta f(x,y) \equiv f(x,y) - \dfrac{x^2+y^2}{2R}$ is nothing but the residual roughness of the mirror (see Fig.4.8).

This residue being small compared to a wavelength, we can write

$$\Gamma(\theta,\phi) = \exp\left[-\frac{2\pi^2 w^2\theta^2}{\lambda^2}\right] + 2ik\int_{\mathbf{R^2}} I(x,y)\,\delta f(x,y) \exp\left[-2ik\theta(x\cos\phi + y\sin\phi)\right]\, dx\, dy$$

$$-2k^2\int_{\mathbf{R^2}} I(x,y)\,\delta f(x,y)^2 \exp\left[-2ik\theta(x\cos\phi + y\sin\phi)\right]\, dx\, dy$$

When the roughness is zero, the first term still remains. It represents the natural overlap of the reflected beam with the phase conjugate beam, due to gaussian divergence. If $\theta = 0$, this overlap is simply unity, expressing the perfect matching of the beam. We can express the natural overlap as :

$$\Gamma_0(\theta) = \exp\left[-2\theta^2/\theta_g^2\right]$$

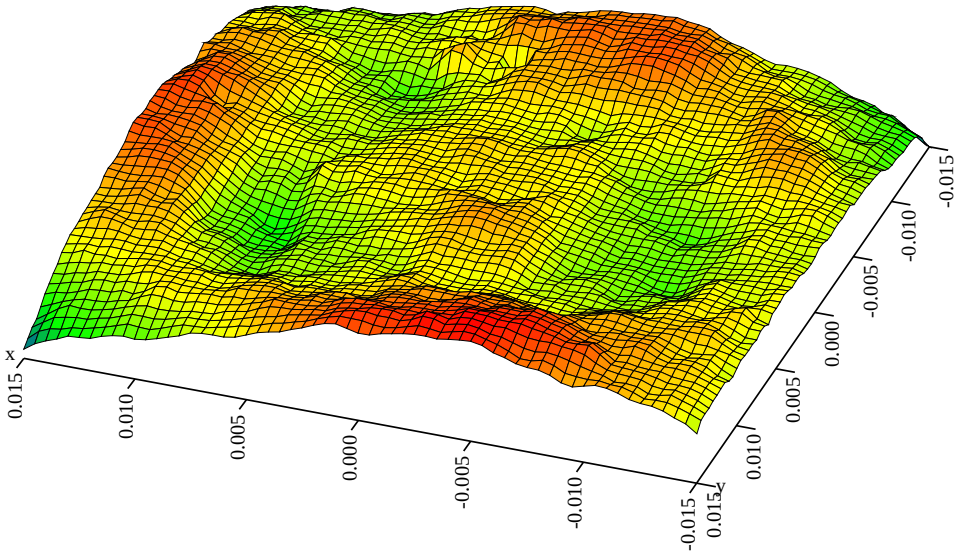

Figure 4.8: Residual roughness in the central zone of the MC spherical mirror, units are m.

where $\theta_g \equiv \lambda/\pi w$. For the Virgo mode-cleaner parameters, we have $\theta_g \sim 3.15\ 10^{-5}$ Rd. For values of θ comparable to the mode-cleaner sharp angle ($\theta_{\rm MC} \sim 3.\ 10^{-4}$ Rd), we see that $|\Gamma_0|^2$ is extremely small and definitely negligible. Within the angular region corresponding to backscattering, it is thus possible to reduce the expression of the coupling factor to the accurate approximation

$$|\Gamma(\theta,\phi)|^2 = 4k^2 \left| \int_{\mathbf{R^2}} I(x,y)\,\delta f(x,y)\,\exp\left[-2ik\theta(x\cos\phi + y\sin\phi)\right]\,dx\,dy + \right.$$

$$\left. + ik \int_{\mathbf{R^2}} I(x,y)\,\delta f(x,y)^2\,\exp\left[-2ik\theta(x\cos\phi + y\sin\phi)\right]\,dx\,dy \right|^2$$

showing that the result reduces eventually to the Fourier transform of the roughness, weighted, as usual, by the intensity distribution of the beam. For numerical computation, it is straightforward to use the exact formula

$$|\Gamma(\theta,\phi)|^2 = \left|\tilde{J}(2k\theta\cos\phi, 2k\theta\sin\phi)\right|^2$$

where $J(x,y) \equiv I(x,y)\,\exp[2ik\delta f(x,y)]$. We give on Fig.4.9 a map of the backcoupling in angular coordinates. The outer thin circle corresponds to coupling with the counterpropagating beam for all azimuth angles of the

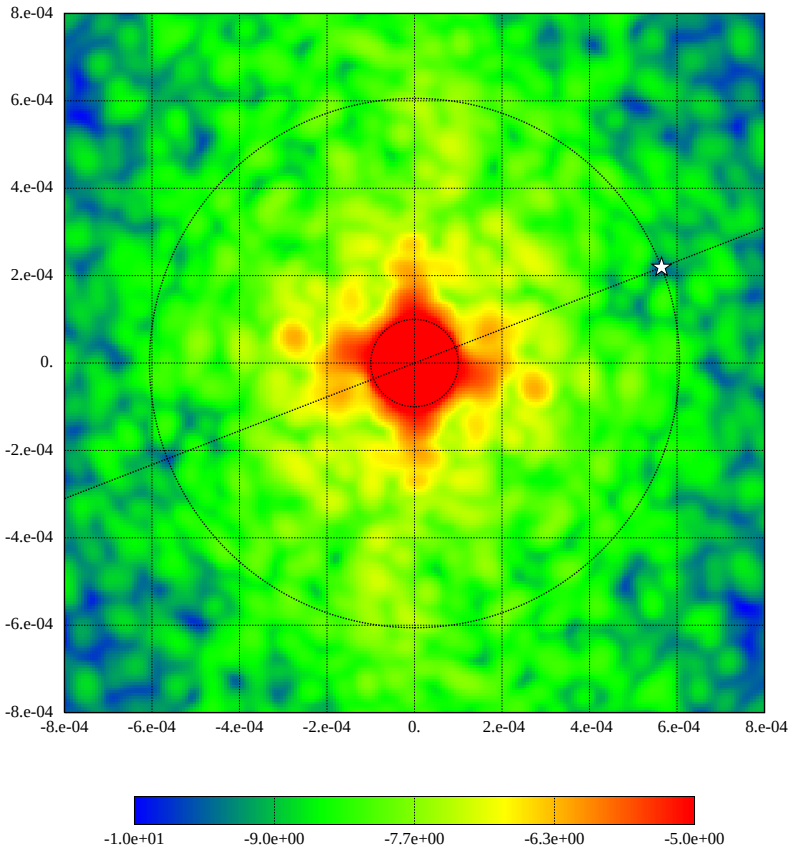

Figure 4.9: Coupling coefficient as a function of (θ, ϕ) (logarithmic scale). The star shows the optimal orientation of the mirror

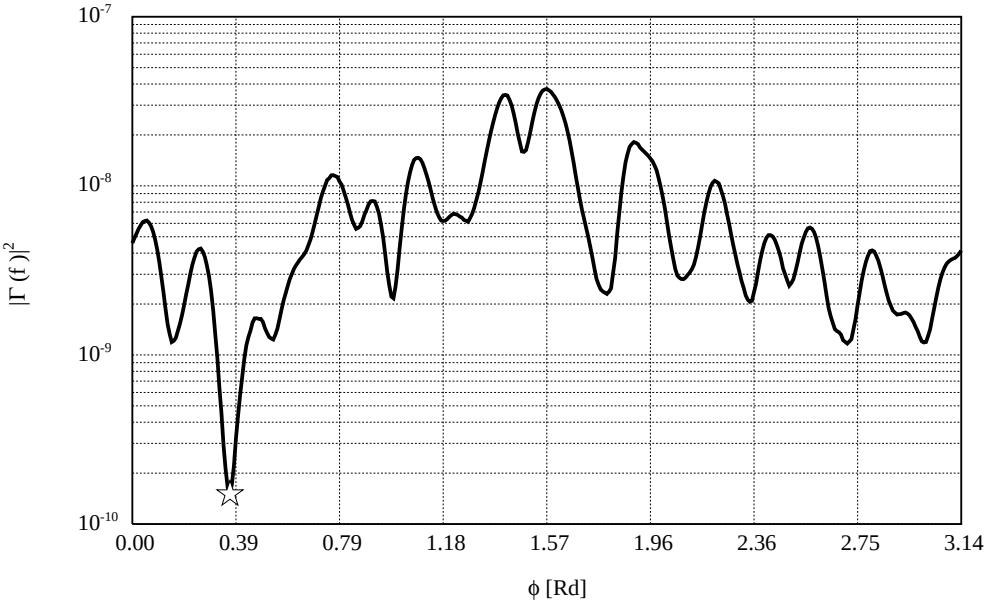

Figure 4.10: Coupling coefficient as a function of ϕ for backscattering

incident beam, or as well for all rotations of the mirror around its axis. The inner thin circle surrounds a non sigificant region where the natural overlap dominates, and has been limited. We see that backcoupling depend sharply on this azimuth angle ϕ. One could rise the question of the sensitivity of this pattern with respect to the centering of the analyzing beam : in other words, has this pattern any physical reality ? The answer can be obtained by varying *via* a small offset the incidence location on the mirror, then taking the average value of $|\Gamma|^2$ over all locations ; we call dithering this operation. If we consider a gaussian distribution of parameter σ of these incidence locations, dithering is strictly equivalent to taking an analyzing beam of width $w' = \sqrt{w^2 + \sigma^2}$. For plausible values of σ (analogous to an error in the centering). The map being rather unsensitive to small variations of w, we conclude that it has an actual physical meaning. It also shows that there are preferred orientations, and that these preferred orientations require a rather accurate positioning. Fig.4.10 represents the variations of $|\Gamma|^2$ along the outer circle, *i.e.* for all possible orientation of the mirror, the incidence angle being fixed. The angle of 0.37 Rd found on the curve corresponds to a hole in the speckle as seen

on Fig.4.9 and marked by a star.

4.2.5 Zernike polynomials

In traditional instrumental optics, there is a need for analyzing and representing the departure of a given mirror surface with respect to the ideal shape. A systematic surface analysis consists firstly in finding a family of orthogonal defects over which a real surface can be expanded. The orthogonality makes possible to treat separately the various defects, and for instance to subtract any one of them without changing the expansion of the remaining surface. The required orthogonality is obtained with a family of functions $Z_{nm}(\rho,\vartheta)$ in polar coordinates. It is necessary to fix the radius a of the mirror, then $\rho \equiv r/a$. The variables (ρ,ϑ) are separate, and in fact,

$$Z_{nm}(\rho,\vartheta) \;=\; R_n^m(\rho) \times \begin{cases} \sin m\vartheta \\ \cos m\vartheta \end{cases}$$

where the $R_n^m(\rho)$ are a family of orthogonal polynomials first introduced by F. Zernike for $n = 0, 1, \ldots$ and $m = n, n-2, \ldots$ (it ends either at 0 or 1 depending on the parity of n):

$$R_n^m(\rho) \;=\; c_{nm} \sum_{p=0}^{(n-m)/2} \frac{(-)^p (n-p)!}{p!\left(\frac{n+m}{2}-p\right)!\left(\frac{n-m}{2}-p\right)!}\,\rho^{n-2p} \qquad (4.7)$$

The c_{nm} are normalization constants. The R_n^m polynomials obey

$$\int_0^1 R_n^m(\rho)\, R_{n'}^m(\rho)\, \rho\, d\rho \;=\; \frac{1}{2(n+1)}\,\delta_{nn'}$$

and the circular functions obey :

$$\int_0^{2\pi} \sin m\vartheta\, \sin m'\vartheta\, d\vartheta \;=\; \pi\delta_{mm'}$$

$$\int_0^{2\pi} \cos m\vartheta\, \cos m'\vartheta\, d\vartheta \;=\; \pi(1+\delta_{m0})\delta_{mm'}$$

sine et cosine being obviously orthogonal. The special behaviour of $cos(0 \times \vartheta) \equiv 1$ forces us to have the following normalization constant :

$$c_{mn} \;=\; \sqrt{\frac{2(n+1)}{\pi(1+\delta_{m0})}}$$

The expansion of a surface of equation $z = f(x, y)$ on the Zernike basis is as follows :

$$f(\rho, \vartheta) \;=\; \sum_{n=0}^{\infty} \sum_{m=0\text{or}1}^{n} f_{nm}\, Z_{nm}(\rho, \vartheta)$$

with

$$f_n^m \;=\; \int_0^1 \int_0^{2\pi} f(\rho, \vartheta)\, Z_{nm}(\rho, \vartheta)\, \rho\, d\rho\, d\vartheta$$

The generating code for calculation of $R_n^m(\rho)$ is very short :

```
c============================================================
      real function zerpol(n,m,rho)
      implicit none
c
      integer n,m,d,s,i
      real facm,rapp,rho
      real alphaz,alpha,rnm,ro2
c
      if (m.gt.n) then
          print*,'ERROR ! : m should be =< n !'
          stop
      endif
c
      d=(n-m)/2
      s=(n+m)/2
      ro2=rho*rho
      rapp=1
      do i=0,n-s-1
        rapp=rapp*(n-i)
      enddo
      facm=1
      do i=2,d
        facm=facm*i
      enddo
      alphaz=rapp/facm
      alpha=alphaz
      rnm=alpha
      do i=0,d-1
         alpha=-alpha*(s-i)*(d-i)/float((n-i)*(i+1))
         rnm=ro2*rnm+alpha
```

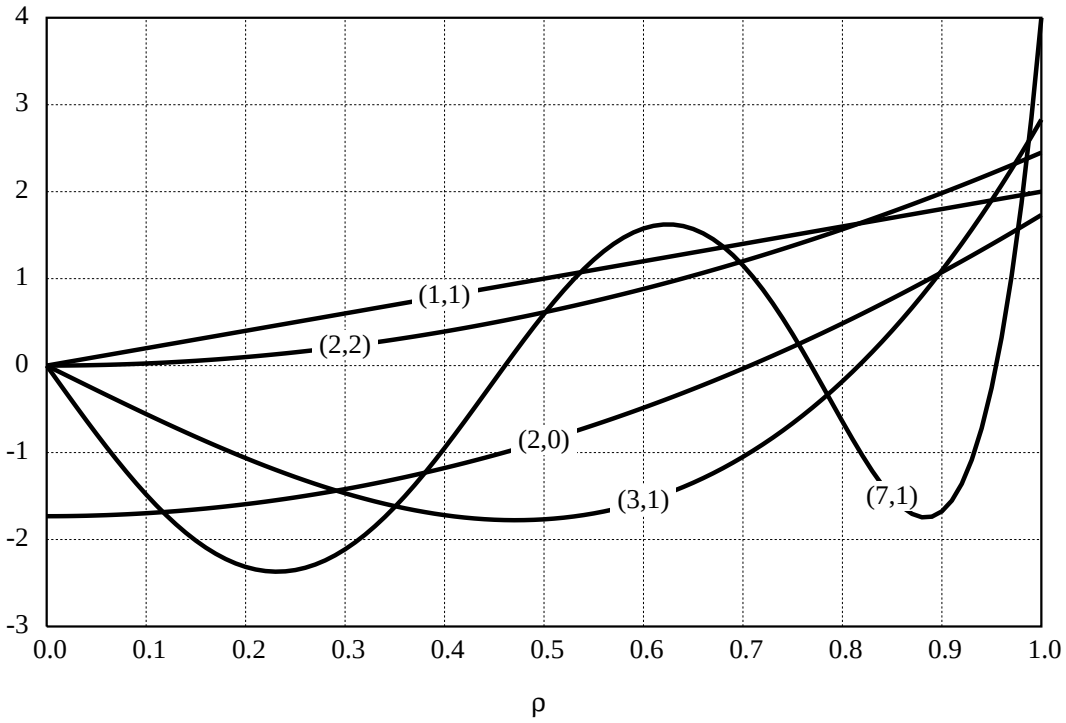

Figure 4.11: Some of the first radial Zernike polynomials

```
      enddo
      if (m.eq.0) then
         zerpol=sqrt(float(n+1))*rnm
      else
         zerpol=sqrt(float(2*(n+1)))*rnm*rho**m
      endif
      return
      end
c=============================================================
```

A plot of the first Zernike radial polynomials is shown on Fig.4.11. The first Zernike functions have the following interpretation, after V.N.Mahajan [21] :

n	m	Z_n^m	*name*
0	0	1	Piston
1	1	$2\rho\cos\vartheta$	x-tilt
1	1	$2\rho\sin\vartheta$	y-tilt
2	0	$\sqrt{3}(2\rho^2-1)$	Defocus
2	2	$\sqrt{6}\rho^2\cos 2\vartheta$	Astigmatism
2	2	$\sqrt{6}\rho^2\sin 2\vartheta$	Astigmatism
3	1	$\sqrt{8}(3\rho^3-2\rho)\cos\vartheta$	Primary x coma
3	1	$\sqrt{8}(3\rho^3-2\rho)\sin\vartheta$	Primary y coma
3	3	$\sqrt{8}\rho^3\cos 3\vartheta$	Triangular astigmatism
3	3	$\sqrt{8}\rho^3\sin 3\vartheta$	Triangular astigmatism
4	0	$\sqrt{5}(6\rho^4-6\rho^2+1)$	Primary spherical
4	2	$\sqrt{10}(4\rho^4-3\rho^2)\cos 2\vartheta$	Secondary astigmatism
4	2	$\sqrt{10}(4\rho^4-3\rho^2)\sin 2\vartheta$	Secondary astigmatism

4.2.6 Roughness and scattering losses

Let $A(x,y)$ be the amplitude of a TEM_{00} gaussian mode falling on a mirror the surface of which is defined by the apex equation $z=f(x,y)-r^2/2R$. The reflected wave is (forgetting the scalar or photometric reflection coefficient)

$$B(x,y) \;=\; \mathrm{e}^{-ikr^2/R+2ikf(x,y)}\,A(x,y)$$

Its coupling with the TEM_{00} mode is given by the hermitian scalar product $< A', B >$, where A' is the phase conjugate of A (reversed wavefront) so that the coupling factor of the TEM_{00} onto itself through reflection is

$$\gamma \;=\; \int A'^{*}(x,y)\,\mathrm{e}^{2ikf(x,y)}\,A(x,y)\,dx\,dy$$

or

$$\gamma \;=\; \frac{2}{\pi w^2}\int \mathrm{e}^{-2r^2/w^2}\mathrm{e}^{2ikf(x,y)}\,dx\,dy$$

If we assume the real surface near the ideal one, then we can expand the phase at second order, and write

$$\gamma \;=\; \frac{2}{\pi w^2}\int \mathrm{e}^{-2r^2/w^2}\left[1+2ik(f(x,y)-2k^2f(x,y)^2+\ldots\right]\,dx\,dy$$

$f(x,y)$ is defined up to a piston (additive constant) which can always be chosen such that

$$\int \mathrm{e}^{-2r^2/w^2}f(x,y)\,dx\,dy \;=\; 0$$

Then the function $f(x,y)$ is nothing but what we called "flattened" surface in a preceding section, and the quantity

$$q \;=\; \frac{2}{\pi w^2} \int \mathrm{e}^{-2r^2/w^2}\, f(x,y)^2 \; dx\, dy$$

is what we called "weighted RMS roughness", so that

$$\gamma \;=\; 1 - 2k^2\, q$$

in terms of power, this is

$$|\gamma|^2 \;=\; 1 - 4k^2\, q$$

and the losses due to the mirror's imperfections are simply

$$p \;=\; 4k^2\, q$$

Chapter 5

Scattered light

5.1 Introduction

Due to the imperfect nature of the surface of the reflecting coating, mirrors not only reflect light and dissipate a part of it into heat, but also scatter light in all directions. In supermirrors as those used in gravitational wave interferometers, the total losses (thermal dissipation + scattering) is very low, of the order of a few ppm, so that the amplitudes of scattered light, unless the mirror surface is polluted, is extremely small. Scattering is a process in which a perfect TEM mode is coupled to partial waves of any direction, depending on the size of the defects of the reflecting surface. The symmetrical process is possible: Diffuse light coming from any direction may be partially coupled into a TEM mode. If that diffuse light is phase modulated for any reason, the modulation will contaminate the stored TEM mode. The most evident scenario is scattering of light off a mirror, reflection of the diffuse light on the metallic walls of the vacuum pipe, then inverse scattering on the emitter or any other mirror. Due to the seismically driven motion of the vacuum pipe, seismic noise is re-entering the readout beam, and we have a by-pass of the seismic isolation system. In order to avoid such a catastrophe, it has been soon seen that a system of baffles for trapping scattered light was necessary. But the design and the nature of these baffles must be such that the remedy makes nothing worse than the disease. It is clear that this double scattering process is extremely weak, but GW interferometers are designed to measure better than 10^{-11} Rd.Hz$^{-1/2}$ phase changes, so that any source of noise, even very weak, must be assessed. This is why models of scattering are useful.

5.2 Scattering mirrors

The scattered light we are faced with, is generated by reflection of light beams on mirrors with weak roughnesses. Mirrors installed in GW interferometers as Virgo have roughnesses of rms value of a few nm, thus very small compared to the usual wavelength (1μm). The departure of the surface of a mirror from its ideal geometrical shape can be represented by a two-dimensional random process $f(\vec{x})$, where $\vec{x}$ represents the coordinates in the plane where we project the surface. We can assume without loss of generality that it is a centered process:

$$\langle f \rangle \;=\; 0$$

we also assume the process stationary:

$$\langle f^2 \rangle \;=\; \sigma^2$$

But the relevant statistics of the process, for studying scattering, is the autocorrelation function:

$$C(\vec{x}-\vec{x'}) \;=\; \langle f(\vec{x}).f(\vec{x'})\rangle/\sigma^2 \tag{5.1}$$

Here the stationarity implies that the autocorrelation function does not depend on the location in the plane, but only on the separation vector. It will be further assumed that the autocorrelation function depends only on the length of the separation vector:

$$C(\vec{x}-\vec{x'}) \;=\; C(\parallel \vec{x}-\vec{x'} \parallel)$$

in words, the roughness is isotropic.

Suppose now that a light beam described by the amplitude $\phi(\vec{r})$ is impinging normally to the reflecting surface, and let us call $\psi(\vec{x})$ the reflected beam's amplitude. We have:

$$\psi(\vec{x}) \;=\; \mathrm{e}^{2ikf(\vec{x})}\phi(\vec{x})$$

By taking the Fourier transform, we have:

$$|\tilde{\psi}(\vec{p})|^2 \;=\; \int \mathrm{e}^{i\vec{p}(\vec{x}-\vec{x'})}\mathrm{e}^{2ik[f(\vec{x})-f(\vec{x'})]}\phi_0(\vec{x})\,\phi_0^*(\vec{x'})d\vec{x}\,d\vec{x'}$$

Owing to the hypothesis that $f \ll \lambda$, we can expand the exponential and write:

$$|\tilde{\psi}(\vec{p})|^2 \;=\; \int \mathrm{e}^{i\vec{p}(\vec{x}-\vec{x'})}\left\{1+2ik[f(\vec{x})-f(\vec{x'})]-2k^2[f(\vec{x})^2+f(\vec{x'})^2-2f(\vec{x}).f(\vec{x'})\right\}\times$$

$$\times \phi_0(\vec{x})\,\phi_0^*(\vec{x'})d\vec{x}\,d\vec{x'}$$

By taking the expectation value, we get:

$$\langle|\tilde{\psi}(\vec{p})|^2\rangle \;=\; (1-4k^2\sigma^2)|\phi(\vec{p})|^2 + 4k^2\sigma^2\int \mathrm{e}^{i\vec{p}(\vec{x}-\vec{x'})}C(\vec{x}-\vec{x'})\,\phi_0(\vec{x})\,\phi_0^*(\vec{x'})d\vec{x}\,d\vec{x'}$$

or as well:

$$\langle|\tilde{\psi}(\vec{p})|^2\rangle \;=\; (1-4k^2\sigma^2)|\phi(\vec{p})|^2 + 4k^2\sigma^2\frac{1}{4\pi^2}\int \tilde{C}(\vec{q}).|\tilde{\phi}(\vec{p}-\vec{q})|^2\,d\vec{q} \qquad (5.2)$$

For gaussian beams, and even more for hypergaussian beams, the angular distribution is sharply peaked, taking significant values only in the neighborood of $\vec{p}=\vec{0}$. We can assume that the Fourier transform of the autocorrelation function (i.e. the power spectral density) does not appreciably vary on angles of the order of the angular width of the beam. In the preceding integral, the beam function can therefore be treated as a Dirac function, and we have:

$$\langle|\tilde{\psi}(\vec{p})|^2\rangle \;=\; (1-4k^2\sigma^2)|\phi(\vec{p})|^2 + 4k^2\sigma^2\tilde{C}(\vec{p}) \qquad (5.3)$$

Under this form, it is clear that the reflected light is the sum of two contributions, one having the same angular distribution as the incoming beam, that we call specularly reflected beam, and one having an angular distribution given by the properties of the surface, namely the power spectral density of f. We identify with scattered light this contribution. It can moreover be seen that the incoming power is shared between specularly reflected light, and scattering. We have:

$$P_{\mathrm{spec}}/P_{\mathrm{in}} \;=\; \frac{1}{4\pi^2}\int(1-4k^2\sigma^2)|\phi(\vec{p})|^2\,d\vec{p} \;=\; 1-4k^2\sigma^2$$

which shows that the scattering losses ϵ are given by:

$$\epsilon \;=\; 4k^2\sigma^2$$

and we have:

$$P_{\mathrm{scatt}}/P_{\mathrm{in}} \;=\; \frac{1}{4\pi^2}\int 4k^2\sigma^2\tilde{C}(\vec{p})\,d\vec{p} \;=\; 4k^2\sigma^2 \;=\; \epsilon$$

We can express the distribution of scattered light as:

$$\frac{1}{P_{\mathrm{in}}}\frac{dP_{\mathrm{scatt}}}{d\vec{p}} \;=\; \frac{\epsilon}{4\pi^2}\,\tilde{C}(\vec{p})$$

and by indentifying the Fourier coordinates to angles according to $\vec{p} \equiv (k \sin\theta \cos\phi,\, k \sin\theta \sin\phi)$, we can write:

$$\frac{d}{d\vec{p}} = \frac{\lambda}{4\pi^2} \frac{d^2}{\sin\theta \, d\theta \, d\phi} = \frac{\lambda}{4\pi^2} \frac{d}{d\Omega}$$

so that

$$\frac{1}{\epsilon P_{\text{in}}} \frac{dP_{\text{scatt}}}{d\Omega} = \frac{1}{\lambda^2} \tilde{C}(k \sin\theta)$$

where we have explicitly taken into acount the isotropy of the autocorrelation. Now,

$$\frac{dP_{\text{scatt}}}{P_{\text{scatt}} \, d\Omega}(\theta)$$

is a normalized function, and we can set

$$\frac{dP_{\text{scatt}}}{P_{\text{scatt}} \, d\Omega}(\theta) = \frac{p(\theta)}{2\pi} \tag{5.4}$$

where

$$\int_0^\pi p(\theta) \, \sin\theta \, d\theta = 1$$

and finally, by comparison between the two last equations:

$$\tilde{C}(k \sin\theta) = \frac{\lambda^2}{2\pi} p(\theta) \tag{5.5}$$

Information on the normalized angular density of scattered power (ADSP) can be obtained by different ways depending on the angular range. For very small angles, corresponding to long correlation distance defects, a direct measurement of the surface by using a profilometer can be carried out. For larger angles, a direct measurement of the ADSP is possible.

5.3 The scattering coherence function

The central concept for a wave optics treatment of light scattered from a beam (gaussian or flat), is the coherence function. We have seen in the preceding section that the light scattered off a mirror of roughness $f(\vec{x})$ can be viewed as emitted by the source

$$s(\vec{x}) = 2k f(\vec{x}) \, \phi(\vec{x})$$

where $\phi(\vec{r})$ is, as above, the incoming optical amplitude. We can consider the wave generated by this elementary source after diffraction along the distance d. It can be computed using the diffraction kernel:

$$K_d(\vec{x}) \;=\; -\frac{i}{\lambda d}\,\mathrm{e}^{ik\vec{x}^2/2d}$$

so that, if we denote by $s_d(\vec{y})$ the propagated wave, we have

$$s_d(\vec{y}) \;=\; \int K_d(\vec{y}-\vec{x}).s(\vec{x})\,d\vec{x}$$

We shall call coherence function of the scattering process, the expectation value

$$\mathcal{C}(d;\vec{y},\vec{y'}) \;=\; \langle s_d(\vec{y}).s_d^*(\vec{y'})\rangle \tag{5.6}$$

This can be computed as follows. Firstly we have

$$s_d(\vec{y}).s_d^*(\vec{y'}) \;=\; 4k^2\int K_d(\vec{y}-\vec{x})K_d^*(\vec{y'}-\vec{x'})\,f(\vec{x})\,f(\vec{x'})\,\phi(\vec{x})\,\phi^*(\vec{x'})\,d\vec{x}d\vec{x'}$$

By taking the expectation value, this becomes:

$$\langle s_d(\vec{y}).s_d^*(\vec{y'}\rangle \;=\; 4k^2\sigma^2\int C(\vec{x}-\vec{x'})\,K_d(\vec{y}-\vec{x})K_d^*(\vec{y'}-\vec{x'})\,\phi(\vec{x})\,\phi^*(\vec{x'})\,d\vec{x}d\vec{x'}$$

after replacing C by its Fourier integral, we get

$$\langle s_d(\vec{y}).s_d^*(\vec{y'}\rangle \;=\; \frac{4k^2\sigma^2}{4\pi^2}\int \tilde{C}(\vec{p})\,\mathrm{e}^{-i\vec{p}(\vec{x}-\vec{x'})}\,K_d(\vec{y}-\vec{x})K_d^*(\vec{y'}-\vec{x'})\,\phi(\vec{x})\,\phi^*(\vec{x'})\,d\vec{x}d\vec{x'}\,d\vec{p}$$

Now, it can be checked that

$$\int K_d(\vec{y}-\vec{x})\mathrm{e}^{-i\vec{p}.\vec{x}}\phi(\vec{x})\,d\vec{x} \;=\; \mathrm{e}^{-id\vec{p}^2/2k}\,\mathrm{e}^{-i\vec{p}.\vec{y}}\phi_d(\vec{y}+d\vec{p}/k)$$

so that

$$\mathcal{C}(d;\vec{y},\vec{y'}) \;=\; \frac{\epsilon}{4\pi^2}\int \tilde{C}(\vec{p})\,\mathrm{e}^{-i\vec{p}.(\vec{y}-\vec{y'})}\phi_d(\vec{y}+d\vec{p}/k)\,\phi_d^*(\vec{y'}+d\vec{p}/k)\,d\vec{p}$$

where ϕ_d is the beam amplitude diffracted at a distance d. Now, it may be noted that if the distance d is larger than a few m, the coordinate $\vec{y}+d\vec{p}/k$ falls outside the actual beam for values of $\vec{p}$ slightly different from the maximum $\vec{p}_0 = -k\vec{y}/d$. This means that the integrand takes non negligible values only in the small domain where the neigborhood of $-k\vec{y}/d$ intersects that

of $-k\vec{y'}/d$. Over this small domain, it can be assumed that the function $\tilde{C}$ has very small variations, and that it differs by a very small amount from the value $\vec{p}_0 = -k\vec{y}/d$. We therefore replace $\tilde{C}(\vec{p})$ by $\tilde{C}(\vec{p}_0) \sim \tilde{C}(\vec{p'}_0)$ in the integral, giving

$$\mathcal{C}(d;\vec{y},\vec{y'}) \;=\; \frac{\epsilon}{4\pi^2}\,\tilde{C}(\vec{p}_0)\int \mathrm{e}^{-i\vec{p}.(\vec{y}-\vec{y'})}\phi_d(\vec{y}+d\vec{p}/k)\,\phi_d^*(\vec{y'}+d\vec{p}/k)\,d\vec{p}$$

When $\mathcal{C}(d;\vec{y},\vec{y'})$ takes significant values, $\vec{y}$ and $\vec{y'}$ are so close together that we can write equally

$$\tilde{C}(-k\vec{y}/d) = \tilde{C}(-k\vec{y'}/d) = \tilde{C}(k\theta) = \frac{\lambda^2}{2\pi}\,p(\theta)$$

where θ is the angle locating the direction of the small domain around $\vec{y}$ and $\vec{y'}$. It is possible to give a shorter version of the preceding integral. by the change of variables

$$\vec{p} = \vec{q} - \frac{k}{2d}\,(\vec{y}+\vec{y'})$$

we obtain

$$\mathcal{C}(d;\vec{y},\vec{y'}) \;=\; \frac{\epsilon\lambda^2}{8\pi^3}\,\mathrm{e}^{ik(y^2-y'2)/2d}\int d\vec{q}\,\mathrm{e}^{-i\vec{q}.\vec{Y}}\,\phi_d\left(\frac{d}{k}\vec{q}+\frac{1}{2}\vec{Y}\right)\,\phi_d^*\left(\frac{d}{k}\vec{q}-\frac{1}{2}\vec{Y}\right)$$

with $\vec{Y} \equiv \vec{y} - \vec{y'}$. By substituting the Fourier transforms of the amplitudes, this is

$$\mathcal{C}(d;\vec{y},\vec{y'}) \;=\; \frac{\epsilon\lambda^2}{8\pi^3}\,\mathrm{e}^{ik(y^2-y'2)/2d}\times$$

$$\frac{1}{16\pi^4}\int d\vec{q}\,d\vec{p}\,d\vec{p'}\,\mathrm{e}^{-i\vec{q}.\vec{Y}}\,\mathrm{e}^{-i\vec{p}(d\vec{q}/k+\vec{Y}/2)}\tilde{\phi_d}(\vec{p})\,\mathrm{e}^{i\vec{p'}(d\vec{q}/k-\vec{Y}/2)}\tilde{\phi}_d^*(\vec{p'})$$

but the Fourier transforms of the progagated amplitudes are equal to the Fourier transforms of the initial amplitudes, times the propagator

$$\mathrm{e}^{-idp^2/2k}$$

so that:

$$\mathcal{C}(d;\vec{y},\vec{y'}) \;=\; =\; \frac{\epsilon\lambda^2}{8\pi^3}\,\mathrm{e}^{ik(y^2-y'2)/2d}\times$$

$$\frac{1}{16\pi^4}\int d\vec{q}\,d\vec{p}\,d\vec{p'}\,\mathrm{e}^{-i\vec{q}.(\vec{Y}+(\vec{p}-\vec{p'})d/k}\,\mathrm{e}^{-i(\vec{p}+\vec{p'}).\vec{Y}/2}\,\mathrm{e}^{-i(p^2-p'^2)d/2k}\,\tilde{\phi}(\vec{p})\,\tilde{\phi}^*(\vec{p'})$$

the $\vec{q}$ integration gives a Dirac function, so that

$$\mathcal{C}(d;\vec{y},\vec{y'}) \;=\; \frac{\epsilon\lambda^2}{8\pi^3}\,\mathrm{e}^{ik(y^2-y'2)/2d}\,\times$$

$$\frac{1}{4\pi^2}\,\frac{k^2}{d^2}\int d\vec{p}\,d\vec{p'}\,\delta(\vec{p'}-\vec{p}-k\vec{Y}/d)\,\mathrm{e}^{-i(\vec{p}+\vec{p'}).\vec{Y}/2}\,\mathrm{e}^{-i(p^2-p'^2)d/2k}\,\tilde{\phi}(\vec{p})\,\tilde{\phi}^*(\vec{p'})$$

$$=\;\frac{\epsilon}{8\pi^3 d^2}\,\mathrm{e}^{ik(y^2-y'2)/2d}\int d\vec{p}\tilde{\phi}(\vec{p})\,\tilde{\phi}^*(\vec{p}+k\vec{Y}/d)$$

which yields the symmetrical expression for the coherence function:

$$\mathcal{C}(d;\vec{y},\vec{y'}) = \;\frac{\epsilon}{8\pi^3 d^2}\,\mathrm{e}^{ik(y^2-y'2)/2d}\int d\vec{p}\,\tilde{\phi}(\vec{p}-k\vec{Y}/2d)\,\tilde{\phi}^*(\vec{p}+k\vec{Y}/2d) \quad (5.7)$$

In the case of a fundamental gaussian beam at its waist w_0, the explicit calculation is straightforward. We have

$$\tilde{\phi}(\vec{p}) \;=\; \sqrt{2\pi w_0^2}\,\mathrm{e}^{-p^2 w_0^2/4}$$

and consequently

$$\int d\vec{p}\,\tilde{\phi}(\vec{p}-k\vec{Y}/2d)\,\tilde{\phi}^*(\vec{p}+k\vec{Y}/2d) \;=\; 4\pi^2\mathrm{e}^{-k^2 w_0^2 Y^2/8d^2}$$

so that finally

$$\mathcal{C}(d;\vec{y},\vec{y'}) \;=\; \frac{\epsilon}{2\pi d^2}\,p(\theta)\,\mathrm{e}^{ik(y^2-y'2)/2d}\,\mathrm{e}^{-(\vec{y}-\vec{y'})^2/2d^2\theta_g^2} \quad (5.8)$$

where $\theta_g \equiv \lambda/\pi w_0$ is the gaussian angular aperture of the initial beam. This shows the memory effect of the initial beam even after diffusion and diffraction.

Chapter 6

Heating issues

The laser beam circulating through or reflected off the mirrors carries high light power, especially in the resonant cavities. These mirrors dissipate a small but non zero rate of this power into heat, increasing their internal temperature. The profile of the beam being sharp (gaussian), the heat generation is practically localized around the optical axis, and the resulting temperature field presents gradients. The non uniform temperature field induces firstly an index field known as a *thermal lens*. It induces secondly distortions of the mirror's surface called *thermal aberrations*. These effects initiate non linear processes : the rate of heating depends on the stored light power, the stored light power depends in turn on the cavities tuning, which in turn depends on the thermal lensing and aberrations. Methods of simulation for these processes need firstly a study of the steady state, then the transient case will be addressed.

6.1 Heating by dissipation in the coating

Consider a cylindrical mirror receiving the beam of a laser : A fraction ϵ of the light power is dissipated in the coating, so that there is a source of heat over one face. If the substrate is crossed by the beam, a fraction of the power is absorbed per unit of length of the path inside, so that there is also a source in the bulk. The mirror being suspended in a vacuum by very thin wires, it cannot appreciably lose heat by conduction nor by convection. The only way for restoring thermal equilibrium with the surrounding walls is to radiate excess energy under the form of infrared radiation, according to

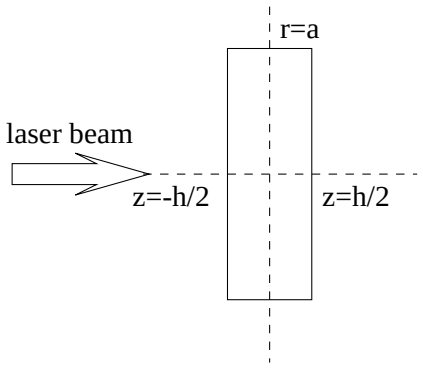

Figure 6.1: Cylindrical mirror heated by laser beam

the blackbody law. Simple analytical solutions can be found in the case of axial symmetry. We address the case of surface heating (bulk heating will be addressed in a coming section). Let z be the coordinate along the symmetry axis (the optical axis), and r the radial coordinate (see Fig.6.1).

6.1.1 The Fourier equation and the boundary conditions

In a general time dependent situation the heat field obeys the Fourier equation :

$$[\rho\, C\, \partial_t - K\Delta]\, T(r,z) \;=\; p(r) \tag{6.1}$$

where K is the thermal conductivity (sorry, don't confuse with the unit K (Kelvin) of absolute temperature !) , ρ the density of the material , C its specific heat , and $p(r)$ the density of power deposited in the material . To be specific, let us give these parameters in the case of silica, a material frequently used for making mirrors, with the notation used throughout this chapter, and the values used in numerical applications :

parameter	name	value	units
ρ	density	2202	$\mathrm{kg\,m^{-3}}$
C	Specific heat	745	$\mathrm{J\,kg^{-1}\,K^{-1}}$
K	Thermal conductivity	1.38	$\mathrm{W\,m^{-1}\,K^{-1}}$
dn/dT	Thermal index coeff.	-0.87 10^{-5}	$\mathrm{K^{-1}}$
ϵ	Dissipation rate (coating)	10^{-6}	dimensionless
β	Linear absorption coeff.	10^{-5}	$\mathrm{m^{-1}}$
α	Thermal expansion coeff.	5.4 10^{-7}	$\mathrm{K^{-1}}$
Y	Young modulus	7.3 10^{10}	$\mathrm{N\,m^{-2}}$
σ	Poisson ratio	0.17	dimensionless

If we assume the stationary state, in which the radiation losses exactly balance the incoming power, the heat field obeys the static homogeneous Fourier equation, and if there is no internal heat sources, this reduces to the Laplace equation :

$$\Delta T(r,z) \;=\; 0$$

We must add to this equation the boundary conditions, namely the balance of heat fluxes on the limiting faces, according to

$$\mathbf{n}\cdot\left[\mathbf{F}+K\,\nabla T\right]_{\mathrm{surf}}=0$$

where $\mathbf{F}$ ($\mathrm{W.m^{-2}}$) is the escaping flux, $-K\nabla T$ the internal flux at boundary and $\mathbf{n}$ the normal. We assume that in case of thermal radiation, the escaping flux is

$$\left[\mathbf{n}\cdot\mathbf{F}\right]_{\mathrm{surf}} \;=\; \sigma'\left[T^4-T_0^4\right]_{\mathrm{surf}}$$

where σ' is related to the Stefan-Boltzmann constant $\sigma_{\mathrm{SB}}\sim 5.67\,10^{-8}\ \mathrm{W\,m^{-2}\,K^{-4}}$ that holds for the true blackbody radiation, by a correction (emissivity correction) taking into account the nature of the material (Please do not confuse the SB constant σ_{SB} with the Poisson ratio σ). T_0 is the temperature of the surrounding wall. $\sigma'=0.8\,\sigma_{\mathrm{SB}}$ is plausible for SiO_2. Let us detail the boundary conditions in the case of a cylindrical body (cf Fig.6.1) :

- On the face $z=h/2$,

$$-K\frac{\partial T}{\partial z}(r,h/2) \;=\; \sigma'(T^4-T_0^4)$$

. The latter expression is non linear, but we hope, in case of low absorption, that the temperature excess with respect to room temperature

will be small. Of course, one must check at the end of the calculation that :

$$T - T_0 \ll T_0$$

was a correct assumption, so that it was reasonable to linearize with respect to T_0. Assume $T - T_0 = \delta T$, this means that

$$T^4 - T_0^4 \sim 4T_0^3\,\delta T$$

It will be understood in what follows, that T is the excess of temperature caused by the laser beam with respect to T_0, so that the boundary condition becomes

$$-K\frac{\partial T}{\partial z}(r, h/2) \;=\; 4\sigma' T_0^3\, T(r, h/2) \tag{6.2}$$

- On the face $z = -h/2$, we have a balance of three heat fluxes :

$$-K\frac{\partial T}{\partial z}(r, -h/2) \;=\; -4\sigma' T_0^3\, T(r, h/2) \;+\; \epsilon\, I(r) \tag{6.3}$$

where ϵ is the loss rate due to dissipation of light power into heat (a few ppm). We assume that the incoming beam is a TEM_{00} wave of half width w, so that the incoming power flux is (P being the beam power) :

$$I(r) = \frac{2P}{\pi w^2}\,\mathrm{e}^{-2r^2/w^2}$$

Note the change in the sign for the radiative part, and the presence of an extra surface heat flux generated by absorption in the coating, represented as a boundary layer.

- On the edge of the cylinder, we find only radiation losses :

$$-K\frac{\partial T}{\partial r}(a, z) \;=\; 4\sigma' T_0^3\, T(a, z) \tag{6.4}$$

6.1.2 Solution as a Dini expansion

In cylindrical coordinates, (still assuming axial symmetry), the Fourier (or Laplace) equation is

$$\left(\partial_r^2 + \frac{1}{r}\partial_r + \partial_z^2\right) T(r, z) \;=\; 0$$

A solution of this equation is called *harmonic*. In cylindrical coordinates, there exist harmonic functions of the form

$$T(r,z) \;=\; J_0(kr)\left(A\,\mathrm{e}^{kz} + B\,\mathrm{e}^{-kz}\right)$$

where k, A, B are arbitrary constants, and the $\{J_n(z)\ ;\ n \in \mathcal{Z}\}$ the Bessel functions. It is probably worth to recall at least that

$$\partial_x J_0(x) \;=\; -J_1(x)$$

$$\left(\partial_x + \frac{1}{x}\right) J_1(x) \;=\; J_0(x)$$

The last boundary condition, expressed by Eq.6.4 reads thus :

$$K\,k\,J_1(ka) \;=\; 4\sigma' T_0^3\,J_0(ka)$$

or, using a reduced radiation constant $\chi \;=\; 4\sigma' T_0^3\,a/K$:

$$kaJ_1(ka) - \chi J_0(ka) = 0$$

An equation like the preceding one has an infinite discrete number of solutions defining the possible values of k. Call $\{\zeta_n\ ;\ n = 1,2,\ldots\}$ the solutions of

$$\zeta J_1(\zeta) - \chi J_0(\zeta) = 0 \tag{6.5}$$

The values of k are the $k_n = \zeta_n/a$. The temperature field can finally be written as an expansion of the type

$$T(r,z) = \sum_n \left(A_n \mathrm{e}^{k_n z} + B_n \mathrm{e}^{-k_n z}\right)\, J_0(k_n r)$$

It is well known from the Sturm-Liouville theorem that the functions $\{J_0(\zeta_n r/a)\ ;\ n = 1,2,\ldots\}$ form a complete orthogonal basis for functions defined in the interval $[0,a]$, having normalization constants c_n [20] such that

$$\int_0^a J_0(\zeta_n r/a) J_0(\zeta_{n'} r/a)\, r\, dr \;=\; \frac{1}{c_n}\,\delta_{nn'}$$

with

$$c_n \;=\; \frac{2\zeta_n^2}{a^2(\chi^2+\zeta_n^2)J_0(\zeta_n)^2}$$

In particular, the intensity profile can be expanded on this basis :

$$I(r) \;=\; \sum_n p_n \, J_0(\zeta_n r/a) \tag{6.6}$$

by inverting the latter relation, one finds :

$$p_n \;=\; c_n \int_0^a I(r)\, J_0(\zeta_n r/a)\, r\, dr$$

and substituting the expression of $I(r)$ yields

$$p_n = \frac{2\zeta_n^2}{a^2(\chi^2+\zeta_n^2)J_0(\zeta_n)^2} \int_0^a \frac{2P}{\pi w^2} J_0(\zeta_n r/a)\, \mathrm{e}^{-2r^2/w^2}\, r\, dr$$

In the cylinders used as mirror substrates, the radius is large enough that the diffraction losses are negligible. This is equivalent to say that in the preceding integral, the bound a may be replaced by ∞ without changing appreciably the result. In this case, the result is [20] :

$$p_n \;=\; \frac{P}{\pi\, a^2} \frac{\zeta_n^2}{(\zeta_n^2+\chi^2)J_0(\zeta_n)^2} \exp\left(-\frac{w^2\zeta_n^2}{8\, a^2}\right) \tag{6.7}$$

Then the boundary conditions 6.2 and 6.3 reduce to a linear system

$$\begin{cases} (\zeta_n-\chi)\Gamma_n^2 A_n - (\zeta_n+\chi)B_n = -\,\epsilon p_n a \Gamma_n / K \\ (\zeta_n+\chi)A_n - (\zeta_n-\chi)\Gamma_n^2 B_n = 0 \end{cases}$$

where for the sake of brevity, $\Gamma_n = \exp(-\zeta_n h/2a)$. This gives the constants $A_n,\ B_n$:

$$A_n = \frac{\epsilon p_n a}{K}\, \mathrm{e}^{-3\zeta_n h/2a}\, \frac{\zeta_n-\chi}{(\zeta_n+\chi)^2-(\zeta_n-\chi)^2\mathrm{e}^{-2\zeta_n h/a}}$$

$$B_n = \frac{\epsilon p_n a}{K}\, \mathrm{e}^{-\zeta_n h/2a}\, \frac{\zeta_n+\chi}{(\zeta_n+\chi)^2-(\zeta_n-\chi)^2\mathrm{e}^{-2\zeta_n h/a}}$$

The temperature field is now fully determined :

$$T(r,z) = \sum_n \frac{\epsilon p_n a}{K}\, \mathrm{e}^{-\zeta_n h/2a}\, \frac{(\zeta_n-\chi)\mathrm{e}^{-\zeta_n(h-z)/a} + (\zeta_n+\chi)\mathrm{e}^{-\zeta_n z/a}}{(\zeta_n+\chi)^2-(\zeta_n-\chi)^2\mathrm{e}^{-2\zeta_n h/a}}\, J_0(\zeta_n r/a) \tag{6.8}$$

The reconstruction of $I(r)$ by expansion on the $J_0(\zeta_n r/a)$ allows to determine the maximum number N of terms to consider for convergence of the above series. The precision improves very fastly with N. On Fig.6.2 one can compare the exact gaussian intensity profile with formula 6.6 with only 10 terms. The error is quite negligible for $N > 30$ (Fig.6.3). Finally the temperature field is shown on Fig.6.4.

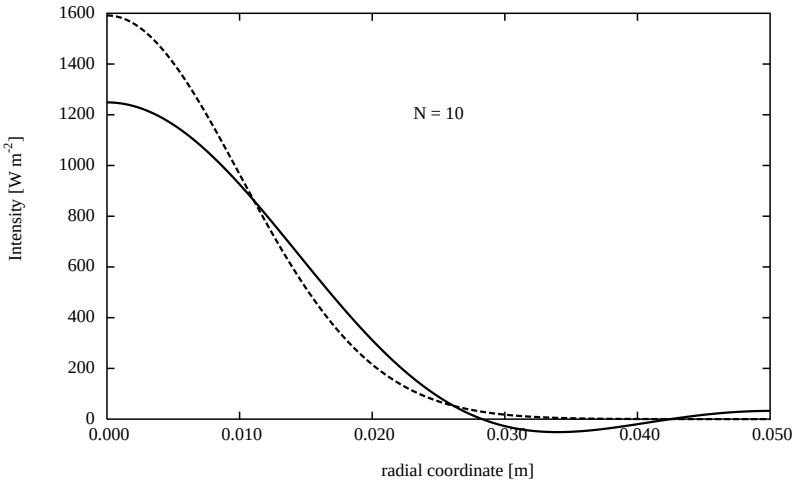

Figure 6.2: dashed line : Beam intensity profile, solid line : reconstruction with only 10 Dini terms

6.1.3 Thermal lensing

The first consequence of a temperature field being installed in the bulk material is to create an index field according to :

$$\Delta n(r,z) \;=\; \frac{dn}{dT}\,T(r,z)$$

where dn/dT is the index temperature coefficient of the material. For Silica we have $dn/dT \sim -0.87\,10^{-5}$ K^{-1}. The effect of the index field is to change the wavefront of a passing optical wave by an extra path, or excess optical thickness $Z(r)$:

$$Z(r) \;=\; \frac{dn}{dT}\int_{-h/2}^{h/2} T(r,z)\,dz$$

With the preceding expression of the temperature field, we find

$$Z(r) \;=\; \frac{dn}{dT}\sum_n \frac{\epsilon p_n a^2}{K\zeta_n}\,\frac{1-\mathrm{e}^{-\zeta_n h/a}}{\zeta_n+\chi-(\zeta_n-\chi)\mathrm{e}^{-\zeta_n h/a}}\,J_0(\zeta_n r/a) \qquad (6.9)$$

Fig.6.5 shows the shape of a plane wavefront after passing through a disk like the Virgo mirrors. We call *thermal lensing* this kind of distortion. The effect

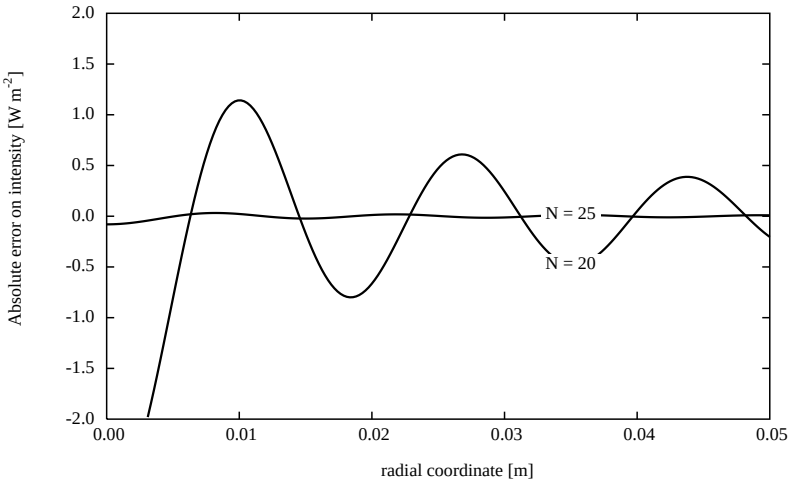

Figure 6.3: Error in the reconstructed intensity profile and order of the Dini expansion

of thermal lensing is as a first approximation to change the curvature of the wavefront, like a real lens. We can estimate the curvature taken by a plane wave after crossing the disk by calculating the nearest paraboloid. The apex equation of such a paraboloid is $z = c\,r^2 + p$, and we want to minimize

$$Q(c,p) \;=\; \int_0^a W(r)\left(Z(r) - c\,r^2 - p\right)^2 r\,dr$$

where

$$W(r) = \frac{4}{w^2}\,\mathrm{e}^{-2r^2/w^2}$$

is the gaussian weighting function, exactly as in the treatment of imperfect mirrors (see preceding chapter). The requirement that the partial derivatives of $Q(c,p)$ vanish, leads to a normal system having the solution

$$c \;=\; \frac{< r^2 Z(r) > - < r^2 >< Z(r) >}{< r^4 > - < r^2 >^2}$$

$$p \;=< Z > - c \;< r^2 >$$

where the weighted average $< f >$ of any function has the definition

$$< f > \equiv \int_0^a W(r)\,f(r)\,r\,dr$$

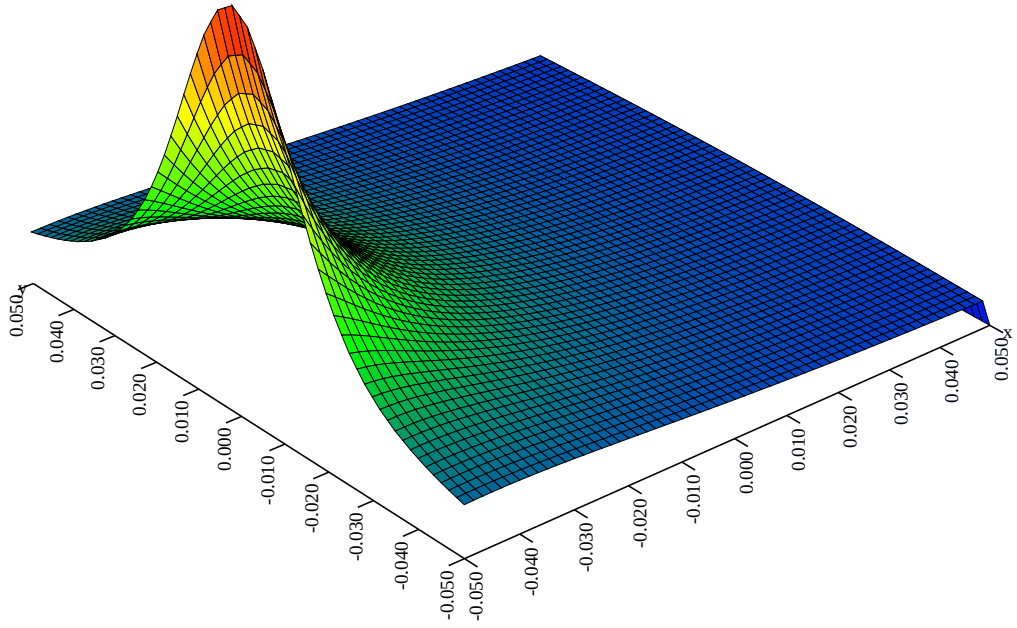

Figure 6.4: Temperature field in a Virgo mirror for 1W dissipated in the coating. Hot point : 13.3K

With the weight $W(r)$ we find (assuming $w \ll a$) :

$$< r^2 > = \frac{w^2}{2}$$

$$< r^4 > = \frac{w^4}{2}$$

so that

$$< r^4 > - < r^2 >^2 = \frac{w^4}{4}$$

Let us derive a useful rule for the computation of the parameters c and p. The equivalent displacement $Z(r)$ being known under the form 6.9

$$Z(r) = \sum_n z_n J_0(\zeta_n r/a)$$

where the coefficients z_n are known by the preceding theory, we find firstly

$$< J_0(\zeta_n r/a) >= \mathrm{e}^{-\zeta_n^2 w^2/8a^2}$$

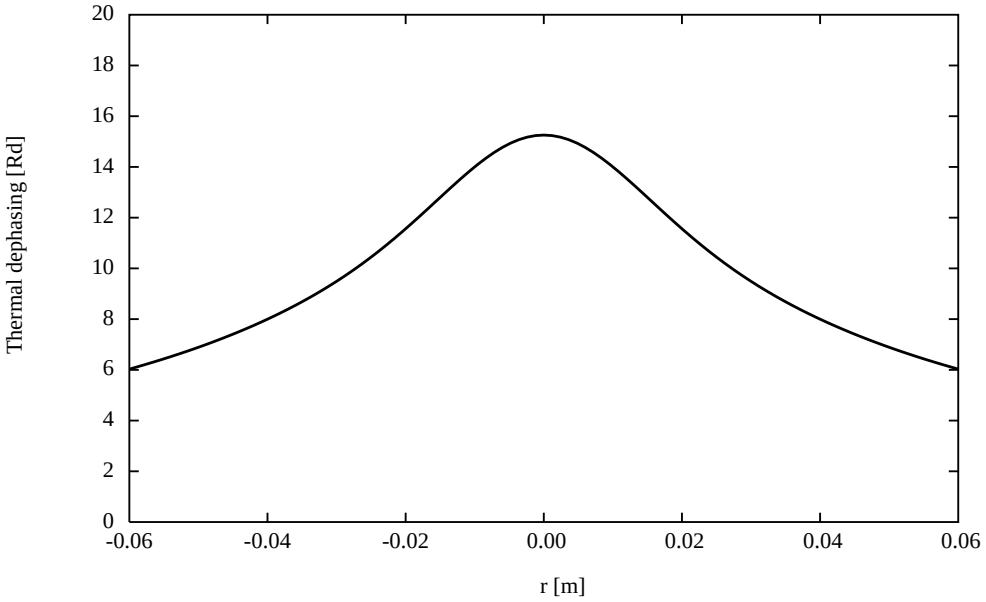

Figure 6.5: Thermal phase lens in a $a = 17.5$ cm, $h = 10$ cm silica mirror for 1W dissipated in the coating (absolute value)

and

$$< r^2 J_0(\zeta_n r/a) >= \frac{w^2}{2}\left(1 - \frac{\zeta^2 w^2}{8a^2}\right) \mathrm{e}^{-\zeta_n^2 w^2/8a^2}$$

so that

$$\frac{< r^2 J_0(\zeta_n r/a) > - < r^2 >< J_0(\zeta_n r/a) >}{< r^4 > - < r^2 >^2} \;=\; -\frac{\zeta_n^2}{4a^2}\,\mathrm{e}^{-\zeta_n^2 w^2/8a^2}$$

and finally, the curvature c is :

$$c = -\frac{1}{4a^2}\sum_n z_n\,\zeta_n^2\,\mathrm{e}^{-\zeta_n^2 w^2/8a^2}$$

The mean optical thickness $< Z >$ is

$$< Z > = \sum_n z_n\,\mathrm{e}^{-\zeta_n^2 w^2/8a^2}$$

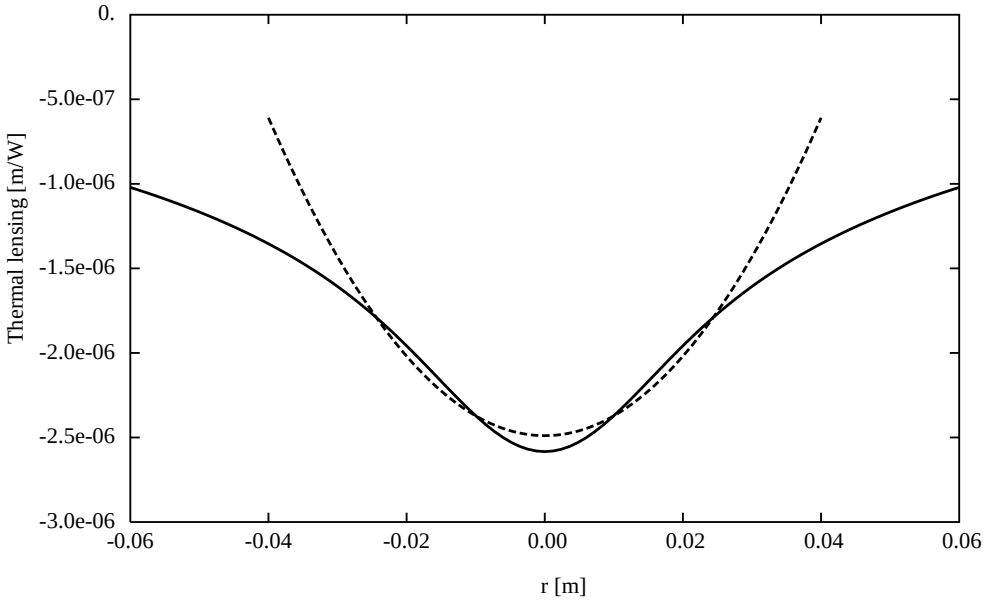

Figure 6.6: Thermal lens and its weighted parabolic approximation for 1 W absorbed in the coating

and the piston :

$$p \;=\; \sum_n z_n \,(1+\zeta_n^2 w^2/8a^2)\,\mathrm{e}^{-\zeta_n^2 w^2/8a^2}$$

The recipe is thus : take the formula giving the thermal lens $Z(r)$, then replace $J_0(\zeta_n r/a)$ by $-\zeta_n^2 \exp(-\zeta_n^2 w^2/8a^2)/4a^2$ and you get the curvature of the wavefront. These formulas will be exploited also in foregoing calculations with other coming definitions of z_n. We can compare the parabolic fit to the original thermal lens on Fig.6.6 ; we have espressed it in m and restablished the sign. For the Virgo parameters, we find a curvature radius of the wavefront, i.e. the focal length of the lens : $R_c = f = 1/2c \sim 425.5$ m.W (Note that f is inversely proportional to the dissipated power).

A perfect parabolic lensing could be compensated by a suitable matching of the beam. We could therefore in principle, ignore it. In fact the curvature is proportional to the absorbed power, which depends in turn of the dissipation rate in the coating. The dissipation rate could easily be different by

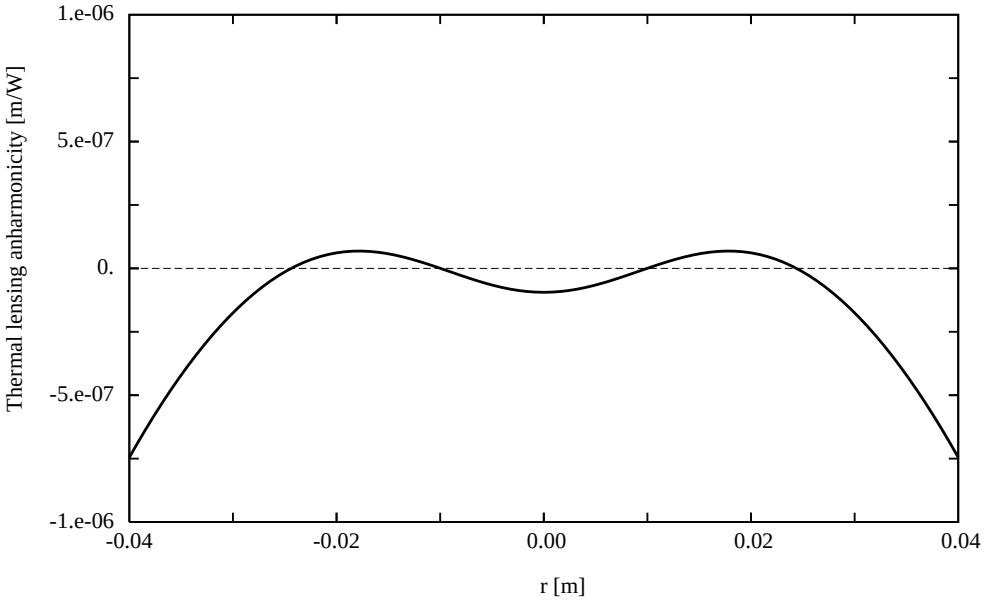

Figure 6.7: Thermal lens : anharmonicity

a factor of the order of 2 between two mirrors, and it is therefore difficult to compensate for the two lenses simultaneously. Moreover, the lensing is not exactly parabolic, and this means that it couples the nominal TEM_{00} mode with higher order modes, resulting in extra losses for the beam. On Fig.6.7, the difference between the actual lens and a paraboloid is plot, we call it *anharmonicity* by analogy with the potential theory. Concerning the losses, we can compute the coupling efficiency of the thermal lens between to matched waves. Consider for instance the incoming wave :

$$\Psi_1 \;=\; \frac{2}{w}\mathrm{e}^{-r^2/w^2}\,\mathrm{e}^{ikr^2/2R_1}$$

and an outgoing wave (after passing the lens)

$$\Psi_2 \;=\; \frac{2}{w}\mathrm{e}^{-r^2/w^2}\,\mathrm{e}^{ikr^2/2R_2}$$

The two waves have equal w for the lens cannot magnify the beam, but

different curvature radii. Both are normalized according to

$$\int_0^\infty \overline{\Psi}(r)\,\Psi(r)\,r\,dr \;=\; 1$$

The lens can be expressed as

$$\Delta\Phi(r) = \frac{r^2}{2f} + p + \epsilon(r)$$

where $\epsilon(r)$ is the anharmonic residue. The efficiency of the coupling depends on the scalar product

$$\gamma \;=\; <\Psi_2, \Psi_1 \mathrm{e}^{i\Delta\Phi}>$$

this gives

$$\gamma \;=\; \frac{4}{w^2}\int_0^\infty \mathrm{e}^{-2r^2/w^2}\,\mathrm{e}^{ik\frac{r^2}{2}(1/R_1+1/f-1/R_2)}\,\mathrm{e}^{ikp}\,\mathrm{e}^{ik\epsilon(r)}$$

The matching condition is precisely

$$\frac{1}{R_2} = \frac{1}{R_1} + \frac{1}{f}$$

and if ϵ is much smaller than the wavelength, we have thus

$$\gamma \;=\; \mathrm{e}^{ikp}\int_0^\infty W(r)\,\left(1 + ik\epsilon(r) - k^2\epsilon^2(r)\right)\,r\,dr$$

the mean $<\epsilon>$ is zero, so that

$$\gamma \;=\; 1 - k^2 <\epsilon^2>/2 \;=\; 1 - k^2 Q(c,p)/2$$

where c and p are the optimal values we just found. the square modulus of γ gives the efficiency :

$$\overline{\gamma}\,\gamma \;=\; 1 - k^2 <\epsilon^2>$$

so that the coupling losses are simply

$$L \;=\; 4\pi^2 <\epsilon^2>/\lambda^2$$

. For our $a = 0.175$ m, $h = 0.1$ m mirror, we find (numerically) $Q(m_0, p_0) \sim 4.15\ 10^{-15}$ m^2/W^2. This is

$$L \sim 0.14\ \mathrm{W}^{-2}$$

Assume $\epsilon = 1$ ppm, $P_{\mathrm{intracavity}} = 10$ kW, one finds $L \sim 5$ ppm. Note that the losses due to mirror roughness were computed exactly the same way, except that an extra factor of 4 appeared, due to that special case of reflection, in which the defects have double weight.

6.2 Heating by dissipation in the bulk substrate

6.2.1 Temperature field

A slightly different model must be used when we consider the heating process caused by dissipation of light power by its propagation through an absorbing medium. Transparent solids as silica have a small but finite linear absorption rate β, so that as a function of z (the optical axis), the intensity obeys :

$$I(r,z) = I_0(r)\,\mathrm{e}^{-\beta z}$$

where I_0 is the lossless solution of Maxwell's equations. The power dissipated in the medium per volume unit is therefore at first order in β :

$$p(r,z) \;=\; -\left[\frac{dI}{dz}\right]_{\text{diss}} \;\sim\; \beta\, I_0(r)$$

We shall neglect diffraction effects inside the medium for the Rayleigh range of the beam ($\sim$ 1 km) is much larger than the medium thickness ($\sim$ 10 cm), so that we can consider a heat source distributed in the bulk material, of the form

$$p(r) \;=\; \frac{2P}{\pi w^2}\,\beta\,\mathrm{e}^{-2r^2/w^2}$$

The heat equation now reads :

$$-K\,\Delta T(r,z) \;=\; \frac{2P}{\pi w^2}\,\beta\,\mathrm{e}^{-2r^2/w^2} \tag{6.10}$$

We know from the coating study that

$$\frac{2P}{\pi w^2}\,\mathrm{e}^{-2r^2/w^2} \;=\; \sum_n p_n\, J_0(\zeta_n r/a)$$

where the ζ_n are the discrete family of zeros of an equation similar to 6.5 (in fact it is the same, as will be seen later), and

$$p_n \;=\; \frac{P}{\pi a^2}\,\frac{\zeta_n^2}{(\zeta_n^2+\chi^2)J_0(\zeta_n)^2}\,\mathrm{e}^{-\zeta_n^2 w^2/8a^2}$$

In fact, it is easy to guess that the ζ_n will be exactly the same as in the coating study. Anyway, eq.6.10 admits a special solution $T_{\rm spec}(r)$ given by

$$T_{\rm spec}(r) \;=\; \sum_n t_n\, J_0(\zeta_n r/a)$$

with

$$t_n \;=\; \frac{\beta P}{\pi K}\,\frac{1}{(\zeta_n^2+\chi^2)J_0(\zeta_n)^2}\,{\rm e}^{-\zeta_n^2 w^2/8a^2}$$

A general solution of 6.10 requires still a general solution of the homogeneous heat equation, that can be taken of the form

$$T_{\rm gen\ eh} = \sum_n A_n \cosh(\zeta_n z/a)\, J_0(\zeta_n r/a)$$

where the coefficients A_n are arbitrary. The particular choice of cosh rather than a combination of $\exp(-\zeta_n z/a)$ and $\exp(\zeta_n z/a)$ is justified by the symmetry of the problem : the heat source is independent of z, and the temperature field must therefore be symmetrical with respect to the meridian plane. The global temperature field is now :

$$T(r,z) = \sum_n \left(A_n \cosh(\zeta_n z/a) + t_n\right)\, J_0(\zeta_n r/a)$$

Now the boundary conditions reduce to radiation losses on the faces and on the edge.

- On the edge

$$-K\,\frac{\partial T}{\partial r}(a,z) \;=\; 4\sigma' T_0^3\, T(a,z)$$

  and this is the same condition as 6.3. It will be satisfied if the ζ_n are the same as in the coating study, as could be foreseen.

- On the face $z = h/2$, we have

$$-K\,\frac{\partial T}{\partial z}(r,h/2) \;=\; 4\sigma' T_0^3\, T(r,h/2)$$

  Owing to the symmetry, the face $z = -h/2$ gives the same condition.

The last boundary condition determines the A_n :

$$A_n \;=\; -t_n\,\frac{\chi}{\zeta_n \sinh(\zeta_n h/2a) + \chi\cosh(\zeta_n h/2a)}$$

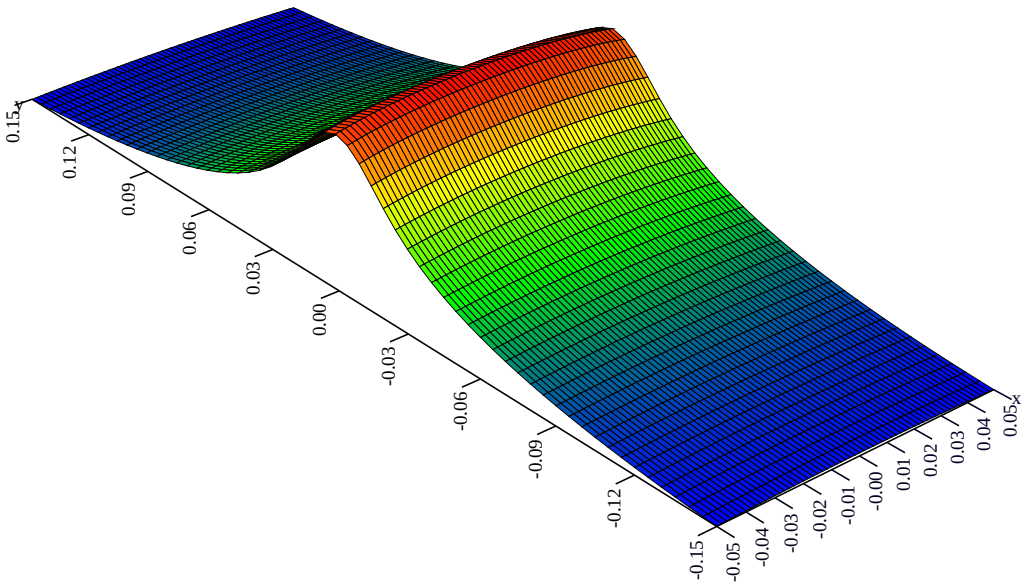

Figure 6.8: Absorption in the bulk : temperature field. Hot point : 3.2 K for 1 W dissipated

and the temperature field is now determined :

$$T(r,z) \;=\; \frac{\beta P}{\pi K}\sum_n \left[1 \;-\; \frac{\chi\cosh(\zeta_n z/a)}{\zeta_n \sinh(\zeta_n h/2a)+\chi\cosh(\zeta_n h/2a)}\right]\times$$
$$\times\; \frac{\exp[-\zeta_n^2 w^2/8a^2)}{(\zeta_n^2+\chi^2)J_0(\zeta_n)^2}\,J_0(\zeta_n r/a) \qquad (6.11)$$

The profile of the temperature field is given on Fig.6.8.

6.2.2 Thermal lensing

We now know how to compute the thermal lens :

$$Z(r) \;=\; \frac{dn}{dT}\int_{-h/2}^{h/2} T(r,z)\,dz$$

this gives :

$$Z(r) \;=\; \frac{dn}{dT}\,\frac{\beta P h}{\pi K}\sum_n \left[1 \;-\; \frac{(2\chi a/\zeta_n h)\,\sinh(\zeta_n h/2a)}{\zeta_n \sinh(\zeta_n h/2a)+\chi\cosh(\zeta_n h/2a)}\right]\times$$

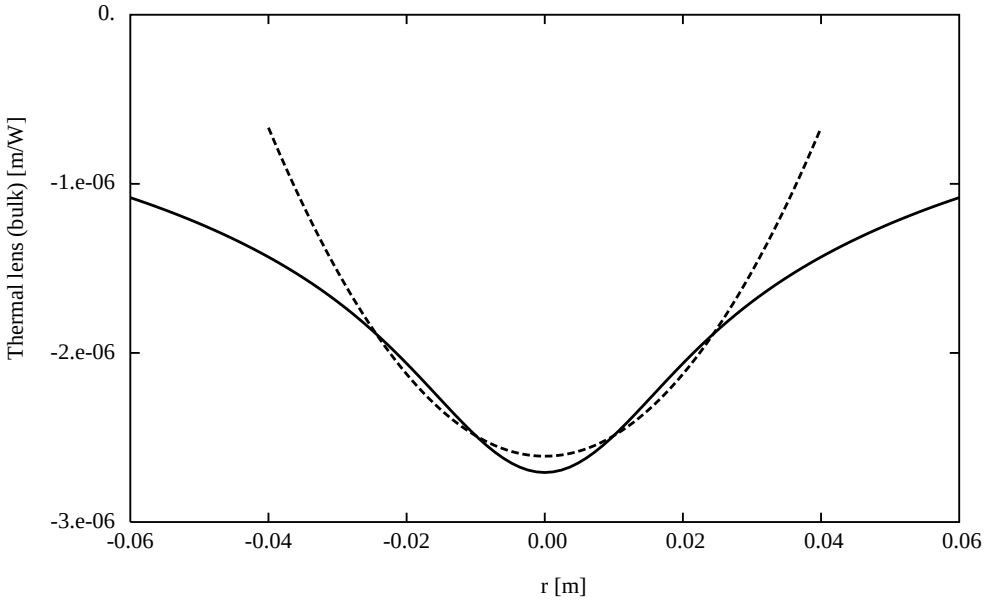

Figure 6.9: Thermal lens and its parabolic approximation (1 W dissipated)- Bulk absorption

$$\times \frac{\exp(-\zeta_n^2 w^2/8a^2)}{(\zeta_n^2+\chi^2)J_0(\zeta_n)^2} J_0(\zeta_n r/a)$$

One sees on Fig.6.9 a plot of the lens profile and of its parabolic best fit, according to methods developped above. The focal length is

$$f \sim 412 \text{ m.W}$$

and the losses

$$L = 0.15 \text{ W}^{-2}$$

Note that these results are very similar to those obtained in the case of coating heating.

6.3 Distortion from coating absorption

An other effect of temperature changes in a solid is its thermal expansion. Moreover, if the temperature is not uniform (we have seen that this is the

case when the heat source is the laser beam) stresses are developed inside causing distortions of the solid. In particular, the mirror reflecting surface is distorted, and we have to estimate the effect both in the case of the coating and bulk heating process. In the case of coating absorption, the fact that the temperature field is harmonic greatly simplifies the solution.

6.3.1 Thermoelastic solution

We first recall the linear thermoelastic equations. The atoms of the distorted solid are displaced with respect to the reference solid by a *displacement* vector $\vec{u}(\vec{r})$. The partial derivatives of $\vec{u}$ define a rank 2 tensor $E_{ij}(\vec{r})$ called *strain* :

$$E_{ij}(\vec{r}) \;=\; \frac{1}{2}[\partial_i u_j(\vec{r}) + \partial_j u_i(\vec{r})]$$

A generalization of Hooke's law linking applied force to displacement in the distortion of a spring, is a linear relation between the *stress* tensor $\Theta_{ij}(\vec{r})$ and the strain tensor via a constant rank 4 tensor :

$$\Theta_{ij} \;=\; \sum_{k,l} C_{ijkl}\, E_{kl}$$

For isotropic solids (e.g. fused silica) , the elastic tensor reduces to only two independent components :

$$\Theta_{ij} \;=\; \lambda\, \delta_{ij}\, E \;+\; 2\mu\, E_{ij}$$

λ and μ are known as the Lamé coefficients. Moreover, if a temperature field T is present, an extra stress arises and this becomes [28]

$$\Theta_{ij} \;=\; \delta_{ij}\,(\lambda\, E - \nu T) + \;2\mu\, E_{ij}$$

ν is the stress temperature modulus, and it is related to the thermal expansion coefficient α by :

$$\nu \;=\; \alpha(3\lambda + 2\mu)$$

The *equilibrium* equation is :

$$\partial_j \Theta_{ij} \;=\; 0$$

In the case of axial symmetry, using cylindrical coordinates, the nonzero strain components are

$$E_{rr} \;=\; \partial_r u_r$$

$$\begin{aligned} E_{rz} &= \frac{1}{2}\left(\partial_r u_z + \partial_z u_r\right) \\ E_{\phi\phi} &= \frac{u_r}{r} \\ E_{zz} &= \partial_z u_z \end{aligned}$$

the stress/strain relations are

$$\begin{cases} \Theta_{rr} &= -\nu\, T + \lambda\, E + 2\mu\, E_{rr} \\ \Theta_{\phi\phi} &= -\nu\, T + \lambda\, E + 2\mu\, E_{\phi\phi} \\ \Theta_{zz} &= -\nu\, T + \lambda\, E + 2\mu\, E_{zz} \\ \Theta_{rz} &= 2\mu\, E_{rz} \end{cases} \tag{6.12}$$

and the equilibrium equation are

$$\begin{cases} \partial_r \Theta_{rr} + (\Theta_{rr} - \Theta_{\phi\phi})/r + \partial_z \Theta_{rz} &= 0 \\ (\partial_r + 1/r)\Theta_{rz} + \partial_z \Theta_{zz} &= 0 \end{cases} \tag{6.13}$$

Recall that the mirror is a cylinder of radius a, of thickness h, that the coordinates are chosen in such a way that $r \in [0, a]$ and $z \in [-h/2, h/2]$, and that the coating is located on the $z = -h/2$ face. One can check that the equilibrium equation is satisfied by a displacement vector of the form

$$u_r = \frac{\nu}{2(\lambda+\mu)} \frac{1}{r} \int_0^r T(r', z)\, r'\, dr'$$

$$u_z = \frac{\nu}{2(\lambda+\mu)} \left[\int_{-h/2}^z T(r, z')\, dz' + \Phi(r) \right]$$

provided a suitable determination of the unknown function $\Phi(r)$. Remark that $\Phi(r)$ is exactly our target, i.e. the displacement of the surface $z = -h/2$ holding the reflective coating. All the following derivations aim to eventually find $\Phi(r)$. We first find the strain tensor :

$$E_{rr}(r, z) = \frac{\nu}{2(\lambda+\mu)} \left[T(r, z) - \frac{1}{r^2} \int_0^r T(r', z)\, r'\, dr' \right]$$

$$E_{\phi\phi}(r, z) = \frac{\nu}{2(\lambda+\mu)} \frac{1}{r^2} \int_0^r T(r', z)\, r'\, dr'$$

$$E_{zz}(r, z) = \frac{\nu}{2(\lambda+\mu)} T(r, z)$$

$$E_{rz}(r,z) = \frac{\nu}{4(\lambda+\mu)}\left[\Phi'(r) + \int_{-h/2}^{z} \frac{\partial T}{\partial r}(r,z')\,dz' + \int_0^r \frac{\partial T}{\partial z}(r',z)\,r'\,dr'\right]$$

The stress tensor is in turn :

$$\Theta_{rr}(r,z) = -\frac{\mu\nu}{\lambda+\mu}\frac{1}{r^2}\int_0^r T(r',z)\,r'\,dr'$$

$$\Theta_{\phi\phi}(r,z) = -\frac{\mu\nu}{\lambda+\mu}\left[T(r,z) - \frac{1}{r^2}\int_0^r T(r',z)\,r'\,dr'\right]$$

$$\Theta_{zz}(r,z) = 0$$

$$\Theta_{rz}(r,z) = \frac{\mu\nu}{2(\lambda+\mu)}\left[\Phi'(r) + \int_{-h/2}^{z} \frac{\partial T}{\partial r}(r,z')\,dz' + \frac{1}{r}\int_0^r \frac{\partial T}{\partial z}(r',z)\,r'\,dr'\right]$$

The equilibrium equations reduce then to :

$$\partial_z \Theta_{rz}(r,z) = 0 \tag{6.14}$$

$$(\partial_r + 1/r)\Theta_{rz}(r,z) = 0 \tag{6.15}$$

By substituting the expression of Θ_{rz} into eq.6.14 we get

$$\frac{\partial \Theta_{rz}}{\partial z}(r,z) = \frac{\mu\nu}{2(\lambda+\mu)}\left[\frac{\partial T}{\partial r}(r,z) + \frac{1}{r}\int_0^r \frac{\partial^2 T}{\partial z^2}(r',z)\,r'\,dr'\right] \tag{6.16}$$

but there is no heat source inside the material, so that T obeys the homogeneous Fourier equation $\Delta T = 0$ i.e.

$$\frac{\partial^2 T}{\partial z^2} = -\frac{1}{r}\,\partial_r\left(r\,\frac{\partial T}{\partial r}\right)$$

so that eq.6.14 is identically satisfied :

$$\partial_z \Theta_{rz} = 0$$

. Now, we have for the same reason (T being harmonic) :

$$(\partial_r + 1/r)\Theta_{rz}(r,z) = \frac{\mu\nu}{2(\lambda+\mu)}\left[\Phi''(r) + \Phi'(r)/r + \frac{\partial T}{\partial z}(r,-h/2)\right]$$

and we have to choose Φ in such a way that the preceding expression vanishes, that is

$$\frac{1}{r}\,\partial r\left(r\,\frac{\partial \Phi}{\partial r}(r)\right) = -\frac{\partial T}{\partial z}(r,-h/2)$$

the solution of which is

$$\Phi(r) \;=\; -\int_0^r \frac{dr'}{r'}\int_0^{r'} \frac{\partial T}{\partial z}(r'',-h/2)\, r''\, dr'' \;+\; C'\ln(r) + C$$

where C and C' are arbitrary constants. Obviously, the regularity of $\vec{u}$ on the axis requires $C'=0$. Now the stress component Θ_{rz} is explicitly known :

$$\Theta_{rz}(r,z) \;=\; \frac{\mu\nu}{2(\lambda+\mu)}\left(\int_{-h/2}^{z}\frac{\partial T}{\partial r}(r,z')\,dz' + \right.$$

$$\left.\frac{1}{r}\int_0^r\left[\frac{\partial T}{\partial z}(r',z)-\frac{\partial T}{\partial z}(r',-h/2)\right]\, r'\, dr'\right)$$

This last form makes it clear that $\Theta_{rz}(r,-h/2)=0$, and since it has been shown that $\partial_z\Theta_{rz}=0$, we have in fact simply

$$\Theta_{rz}(r,z) \;=\; 0$$

The boundary conditions express the balance of applied forces and torques at the limiting surfaces. These conditions are here :

$$\Theta_{rr}(a,z) \;=\; 0$$

$$\Theta_{rz}(a,z) \;=\; 0$$

$$\Theta_{rz}(r,\pm h/2) \;=\; 0$$

$$\Theta_{zz}(r,\pm h/2) \;=\; 0$$

all are identically fulfilled except the first one. It is easy to compute $\Theta_{rr}(a,z)$. We recall the expression found in the preceding section for the temperature field 6.8

$$T(r,z) = \sum_n \frac{\epsilon p_n a}{K}\,\mathrm{e}^{-\zeta_n h/2a}\,\frac{(\zeta_n-\chi)\mathrm{e}^{-\zeta_n(h-z)/a}+(\zeta_n+\chi)\mathrm{e}^{-\zeta_n z/a}}{(\zeta_n+\chi)^2-(\zeta_n-\chi)^2\mathrm{e}^{-2\zeta_n h/a}}\,J_0(\zeta_n r/a)$$

We have

$$\int_0^a J_0(\zeta_n r/a)\, r\, dr \;=\; \frac{a^2}{\zeta_n^2}\int_0^{\zeta_n} J_0(x)\, x\, dx \;=\; \frac{a^2}{\zeta_n^2}\,\zeta_n J_1(\zeta_n) \;=\; \frac{a^2}{\zeta_n^2}\,\chi\, J_0(\zeta_n)$$

where we have used the definition 6.5 of ζ_n. This gives

$$\Theta_{rr}(a,z) \;=\; -\,\frac{\mu\nu}{\lambda+\mu}\,\frac{\epsilon P\chi}{\pi a K}\,\times$$

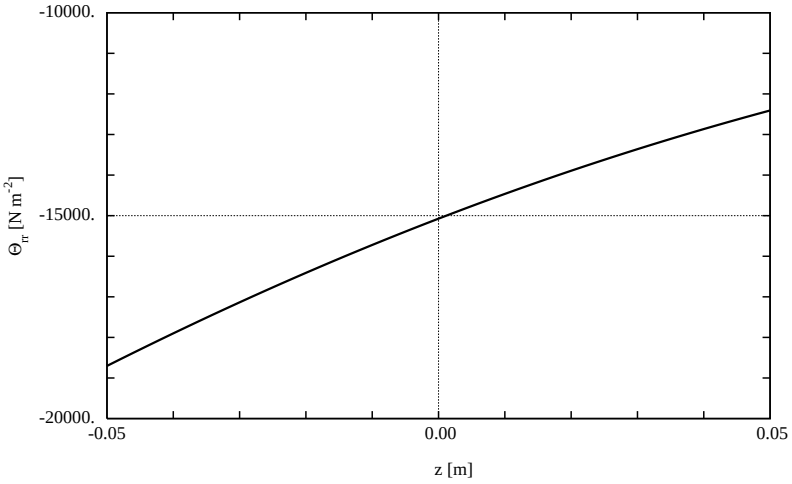

Figure 6.10: The radial stress Θ_{rr} on the edge is a quasi-linear function of z

$$\times \sum_n \frac{\mathrm{e}^{-w^2\zeta_n^2/8a^2}}{(\zeta_n^2+\chi^2)J_0(\zeta_n)} \frac{(\zeta_n-\chi)\mathrm{e}^{-\zeta_n(h-z)/a}+(\zeta_n+\chi)\mathrm{e}^{-\zeta_n z/a}}{(\zeta_n+\chi)^2-(\zeta_n-\chi)^2\mathrm{e}^{-2\zeta_n h/a}}$$

A plot of $\Theta_{rr}(a,z)$ (see fig.6.10) shows that the dependence on z is quasi linear, and by adding a stress of the form $\theta_{rr}(a,z) = A + B\,z$, it will be possible to almost exactly cancel the edge stress. But we have to find a new solution of the elastic equations satisfying the boundary conditions and giving a linear $\theta_{rr}(a,z)$. This is done by the new displacement vector

$$\delta u_r(r,z) \;=\; \frac{\lambda+2\mu}{2\mu(3\lambda+2\mu)}\,(A\,r + B\,rz)$$

$$\delta u_z(r,z) \;=\; -\,\frac{\lambda}{\mu(3\lambda+2\mu)}\,(A\,z + B\,z^2/2) \;-\; \frac{\lambda+2\mu}{4\mu(3\lambda+2\mu)}\,B\,r^2$$

some calculation shows that θ_{rz} as well as θ_{zz} are identically zero, and $\theta_{rr}(a,z) = A + B\,z$. By suitably chosing the arbitrary constants A and B, and adding the correction $\delta\vec{u}$ to $\vec{u}$, we can remove the global resultant radial force exerted on the edge and the resultant torque. Then the Saint-Venant principle tells us that the resulting solution is almost everywhere near the exact solution, except maybe in a small neighborhood of the edge. But we are

interested in the region "seen" by the light beam, so that the approximation should work quite well. By minimizing

$$Q \;=\; \int_{-h/2}^{h/2} \left(\Theta_{rr}(a,z) + A + B\,z\right)^2 dz$$

one finds

$$A \;=\; -\frac{1}{h}\int_{-h/2}^{h/2} \Theta_{rr}(a,z)\,dz$$

and

$$B \;=\; -\frac{12}{h^3}\int_{-h/2}^{h/2} z\,\Theta_{rr}(a,z)\,dz$$

By substituting the expression of $\Theta_{rr}(a,z)$, we get

$$A \;=\; \frac{\alpha Y \epsilon P \chi}{\pi K h} \sum_n \frac{\mathrm{e}^{-w^2\zeta_n^2/8a^2}}{(\zeta_n^2+\chi^2)\zeta_n J_0(\zeta_n)} \frac{1-\mathrm{e}^{-\zeta_n h/a}}{\zeta_n + \chi - (\zeta_n - \chi)\mathrm{e}^{-\zeta_n h/a}} \tag{6.17}$$

and

$$B \;=\; -\frac{12\alpha Y \epsilon P \chi a}{\pi K h^3} \sum_n \frac{\mathrm{e}^{-w^2\zeta_n^2/8a^2}}{(\zeta_n^2+\chi^2)\zeta_n^2 J_0(\zeta_n)} \frac{\frac{\zeta_n h}{2a}\left(1-\mathrm{e}^{-\zeta_n h/a}\right) - 1 + \mathrm{e}^{-\zeta_n h/a}}{\zeta_n + \chi + (\zeta_n - \chi)\mathrm{e}^{-\zeta_n h/a}} \tag{6.18}$$

It has been found more convenient to use the Young modulus Y and the Poisson ratio σ instead of the Lamé coefficients. The relation is

$$\lambda \;=\; \frac{Y\sigma}{(1+\sigma)(1-2\sigma)}$$

$$\mu \;=\; \frac{Y}{2(1+\sigma)}$$

so that

$$\frac{\nu}{2(\lambda+\mu)} = \alpha(1+\sigma)$$

and

$$\frac{\mu\nu}{\lambda+\mu} \;=\; \alpha Y$$

On fig.6.11, one can see the linear function $-A - B\,z$ superimposed to the function $\Theta_{rr}(a,z)$. On the following figure 6.12 one sees the error $\Theta_{rr}(a,z) + A + Bz$. The displacement is now fully determined, and the total displacement vector field is $\vec{U} \;=\; \vec{u} + \delta\vec{u}$. The displacement is defined up to a constant

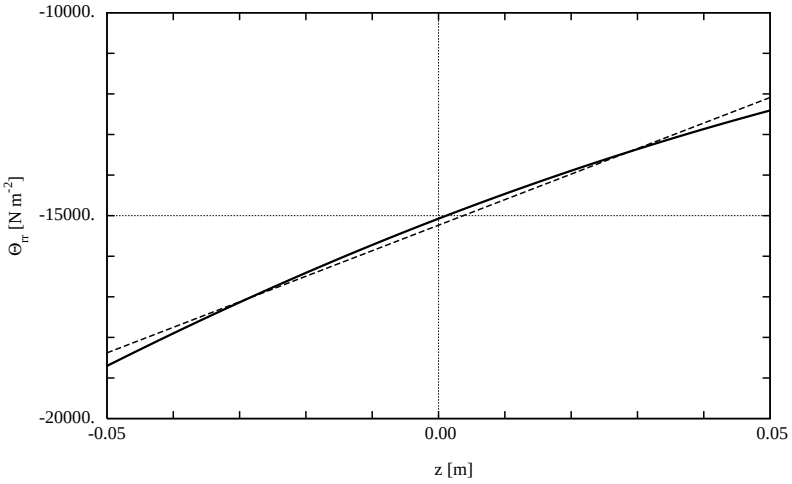

Figure 6.11: Edge stress function (solid line) and its linear fit (dashed line)

vector. We arbitrarily choose a displacement zero for $r = 0$ and $z = -h/2$. We have thus the special result

$$u_z(r,-h/2) \;=\; \frac{\alpha(1+\sigma)\epsilon P}{\pi K}\sum_n \frac{\zeta_n \mathrm{e}^{-\zeta_n^2 w^2/8a^2}}{(\zeta_n^2+\chi^2)J_0^2(\zeta_n)}$$
$$\frac{\zeta_n+\chi-(\zeta_n-\chi)\mathrm{e}^{-2\zeta_n h/a}}{(\zeta_n+\chi)^2-(\zeta_n-\chi)^2\mathrm{e}^{-2\zeta_n h/a}}\,[J_0(\zeta_n r/a)-1] \qquad (6.19)$$

and

$$\delta u_z(r,-h/2) \;=\; \frac{1-\sigma}{2Y}\,B\,r^2$$

But the Saint-Venant correction appears very small in the region of optical interest, as can be seen on Fig6.13.

6.3.2 Surface analysis

As in the case of thermal lensing, we wish to estimate the departure of the distorted face from an ideally parabolic surface. The apex equation of the paraboloid being

$$\hat{Z}(r) \;=\; c\,r^2 + \;p$$

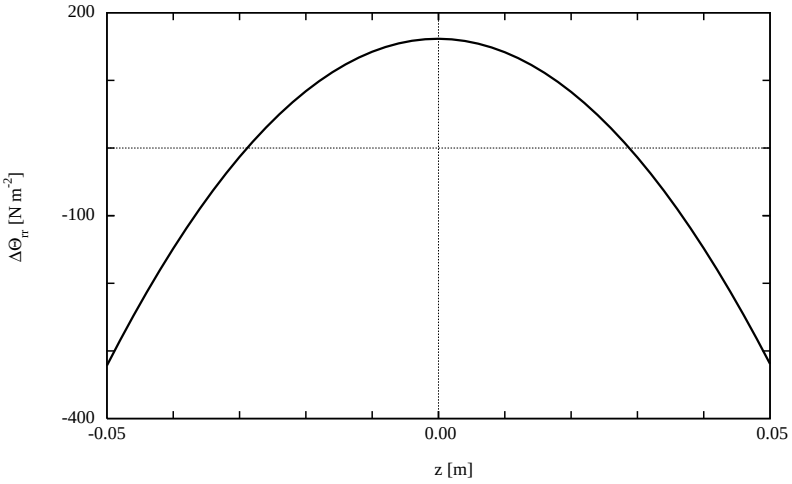

Figure 6.12: Residual edge stress

we find the parameters c (curvature) and p (piston) by minimizing

$$Q(c,p) \;=\; \int_0^a W(r)\left[u_z(r,-h/2) - c\,r^2 - p\right]^2$$

where $W(r)$ is the normalized intensity of the light spot. This yields

$$c \;=\; -\frac{\alpha(1+\sigma)\epsilon P}{4\pi a^2 K}\sum_n \frac{\zeta_n^3 \mathrm{e}^{-\zeta_n^2 w^2/4a^2}}{(\zeta_n^2+\chi^2)J_0^2(\zeta_n)}\frac{\zeta_n+\chi-(\zeta_n-\chi)\mathrm{e}^{-2\zeta_n h/a}}{(\zeta_n+\chi)^2-(\zeta_n-\chi)^2\mathrm{e}^{-2\zeta_n h/a}} \quad (6.20)$$

and, with the notation $x_n = \zeta_n^2 w^2/8a^2$:

$$p \;=\; -\frac{\alpha(1+\sigma)\epsilon P}{\pi K}\sum_n \frac{\zeta_n \mathrm{e}^{-x_n}}{(\zeta_n^2+\chi^2)J_0^2(\zeta_n)}\left[1-(1+x_n)\mathrm{e}^{-x_n}\right]\times$$

$$\times\frac{\zeta_n+\chi-(\zeta_n-\chi)\mathrm{e}^{-2\zeta_n h/a}}{(\zeta_n+\chi)^2-(\zeta_n-\chi)^2\mathrm{e}^{-2\zeta_n h/a}} \quad (6.21)$$

for the Virgo corner mirrors ($a = 0.175$ m, $h = 0.1$ m and $w = 0.02$ m), we find for instance a curvature

$$c \sim -8.6\,10^{-5}\ \mathrm{m}^{-1}\mathrm{W}^{-1}$$

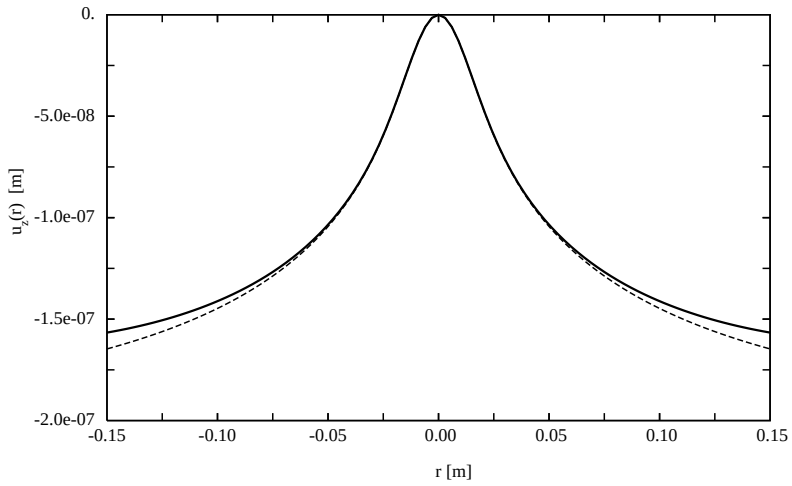

Figure 6.13: Distortion of the reflecting surface. Without S-V corection (dashed line) and with S-V correction (solid line). The beam half-width was $w = 0.02$ m

and for the curvature radius ($R_c = 1/2c$):

$$R_c \sim -5818 \text{ m.W}$$

On Fig.6.14, we show the distorted surface in the optically interesting region, and the nearest paraboloid. This distorted surface couples the TEM_{00} mode with higher order modes causing coupling losses. One can evaluate these coupling losses as customary by

$$L = 16\pi^2 \, Q(c,p)/\lambda^2$$

where c and p have their optimal values, defined above. For the Virgo corner mirrors, one finds the loss rate

$$L \sim \; 3 \; 10^{-3} \; /\text{W}^2$$

Recall that the displacement being linear with respect to the absorbed power, the losses are *quadratic*.

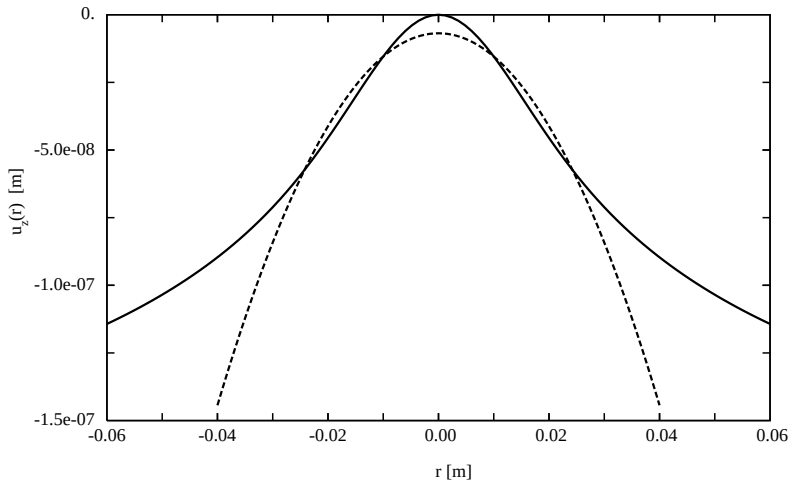

Figure 6.14: Distortion $Z(r)$ of the reflecting surface and the nearest (intensity weighted) paraboloid

6.4 Distortion caused by bulk absorption

In the case of bulk absorption, the temperature field is not any more harmonic, and the preceding short method cannot be employed. We are bound to solve the full system of thermo-elastic equations. Let us recall that the temperature field is given by :

$$T(r,z) \;=\; \sum_n t_n(z)\, J_0(k_n r)$$

where $k_n \equiv \zeta_n/a$. The functions $t_n(z)$ are of the form

$$t_n(z) = p_n\,[1 - \rho_n\,\cosh(k_n z)]$$

namely,

$$p_n \;=\; \frac{\beta P}{\pi K}\frac{\exp(-\zeta_n^2 w^2/8a^2)}{(\chi^2+\zeta_n^2)J_0^2(\zeta_n)}$$

and

$$\rho_n \;=\; \frac{\chi}{\zeta_n\,\sinh(\zeta_n h/2a) + \chi\,\cosh(\zeta_n h/2a)}$$

6.4.1 Thermoelastic solution

We search for a solution of the form

$$\begin{cases} u_r(r,z) &= \sum_n A_n(z)\, J_1(k_n r) \\ u_z(r,z) &= \sum_n B_n(z)\, J_0(k_n r) \end{cases}$$

where $A_n(z)$ and $B_n(z)$ are unknown functions to be determined according to the equilibrium equations and the boundary conditions. The strain tensor components are :

$$\begin{array}{rcl} E_{rr}(r,z) &=& \sum_n k_n A_n(z)\, J_1'(k_n r) \\ E_{\phi\phi}(r,z) &=& \sum_n k_n A_n(z)\, J_1(k_n r)/k_n r \\ E_{zz}(r,z) &=& \sum_n B_n'(z)\, J_0(k_n r) \\ E_{rz}(r,z) &=& \frac{1}{2}\sum_n (A_n'(z) - k_n B_n(z))\, J_1(k_n r) \end{array}$$

so that the trace is

$$E(r,z) \;=\; \sum_n (k_n A_n(z) + B_n'(z))\, J_0(k_n r)$$

The stress tensor is in turn :

$$\begin{array}{rcl} \Theta_{rr}(r,z) &=& \sum_n \left[\lambda(k_n A_n(z) + B_n'(z)) - \nu t_n(z)\right]\, J_0(k_n r) + 2\mu \sum_n k_n A_n(z)\, J_1'(k_n r) \\ \Theta_{\phi\phi}(r,z) &=& \sum_n \left[\lambda(k_n A_n(z) + B_n'(z)) - \nu t_n(z)\right]\, J_0(k_n r) + 2\mu \sum_n k_n A_n(z)\, J_1(k_n r)/k_n r \\ \Theta_{zz}(r,z) &=& \sum_n \left[\lambda(k_n A_n(z) + B_n'(z)) - \nu t_n(z)\right]\, J_0(k_n r) + 2\mu \sum_n B_n'(z)\, J_0(k_n r) \\ \Theta_{rz}(r,z) &=& \mu \sum_n (A_n'(z) - k_n B_n(z))\, J_1(k_n r) \end{array}$$

after some algebra, we find the equilibrium equations :

$$\begin{cases} \mu\left[A_n'' - k_n^2 A_n\right] - k_n\, \left[(\lambda+\mu)\,(B_n' + k_n A_n) - \nu t_n\right] &= 0 \\ \mu\left[B_n'' - k_n^2 B_n\right] + \partial_z \left[(\lambda+\mu)(B_n' + k_n A_n) - \nu t_n\right] &= 0 \end{cases}$$

The first consequence is that

$$\left[\partial_z^2 - k_n^2\right]\,(A_n' + k_n B_n) \;=\; 0$$

of which the odd solution is

$$A_n' + k_n B_n \;=\; k_n C_n' \sinh(k_n z) \tag{6.22}$$

where C_n' is an arbitrary constant. The source of heat being independent on z and the temperature, consequently, an even function of z, we expect A_n

being an even function and B_n an odd one. This result (Eq.6.22) allows to express B_n as a function of A_n and to insert it in any of the two equilibrium equations. For instance, inserting in the first, yields

$$(\lambda+2\mu)\left[\partial_z^2 - k_n^2\right] A_n \;=\; (\lambda+\mu)k_n^2 C'_n \cosh(k_n z) - \nu k_n p_n \left[1-\rho_n \cosh(k_n z)\right]$$

of which the even solution including one more arbitrary constant C''_n is :

$$A_n(z) \;=\; C''_n \cosh(k_n z) + \frac{\lambda+\mu}{2(\lambda+2\mu)}\, C'_n\, k_n z\, \sinh(k_n z) +$$

$$+\; \frac{\nu p_n}{k_n(\lambda+2\mu)}\left[1+\rho_n\, k_n z\, \sinh(k_n z)/2\right]$$

then, using 6.22 :

$$B_n(z) \;= (C'_n - C''_n)\sinh(k_n z) - \frac{\lambda+\mu}{2(\lambda+2\mu)}\, C'_n\, \left[\sinh(k_n z) + k_n z\, \cosh(k_n z)\right] \;-$$

$$-\; \frac{\nu p_n \rho_n}{2k_n(\lambda+2\mu)}\left[\sinh(k_n z) + k_n z\, \cosh(k_n z)\right]$$

The arbitrary constants are determined by the boundary conditions on the surfaces $z = \pm h/2$. The conditions on the edge $r = a$ are ignored. We have seen indeed on the preceding case that the needed correction to the displacement is practically negligible on the central area of the mirror, where light is actually interacting with the surface. The condition $\Theta_{rz}(r, \pm h/2) = 0$ gives

$$\left[\frac{\lambda+\mu}{\lambda+2\mu}\,\gamma_n \cosh\gamma_n - \frac{\mu}{\lambda+2\mu}\,\sinh\gamma_n\right]\, C'_n \;+\; 2\sinh\gamma_n\, C''_n \;=$$

$$-\; \frac{\nu p_n \rho_n}{k_n(\lambda+2\mu)}(\sinh\gamma_n + \gamma_n \cosh\gamma_n) \qquad (6.23)$$

and the condition $\Theta_{zz}(r, \pm h/2) = 0$ yields

$$\left[\cosh\gamma_n - \frac{\lambda+\mu}{\lambda+2\mu}\,\gamma_n \sinh\gamma_n\right]\, C'_n \;-\; 2\cosh\gamma_n\, C''_n \;=$$

$$\frac{2\nu p_n}{k_n(\lambda+2\mu)} \;+\; \frac{\nu p_n \rho_n}{k_n(\lambda+2\mu)}\,\gamma_n \sinh\gamma_n$$

where, $\gamma_n \equiv \zeta_n h/2a$. This is a linear system in $(C',\ C'')$ the solution of which is is

$$C'_n = \frac{\nu p_n}{k_n(\lambda+\mu)}\left[\frac{2\sinh\gamma_n}{\gamma_n+\sinh\gamma_n\cosh\gamma_n} - \rho_n\right]$$

$$C''_n = -\frac{\nu p_n}{2k_n(\lambda+\mu)}\left[\frac{2}{\lambda+2\mu}\frac{(\lambda+\mu)\gamma_n\cosh\gamma_n-\mu\sinh\gamma_n}{\gamma_n+\sinh\gamma_n\cosh\gamma_n}+\rho_n\right]$$

Now, it is possible to compute $B_n(\pm h/2)$:

$$B_n(h/2) = \frac{\nu p_n}{k_n(\lambda+\mu)}\sinh\gamma_n\left[\frac{\sinh\gamma_n}{\gamma_n+\sinh\gamma_n\cosh\gamma_n}-\frac{\rho_n}{2}\right]$$

so that the displacement at $z = h/2$ (symmetrical to the displacement at $z = -h/2$, is

$$u_z(r,h/2) = \frac{\nu}{\lambda+\mu}\sum_n \frac{p_n\sinh\gamma_n}{k_n}\left[\frac{\sinh\gamma_n}{\gamma_n+\sinh\gamma_n\cosh\gamma_n}-\frac{\rho_n}{2}\right]J_0(k_n r)$$

Calling $Z(r)$ the apex of the distorted surface, this is in detail

$$Z(r) = \frac{\alpha(1+\sigma)\beta Pa}{\pi K}\sum_n \frac{\exp\left(-\zeta_n^2 w^2/8a^2\right)}{\left(\zeta_n^2+\chi^2\right)\zeta_n J_0^2(\zeta_n)}$$

$$\left[\frac{2\sinh\gamma_n}{\gamma_n+\sinh\gamma_n\cosh\gamma_n} - \frac{\chi}{\zeta_n\sinh\gamma_n+\chi\cosh\gamma_n}\right]J_0(\zeta_n r/a)$$

where we have replaced the Lamé coefficients (λ, μ and ν) by the Poisson ratio σ and the linear thermal expansion coefficient α.

6.4.2 Surface analysis

One can see on Fig.6.15 the shape of the distorted surface in the center region, with the nearest paraboloid, computed according to the method already experimented in the previous problems. The curvature radius is

$$r_c = -16388\,\mathrm{m.W}$$

and the losses

$$L = 9.3\,10^{-5}\,W^{-2}$$

These figures are significantly different from the case of coating heating, by a rough factor of 3 for the focal length, and even by two orders of magnitude for the losses, due to the nearly parabolic profile.

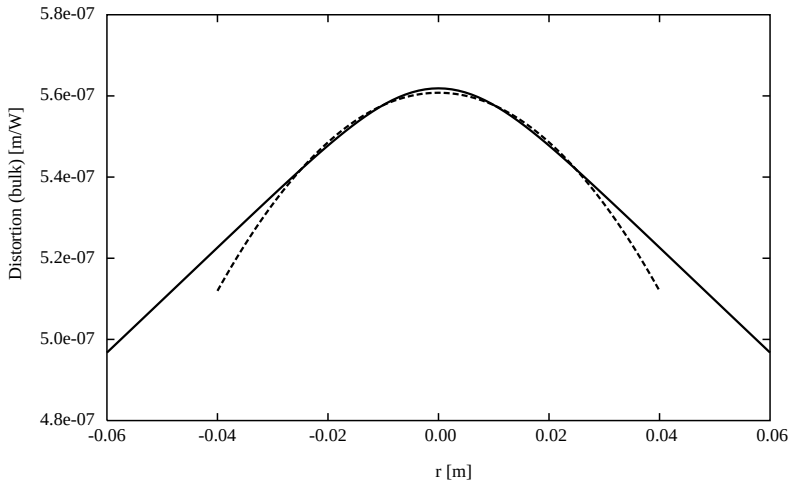

Figure 6.15: Distortion of the reflecting surface and the nearest (intensity weighted) paraboloid

6.5 Heating processes

6.5.1 Transient temperature fields : general method

Up to now we have treated the steady state solution supposed to be reached at thermal equilibrium between the mirror and the world around the vacuum vessel. Now we turn to the question of temperature *evolution* from a given state to a new one. For instance the mirror is at a uniform temperature T_0, then we switch on the laser, and the temperature begins to increase until the steady state. In the time dependent case the heat equation is (we keep axial symmetry) :

$$\left[\rho C \frac{\partial}{\partial t} - K\Delta\right] T(t,r,z) = S_1(t,r,z) \tag{6.24}$$

where $S_1(t,r,z)$ refers to the internal source of heat. The boundary conditions remain

$$-K\left[\frac{\partial}{\partial z}T\right]_{z=-h/2} = -4\sigma' T_0^3 T(t,r,h/2) + S_2(t,r)$$

$$-K\left[\frac{\partial}{\partial z}T\right]_{z=h/2} = 4\sigma' T_0^3 T(t,r,h/2)$$

$$-K\left[\frac{\partial}{\partial r}T\right]_{r=a} = 4\sigma' T_0^3 T(t,a,z)$$

where $S_2(t,r)$ is the surface source of heat localized on the coating (at $z = -h/2$). In the special case of a static source (a constant power laser beam), the sources are time independent, and a special static solution $T_\infty(r,z)$ of 6.24 satisfying the boundary conditions is known since the preceding sections. The general solution of 6.24 is therefore of the form

$$T(t,r,z) = T_\infty(r,z) + T_{\rm tr}(t,r,z)$$

where $T_{\rm tr}(t,r,z)$ is the transient part, satisfying the homogeneous heat equation and the homogeneous boundary conditions (i.e. reduced to outgoing radiation). The transient temperature can be searched under the separated form

$$T_{\rm tr}(t,r,z) = \sum_{n,m} \left[\theta'_{nm}(t)\cos(\kappa'_m z) + \theta''_{nm}(t)\sin(\kappa''_m z)\right] J_0(k_n r)$$

where κ'_m, κ''_m, and k_n are arbitrary constants. The functions $\theta'_{nm}(t)$ and $\theta''_{nm}(t)$ must satisfy

$$\frac{\partial \theta'_{nm}}{\partial t} + \frac{K}{\rho C}(k_n^2 + \kappa'^2_m)\,\theta'_{nm} = 0$$

$$\frac{\partial \theta''_{nm}}{\partial t} + \frac{K}{\rho C}(k_n^2 + \kappa''^2_m)\,\theta''_{nm} = 0$$

whose non exploding solutions are

$$\theta'_{nm}(t) = \theta'_{nm}\,\exp\left[-\frac{K}{\rho C}(k_n^2 + \kappa'^2_m)t\right]$$

$$\theta''_{nm}(t) = \theta''_{nm}\,\exp\left[-\frac{K}{\rho C}(k_n^2 + \kappa''^2_m)t\right]$$

where the θ_{nm} are extra arbitrary constants. It is convenient to define the following time constants :

$$\tau'_{nm} = \frac{\rho C}{K(\kappa'^2_m + k_n^2)}$$

$$\tau''_{nm} = \frac{\rho C}{K(\kappa''^{\,2}_m + k_n^2)}$$

Now, the boundary conditions impose

$$k_n \;=\; \zeta_n/a$$

where the ζ_n have the same definition (6.5) as in the whole present chapter, whereas for satisfying the boundary conditions on the circular faces, κ'_m and κ''_m must respectively verify

$$\kappa'_m \frac{h}{2} \sin(\kappa'_m h/2) - \frac{4\sigma' T_0^3 h}{2K} \cos(\kappa'_m h/2) = 0$$

$$\kappa''_m \frac{h}{2} \cos(\kappa''_m h/2) + \frac{4\sigma' T_0^3 h}{2K} \sin(\kappa''_m h/2) = 0$$

Let us introduce the new radiation constant $\chi' \equiv \chi h/2a$, The first equation has the form

$$u \sin u - \chi' \cos u = 0 \tag{6.25}$$

It admits an infinite discrete family $\{u_m \;;\; m \in \mathcal{Z}\}$ of solutions, that can be easily computed, then we have

$$\kappa'_m \;=\; 2u_m/h$$

The same way, the equation

$$v \cos v + \chi' \sin v = 0 \tag{6.26}$$

admits an infinite discrete family $\{v_m \;;\; m \in \mathcal{Z}\}$ of solutions, and

$$\kappa''_m \;=\; 2v_m/h$$

It is essential to note that the functions $\{J_0(\zeta_n r/a);\; n \in \mathcal{N}\}$ form an orthogonal complete basis for functions of r defined on $r \in [0, a]$, as already remarked, and for the same theoretical reasons, the functions $\{\cos(2u_m z/h);\; m \in \mathcal{N}\}$ and $\{\sin(2v_m z/h);\; m \in \mathcal{N}\}$ on $z \in [-h/2, h/2]$. For the two last cases, this is a consequence of the relations 6.25 and 6.26. The orthogonality of the sine family with respect to cosine is obvious over a symmetrical interval. But moreover, we have

$$\int_{-h/2}^{h/2} \cos(\kappa'_m z) \cos(\kappa'_n z)\, dz \;=\; \delta_{nm} g'_m$$

$$\int_{-h/2}^{h/2} \sin(\kappa''_m z)\sin(\kappa''_n z)\,dz \;=\; \delta_{nm} g''_m$$

where

$$g'_m \;=\; \frac{h}{2}\left[1+\frac{\sin(2u_m)}{2u_m}\right], \quad g''_m \;=\; \frac{h}{2}\left[1-\frac{\sin(2v_m)}{2v_m}\right]$$

At this point, all constants are determined except θ'_{mn} and θ''_{mn}. This is done depending on the initial condition on the temperature. Assume for instance the excess temperature is zero at $t=0$. The steady state temperature (see preceding sections) is generally known under the form

$$T_\infty(r,z) = \sum_n t_n(z)\,J_0(k_n r)$$

requiring $T(0,r,z)=0$ yields

$$\sum_n t_n(z)\,J_0(k_n r) + \sum_{n,m}\left[\theta'_{nm}\cos(\kappa'_m z) + \theta''_{nm}\sin(\kappa''_m z)\right]\,J_0(k_n r) = 0$$

Owing to the orthogonality of the $J_0(k_n r)$ this is equivalent to

$$t_n(z) + \sum_m \left[\theta'_{nm}\cos(\kappa'_m z) + \theta''_{nm}\sin(\kappa''_m z)\right] \;= 0$$

and now, owing to the orthogonality of the $\sin(\kappa''_m z)$ and the $\cos(\kappa'_m z)$, this gives

$$\theta'_{nm} \;=\; -\,\frac{1}{g'_m}\int_{-h/2}^{h/2} t_n(z)\cos(\kappa'_m z)\,dz$$

$$\theta''_{nm} \;=\; -\,\frac{1}{g''_m}\int_{-h/2}^{h/2} t_n(z)\sin(\kappa''_m z)\,dz$$

which completes the determination. The temperature field is then

$$T(t,r,z) \;=\; -\sum_{n,m}\left[\theta'_{nm}\left(1-\mathrm{e}^{-t/\tau'_{nm}}\right)\cos(\kappa'_m z) + \right.$$

$$\left.\theta''_{nm}\left(1-\mathrm{e}^{-t/\tau''_{nm}}\right)\sin(\kappa''_m z)\right]\,J_0(k_n r) \qquad (6.27)$$

case of coating absorption

In the case of heating by dissipation in the coating, we have seen that

$$t_n(z) \;=\; \frac{\epsilon p_n a}{K}\,\mathrm{e}^{-\gamma_n}\,\frac{(\zeta_n-\chi)\mathrm{e}^{-2\gamma_n}\mathrm{e}^{\zeta_n z/a}+(\zeta_n+\chi)\mathrm{e}^{-\zeta_n z/a}}{(\zeta_n+\chi)^2-(\zeta_n-\chi)^2\mathrm{e}^{-4\zeta_n z/a}}$$

where $\gamma_n \equiv \zeta_n h/2a$. We clearly need the following parameters :

$$C'_{nm} \;\equiv\; \frac{1}{g'_m}\int_{-h/2}^{h/2}\cos(\kappa'_m z)\exp(\pm\zeta_n z/a)\,dz$$

and

$$C''_{nm} \;\equiv\; \pm\,\frac{1}{g''_m}\int_{-h/2}^{h/2}\sin(\kappa''_m z)\exp(\pm\zeta_n z/a)\,dz$$

after some algebra, we find

$$C'_{nm} \;=\; \frac{2\cos(u_m)}{1+\sin(2u_m)/2u_m}\,\mathrm{e}^{\gamma_n}\,\frac{\gamma_n+\chi'-(\gamma_n-\chi')\,\mathrm{e}^{-2\gamma_n}}{\gamma_n^2+u_m^2}$$

and

$$C''_{nm} \;=\; \frac{2\sin(v_m)}{1-\sin(2v_m)/2v_m}\,\mathrm{e}^{\gamma_n}\,\frac{\gamma_n+\chi'+(\gamma_n-\chi')\,\mathrm{e}^{-2\gamma_n}}{\gamma_n^2+u_m^2}$$

so that

$$\theta'_{nm} \;=\; \frac{\epsilon h p_n}{K}\,\frac{\cos(u_m)}{1+\sin(2u_m)/2u_m}\,\frac{1}{\gamma_n^2+u_m^2}$$

$$\theta''_{nm} \;=\; -\frac{\epsilon h p_n}{K}\,\frac{\sin(v_m)}{1-\sin(2v_m)/2v_m}\,\frac{1}{\gamma_n^2+v_m^2}$$

and the temperature field is (by substituting the explicit expression of p_n) :

$$T(t,r,z) \;=\; \frac{4\epsilon P}{MC}\sum_{n,m}\frac{\zeta_n^2\exp(-\zeta_n^2 w^2/8a^2)}{(\zeta_n^2+\chi^2)J_0^2(\zeta_n)}\;\times$$

$$\left[\frac{\cos(u_m)}{1+\sin(2u_m)/2u_m}\,\tau'_{nm}\left(1-\mathrm{e}^{-t/\tau'_{nm}}\right)\cos(\kappa'_m z)-\right.$$

$$\left.\frac{\sin(v_m)}{1-\sin(2v_m)/2v_m}\,\tau''_{nm}\left(1-\mathrm{e}^{-t/\tau''_{nm}}\right)\sin(\kappa''_m z)\right]\,J_0(\zeta_n r/a) \qquad (6.28)$$

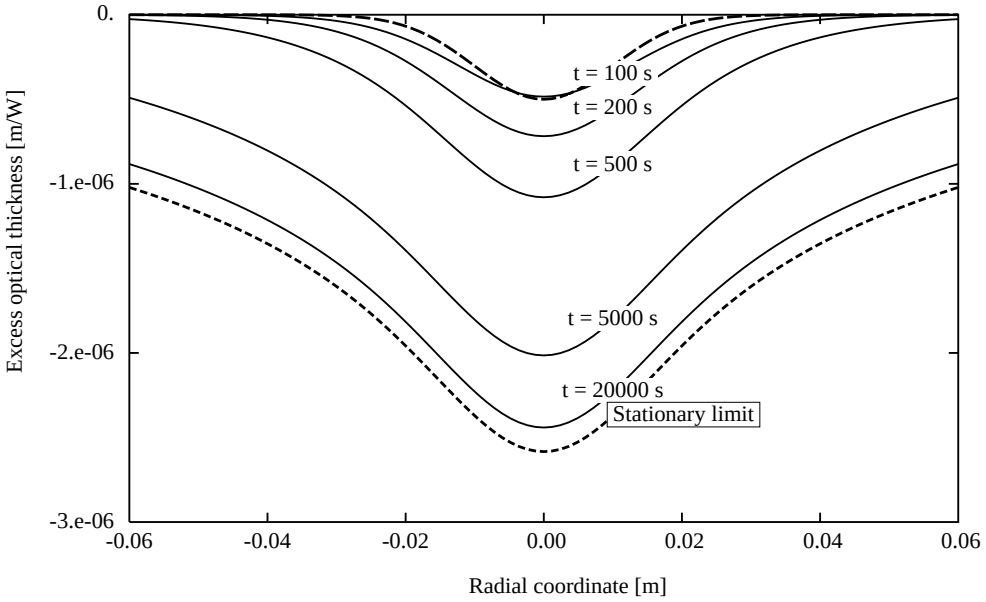

Figure 6.16: Transient thermal lensing in a standard Virgo mirror, case of coating absorption. Long dashed line : beam profile. Short dashed line : Stationary case of fig6.6.

where $M = \rho\pi a^2 h$ is the mass of the mirror. The thermal lens, defined by

$$Z(t,r) \;=\; \frac{dn}{dT}\int_{-h/2}^{h/2} T(t,r,z)\,dz$$

obviously, only the even part contributes, giving

$$Z(t,r) \;=\; \frac{dn}{dT}\,\frac{2\epsilon P h}{MC}\sum_{n,m}\frac{\zeta_n^2\exp(-\zeta_n^2 w^2/8a^2)}{(\zeta_n^2+\chi^2)J_0^2(\zeta_n)}\;\times$$

$$\frac{\sin(2u_m)/2u_m}{1+\sin(2u_m)/2u_m}\;\tau'_{nm}\left(1-\mathrm{e}^{-t/\tau'_{nm}}\right)J_0(\zeta_n r/a) \qquad (6.29)$$

On Fig.6.16, one can see the time scale of the evolution of the lens profile. The steady state is reached after hours. We get the time variable focal length $f(t)$ defined by

$$\frac{1}{f(t)} \;=\; -\frac{dn}{dT}\,\frac{\epsilon P h}{MCa^2}\sum_{n,m}\frac{\zeta_n^4\exp(-\zeta_n^2 w^2/4a^2)}{(\zeta_n^2+\chi^2)J_0^2(\zeta_n)}\;\times$$

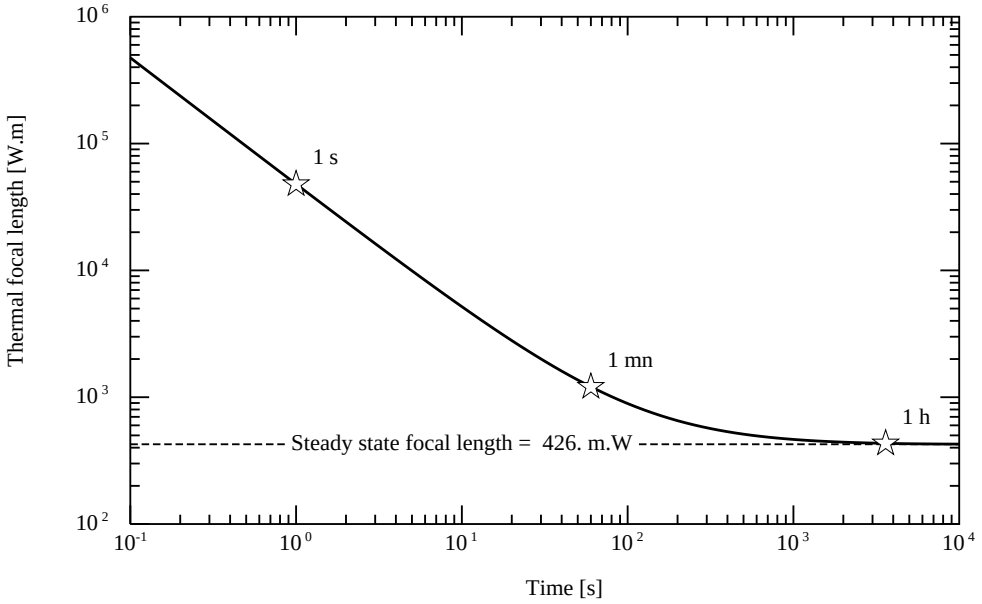

Figure 6.17: Evolution of the thermal focal length (heat source on the coating)

$$\frac{\sin(2u_m)/2u_m}{1+\sin(2u_m)/2u_m}\,\tau'_{nm}\left(1-\mathrm{e}^{-t/\tau'_{nm}}\right) \tag{6.30}$$

It is interesting to realize that though the heating process takes hours to reach the steady state, the focal length takes only a few minutes (see Fig. 6.17)to reach its stationary value. This is due to the fact that the temperature field reaches soon its final profile, and spends further time growing uniformly without noticeably changing the gradients. The situation is different for the piston, which follows the evolution of the temperature on a long time scale, but is automatically corrected by the servo loops.

case of bulk absorption

In this case, as seen above,

$$t_n(z) \;=\; \frac{\beta a^2}{K}\,\frac{p_n}{\zeta_n^2}\left[1-\frac{2\chi \mathrm{e}^{-\gamma_n}\cosh(\zeta_n z/a)}{\chi+\zeta_n+(\chi-\zeta_n)\mathrm{e}^{-2\gamma_n}}\right]$$

so that, using previous results,

$$\int_{-h/2}^{h/2} t_n(z)\, cos(\kappa'_m z)\, dz \;=\; \frac{\beta a^2 h}{K}\,\frac{p_n}{\zeta_n^2}\left[\frac{\sin u_m}{u_m} - \frac{h}{2a}\,\frac{\chi\cos u_m}{u_m^2+\gamma_n^2}\right]$$

$$= \frac{\beta a^2 h}{K}\, p_n\, \gamma_n^2\, \frac{\sin u_m/u_m}{u_m^2+\gamma_n^2}$$

If we define

$$\theta_{nm} \;= \frac{1}{g'_m}\int_{-h/2}^{h/2} t_n(z)\, cos(\kappa'_m z)\, dz$$

we have, after susbtitution of the expression for p_n :

$$\theta_{nm} \;=\; \frac{\beta P h^2}{2\pi K a^2}\,\frac{\zeta_n^2 \exp(-\zeta_n^2 w^2/8a^2)}{(\chi^2+\zeta_n^2)J_0^2(\zeta_n)}\,\frac{1}{1+\sin(2u_m)/2u_m}\,\frac{\sin u_m/u_m}{u_m^2+\gamma_n^2}$$

and finally, using the definition of τ'_{nm} :

$$T(t,r,z) \;=\; \frac{2\beta h P}{MC}\sum_{n,m}\frac{\zeta_n^2\exp(-\zeta_n^2 w^2/8a^2)}{(\chi^2+\zeta_n^2)J_0^2(\zeta_n)}\times$$

$$\frac{\sin u_m/u_m}{1+\sin(2u_m)/2u_m}\,\tau'_{nm}\,\left(1-\mathrm{e}^{-t/\tau'_{nm}}\right)\,\cos(\kappa'_m z)\,J_0(\zeta_n r/a) \qquad (6.31)$$

where $M=\rho\pi a^2 h$ is the mass of the mirror. The thermal lens is

$$Z(t,r) \;=\; \frac{dn}{dT}\,\frac{2\beta h^2 P}{MC}\sum_{n,m}\frac{\zeta_n^2\exp(-\zeta_n^2 w^2/8a^2)}{(\chi^2+\zeta_n^2)J_0^2(\zeta_n)}\times$$

$$\frac{(\sin u_m/u_m)^2}{1+\sin(2u_m)/2u_m}\,\tau'_{nm}\,\left(1-\mathrm{e}^{-t/\tau'_{nm}}\right)\;J_0(\zeta_n r/a) \qquad (6.32)$$

Fig.6.18, show almost exactly the same behavior as in the case of coating absorption. The focal length is defined by

$$\frac{1}{f(t)} \;=\; -\,\frac{dn}{dT}\,\frac{\beta h^2 P}{MCa^2}\sum_{n,m}\frac{\zeta_n^4\exp(-\zeta_n^2 w^2/4a^2)}{(\chi^2+\zeta_n^2)J_0^2(\zeta_n)}\times$$

$$\frac{(\sin u_m/u_m)^2}{1+\sin(2u_m)/2u_m}\,\tau'_{nm}\,\left(1-\mathrm{e}^{-t/\tau'_{nm}}\right) \qquad (6.33)$$

Fig.6.19 is almost identical to Fig.6.17 and the same comments apply.

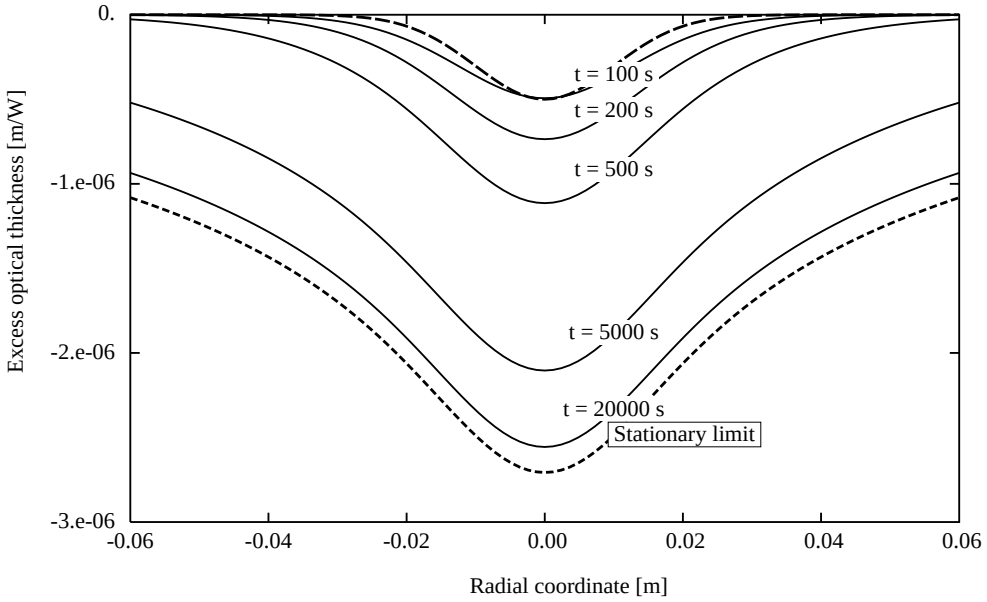

Figure 6.18: Transient thermal lensing in a standard Virgo mirror, case of bulk absorption. Long dashed line : beam profile. Short dashed line : Stationary case of fig6.9.

6.5.2 Transient thermoelastic deformations

When time enter elasticity problems, the relevant theory is elastodynamics. The basic elastodynamics equations are the equilibrium equations, modified in order to take into account inertial forces and generalizing Newton's second law :

$$\mathrm{div}\Theta \;=\; \rho\, \partial_t^2\, \mathbf{u}$$

The boundary conditions remain the same as in elasticity. Considering motions of matter caused by a constant low rate heating, the velocities of matter are so small, about one μm in tens of minutes, that we can neglect the inertial forces. The equations return to the form of static elasticity, except that the time enters as an evolution parameter through temperature. This is the quasi-static regime. It will be assumed for finding the slow evolution of the shape of the mirrors faces. We shall start from the expression of the time dependent temperature field which is never harmonic (even in the case of

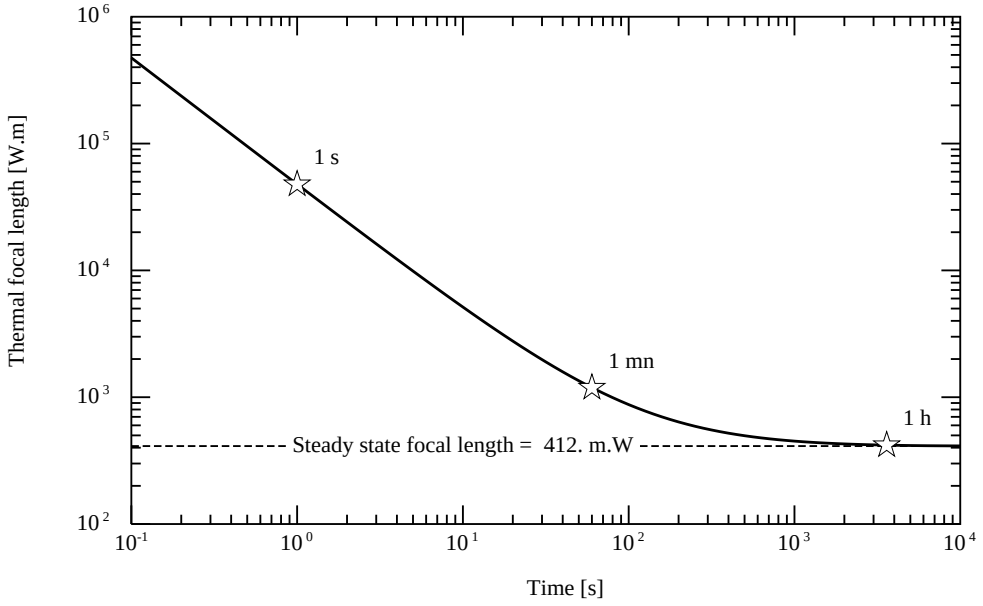

Figure 6.19: Transient thermal focal length (heat source in the bulk)

coating dissipation) so that we must tackle the thermoelastic equations, and assume that the temperature field is given under the form

$$T(t,r,z) \;=\; \sum_n t_n(t,z)\, J_0(k_n r)$$

As in the static study, we search the displacement vector under the form

$$\begin{cases} u_r(t,r,z) \;=\; \sum_n A_n(t,z)\, J_1(k_n r) \\ u_z(t,r,z) \;=\; \sum_n B_n(t,z)\, J_0(k_n r) \end{cases}$$

We know from the study of distortions caused by bulk absorption that the unknown functions A_n and B_n obey

$$\left(\partial_z^2 - k_n^2\right)\, (A_n' + k_n\, B_n) \;=\; 0$$

In general, there is no symmetry with respect to the meridian plane, so that we must take the general solution depending on two arbitrary functions of t, C_n and D_n :

$$A_n' + k_n\, B_n \;=\; k_n C_n \cosh(k_n z) + k_n D_n \sinh(k_n z) \qquad (6.34)$$

then we are led to solve the differential equation

$$\left(\partial_z^2 - k_n^2\right) A_n \;=\; \frac{k_n^2(\lambda+\mu)}{\lambda+2\mu}\left[C_n \sinh(k_n z) + D_n \cosh(k_n z)\right] - \frac{k_n \nu t_n}{\lambda+2\mu}$$

the general solution of which, involving two more arbitrary functions of t is

$$A_n(t,z) \;=\; M_n \sinh(k_n z) + P_n \cosh(k_n z) +$$

$$+\; \frac{\lambda+\mu}{2(\lambda+2\mu)}\, k_n z \left[C_n \cosh(k_n z) + D_n \sinh(k_n z)\right] - \frac{k_n \nu \theta_n}{\lambda+2\mu}$$

where $\theta_n(t,z)$ represents a special solution of

$$\left(\partial_z^2 - k_n^2\right)\theta_n \;=\; t_n$$

then it is possible to deduce $B_n(t,z)$ from 6.34 :

$$B_n(t,z) \;=\; (C_n - M_n)\cosh(k_n z) + (D_n - P_n)\sinh(k_n z) + \frac{\lambda+\mu}{2(\lambda+2\mu)}\times$$

$$\left[C_n\left(\cosh(k_n z) + k_n z \sinh(k_n z)\right) + D_n\left(\sinh(k_n z) + k_n z \cosh(k_n z)\right)\right] + \frac{\nu \theta_n'}{\lambda+2\mu}$$

The stress tensor is now explicitly defined, depending on 4 families of constants to be determined from the boundary conditions. These boundary conditions on the circular faces (recall that we neglect conditions on the edge) give a rank 4 linear system, namely

$$\left[\frac{\lambda+\mu}{\lambda+2\mu}\gamma_n \sinh\gamma_n - \frac{\mu}{\lambda+2\mu}\cosh\gamma_n\right] C_n + \left[\frac{\lambda+\mu}{\lambda+2\mu}\gamma_n \cosh\gamma_n - \frac{\mu}{\lambda+2\mu}\sinh\gamma_n\right] D_n$$

$$+\, 2\cosh\gamma_n\, M_n + 2\sinh\gamma_n\, P_n \;=\; \frac{2\nu\theta_n'(t,h/2)}{\lambda+2\mu}$$

$$\left[\frac{\lambda+\mu}{\lambda+2\mu}\gamma_n \sinh\gamma_n - \frac{\mu}{\lambda+2\mu}\cosh\gamma_n\right] C_n - \left[\frac{\lambda+\mu}{\lambda+2\mu}\gamma_n \cosh\gamma_n - \frac{\mu}{\lambda+2\mu}\sinh\gamma_n\right] D_n$$

$$+\, 2\cosh\gamma_n\, M_n - 2\sinh\gamma_n\, P_n \;=\; \frac{2\nu\theta_n'(t,-h/2)}{\lambda+2\mu}$$

$$\left[\sinh\gamma_n - \frac{\lambda+\mu}{\lambda+2\mu}\gamma_n\cosh\gamma_n\right] C_n + \left[\cosh\gamma_n - \frac{\lambda+\mu}{\lambda+2\mu}\gamma_n\sinh\gamma_n\right] D_n$$

$$-2\sinh\gamma_n\, M_n - 2\cosh\gamma_n\, P_n \;=\; -\frac{2\nu k_n \theta(t,h/2)}{\lambda+2\mu}$$

$$-\left[\sinh\gamma_n - \frac{\lambda+\mu}{\lambda+2\mu}\gamma_n\cosh\gamma_n\right] C_n + \left[\cosh\gamma_n - \frac{\lambda+\mu}{\lambda+2\mu}\gamma_n\sinh\gamma_n\right] D_n$$

$$2\sinh\gamma_n\, M_n - 2\cosh\gamma_n\, P_n \;=\; -\frac{2\nu k_n \theta_n(t,-h/2)}{\lambda+2\mu}$$

where as usual, $\gamma_n \equiv \zeta_n h/2a$. After solving the system and some tedious but elementary algebra, one can express the displacement amplitude :

$$B_n(t,-h/2) \;=\; \frac{\nu}{\lambda+\mu}\frac{\cosh\gamma_n}{\sinh(\gamma_n)\cosh(\gamma_n)-\gamma_n}\left[\sinh\gamma_n e'_n(t) - \cosh\gamma_n k_n o(t)\right] -$$

$$\frac{\nu}{\lambda+\mu}\frac{\sinh\gamma_n}{\sinh(\gamma_n)\cosh(\gamma_n)+\gamma_n}\left[\cosh\gamma_n o'_n(t) - \sinh\gamma_n k_n e(t)\right]$$

where we have introduced the even and odd parts of the temperature field and its gradients :

$$e_n(t) = \frac{1}{2}\left[\theta_n(t,h/2) + \theta_n(t,-h/2)\right]$$

$$o_n(t) = \frac{1}{2}\left[\theta_n(t,h/2) - \theta_n(t,-h/2)\right]$$

$$e'_n(t) = \frac{1}{2}\left[\theta'_n(t,h/2) + \theta'_n(t,-h/2)\right]$$

$$o'_n(t) = \frac{1}{2}\left[\theta'_n(t,h/2) - \theta'_n(t,-h/2)\right]$$

Then the shape $Z(t,r)$ of the mirror's surface (at $z=-h/2$) is

$$Z(t,r) \;=\; \sum_n B_n(t,-h/2)\, J_n(\zeta_n r/a)$$

case of coating absorption

The time dependent temperature field has been derived in a preceding section. In the case of absorption in the coating, we found

$$T(t,r,z) \;=\; \frac{4\epsilon P}{MC}\sum_{n,m}\frac{\zeta_n^2\exp(-\zeta_n^2 w^2/8a^2)}{(\zeta_n^2+\chi^2)J_0^2(\zeta_n)}\;\times$$

$$\left[\frac{\cos(u_m)}{1+\sin(2u_m)/2u_m}\,\tau'_{nm}\left(1-\mathrm{e}^{-t/\tau'_{nm}}\right)\cos(\kappa'_m z)-\right.$$

$$\left.\frac{\sin(v_m)}{1-\sin(2v_m)/2v_m}\,\tau''_{nm}\left(1-\mathrm{e}^{-t/\tau''_{nm}}\right)\sin(\kappa''_m z)\right]\,J_0(\zeta_n r/a) \qquad (6.35)$$

using the preceding principles gives the apex equation

$$Z(t,r) \;=\; -\,\frac{\epsilon P\alpha(1+\sigma)h^2}{\pi K a^2}\times$$

$$\sum_{n,m} p_n\left\{\frac{\sinh\gamma_n\,(\chi'\cosh\gamma_n+\gamma_n\sinh\gamma_n)}{\sinh\gamma_n\cosh\gamma_n+\gamma_n}\left[\frac{\cos^2 u_m}{1+\sin(2u_m)/2u_m}\,\frac{1-\exp(-t/\tau'_{nm})}{(u_m^2+\gamma_n^2)^2}\right]+\right.$$

$$\left.\frac{\cosh\gamma_n\,(\chi'\sinh\gamma_n+\gamma_n\cosh\gamma_n)}{\sinh\gamma_n\cosh\gamma_n-\gamma_n}\left[\frac{\sin^2 v_m}{1-\sin(2v_m)/2v_m}\,\frac{1-\exp(-t/\tau''_{nm})}{(v_m^2+\gamma_n^2)^2}\right]\right\}\,J_0(\zeta_n r/a)$$

case of bulk absorption

In this case, the temperature field is, according to the previous section,

$$T(t,r,z) \;=\; \frac{2\beta h P}{MC}\sum_{n,m}\frac{\zeta_n^2\exp(-\zeta_n^2 w^2/8a^2)}{(\chi^2+\zeta_n^2)J_0^2(\zeta_n)}\times$$

$$\frac{\sin u_m/u_m}{1+\sin(2u_m)/2u_m}\,\tau'_{nm}\,\left(1-\mathrm{e}^{-t/\tau'_{nm}}\right)\,\cos(\kappa'_m z)\,J_0(\zeta_n r/a)$$

and the corresponding apex equation for the time-evoluting surface is

$$Z(t,r) \;=\; -\frac{\beta h P\alpha(1+\sigma)h^2}{2\pi K a^2}\sum_{n,m} p_n\frac{\sinh\gamma_n\,(\chi'\cosh\gamma_n+\gamma_n\sinh\gamma_n)}{\sinh\gamma_n\cosh\gamma_n+\gamma_n}$$

$$\frac{\sin(2u_m)/2u_m}{1+\sin(2u_m)/2u_m}\,\frac{1-\exp(-t/\tau'_{nm})}{(u_m^2+\gamma_n^2)^2}\,J_0(\zeta_n r/a)$$

6.6 Thermoelastic coupling : Coating absorption

Deformation of the wavefront after reflection on a mirror due either to thermal lensing or to distortion of the reflecting coating obviously affect the tuning of cavities involving such temperature sensitive mirrors. The tuning

affects, as a feedback loop, the stored power and thus the heating rate of the mirrors. We are thus faced with the question of time varying power fluxes on mirrors. The first step is to study the time dependent temperature field, and the resulting dynamical thermal lens, the second step is to derive the dynamical distortion of the reflecting face.

6.6.1 Dynamical temperature

Temperature field

We assume here an incoming optical beam having for any reason a time varying integrated power. The causes may be technological (an unperfect power stabilization) or fundamental : The absorbed power fluctuates due to shot noise, and the situation is equivalent to a varying power flux. Let us firstly evaluate the result from a coating absorption. With no internal source of heat, The Fourier-heat equation reads:

$$[\rho C \partial_t - K \Delta] \, T(t,r,z) \;=\; 0$$

Let us recall that C is the specific heat of the material, K its thermal conductivity, and ρ its density. We take the time-Fourier transform:

$$\left[\Delta + i \, \frac{\omega \rho C}{K}\right] \, T(\omega,r,z) \;=\; 0 \tag{6.36}$$

We separate the space variable by taking

$$T(\omega,r,z) \;=\; t(\omega,z) J_0(kr)$$

where J_0 is the Bessel function, and k an arbitrary constant. Eq.6.36 becomes

$$\left[\partial_z^2 - \kappa^2\right] t(\omega,z) \;=\; 0$$

where

$$\kappa \;=\; \sqrt{k^2 - i \, \frac{\omega \rho C}{K}}$$

The general solution is:

$$t(\omega,z) \;=\; \theta'(\omega) \exp(-\kappa z) + \theta''(\omega) \exp(\kappa z)$$

where θ' and θ'' are two arbitrary functions. We have now a solution of Eq.6.36 under the form:

$$T(\omega, r, z) \;=\; [\theta'(\omega)\exp(-\kappa z) + \theta''(\omega)\exp(\kappa z)]\; J_0(kr)$$

The various arbitrary constants and functions can now be determined by the boundary conditions as usual. We take the coordinates as follows: The radial coordinate is such that $0 \leq r \leq a$ (a is the radius of the cylindrical mirror), the axial coordinate is such that $0 \leq z \leq h$ (h is the thickness of the mirror). The absorbing coating is assumed at $z = 0$. We firstly address the condition of an outgoing radiating heat flux off the circular edge ($r = a$). This yields:

$$-K\frac{\partial T}{\partial r}(\omega, a, z) \;=\; 4\sigma' T_0^3 T(\omega, a, z)$$

The z dependent factor cancels out from the equation, and we are left with

$$KkJ_1(ka) \;=\; 4\sigma' T_0^3 J_0(ka)$$

or, by setting $ka = \zeta$ and $\chi = 4\sigma' T_0^3 a/K$:

$$\zeta J_1(\zeta) - \chi J_0(\zeta) \;=\; 0 \tag{6.37}$$

An equation like 6.37 has an infinite family of discrete solutions we note $\{\zeta_n,\ n = 1, 2, ...\}$. A consequence of this quantization is that now, the family of functions $J_0(\zeta_n r/a)$ form an othonormal and closed family of functions on which any reasonably behaviored function (for instance an optical intensity) can be expanded. We have namely:

$$\int_0^a J_0(\zeta_n r/a)\, J_0(\zeta_m r/a)\, r\, dr \;=\; \frac{a^2(\chi^2 + \zeta_n^2) J_0^2(\zeta_n)}{2\zeta_n^2}\; \delta_{nm}$$

(see for instance [20] p.485, formula 11.4.5). We shall therefore consider the solution of Eq.6.36 as a sum over all indices n:

$$T(\omega, r, z) \;=\; \sum_n [\theta'_n(\omega)\exp(-\kappa_n z) + \theta''_n(\omega)\exp(\kappa_n z)]\; J_0(\zeta_n r/a) \tag{6.38}$$

where

$$\kappa_n \;=\; \sqrt{\frac{\zeta_n^2}{a^2} - i\,\frac{\omega\rho C}{K}}$$

Now we can address the boundary condition on the face $z = 0$:

$$-K\frac{\partial T}{\partial z}(\omega, r, 0) \;=\; -4\sigma' T_0^3 T(\omega, r, 0) + I(\omega, r)$$

Where $I(\omega, r)$ is the Fourier transform of the incoming absorbed intensity flow on the absorbing face. $p(\omega, r)$ can be expanded in a Dini series:

$$I(\omega, r) \;=\; \frac{P(\omega)}{2\pi a^2} \sum_n p_n J_0(\zeta_n r/a)$$

where $P(\omega)$ refers to the integrated absorbed power flow. The boundary condition is now:

$$\kappa_n K(\theta'_n - \theta''_n) \;=\; P(\omega)p_n/2\pi a^2 - 4\sigma' T_0^3(\theta'_n + \theta''_n)$$

The boundary condition on the face $z = h$ is simply:

$$\kappa_n K(\theta'_n \mathrm{e}^{-\gamma_n} - \theta''_n \mathrm{e}^{\gamma_n}) \;=\; 4\sigma' T_0^3(\theta'_n \mathrm{e}^{-\gamma_n} + \theta''_n \mathrm{e}^{\gamma_n})$$

where $\gamma_n \equiv \kappa_n h$. By introducing the constant

$$\chi' \;\equiv\; 4\sigma' T_0^3 h/K$$

we get the system:

$$\begin{cases} (\gamma_n + \chi')\theta'_n - (\gamma_n - \chi')''_n \;=\; P(\omega)p_n h/2\pi K a^2 \\ (\gamma_n - \chi')\,\mathrm{e}^{-\gamma_n}\,\theta'_n - (\gamma_n + \chi')\,\mathrm{e}^{\gamma_n}\,\theta''_n \;=\; 0 \end{cases} \tag{6.39}$$

so that the solution is now fully determined, and quite analogous to the one obtained in the static domain, except that now some quantities are complex. We have:

$$T(\omega, r, z) \;=\; \frac{P(\omega)h}{2\pi K a^2} \sum_n p_n \frac{(\gamma_n + \chi')\mathrm{e}^{-\kappa_n z} + (\gamma_n - \chi')\mathrm{e}^{\kappa_n(z-2h)}}{(\gamma_n + \chi')^2 - (\gamma_n - \chi')^2\,\mathrm{e}^{-2\gamma_n}}\; J_0(\zeta_n r/a) \tag{6.40}$$

In the case of a gaussian beam of half width w, we have:

$$I(\omega, r) \;=\; \frac{2P(\omega)}{\pi w^2}\,\exp(-2r^2/w^2)$$

We get:

$$p_{n,\mathrm{gauss}} \;=\; \frac{2\zeta_n^2}{(\chi^2 + \zeta_n^2)J_0^2(\zeta_n)}\;\exp(-w^2\zeta_n^2/8a^2)$$

so that the solution corresponding to a gaussian beam is explicitly:

$$T_{\text{Gauss}}(\omega,r,z) \;=\; \frac{P(\omega)h}{\pi a^2 K}\sum_n \frac{\zeta_n^2\,\exp(-w^2\zeta_n^2/8a^2)}{(\chi^2+\zeta_n^2)J_0^2(\zeta_n)}\times \tag{6.41}$$

$$\times\,\frac{(\gamma_n+\chi')\mathrm{e}^{-\kappa_n z}+(\gamma_n-\chi')\mathrm{e}^{\kappa_n(z-2h)}}{(\gamma_n+\chi')^2-(\gamma_n-\chi')^2\,\mathrm{e}^{-2\gamma_n}}\;J_0(\zeta_n r/a)$$

In the case of an ideally flat beam of half width b, we have:

$$I(r)=\begin{cases} P(\omega)/\pi b^2 & (r\le b)\\ 0 \quad \text{otherwise}\end{cases}$$

so that

$$p_{n,\text{flat}} \;=\; \frac{4a\zeta_n\,J_1(\zeta_n b/a)}{b(\chi^2+\zeta_n^2)J_0^2(\zeta_n)}$$

and the solution is explicitly:

$$T_{\text{Flat}}(\omega,r,z) \;=\; \frac{2P(\omega)h}{\pi abK}\sum_n \frac{\zeta_n\,J_1(\zeta_n b/a)}{(\chi^2+\zeta_n^2)J_0^2(\zeta_n)}\times \tag{6.42}$$

$$\times\,\frac{(\gamma_n+\chi')\mathrm{e}^{-\kappa_n z}+(\gamma_n-\chi')\mathrm{e}^{\kappa_n(z-2h)}}{(\gamma_n+\chi')^2-(\gamma_n-\chi')^2\,\mathrm{e}^{-2\gamma_n}}\;J_0(\zeta_n r/a)$$

The temperature field, at frequencies higher than 1 Hz, is significant only in the close neighborhood of the hot spot. See on Fig.6.20 the distribution of the transfer function $|T|/P(\omega)$ for $f=0.1$ Hz. and on Fig.6.21 the same for 1 Hz. Moreover, as can be seen, the temperature field tends to a pure skin effect, as the frequency increases. We can see the results for an ideally flat mode on Figs.6.22, 6.23. We already see that the dynamic temperature field has a much lower amplitude in the case of a flat beam.

Thermal lens

The first effect of the varying temperature field is to create a variable thermal lensing. The apex equation $Z(\omega,r)$ giving the lens profile is obtained by integrating the temperature along the optical path. This is:

$$Z(\omega,r) \;=\; \frac{dn}{dT}\int_0^h T(\omega,r,z)\,dz$$

Where dn/dT is the temperature refractive index coefficient. This gives:

$$Z(\omega,r) \;=\; \frac{dn}{dT}\,\frac{h^2P(\omega)}{2\pi Ka^2}\sum_n \frac{p_n(1-\mathrm{e}^{-\gamma_n})}{\gamma_n\,[\gamma_n+\chi'-(\gamma_n-\chi')\mathrm{e}^{-\gamma_n}]}\,J_0(\zeta_n r/a) \qquad (6.43)$$

We can finally address the question of effective length variations. The beam that crosses the mirror substrate undergoes a global length change, as seen in apreceding chapter, given by:

$$Z(\omega) \;=\; 2\pi\int_0^\infty Z(\omega,r)\,I(r)\,r\,dr$$

where $I(r)$ is the normalized intensity profile of the beam. This results here in:

$$Z(\omega) \;=\; \frac{dn}{dT}\,\frac{h^2P(\omega)}{4\pi Ka^2}\sum_n \frac{p_n^2(1-\mathrm{e}^{-\gamma_n})(\chi^2+\zeta_n^2)J_0(\zeta_n)^2}{\gamma_n\,[\gamma_n+\chi'-(\gamma_n-\chi')\mathrm{e}^{-\gamma_n}]\,\zeta_n^2} \qquad (6.44)$$

If we interpret $P(\omega)$ as the spectral density of absorbed power fluctuations, and $Z(\omega)$ as the spectral density of path length fluctuations, we see that the two SD are related by the transfer function:

$$F(\omega) \;=\; \frac{dn}{dT}\,\frac{h^2}{4\pi Ka^2}\sum_n \frac{p_n^2(1-\mathrm{e}^{-\gamma_n})(\chi^2+\zeta_n^2)J_0(\zeta_n)^2}{\gamma_n\,[\gamma_n+\chi'-(\gamma_n-\chi')\mathrm{e}^{-\gamma_n}]\,\zeta_n^2}$$

On Fig.6.24, one can see the frequency dependence of the modulus transfer function. This dependence is clearly in $1/f$ for frequencies larger than a fraction of a Hz, the TF is much lower for a flat beam. One sees moreover that the knee frequency is different for the two types of mode. or a gaussian beam of radius $w = 2$ cm, it is:

$$F(f) \;\sim\; \frac{6.7\ 10^{-10}}{f}\ \ \mathrm{m/absorbedW.}$$

while for a flat beam of radius $b = 10$ cm:

$$F(f) \;\sim\; \frac{2.7\ 10^{-11}}{f}\ \ \mathrm{m/absorbedW.}$$

If we assume the power fluctuations caused by the shot noise (the power is absorbed by quanta in the coating), the spectral density of absorbed power fluctuation is given by:

$$\epsilon P(\omega) \;=\; \sqrt{2\epsilon P_0 h_P \nu}$$

where P_0 is the nominal power of the incoming beam (even highly stable!), and ϵ the losses in the mirror due to thermal dissipation. This allows to give an order of magnitude for the optical path fluctuations caused by the shot noise. We assume the Silica parameters already given, and a power of the order of magnitude of that stored in the long cavities, i.e. 20 kW, coating thermal losses of about 1 ppm:

$$Z(f) \sim \frac{4\,10^{-20}}{f} \text{ m.Hz}^{-1/2}$$

This represents the optical path fluctuations by passing for instance through the Fabry-Perot input mirrors. This is negligible in the present configuration of Virgo, but should be reexamined in an advanced detector with high recycled power.

Asymptotic solution

The exact model presented above can be hugely simplified in some realistic cases. If we consider the paramters

$$\kappa_n = \sqrt{\frac{\zeta_n^2}{a^2} - i\,\frac{\omega\rho C}{K}}$$

we see that in general, the second imaginary contribution will be much larger than the real one. Namely, even for a frequency of 10 Hz, we have

$$\frac{\omega\rho C a^2}{K} \sim 2.3\ 10^5$$

which is to be compared with $\zeta_n^2 \sim n^2\pi^2$. If the p_n are rapidly decreasing (as in the case of a gaussian beam), the index at which the real contribution becomes non negligible compared to the imaginary, is never reached, and we can write:

$$\kappa_n = \kappa = \sqrt{-i\,\frac{\omega\rho C}{K}} = k(1-i)$$

and the same way

$$\gamma_n = \gamma = kh(1-i)$$

where $k \equiv \sqrt{\omega\rho C/2K}$. Expressions like $\exp(-\kappa h)$ vanish, and we have simply, instead of 6.40:

$$T(\omega, r, z) = \frac{P(\omega)h}{2\pi K a^2} \sum_n p_n \frac{\exp(-\kappa z)}{\gamma} J_0(\zeta_n r/a) \qquad (6.45)$$

and due to the fact that

$$I(r) \;=\; \frac{P(\omega)}{2\pi a^2}\sum_n p_n J_0(\zeta_n r/a)$$

we have finally

$$T_{\rm asymp}(\omega,r,z) \;=\; \frac{1}{K\kappa}I(r)\mathrm{e}^{-\kappa z} \tag{6.46}$$

Recall that $I(r)$ is the absorbed intensity profile. Numerical tests show that there is no difference between 6.40 and 6.46 in the case of a gaussian beam. In the case of an ideally flat beam, there are some differences due to the weak decreasing rate of the p_n in this case, but the accuracy is sufficient for further purposes. A simplified version of the thermal lens immediately follows:

$$Z(\omega,r) \;=\; \frac{dn}{dT}\,\frac{1}{K\kappa^2}\,I(r)$$

For the effective displacement:

$$Z(\omega) \;=\; \frac{dn}{dT}\,\frac{1}{K\kappa^2}\int I(r)I_0(r)^2 r\,dr\,d\phi$$

where $I_0(r)$ is the same intensity profile, but normalized to 1 W. in the case of a gaussian beam of half-width w, we have:

$$\int I_{0,\rm Gauss}(r)^2 r\,dr\,d\phi \;=\; \frac{1}{\pi w^2}$$

so that

$$Z(\omega) \;=\; i\,\frac{dn}{dT}\,\frac{P(\omega)}{\pi w^2 K\,\rho C\omega} \tag{6.47}$$

and we see explicitly the dependence in $1/f$, whereas in the case of a flat beam of radius b, we have

$$\int I_{\rm Flat}(r)^2 r\,dr\,d\phi \;=\; \frac{1}{\pi b^2}$$

so that the formula is the same with w replaced by b, and we see that the optical path fluctuations are reduced by a factor of $(w/b)^2$.

6.6.2 Dynamical thermal surface distortions

The obvious other effect of a fluctuating temperature field in the substrate is to induce fluctuating distortions in the bulk, resulting in surface flcutuations, and consequently to a fluctuation of the effective position of the mirror. We consider again the elastodynamics equation:

$$\mathrm{div}\Theta \;=\; \rho\,\partial_t^2\mathbf{u}$$

We take as usual the displacement vector under the form (after a Fourier transform) :

$$\begin{cases} u_r(\omega,r,z) \;=\; \sum_n A_n(\omega,z)\,J_1(k_n r) \\ u_z(\omega,r,z) \;=\; \sum_n B_n(\omega,z)\,J_0(k_n r) \end{cases}$$

The temperature field being given under the form

$$T(\omega,r,z) \;=\; \sum_n t_n(\omega,z)\,J_0(k_n r)$$

The elastodynamics equations reduce to

$$\left[\mu\left(\partial_z^2-k_n^2\right)+\rho\omega^2\right]\,A_n - k_n\left[(\lambda+\mu)(\partial_z B_n + k_n A_n)-\nu t_n\right] \;=\; 0 \qquad (6.48)$$

$$\left[\mu\left(\partial_z^2-k_n^2\right)+\rho\omega^2\right]\,B_n + \partial_z\left[(\lambda+\mu)(\partial_z B_n + k_n A_n)-\nu t_n\right] \;=\; 0 \qquad (6.49)$$

from what we get

$$\left(\partial_z^2-k_n^2+\rho\omega^2/\mu\right)\,(\partial_z A_n + k_n B_n) \;=\; 0$$

We have seen in the preceding section that even for frequencies as low as a few Hz, the temperature field is negligible outside a thin neighborhood of the beam spot. We shall therefore consider the mirror in this regime, as an infinite medium. We assume the displacement vector to decrease exponentially, and we take the solution of the preceding equation as:

$$\partial_z A_n + k_n B_n \;=\; k\,M_n\,\mathrm{e}^{-\kappa_{T,n} z}$$

where

$$\kappa_{T,n} \;=\; \sqrt{k_n^2-\frac{\rho\omega^2}{\mu}}$$

is the transverse elastic wave vector. We have thus:

$$B_n \;=\; M_n\,\mathrm{e}^{-\kappa_{T,n} z} - \frac{\partial_z A_n}{k_n}$$

and by substituting in 6.48 we obtain:

$$\left[(\lambda+2\mu)\left(\partial_z^2-k_n^2\right)+\rho\omega^2\right]\,A_n \;=\; -k_n\,\kappa_{T,n}\,(\lambda+\mu)M_n\,\mathrm{e}^{-\kappa_{T,n}z}-k\nu t_n \quad (6.50)$$

The solution of which is:

$$A_n \;=\; Q_n\,\mathrm{e}^{-\kappa_{L,n}z} \;-\; \frac{k_n\,\kappa_{T,n}(\lambda+\mu)}{(\lambda+2\mu)(\kappa_{T,n}^2-\kappa_{L,n}^2)}\,M_n\,\mathrm{e}^{-\kappa_{T,n}z} \;-\; \frac{k_n\nu\theta_n}{\lambda+2\mu} \quad (6.51)$$

where

$$\kappa_{L,n} \;=\; \sqrt{k_n^2-\frac{\rho\omega^2}{\lambda+2\mu}}$$

is the longitudinal elastic wave vector. But

$$\kappa_{T,n}^2-\kappa_{L,n}^2 \;=\; -\rho\omega^2\frac{\lambda+\mu}{\mu(\lambda+2\mu)}$$

so that:

$$A_n \;=\; Q_n\,\mathrm{e}^{-\kappa_{L,n}z} \;+\; \frac{\kappa_{T,n}}{2k_nX_n} \;-\; \frac{k_n\nu\theta_n}{\lambda+2\mu} \quad (6.52)$$

with the notation

$$X_n \;\equiv\; \frac{\rho\omega^2}{2k_n^2\mu}$$

Having A_n, we can calculate B_n:

$$B_n \;=\; \frac{\kappa_{L,n}}{k_n}\,Q_n\,\mathrm{e}^{-\kappa_{L,n}z} \;+\; \frac{1}{2X_n}\,M_n\,\mathrm{e}^{-\kappa_{T,n}z} \;+\; \frac{\nu\partial_z\theta_n}{\lambda+2\mu} \quad (6.53)$$

The medium being assumes infinite, the only boundary conditions are the vanishing of the axial pressure on the heated surface, i.e.:

$$\Theta_{rz}(\omega,r,z=0) \;=\; \Theta_{zz}(\omega,r,z=0) \;=\; 0 \quad (6.54)$$

this leads to two equations allowing to determine the Q_n and the M_n. We have

$$\Theta_{n,rz} \;=\; \mu(\partial_z A_n-k_nB_n)$$

and

$$\Theta_{n,zz} \;=\; -\nu t_n+\lambda k_nA_n \;+\; (\lambda+2\mu)\partial_z B_n$$

We get the system:

$$\begin{cases} \frac{\kappa_{T,n}}{2k_nX_n}\,M_n + (1-X_n)\,Q_n &= \frac{\nu}{\lambda+2\mu}(1-X_n)k_n\theta_n(0) \\ \frac{1-X_n}{2X_n}\,M_n + \frac{\kappa_{L,n}}{k_n}\,Q_n &= -\frac{\nu}{\lambda+2\mu}k_n\partial_z\theta_n(0) \end{cases} \tag{6.55}$$

The solution of which is:

$$M_n = \frac{2\nu X_n(1-X_n)}{\lambda+2\mu}\,\frac{\partial_z\theta_n(0)+\kappa_{L,n}\theta_n(0)}{\kappa_{L,n}\kappa_{T,n}/k_n^2-(1-X_n)^2} \tag{6.56}$$

and

$$Q_n = -\frac{\nu}{\lambda+2\mu}\,\frac{\frac{\kappa_{T,n}}{k_n}\partial_z\theta_n(0)+(1-X_n)^2k_n\theta_n(0)}{\kappa_{L,n}\kappa_{T,n}/k_n^2-(1-X_n)^2} \tag{6.57}$$

Our target is the displacement of the surface, or in other words the function

$$\sum_n B_n(\omega, z=0)J_0(k_nr)$$

We have:

$$B_n(\omega,0) = \frac{1}{2X_n}M_n + \frac{\kappa_{L,n}}{k_n}\,Q_n + \frac{\nu}{\lambda+2\mu}\partial_z\theta_n(0)$$

by substituting the values found for the Q_n and the M_n, this is, after some algebra:

$$B_n(\omega,0) = \frac{\nu}{\lambda+2\mu}\,\frac{X_n(1-X_n)\left[\partial_z\theta_n(0)+\kappa_{L,n}\theta_n(0)\right]}{\kappa_{L,n}\kappa_{T,n}/k_n^2-(1-X_n)^2} \tag{6.58}$$

Let us now consider some figures. It is easily seen that the parameters X_n are very small in realistic cases. Recall that

$$X_n = \frac{\rho\omega^2a^2}{2\mu\zeta_n^2}$$

The largest X_n is obviously X_1, in which $\zeta_1 \sim 1$. For the silica parameters, at a frequency of 10 Hz, we have

$$X_1 \sim 4\,10^{-6}$$

it is therefore quite allowed to compute B_n at the lowest order in X_n. We have:

$$\kappa_{L,n}\kappa_{T,n}/k_n^2-(1-X_n)^2 = X_n\frac{\lambda+\mu}{\lambda+2\mu} + \mathcal{O}(X_n^2)$$

so that:

$$B_n(\omega,0) \;=\; \frac{\nu}{\lambda+\mu}\left[\partial_z\theta_n(0)+\kappa_{L,n}\theta_n(0)\right] \tag{6.59}$$

Now, if we introduce the temperature field found in the preceding section, in the asymptotic regime:

$$t_n(\omega,z) \;=\; \frac{P(\omega)h}{2\pi Ka^2}\,\frac{\mathrm{e}^{-\kappa_n z}}{\gamma_n+\chi'}\,p_n$$

we have

$$\theta_n(\omega,z) \;=\; \frac{P(\omega)h}{2\pi Ka^2}\,\frac{\mathrm{e}^{-\kappa_n z}}{\gamma_n+\chi'}\,\frac{1}{\kappa_n^2-\kappa_{L,n}^2}\,p_n$$

so that

$$\partial_z\theta_n(0)+\kappa_{L,n}\theta_n(0) \;=\; -\,\frac{P(\omega)h}{2\pi Ka^2}\,\frac{1}{\gamma_n+\chi'}\,\frac{1}{\kappa_n+\kappa_{L,n}}\,p_n$$

Recall now that the heat wave vector κ_n is very large compared to the elastical ones. We have namely:

$$\kappa_{L,n}/\kappa_n \;\sim\; 4\;10^{-6}\,\frac{\zeta_n^2}{f}$$

By keeping only the leading terms, we obtain:

$$B_n(\omega,0) \;=\; -i\,\frac{\nu}{\lambda+\mu}\,\frac{P(\omega)}{2\pi a^2\rho C\omega}\,p_n$$

If we express this in terms of the linear dilatation coefficient α and the Poisson ratio σ, we have:

$$B(\omega,0) \;=\; -i\,\frac{\alpha(1+\sigma)P(\omega)}{\pi a^2\rho C\omega}\,p_n \tag{6.60}$$

and finally, for the surface apex equation:

$$Z(\omega,r) \;=\; -i\,\frac{2\alpha(1+\sigma)P(\omega)}{\rho C\omega}\;I(r)$$

where $I(r)$ is the absorbed intensity. The surface distortion is thus proportional to the temperature field. For the effective displacement, we have:

$$Z(\omega) \;=\; \int Z(\omega,r)\,I(r)\,r\,dr\,d\phi$$

or

$$Z(\omega) \;=\; -\,\frac{2i\alpha(1+\sigma)P(\omega)}{\rho C\omega}\int I(\omega,r)^2 r\,dr\,d\phi \tag{6.61}$$

For a gaussian beam of half-width w, the transfer function from the power variations to the mirror displacement is:

$$Z(\omega)/P(\omega) \;=\; -\,\frac{2i\alpha(1+\sigma)}{\pi w^2\rho C\omega} \tag{6.62}$$

to be specific, in the case of silica, for $w \sim 2$ cm, this is

$$Z(f)/P(f) \;\sim\; \frac{2\ 10^{-10}}{f}\ \ \mathrm{m/W}$$

In the case of a flat beam of radius b, the formula is the same, with w replaced by b.

6.7 Thermoelastic coupling : Bulk absorption

The same work can be carried out in the case where the incident power is dissipated in the bulk material. As usual, we get a temperature field which generates a thermal lens and a distortion of the solid. We follow the same scheme as in the preceding section.

6.7.1 Dynamical temperature

Temperature field

We again assume an incoming light beam of power $P(\omega,z)$ (either a Fourier component or a spectral density), and normalized intensity profile $I(r)$. As usual in this chapter, the mirror is assumed to have a radius a and a thickness h. The radial coordinate is $r \le a$, and the axial coordinate is $-h/2 \le z \le h/2$. The beam is weakly absorbed during its crossing the mirror substrate, so that its intensity is assumed constant with respect to z : $P(\omega,z) = P(\omega)$. We have thus a new definition of the axial coordinate, in order to benefit from the symmetry of the problem. The intensity being constant along z, the result is that the temperature field will be symmetrical with respect to z. As usual, the normalized intensity profile can be expanded on the basis

of the Bessel functions $J_0(k_n z)$, where the family of constants k_n are to be determined. We have:

$$I(r) \;=\; \frac{1}{2\pi a^2} \sum_n p_n J_0(k_n r)$$

If we note $T(\omega, r, z)$ the temperature field, it obeys the inhomogeneous Fourier-heat equation:

$$[i\omega\rho C - K\Delta]\, T(\omega, r, z) \;=\; \beta P(\omega) I(r) \tag{6.63}$$

where β is as usual the linear absorption coefficient (m^{-1}). In order to separate the variables, we can write:

$$T(\omega, r, z) \;=\; \sum_n t_n(\omega, z)\, J_0(k_n r)$$

where the functions $t_n(\omega, z)$ remain to be determined. We have exchanged the partial differential equation for a set of differential equations:

$$(\partial_z^2 - \kappa_n^2) t_n(\omega, z) \;=\; -\frac{\beta P(\omega)}{2\pi K a^2}\, p_n \tag{6.64}$$

where

$$\kappa \;=\; \sqrt{k_n^2 - i\rho C\omega / K}$$

The z-symmetrical solution is obviously:

$$t_n(z) \;=\; A_n \cosh(\kappa_n z) \;+\; \frac{\beta P(\omega)}{2\pi K a^2 \kappa_n^2}\, p_n \tag{6.65}$$

and the arbitrary constants A_n are to be determined by the boundary conditions. These conditions are the vanishing of heat flows on the faces and on the edge. On the edge, we get the condition

$$-K \frac{\partial T}{\partial r} \;=\; 4\sigma' T_0^3\, T$$

(the notations are the same as throughout all this chapter). This gives the same equation as in the preceding section and determines the k_n, namely:

$$k_n \;=\; \zeta_n / a$$

where the ζ_n are the zeroes of the equation:

$$\zeta J_1(\zeta) - \chi J_0(\zeta) \;=\; 0 \quad (\chi \;\equiv\; 4\sigma' T_0^3 a / K)$$

so that the p_n are the same as in all preceding sections. Now the conditions on each circular faces reduce, thanks to symmetry to one condition on the face $z = h/2$:

$$-K \frac{\partial T}{\partial z} \;=\; 4\sigma' T_0^3 \, T$$

and the result determines the A_n:

$$A_n(\omega) \;=\; -\frac{\chi'' \beta P(\omega) p_n}{2\pi K \kappa_n^2 a^2} \frac{1}{\gamma_n \sinh \gamma_n \;+\; \chi' \cosh \gamma_n} \tag{6.66}$$

where the notation being:

$$\gamma_n \;\equiv\; \kappa_n h/2 \quad , \quad \chi'' \;\equiv\; \chi \, h/2a$$

And finally, the temperature field is:

$$T(\omega, r, z) \;=\; \frac{\beta P(\omega)}{2\pi K a^2} \sum_n \frac{p_n}{\kappa_n^2} \left[1 \;-\; \frac{\chi'' \cosh(\kappa_n z)}{\gamma_n \sinh \gamma_n + \chi'' \cosh \gamma_n} \right] J_0(\zeta_n r/a) \tag{6.67}$$

Again, we note that for frequencies larger than a few Hz, the κ_n are almost all equal:

$$\kappa_n \;\sim\; \sqrt{-i\omega C\rho/K} \;=\; \kappa \;\Rightarrow\; \gamma_n \;\sim\; \gamma \equiv \kappa h/2$$

so that the temperature field reproduces the same profile as the beam intensity:

$$T(\omega, r, z) \;\sim\; \frac{\beta P(\omega)}{K\kappa^2} \left[1 \;-\; \frac{\chi'' \cosh(\kappa z)}{\gamma \sinh \gamma + \chi'' \cosh \gamma} \right] I(r)$$

Thermal lens

By integrating along z, we find the thermal lens:

$$Z(\omega, r) \;=\; \frac{dn}{dT} \frac{\beta P(\omega) h}{K\kappa^2} \left[1 \;-\; \frac{\chi'' \sinh \gamma}{\gamma(\gamma \sinh \gamma + \chi'' \cosh \gamma)} \right] I(r) \tag{6.68}$$

or simply, owing to the fact that $\gamma \gg 1$:

$$Z(\omega, r) \;=\; \frac{dn}{dT} \frac{\beta P(\omega) h}{\rho C \omega} I(r) \tag{6.69}$$

The effective length of the path in the substrate is as usual the average of the thermal lens weighted by the intensity profile:

$$Z(\omega) \;=\; \int I(r) Z(\omega, r)\, r\, dr\, d\phi \tag{6.70}$$

which gives:

$$Z(\omega) \;=\; i\, \frac{dn}{dT}\, \frac{\beta P(\omega) h}{\pi w^2 \rho C \omega} \tag{6.71}$$

This is identical to eq.6.47, which shows that for equal absorbed power in the coating and in the bulk, the two contributions to thermal lensings are equal. in the case of a gaussian beam of half-width w. In the case of a flat beam of radius b, the formula is the same, with w replaced by b. In the case of the Silica parameters, the transfer function is:

$$Z(\omega)/\beta h P(\omega) \;\sim\; 6.7\ 10^{-10} \left[\frac{1\mathrm{Hz}}{f}\right] \ \mathrm{m/absorbedW}$$

6.7.2 Dynamical thermal distortions

General solution

We have to carry out the same calculations as in the coating absorption case, except that the definition of p_m is changed, and that the symmetry is different. In the coating absorption case, the temperature field was localized in the neighborhood of the hot spot. Now, the temperature field extends throughout the mirror. We take the same coordinate system as above, and write the displacement vector as:

$$u_r(\omega, r, z) \;=\; \sum_n A_n(\omega, z) J_1(k_n r) \tag{6.72}$$

and

$$u_z(\omega, r, z) \;=\; \sum_n B_n(\omega, z) J_0(k_n r)$$

where $A_n(\omega, z)$ is assumed an even function of z, and $B_n(\omega, z)$ an odd function of z. The temperature field is assumed expanded as:

$$T(\omega, r, z) \;=\; \sum_n t_n(\omega, z)\, J_0(k_n z)$$

In all the following calculations, the k_n are the same as in the preceding section. The elastodynamic equations are identical to eq.6.48 and 6.49. We find again that:

$$(\partial_z^2 - \kappa_{T,n}^2)(\partial_z A_n + k_n B_n) \;=\; 0$$

and we choose the odd solution:

$$\partial_z A_n + k_n B_n \;=\; kQ_n \sinh(\kappa_{T,n} z) \tag{6.73}$$

and by substituting in eq.6.48, we get:

$$(\partial_z^2 - \kappa_{L,n}^2)A_n \;=\; \frac{k\kappa_{T,n}(\lambda+\mu)}{(\lambda+2\mu)(\kappa_{T,n}^2 - \kappa_{L,n}^2)} Q_n \cosh(\kappa_{T,n} z) - \frac{k_n \nu t_n}{\lambda+2\mu} \tag{6.74}$$

By using again the notation $X_n \equiv \rho\omega^2/2k_n^2\mu$, and taking the even solution, we get:

$$A_n \;=\; M_n \cosh(\kappa_{L,n} z) - \frac{\kappa_{T,n}}{2k_n X_n} Q_n \cosh(\kappa_{T,n} z) - \frac{k_n \nu \theta_n}{\lambda+2\mu} \tag{6.75}$$

and, owing to eq.6.73, this gives in turn:

$$B_n \;=\; -\frac{\kappa_{L,n}}{k_n} M_n \sinh(\kappa_{L,n} z) + \frac{1}{2X_n} Q_n \sinh(\kappa_{T,n} z) + \frac{\nu \partial_z \theta_n}{\lambda+2\mu} \tag{6.76}$$

where $\theta(\omega, z)$ is assumed a particular solution of

$$(\partial_z^2 - \kappa_{L,n}^2)\theta_n \;=\; t$$

We have seen that the temperature field, in practice, for frequencies higher than a few Hz, has the same profile as the beam's intensity. We therefore consider only boundary conditions on the two circular faces of the mirror (infinite slab of finite width), and due to symmetry, there are only two equations, allowing to determine the Q_n and the M_n. The condition

$$\Theta_{rz} \;=\; 0 \quad (z = \pm h/2)$$

yields the equation:

$$\frac{\kappa_{L,n}}{k_n} M_n \sinh\phi_{L,n} \;-\; \frac{1-X_n}{2X_n} Q_n \sinh\phi_{T,n} \;=\; \frac{\nu \partial_z \theta_n(h/2)}{\lambda+2\mu} \tag{6.77}$$

and the condition

$$\Theta_{zz} \;=\; 0 \quad (z = \pm h/2)$$

yields the equation

$$(1-X_n)\, M_n \,\cosh\phi_{L,n} - \frac{\kappa_{T,n}}{2k_n X_n}\, Q_n \,\cosh\phi_{T,n} \;=\; (1-X_n)\,\frac{k_n \nu \theta_n(h/2)}{\lambda+2\mu} \quad (6.78)$$

with the notation $\phi_{L,T,n} \equiv \kappa_{T,L,n} h/2$. The solution of the system (6.77,6.78) is:

$$M_n \;=\; \frac{\nu}{(\lambda+2\mu)D_n}\left[\frac{\kappa_{T,n}}{k_n}\,\cosh\phi_{T,n}\theta'_n - (1-X_n)^2\,\sinh\phi_{T,n}\,k_n\theta_n\right] \quad (6.79)$$

(we have written θ'_n for $\partial_z\theta_n(h/2)$, and θ_n for $\theta_n(h/2)$) we have also set:

$$D_n \;=\; \frac{\kappa_{T,n}\kappa_{L,n}}{k_n^2}\,\sinh\phi_{L,n}\,\cosh\phi_{T,n} - (1-X_n)^2\,\cosh\phi_{L,n}\,\sinh\phi_{T,n}$$

The same way, we get:

$$Q_n \;=\; X_n(1-X_n)\,\frac{\nu}{(\lambda+2\mu)D_n}\,\left[\cosh\phi_{L,n}\,\theta'_n - \kappa_{L,n}\,\sinh\phi_{L,n}\,\theta_n\right] \quad (6.80)$$

But we are interested in the displacement of the surface $z = -h/2$. (or $h/2$ as well, owing to the symmetry). We need:

$$B_m(\omega,-h/2) \;=\; \frac{\kappa_{L,n}}{k_n}\,\sinh\phi_{L,n}\,M_n - \frac{1}{2X_n}\,\sinh\phi_{T,n}\,Q_n - \frac{\nu\theta'_n}{\lambda+2\mu}$$

(this because $\partial_z\theta_n(-h/2) \;=\; -\theta'_n$). After some straightforward algebra, it comes:

$$B_n(\omega,-h/2) \;=\; \frac{\nu}{(\lambda+2\mu)D_n}\,X_n(1-X_n)\,\sinh\phi_{T,n}\,\times \quad (6.81)$$

$$\times\;\left[\kappa_{L,n}\,\sinh\phi_{L,n}\theta_n - \cosh\phi_{L,n}\,\theta'_n\right]$$

The constants θ_n and θ'_n are derived from the preceding section:

$$\theta_n \;=\; -\,\frac{\beta P(\omega)\,p_n}{2\pi K\kappa_n^2 a^2}\,\left[\frac{1}{\kappa_{L,n}^2} + \frac{1}{\kappa_n^2-\kappa_{L,n}^2}\,\frac{\chi''\cosh\gamma_n}{\gamma_n\sinh\gamma_n + \chi''\cosh\gamma_n}\right]$$

and

$$\theta'_n \;=\; -\,\frac{\beta P(\omega)\,p_n\kappa_n}{2\pi K\kappa_n a^2\,(\kappa_n^2-\kappa_{L,n}^2)}\,\frac{\chi''\sinh\gamma_n}{\gamma_n\sinh\gamma_n + \chi''\cosh\gamma_n}$$

Asymptotic regime

Now, the same considerations on the order of magnitude of κ_n that becomes practically independent of its index at frequencies larger than a few Hz, and much larger than $\kappa_{T,L,n}$, leads to:

$$\theta_n \sim -\frac{\beta P(\omega) p_n}{2\pi K \kappa^2 a^2 \kappa_L}$$

and

$$\theta'_n \sim -\frac{\beta P(\omega)\, p_n \chi''}{2\pi K \kappa^2 a^2 h} \frac{\chi''}{\gamma} \frac{1}{\kappa}$$

so that in the combination involved in $B_n(\omega, -h/2)$, θ'_n can be neglected in regard of θ_n. We also remark that the parameters X_n are very small, so that an expansion of the various expressions is needed. At the lowest order we find:

$$D_n = \frac{\lambda+\mu}{\lambda+2\mu} X_n (x_n + \sinh x_n \cosh x_n)$$

where $x_n \equiv k_n h/2$. The asymptotic expression for B_n is now:

$$B_n \sim -\frac{\nu}{\lambda+\mu} \frac{\beta P(\omega) p_n}{2\pi K \kappa^2 a^2 k_n} \frac{\sinh^2 x_n}{x_n + \sinh x_n \cosh x_n}$$

Finally, we find the asymptotic apex equation:

$$Z(\omega, r) = -\frac{\alpha(1+\sigma)\beta P(\omega) h}{2\pi K \kappa^2 a^2} \sum_n \frac{\sinh^2 x_n\, p_n}{x_n(x_n + \sinh x_n \cosh x_n)} J_0(\zeta_n r/a) \tag{6.82}$$

The difference between the exact calculation and the preceding asymptotic formula is negligible for frequencies lager than 1 Hz. An example of the surface profile is shown on fig.6.25, where it can be seen that contrarily to the previous asymptotic cases, the surface profile does not reproduces the intensity profile. By taking the average of the surface weighted by the intensity profile, we get the effective displacement. The transfer function from the absorbed power $\beta P(\omega) h$ to the effective displacement $Z(\omega)$ is:

$$Z(\omega)/\beta h P(\omega) = -i \frac{\alpha(1+\sigma)}{4\pi\rho C \omega a^2} \sum \frac{(1+\chi^2/\zeta_n^2)\, J_0^2(\zeta_n)\, \sinh^2 x_n\, p_n^2}{x_n(x_n + \sinh x_n \cosh x_n)} \tag{6.83}$$

For an input Virgo mirror, this is:

$$Z(f)/\beta h P(f) = \frac{1.3\, 10^{-11}}{f} \text{ m/absorbedW} \tag{6.84}$$

and for a flat beam of radius 10 cm, we get:

$$Z(f)/\beta h P(f) \;=\; \frac{8.8\,10^{-13}}{f}\ \mathrm{m/absorbedW} \tag{6.85}$$

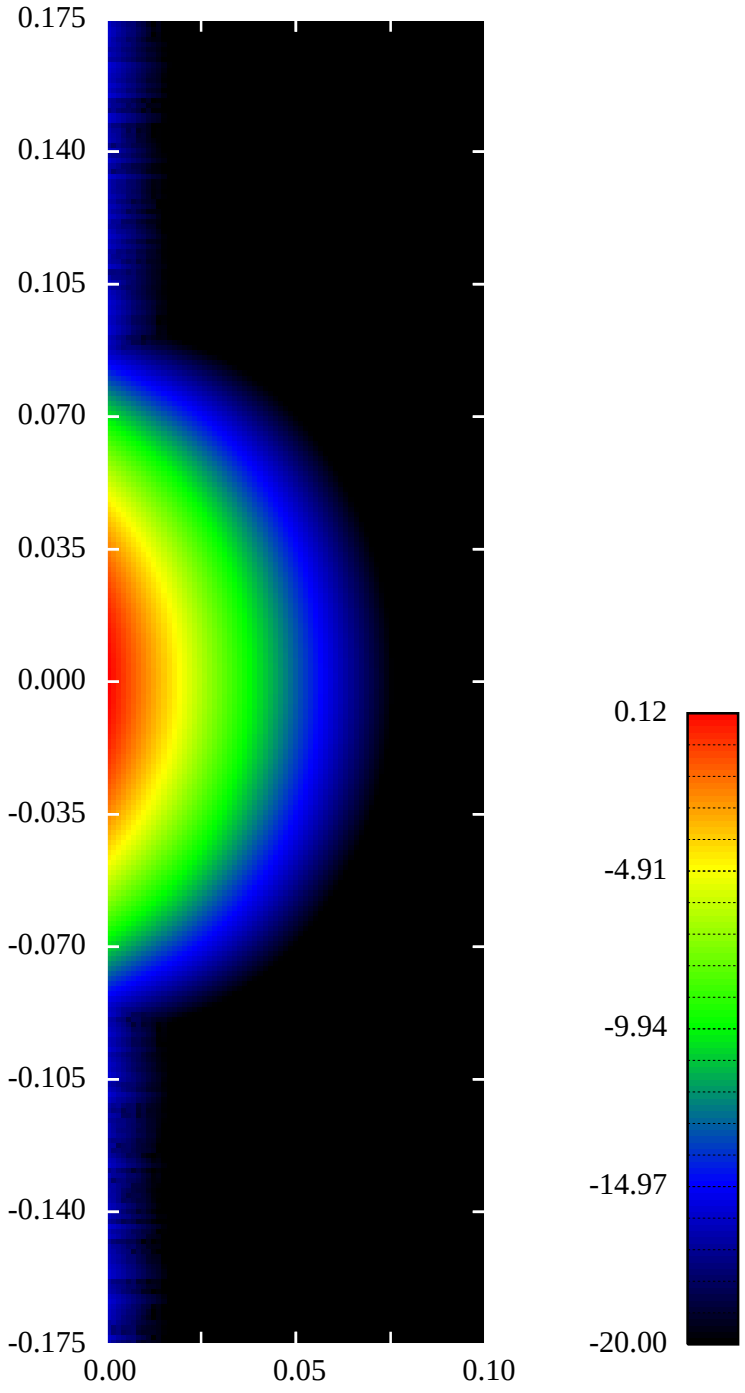

Figure 6.20: Opto-thermal transfer function: $f = 0.1$ Hz, case of gaussian beam $w = 2$ cm

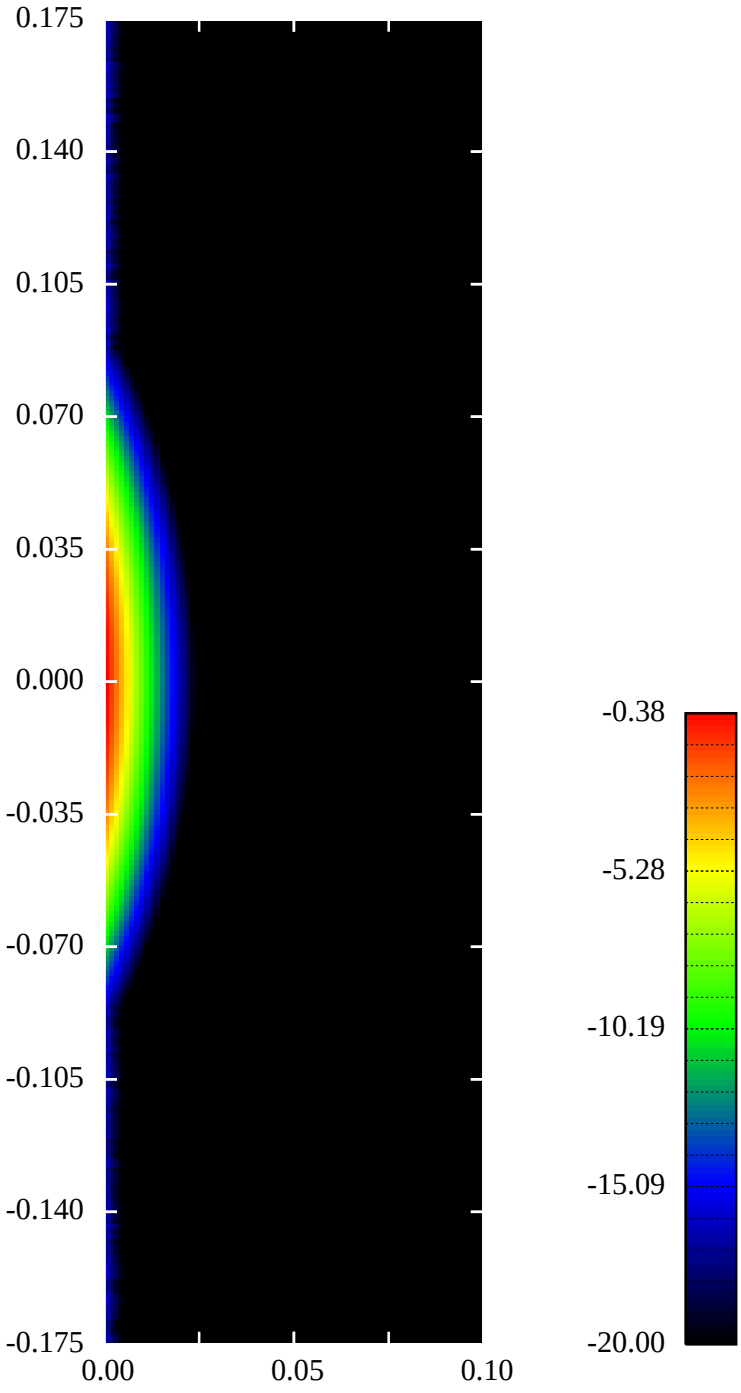

Figure 6.21: Opto-thermal transfer function: $f = 1$ Hz, case of a gaussian beam $w = 2$ cm

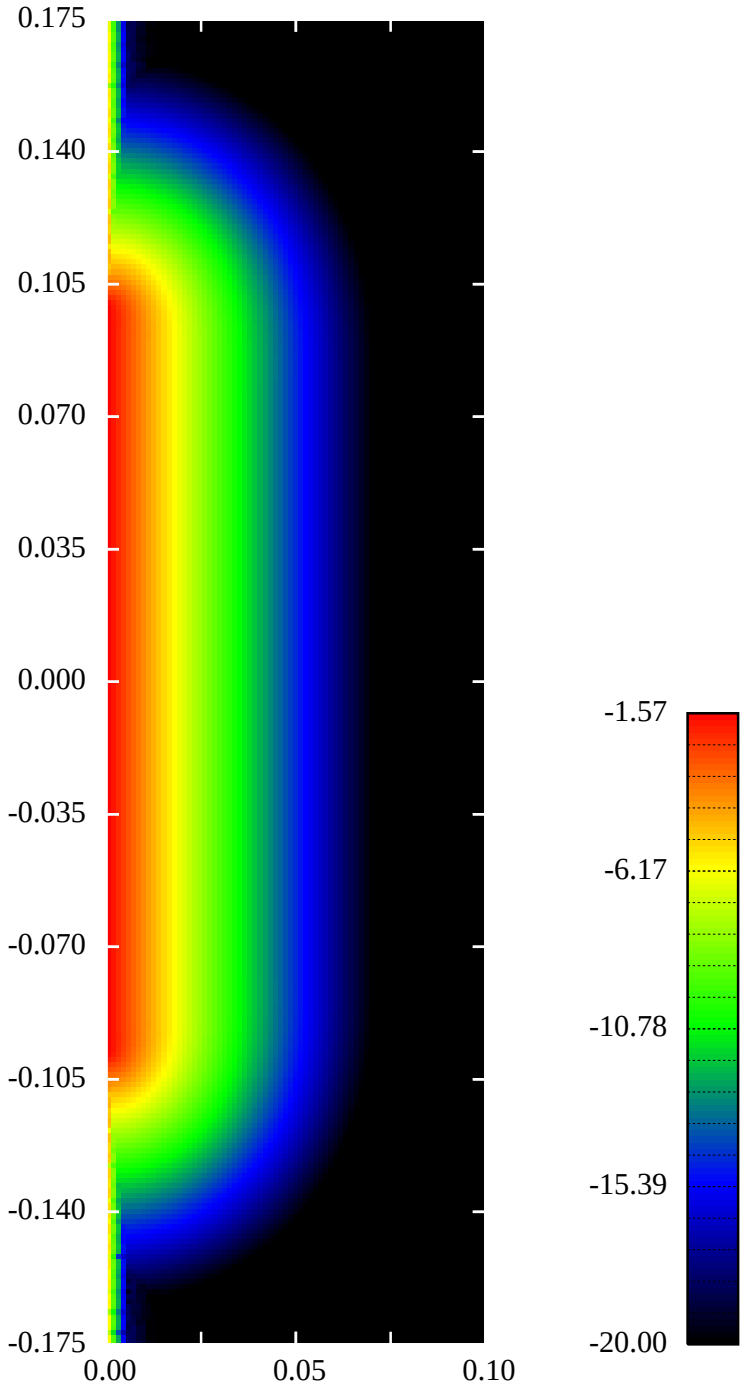

Figure 6.22: Opto-thermal transfer function: $f = 0.1$ Hz, case of a flat beam, $b = 10$ cm

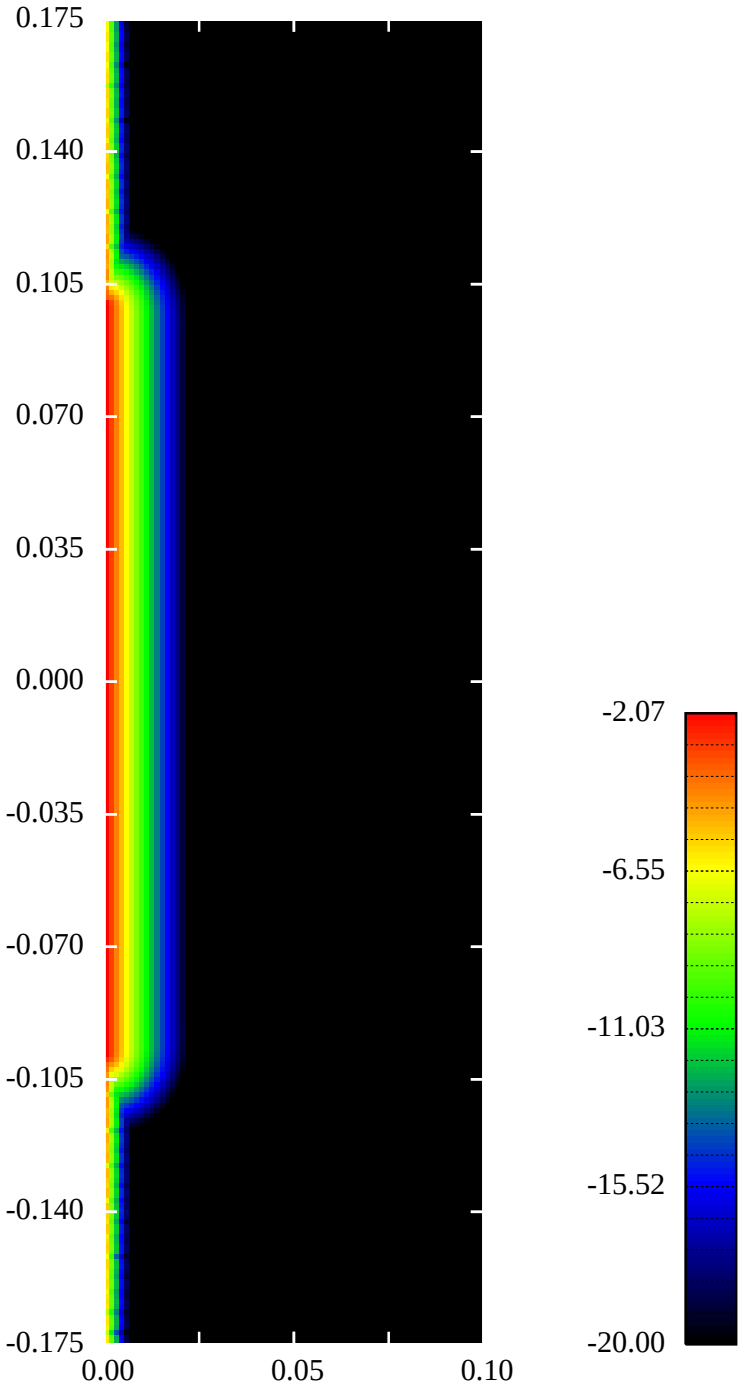

Figure 6.23: Opto-thermal transfer function: $f = 1$ Hz,, case of a flat beam, $b = 10$ cm

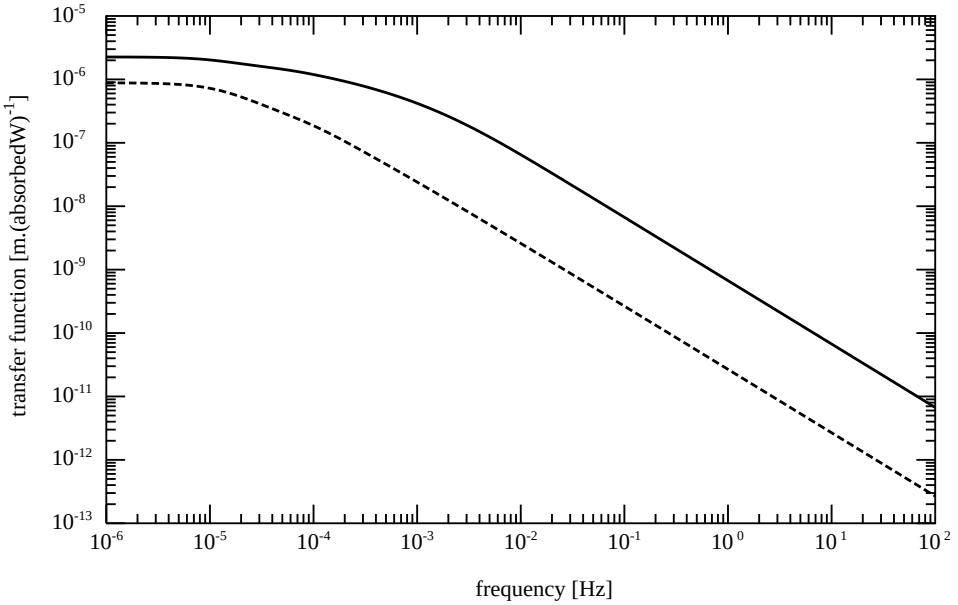

Figure 6.24: Opto-thermal transfer function. Solid line: gaussian beam, w = 2 cm. Dashed line: flat beam, b = 10 cm

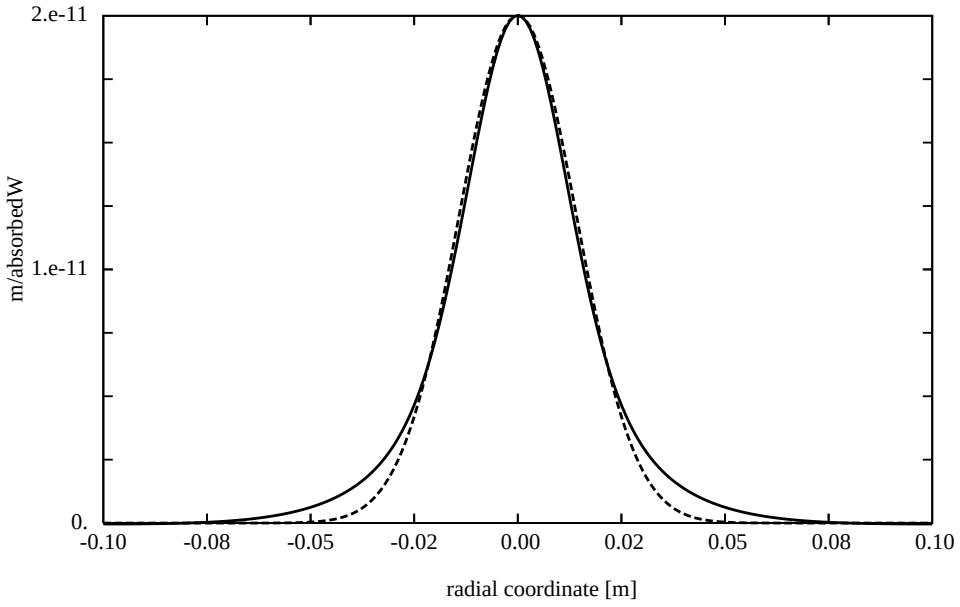

Figure 6.25: Bulk absorption. Surface distortion at 1 Hz for a gaussian beam of width $w = 2$ cm. Solid line: asymptotic solution. Dashed line: intensity profile for comparison

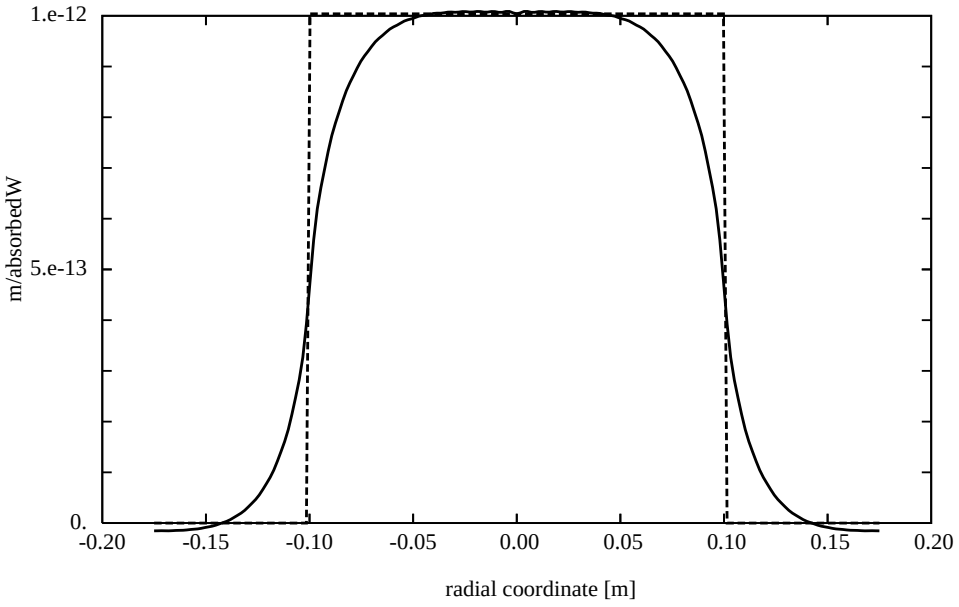

Figure 6.26: Bulk absorption. Surface distortion at 1 Hz for a flat beam of radius $b = 10$ cm. Solid line: asymptotic solution. Dashed line: intensity profile for comparison

Chapter 7

Mirrors standard thermal noise

standard thermal noise is the phase noise caused by random motions of the reflecting faces of mirrors in a GW interferometer. A reflecting face can move either because it is displaced by its suspension system, or because it undergoes internal stresses. At finite temperature, the two effects are possible. We address here the internal stresses. Consider a massive body at temperature T. If $T > 0$, the atoms constituting the body are excited and have random motions around their equibrium position. The fact that they are strongly coupled to neighboring atoms makes possible propagation of elastic waves of various types, reflecting on the faces and the onset of stationary waves. One can show that, for a finite body (like for instance a cylinder of silica), there is a discrete infinity of such stationary waves, each corresponding to a particular elastic *normal mode*. At thermal equilibrium, the state of the body can be represented by a linear superposition of all the modes, with random relative phases, and, due to the energy equipartition theorem, the same energy $k_B T$ (k_B is the Boltzmann constant). The motion of atoms near a limiting surface of the body will slightly modify its shape, and if we consider the reflecting face of a mirror, a surface distortion is a possible cause of phase change in the reflected beam, in other words, of a noise. Estimation of the resulting spectral density of phase noise is the *internal thermal noise* problem in massive mirrors.

7.1 Damped harmonic oscillator

Each internal mode is characterized by its eigenfrequency, its geometry and its amplitude. Determination of the eigenfrequencies and of the eigenmodes of an arbitrary body is in general difficult, but the amplitude is a scalar x obeying a dynamical equation analogous to the harmonic oscillator's. If we consider the decoupled and undamped oscillator, this is :

$$\frac{d^2x}{dt^2} + \omega_0^2 x \;=\; 0$$

where $\omega_0/2\pi$ is the eigenfrequency of the mode. At thermal equilibrium with the environment (the heat bath), the amplitude follows a random walk so that the potential and kinetic energies have equal means, each being equal to $k_BT/2$ ($k_B \sim 1.38 \times 10^{-23}$J.K^{-1} is the Boltzmann constant). For the potential energy, we have

$$E_P \;=\; \frac{1}{2} m\omega_0^2 x^2$$

by taking the expectation value, and assuming a zero mean of x, this gives

$$V(x) \;=\; \frac{k_BT}{m\omega_0^2}$$

It is important to understand that though very small, the displacement-like variable x is, at room temperature much larger than GW induced ($x_{gw} \sim 10^{-18}$ m) displacements. Assume for instance a frequency of $2\pi \times 1000$ Hz and an equivalent mass of 10 kg (in fact the masses equivalent to modes are even smaller), we get a standard deviation

$$\sigma(x) \;=\; 3 \times 10^{-15} \text{ m}$$

At first sight, this seems to definitely forbid any GW detection. Even by cooling at very low temperature (say 1 mK), the result is still much too high.

In fact and fortunately, this is not true if we take into account the frequency distribution of the noise. If we introduce simultaneously a random driving force (Langevin force) $F(t)$ and a damping factor γ accounting for dissipation, we couple the oscillator to the heat bath : the driving force expresses action of the external world on the oscillator, whereas the damping factor releases the received energy, so that the energy of the oscillator is statistically stationary. The motion equation is (case of viscous damping) :

$$\frac{d^2x}{dt^2} + \gamma\,\frac{dx}{dt} + \omega_0^2\, x \;=\; F(t)/m$$

By taking the Fourier transform, this is

$$\tilde{x}(\omega) \;=\; \frac{1}{m}\,\frac{\tilde{F}(\omega)}{\omega_0^2-\omega^2+i\gamma\,\omega}$$

The relation between the spectral densities of x and F must therefore be :

$$S_x(f) \;=\; S_F(f)\,\frac{1}{m^2}\,\frac{1}{(\omega^2-\omega_0^2)^2+\gamma^2\omega^2}$$

S_F is a constant (white noise) , its value can be determined by requiring that

$$\int_0^\infty S_x(f)\,df \;=\; V(x) \;=\; \frac{k_BT}{m\omega_0^2}$$

We have obviously

$$\int_0^\infty S_x(f)\,df \;=\; \frac{1}{2}\int_{-\infty}^\infty S_x(\omega)\,\frac{d\omega}{2\pi}$$

so that

$$S_F\int_{-\infty}^\infty \frac{d\omega}{(\omega^2-\omega_0^2)^2+\gamma^2\omega^2} \;=\; \frac{4\pi k_BTm}{\omega_0^2}$$

For carrying out the integration, it is convenient to set

$$(\omega^2-\omega_0^2)^2+\gamma^2\omega^2=(\omega^2-\Omega^2)(\omega^2-\overline{\Omega}^2)$$

where

$$\Omega^2=\omega_0^2-\gamma^2/2+i\,\gamma\sqrt{\omega_0^2-\gamma^2/4}$$

so that

$$\Omega \;=\; \sqrt{\omega_0^2-\gamma^2/4}+i\,\gamma/2$$

then the integral can be split into two terms, giving

$$S_F\int_{-\infty}^\infty\left[\frac{1}{\omega^2-\Omega^2}-\frac{1}{\omega^2-\overline{\Omega}^2}\right]\frac{d\omega}{\Omega^2-\overline{\Omega}^2} \;=\; \frac{4\pi k_BTm}{\omega_0^2}$$

The Cauchy theorem gives (provided that $\gamma>0$) :

$$\int_{-\infty}^\infty \frac{d\omega}{\omega^2-\Omega^2} \;=\; \frac{i\pi}{\Omega}$$

so that the integral reduces to $\pi/\gamma\omega_0^2$, and the result for the spectral density of Langevin force is:

$$S_F = 4k_BTm\gamma$$

The spectral density of displacement is finally:

$$S_x(f) = \frac{4k_BT\gamma/m}{(\omega^2-\omega_0^2)^2+\gamma^2\omega^2} \tag{7.1}$$

The mechanical *quality factor* Q is defined as

$$Q = \omega_0/\gamma \tag{7.2}$$

The main features are:

$$\omega \to 0 \Rightarrow S_x(f) \to \frac{4k_BT}{mQ\omega_0^3}$$

$$\omega \to \omega_0 \Rightarrow S_x(f) \to \frac{4k_BQ}{m\omega_0^3}$$

$$\omega \to \infty \Rightarrow S_x(f) \to \frac{4k_BT\omega_0}{mQ\omega^4}$$

so that the spectral density is a constant for low frequencies, and the root spectral density is $1/Q$ the value at resonance. On Fig.7.1, one sees the general philosophy of thermal noise. The integral of the spectral density S_x is independent on Q, but by increasing Q, we can concentrate the SD in the neighborhood of the resonance, which becomes more and more narrow, and reduce the thermal noise outside the resonance. This is why high-Q material and fixations are searched for, in GW experiments. Heavy test masses and low temperatures have been also obviously proposed a number of times.

7.2 The FD theorem

There is a more general derivation of the spectral density, based on the *Fluctuation-Dissipation Theorem* (FD), due to Callen and Welton [25] : For an elementary dynamical system described by a degree of freedom x and any driving force F, one can consider the resulting velocity $\tilde{v} = i\omega\tilde{x}$, and compute a mechanical impedance as $Z = \tilde{v}/\tilde{F}$. Then, (this is the FD theorem):

$$S_x(f) = \frac{4k_BT}{\omega^2}\Re e[Z] \tag{7.3}$$

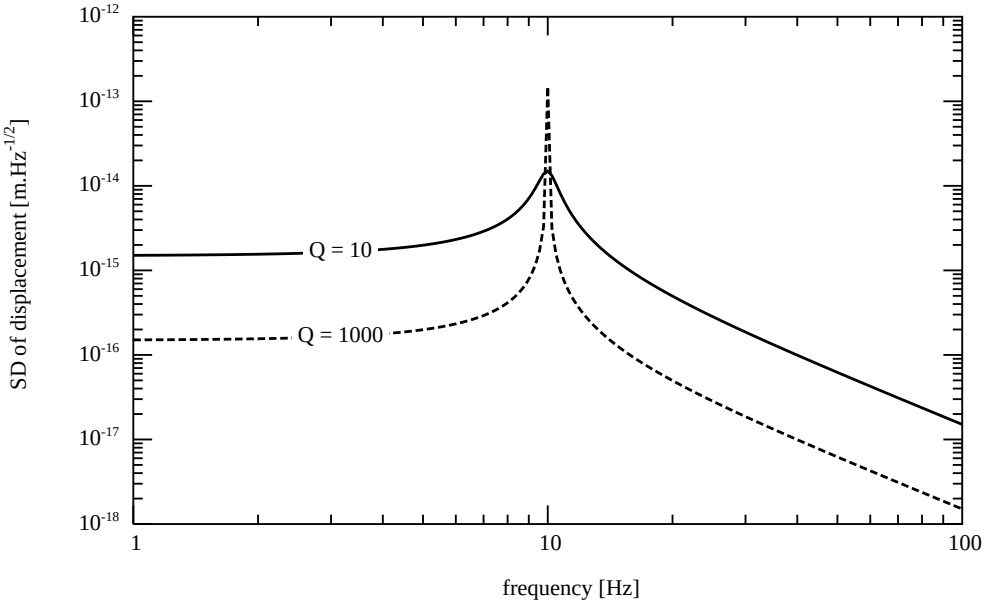

Figure 7.1: sqrt of spectral density of thermal displacement : viscous damping

In the preceding case, for instance, we had

$$Z(\omega) \;=\; \frac{i\,\omega/m}{\omega_0^2 - \omega^2 + i\,\gamma\omega}$$

from where 7.1 follows directly. But this approach allows to obtain results more difficult to derive by other means. For instance, if we consider a solid resonator, as for instance a mirror substrate, dissipation of the elastic energy is not caused by viscosity, but rather by thermoelastic processes: stressed regions are heated, and there is a heat flow from hot to cold regions due to finite thermal consuctivity leading to irreversibility. A very simple model of thermoelastic dissipation is given by a complex elastic stiffness, the motion equation being in some frequency domain:

$$\left[-\omega^2 + \omega_0^2\,(1 + i\Phi)\right]\,\tilde{x}(\omega) \;=\; \tilde{F}/m$$

where Φ is the so-called loss angle, often considered as independent on the frequency. It may be seen as the inverse of the quality factor. We have thus:

$$\tilde{x}(\omega) = \frac{\tilde{F}/m}{\omega_0^2 - \omega^2 + i\Phi\omega_0^2} \tag{7.4}$$

In order to determine the function F, we can no more use the direct approach of integrating over frequencies to recover the variance, because we know that the eq. 7.4 is only valid in some frequency domain. However, by using the FD theorem (eq.7.3), we get

$$S_x(f) = \frac{4k_BT\omega_0^2\Phi}{m\omega} \frac{1}{(\omega^2 - \omega_0^2)^2 + \omega_0^4\,\Phi^2}$$

This formula clearly holds above some cut-off frequency. It is essential to note the very different behavior of this thermoelastic spectral density with respect to the viscoelastic.

$$\omega \to 0 \;\Rightarrow\; S_x(f) \to \frac{4k_BT}{mQ\omega\omega_0^2}$$

$$\omega \to \omega_0 \;\Rightarrow\; S_x(f) \to \frac{4k_BQ}{m\omega_0^3}$$

$$\omega \to \infty \;\Rightarrow\; S_x(f) \to \frac{4k_BT\omega_0^2}{mQ\omega^5}$$

(see Fig.7.2) This is a common behavior for all internal modes of solid resonators, each being viewed as a thermoelastically damped harmonic oscillator. It is possible to numerically compute resonance frequencies of a cylindrical solid (as the mirror substrates), associate such a model to each corresponding mode (the question of the effective mass of the mode is raised), and sum up to find the global noise. Anyway, the increase of the thermal noise at low frequency is presently the main limitation to GW detectors.

7.3 The Levin generalized coordinate method

We can now address the problem of internal degrees of freedom in the mirrors. Internal elastic waves eventually distort the reflecting surface, causing a phase noise. We have already discussed the way of obtaining the information on

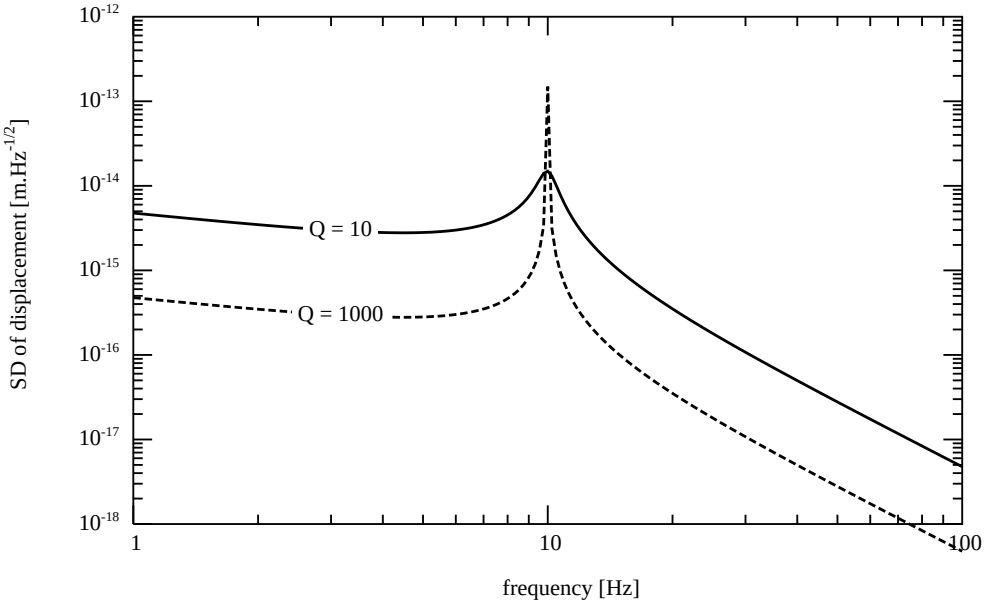

Figure 7.2: sqrt of spectral density of thermal displacement : thermoelastic damping

the surface relevant for the beam. Let $u_z(t,x,y)$ be the z component of the displacement vector of matter at the surface of the mirror. The equivalent displacement (generalized coordinate x) is

$$x(t) \;=\; \iint u_z(t,x,y)\, I(x,y)\, dx\, dy$$

where $I(x,y)$ is the normalized light intensity distribution in the TEM_{00} mode assumed to be the readout beam. We now follow the method proposed by Levin ([24]). Let $F(t)$ be the corresponding driving force. The interaction energy is

$$\mathcal{E} \;=\; -F(t)\, x(t)$$

or

$$\mathcal{E} \;=\; \iint u_z(t,x,y)\, F(t)\, I(x,y)\, dx\, dy$$

where the displacement u may be thought of as beeing caused by the pressure distribution $F \times I$. We address now the case of low frequencies. This case is

very relevant, because resonances of mirrors are at relatively high frequencies (several kHz) and the region where internal thermal noise is disturbing lies long before the first resonance, in the low frequency regime. Thus, although a general knowledge on internal thermal noise is useful, it is nevertheless extremely interesting to have the low frequency tail. This can be obtained as follows. If we consider a force $F(t) = F\mathrm{e}^{i\omega t}$ oscillating at very low frequency, the frequency will be lower than the cut-off for any standing waves. the pressure $F \times I$ will produce an oscillating stationary displacement u, of the form

$$u_z(t,x,y) = \mathrm{e}^{i(\omega t - \phi)} u(x,y)$$

this is equivalent to neglecting inertial forces in the motion of matter. The phase ϕ represents a retardation effect that dissipation may cause. In the Fourier domain, this is

$$u_z(\omega,x,y) \;=\; (1 - i\phi) u_z(x,y)$$

the impedance is

$$Z(f) \;=\; i\omega \, \frac{(1-i\phi) \int\int u_z(x,y)\, I(x,y)\, dx\, dy}{F}$$

so that

$$\Re e[Z] \;=\; \omega\, \phi \, \frac{\int\int u_z(x,y)\, F.I(x,y)\, dx\, dy}{F^2}$$

where the numerator of the fraction appears as the elastic energy stored in the solid stressed by the pressure distribution $F.I$. The strain energy is defined in classical elasticity theory by

$$W \;=\; \frac{1}{2} \int\int u_z(x,y) p(x,y)\, dx\, dy$$

where $p(x,y)$ is the pressure distribution causing the displacement $u_z(x,y)$ at the surface where it is applied. We can thus write for the spectral density of displacement :

$$S_x(f) \;=\; \frac{4k_B T}{\pi f}\, \phi\, \frac{W}{F^2}$$

in fact, W is proportional to F^2, so that $U \equiv W/F^2$ is the strain energy for a static pressure normalized to 1 N. The SD of displacement takes the general (low frequency) form :

$$S_x(f) \;=\; \frac{4k_B T}{\pi f}\, \phi\, U \tag{7.5}$$

The problem is reduced to the computation of U. This can be difficult in the general case of an arbitrary solid, but numerical finite element codes are able to give more or less accurate estimates. It is however possible to obtain analytic solutions in the case of axial symmetry.

7.4 Basic linear elasticity

We recall here the principles and master formulas of the linear elasticity theory.

7.4.1 displacement, strain, stress

Let a solid be decribed in the (x,y,z) coordinate system by its reference state, and its deformed state

$$x_i \to x_i + u_i(x_k)$$

The vector **u** is called *displacement* vector. The strain tensor E_{ij} is defined as

$$E_{ij} = \frac{1}{2}(\partial_i u_j + \partial_j u_i)$$

Its trace is

$$E = \sum_{i=1}^{3} E_{ii}$$

The stress tensor Θ_{ij} is linearly related to the strain tensor in a way generalizing Hooke's law. For isotropic solids (like silica), the relation is very simple :

$$\Theta_{ij} = \lambda \, \delta_{ij} E + 2\mu \, E_{ij}$$

the two parameters (λ, μ) are called Lamé coefficients. They are related to the Young modulus Y and the Poisson ratio σ by

$$\lambda = \frac{Y\sigma}{(1+\sigma)(1-2\sigma)}$$

$$\mu = \frac{Y}{2(1+\sigma)}$$

7.4.2 Elastodynamics equation

The elastodynamics equation is :

$$\partial_j \Theta_{ij} \;=\; \rho\, \partial_t^2 u_i$$

which in the static case reduces to the equilibrium equation

$$\partial_j \Theta_{ij} \;=\; 0$$

In polar coordinates (r, ϕ, z), the strain tensor has coordinates

$$E_{rr},\ E_{r\phi},\ E_{rz},\ E_{\phi\phi},\ E_{z\phi},\ E_{zz}$$

defined by :

$$\begin{aligned}
E_{rr} &= \partial_r u_r \\
E_{r\phi} &= \frac{1}{2}\left(\partial_r u_\phi - \frac{u_\phi}{r} + \frac{1}{r}\,\partial_\phi u_r\right) \\
E_{rz} &= \frac{1}{2}\left(\partial_r u_z + \partial_z u_r\right) \\
E_{\phi\phi} &= \frac{1}{r}\partial_\phi u_\phi + \frac{u_r}{r} \\
E_{z\phi} &= \frac{1}{2}\left(\frac{1}{r}\partial_\phi u_z + \partial_z u_\phi\right) \\
E_{zz} &= \partial_z u_z
\end{aligned}$$

The elastodynamics equation reads in detail

$$\left\{\begin{array}{l}
\partial_r \Theta_{rr} + \frac{1}{r}\left(\Theta_{rr} - \Theta_{\phi\phi}\right) + \frac{1}{r}\partial_\phi \Theta_{r\phi} + \partial_z \Theta_{rz} \;=\; \rho\, \partial_t^2 u_r \\
(\partial_r + \frac{2}{r})\Theta_{r\phi} + \frac{1}{r}\partial_\phi \Theta_{\phi\phi} + \partial_z \Theta_{\phi z} \;=\; \rho\, \partial_t^2 u_\phi \\
(\partial_r + \frac{1}{r})\Theta_{rz} + \frac{1}{r}\partial_\phi \Theta_{\phi z} + \partial_z \Theta_{zz} \;=\; \rho\, \partial_t^2 u_z
\end{array}\right. \tag{7.6}$$

In the special case of static axial symmetry, the system reduces to the *equilibrium* equation :

$$\left\{\begin{array}{l}
\partial_r \Theta_{rr} + \frac{1}{r}\left(\Theta_{rr} - \Theta_{\phi\phi}\right) + \partial_z \Theta_{rz} \;=\; 0 \\
(\partial_r + \frac{1}{r})\Theta_{rz} + \partial_z \Theta_{zz} \;=\; 0
\end{array}\right. \tag{7.7}$$

7.4.3 Boundary conditions

The boundary conditions express the balance between internal stresses and external pressures at the limiting surfaces :

$$[\sum_j \Theta_{ij} n_j]_\Sigma \;=\; p_i$$

where n_i is the normal to surface Σ

7.5 Mirror as a half-space

If the spot of the readout beam on a mirror is centered and small compared to the mirror's dimensions (radius, thickness), we can consider the substrate as an infinite half-space limited by a plane (the optical curvature is negligible here). The problem obeys the axial symmetry and it is easy to verify that there is a solution of 7.7 of the form :

$$u_r(r,z) \;=\; \left(\alpha - \frac{\lambda+2\mu}{\lambda+\mu}\,\beta + \beta\, kz\right)\, \mathrm{e}^{-kz} J_1(kr)$$

$$u_z(r,z) \;=\; \left(\alpha + \frac{\mu}{\lambda+\mu}\,\beta + \beta\, kz\right)\, \mathrm{e}^{-kz} J_0(kr)$$

where (α, β, k) are arbitrary constants. The J_n are the Bessel functions. The region occupied by the substrate is supposed to extend from $z = 0$ till infinity. The boundary conditions are

$$[\Theta_{rz}]_{z=0} \;=\; 0$$

and

$$[\Theta_{zz}]_{z=0} \;=\; p(r)$$

where $p(r)$ is the gaussian pressure having the beam's profile and normalized to 1 N (the integral over the whole plane of a pressure is a force):

$$p(r) \;=\; \frac{2}{\pi w^2} \mathrm{e}^{-2r^2/w^2}$$

It is easy to compute the stresses :

$$\Theta_{rz} \;=\; 2\mu\, k\, (\beta - \alpha - \beta\, kz) J_1(kr)$$

$$\Theta_{zz} \;=\; -2\mu\, k\,(\alpha + \beta\, kz) J_0(kr)$$

The first boundary condition gives $\alpha = \beta$. The solution depends now on two arbitrary constants $(\alpha,\, k)$. In fact the most general solution will be an integral over k :

$$u_r(r,z) \;=\; \int_0^\infty \alpha(k)\, \left(-\frac{\mu}{\lambda+\mu} + kz\right) \mathrm{e}^{-kz} J_1(kr) k\, dk$$

$$u_z(r,z) \;=\; \int_0^\infty \alpha(k)\, \left(\frac{\lambda+2\mu}{\lambda+\mu} + kz\right) \mathrm{e}^{-kz} J_0(kr) k\, dk$$

and now, $\alpha(k)$ refers to an arbitrary function of k. The Θ_{zz} stress component becomes :

$$\Theta_{zz}(r, z=0) \;=\; -2\mu \int_0^\infty \alpha(k) J_0(kr)\, k^2\, dk$$

so that the last boundary condition becomes

$$\int_0^\infty \alpha(k) J_0(kr)\, k^2\, dk \;=\; -\frac{1}{2\mu}\, p(r) \tag{7.8}$$

This expresses a Bessel transform. Recall that for functions admitting a Fourier transform, the two reciprocal Fourier transforms become, for axially symmetrical functions, reciprocal Bessel transforms :

$$\tilde{f}(\rho) \;=\; \int_0^\infty J_0(\rho r) f(r)\, r\, dr$$

and

$$f(r) \;=\; \int_0^\infty J_0(\rho r) \tilde{f}(\rho)\, \rho\, d\rho$$

we have thus, inverting the Bessel transform in 7.8 :

$$k\alpha(k) \;=\; -\frac{1}{2\mu} \int_0^\infty p(r)\, J_0(kr)\, r\, dr$$

It is possible to carry out the integration (see [20], Eq. **11.4.29**), obtaining

$$\alpha(k) \;=\; -\frac{1}{4\pi\mu k}\, \mathrm{e}^{-k^2 w^2/8}$$

and consequently a displacement

$$u_z(r, z=0) \;=\; -\frac{\lambda+2\mu}{\mu(\lambda+\mu)}\, \frac{1}{4\pi} \int_0^\infty \mathrm{e}^{-k^2 w^2/8}\, J_0(kr)\, dk \tag{7.9}$$

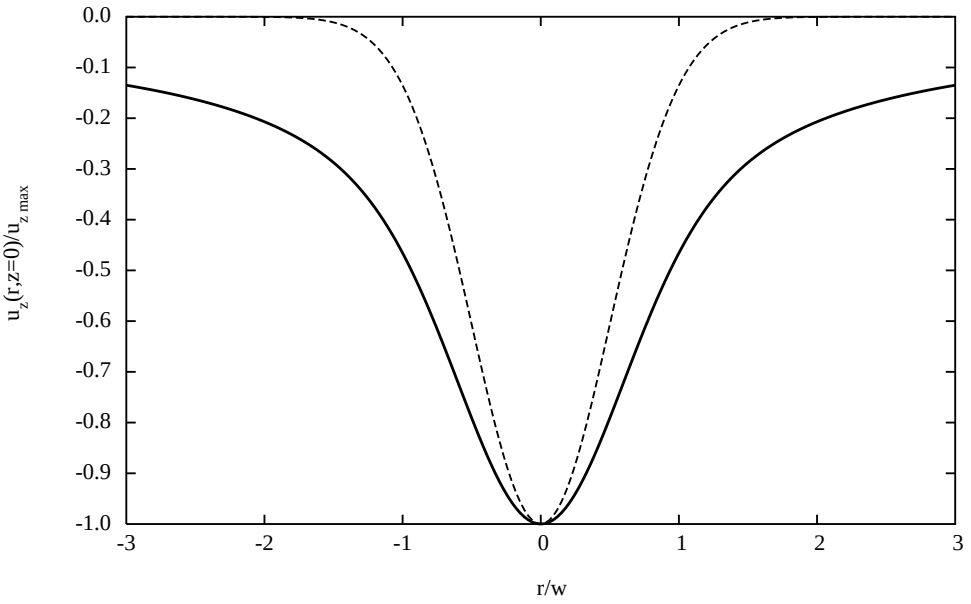

Figure 7.3: Displacement of the surface of an infinite substrate under gaussian pressure. The dashed line recalls the beam profile. The surface is assumed infinite (radius much larger than the beam width)

the integral can be found in tables of Bessel transforms [26], then converting (λ, μ) into (Y, σ) leads to :

$$u_z(r, z=0) \;=\; -\frac{1-\sigma^2}{Y}\sqrt{\frac{2}{\pi w^2}}\, I_0(r^2/w^2)\, \mathrm{e}^{-r^2/w^2}$$

where I_0 refers to the modified Bessel function. The profile of the displacement is shown in Fig.7.3. But we are interested in the strain energy, which can be calculated using

$$U \;=\; -\frac{1}{2}\int\int u_z(r, z=0)\, p(r)\, r\, dr\, d\phi$$

that is

$$U \;=\; \frac{1-\sigma^2}{Y}\,\frac{2}{\pi w^2}\int_0^\infty r\, dr\, \mathrm{e}^{-2r^2/w^2} \int_0^\infty dk\, \mathrm{e}^{-k^2 w^2/8} J_0(kr)$$

$$= \frac{1-\sigma^2}{Y}\frac{2}{\pi w^2}\int_0^\infty dk\,\mathrm{e}^{-k^2w^2/8}\int_0^\infty r\,dr\,\mathrm{e}^{-2r^2/w^2}\,J_0(kr)$$
$$= \frac{1-\sigma^2}{Y}\frac{2}{\pi w^2}\int_0^\infty dk\,\mathrm{e}^{-k^2w^2/8}\,\frac{w^2}{4}\,\mathrm{e}^{-k^2w^2/8}$$
$$= \frac{1-\sigma^2}{2\sqrt{\pi}Yw}$$

And finally, the spectral density of internal thermal noise takes the very simple expression

$$S_z(f) = \frac{4k_BT}{\pi f}\,\Phi\,\frac{1-\sigma^2}{2\sqrt{\pi}Yw} \tag{7.10}$$

with values such that $Y \sim 7.3\times10^{10}\mathrm{Nm}^{-2}$, $\sigma \sim 0.17$, $w = 0.02$ m, and a loss angle of $\Phi \sim 10^{-6}$, we get a root spectral density

$$S_z^{1/2}(f) \sim 10^{-18}\left[\frac{1\mathrm{Hz}}{f}\right]^{1/2}\ \mathrm{m\,Hz}^{-1/2}$$

7.6 Finite mirrors

The preceding calculation does not allow to study the effect of the aspect ratio of the actual mirror on the spectral density of thermal noise. We propose here an approximate model for a cylindrical mirror having a radius a and a thickness h. This model has been published in the BHV paper [33] with one wrong boundary condition. Then Yuk Tung Liu et al. (YT) have derived a correction to the BHV result.

7.6.1 A solution to the equilibrium equations

We consider a cylindrical mirror limited by:

$$0 \le r \le a, \quad 0 \le z \le h$$

The reflecting face is assumed at $z = 0$ In the case of a finite solid, we expect the displacement vector to be a discrete sum of Bessel modes, of the form:

$$\begin{cases} u_r(r,z) = \sum_m A_m(z)J_1(k_mr) \\ u_\phi(r,z) = 0 \\ u_z(r,z) = \sum_m B_m(z)J_0(k_mr) \end{cases} \tag{7.11}$$

Where A_m, B_m are arbitrary functions of z, and k_m arbitrary constants. The equilibrium equations however imply for each order:

$$\begin{cases} \mu(A''_m - k_m^2 A_m) - (\lambda+\mu)k_m(B'_m + k_m A_m) &= 0 \\ \mu(B''_m - k_m^2 B_m) + (\lambda+\mu)(B''_m + k_m A'_m) &= 0 \end{cases} \tag{7.12}$$

so that by combining the two, we get:

$$[\partial_z^2 - k_m^2](A'_m + k_m B_m) = 0$$

the solution of which is:

$$A'_m + k_m B_m = k_m \left(\alpha_m \mathrm{e}^{-k_m z} + \beta_m \mathrm{e}^{k_m z}\right)$$

where α_m, β_m are arbitrary constants. This allows to substitute B_m in the first of eq.7.12, and yields:

$$A''_m - k_m^2 A_m = -\frac{\lambda+\mu}{\lambda+2\mu} k_m^2 \left(\alpha_m \mathrm{e}^{-k_m z} - \beta_m \mathrm{e}^{k_m z}\right)$$

the solution of which is:

$$A_m(z) = \gamma_m \mathrm{e}^{-k_m z} + \delta_m \mathrm{e}^{k_m z} + \frac{\lambda+\mu}{2(\lambda+2\mu)} k_m z \left(\alpha_m \mathrm{e}^{-k_m z} + \beta_m \mathrm{e}^{k_m z}\right) \tag{7.13}$$

introducing two new series (γ_m, δ_m) of arbitrary constants. Now B_m is determined:

$$\begin{aligned} B_m(z) = &\left(\frac{\lambda+3\mu}{2(\lambda+2\mu)}\alpha_m + \gamma_m\right)\mathrm{e}^{-k_m z} + \left(\frac{\lambda+3\mu}{2(\lambda+2\mu)}\beta_m - \delta_m\right)\mathrm{e}^{k_m z} + \\ &+ \frac{\lambda+\mu}{2(\lambda+2\mu)} k_m z \left(\alpha_m \mathrm{e}^{-k_m z} - \beta_m \mathrm{e}^{k_m z}\right) \end{aligned} \tag{7.14}$$

The stress tensor has the following non zero components of order m:

$$\begin{cases} \Theta_{m,rr} &= \lambda(B'_m + k_m A_m)J_0(k_m r) + 2\mu k_m A_m J'_1(k_m r) \\ \Theta_{m,\phi\phi} &= \lambda(B'_m + k_m A_m)J_0(k_m r) + +2\mu\frac{A_m}{r}J_1(k_m r) \\ \Theta_{m,zz} &= [(\lambda+2\mu)B'_m + \lambda k_m A_m]\, J_0(k_m r) \\ \Theta_{m,rz} &= \mu(A'_m - k_m B_m)J_1(k_m r) \end{cases} \tag{7.15}$$

7.6.2 Boundary conditions

The boundary conditions we assume are:

- No shear on the cylindrical edge, i.e.

$$\Theta_{rz}(r = a, z) \;=\; 0$$

  this can be satisfied by requiring that $k_m a$ is a zero of J_1

$$k_m \equiv \zeta_m / a$$

  where the ζ_m are the strictly positive zeros of J_1.

- No shear on the two circular faces, i.e.

$$\Theta_{rz}(r, z = 0) \;=\; 0, \quad \Theta_{rz}(r, z = h) \;=\; 0 \tag{7.16}$$

- Pressure of the beam on the first face:

$$\Theta_{zz}(r, z = 0) \;=\; -p(r) \tag{7.17}$$

- No pressure on the second face:

$$\Theta_{zz}(r, z = h) \;=\; 0 \tag{7.18}$$

- No radial stress on the cylindrical edge:

$$\Theta_{rr}(r = a, z) \;=\; 0 \tag{7.19}$$

To the preceding constraints, Yuk Tung Liu et al. have pointed out that the pressure acting on the face $z = h$ results in a global force accelerating the solid, so that an acceleration field must be added to the equilibrium equations. This will be treated later. Now the pressure distribution can be expanded on the orthogonal family of functions $J_0(\zeta_m r/a)$:

$$p(r) \;=\; p_0 \sum_m p_m J_0(\zeta_m r/a)$$

where $p_0 \;=\; 1/\pi a^2$ is a normalisation constant such that the p_m are dimensionless. The orthogonality relations are:

$$\int_0^a J_0(\zeta_m r/a) J_0(\zeta_n r/a)\, r\, dr \;=\; \frac{1}{2} a^2 J_0^2(\zeta_m)$$

so that the p_m are obtained as:

$$p_m = \frac{2\pi}{J_0^2(\zeta_m)} \int_0^a p(r) J_0(\zeta_m r/a)\, r\, dr \tag{7.20}$$

The Θ_{rz} and Θ_{zz} components of the stress tensor are easily found from A_m and B_m:

$$\Theta_{m,rz}/k_m\mu = \left(2\delta_m - \frac{\mu}{\lambda+2\mu}\beta_m\right) \mathrm{e}^{k_m z} - \left(2\gamma_m + \frac{\mu}{\lambda+2\mu}\alpha_m\right) \mathrm{e}^{-k_m z} +$$

$$-\frac{\lambda+\mu}{\lambda+2\mu} k_m z \left(\alpha_m \mathrm{e}^{-k_m z} - \beta_m \mathrm{e}^{k_m z}\right) \tag{7.21}$$

and

$$\Theta_{m,zz}/k_m\mu = (\beta_m - 2\delta_m)\mathrm{e}^{k_m z} - (\alpha_m + 2\gamma_m)\mathrm{e}^{-k_m z} -$$

$$-\frac{\lambda+\mu}{\lambda+2\mu} k_m z \left(\alpha_m \mathrm{e}^{-k_m z} + \beta_m \mathrm{e}^{k_m z}\right) \tag{7.22}$$

The boundary conditions provide 4 equations. The two first are:

$$\beta_m - 2\delta_m - \alpha_m - 2\gamma_m = -p_m/k_m\mu \tag{7.23}$$

and

$$2\delta_m - \frac{\mu}{\lambda+2\mu}\beta_m - 2\gamma_m - \frac{\mu}{\lambda+2\mu}\alpha_m = 0 \tag{7.24}$$

They allow to compute γ_m and δ_m in terms of α_m, β_m:

$$\gamma_m = \frac{1}{4}\left[\frac{\lambda+\mu}{\lambda+2\mu}\beta_m - \frac{\lambda+3\mu}{\lambda+2\mu}\alpha_m + \frac{p_m}{k_m\mu}\right]$$

$$\delta_m = \frac{1}{4}\left[\frac{\lambda+3\mu}{\lambda+2\mu}\beta_m - \frac{\lambda+\mu}{\lambda+2\mu}\alpha_m + \frac{p_m}{k_m\mu}\right]$$

The next two boundary conditions imply:

$$\left[2\delta_m - \frac{\mu}{\lambda+2\mu}\beta_m\right] \mathrm{e}^{k_m h} - \left[2\gamma_m + \frac{\mu}{\lambda+2\mu}\alpha_m\right] \mathrm{e}^{-k_m h} +$$

$$+k_m h \frac{\lambda+\mu}{\lambda+2\mu}\left[\beta_m \mathrm{e}^{k_m h} - \alpha_m \mathrm{e}^{-k_m h}\right] = 0$$

and

$$(\beta_m - 2\delta_m)\mathrm{e}^{k_m h} - (\alpha_m + 2\gamma_m)\mathrm{e}^{-k_m h} - \frac{\lambda+\mu}{\lambda+2\mu} k_m h \left[\beta_m \mathrm{e}^{k_m h} + \alpha_m \mathrm{e}^{-k_m h}\right] = 0$$

by substituting the values found for γ_m, δ_m, we find

$$\alpha_m = p_0 \frac{p_m(\lambda+2\mu)}{k_m \mu(\lambda+\mu)} \frac{1 - q_m + 2q_m x_m}{(1-q_m)^2 - 4q_m x_m^2} \tag{7.25}$$

$$\beta_m = p_0 \frac{p_m(\lambda+2\mu)}{k_m \mu(\lambda+\mu)} \frac{q_m(1 - q_m + 2x_m)}{(1-q_m)^2 - 4q_m x_m^2} \tag{7.26}$$

then

$$\gamma_m = -p_0 \frac{p_m}{2k_m \mu} \frac{2q_m x_m^2 + \frac{\mu}{\lambda+\mu}(1 - q_m + 2q_m x_m)}{(1-q_m)^2 - 4q_m x_m^2} \tag{7.27}$$

$$\delta_m = -p_0 \frac{p_m q_m}{2k_m \mu} \frac{2x_m^2 - \frac{\mu}{\lambda+\mu}(1 - q_m + 2x_m)}{(1-q_m)^2 - 4q_m x_m^2} \tag{7.28}$$

with the notation $x_m \equiv k_m h$ and $q_m \equiv \exp(-2x_m)$. At this point, YT pointed out that the component of spatial frequency zero of the pressure has not been taken into account. Because the series involves only strictly positive zeros of J_1, the preceding displacement has a zero average on the strained face. One must consider the resulting force acting on the body under the uniform pressure

$$p_0 = 1/\pi a^2$$

producing a force of 1 N after integration on the disk. But this force produces an acceleration, so that an acceleration field should be added in the equilibrium equations (recall that our mirrors are practically free falling in the z direction). This can be done by adding to the preceding displacement an extra displacement of the form:

$$\begin{cases} \delta u_r(r,z) = \frac{\lambda p_0 r}{2\mu(3\lambda+2\mu)}(1 - z/h) \\ \delta u_\phi(r,z) = 0 \\ \delta u_z(r,z) = \frac{\lambda p_0 r^2}{4\mu h(3\lambda+2\mu)} - \frac{(\lambda+\mu)p_0}{\mu(3\lambda+2\mu)}(z - z^2/2h) \end{cases} \tag{7.29}$$

This extra displacement contributes only the axial stress:

$$\delta\Theta_{zz} = -p_0(1 - z/h)$$

all other stress components are identically zero. The equilibrium equations remain satisfied:

$$\partial_z \delta\Theta_{zz} \;=\; p_0/h \;=\; \rho \times \frac{1N}{\rho\pi a^2 h} \;=\; \rho \times (1\,N)/M \;=\; \rho\ddot{z}$$

where M is the mirror mass and ρ the density. Now the sum of the displacement 7.11 and the extra displacement 7.28 satisfies all boundary conditions, except the vanishing of the radial stress on the cylindrical edge. We have indeed

$$\Theta_{m,rr}(r=a,z) \;=\; \lambda(k_m A_m(z) + B'_m(z))J_0(\zeta_m) + 2\mu k_m A_m(z) J'_1(\zeta_m)$$

but due to the fact that $J'_1(\zeta_m) = J_0(\zeta_m)$, and after substituting the explicit values of A_m and B_m, we get

$$\begin{aligned}\Theta_{m,rr}(r=a,z) \;=\; p_0 \frac{J_0(\zeta_m)p_m}{(1-q_m)^2 - 4q_m x_m^2}\Big[&(1-q_m+2q_m x_m(1+x_m))\,\mathrm{e}^{-k_m z} - \\ &-q_m\,(1-q_m+2x_m(1-x_m))\,\mathrm{e}^{k_m z} - \\ &-k_m z q_m(1-q_m+2x_m)\mathrm{e}^{k_m z} - k_m z(1-q_m+2q_m x_m)\mathrm{e}^{-k_m z}\Big]\end{aligned} \tag{7.30}$$

It is numerically easy to check that this function of z is not very different from linear. It has even a vanishing average. It is therefore possible to find an approximate solution of the problem by using the De Saint-Venant principle: If we add to our displacement vector one more extra displacement giving a linear stress with suitable parameters, we compensate for the mean stress and torque on the edge, and the resulting solution is very accurate everywhere in the body, except maybe in the neighborhood of the edge, where the strain energy is likely weak. The second extra displacement is of the form:

$$\begin{cases} \Delta u_r(r,z) \;=\; \frac{\lambda+2\mu}{2\mu(3\lambda+2\mu)}(c_0 r + c_1 r z) \\ \Delta u_\phi(r,z) \;=\; 0 \\ \Delta u_z(r,z) \;=\; -\frac{\lambda}{\mu(3\lambda+2\mu)}(c_0 z + c_1 z^2/2) - \frac{\lambda+2\mu}{4\mu(3\lambda+2\mu)} c_1 r^2 \end{cases} \tag{7.31}$$

This displacement induces zero stresses, and thus leaves unchanged the boundary conditions, except for a radial contribution:

$$\Delta\Theta_{rr}(z) \;=\; c_0 + c_1 z$$

This linear stress can be adjusted to compensate for the first moments of the residual stress $\Theta_{rr}(r=a,z)$. We require for instance a minimum value for the integral

$$\int_0^h \left[\Theta_{rr}(r=a,z)+\Delta\Theta_{rr}(z)\right]^2 dz$$

If we define

$$I_0 = \frac{1}{h}\int_0^h \Theta_{rr}(r=a,z)dz$$

$$I_1 = \frac{1}{h^2}\int_0^h \Theta_{rr}(r=a,z)z\,dz$$

we have the values of c_0, c_1:

$$c_0 = 6I_1-4I_0, \quad c_1 = 6(I_0-2I_1)/h$$

The explicit expression of $\Theta_{rr}(r=a,z)$ (eq.7.30) allows to compute I_0, I_1. Firstly, one finds $I_0 = 0.$ and secondly

$$I_{1,m} = p_0\, J_0(\zeta_m)p_m/k_m^2h^2$$

so that

$$I_1 = p_0 \times s$$

where

$$s = \frac{a^2}{h^2}\sum_m \frac{p_m J_0(\zeta_m)}{\zeta_m^2}$$

then

$$c_0 = 6sp_0, \quad c_1 = -12sp_0/h$$

7.6.3 Strain Energy

The global displacement vector has the form

$$\begin{cases} u_r(r,z) &= \sum_m A_m(z)J_1(\zeta_m r/a)+Pr+Qrz \\ u_\phi(r,z) &= 0 \\ u_z(r,z) &= \sum_m B_m(z)J_0(\zeta_m r/a)+Wr^2+Tz+Sz^2 \end{cases}$$

where P,Q,W,T,S are known coefficients related to the two extra displacement terms defined above. The strain components are:

$$E_{rr}(r,z) = \sum_m k_m A_m(z)J_1'(\zeta_m r/a)+P+Qz$$

$$
\begin{aligned}
E_{\phi\phi}(r,z) &= \sum_m A_m(z)\frac{J_1(\zeta_m r/a)}{r} + P + Qz \\
E_{zz}(r,z) &= \sum_m B'_m(z) J_0(\zeta_m r/a) + T + 2Sz \\
E_{rz}(r,z) &= \sum_m \left(A'_m(z) - k_m B_m(z)\right) J_1(\zeta_m r/a)
\end{aligned}
$$

the trace of the strain tensor is thus:

$$
E(r,z) = \sum_m (B'_m(z) + k_m A_m(z))\, J_0(\zeta_m r/a) + 2P + T + 2(Q+S)z
$$

The strain energy per N^2(our target) is given by

$$
U = \int_0^{2\pi} d\phi \int_0^h dz \int_0^a r\, dr\, w(r,z)
$$

where the energy density w is defined as:

$$
w = \frac{1}{2}\left[\lambda E^2 + 2\mu\left(E_{rr}^2 + E_{\phi\phi}^2 + E_{zz}^2 + 2E_{rz}^2\right)\right] \tag{7.32}
$$

The squares of the stress components involve the squares of the main stresses, the squares of the extra stresses, plus crossed terms. It is possible to show that crossed terms vanish in the r integration. There is thus a perfect decoupling,and the extra terms in the displacement vector result in corrections to the global energy.

Main contribution to the strain energy

Now we can compute the main contribution. We recall the following integrals:

$$
\begin{aligned}
\int_0^a J_0(\zeta_m r/a) J_0(\zeta_m r/a) r\, dr &= \frac{a^2}{2} J_0^2(\zeta_m) \\
\int_0^a J_1(\zeta_m r/a) J_1(\zeta_m r/a) r\, dr &= \frac{a^2}{2} J_0^2(\zeta_m)
\end{aligned}
$$

For the Bessel modes contribution we have thus:

$$
U = \frac{\pi a^2}{2} \sum_m J_0(\zeta_m)^2 \int_0^h U_m(z)\, dz
$$

where

$$U_m = \lambda(B'_m + k_m A_m)^2 + 2\mu\left(k_m^2 A_m^2 + B_m'^2 + \frac{1}{2}(A'_m - k_m B_m)^2\right)$$

All the terms being known, the integration is straightforward, and the result is:

$$U = \frac{\pi a^3}{4}\frac{\lambda+2\mu}{\mu(\lambda+\mu)}\sum_m \frac{J_0^2(\zeta_m)p_m^2}{\zeta_m}\frac{1-q_m^2+4q_m x_m}{(1-q_m)^2-4q_m x_m^2}$$

or as well, using the Young modulus Y and the Poisson ratio σ instead of the Lamé coefficients:

$$U = \frac{1-\sigma^2}{\pi a Y}\sum_m \frac{J_0^2(\zeta_m)p_m^2}{\zeta_m}\frac{1-q_m^2+4q_m x_m}{(1-q_m)^2-4q_m x_m^2} \tag{7.33}$$

The dimension of U is J.N^{-2}.

Correction to strain energy

The contribution of the extra stresses to the strain energy is:

$$\Delta U = \int_0^{2\pi} d\phi \int_0^a r\,dr \int_0^h \Delta w(z) dz$$

where $\Delta w(z)$ is the extra density:

$$\Delta w(z) = \frac{1}{2}\left[\lambda\left(((2P+T+2(Q+S)z)^2 + 2\mu\left(2(P+Qz)^2 + (T+2Sz)^2\right)\right]\right.$$

The coefficients are:

$$P = \frac{p_0}{2\mu(3\lambda+2\mu)}(\lambda + 6s(\lambda+2\mu))$$

$$Q = -\frac{p_0}{2\mu(3\lambda+2\mu)h}(\lambda + 12s(\lambda+2\mu))$$

$$T = -\frac{p_0}{\mu(3\lambda+2\mu)}(\lambda+\mu+6s\lambda)$$

$$S = \frac{p_0}{2\mu(3\lambda+2\mu)h}(\lambda+\mu+12s\lambda)$$

The result is:

$$\Delta U = \frac{\pi a^2 h p_0^2}{6\mu(3\lambda+2\mu)}\left[6\lambda s + \lambda + \mu + 36(\lambda+2\mu)s^2\right]$$

After replacing the Lamé coefficients by Y, σ, this is:

$$\Delta U \;=\; \frac{a^2}{6\pi h^3 Y}\left[\left(\frac{h}{a}\right)^4 + 12\sigma\xi\left(\frac{h}{a}\right)^2 + 72(1-\sigma)\xi^2\right] \qquad (7.34)$$

with

$$\xi \;\equiv\; \sum_{m>0} p_m J_0(\zeta_m)/\zeta_m^2$$

Explicit coating displacement and edge stress

It is interesting to have the explicit expression for the reflecting surface displacement:

$$u_z(r, z=0) \;=\; \frac{2(1-\sigma^2)}{\pi a Y}\sum_{m>0}\frac{1-q_m^2+4q_m x_m}{(1-q_m)^2-4q_m x_m^2}\frac{p_m J_0(\zeta_m r/a)}{\zeta_m} +$$

$$+\frac{r^2/a^2}{2\pi h Y}\left[\sigma + 12\xi\frac{a^2}{h^2}(1-\sigma)\right]$$

units are m/N. See the displacement profile on figure 7.4

For the stress on the cylindrical edge before correction, we have as seen above (7.30):

$$\Theta_{rr}(r=a,z) \;=\; \frac{1}{\pi a^2}\sum_{m>0}\frac{J_0(\zeta_m)p_m}{(1-q_m)^2-4q_m x_m^2}\Big[(1-q_m+2q_m x_m(1+x_m))\,\mathrm{e}^{-\zeta_m z/a} -$$

$$-q_m\,(1-q_m+2x_m(1-x_m))\,\mathrm{e}^{\zeta_m z/a} -$$

$$-\zeta_m\frac{z}{a}\left[q_m(1-q_m+2x_m)\mathrm{e}^{\zeta_m z/a} + (1-q_m+2q_m x_m)\mathrm{e}^{-\zeta_m z/a}\right]\Big]$$

A plot of $\Theta_{rr}(r=a,z)$ (fig.7.5) shows the its quasi-linear behavior, justifying a posteriori the De Saint-Venant approximation.

Case of gaussian beams

if the beam intensity comes from a TEM_{00} wave of width w, we have

$$p_m \;=\; \frac{2\pi}{J_0(\zeta_m)^2}\frac{2}{\pi w^2}\int_0^a \exp(-2r^2/w^2)J_0(\zeta_m r/a)\,r\,dr$$

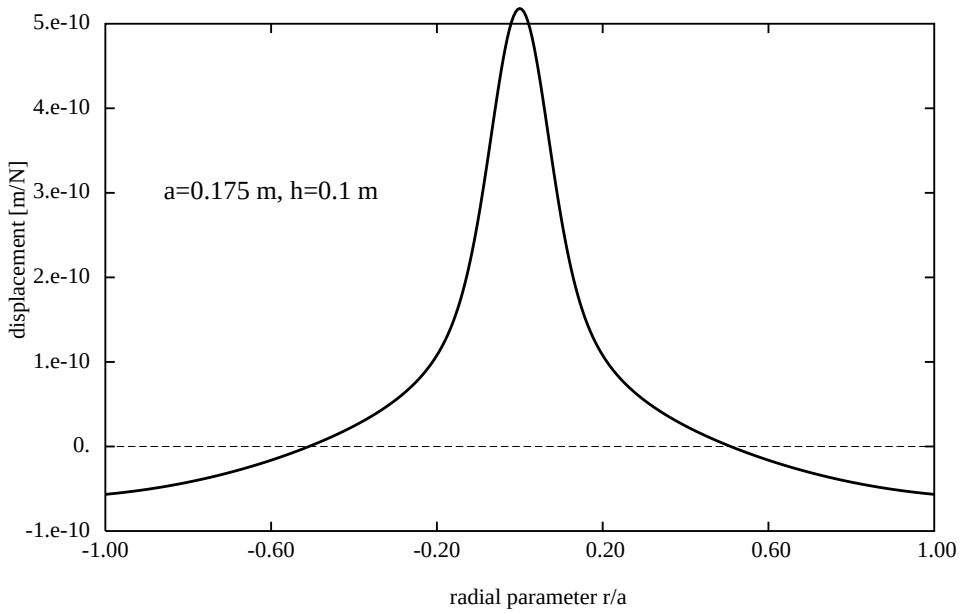

Figure 7.4: Displacement of the surface of a finite substrate under a gaussian pressure

The upper integration bound can be replaced by $+\infty$ if, as a mirror, the cylinder has negligible diffraction losses. Then the result can be found in [20] (eq. 11.4.29).

$$p_m = \frac{1}{J_0(\zeta_m)^2} \exp\left[-\frac{\zeta_m^2 w^2}{8a^2}\right]$$

The expansion of $p(r)$ on the orthogonal family $J_0(\zeta_m r/a)$ is rapidly convergent. A plot of $p(r)$ reconstructed from only 12 terms is shown on fig.7.6. A good accuracy is obtained for all the numerical calculations with only 50 terms. The expression 7.33 for U takes the special form

$$U_{\text{Gauss}} = \frac{1-\sigma^2}{\pi a Y} \sum_{m>0} \frac{\exp(-\zeta_m^2 w^2/4a^2)}{\zeta_m J_0(\zeta_m)^2} \frac{1-q_m^2+4q_m x_m}{(1-q_m)^2-4q_m x_m^2} \qquad (7.35)$$

the ξ parameter involved in expression 7.34 for ΔU takes the special form:

$$\xi_{\text{Gauss}} = \sum_{m>0} \frac{\exp(-\zeta_m^2 w^2/8a^2)}{\zeta_m^2 J_0(\zeta_m)}$$

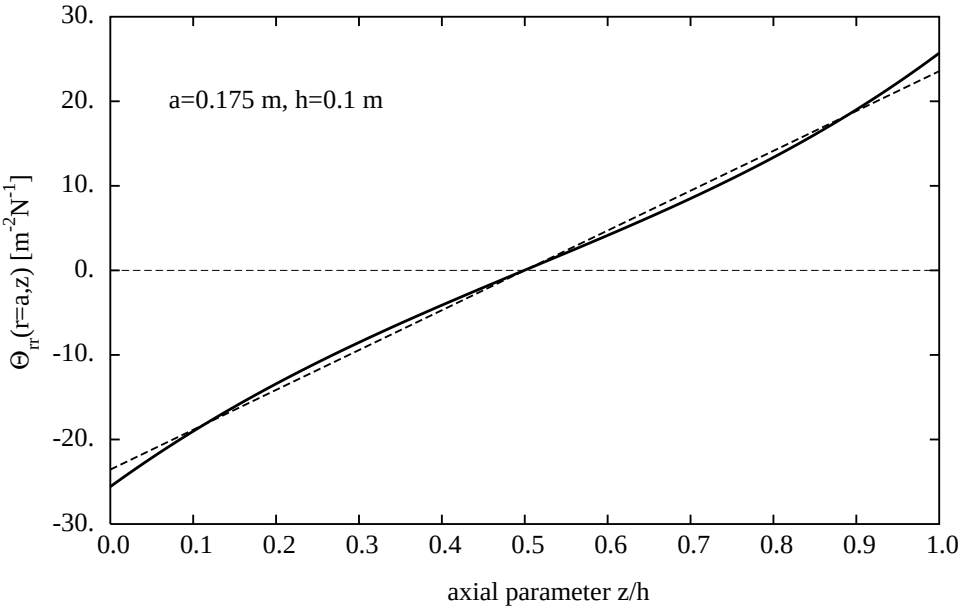

Figure 7.5: Radial stress along the edge of the cylindrical solid. Solid line : $\Theta_{rr}(r = a, z)$, Dashed line: linear fit $c_0 + c_1 z$

It is interesting to compare the results with the case discussed in the preceding section, of the half-space (infinite mirror) appproximation. If we note U_{HS} the corresponding strain energy and U_{FM} that of the finite mirror, we can plot the ratio for varying aspect ratios (see Fig.7.7). and it is clear that for a given thickness h, values of a as small as possible are desirable. Gong-like mirrors are worse than bar-like ones.

7.6.4 Some numerical results

For a Virgo input mirror, a =0.175m, h =0.1m, w =0.02m, we get

$$U \sim 1.81 \times 10^{-10} \text{ J.N}^{-2}$$

$$\Delta U \sim 2.08 \times 10^{-11} \text{ J.N}^{-2}$$

$$U_{\text{tot}} = U + \Delta U \sim 2.02 \times 10^{-10} \text{ J.N}^{-2}$$

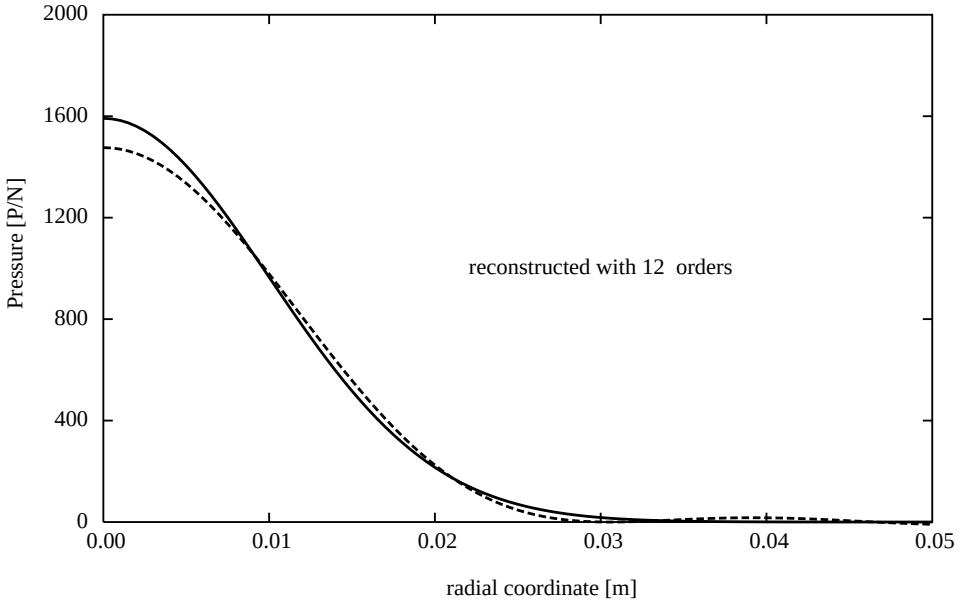

Figure 7.6: Solid line : gaussian pressure. Dashed line : reconstruction

The infinite mirror approximation was:

$$U_\infty \sim 1.88 \times 10^{-10} \text{ J.N}^{-2}$$

so that $U/U_\infty \sim 1.07$. The corresponding root spectral density of thermal noise is given by

$$S_x(f)^{1/2} = \sqrt{\frac{4k_BT}{\pi f}\Phi U_{\rm tot}}$$

so that we find (the loss angle being 10^{-6}:

$$S_x(f)^{1/2} \sim 1.03 \times 10^{-19} \text{ m.Hz}^{-1/2} \text{ at 100 Hz}$$

For a Virgo end mirror (a =0.175m, h =0.1m, w =0.0554m) we find:

$$U \sim 5.55 \times 10^{-11} \text{ J.N}^{-2}$$

$$\Delta U \sim 1.75 \times 10^{-11} \text{ J.N}^{-2}$$

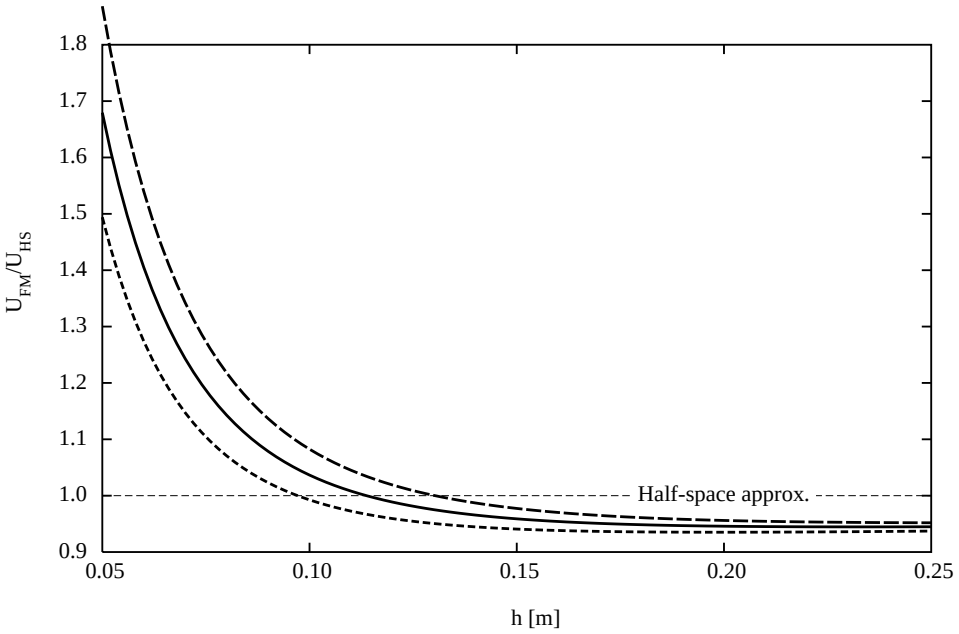

Figure 7.7: relative spectral density of Thermal noise for various aspect ratios. Solid line: a=0.175m, long dashed line: a=0.2m, short dashed line: a=0.15m

$$U_{\rm tot} \sim 7.30 \times 10^{-11} \text{ J.N}^{-2}$$

The beam width has changed (w=5.54cm), so that

$$U_\infty \sim 6.77 \times 10^{-11} \text{ J.N}^{-2}$$

so that $U/U_\infty \sim 1.08$. and

$$S_x(f)^{1/2} \sim 6.21 \times 10^{-20} \text{ m.Hz}^{-1/2} \text{ at 100 Hz}$$

Finally, it is interesting to check the convergence of $U_{\rm tot}$ to the infinite mirror approximation when the size of the mirror increases. This is shown on Fig.7.8.

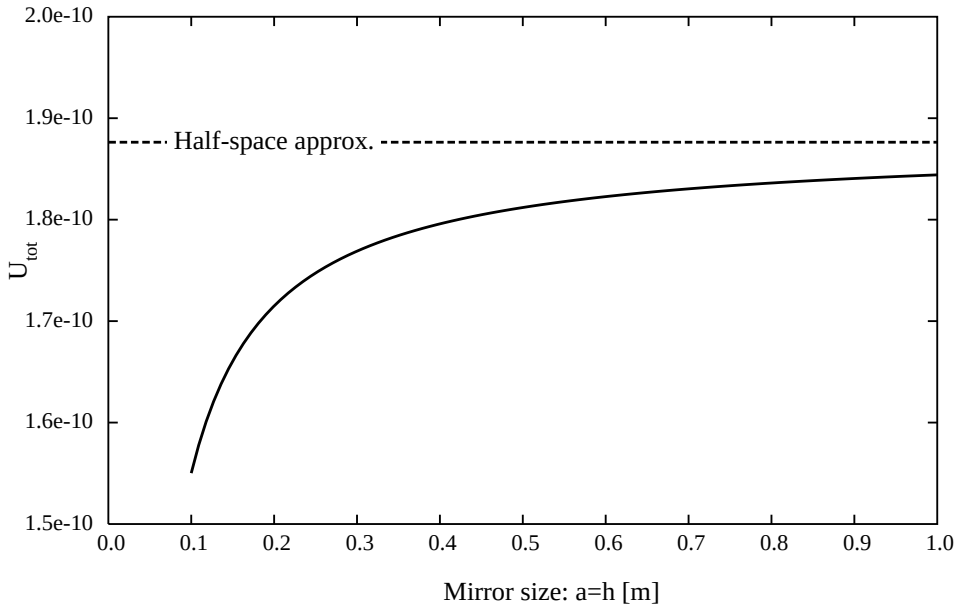

Figure 7.8: Convergence of the finite mirror model to the infinite, when the size of the mirror increases.

7.7 Non gaussian beams

7.7.1 Half-space approximation

It has been suggested ([37]) to use light beams with a flat profile in the long cavities instead of gaussian modes, in order to reduce the thermoelastic noise. It is expected that widen the beam will average the surface fluctuations and. The idea is convincing, but a quantitative model is obviously needed. We have addressed the question of how to generate these modes in a preceding section. For any pressure profile $p(r)$, the general expression of $\alpha(k)$ is, as already seen:

$$k\alpha(k) \;=\; -\,\frac{1}{2\mu}\int_0^\infty p(r)\,J_0(kr)\,r\,dr$$

so that the displacement of the surface of the half-space is:

$$u_z(r,z=0) \;=\; -\,\frac{\lambda+2\mu}{2\mu(\lambda+\mu)}\int_0^\infty dk\,J_0(kr)\int_0^\infty r'dr'\,J_0(kr')\,p(r')$$

or as well, using the Poisson ratio and the Young modulus:

$$u_z(r, z=0) \;=\; -\,\frac{2(1-\sigma^2)}{Y}\int_0^\infty dk\, J_0(kr)\int_0^\infty r'dr'\, J_0(kr')\, p(r') \qquad (7.36)$$

It is easy to see that the strain energy per N^2 is then given by

$$U \;=\; \frac{2\pi(1-\sigma^2)}{Y}\int_0^\infty dk\, \tilde{p}(k)^2$$

where

$$\tilde{p}(k) \;=\; \int_0^\infty r\, dr\, p(r)\, J_0(kr)$$

is nothing but the Fourier transform of the pressure distribution. In the special case of a distribution uniform on the disk $r < b$, representing a simplified version of a realistic mode (which would be only almost flat), we have

$$p(r) \;=\; \begin{cases} 1/\pi b^2 & (r < b) \\ 0 & (r \geq b) \end{cases}$$

so that

$$\tilde{p}(k) \;=\; \frac{J_1(kb)}{\pi kb}$$

and the energy integral reduces to

$$U \;=\; \frac{2(1-\sigma^2)}{\pi Y b}\int_0^\infty dx\, \left(\frac{J_1(x)}{x}\right)^2$$

the integral is of the Weber-Schafheitlin type (see [20] p.487), thus expressible in terms of a hypergeometric series:

$$\int_0^\infty dx\, \left(\frac{J_1(x)}{x}\right)^2 \;=\; \frac{1}{2}\, F\left(\frac{1}{2},\; -\frac{1}{2};\; 2\;;\; 1\right)$$

now (see [20] p.556),

$$F\left(\frac{1}{2},\; -\frac{1}{2};\; 2,\; 1\right) \;=\; \frac{8}{3\pi}$$

so that we have

$$\int_0^\infty dx\, \left(\frac{J_1(x)}{x}\right)^2 \;=\; \frac{4}{3\pi}$$

which yields the final result:

$$U = \frac{8(1-\sigma^2)}{3\pi^2 Y b}$$

It is worth to compare this value, denoted by $U_{\rm flat}$ with the gaussian value, denoted by $U_{\rm Gauss}$:

$$\frac{U_{\rm flat}}{U_{\rm Gauss}} = \frac{16}{3\pi^{3/2}}\frac{w}{b} \approx .96\,\frac{w}{b}$$

If it is possible to establish a flat mode of radius 10 cm where a gaussian mode of half-width 2 cm was used, the gain in thermal noise could be

$$\sqrt{\frac{U_{\rm flat}}{U_{\rm Gauss}}} \approx 0.44$$

which means a factor better than 2 in sensitivity, therefore 1 order of magnitude in the analyzed volume of space in the frequency band around 100 Hz. For curious readers, and though it is of no practical interest for our present purpose (but any result may always be re-used one day in a different context), we show the (virtual) distorted surface on Fig.7.9, and give the apex equation of the surface as:

$$u_z(r, z=0) = -\frac{2(1-\sigma^2)}{\pi Y b}\begin{cases} 1 & (r=0) \\ F\left(\frac{1}{2},\ -\frac{1}{2};\ 1\ ;\ r^2/b^2\right) & (0<r<b) \\ 2/\pi & (r=b) \\ bF\left(\frac{1}{2},\ \frac{1}{2};\ 2\ ;\ b^2/r^2\right)/2r & (r>b) \end{cases}$$

where $F(a,b;c;z)$ denotes the Gauss hypergeometric series.

In this case, the pressure distribution takes however significant values probably near the edge of the mirror, because the reduction of thermal noise operates only if a is much larger than w, and secondly because the size of actual mirrors has been defined as the minimum consistent with small diffraction losses, so that say 5 times w is near the physical edge for input mirrors, and outside the mirror for end mirrors of radius 35 cm. Approximate representation of the mirror as an infinite half-space is thus questionable in this case, and a theory with a finite mirror radius is needed.

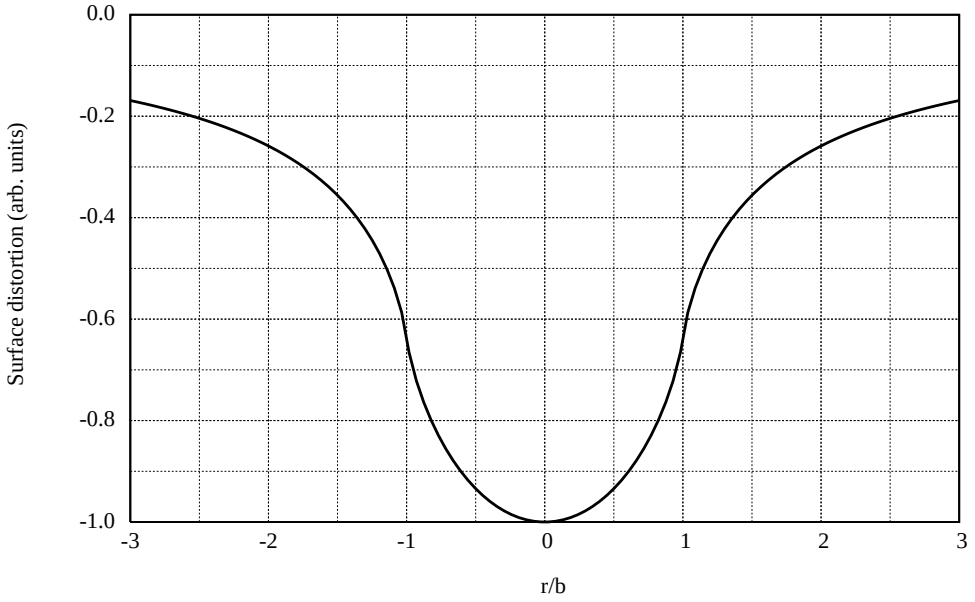

Figure 7.9: Displacement of the surface of an infinite substrate under a pressure uniform on the disk $r < b$. The surface is assumed infinite

7.7.2 Finite test mass approximation

The model developped for a finite mirror of radius a and thickness h can be extended to the case of a flat pressure

$$\begin{cases} p(r) &= 1/\pi b^2 \quad (r \leq b) \\ p(r) &= 0 \quad (r > b) \end{cases}$$

representing approximately a flat mode. The pressure coefficients are:

$$p_m = \frac{2a J_1(\zeta_m b/a)}{b\zeta_m J_0^2(\zeta_m)}$$

The p_m decrease much less rapidly for increasing m than in the case of a gaussian profile, so that reconstruction of $p(r)$ is numerically difficult. But The series giving U and ξ are still convergent, despite the new values for the p_m. In fact, these new p_m are decreasing like $1/\sqrt{m}$, so that the formal series giving $p(r)$ is valid in the sense of the distribution theory. But the terms in

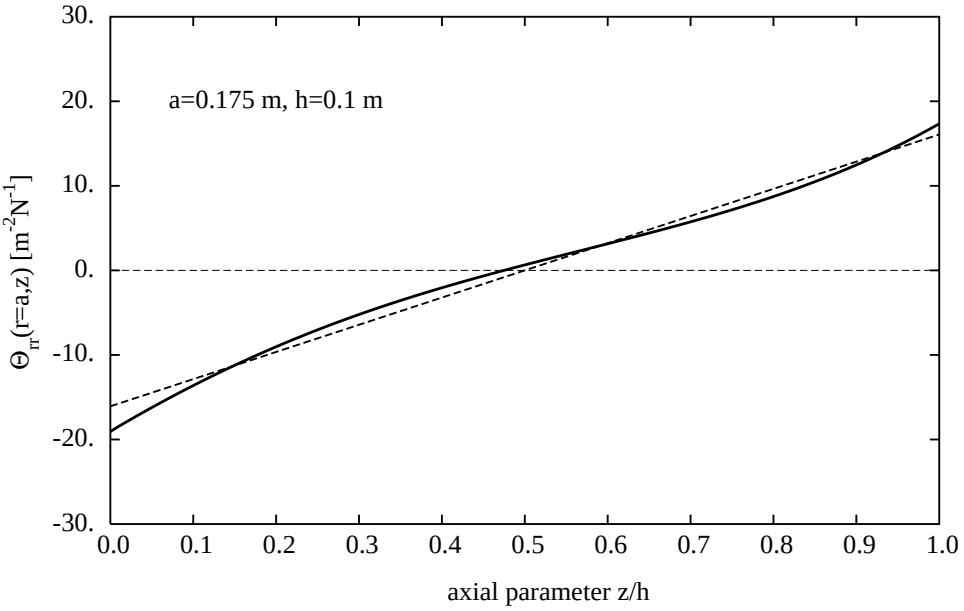

Figure 7.10: Radial stress and corresponding linear fit. b=0.1m

the series 7.33 fo r U, and in the series defining ξ are nevertheless decreasing like $1/m^3$, so that ordinary convergence is secured. All the formulas derived in the preceding section are unchanged, apart from the new values for p_m. It is nevertheless necessary to check that the correction for the radial stress on the edge is still reasonable. If we compute the stress $\Theta_{rr}(r = a, z)$ with the new coefficients, we get the following plot (fig.7.10), in the case of a mirror of radius 0.175m and a pressure flat in a disk of radius 0.1m. showing that the De Saint-Venant correction is still realistic. Even with a spot radius of 0.15m, the linear correction seems to make sense (see fig.7.11). The displacement of the reflecting surface is much less than in the gaussian case (fig.7.12), and distortion is very similar to the infinite case. It is especially intersting to compare the spectral densities of thermal noise in the gaussian mode regime to the flat mode regime. The following plot (7.13) shows again the large gain that could be achieved by increasing the spot radius. Comparison is made with a gaussian beam of width 2cm. It is interesting to remark that the case $b = a$ (the flat mode has the same radius as the mirror) leads to $U = 0$

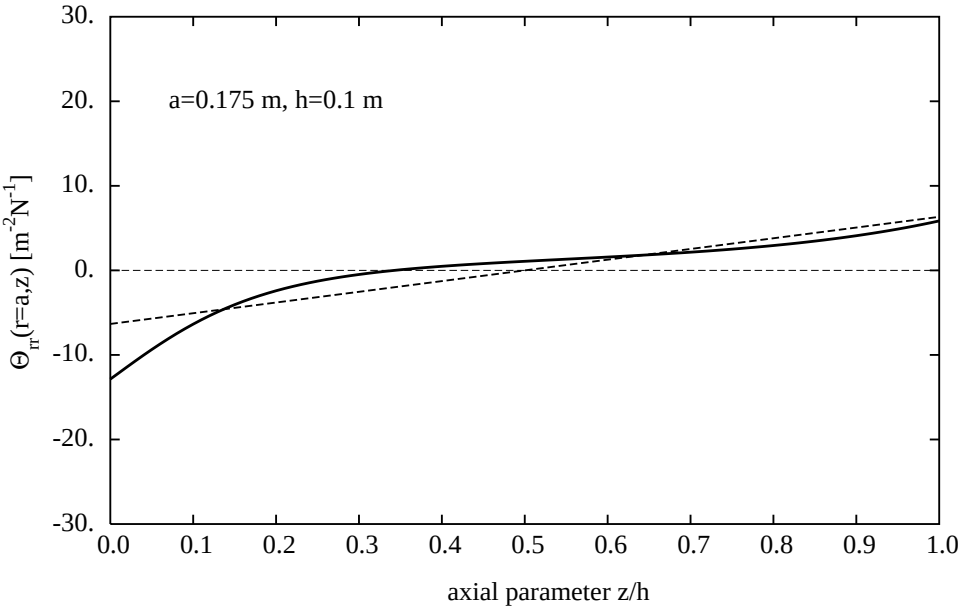

Figure 7.11: Radial stress and corresponding linear fit.b=0.15m

and $\xi = 0$. In this case the solution is exact, and the strain energy reduces, according to 7.34 to

$$\Delta U \;=\; h/6\pi a^2 Y$$

7.7.3 Numerical results

Let us assume such a flat mode in the Virgo cavities whose mirrors are assumed identical in size to the current situation. For the input mirrors, we find:

$$U \;\sim\; 1.60 \times 10^{-11}\ \text{J.N}^{-2}$$

$$\Delta U \;\sim\; 1.06 \times 10^{-11}\ \text{J.N}^{-2}$$

$$U_{\text{tot}} \;\sim\; 2.65 \times 10^{-11}\ \text{J.N}^{-2}$$

The infinite mirror approximation was:

$$U_{\infty} \;\sim\; 3.59 \times 10^{-11}\ \text{J.N}^{-2}$$

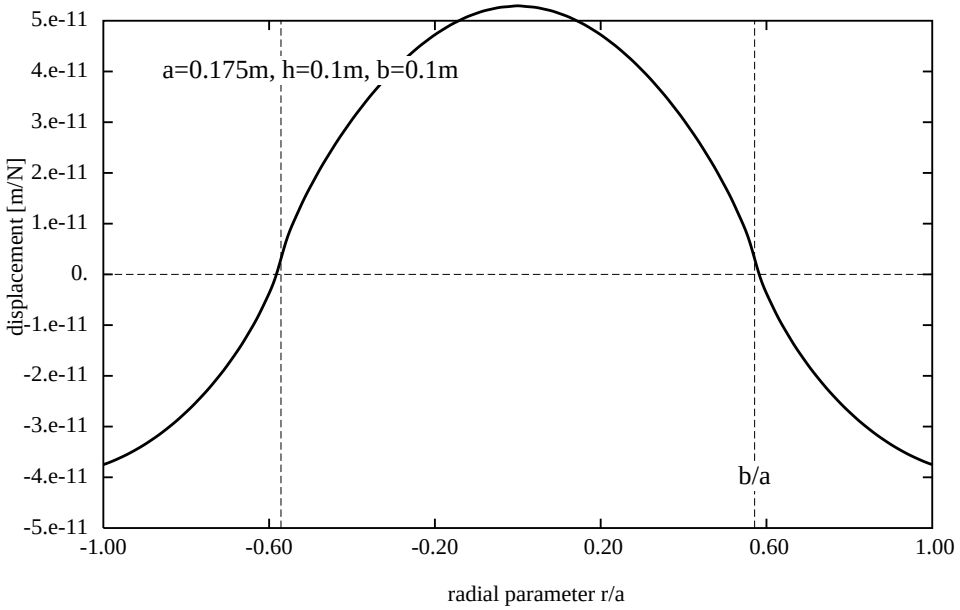

Figure 7.12: Displacement of the reflecting surface under a pressure uniform in a disk of radius 0.1m. (a=0.175m, h=0.1m)

so that $U/U_\infty \sim 0.74$. We find the spectral density (the loss angle being still 10^{-6}:

$$S_x(f)^{1/2} \sim 3.74 \times 10^{-20} \text{ m.Hz}^{-1/2} \text{ at 100 Hz}$$

For the end mirrors, the mode having almost exactly the same spot size after propagation, the numerical results are almost identical.

7.7.4 Realistic modes

The preceding approach is still questionable because the pressure distribution, as represented by an ideal flat top function is unrealistic from an optical point of view. It is thus necessary to check that taking a more realistic flat mode does not destroy the preceding conclusions. The more realistic model proposed by D'ambrosio et al.[37] consists in a superposition of elementary gaussian modes of waist w_0 on a disk of radius b. If we adapt the model to the Virgo parameters, for the sake of definiteness, we would have an amplitude

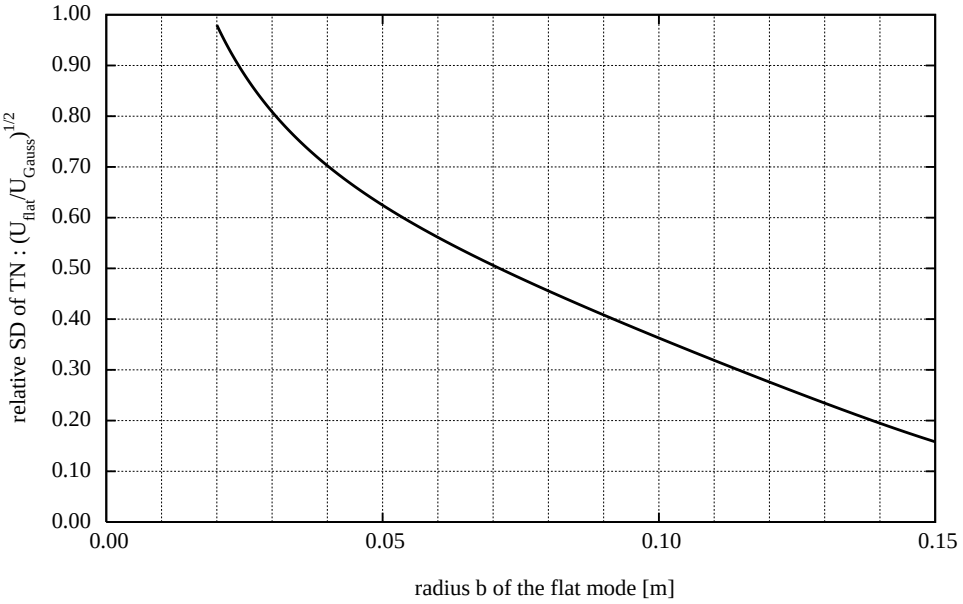

Figure 7.13: gain in SD of thermal noise vs spot radius.(a=0.175m, h=0.1m)

on the flat input mirror of the form:

$$A(x,y,0) \;=\; \int_{\Delta} \phi(x-x_0, y-y_0, 0)\, dx_0\, dy_0$$

where Δ is the disk of radius b, and $\phi(x,y,z)$ a gaussian TEM_{00} wave:

$$\phi(x,y,0) \;=\; \exp\left(-\frac{x^2+y^2}{w_0^2}\right)$$

The resulting amplitude has a quite flat maximum, with a gaussian-like edge Parameter w_0 determines the sharpness of this edge. It is easy to show that after propagation at a distance L, the amplitude is (up to a normalization factor):

$$A(x,y,L) \;\propto\; \int_0^{b/w} \exp\left[-Z(\rho-\rho_0)^2\right]\, \exp(-2Z\rho\rho_0)\, I_0(2Z\rho\rho_0)\, \rho_0\, d\rho_0$$

$z_R = \pi w_0^2/\lambda$ being the Rayleigh parameter, w is the beam half-width after propagation on the distance L:

$$w = w_0\sqrt{1+L^2/z_R^2}$$

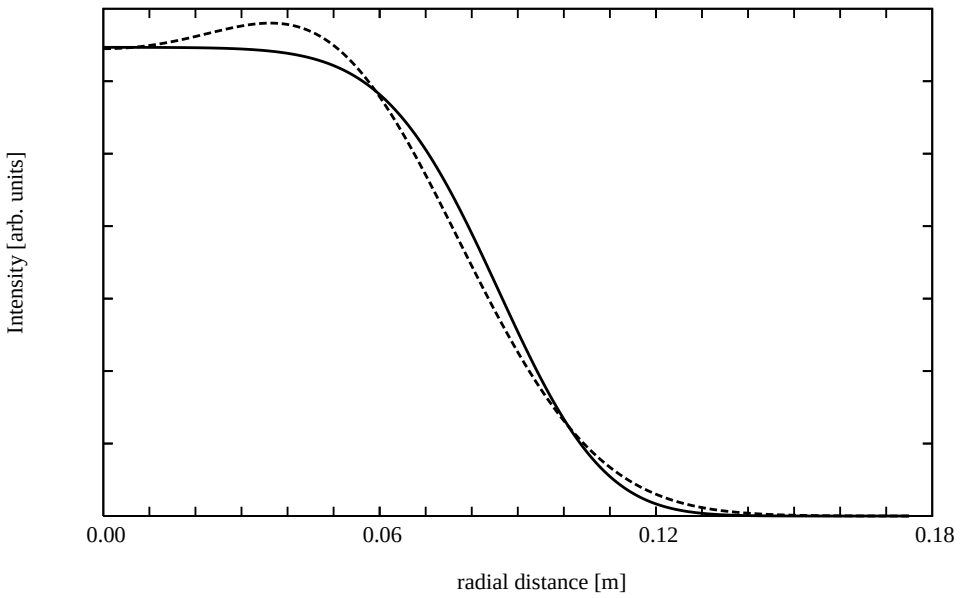

Figure 7.14: Intensity profile in the flat mode. Solid line : Profile on the input flat cavity mirror. Dashed line : Profile on the far mirror (3 km away).

$\rho \equiv \sqrt{x^2+y^2}/w$, and $Z \equiv 1 - iL/z_R$. $I_0(z)$ is the modified Bessel function of the first kind. There is no better analytical expression for the amplitude, but a numerical integration is straightforward, because the function $\exp(-z)I_0(z)$ has an easy behavior. On Fig.7.14, we have plotted the mode intensity profile for the following parameters: $w_0 \sim 3.2$ cm, $b = 0.1$ m, at the two ends of a cavity of length 3 km. Knowing A, we can compute numerically the p_m from $|A|^2$ after normalization. This can be done for the input mirrors (flat wavefront, $L = 0$) and for the end mirrors ('mexican hat' wavefront, L =3 km). The corresponding strain energies are almost the same, because the intensity distribution is weakly modified by diffraction for not too small w_0. Even for smaller w_0 resulting in more distorted intensity profiles on the end mirror, the strain energies are nearly identical at the two ends. In Fig.7.15, we plot the values found for several particular radii and several values of the parameter w_0. It is clear that by decreasing the parameter w_0 (sharping the edge), we get more and more close to the ideally flat model. However a too sharp edge is not desirable from an optical point of view, giving a too

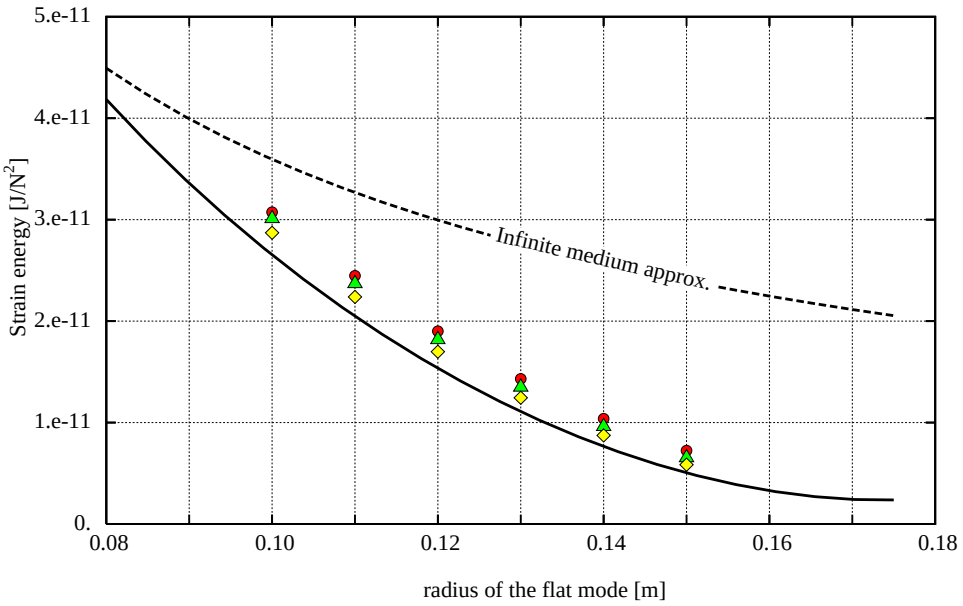

Figure 7.15: Strain energy U vs radius of the flat mode. Dashed line: Infinite mirror and ideally flat mode, Solid line : Mirror of radius 0.175 m, thickness 0.1 m and ideally flat mode. Circles: same finite mirror with realistic mode $w_0 \sim 3.2$ cm. Triangles: same finite mirror with realistic mode $w_0 \sim 2$ cm. Diamonds: same finite mirror with realistic mode $w_0 \sim 1$ cm

distorted wavefront (and consequently unfeasible mirrors). However, in the limit of reasonable parameters, we remark a good agreement between the ideal and realistic models.

7.8 Mirror distortions and energy maps

It is interesting to write explicitly the solution of the elastical problem. The expressions of the displacement vector components in the case of finite cylindrical mirrors are:

$$u_r(r,z) = u_{\mathrm{main},r}(r,z) + \Delta u_r(r,z)$$

$$u_z(r,z) = u_{\mathrm{main},z}(r,z) + \Delta u_z(r,z)$$

with the following expressions:

$$\Delta u_z(r,z) = \frac{1}{2\pi a^2 h Y}\left\{\left[\sigma+12s(1-\sigma)\right]r^2+(1+24s\sigma)z^2-2(1+12s\sigma)hz\right\}$$

(with $s \equiv \xi a^2/h^2$),

$$\Delta u_r(r,z) = \frac{r}{\pi a^2 Y}\left\{\sigma+6s(1-\sigma)-z\left[\sigma+12s(1-\sigma)\right]/h\right\}$$

$$u_{\mathrm{main},r}(r,z) = \frac{1+\sigma}{\pi a Y}\sum_{m>0}\frac{p_m J_1(\zeta_m r/a)}{\zeta_m D_m}P_m(z)$$

with $D_m \equiv (1-q_m)^2 - 4q_m x_m^2$, and

$$-P_m(z) = \left[2q_m x_m^2+(1-2\sigma)(1-q_m+2q_m x_m)\right]\exp(-\zeta_m z/a)+$$

$$+q_m\left[2x_m^2-(1-2\sigma)(1-q_m+2x_m)\right]\exp(\zeta_m z/a)-$$

$$-\zeta_m\frac{z}{a}\left[(1-q_m+2q_m x_m)\exp(-\zeta_m z/a)+q_m(1-q_m+2x_m)\exp(\zeta_m z/a)\right]$$

and

$$u_{\mathrm{main},z}(r,z) = \frac{(1+\sigma)}{\pi a Y}\sum_{m>0}\frac{p_m J_0(\zeta_m r/a)}{\zeta_m D_m}Q_m(z)$$

where

$$\frac{1}{2}Q_m(z) = \left[(1-\sigma)(1-q_m+2q_m x_m)-q_m x_m^2)\right]\exp(-\zeta_m z/a)+$$

$$+q_m\left[(1-\sigma)(1-q_m+2x_m)+x_m^2\right]\exp(\zeta_m z/a)+$$

$$+\zeta_m\frac{z}{2a}\left[(1-q_m+2q_m x_m)\exp(-\zeta_m z/a)-q_m(1-q_m+2x_m)\exp(\zeta_m z/a)\right]$$

Despite the apparent complexity, this is extremely fast to compute (see the "Heating issues" chapter for algorithmic details). These formulas allow to draw (see Fig.7.25) the distorted shape of the solid, and to check that the distortion is minimized by the flat mode. It is also possible to give the strain components. By derivating the preceding expressions, we get:

$$E_{i,j}(r,z) = E_{\mathrm{main},i,j}(r,z)+\Delta E_{i,j}(r,z)$$

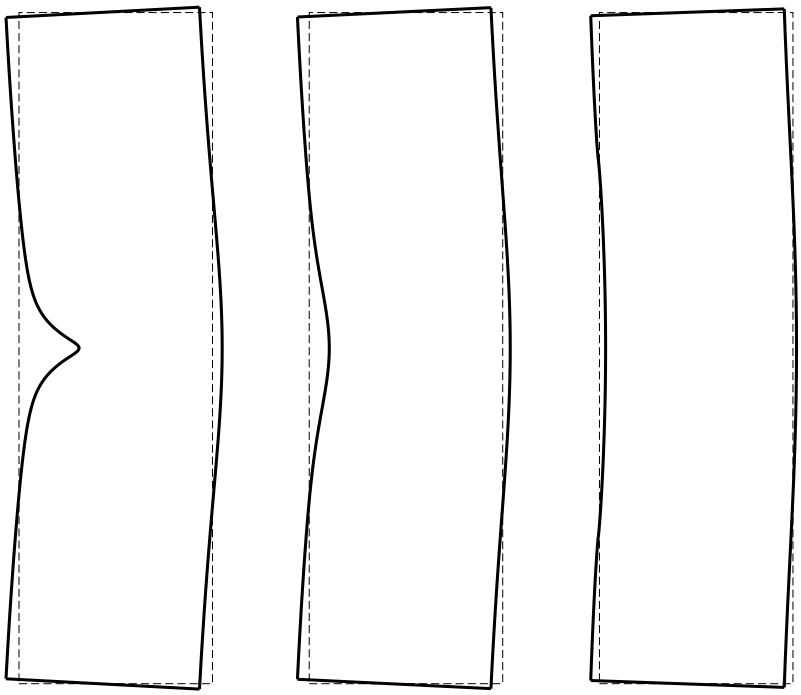

Figure 7.16: Distorted mirror for 1 N normalized pressure. From left to right: Gaussian mode, w=2cm, Gaussian mode w=5.54cm, flat mode of radius b =10cm. (exaggerated by a factor of 6×10^7)

with, in detail:

$$E_{\mathrm{main},rr}(r,z) = \frac{1+\sigma}{\pi a^2 Y}\sum_{m>0}\frac{p_m}{D_m}J_1'(\zeta_m r/a)\,P_m(z)$$

$$E_{\mathrm{main},\phi\phi}(r,z) = \frac{1+\sigma}{\pi a^2 Y}\sum_{m>0}\frac{p_m}{D_m}\,\frac{J_1(\zeta_m r/a)}{\zeta_m r/a}\,P_m(z)$$

$$E_{\mathrm{main},zz}(r,z) = \frac{1+\sigma}{\pi a^2 Y}\sum_{m>0}\frac{p_m}{D_m}J_0(\zeta_m r/a)\,\frac{a}{\zeta_m}Q'_m(z)$$

$$E_{\mathrm{main},rz}(r,z) = \frac{1+\sigma}{\pi a^2 Y}\sum_{m>0}\frac{p_m}{D_m}J_1(\zeta_m r/a)\,\frac{1}{2}\left[\frac{a}{\zeta_m}P'_m(z)-Q_m(z)\right]$$

$$E_{\mathrm{main}}(r,z) = \frac{1+\sigma}{\pi a^2 Y}\sum_{m>0}\frac{p_m}{D_m}J_0(\zeta_m r/a)\,\left[P_m(z)+\frac{a}{\zeta_m}Q'_m(z)\right]$$

The functions $P_m(z),\ Q_m(z)$ have been defined above. Moreover we have:

$$\frac{a}{\zeta_m}\,Q'_m(z)+P_m(z) = -2(1-2\sigma)\left[(1-q_m+2q_m x_m)\mathrm{e}^{-\zeta_m z/a}-q_m(1-q_m+2x_m)\mathrm{e}^{\zeta_m z/a}\right]$$

and

$$\frac{1}{2}\left[\frac{a}{\zeta_m}\,P'_m(z)-Q_m(z)\right] = \left(2q_m x_m^2-(1-q_m+2q_m x_m)\frac{\zeta_m}{a}z\right)\mathrm{e}^{-\zeta_m z/a}-$$

$$-\left(2q_m x_m^2-q_m(1-q_m+2x_m)\frac{\zeta_m}{a}z\right)\mathrm{e}^{\zeta_m z/a}$$

For the extra contributions, we have

$$\Delta E_{rr}(r,z) = \frac{1}{\pi a^2 Y}\left[\sigma+6s(1-\sigma)-z\left(\sigma+12s(1-\sigma)\right)/h\right]$$

$$\Delta E_{\phi\phi}(r,z) = \Delta E_{rr}(r,z)$$

$$\Delta E_{zz}(r,z) = \frac{1}{\pi a^2 Y}\left[(1+24s\sigma)z/h-1-12s\sigma)\right]$$

$$\Delta E_{rz}(r,z) = 0$$

$$\Delta E(r,z) = -\frac{1-2\sigma}{\pi a^2 Y}\left[1-12s-(1-24s)z/h\right]$$

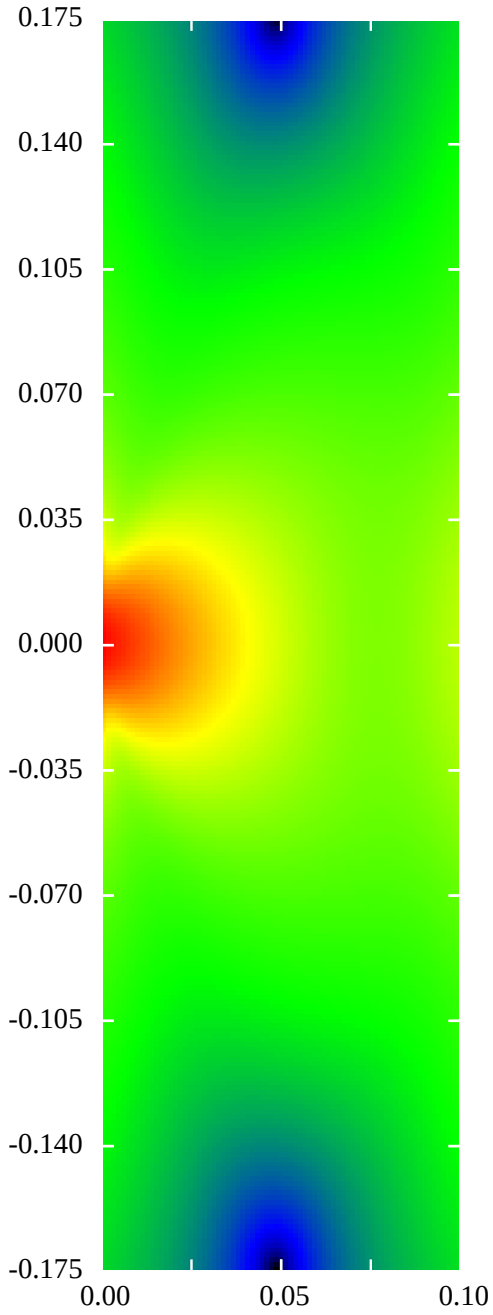

Figure 7.17: Distribution of strain energy in a cylindical mirror of radius a=17.5 cm, of thickness h=10 cm, under a gaussian pressure w=2 cm. Logarithmic scale

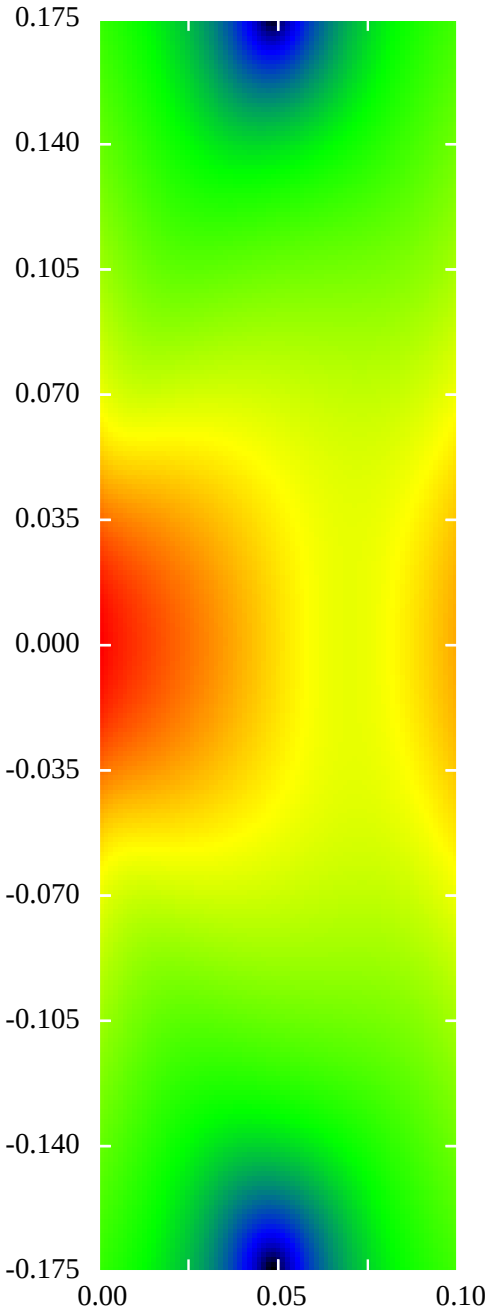

Figure 7.18: Distribution of strain energy in a cylindical mirror of radius a=17.5 cm, of thickness h=10 cm, under a gaussian pressure w=5.54 cm.Logarithmic scale

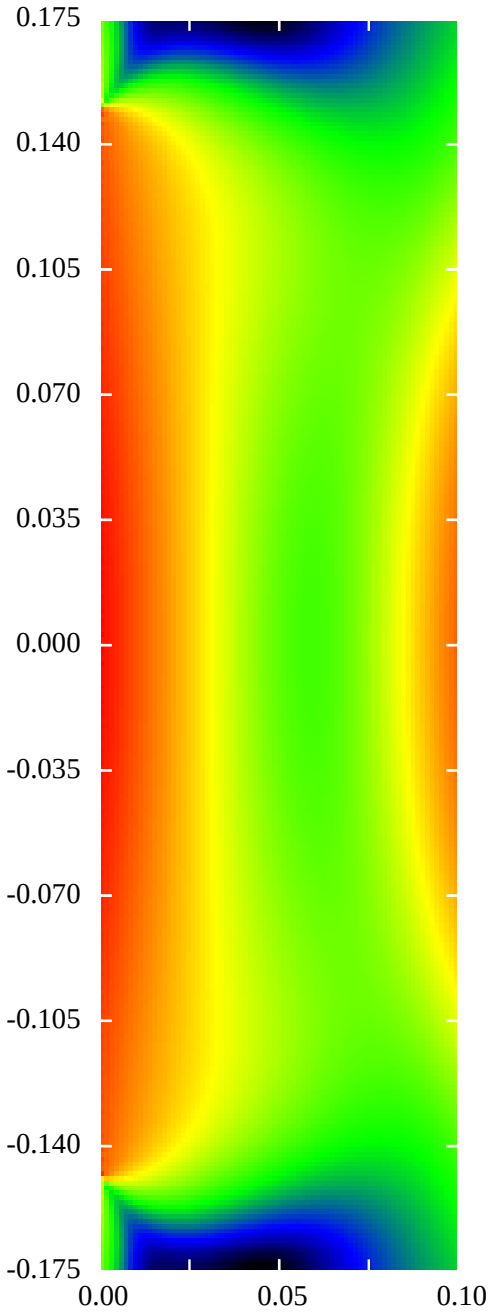

Figure 7.19: Distribution of strain energy in a cylindical mirror of radius a=17.5 cm, of thickness h=10 cm, under a flat top pressure b=15 cm.Logarithmic scale

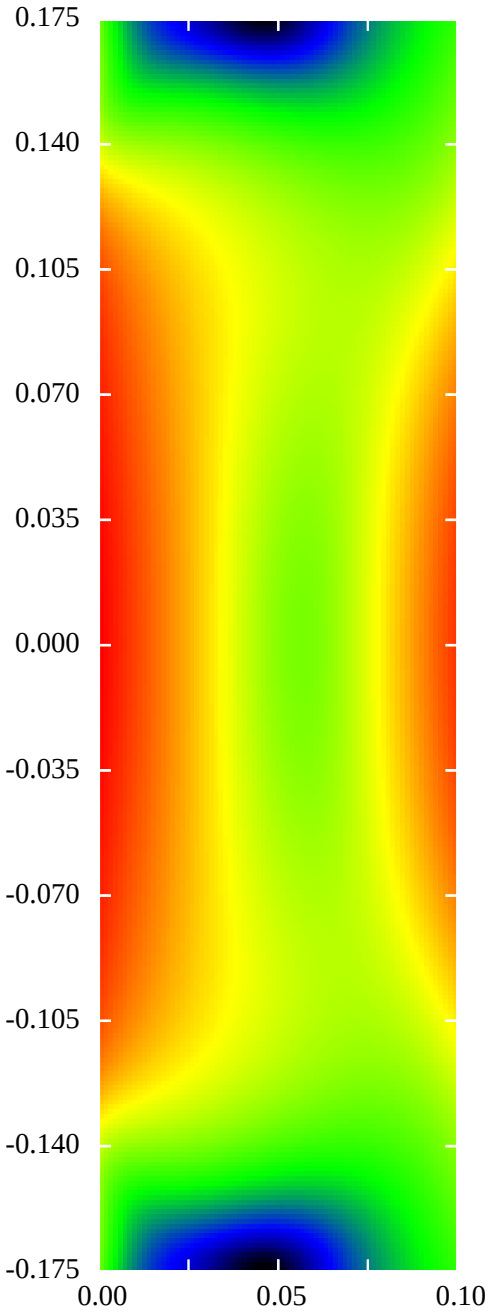

Figure 7.20: Distribution of strain energy in a cylindical mirror of radius a=17.5 cm, of thickness h=10 cm, under a realistically flat pressure b=15 cm.

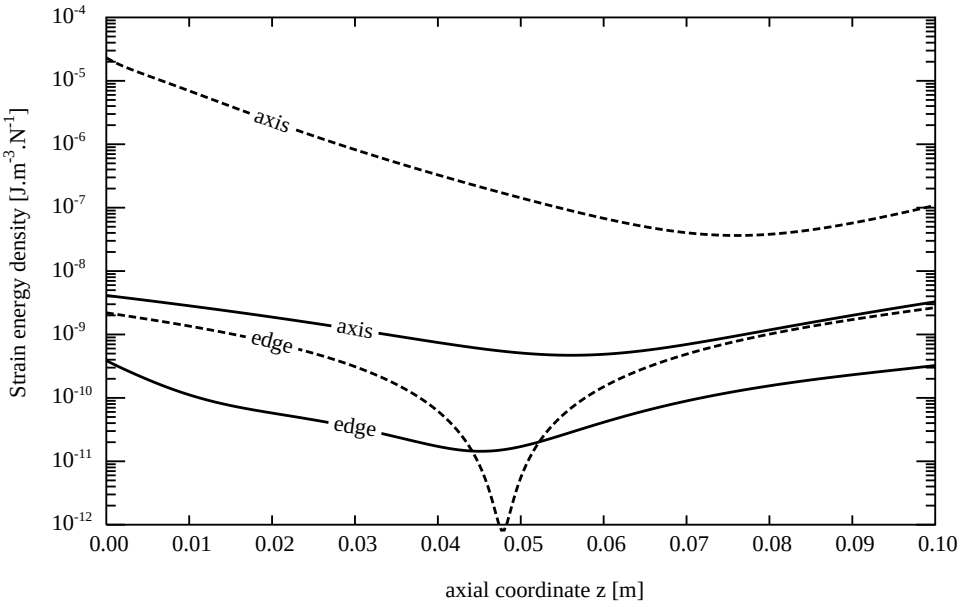

Figure 7.21: Distribution of strain energy on the axis and on the edge of a cylindrical mirror (a=17.5 cm, h=10 cm). Case of a gaussian (w=2 cm) beam (dashed lines), and of a realistic flat beam (b=0.15 m) (solid lines)

so that it is possible to compute explicitly the strain energy density:

$$w(r,z) \;=\; \frac{Y}{2(1+\sigma)}\left[\frac{E(r,z)^2}{1-2\sigma} + E_{rr}(r,z)^2 + E_{\phi\phi}(r,z)^2 + E_{zz}(r,z)^2 + 2E_{r,z}(r,z)^2\right]$$

The following pictures (Fig.7.17,7.18,7.19,7.20) show the distribution of w in some cases examined above. The energy density is weak on the edge, and this is even more clear for wider w and a fortiori, in average for flat beams and realistic flat beams. We show in Fig.7.21 the energy density on the axis and on the edge in the two extreme cases, namely a gaussian beam of width 2 cm, and a realistic flat mode of radius 15 cm. It can be seen that the energy density is much lower on the edge than on the hot point on the axis, in both cases, even if there is a sharp minimum for the gaussian beam, locally lower than the flat beam average.

7.9 Higher order LG modes

7.9.1 Introduction

Another interesting possibility is to spread power on the mirror's surface by using high order gaussian TEM modes. We restrict here our attention to axisymmetrical modes, for which the BHV model is relevant. The interest of using gaussian modes is to keep using spherical mirrors, instead of exotic surfaces. We hope the effect of misalignments to be significantly lower than with flat modes.

7.9.2 The BHV model

In the case where both the mirrors and the beam are assumed axisymmetrical, there exists a model allowing an accurate calculation of the low frequency tail of the spectral densities of internal noises. As a result of Levin's [?] theory The power spectral density (PSD) of displacement equivalent to thermal noise takes the general (low frequency) form :

$$S_x(f) \;=\; \frac{4k_BT}{\pi f}\,\phi\,U \tag{7.37}$$

where ϕ is a loss angle, and where U is the strain energy of the mirror under a pressure distribution having the same profile as the readout beam, and normalized to 1 N.

Let us summarize the results of the preceding chapter. the total internal energy is the sum of two contributions:

$$U \;=\; U_0 \;+\; \Delta U$$

that can be computed separately. Let a be the radius of the mirror and h its thickness. Let $J_\nu(x)$ be the Bessel functions, and $\{\zeta_k,\, k > 0\}$ the family of all non-zero solutions of $J_1(\zeta) = 0$. Let us note $x_k \equiv \zeta_k h/a$, and $q_k \equiv \exp(-2x_k)$. Let Y be the Young modulus of the mirror's material and σ its Poisson ratio.

Then we have:

$$U_0 \;=\; \frac{1-\sigma^2}{\pi a Y} \sum_{k>0} \frac{J_0^2(\zeta_k) p_k^2}{\zeta_k} \frac{1 - q_k^2 + 4q_k x_k}{(1-q_k)^2 - 4q_k x_k^2} \tag{7.38}$$

The dimension of U is J.N^{-2}.

In the preceding expression the Fourier-Bessel coefficients $\{p_k,\, k > 0\}$ are determined by the pressure profile. If we denote by $p(r)$ this pressure distribution, we have:

$$p_k \;=\; \frac{2\pi}{J_0^2(\zeta_k)} \int_0^a p(r) J_0(\zeta_k r/a)\, r\, dr \tag{7.39}$$

For the second contribution, we have:

$$\Delta U \;=\; \frac{a^2}{6\pi h^3 Y} \left[\left(\frac{h}{a}\right)^4 + 12\sigma\xi \left(\frac{h}{a}\right)^2 + 72(1-\sigma)\xi^2 \right] \tag{7.40}$$

with

$$\xi \;\equiv\; \sum_{k>0} p_k J_0(\zeta_k)/\zeta_k^2$$

At this level, the computation amounts to find the p_k.

7.9.3 Power profiles

In the case of an ideal flat-top mode of radius b, the pressure distribution is:

$$p_{\text{flat}}(r) \;= \begin{cases} 1/\pi b^2 & (r \le a) \\ 0 & (r > a) \end{cases} \tag{7.41}$$

As seen in the preceding section, the p_k coefficients are [?]

$$p_{k,\mathrm{flat}} \;=\; \frac{2aJ_1(\zeta_k b/a)}{b\zeta_k\, J_0^2(\zeta_k)}$$

In the case of a Gaussian TEM_{00} readout mode of normalized amplitude

$$\Psi_{0,0}(r) \;=\; \sqrt{\frac{2}{\pi w^2}}\,\exp(-r^2/w^2),$$

the pressure distribution is:

$$p(r) \;=\; |\Psi_{0,0}(r)|^2$$

and the p_k coefficients are:

$$p_{k,0}^{(0)} \;=\; \frac{1}{J_0(\zeta_k)^2}\,\exp\left[-\frac{\zeta_k^2 w^2}{8a^2}\right]$$

The preceding result can be extended to the case of any axisymmetrical Laguerre-Gauss mode $\mathrm{LG}_{n,m}$. It is well known that the paraxial diffraction equation (relevant for finding the eigenmodes of a resonant cavity with weakly spherical mirrors) admits solutions of the form (in polar coordinates)

$$\Psi_{n,m}(r,\phi,z) \;=\; \sqrt{\frac{2}{\pi w(z)^2}\,\frac{m!}{(m+n)!}}\,\exp(-r^2/w(z)^2)\,(2r^2/w(z)^2)^{n/2}\,L_m^{(n)}[2r^2/w(z)^2]\,\times$$

$$\times\;\exp(in\phi)\;\exp[-i(2m+n+1)\arctan(z/z_R)]\,\exp[i\pi r^2/\lambda R(z)]\,\exp(2i\pi z/\lambda) \tag{7.42}$$

where the $L_m^{(n)}(x)$ are the Generalized Laguerre polynomials. λ is the wavelength and z_R the Rayleigh parameter. The functions $w(z)$ and $R(z)$ determine respectively the width of the mode, and the curvature radius of its wavefront. In what follows, we only need $w(z)$. At the location z_M of a mirror, the normalized pressure distribution has therefore the general expression:

$$p_m^{(n)}(r) \;=\; \frac{2}{\pi w^2}\frac{m!}{(m+n)!}\,\exp(-2r^2/w^2)\,(2r^2/w^2)^n\,L_m^{(n)}(2r^2/w^2)^2$$

depending on the parameter $w \equiv w(z_M)$. If the ratio a/w is large enough that the diffraction losses are small, we can replace the finite upper bound of integral (7.39) by $+\infty$, and the Fourier-Bessel coefficients are simply:

$$p_{k,m}^{(n)} \;=\; \frac{1}{J_0(\zeta_k)^2}\,\exp\left[-\frac{\zeta_k^2 w^2}{8a^2}\right]\;L_m^{(0)}\left(\frac{\zeta_k^2 w^2}{8a^2}\right)\,L_{n+m}^{(0)}\left(\frac{\zeta_k^2 w^2}{8a^2}\right)$$

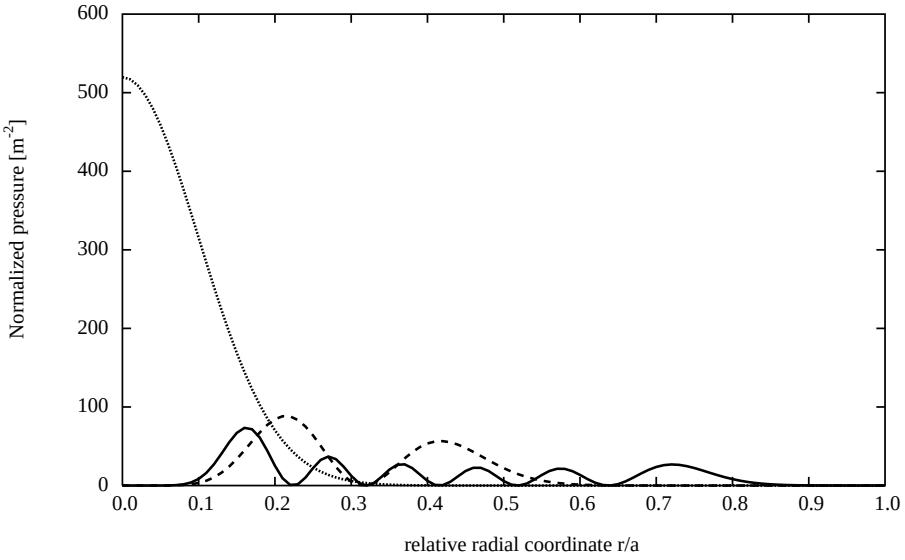

Figure 7.22: Pressure profiles. (0,0): dotted, (4,1): dashed, (5,5): solid

If the diffraction losses are not small, the preceding expression losses some accuracy, but simultaneously the corresponding mode losses its practical interest. The pressure profiles on the input mirror for some among the first Laguerre-Gauss modes of parameter $w = 3.5$ cm are represented on Fig.7.22. See on Fig.7.23 the intensity pattern of a $LG_{5,5}$ (for instance) mode. The integrated power (Fig.7.24) clearly shows a smoother distribution of power on the mirror's surface. Some examples of the virtual deformation of the mirror's surface under a pressure normalized to 1 N can be seen on Fig.7.25 with again w=3.5 cm. For the mirror's size, we assume a radius a= 17.5 cm and a thickness h= 10 cm. One clearly sees that the strain is a decreasing function of the orders (n, m) of the mode.

7.10 Relative gains on thermal noise

With the current parameters a= 17.5 cm, h = 10 cm, w= 2 cm of the Virgo input mirrors, if we insert the preceding $p_{k,m}^{(n)}$ in equations 7.38 and 7.40, we

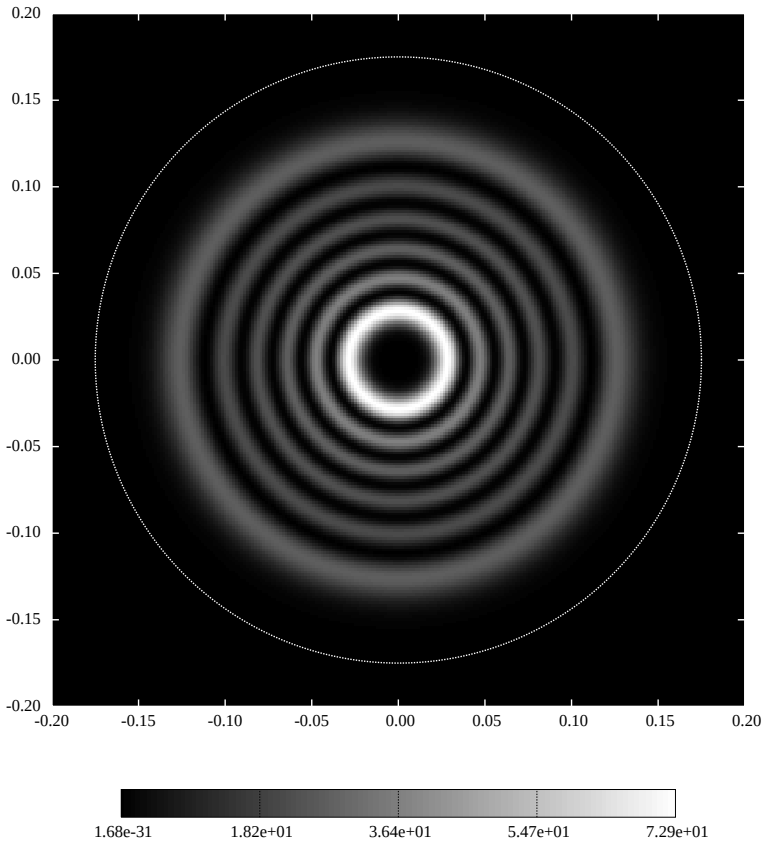

Figure 7.23: Intensity pattern of a $LG_{5,5}$ mode of Gaussian parameter $w = 3.5$ cm. The faint circle represents the edge of a 17.5 cm radius mirror (units: m).

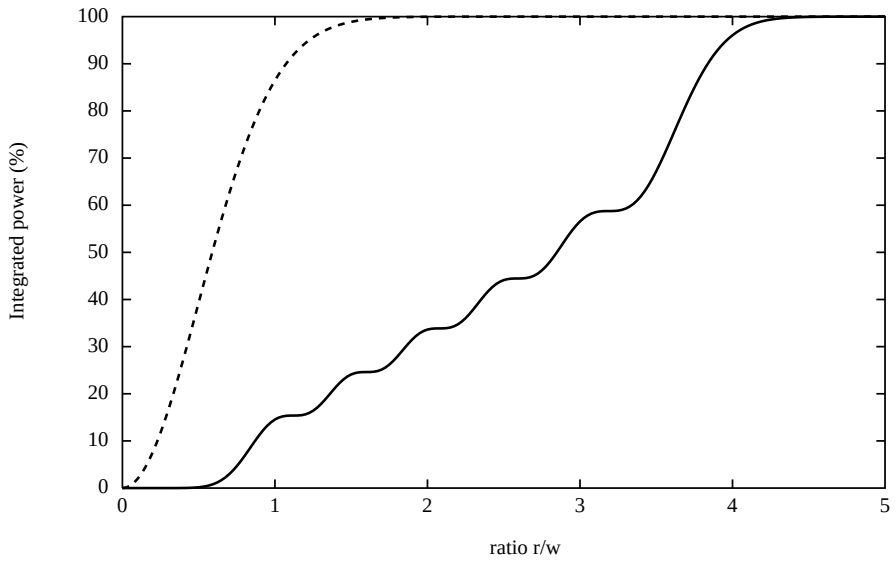

Figure 7.24: Integrated power for $LG_{5,5}$ (solid line) and $LG_{0,0}$ (dashed line) (w=3.5 cm)

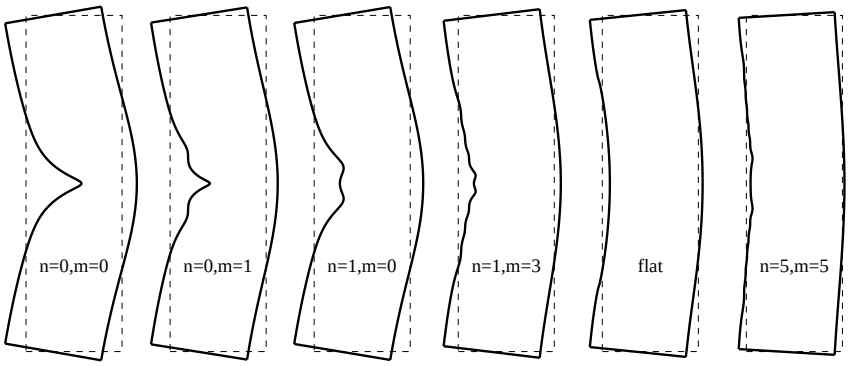

Figure 7.25: Deformation of a cylindrical mirror (a= 17.5 cm, h= 10 cm) under a $\mathrm{LG}_{n,m}$ readout beam (w = 3.5 cm) normalized to 150 MW (1 N integrated radiation pressure), exaggerated by a factor of 2×10^8. The case of a flat beam b = 11.3 cm is also shown

find for the fundamental:

$$U^{(0)}_{\text{input},0} \;=\; 2.02\ 10^{-10}\text{J.N}^{-2} \tag{7.43}$$

then, for the Virgo end mirrors (w= 5.54 cm):

$$U^{(0)}_{\text{end},0} \;=\; 7.43\ 10^{-11}\text{J.N}^{-2} \tag{7.44}$$

For comparison, with a flat mode of radius 11.3 cm, we have

$$U_{\text{flat}} \;=\; 1.88\ 10^{-11}\text{J.N}^{-2} \tag{7.45}$$

The gain in thermal noise are:

$$g_{\text{end/input}} \;=\; \sqrt{\frac{U^{(0)}_{\text{end},0}}{U^{(0)}_{\text{input},0}}} \;\sim\; 0.6$$

$$g_{\text{flat/input}} \;=\; \sqrt{\frac{U_{\text{flat}}}{U^{(0)}_{\text{input},0}}} \;\sim\; 0.3$$

By increasing the order of the LG mode and the beam parameter w, it is possible to reach gains comparable to this flat mode. For instance, with a $\text{LG}_{0,3}$ mode of parameter w = 4.5 cm, or a $\text{LG}_{1,2}$ mode of parameter w = 4.78 cm, we get in both cases

$$U \;=\; 1.85\ 10^{-11}\text{J.N}^{-2}$$

meaning a gain of ~ 0.3, and it is possible to do better. One must however consider the diffraction losses when the width w of the mode becomes too large compared to the mirror's radius a (see Fig.7.26). For each mode, there is a ratio a/w such that the losses fall to 1 ppm, and when comparing the gains for various orders, it is more relevant to take equal losses modes. On Fig.7.27 we show the ratio a/w insuring diffraction losses of 1 ppm, versus orders of the mode. We finally show (Fig.7.28) the gains relative to the worse situation of Virgo (input mirrors, $\text{LG}_{0,0}$, w=2 cm) for several higher order modes having each a w parameter adjusted to set diffraction losses at 1 ppm; the gain of the flat mode of size 11.3 cm (having the same losses) is also shown. Optimization of the beam parameter leads to symmetrical cavities having equally curved mirrors. Modes with $m \geq 2$ give already similar or better results than the flat mode.

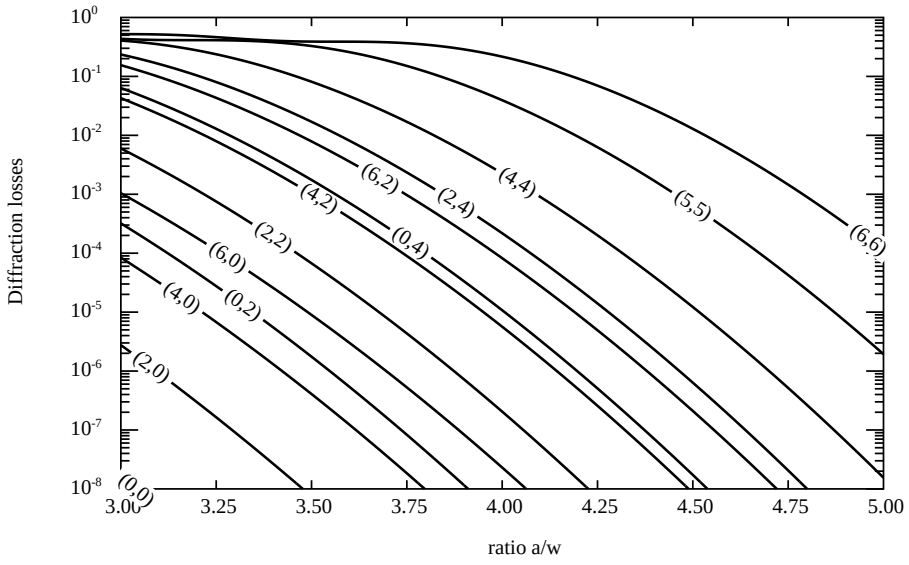

Figure 7.26: Diffraction losses vs ratio a/w for several LG modes

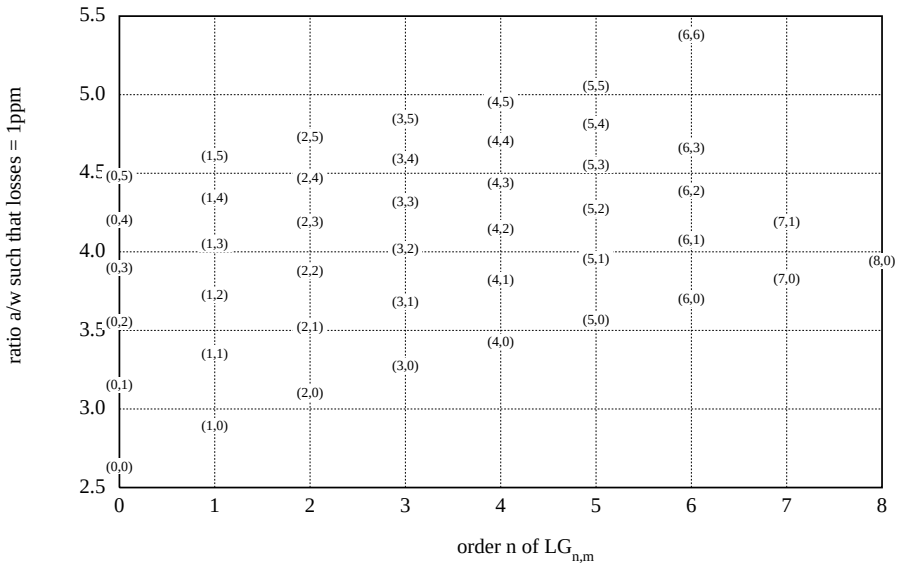

Figure 7.27: ratio a/w insuring 1 ppm diffraction losses vs order of the LG mode

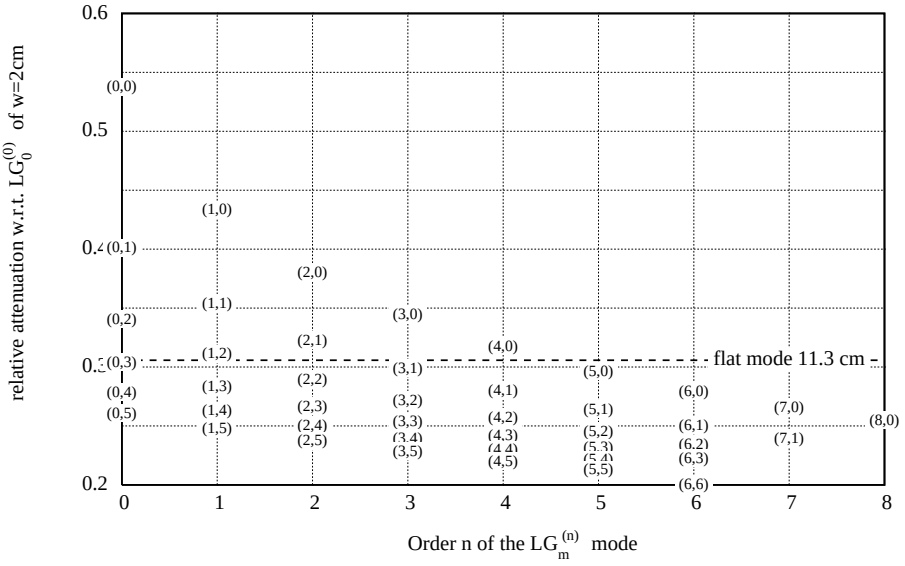

Figure 7.28: Relative reduction in root spectral density of thermal noise vs order (n, m) of the LG mode (each having a w tuned for 1 ppm diffraction losses).

To be specific, let us compute the spectral densities of displacement equivalent to thermal noise in some cases. We assume a loss angle of $\phi = 10^{-6}$. Firstly, in the case of a $\mathrm{TEM}_{0,0}$, $w = 2$ cm beam on a Virgo input mirror:

$$S_x^{1/2}(f) = 1.03\,10^{-19} \left[\frac{100\,\mathrm{Hz}}{f}\right]^{1/2} \mathrm{m.Hz}^{-1/2} \tag{7.46}$$

for $w = 3.5$ cm:

$$S_x^{1/2}(f) = 7.90\,10^{-20} \left[\frac{100\,\mathrm{Hz}}{f}\right]^{1/2} \mathrm{m.Hz}^{-1/2} \tag{7.47}$$

then for a flat mode of radius 11.3 cm:

$$S_x^{1/2}(f) = 3.15\,10^{-20} \left[\frac{100\,\mathrm{Hz}}{f}\right]^{1/2} \mathrm{m.Hz}^{-1/2} \tag{7.48}$$

and now for a $\mathrm{LG}_{5,5}$, $w = 3.5$ cm:

$$S_x^{1/2}(f) = 2.13\,10^{-20} \left[\frac{100\,\mathrm{Hz}}{f}\right]^{1/2} \mathrm{m.Hz}^{-1/2} \tag{7.49}$$

If we compare the 1st example (standard Virgo) to the third (in some "advanced Virgo"), we note a gain factor of ~ 5 in sensitivity in the 100 Hz region.

7.11 Conclusion and perspectives

It is possible to have a reduction of thermal noise comparable to or even better than that obtained with flat modes, by using moderately high order Laguerre-Gauss axisymmetrical modes. It seems beneficial that these modes are compatible with spherical cavity mirrors instead of "Mexican" surface shapes. The diffraction losses on the end mirror would however be too large in the present design (flat/spherical) of the Virgo cavities (2 cm waist on flat input mirror). If the flat/spherical cavities are replaced by symmetrical spherical/spherical cavities, that issue could be overcome. The question of generation of such modes having complex annular patterns could be solved by the recently developed fiber technology (Bragg fibers)[**?**], allowing to design fiber-lasers with analogous mode structures. A study of the optical stability of such a cavity operating with a $\mathrm{LG}_{n,m}$ mode is now necessary to confirm that it could be practically operated this way. In particular, the issue of the degeneracy of $\mathrm{LG}_{n,m}$ modes having the same $n + 2m$ is to be addressed.

Chapter 8

Thermoelastic noise

8.1 Introduction

The brownian motion of matter inside the substrates is not the only cause of noise in the optical readout. There is another cause due to temperature fluctuations in a finite volume of material. These fluctuations are called thermodynamical and can couple with strain via the thermal dilatation constant α, producing eventually random motions of the surface. A good way for modeling this kind of noise is to start from the general thermodynamical formulas as detailed by Landau and Lifshitz [36], and use the Levin approach already presented. As in the preceding chapter, we shall consider the low frequency tail of the spectral density of the effective motion of the surface (i.e. the readout noise) as depending on the energy dissipated when the body is under a virtual pressure having the same profile as the optical beam and excited at low frequency. In this case, the spectral density is still of the form (Levin's formula):

$$S_x(f) \;=\; \frac{4k_BT}{\omega^2}\,W \tag{8.1}$$

where W is the average dissipated energy. For the standard thermal noise, we had $W = 2U\omega\Phi$ as average dissipated energy, Φ being a global loss angle and U the static strain energy. But now W must be interpreted as the energy dissipated via coupling of the strain with the temperature field in the bulk. Obviously, the temperature field itself depends on the strain field. Using the same approach as used in [34], we first solve the static linear elastical problem (it is done in the preceding chapter), then we compute the resulting temperature field, and use it to compute the dissipated energy. For

computing the dissipated energy, we use the time dependence of the entropy S. The variations of the entropy density are related to the heat flux $\vec{q}$ by requiring conservation of the energy in the body:

$$T\,\frac{\partial S}{\partial t} \;=\; -\,\mathrm{div}(\vec{q}) \tag{8.2}$$

where $\vec{q} = -K\,\mathrm{grad}T$, K being the thermal conductivity of the material (cf.Landau and Lifshitz [36]). Or, as well:

$$\frac{\partial S}{\partial t} \;=\; -\,\frac{1}{T}\mathrm{div}(\vec{q})$$

The total entropy variation in the body is therefore:

$$\frac{dS_{\mathrm{tot}}}{dt} \;=\; -\int \frac{1}{T}\mathrm{div}(\vec{q})\,dV$$

where the integral is extended to the whole body. this is as well:

$$\frac{dS_{\mathrm{tot}}}{dt} \;=\; -\int \mathrm{div}\frac{\vec{q}}{T}\,dV + \int \vec{q}.\mathrm{grad}\left(\frac{1}{T}\right)\,dV$$

Owing to the fact that the heat flux is zero on the surface of the body, the first integral vanishes, and we have:

$$\frac{dS_{\mathrm{tot}}}{dt} \;=\; -\int \frac{1}{T^2}\,\vec{q}.\mathrm{grad}\,T\,dV$$

but using the definition of $\vec{q}$, this is:

$$\frac{dS_{\mathrm{tot}}}{dt} \;=\; \int \frac{K}{T^2}\,(\mathrm{grad}\,T)^2\,dV$$

so that the energy variation is :

$$W \;=\; T\,\frac{dS_{\mathrm{tot}}}{dt} \;=\; \int \frac{K}{T}\,(\mathrm{grad}\,T)^2\,dV \tag{8.3}$$

We shall say now that the temperature gradient field is caused by the small deformations of the body that we have computed precedingly, while T is the mean temperature. This becomes:

$$W \;=\; T\,\frac{dS_{\mathrm{tot}}}{dt} \;=\; \frac{K}{T}\int (\mathrm{grad}\,\delta T)^2\,dV \tag{8.4}$$

Where we have replaced T by a δT in the gradient for more clarity. On the other hand, it is well known (cf. Landau-Lifshitz) that the total entropy is the sum of two terms, one being the entropy in the reference state, and a second one proportional to the trace E of the strain tensor:

$$S = S_0 + \nu E$$

ν being the thermoelastic coefficient. so that there is in the bulk material a power source given by

$$P \;=\; T.\frac{dS}{dt} \;=\; \nu\, T\, \frac{dE}{dt}$$

where E is the trace of E_{ik}. The resulting temperature field obeys the Heat (Fourier) equation:

$$(\rho C \partial_t - K\,\Delta)\,\delta T \;=\; \nu\, T\, \frac{dE}{dt} \tag{8.5}$$

The trace of the strain tensor E_{ik} found in the preceding chapter is in any case a harmonic function, so that there is a trivial solution:

$$\delta T \;=\; \frac{\nu T}{\rho C}\, E$$

The boundary conditions (null heat flux on the surfaces) are considered satisfied in time average (δT is assumed oscillating at a few tens of Hz).In fact, they are exactly satisfied on the circular edge of the mirror. Now we reach the relevant equation for the dissipated energy:

$$W \;= \frac{K\nu^2 T}{\rho^2 C^2} \int (\text{grad}\; E)^2\, dV \tag{8.6}$$

ν is related to the linear dilatation coefficient α by

$$\nu \;=\; \frac{\alpha\, Y}{1-2\sigma}$$

where Y is the Young modulus, and σ the Poisson ratio. Finally:

$$W \;=\; KT\, \left[\frac{\alpha Y}{(1-2\sigma)\rho C}\right]^2 \int (\text{grad}\; E)^2\, dV \tag{8.7}$$

(see [34]). We have after the preceding chapter on standard thermal noise all the material for computing W.

8.2 Case of infinite mirrors

Let us recall the results obtained in the preceding chapter on standard thermal noise. Under beam pressure, the displacement vector is:

$$u_r(r,z) \;=\; \int_0^\infty u(k)\,[kz-1+2\sigma]\exp(-kz)\,J_1(kz)\,k\,dk \tag{8.8}$$

$$u_z(r,z) \;=\; \int_0^\infty u(k)\,[kz+2-2\sigma]\exp(-kz)\,J_0(kz)\,k\,dk \tag{8.9}$$

so that:

$$E(r,z) \;=\; \mathrm{div}\,\vec{u}(r,z) \;=\; -2(1-2\sigma)\int_0^\infty u(k)\,\exp(-kz)\,J_0(kz)\,k^2\,dk \tag{8.10}$$

The function $u(k)$ is determined by the virtual pressure distribution $p(r)$. Namely:

$$u(k) \;=\; -\frac{1+\sigma}{Y}\,\frac{\tilde{p}(k)}{k} \tag{8.11}$$

where $\tilde{p}(k)$ is the Fourier-Bessel transform of $p(r)$. As a result,

$$E(r,z) \;=\; -\,\frac{2(1-2\sigma)(1+\sigma)}{Y}\int_0^\infty \tilde{p}(k)\,\exp(-kz)\,J_0(kr)\,k\,dk$$

Which shows, in passing, that

$$E(r,0) \;=\; -\,\frac{2(1-2\sigma)(1+\sigma)}{Y}\,p(r)$$

We can thus already foresee that in the case of an ideally flat top beam, the gradient will involve Dirac distributions, and therefore the volume integration of its square will be problematic. Let us compute the gradient of E:

$$\frac{\partial E}{\partial r} \;=\; \frac{2(1-2\sigma)(1+\sigma)}{Y}\int_0^\infty \tilde{p}(k)\,\exp(-kz)\,J_1(kz)\,k^2\,dk$$

$$\frac{\partial E}{\partial z} \;=\; \frac{2(1-2\sigma)(1+\sigma)}{Y}\int_0^\infty \tilde{p}(k)\,\exp(-kz)\,J_0(kz)\,k^2\,dk$$

Now, using the closure relation

$$\int_0^\infty J_\nu(kr)\,J_\nu(k'r)\,r\,dr \;=\; \frac{\delta(k-k')}{k} \tag{8.12}$$

for $\nu = 0, 1$. It is now possible to carry out the volume integration:

$$2\pi \int_0^\infty r\,dr \int_0^\infty dz\ (\vec{\mathrm{grad}}E)^2 \ = \ 8\pi \frac{(1-2\sigma)^2(1+\sigma)^2}{Y^2} \int_0^\infty \tilde{p}(k)^2\, k^2\, dk \quad (8.13)$$

so that

$$W \ = \ \frac{KT\alpha^2(1+\sigma)^2}{\rho^2 C^2} \int_0^\infty \tilde{p}(k)^2\, k^2\, dk \quad (8.14)$$

This expression shows that the function $\tilde{p}(k)$ must have an asymptotic behavior better than $k^{-3/2}$ for the integral to converge. This is a strong requirement on the Fourier transform of the pressure distribution.

8.2.1 Gaussian beams

For a gaussian profile of half width w, we have seen that:

$$\tilde{p}(k) \ = \ \frac{1}{2\pi} \exp\left[-k^2 w^2/8\right]$$

giving

$$\int (\vec{\mathrm{grad}}E)^2\, dV \ = \ \frac{4(1-2\sigma)^2(1+\sigma)^2}{\sqrt{\pi} Y^2 w^3} \quad (8.15)$$

so that the spectral density of thermoelastic noise is, using (8.1) and (8.7):

$$S_x(f) \ = \ \frac{4k_B KT^2\alpha^2(1+\sigma)^2}{\sqrt{\pi}\,\rho^2\, C^2\, f^2 w^3} \quad (8.16)$$

This result has been found firstly by Braginsky et al.[35], then by Liu et al.[34], using the preceding approach. For silica parameters:

$$K \ \sim \ 1.4 \ \mathrm{W.m^{-1}.K^{-1}}$$
$$\alpha \ \sim \ 5.4\,10^{-7} \ \mathrm{K^{-1}}$$
$$\rho \ \sim \ 2,202 \mathrm{kg.m^{-3}}$$
$$C \ \sim \ 7,500 \ \mathrm{J.kg^{-1}.K^{-1}}$$

on finds:

$$S_x(f)^{1/2} \ = \ 2.68\,10^{-20} \left[\frac{1\ \mathrm{Hz}}{f}\right] \mathrm{m.Hz^{-1/2}}$$

which is lower than the standard thermal noise, but almost significant. For the end mirrors ($w = 5.54$ cm) , this is:

$$S_x(f)^{1/2} \ = \ 5.81\,10^{-21} \left[\frac{1\ \mathrm{Hz}}{f}\right] \mathrm{m.Hz^{-1/2}}$$

8.2.2 Flat beams

If we now consider a flat beam modeled by its ideal representation:

$$p(r) \;=\; \begin{cases} 1/\pi b^2 & (r < b) \\ 0 & (r \geq b) \end{cases}$$

we have the Fourier-Bessel transform:

$$\tilde{p}(k) \;=\; \frac{J_1(kb)}{\pi\, kb}$$

which shows that the requirement on the decreasing rate for large k is not fulfilled, $J_\nu(k)$ having an asymptotic behavior in $k^{-1/2}$. If we try to compute the integral, we get:

$$\int (\vec{\mathrm{grad}}\, E)^2\, dV \;=\; \frac{8(1-2\sigma)^2(1+\sigma)^2}{\pi b^3} \int_0^\infty J_1(x)^2\, dx$$

wich is a divergent integral.This is the consequence of our preceding remark on the discontinuity of the pressure. For fun, we note that "Mathematica" nevertheless gives a finite (and rather strange) result:

$$\int_0^\infty J_1(x)^2\, dx \;=\; \frac{\mathrm{Ln}(64) - 4 + 2\gamma}{2\pi}$$

(γ = Euler's constant). We meet two conclusions: the first is that we must carry out a numerical integration with the "realistic" flat modes detailed in the preceding chapter, the second is that we must be cautious with results of symbolic computation softwares.

8.3 Case of finite mirrors

In the case of finite mirrors, the model developped for standard thermal noise provides the explicit expressions for the trace E of the strain tensor:

$$E(r,z) \;=\; E_0(r,z) + \Delta E(r,z)$$

with

$$E_0(r,z) \;=\; -\,\frac{2(1-2\sigma)(1+\sigma)}{\pi a^2 Y} \sum_{m>0} \frac{p_m}{D_m} J_0(\zeta_m r/a) \left[u_m\, \mathrm{e}^{-\zeta_m z/a} - v_m\, \mathrm{e}^{\zeta_m z/a} \right]$$

where the p_m are the Fourier-Bessel coefficients of the pressure distribution, and where the D_m have been defined in the preceding chapter. The u_m, v_m are:

$$u_m = 1 - q_m + 2q_m x_m, \quad v_m = q_m(1 - q_m + 2x_m)$$

q_m and x_m have also the same definitions. Moreover,

$$\Delta E(r,z) = -\frac{1-2\sigma}{\pi a^2 Y}\left[1 - 12s - (1-24s)z/h\right]$$

so that the gradient of E is:

$$\frac{\partial E_0}{\partial r} = \frac{2(1-2\sigma)(1+\sigma)}{\pi a^3 Y}\sum_{m>0}\frac{p_m\zeta_m}{D_m}J_1(\zeta_m r/a)\left[u_m\,\mathrm{e}^{-\zeta_m z/a} - v_m\,\mathrm{e}^{\zeta_m z/a}\right] \tag{8.17}$$

$$\frac{\partial E_0}{\partial z} = \frac{2(1-2\sigma)(1+\sigma)}{\pi a^3 Y}\sum_{m>0}\frac{p_m\zeta_m}{D_m}J_0(\zeta_m r/a)\left[u_m\,\mathrm{e}^{-\zeta_m z/a} + v_m\,\mathrm{e}^{\zeta_m z/a}\right] \tag{8.18}$$

$$\frac{\partial \Delta E}{\partial z} = \frac{1-2\sigma}{\pi a^2 h Y}(1-24s) \tag{8.19}$$

Owing to the orthogonality relations for the $J_\nu(\zeta_m r/a)$, we get

$$\int(\vec{\mathrm{grad}}\,E_0)^2\,dV = \frac{4(1-2\sigma)^2(1+\sigma)^2}{\pi a^3 Y^2}\sum_{m>0} w_m \tag{8.20}$$

where

$$w_m = \frac{p_m^2\zeta_m}{D_m^2}J_0(\zeta_m)^2\,(1-q_m)\times$$

$$\times\left[(1-q_m)(1-q_m^2) + 8q_m(1-q_m)x_m + 4q_m(1+q_m)x_m^2\right]$$

and obviously,

$$\int(\vec{\mathrm{grad}}\Delta E)^2\,dV = \frac{(1-2\sigma)^2}{\pi a^2 h Y^2}(1-24s)^2$$

(NB: $\vec{\mathrm{grad}}\Delta E$ and $\vec{\mathrm{grad}}\,E_0$ are orthogonal in the r integration). We have successively:

$$W = \frac{4KT\alpha^2}{\pi a^3\rho^2 C^2}\left[(1+\sigma)^2\sum_{m>0} w_m + (1-24s)^2\frac{a}{4h}\right]$$

And for the spectral density:

$$S_x(f) = \frac{4k_B KT^2\alpha^2}{\pi a^3\rho^2 C^2 f^2}\left[(1+\sigma)^2\sum_{m>0} w_m + (1-24s)^2\frac{a}{4h}\right] \tag{8.21}$$

8.3.1 Gaussian beams

For gaussian beams, we substitute the p_m's in the preceding formulae. For the parameters corresponding to Virgo input mirrors (w =2 cm, a = 17.5 cm, h = 10 cm, we find:

$$S_x^{1/2}(f) \;=\; 2.76\,10^{-20}\ \mathrm{m.Hz^{-1/2}}\left[\frac{1\ \mathrm{Hz}}{f}\right]$$

slightly worse than the infinite case. For w = 5.54 cm (end mirrors):

$$S_x^{1/2}(f) \;=\; 8.20\,10^{-21}\ \mathrm{m.Hz^{-1/2}}\left[\frac{1\ \mathrm{Hz}}{f}\right]$$

in Fig.8.1, one sees the distribution of $(\mathrm{grad}E)^2$ in the case of an input Virgo mirror. which is worse than the infinite case.

8.3.2 Flat modes

The same drawback happens in the case of ideally flat modes. The sharp edge generates high spatial frequencies that forbid the Fourier-Bessel coefficients p_m to have a decreasing rate able to secure the convergence of the series. One more time we have to numerically compute the p_m for realistic flat modes. The result for a Virgo-like mirror (a = 17.5 cm, h = 10 cm) and for a realistic mode (b = 10 cm, w_0 = 3.2 cm), is:

$$S_x^{1/2}(f) \;=\; 4.89\,10^{-21}\ \mathrm{m.Hz^{-1/2}}\left[\frac{1\ \mathrm{Hz}}{f}\right] \tag{8.22}$$

It is weakly dependent on the parameter w_0 (sharpness of the beam's edge). To be specific, for w_0 = 1 cm, this is

$$S_x^{1/2}(f) \;=\; 4.92\,10^{-21}\ \mathrm{m.Hz^{-1/2}}\left[\frac{1\ \mathrm{Hz}}{f}\right]^2$$

On Fig.8.2, we have represented the distribution of $(\mathrm{grad}E)^2$ for a realistic flat mode (b = 10 cm, w_0 = 1 cm). Note the two "hot" points corresponding to the regions where the gradient is the largest. When sharping the edge, these points become hoter and hoter, yielding a singularity in the limit of an ideal flat top beam.

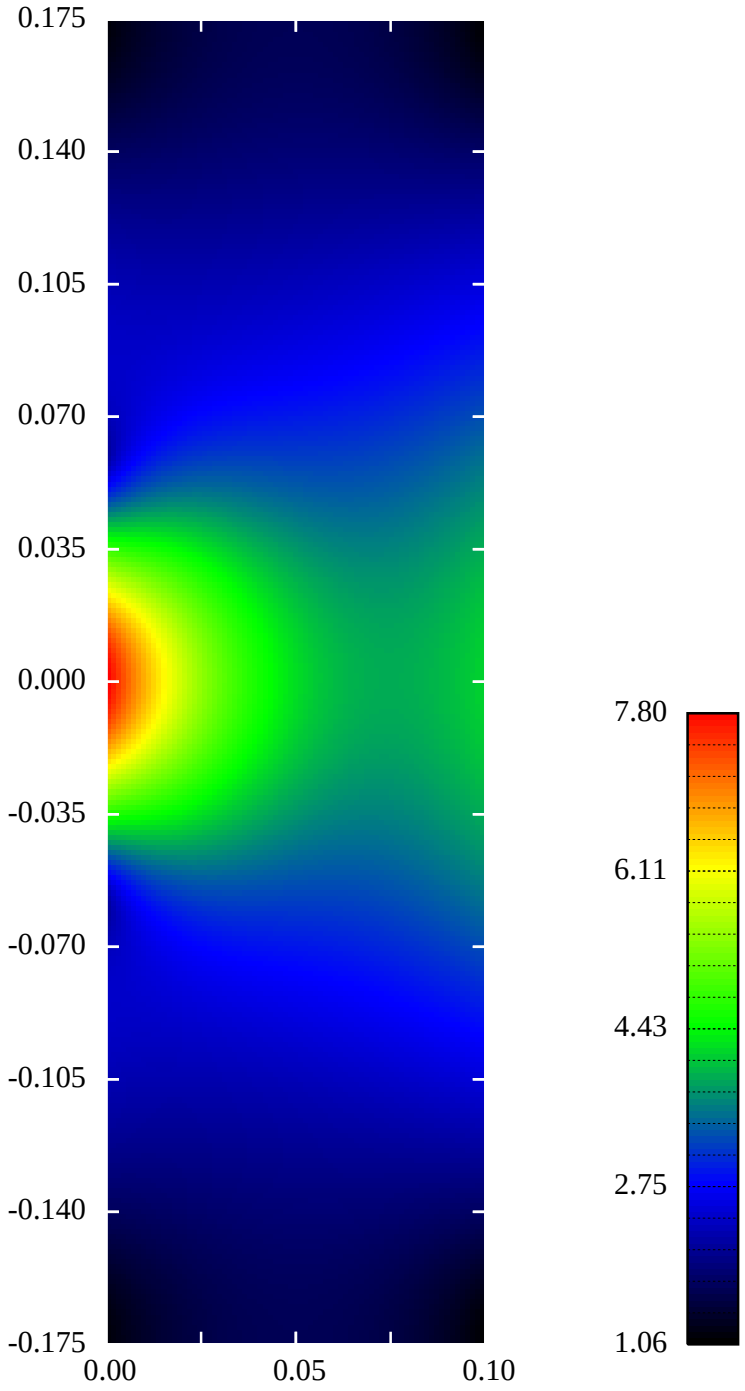

Figure 8.1: Distribution of the square gradient of the temperature in the case of a gaussian beam. (Logarithmic scale, arbitrary units)

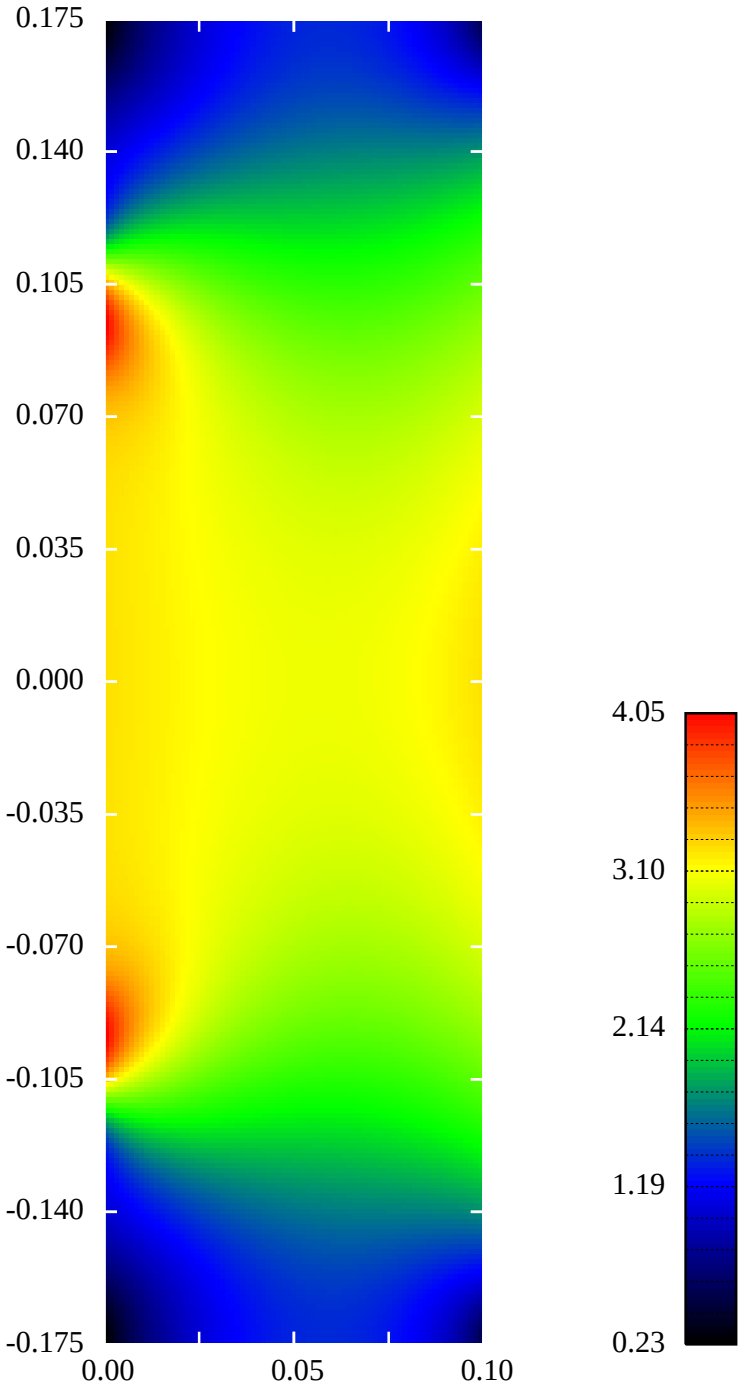

Figure 8.2: Distribution of the square gradient of the temperature in the case of a realistic flat beam. (Logarithmic scale, arbitrary units)

Chapter 9

Modulation and Transfer functions

9.1 Introduction

Analysis of the statistical structure of noise at the output of gravitational wave interferometers like LIGO or Virgo is essential regarding two different tasks, that are the commissionning of the instrument and the signal processing. During the first test runs of the new instrument, identification of special types of noise will be a valuable aid to diagnostics and correction for bias. During the regular exploitation period, many filtering techniques requiring a good knowledge of the spectral density of the instrument noise will be running on line. Moreover, it will be necessary to permanently control the stationarity of statistical parameters. A correct association between noise characteristics and parts of the instrument requires information about the transfer functions relating elementary perturbations of these elements and output at the different ports of the interferometer. In the present study, we show how to systematically construct these transfer functions, starting from elementary objects like mirrors and space between them, in a way easily done numerically, increasing the reliability of the results with respect to long special analytical formulas. These elementary objects are so simple that one can rely on them, then the proper algebra being defined, one has simply to code the simple general analytical formulas, and the correct result is automatically obtained. We shall present as first results and examples, transfer functions for the motions of mirrors, for laser frequency fluctuations, for the modulator

frequency fluctuations, and for a gravitational wave. The last one is necessary for evaluating the spectral densities of gravitational amplitudes equivalent to the various sources of noise and add them in a consistent way for obtaining the spectral sensivity of the instrument. The modulation/demodulation system plays an essential role in the derivation of transfer functions, and we give the expressions for a lock in detection with a given phase lag. A special attention is devoted to the question of modulated quantum noise. This approach is especially well adapted to object-oriented coding.

9.2 Elementary perturbations and audio sidebands

The basic elements constituting an interferometer are the mirrors and the vacuum space in between them. The possible perturbations reduce consequently to two kinds : changes in position of the mirrors, and changes in the vacuum properties due to a passing GW. In the present approach, we shall describe the light beams circulating in the instrument as plane waves and mirrors as flat surfaces. In other words, we consider only the projection of the amplitudes on the TEM_{00} mode.

9.2.1 Perturbation of mirrors by small displacements

Small displacements of mirrors must be considered either for actual displacements (e.g. pendulum thermal noise), for distortions globally equivalent to a displacement of the hot spot on the coating (e.g. substrate thermal noise) or for any phase perturbation mathematically equivalent to a displacement (e.g. scattered light recombination). This comprises a large class of phenomena. We shall assume infinite flat mirrors, and as only allowed perturbation, a displacement of the reflecting surface along its normal. This is not a loss of generality because other perturbations can be shown to eventually reduce to an equivalent longitudinal displacement. For instance this has been shown in detail [29],[30] for excited internal degrees of freedom of a real mirror if coupled to the beam phase (internal thermal noise). In the case of scattered light, the noisy recombination effect takes place on the mirror's surface and generate a phase that cannot be distinguished from a displacement phase. We restrict our attention to motions, or equivalent motions, $x(t)$ of amplitude very small compared to a wavelength, so that a first order expansion is

allowed, and all further computations are linear with respect to the displacement x. We shall moreover consider $x(t)$ as a zero mean random process of spectral density $x^2(f)$ and will refer to $x(f)$ as its "root spectral density" (RSD). Thanks to the linarity of the calculations, it is allowed and convenient to consider $x(f)$ as the amplitude of a Fourier component of the motion at frequency f, and study the situation created by this elementary harmonic perturbation : The result is to add two sidebands to the main wave, so that the amplitude of light anywhere in the interferometer is modulated, i.e. of the form

$$A(t) \;=\; \left(A_0 + \frac{1}{2}\Phi(f)\,A_1 \mathrm{e}^{-i\Omega t} + \frac{1}{2}\Phi(f)\,A_2 \mathrm{e}^{i\Omega t}\right) \mathrm{e}^{-i\omega_L t} \tag{9.1}$$

where $\omega_L/2\pi$ is the laser frequency, and $\Omega \equiv 2\pi f$. $\Phi(f) = 4\pi x(f)/\lambda$ is the RSD of phase equivalent to the displacement. This form will hold quite generally, whatever the cause of the phase fluctuation is. Because we intend to study the noise in the detection band (a few Hz to a few kHz), we call these "audio" sidebands. Assume a wave of the preceding form is reflected by our moving mirror, the incidence angle being θ (almost all incidence angles in the interferometer are zero, except on the splitter, which leads us to consider the general case); provided that the incident wave is propagating to the right, the reflected amplitude B(t) is given by $B(t) = i\ r\ A[t - 2x(t)\cos\theta/c]$, because the reflected wave experiences then an extra delay. Obviously, if the incident wave now comes from the right, we have to replace x by $-x$. We have

$$\begin{aligned} B(t) \;= i\ r\ \Big(& A_0\, \mathrm{e}^{-i\omega_L(t-2x\cos\theta/c)} + \frac{1}{2}\,\Phi(f)\,A_1 \mathrm{e}^{i[(\omega_L+\Omega)(t-2x\cos\theta/c)} \\ & + \frac{1}{2}\,\Phi(f)\,A_2 \mathrm{e}^{i[(\omega_L-\Omega)(t-2x\cos\theta/c)}\Big) \end{aligned} \tag{9.2}$$

The factor of i is inserted for taking into account the necessary relative phase of $\pi/2$ between the reflected and the transmitted wave at each partial reflection (all transmission coefficients will be thus taken real). Substituting $x(t) = x(f)\cos(\Omega t)$ and expanding this expression at first order leads to

$$\begin{aligned} B(t) \;=\; & A_0\, \mathrm{e}^{-i\omega_L t}\left(1 + \frac{2\,i\,\pi x(f)\,cos\theta}{\lambda}\ \mathrm{e}^{-i\Omega t} + \frac{2\,i\,\pi x(f)\,cos\theta}{\lambda}\ \mathrm{e}^{i\Omega t}\right) \\ & + \frac{1}{2}\ \Phi(f)\,A_1 \mathrm{e}^{-i[(\omega_L+\Omega)t} + \frac{1}{2}\ \Phi(f)\,A_2 \mathrm{e}^{-i[(\omega_L-\Omega)t} \end{aligned} \tag{9.3}$$

This verifies that the structure (carrier+2 sidebands) is stable and consequently it is allowed representing the modulated amplitudes by 3-vectors as : $A = (A_0, A_1, A_2)$. Reflection is then a linear operator, and we can write, for a mirror of photometric reflectivity r, and for a wave coming from the left :

$$B = i\, r\, R\, A$$

the operator R having the form

$$R = \begin{pmatrix} 1 & 0 & 0 \\ i\cos\theta & 1 & 0 \\ i\cos\theta & 0 & 1 \end{pmatrix} \tag{9.4}$$

If the wave is coming from the right, we have to change the sign of the non diagonal elements. This means that a mirror has two operators : a left side reflection operator R, and a right side operator $\overline{R} = R^{-1}$. This sign convention is quite arbitrary, and is of no consequence if we consider only one perturbed mirror in a given configuration. But if we intend to study coherent motions of pairs of mirrors, (common modes, or differential modes, for instance), we have to be careful with the signs. With this operator notation, R_{10} for instance, is a transfer function relating the upper sideband amplitude to the RSD of phase $\Phi(f) = 2kx(f)$.

9.2.2 Perturbation of a vacuum by a gravitational wave

A passing gravitational wave will perturb light-distance measurements due to small changes in the space-time metrics. Assume a GW of amplitude h and frequency $f = \Omega/2\pi$ propagating along the z direction, having the + polarization. A photon travelling along the x or y direction and detected at time t after a round trip of length $2L$, was emitted at the retarded time

$$t_r = t - \frac{2L}{c} - \epsilon\, \frac{hL}{c}\, \mathrm{sinc}(\Omega L/c) \cos[\Omega(t - L/c)]$$

where $\epsilon = \pm 1$ depending on the direction x or y ([27]). Consider now a wave already modulated at the gravitational frequency f, i.e. having two sidebands proportional to h, of the form

$$A(t) = \left(A_0 + \frac{h}{2}\, A_1 \mathrm{e}^{-i\Omega t} + \frac{h}{2}\, A_2 \mathrm{e}^{i\Omega t} \right) \mathrm{e}^{-i\omega t}$$

The propagated amplitude $B(t)$ is nothing but the incoming wave taken at the retarded time, i.e.

$$B(t) \;=\; A(t_r)$$

so that we obtain

$$B(t) \;=\; \left(B_0 \;+\frac{h}{2}\; B_1\; \mathrm{e}^{-i\Omega t} + \frac{h}{2}\; B_2\; \mathrm{e}^{i\Omega t}\right) \mathrm{e}^{-i\omega t}$$

with (we set $K \;\equiv\; \Omega L/c$):

$$\begin{aligned} B_0 \;&= \mathrm{e}^{2ikL}\;\; A_0 \\ B_1 \;&=\; \mathrm{e}^{2i(k+K)L}\; A_1 \;-\; i\epsilon kL\; \mathrm{sinc}(KL)\mathrm{e}^{i(2k+K)L}\; A_0 \\ B_2 \;&=\; \mathrm{e}^{2i(k-K)L}\; A_2 \;-\; i\epsilon kL\; \mathrm{sinc}(KL)\mathrm{e}^{i(2k-K)L}\; A_0 \end{aligned}$$

This can be represented as the action of the operator (see [1]) :

$$P(2L) \;=\; \begin{pmatrix} \mathrm{e}^{2ikL} & 0 & 0 \\ i\,\epsilon\,\mathrm{e}^{i(2k+K)L}\mathrm{sinc}(KL) & \mathrm{e}^{2i(k+K)L} & 0 \\ i\,\epsilon\,\mathrm{e}^{i(2k-K)L}\mathrm{sinc}(KL) & 0 & \mathrm{e}^{2i(k-K)L} \end{pmatrix} \tag{9.5}$$

on vector amplitudes. According to the above outlined philosophy, the diagonal terms express the phase factor corresponding to ordinary propagation in a vacuum of waves of frequency $\nu_L, \nu_L + f, \nu_L - f$ respectively, whereas $P(2L)_{10}$ must be understood as the transfer function relating the upper sideband amplitude to the RSD of phase $\Phi(f) \;=\; kh(f)L$. Obviously, the off-diagonal terms evaluate the creation of sidebands by the GW, and are the seed of the whole detection process in an interferometer; however they may be significantly different from zero only on very long distances. Though the preceding expression is valid in general, the off-diagonal terms will be considered only in the case of propagation in the km long Fabry-Perot cavities.

9.2.3 Algebra of first order perturbations

Any history of modulated light through the interferometer is thus represented by a product of propagation and reflection rank 3 operators, and consequently, a matter of algebra. The general form of any operator is :

$$O \;=\; \begin{pmatrix} O_{00} & 0 & 0 \\ O_{10} & O_{11} & 0 \\ O_{20} & 0 & O_{22} \end{pmatrix} \tag{9.6}$$

The product of two operators A, B is

$$(AB) = \begin{pmatrix} (AB)_{00} = A_{00}B_{00} & 0 & 0 \\ (AB)_{10} = A_{10}B_{00} + A_{11}B_{10} & (AB)_{11} = A_{11}B_{11} & 0 \\ (AB)_{20} = A_{20}B_{00} + A_{22}B_{20} & 0 & (AB)_{22} = A_{22}B_{22} \end{pmatrix} \tag{9.7}$$

For the inverse A^{-1} of any operator A, we have :

$$A^{-1} = \begin{pmatrix} (A^{-1})_{00} = 1/A_{00} & 0 & 0 \\ (A^{-1})_{10} = -A_{10}/A_{00}A_{11} & (A^{-1})_{11} = 1/A_{11} & 0 \\ (A^{-1})_{20} = -A_{20}/A_{00}A_{22} & 0 & (A^{-1})_{22} = 1/A_{22} \end{pmatrix} \tag{9.8}$$

This is a non commutative algebra we call $\mathcal{A}$ for brevity, isomorphous to the algebra of first order expansions, it is very simple, very fast (there is no need of a general matrix inversion) , and easy to implement in a numerical code. We show hereafter how for any complex optical scheme, it is possible using $\mathcal{A}$ to compute global transmission and reflection operators between an input point and any output point. We have presented for the sake of clarity the full three dimensional version of this algebra, and one could argue a redundancy, due to the fact that (02) (resp. (22)) components can be deduced from (01) (resp (11)) components by simply changing Ω into $-\Omega$. In a numerical scheme, however, it is anyway necessary to evaluate all the components, and consequently using rank 3 operators (in practice 5 components objects) is not a waste of time nor memory.

9.3 Interferometer operators

9.3.1 Cavity

The basic parameters of a mirror are the reflection coefficient r, the transmission coefficient t and the loss rate p. The power balance reads $r^2 + t^2 = 1 - p$. A Fabry-Perot cavity consists of two mirrors, a coupling mirror M_1 of parameters r_1, t_1, p_1 and a maximum reflectance mirror M_2 of parameters r_2, t_2, p_2, separated by a vacuum gap of length L. The equation relating the incoming field A_{in} and the intracaviy field B is

$$B = t_1 A_{in} - r_1 r_2 \overline{R_1} P(L) R_2 P(L)\ B \tag{9.9}$$

in this expression we note that the transmission is represented by a pure scalar, owing to the fact that a motion of the transparent sustrate of the

mirror does not affect the phase of a transmitted wave, we note that the R_2 operator has been conjugated (or inverted) because the normal to M_2 is in the opposite direction with respect to that of M_1. We shall consider separately the effects of perturbations, so that either $P(L)$ is gravitationnally perturbed and then R_1, R_2 reduce to identity, or M_1 or M_2 is moving and then $P(L)$ is diagonal. We have

$$B \;=\; \left(1 + r_1 r_2 \overline{R_1} P(L) R_2 P(L)\right)^{-1} \; t_1 A_{in} \tag{9.10}$$

Concerning the field A_{ref} reflected off the cavity, we have

$$A_{ref} \;=\; i\; r_1 R_1 A_{in} + i\; t_1^2 r_2 P(L) \overline{R_2} P(L)\, B \tag{9.11}$$

(remember that R_1 corresponds to a reflection at the left side, and $\overline{R_1}$ at the right side of M_1). We find $A_{ref} \;=\; i\; F\; A_{in}$ with the general formula :

$$F \;=\; R_1 \left[r_1 + (1-p_1) r_2 \overline{R_1} P(L) R_2 P(L)\right] \left[1 + r_1 r_2 \overline{R_1} P(L) R_2 P(L)\right]^{-1} \tag{9.12}$$

We can say that F is the Fabry-Perot reflectance operator. It contains three possible pertubations we enumerate below. Though it is quite useless to know the details of the operators in a numerical scheme, where we stick to synthetic algebraic expressions as the preceding one, instead of long special analytical formulas, it is nevertheless interesting to see the effect of these perturbations on the cavity $\mathcal{A}$ operator. We have the following general structure :

$$F \;=\; \begin{pmatrix} F_0 & 0 & 0 \\ G_1 & F_1 & 0 \\ G_{-1} & 0 & F_{-1} \end{pmatrix} \tag{9.13}$$

- GW event :

$$F \;=\; \left[r_1 + (1-p_1) r_2 P(2L)\right] \left[1 + r_1 r_2 P(2L)\right]^{-1} \tag{9.14}$$

M_1 and M_2 are pure scalars and $P(2L)$ is the perturbed propagator. we have here,

$$F_\mu \;=\; \frac{r_1 + (1-p_1) r_2 \mathrm{e}^{2i(k+\mu K)L}}{1 + r_1 r_2 \mathrm{e}^{2i(k+\mu K)L}} \quad (\mu = -1, 0, 1) \tag{9.15}$$

(ordinary reflectance for the carrier and the two sidebands),

$$G_\mu \;=\; i\; \epsilon \frac{r_2 t_1^2 \mathrm{e}^{i(2k+\mu K)L} \mathrm{sinc}(KL)}{\left(1 + r_1 r_2 \mathrm{e}^{2ikL}\right)\left(1 + r_1 r_2 \mathrm{e}^{2i(k+\mu K)L}\right)} \quad (\mu = -1, 1) \tag{9.16}$$

which represents the sidebands amplitudes created by the cavity while the GW event, with respect to the incoming carrier's.

- Motion of the coupling mirror M_1

$$F = \overline{R_1}\left[r_1 + (1-p_1)r_2 R_1 P(2L)\right]\left[1 + r_1 r_2 R_1 P(2L)\right]^{-1} \tag{9.17}$$

$P(2L)$ is diagonal and M_2 scalar. The components F_μ are the same as in the precedent item, but now :

$$G_\mu = -\,i\,\left(\frac{r_2 t_1^2 \mathrm{e}^{2ikL}}{(1 + r_1 r_2 \mathrm{e}^{2ikL})\,(1 + r_1 r_2 \mathrm{e}^{2i(k+\mu K)L})} - F_0\right) \tag{9.18}$$

- Motion of the far mirror M_2

$$F = \left[r_1 + (1-p_1)r_2 P(L)\overline{R_2}P(L)\right]\left[1 + r_1 r_2 P(L)\overline{R_2}P(L)\right]^{-1} \tag{9.19}$$

$P(L)$ is diagonal and M_1 scalar. The elements F_μ are still unchanged, and the G_μ are now :

$$G_\mu = i\,\frac{r_2 t_1^2 \mathrm{e}^{i(2k+\mu K)L}}{(1 + r_1 r_2 \mathrm{e}^{2ikL})\,(1 + r_1 r_2 \mathrm{e}^{2i(k+\mu K)L})} \tag{9.20}$$

(The change of sign with respect to the coupler formula comes from the opposite orientation of the normal). Note the close similarity between the GW case and an M_2 far mirror motion of amplitude $x(f) = \frac{1}{2}h(f)L$. At low frequencies the sinc function can be replaced by 1 and the two formulas become identical.

9.3.2 Michelson

A GW Michelson interferometer like LIGO or Virgo involves two arms containing each a Fabry-Perot cavity. For more clarity we can denote by "North" and "West" the directions of the arms without loss of generality. Knowing the operators F_{north}, F_{west} of both cavities, maybe having different parameters M_1, M_2, L due to unavoidable asymmetries, it is easy to compute the transmittance T_{mic} and the reflectance R_{mic} of the Michelson. We denote by M_s the splitter of parameters r_s, t_s, p_s, by a and b the short distances (see Fig.9.1) then the transmittance is

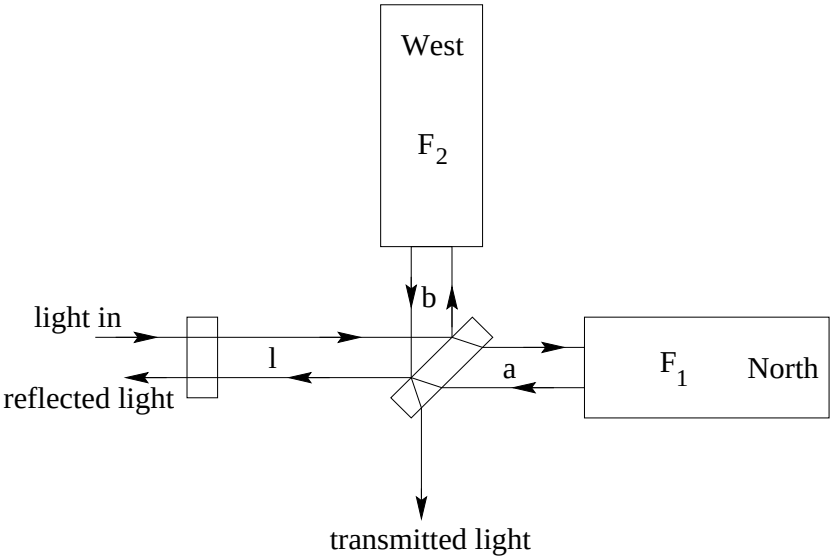

Figure 9.1: General setup for a Power recycled interferometer

$$T_{mic} = -r_s t_s \left(R_s^{-1} P(a) F_{north} P(a) + P(b) F_{west} P(b) R_s \right) \tag{9.21}$$

Let us note that the motion of any mirror can be considered as the sum of a motion along its normal, and a motion orthogonal to it. Only the normal part gives rise to a phase lag. There is therefore no ambiguity in the definition of the left and right sides of the splitter M_s : these are determined with respect to the right oriented normal. For the reflectance, we get

$$R_{mic} = t_s^2 P(a) F_{north} P(a) - r_s^2 R_s P(b) F_{west} P(b) R_s \tag{9.22}$$

In these expressions, $P(a)$ and $P(b)$ can be understood as diagonal, neglecting a possible GW perturbation on so short distances. In the operator R_s, the incidence angle is taken as $\pi/4$.

9.3.3 Recycled interferometer transmittance and reflectance

A recycling interferometer is a cavity involving a recycling mirror M_r of parameters r_r, t_r, p_r at a distance l of a Michelson (see Fig.9.1). Elementary calculations lead to the transmittance T_{itf} and the reflectance R_{itf} of the whole system.

$$T_{itf} = t_r T_{mic} P(l) \left[1 + r_r R_r^{-1} P(l) R_{mic} P(l)\right]^{-1} \tag{9.23}$$

$$R_{itf} = R_r \left[r_r + (1-p_r) R_r^{-1} P(l) R_{mic} P(l)\right] \left[1 + r_r R_r^{-1} P(l) R_{mic} P(l)\right]^{-1} \tag{9.24}$$

At this point, we are able to compute the transmission of a wave of arbitrary frequency through the interferometer, and moreover the amplitude of the sidebands created inside by the motion of any mirror or a passing GW. Moreover, we can do it by a constructive approach, without handling intricate analytical formulas : Once given the elementary operators (mirrors, propagator), a code can build the cavity operators, the Michelson operators and eventually the interferometer's by using $\mathcal{A}$ and synthetic expressions like (9.23,9.24). Any other port inside the interferometer can be treated the same way. It is straightforward, using the same principles, to insert an input or output mode-cleaner. For instance, T_{MC} being the mode-cleaner $\mathcal{A}$ operator, We have simply for the global transmission of the system :

$$T_{glob} = T_{itf}\ T_{MC}$$

because mode-cleaners are designed (ring cavities) for suppressing reflected waves, there is no cavity between the MC and the interferometer.

The same way, it is possible to associate a global operator describing the transfer from input light to any point of the interferometer. For instance, apart from the main port on which we have focused unitl now, at least two other ports are of interest (see Fig.9.2), namely the detector receiving a part of the light reflected by the interferometer (port #2), and the detector receiving the light coming from the unavoidable spurious reflection off the back face (coated for anti-reflection) of the splitter (port #5). The operator associated with port #2 is clearly

$$T_{2,glob} = R_{itf}\ T_{MC}$$

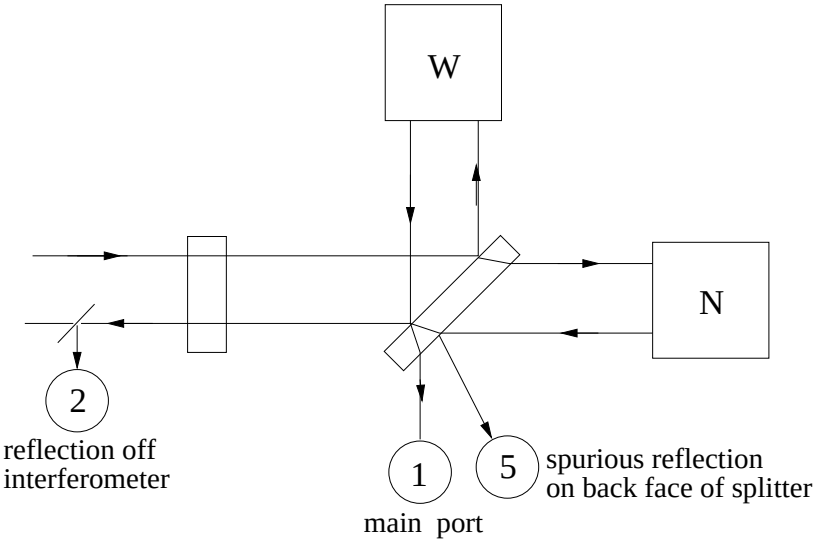

Figure 9.2: Location of the interferometer ports

(this is why it is necesary to compute R_{itf}). For port #5, it is convenient to define, baside the operators R_{mic} and T_{mic} related to the Michelson part, a new operator :

$$T_{5,mic} \;=\; iP_a\, F_{north}\, P_a$$

This allows to compute the corresponding operator when recycling is applied (formula formally identical to 9.23) :

$$T_{5,itf} \;=\; t_r T_{5,mic} P(l) \left[1 + r_r R_r^{-1} P(l) R_{mic} P(l)\right]^{-1}$$

then the operator associated with port 5 is simply

$$T_{5,glob} \;=\; T_{5,itf}\; T_{MC}$$

9.4 Tuning the interferometer

It is essential for understanding the results that we report below, to describe how the various cavities and the interferometer itself are tuned. All information on the tuning is contained in the various propagators encountered. In

these propagators, especially in long (km) distance operators, huge phases involving the laser frequency, as $2\pi\nu_L L/c$ appear, and are difficult to numerically take into account without a special care. For a light of wavelength 1.064 μm, and 3 km propagation, we get $kL \sim 17,715,748,046.558,983$ Rd, value in which a variation of the last digit is enough to change the phase reflectance of a high finesse cavity by $\pi/2$. If we keep the full value of phases, we loss any precision on the fine tuning. In other words, it is difficult to handle the same way kilometers and picometers. We try therefore to extract from all phases a large static value that proves irrelevant in the calculations. To obtain this result, we shall consider that the lengths of the various cavities present in the interferometer are kept nearly resonant for the laser light (carrier). Possible departures from resonance will be expressed with respect to the resonant length. This way it is possible to get rid of the exact carrier frequency, and consider only offsets with respect to that frequency for describing for instance the transmission of sidebands.

9.4.1 Tuning long cavities

The optical length L of a long cavity can be considered as the sum of a resonant part L_0, plus a small detuning δL that we can express as a fraction σ of the linewidth of the cavity (of finesse $\mathcal{F}$) :

$$\delta L \;=\; \sigma \times \frac{\lambda}{2\mathcal{F}}$$

with $-1 \leq \sigma \leq 1$. The parameter σ allows to examine special modes of operation of the interferometer assuming detuned cavities, or to represent DC servo errors. Resonance obviously corresponds to $\sigma = 0$. We may assume $L_0 = (4n+1)\lambda/4$ where n is the largest integer less than $4L/\lambda$. The propagator's phase kL appearing in $P(L)$ (see Eq.9.5) is thus :

$$kL \;=\; \frac{2\pi}{c}(\nu_L + \delta\nu)\left(L_0 + \;\sigma\frac{\lambda}{2\mathcal{F}}\right)$$

where $\delta\nu$ represents an offset with respect to the laser frequency caused for instance, as will be seen in the next section, by the modulation. The result is

$$kL \;=\; \frac{\pi}{2} \;+\; \pi\left[\frac{\delta\nu}{\Delta\nu_{FSR}} + \left(1+\frac{\delta\nu}{\nu_L}\right)\frac{\sigma}{\mathcal{F}}\right] \pmod{2\pi} \qquad (9.25)$$

$\Delta\nu_{FSR} = c/2L$ is the free spectral range of the cavity. It might be thought that we failed to get rid of the laser frequency ν_L, but the way it enters the last formula is now much less dangerous, because is appears in a small correction factor (even negligible in certain cases), and a high precision value is no more needed for it. The argument KL appearing in some components of $P(L)$ is simply

$$KL = \pi \frac{f}{\Delta\nu_{FSR}} \pmod{2\pi} \tag{9.26}$$

9.4.2 Tuning at a dark fringe

At the main output of the interferometer, two partial waves returning from the two arms interfere, and it is well known that the optimum signal to noise ratio is obtained when the the optical path difference between the two arms is such that the extinction is a maximum. The relevant information on this is contained in the (00) component of the T_{mic} operator, namely

$$[T_{mic}]_{00} = r_s t_s \left(\mathrm{e}^{2ika} [F_{north}]_{00} + \mathrm{e}^{2ikb} [F_{west}]_{00} \right)$$

Assume that the short arms lengths a, b are integer multiples of the laser wavelength plus a small offset δ :

$$a = a_0 + \delta\lambda/4 \quad , \quad b = b_0 - \delta\lambda/4$$

with $a_0 = n_a\lambda$, $b_0 = n_b\lambda$. At the laser frequency ($\delta\nu = 0$), we have

$$|[T_{mic}]_{00}(\nu_L)| = r_s t_s \left(|[F_{north}]_{00}(\nu_L)| + \mathrm{e}^{i\varphi} |[F_{west}]_{00}(\nu_L)| \right)$$

where

$$\varphi = \frac{4\pi\nu_L}{c}(b-a) - \mathrm{Arg}[F_{north}]_{00}(\nu_L) + \mathrm{Arg}[F_{west}]_{00}(\nu_L)$$

The dark fringe at the laser frequency corresponds to $\varphi = \pi \pmod{2\pi}$. This is obtained if

$$\delta = \delta_0 + \frac{1}{2} + \frac{\mathrm{Arg}[F_{west}]_{00}(\nu_L) - \mathrm{Arg}[F_{north}]_{00}(\nu_L)}{2\pi} \tag{9.27}$$

where δ_0 represents a possible offset with respect to the dark fringe caused for instance by a DC servo error. This being calculated, the phase factors ka, kb of the propagators $P(a)$, $P(b)$ are given by

$$\begin{aligned} ka &= 2\pi \tfrac{a_0}{c}\delta\nu + \tfrac{\pi}{2}\left(1 + \tfrac{\delta\nu}{\nu_L}\right)\delta \pmod{2\pi} \\ kb &= 2\pi \tfrac{b_0}{c}\delta\nu - \tfrac{\pi}{2}\left(1 + \tfrac{\delta\nu}{\nu_L}\right)\delta \pmod{2\pi} \end{aligned} \tag{9.28}$$

9.4.3 Tuning the recycling cavity

The recycling resonance allows to increase the power reaching the splitter. The recycling cavity (recycling mirror + Michelson) , of length l, is at resonance when

$$D \;=\; |1 + r_{rec}[R_{mic}]_{00}\mathrm{e}^{2ikl}|$$

is a minimum. At the laser frequency, this is

$$D(\nu_L) \;=\; 1 + r_{rec}|[R_{mic}]_{00}(\nu_L)|\,\mathrm{e}^{i\psi}$$

where

$$\psi \;=\; 4\pi\nu_L l/c + \mathrm{Arg}[R_{mic}]_{00}(\nu_L)$$

We assume a length $l \;=\; l_0 + \mu\lambda/4$ where l_0 is an integer multiple of λ and μ an adjustable parameter. We get

$$\psi \;=\; \mu\pi + \mathrm{Arg}[R_{mic}]_{00}(\nu_L)$$

The minimum of $D(\nu_L)$ is attained when $\psi = \pi \pmod{2\pi}$, which yields

$$\mu \;=\; \mu_0 + 1 - \frac{\mathrm{Arg}[R_{mic}]_{00}(\nu_L)}{\pi}$$

μ_0 allowing to take into account a possible offset with respect to resonance. We have thus for the argument kl entering the propagator $P(l)$:

$$kl \;=\; \frac{2\pi l_0}{c}\,\delta\nu + \frac{\pi}{2}\left(\mu_0 + 1 - \frac{\mathrm{Arg}[R_{mic}]_{00}(\nu_L)}{\pi}\right)\left(1 + \frac{\delta\nu}{\nu_L}\right) \pmod{2\pi} \tag{9.29}$$

9.5 Modulation, Detection, Demodulation and Transfer functions

9.5.1 General case

The optical wave entering the interferometer is not a simple monochromatic wave. It is passed through a phase modulator in order to translate the detection band in a high frequency region where the laser frequency noise is

lower. The action of an ideal phase modulator is analogous to a transmittance of the form

$$T(t) \;=\; \mathrm{e}^{-i\kappa \sin \omega t} \tag{9.30}$$

where $\omega = 2\pi f_m$, f_m being the modulation frequency. The parameter κ is the modulation depth. If the laser output amplitude is $A\mathrm{e}^{-i\omega_L t}$, the modulated amplitude $A'(t)$ is a sum of a carrier and partial waves we call "rf sidebands" because f_m is of the order of a few MHz.

$$A'(t) \;=\; A \sum_{p\in\mathbf{Z}} J_p(\kappa)\mathrm{e}^{-i(\omega_L + p\omega)t} \tag{9.31}$$

The interferometer contains a number of points where it is useful to detect the light amplitude. The main is obviously the dark fringe, from where the gravitational information is expected to come, but the field reflected by the recycling mirror, the field weakly transmitted by the end mirrors, some spurious reflections, are also of some interest for the control of the instrument. Each of these amplitudes can be computed by the constructive way outlined above, giving a suitable operator $S \in \mathcal{A}$. The component $S_{00}(\nu)$ depends only on the frequency ν of the light source, whereas $S_{10}(\nu, f)$, $S_{20}(\nu, f)$ depend also on the perturbation frequency. We shall use the following notation, defining transfer coefficients for each discrete Fourier component of the light amplitude :

$$\begin{aligned} t_p &= S_{00}(\nu_L + p\, f_m) \\ t_p^+ &= S_{10}(\nu_L + p\, f_m,\ f) \\ t_p^- &= S_{20}(\nu_L + p\, f_m,\ f) \end{aligned} \tag{9.32}$$

We can then write the amplitude $B(t)$ at the considered port :

$$\begin{aligned} B(t) \;=\; A\mathrm{e}^{-i\omega_L t} \;\Bigg(& \sum_{p\in\mathbf{Z}} t_p\, J_p(\kappa)\mathrm{e}^{-ip\omega t} + \frac{1}{2}\,\Phi(f) \sum_{p\in\mathbf{Z}} t_p^+\, J_p(\kappa)\mathrm{e}^{-i(p\omega+\Omega)t} \\ & + \frac{1}{2}\,\Phi(f) \sum_{p\in\mathbf{Z}} t_p^-\, J_p(\kappa)\mathrm{e}^{-i(p\omega-\Omega)t} \Bigg) \end{aligned} \tag{9.33}$$

where we see that the effect of the perturbed interferometer is to add two audio sidebands to every rf sideband. The power is, treating the $t_p^{\pm}$ as first order terms :

$$P(t) \;=\; B(t)\overline{B(t)} \;=\; P_0 \left(\sum_{p,q\in\mathbf{Z}} t_p \overline{t_q} J_p J_q \mathrm{e}^{-i(p-q)\omega t} + \right.$$

$$\frac{1}{2}\,\Phi(f)\,\sum_{p,q\in\mathbf{Z}}(t_p^+\overline{t_q}+t_p\overline{t_q^-})J_pJ_q\mathrm{e}^{-i[(p-q)\omega+\Omega]t}+$$

$$\frac{1}{2}\,\Phi(f)\,\sum_{p,q\in\mathbf{Z}}(t_p^-\overline{t_q}+t_p\overline{t_q^+})J_pJ_q\mathrm{e}^{-i[(p-q)\omega-\Omega]t}\Bigg) \tag{9.34}$$

where J_p is a shorthand notation for $J_p(\kappa)$. The end of the process is a mixing with a demodulation current of the form

$$D(t) \;=\; \sin(\omega t+\xi)$$

where ξ denotes the demodulation phase, followed by a low pass filtering suppressing frequencies equal or higher than f_m. $\xi=0$ gives the in-phase demodulation current, and $\xi=\pi/2$ the quadrature. It is therefore clear that in the preceding sum, only terms such that $p-q=\pm1$ will contribute the demodulated filtered current. We can thus write the contributing part P_{eff} of the detected power as :

$$P_{eff}(t)/P_0 \;=\; a_0\mathrm{e}^{-i\omega t}+\left(\frac{1}{2}\Phi(f)\,a^+\,\mathrm{e}^{-i(\omega+\Omega)t}+\frac{1}{2}\Phi(f)\,a^-\,\mathrm{e}^{-i(\omega-\Omega)t}\right)+\text{c.c} \tag{9.35}$$

where the coefficients a_k have the following definitions :

$$\begin{array}{rcl} a_0 &=& \sum_{p\in\mathbf{Z}}J_pJ_{p-1}t_p\overline{t_{p-1}} \\ a^+ &=& \sum_{p\in\mathbf{Z}}J_pJ_{p-1}(t_p^+\overline{t_{p-1}}+t_p\overline{t_{p-1}^-}) \\ a^- &=& \sum_{p\in\mathbf{Z}}J_pJ_{p-1}(t_p^-\overline{t_{p-1}}+t_p\overline{t_{p-1}^+}) \end{array} \tag{9.36}$$

The demodulated, filtered current (DFC) at frequency f is :

$$DFC(t) \;=\; \frac{1}{4i}\left[(a^+\,\mathrm{e}^{i\xi}-\overline{a^-}\,\mathrm{e}^{-i\xi})\mathrm{e}^{-2i\pi ft}+\text{c.c}\right]\;\Phi(f) \tag{9.37}$$

The function $DFC(t)$ is given up to an arbitrary amplitude depending on the tuning of the various amplifiers of the detection chain. Anyway, we are going to compare one another the DFC's due to different causes, and the undetermined common amplitude plays no role in the discussion. The function $\Theta(f)$, defined as

$$\Theta(f) \;=\; \frac{1}{2}\left[a^+\,\mathrm{e}^{i\xi}-\overline{a^-}\,\mathrm{e}^{-i\xi}\right] \tag{9.38}$$

is thus the (complex) transfer function relating the RSD of DFC to the RSD of special phase noise :

$$DFC(f) \;=\; \Theta(f)\;\times\;\Phi(f) \tag{9.39}$$

- $\Phi(f) = 2k\,x(f)$ for a moving mirror. So that

$$DFC(f) = \Theta_{x\to DFC}(f)\frac{4\pi}{\lambda}x(f) \tag{9.40}$$

  where in $\Theta_{x\to DFC}$, the t_p^k coefficients have been calculated from operators all diagonal except the special one corresponding to the perturbed mirror

- $\Phi(f) = k\,h(f)L$ for a GW event, so that

$$DFC(f) = \Theta_{h\to DFC}(f)\frac{2\pi L}{\lambda}h(f) \tag{9.41}$$

  where in $\Theta_{h\to DFC}$, the t_p^k coefficients have been calculated from operators all diagonal except the propagators $P(2L_{north})$ and $P(2L_{west})$.

From $\Theta(f)$, one can extract the modulus and phase transfer functions, both useful in servo loops studies.

9.5.2 The special case of quantum noise

Our discussion of the quantum noise calculation is based on the approach by Niebauer et al. [31] about non stationary shot noise. Consider a time interval Δt, around time t, very short compared to the modulation period $1/f_m$. The number $n(t)$ of photons reaching the photodiode during this time is a random variable obeying a Poisson statistics, having an expectation value $E[n(t)] = n_0(t)$, so that its variance is $V[n(t)] = n_0(t)$. The statistical parameter $n_0(t)$ is related to the averaged power $P_0(t)$ during Δt by (h_P denoting the Planck constant) :

$$n_0(t) \;=\; \frac{P_0(t)\Delta t}{h_P\nu_L}$$

We can reverse as well the point of view and consider the detected power as a random process, and we consider the associated centered process

$$\delta P(t) \;=\; \frac{h_P\nu_L}{\Delta t}\,(n(t) - n_0(t))$$

Having the variance

$$V[\delta P(t)] \;=\; \left(\frac{h_P\nu_L}{\Delta t}\right)^2 n_0(t) \;=\; \frac{h_P\nu_L}{\Delta t}\,P_0(t)$$

Assuming a quantum efficiency of 1, the detection current generated by the diode is (for its centered part) :

$$I(t) \;=\; \frac{e}{h_P \nu_L}\,\delta P(t)$$

where e is the elementary charge. The process $I(t)$ has a variance

$$V[I(t)] \;=\; \frac{e^2}{h_P \nu_L \Delta t}\,P_0(t)$$

D(t) being the demodulation current, the demodulated current $J(t)$ is given by

$$J(t) \;=\; D(t)\,I(t)$$

This defines a new centered process, of variance:

$$V[J(t)] \;=\; D(t)^2 V[I(t)] \;=\; D(t)^2\,\frac{e^2}{h_P \nu_L \Delta t}\,P_0(t)$$

Moreover, we can consider the fluctuations δP as uncorrelated between any two different time intervals, so that if t, t' are the centers of two time slices, we have

$$E[J(t)J(t')] \;=\; \frac{e^2}{h_P \nu_L \Delta t} D^2(t) P_0(t)\,\delta_{t,t'} \tag{9.42}$$

where $\delta_{t,t} = 1$, and $\delta_{t,t' \neq t} = 0$. The output current being periodic, it admits an expansion in a Fourier series, and the coefficients are

$$\tilde{J}(\omega) \;=\; \frac{1}{\mathcal{T}} \int_{\mathcal{T}} J(t)\,\mathrm{e}^{i\omega t}$$

where $\mathcal{T}$ is any multiple of $1/f_m$ and consequently much longer than Δt. The integral is thus fairly approximated by the discrete sum

$$\tilde{J}(\omega) \;=\; \frac{\Delta t}{\mathcal{T}} \sum_{t \in \mathcal{T}} J(t)\,\mathrm{e}^{i\omega t}$$

and we get

$$E[\tilde{J}(\omega)\,\tilde{J}(\omega)^*] \;=\; \left(\frac{\Delta t}{\mathcal{T}}\right)^2 \sum_{t,t' \in \mathcal{T}} E[J(t)J(t')]\,\mathrm{e}^{i(\omega t - \omega' t')}$$

thanks to eq.9.42, we find

$$E[\tilde{J}(\omega)\,\tilde{J}(\omega)^*] \;=\; \frac{e^2}{h_P\nu_L\mathcal{T}}\,\frac{\Delta t}{\mathcal{T}}\sum_{t\in\mathcal{T}} D(t)^2 P_0(t)\,\mathrm{e}^{i(\omega-\omega')t} \;=\; \frac{e^2}{h_P\nu_L\mathcal{T}}\,\widetilde{D^2P}_0(\omega-\omega')$$

In particular,

$$E[|\tilde{J}(\omega)|^2] \;=\; \frac{e^2}{h_P\nu_L\mathcal{T}}\,\widetilde{D^2P}_0(0) \tag{9.43}$$

This result is independent on Δt that we can take arbitrarily small, therefore, eq.(9.43) is exact. It follows that the spectral density of demodulated current is

$$Q(\omega) \;=\; \frac{e^2}{h_P\nu_L}\,\widetilde{D^2P}_0(0) \tag{9.44}$$

The mean detected power being :

$$P_0(t) \;=\; P_L\sum_{p,q\in\mathbf{Z}} J_p\,J_q\,t_p,\overline{t_q}\,\mathrm{e}^{-i(p-q)\omega t}$$

and the squared demodulation current

$$D(t)^2 \;=\; \sin(\omega t+\xi)^2 \;=\; \frac{1}{4}\left(2-\mathrm{e}^{2i\omega t+2i\xi}-\mathrm{e}^{-2i\omega t-2i\xi}\right)$$

we get

$$D^2P_0(t) \;=\; \frac{1}{4}\left(2\sum_{p,q\in\mathbf{Z}} J_pJ_q\,t_p\overline{t_q}\,\mathrm{e}^{-i(p-q)\omega t} \;-\; \mathrm{e}^{2i\xi}\sum_{p,q\in\mathbf{Z}} J_pJ_q\,t_p\overline{t_q}\,\mathrm{e}^{-i(p-q-2)\omega t} \;-\right.$$

$$\left.\mathrm{e}^{-2i\xi}\sum_{p,q\in\mathbf{Z}} J_pJ_q\,t_p\overline{t_q}\,\mathrm{e}^{-i(p-q+2)\omega t}\right)$$

so that the Fourier coefficient of the zero frequency is

$$\widetilde{D^2P}_0(0) \;=\; \frac{1}{4}\left[2\sum_{p\in\mathbf{Z}} J_p^2t_p\overline{t_p} \;-\; \mathrm{e}^{-2i\xi}\sum_{p\in\mathbf{Z}} J_pJ_{p-2}\overline{t_p}t_{p-2} \;-\; \mathrm{e}^{2i\xi}\sum_{p\in\mathbf{Z}} J_pJ_{p-2}\overline{t_{p-2}}t_p\right]$$

once substituted in (9.44), the RSD of quantum noise current is determined. Note that in the calculation of the DFC's due to classical perturbations (precedent subsection) a factor of $eP_0/h_P\nu_L$ was ignored, as a part of a common arbitrary scale factor. It is necessary to remember it here : ignoring

this factor is equivalent to take 1 as the amplitude of the demodulating current, and divide all DFC's by $eP_0/h_P\nu_L$. If we keep this convention, we must finally take for the spectral density of modulated quantum noise :

$$DFC_{qn}(f) \;=\; \sqrt{\frac{2h_P\nu_L}{P_0}}\;\Theta_{qn\to DFC}$$

The factor of 2 is necessary for passing to a one sided spectral density. We have otherwise :

$$\Theta_{qn\to DFC} \;=\; \frac{1}{4}\left[2a - b\;\mathrm{e}^{-2i\xi} - \overline{b}\;\mathrm{e}^{2i\xi}\right]$$

$$a \;=\; \sum_{p\in\mathbf{Z}} J_p^2 t_p \overline{t_p}$$

$$b \;=\; \sum_{p\in\mathbf{Z}} J_p J_{p-2} \overline{t_p} t_{p-2}$$

9.5.3 Transfer functions to an equivalent h(f)

An essential point is to compare the various perturbations acting on the interferometer to the expected gravitational signals. One way for doing it is to express these perturbations in terms of an equivalent spectral density $h(f)$ of gravitational amplitude. This is often implicitly done in papers. The method we propose is to identify the DFC produced by a GW to the DFC produced by any perturbation X of RSD $X(f)$:

$$DFC_h(f) \;=\; DFC_X(f)$$

or, introducing the transfer functions

$$\Theta_{h\to DFC}\;h(f) \;=\; \Theta_{X\to DFC}\;X(f)$$

This allows to express the $h_X(f)$ equivalent to $X(f)$ as

$$h_X(f) \;=\; \Theta_{X\to h}\;X(f)$$

and define a new class of transfer functions :

$$\Theta_{X\to h} \;=\; \frac{\Theta_{X\to DFC}}{\Theta_{h\to DFC}}$$

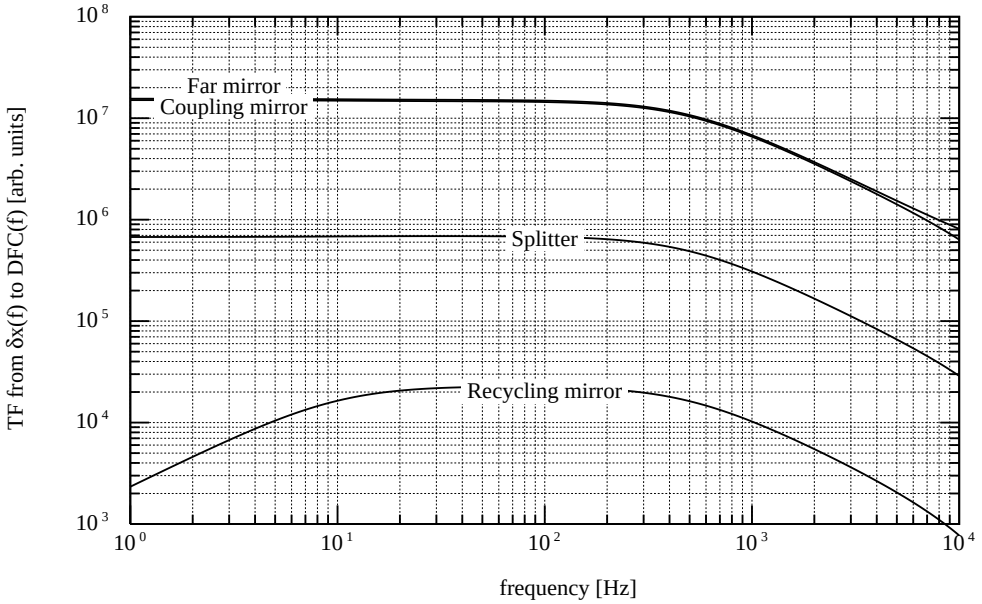

Figure 9.3: Transfer functions from $\delta x(f)$ to $DFC(f)$ for 4 types of mirrors, 5% finesse asymmetry

9.6 Interferometer noises

9.6.1 Proof masses position noise

A first possible use of our method could be to find the transfer functions corresponding to motions of every mirror involved in a given instrument. This could help in the commissionning phase, when we are free to test the response of the interferometer to given, calibrated excitations. We show below (Fig.9.3) the behavior of the transfer functions

relating the RSD of motion $x(f)$ of each mirror of a perfectly tuned interferometer to the resulting DFC root spectral density. The transfer function from the GW RSD to DFC is mostly identical to that of an end mirror, as already seen, apart from an extra cause of cutoff, due to the $\mathrm{sinc}(2\pi fL/c)$ factor, representing the averaging effect of propagation inside the cavity during a time comparable to the GW period. This is why the transfer functions

from the displacements RSD to an equivalent $h(f)$ are not exactly constant (see Fig.9.4). We see that the transfer functions for the cavity mirrors are almost identical, the end mirror's one being slightly larger. The splitter's and the recycler's are much smaller (at least in the detection band). If furthermore we assume the laser locked in frequency to the recycling cavity, the laser frequency is correlated with the recycler's motions (error signal is taken a port 2). A simple approach assuming an infinite gain in the servo loop is to adopt the transfer function

$$\Theta_{\delta x_R \to h,1} \;=\; \frac{\Theta_{\delta x_R \to DFC,1} - \frac{\Theta_{\delta x_R \to DFC,2}}{\Theta_{\delta \nu_L \to DFC,2}}\,\Theta_{\delta \nu_L \to DFC,1}}{\Theta_{h \to DFC,1}}$$

where the numerical indices refer to the corresponding port. The transfer function $\Theta_{\delta \nu_L \to DFC,p}$ expresses the relation between the laser frequency noise and the DFC on port p, and will be expressed in detail in a coming section. It follows that the recycler's position noise is almost cancelled (see Fig.9.4), at least in the detection band.

The irreducible part of the position noise is caused by small motions of the mirrors, essentially driven by excitation of all degrees of freedom of the various oscillators coupled to each. If we restrict ourselves to the main features, we can take into account the motion of the suspension (the mirrors are suspended like pendulums) and the motion of the reflecting face resulting from excitation of the internal modes. For the pendulum thermal noise, we adopt the following model ([32]) assuming that the dissipation occurs due to a finite thermal conductivity in the wires :

$$x(f)^2 \;=\; \frac{2k_B T \Phi \omega_w^2}{m\Omega}\,\frac{1}{(\Omega^2 - \omega_p^2)^2 + \Phi^2 \omega_w^4}$$

with the following definitions : k_B is the Boltzmann constant, T the temperature, $\Omega = 2\pi f$ as usual. The loss angle $\Phi(f)$ is of the thermoelastic form

$$\Phi(f) \;=\; \Phi_0 + \frac{\Delta \Omega \tau}{1 + (\Omega\tau)^2}$$

with the Virgo parameters (case of an end mirror) ($\Delta = 3\ 10^{-3}$, $\tau = 2.34\ 10^{-4}$ s. The frequency corresponding to the elasticity of the steel wires (pendulum frequency in zero gravity) is $\omega_w = 2\pi \times 0.017$ Hz. The resultant pendulum frequency is $\omega_p^2 = \frac{g}{L} + \omega_w^2$.

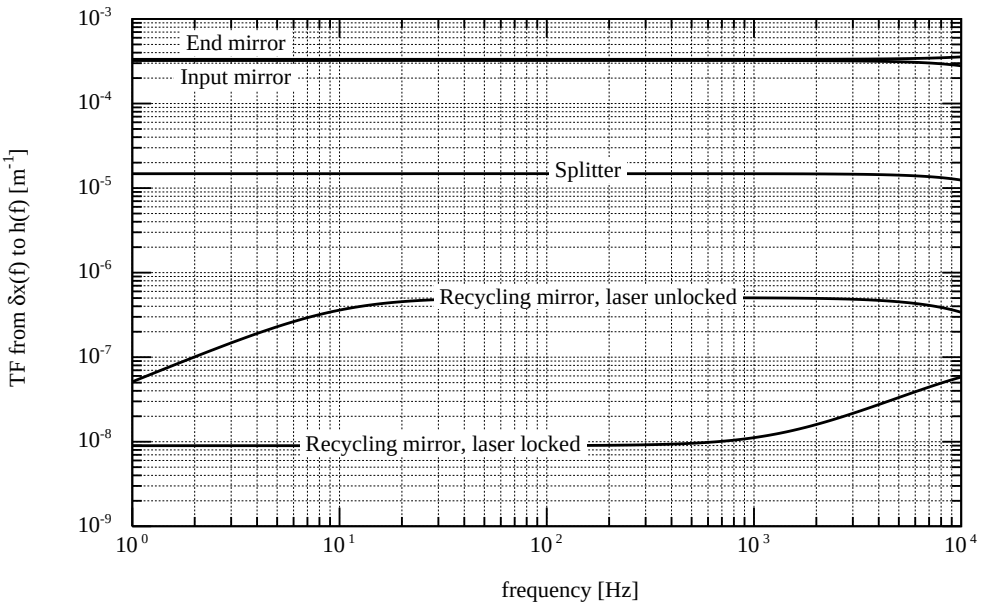

Figure 9.4: Transfer functions from $\delta x(f)$ to $h(f)$ for 4 types of mirrors,5% finesse asymmetry

where l is the pendulum length. Obviously, the parameters must be slightly modified according to the type of the considered mirror. For the internal thermal noise, we take a very simple model (see [33],[34]) valid for the low frequency tail :

$$x^2(f) = \frac{4k_BT}{\pi f} U\phi_M$$

Where U is proportional to the strain energy stored in the assumed cylindrical substrate when a static pressure is applied having the same profile as the light power flux (gaussian). It depends on the size of the blank and on the radius of the light spot. This model does not take into account resonances, that are likely at frequencies (several kHz) where only thin peaks will emerge from the shot noise. For instance, for the Virgo end or corner mirror, we find $U = 7.32\ 10^{-11}\text{J.N}^{-2}$. The loss angle ϕ_M can be as low as 10^{-6} for silica mirrors. Suspension wires have also a special thermal noise spectrum (violin modes), but essentially concentrated on thin resonance lines non essential for data analysis since a number of papers [38] have been devoted to removal from data of that kind of component. By taking for a given mirror the sum of all these contributions, applying its transfer function, we get the equivalent GW amplitude $h_i(f)$ (i enumerates the mirrors).

9.6.2 Quantum noise

The shot noise RSD is a constant, and therefore, the transfer function from shot noise to an equivalent $h_{QN}(f)$ is the inverted transfer function from $h(f)$ to DFC (see Fig.9.5).

$$\Theta_{QN\to h} = \frac{\Theta_{QN\to DFC}}{\Theta_{h\to DFC}}$$

then the $h(f)$ equivalent to shot noise is

$$h_{QN}(f) = \Theta_{QN\to h} \times \sqrt{\frac{2h_P\nu_L}{P_0}}$$

9.6.3 Sensitivity curve

Then the (incoherent) sum of all $h_i(f)$ thermal contributions gives a global $h_{THN}(f)$ equivalent to thermal noise. A new incoherent sum with the h_{QN} gives an estimate of the sensitivity of the interferometer (see Fig.9.6), to be

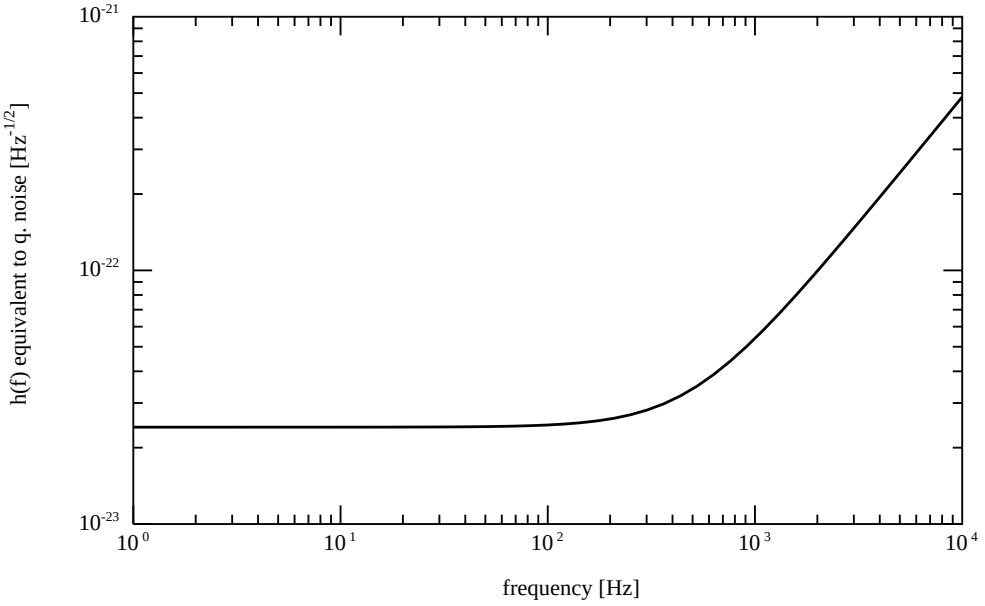

Figure 9.5: h(f) equivalent to quantum noise

taken into account, for instance when evaluating the efficiency of matched filters. This sensitivity curve is very well approximated by the fit function :

$$h(f) \;=\; \left(\frac{4.5\ 10^{-43}}{f} + \frac{9\ 10^{-37}}{f^5} + 3.24\ 10^{-46} \left[1 + \left(\frac{f}{500\ \mathrm{Hz}} \right)^2 \right] \right)^{1/2}$$

9.7 Upstream noises

Some noises are caused by perturbations acting before entrance of light in the interferometer. We consider here the three main sources of upstream noise, the laser itself and the modulator.

9.7.1 Laser frequency noise

The laser may be noisy in phase and in amplitude (in power). Let us consider these two cases. The frequency noise will be described by a noisy optical

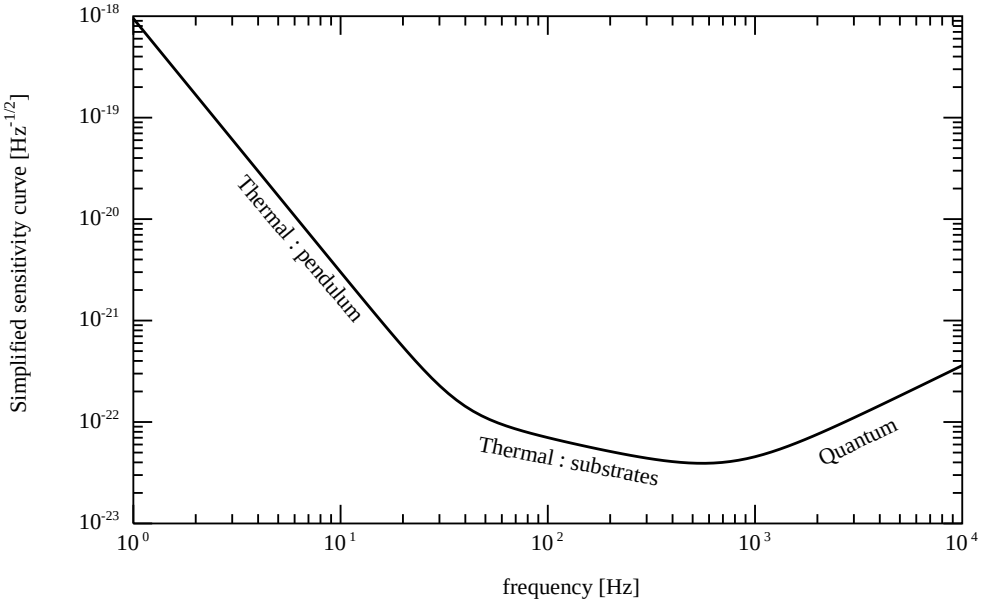

Figure 9.6: $h(f)$ equivalent to the global noise SD

phase $\phi(t)$:

$$\frac{1}{2\pi}\frac{\partial\phi}{\partial t} \;=\; \nu_L \;+\; \delta\nu(t)$$

Where ν_L is the averaged frequency, and $\delta\nu(t)$ a centered stationnary random process of RSD $\delta\nu(f)$. We shall as usual consider a special Fourier component of the frequency noise and write

$$\delta\nu(t) \;=\; \delta\nu(f)\cos(2\pi f t)$$

so that the phase is

$$\phi(t) \;=\; \omega_L t + \frac{\delta\nu(f)}{f}\sin(\Omega t)$$

We could have directly introduced a RSD of "laser phase noise" $\phi(f)$, instead of its equivalent $\delta\nu(f)/f$. After a first order expansion (in the frequency region of interest, $\delta\nu(f)$ is very small compared even to small values of f), we get the laser output amplitude as the sum of a carrier plus two sidebands :

$$A(t) \;=\; A_0\left[\mathrm{e}^{-i\omega_L t} + \frac{\delta\nu(f)}{2f}\mathrm{e}^{-i(\omega_L+\Omega)t} - \frac{\delta\nu(f)}{2f}\mathrm{e}^{-i(\omega_L-\Omega)t}\right]$$

After passing the phase modulator, the amplitude becomes

$$A'(t) \;=\; A_0\,\mathrm{e}^{-i\omega_L t}\left[\sum_{p\in\mathbf{Z}} J_p\,\mathrm{e}^{-ip\omega t} + \frac{\delta\nu(f)}{2f}\sum_{p\in\mathbf{Z}} J_p\,\mathrm{e}^{-i(p\omega+\Omega)t} - \frac{\delta\nu(f)}{2f}\sum_{p\in\mathbf{Z}} J_p\,\mathrm{e}^{-i(p\omega-\Omega)t}\right]$$

each of these partial waves is transmitted by the interferometer according to their frequency. S being as above the $\mathcal{A}$ operator associated with the comsidered port of the interferometer, the transfer coefficients are :

$$\begin{aligned} t_p &= S_{00}(\nu_L + p\,f_m) \\ t_{p+} &= S_{11}(\nu_L + p\,f_m, f) \\ t_{p-} &= S_{22}(\nu_L + p\,f_m, f) \end{aligned} \qquad (9.45)$$

The interferometer being static, the transmittance is the ordinary scalar transmittance. The purpose of the $t_{p\pm}$ notation is to avoid confusion with the $t_p^{\pm}$ of the preceding section that have a different meaning. The $t_p^{\pm}$ express the

rate of creation of sidebands inside the interferometer, whereas the $t_{p\pm}$ express the transmission by the interferometer of sidebands already generated The transmitted amplitude is now :

$$B(t) = A_0\,\mathrm{e}^{-i\omega_L t}\left[\sum_{p\in\mathbf{Z}} J_p\,t_p\,\mathrm{e}^{-ip\omega t} + \frac{\delta\nu(f)}{2f}\sum_{p\in\mathbf{Z}} J_p\,t_{p+}\,\mathrm{e}^{-i(p\omega+\Omega)t} - \frac{\delta\nu(f)}{2f}\sum_{p\in\mathbf{Z}} J_p\,t_{p-}\,\mathrm{e}^{-i(p\omega-\Omega)t}\right]$$

And the power reaching the photodiode :

$$P(t) = P_0\left[\sum_{p,q\in\mathbf{Z}} J_p\,J_q\,t_p\,\overline{t_q}\,\mathrm{e}^{-i(p-q)\omega t} + \frac{\delta\nu(f)}{2f}\sum_{p,q\in\mathbf{Z}} J_p\,J_q\,(t_{p+}\overline{t_q} - t_p\overline{t_{q-}})\mathrm{e}^{-i[(p-q)\omega+\Omega]t}\right.$$
$$\left. - \frac{\delta\nu(f)}{2f}\sum_{p,q\in\mathbf{Z}} J_p\,J_q\,(t_{p-}\overline{t_q} - t_p\overline{t_{q+}})\mathrm{e}^{-i[(p-q)\omega-\Omega]t}\right]$$

Applying the demodulation/filtering scheme already detailed above, we obtain the RSD of DFC as :

$$DFC(f) = \Theta_{\delta\nu\to DFC}(f)\,\frac{\delta\nu(f)}{f}$$

where the complex transfer function is defined as in the precedent section (Eq.9.38) by

$$\Theta_{\delta\nu\to DFC}(f) = \frac{1}{2}[a_+\mathrm{e}^{i\xi} - \overline{a_-}\mathrm{e}^{-i\xi}]$$

where $a_\pm$ have the following definitions :

$$\begin{array}{rcl} a_+ & = & \sum_{p=-\infty}^{\infty} J_p\,J_{p-1}(t_{p+}\overline{t_{p-1}} - t_p\overline{t_{p-1-}}) \\ a_- & = & \sum_{p=-\infty}^{\infty} J_p\,J_{p-1}(t_p\overline{t_{p-1+}} - t_{p-}\overline{t_{p-1}}) \end{array} \qquad (9.46)$$

Fig.9.7 shows the behavior of the transfer function in the case where some asymmetry in the arms (different finesses) makes the interferometer sensitive to frequency noise

9.7.2 Laser amplitude noise

Assume now fluctuations of the laser power, such that the averaged power is P and the instantaneous power $P(t)$ the sum of P plus a centered random process of RSD $\delta P(f)$:

$$P(t) = P_0 + \delta P(f)\sin(2\pi f t) \qquad (9.47)$$

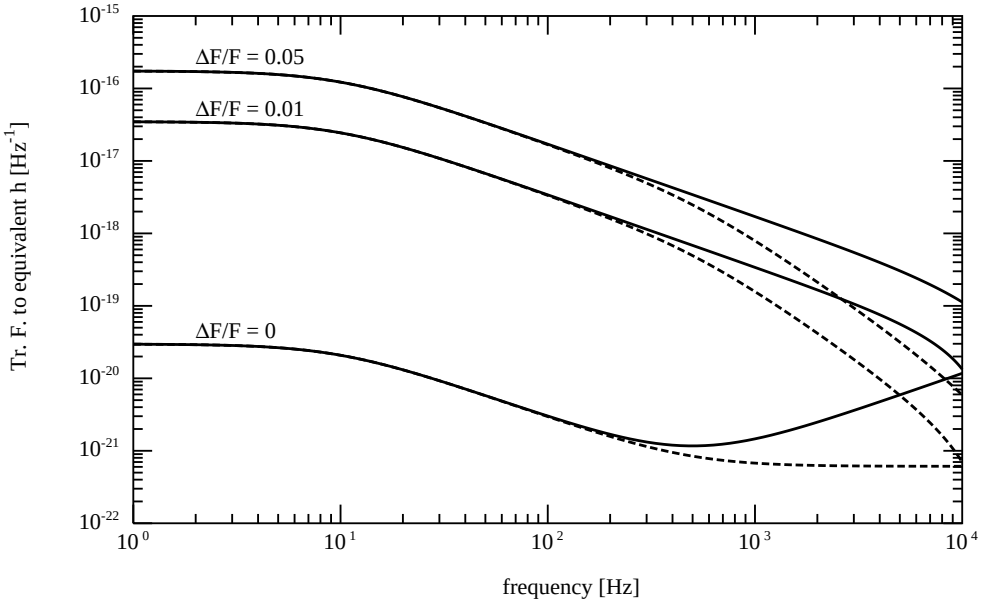

Figure 9.7: Transfer function for laser frequency noise with and without mode-cleaner

The modulus of the amplitude is thus

$$P(t)^{1/2} = A_0 \left(1 + \frac{\delta P(f)}{2P_0} \sin(\Omega t)\right) \tag{9.48}$$

So that the complex amplitude can be written as

$$A(t) = A_0 \mathrm{e}^{-i\omega_L t} \left(1 + i\frac{\delta P(f)}{4P_0} \mathrm{e}^{-i\Omega t} - i\frac{\delta P(f)}{4P_0} \mathrm{e}^{i\Omega t}\right) \tag{9.49}$$

The quantity $\delta P(f)/2P_0$ plays here the role of a phase RSD. Then, a treatment similar to the preceding leads to the transfer function

$$DFC(f) \;=\; \Theta_{\delta P \to DFC}(f)\, \frac{\delta P(f)}{2P_0} \tag{9.50}$$

with

$$\Theta_{\delta P \to DFC}(f) \;=\; \frac{1}{2}\left[a_+ \mathrm{e}^{i\xi} - \overline{a_-}\mathrm{e}^{-i\xi}\right]$$

where the $a_\pm$ have the following definitions :

$$\begin{array}{rcl} a_+ & = & \sum_{p=-\infty}^{\infty} J_p\, J_{p-1}(t_{p+}\overline{t_{p-1}} + t_p \overline{t_{p-1-}}) \\ a_- & = & \sum_{p=-\infty}^{\infty} J_p\, J_{p-1}(t_{p-}\overline{t_{p-1}} + t_p \overline{t_{p-1+}}) \end{array} \tag{9.51}$$

The coefficients t_p, $t_{p\pm}$ have the same definition as above (Eq.9.45). Fig.9.8 show the transfer function in the case where some detuning of the cavities makes the interferometer is sensitive to laser power noise. It uses an experimental spectral density of laser power noise measured on the Virgo laser, that can be fit by the following expression :

$$\frac{\delta P}{P}(f) \;=\; \frac{3.1\ 10^{-6}}{f^{1.5}} + 1.82\ 10^{-9} + 8.18\ 10^{-17}\ f^2$$

9.7.3 Modulator noise

If the oscillator driving the phase modulator presents some frequency noise, some effects could be a priori expected on the interferometer noise. These effects should however be small, if the demodulation current comes from the same oscillator. Roughly speaking, what matters are the differences between

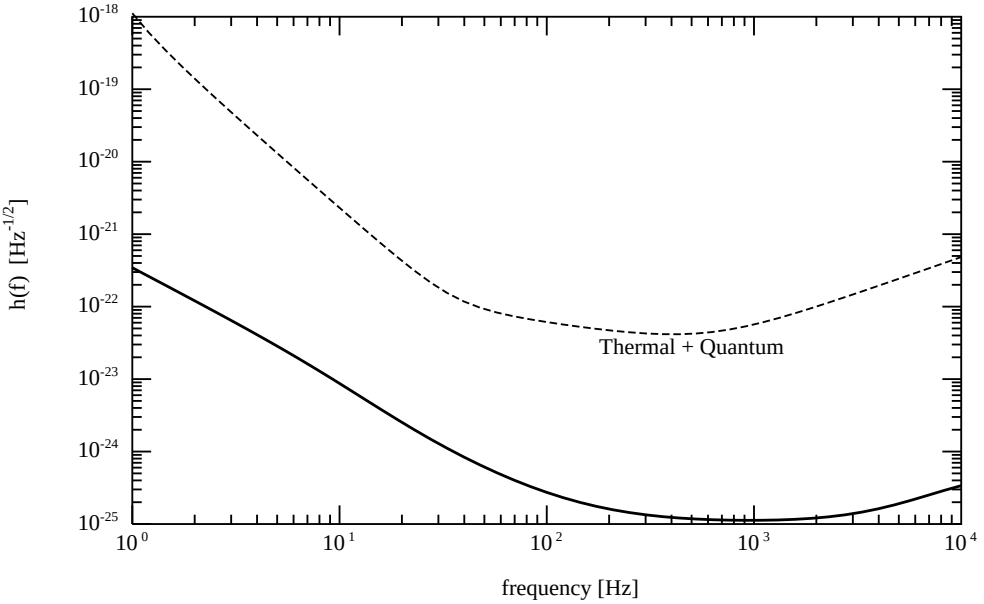

Figure 9.8: Transfer function for laser amplitude noise. 10^{-11}m detuning of the black fringe

the frequencies of the rf sidebands and that of the demodulator, and they are constants unless some extra noise is fed into the demodulator. The modulator has the transmittance

$$T(t) \;=\; \mathrm{e}^{-i\kappa \sin\phi(t)}$$

where the phase $\phi(t)$ obeys

$$\frac{1}{2\pi}\frac{\partial\phi}{\partial t} \;=\; f_m \;+\; \delta\nu(f)\,\sin(2\pi f t)$$

so that

$$\phi(t) \;=\; \omega t - \frac{\delta\nu(f)}{f}\cos\Omega t$$

and $(J_p \equiv J_p(\kappa))$

$$T(t) \;=\; \mathrm{e}^{-i\kappa\sin\omega t}\mathrm{e}^{i\kappa\frac{\delta\nu(f)}{f}\,\cos\omega t\,\cos\Omega t}$$

$$= \sum_{p\in\mathbf{Z}} J_p \mathrm{e}^{-i\,p\omega t} + \frac{i\kappa\phi(f)}{2}\cos\Omega t \left(\sum_{p\in\mathbf{Z}} J_p\,\mathrm{e}^{-i\,(p+1)\omega t} + \sum_{p\in\mathbf{Z}} J_p\,\mathrm{e}^{-i\,(p-1)\omega t}\right)$$

where $\phi(f) = \delta\nu(f)/f$ is the RSD of phase noise. Thanks to well known properties of the Bessel functions, we can write as well :

$$T(t) = \sum_{p\in\mathbf{Z}} J_p \mathrm{e}^{-i\,p\omega t} + \frac{i\phi(f)}{2}\sum_{p\in\mathbf{Z}} pJ_p\,\mathrm{e}^{-i\,(p\omega+\Omega)t} + \frac{i\phi(f)}{2}\sum_{p\in\mathbf{Z}} pJ_p\,\mathrm{e}^{-i\,(p\omega-\Omega)t}$$

The wave transmitted by the interferometer is thus

$$B(t) = A_0\left[\sum_{p\in\mathbf{Z}} t_p\,J_p\,\mathrm{e}^{-i\,(\omega_L+p\omega)t} + \frac{i\phi(f)}{2}\sum_{p\in\mathbf{Z}} p\,t_{p+}\,J_p\,\mathrm{e}^{-i\,(\omega_L+p\omega+\Omega)t} + \sum_{p\in\mathbf{Z}} p\,t_{p-}\,J_p\,\mathrm{e}^{-i\,(\omega_L+p\omega-\Omega)t}\right]$$

with the same definition as above (Eq.9.45) for the $t_p, t_{p\pm}$. The demodulation current must contain the frequency noise :

$$D(t) = \sin\left(\omega t - \frac{\delta\nu(f)}{f}\,cos\Omega t + \xi\right)$$

After some straightforward algebra, we find for the RSD of DFC

$$DFC(f) = \Theta(f) \times \frac{\delta\nu(f)}{f}$$

with as customary

$$\Theta(f) = \frac{1}{2}\left[a^+\mathrm{e}^{i\xi} - \overline{a^-}\mathrm{e}^{-i\xi}\right]$$

and in this special case :

$$\begin{array}{rcl} a^+ & = & \sum_{p\in\mathbf{Z}} J_pJ_{p-1}\left(pt_{p+}\overline{t_{p-1}} - (p-1)t_p\overline{t_{p-1-}} - t_p\overline{t_{p-1}}\right) \\ a^- & = & -\sum_{p\in\mathbf{Z}} J_pJ_{p-1}\left(pt_{p-}\overline{t_{p-1}} - (p-1)t_p\overline{t_{p-1+}} - t_p\overline{t_{p-1}}\right) \end{array} \qquad (9.52)$$

The third term in each parenthesis represents the demodulator's noise. The essential feature is that independently taken, the modulator and the demodulator noises have the same $1/f$ behavior at low frequencies, but in the above formula, assuming a perfect coherence of phase between the modulating and the demodulating currents, they almost exactly cancel each other at low frequency. This is apparent on Fig.9.9. Anyway, even with large perturbations, the noise level remains negligible, well below the sentitivity curve (see Fig.9.10).

.

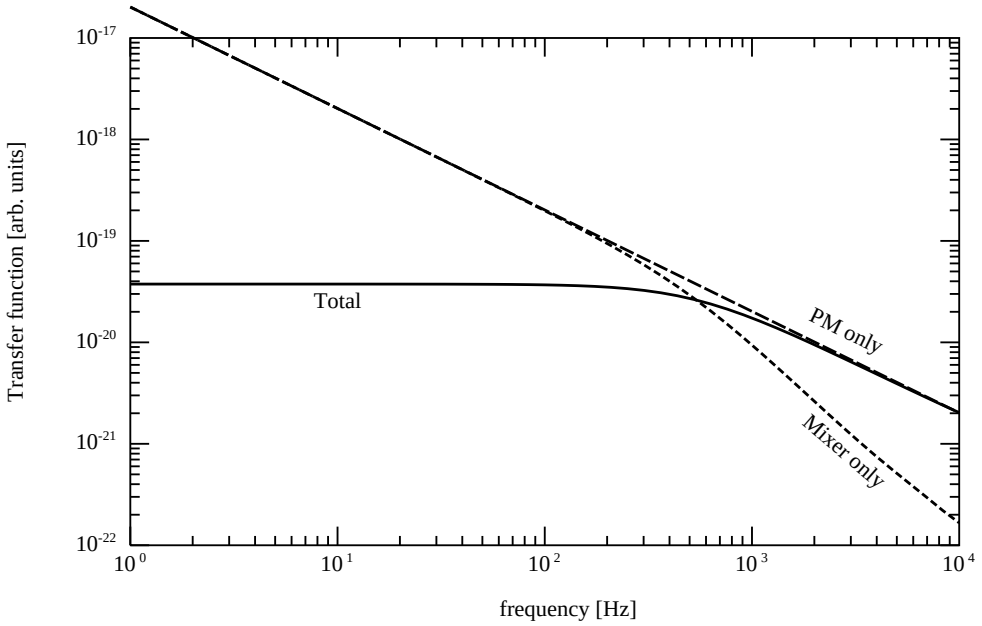

Figure 9.9: Transfer function for modulation frequency noise. 10^{-12}m detuning of 1 cavity

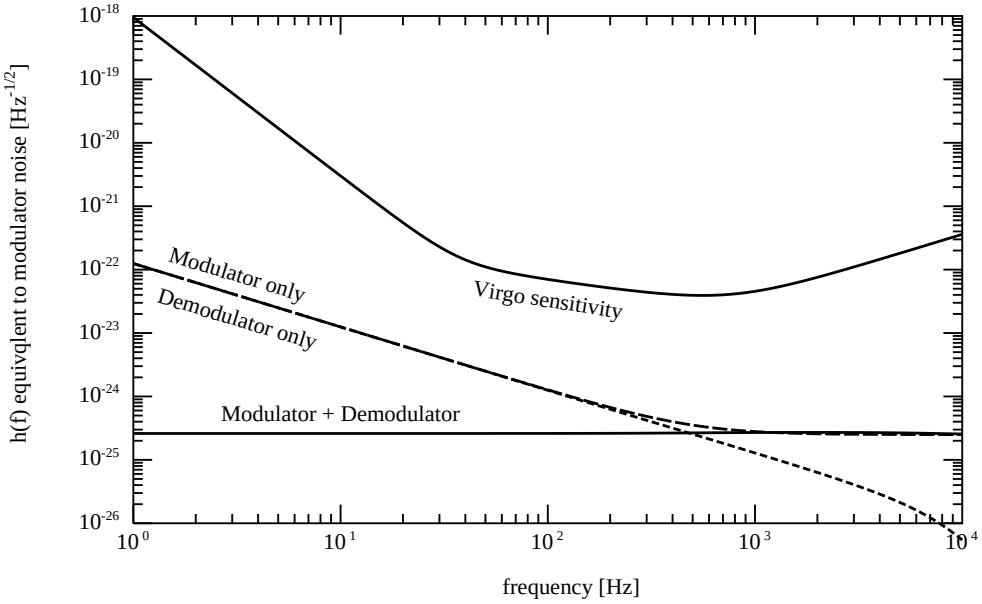

Figure 9.10: h(f) equivalent to modulator frequency noise for $\lambda/1000$ detuning of one cavity

Bibliography

[1] **Jean-Yves Vinet, Brian Meers, Catherine Nary Man and Alain Brillet**
Optimization of long-baseline interferometers for gravitational-wave detection
Phys. Rev. D , Vol **38**, N.2 (1988) p. 433

[2] **Brian J. Meers**
Recycling in laser-interferometric GW detectors
Phys. Rev. D , Vol **38**, N.2 (1988) p. 2317

[3] **Ronald Drever**
in *Gravitational Radiation*
edited by N. Deruelle and T. Piran (North Holland 1983) p.321

[4] **F. Pegoraro, L.A. RAdicati, Ph. Bernard and E. Picasso**
Phys. Lett. **A68** (1978) p.165

[5] **J. Mizuno, K.A. Strain, P.G. Nelson, J.M. Chen, R. Schilling, A. Rüdiger, W. Winkler and K. Danzmann**
Phys. Lett. **A175** (1993) p.273

[6] **Jun Mizuno** in
Comparison of optical configurations for laser-interferometric gravitational-wave detectors
PHD Thesis, Max-Planck-Institut für Quantenoptik (MPQ 203) 1995

[7] **Max BORN & Emil WOLF**
Principles of Optics
Pergamon Press 1980

[8] **Fritz Oberhettinger**
Tables of Bessel Transforms
Springer 1972

[9] **Fritz Oberhettinger**
Tabellen zur Fourier Transformation
Springer 1957

[10] **J.W. Cooley and J.W. Tukey**
An algorithm for the machine calculation of complex Fourier series
Math. Comput.**19**, pp.297-301 (1965)

[11] **Anthony E. Siegman**
Lasers
Univ. Sc. Book (Oxford University Press) 86

[12] **H. Kogelnik, Tingye Li**
Laser beams and resonators Appl. Opt. **5**, p.1550 (1966)

[13] **E. Sziklas, A. E. Siegman**
Mode calculation in unstable resonators with flowing saturable gain I : Hermite-Gaussian expansion
Appl. Opt.**13**, p.2775 (1974)
Mode calculation in unstable resonators with flowing saturable gain II : FFT methods
Appl. Opt.**14**, p.1874 (1975)

[14] **Patrice Hello, jean-Yves Vinet**
Simulation of beam propagation in off-axis optical sytems J. Opt. Paris, 1996 vol 27, N6, pp.265-276

[15] **Michael Hercher**
The spherical mirror Fabry-Perot interferometer
Appl. Opt. **7**, p.951 (1968)

[16] **Erika D'Ambrosio**
to be published in Phys. Rev. D .....

[17] **Patrice Hello**
Modèle physique et simulation de l'antenne interférométrique gravitationnelle Virgo
Thèse de Doctorat en Sciences, Université Paris-Sud (1990)

[18] **G.D. Bergland**
A guided tour of the fast Fourier Transform
IEEE spectrum, July 1969

[19] **B.K. Likeness**
Stray light simulation with advanced Monte-Carlo techniques
Proc. Soc. of Photo-optical Instrumentation Engineers
April 18-21, 1977, Reston (Virginia/USA)

[20] **M. Abramowitz and I. Stegun**
Handbook of mathematical functions
Dover

[21] **Virendra N. Mahajan**
Zernike circle polynomials and optical aberrations of systems with circular pupils
Engineers & Laboratory Notes (Aug. 1994) pp. 21-24

[22] **Patrice Hello and Jean-Yves Vinet**
Analytical models of thermal aberrations in massive mirrors heated by high power laser beams
J. Phys. France 51 (1990) p.1267

[23] **Patrice Hello and Jean-Yves Vinet**
Analytical models of transient thermoelastic deformations of mirrors heated by high power cw laser beams
J. Phys. France 51 (1990) p. 2243

[24] **Yu. Levin**
Internal thermal noise in the LIGO test masses : a direct approach
Phys. Rev. D 57 (1998) p.659

[25] **H.B. Callen and T.A. Welton**
Phys. Rev. 83 (1951) p.34

[26] **Fritz Oberhettinger**
Tables of Bessel Transforms
Springer-Verlag (1972)

[27] **Jean-Yves Vinet**
Journal de Physique (Paris) 10 (1985) p.252

[28] **Timoshenko S. and Goodier J.N.**
Theory of elasticity
Mc Graw & Hill 1951

[29] **F.Bondu and J-Y. Vinet**
Phys. Lett. A 198 (1995) p. 74-78

[30] **A.Gillespie and F. Raab**
Phys. Lett. A 178 (1993) P. 357

[31] **T.M. Niebauer et al.**
Phys. Rev. A **43** (1991) p. 5052

[32] **C. Cagnoli, L. Gammaitoni, F. Marchesoni, M. Punturo**
Virgo note PJT94/032

[33] **F. Bondu, P. Hello, J-Y. Vinet**
Phys. Lett. A 246 (1998) p.227

[34] **Yuk Tung Liu, Kip S. Thorne**
in press for Phys. Rev D (gr-qc/0002055)

[35] **V.B Braginsky, M.L. Gorodetsky and S.P. Vyatchanin**
Phys. Lett. A 264 (1999)

[36] **Landau & Lifshitz**
Course of theoretical physics, Vol.7 Pergamon, 1959

[37] **Erika D'ambrosio, Kip S. Thorne**
Phys. Rev. D 67 102004

[38] **Soma Mukherjee and Lee Samuel Finn**
To be published in the proceedings of the third Amaldi Meeting
(AIP Press) bibitembragg **S. Ramachandran et al.**
Proceedings of the optical fibre communication conference, paper K2
(March 5-10 2006)